Synthese funktionalisierter Linker

und

prä- und postsynthetische Modifikationen von MOFs

Dissertation

zur Erlangung des Doktorgrades

der Mathematisch-Naturwissenschaftlichen Fakultät

der Christian-Albrechts-Universität zu Kiel

vorgelegt von

Ole Beyer

Kiel, 2017

Erster Gutachter:	Prof. Dr. U. Lüning
Zweiter Gutachter:	Prof. Dr. N. Stock
Tag der mündlichen Prüfung:	13.07.2017
Zum Druck genehmigt:	13.07.2017

gez. Prof. Dr. Natascha Oppelt, Dekanin

Die vorliegende Arbeit wurde unter Anleitung von

Prof. Dr. Ulrich Lüning

am Otto-Diels-Institut für Organische Chemie

der Christian-Albrechts-Universität zu Kiel

in der Zeit von März 2014 bis April 2017 angefertigt.

Eidesstattliche Erklärung

Hiermit erkläre ich, Ole Beyer, an Eides statt, dass ich die vorliegende Dissertation selbstständig und nur mit den angegebenen Hilfsmitteln angefertigt habe. Inhalt und Form dieser Arbeit sind, abgesehen von der Beratung durch meinen Betreuer Prof. Dr. Ulrich Lüning, durch mich eigenständig erarbeitet und verfasst worden. Die Arbeit entstand unter Einhaltung der Regeln guter wissenschaftlicher Praxis der Deutschen Forschungsgemeinschaft. Weder die gesamte Arbeit noch Teile davon habe ich an anderer Stelle im Rahmen eines Prüfungsverfahrens eingereicht. Dies ist mein erster Promotionsversuch.

Kiel, den 23.05.2017

_____

Ole Beyer

Danksagung

Als Erstes möchte ich mich bei meinem Doktorvater Prof. Dr. Ulrich Lüning für dieses interessante und vielseitige Thema, die permanent großartige Unterstützung und die schöne Zeit während und neben der Arbeit bedanken.

Großer Dank gilt außerdem meinen Kooperationspartnern Prof. Dr. Norbert Stock, Thomas Homburg, Milan Köppen, Martin Albat, Erika Virmani und Dr. Stefan Wuttke für die ausgezeichnete Zusammenarbeit vor allem gegen Ende dieser Arbeit. Auch Arne Klinkebiel möchte ich danken, für seine Unterstützung zu Beginn dieser Arbeit und für die Ablenkungen neben dem Laboralltag. Ohne Eure Hilfe wäre diese Arbeit in dieser Form nicht möglich gewesen.

Ich möchte dem ganzen AK Lüning für die angenehme Arbeitsatmosphäre und vor allem fürs Korrekturlesen danken. Meinen Laborkollegen Arne, Svenja, Laura, Nelli, Achim, Torben und Julian, meinen F-3-Praktikanten Jesper und Barbara und meiner Bachelorette Chrissy danke ich für die gute Zusammenarbeit, die Unterstützung (vor allem beim Lösungsmittel destillieren) und dafür, dass ihr meine Musik ertragen habt.

Ich möchte mich bei allen Kollegen, Kommilitonen und Freunden, die mich während meines Studiums und meiner Doktorarbeit begleitet und für die eine oder andere Ablenkung gesorgt haben, bedanken. Bei allen Teilnehmern des Stammtisches, aber vor allem Dennis, Roland und Britta, möchte ich mich für die unterhaltsamen Freitage bedanken. Besonders möchte ich meinen Freunden Konradin, Sonja, Andreas, Julia, Antonia, Jan, Thowas W., Mareike und Thomas H. für die schönen gemeinsamen letzten Jahre danken. Ich freue mich, dass wir es trotz teilweise großer Distanz immer wieder schaffen, uns regelmäßig zu treffen.

Besonderer Dank gilt meinen drei Brüdern, meinen Eltern und meinen Großeltern, ohne die das Studium und diese Arbeit nicht möglich gewesen wären. Danke für euren Zuspruch und eure Unterstützung!

Mein allergrößter Dank geht an Ruth! Dafür dass du mich immer wieder motiviert hast, dass du dir geduldig meine Probleme angehört hast und mich, wo auch immer du konntest, unterstützt hast. Ohne die erholsamen Wochenenden mit dir wäre die Arbeit nie so schnell fertig geworden. Die Vorteile überwiegen ganz klar!

Zusammenfassung

Im Rahmen dieser Arbeit sollten funktionalisierte IRMOFs und protonenleitfähige MOFs durch prä- oder postsynthetische Modifikation dargestellt werden.

Für die präsynthetische Darstellung von funktionalisierten IRMOFs wurden in dieser Arbeit verschiedene amino-, nitro-, methoxy- und hydroxyfunktionalisierte Triazin-Linker synthetisiert und für die MOF-Synthese zur Verfügung gestellt. Einige der Linker konnten erfolgreich zur Darstellung von funktionalisierten IRMOFs, basierend auf PCN-6-, MIL-143- und CAU-7-Topologie, verwendet werden.

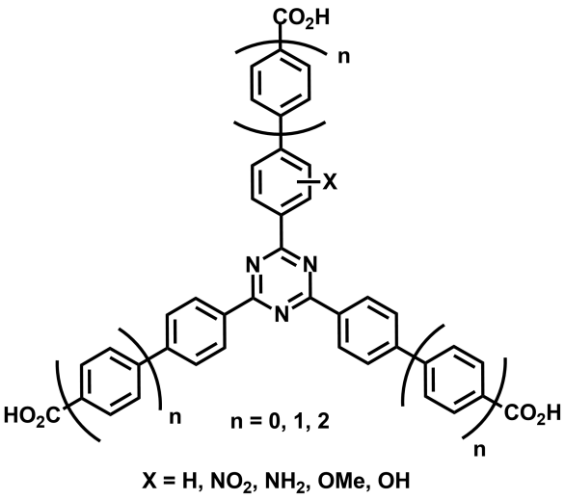

Für einen aminofunktionalisierten Bismut-IRMOF mit CAU-7 Topologie konnten außerdem Methoden zur postsynthetischen Modifikation entwickelt werden. Die Aminogruppen konnten erfolgreich mit aliphatischen Anhydriden, cyclischen Anhydriden und 1,3-Propansulton umgesetzt werden. Auf diese Weise konnten sowohl Carbonsäure- als auch Sulfonsäure-Gruppen in den IRMOF implementiert werden.

Für die präsynthetische Darstellung von protonenleitfähigen MOFs wurden im Rahmen dieser Arbeit zehn unterschiedliche Phosphosulfonsäure-Linker synthetisiert und für die MOF-Synthese zur Verfügung gestellt. In ersten Versuchen konnten einige Linker bereits erfolgreich zu Lanthan-basierten MOFs umgesetzt werden.

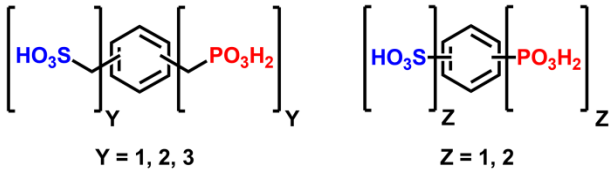

Für die postsynthetische Darstellung von protonenleitfähigen MOFs wurden Methoden zur Implementierung von Phosphonsäure-Gruppen in Cr-MIL-101-Derivate entwickelt. Phosphonsäurediethylester-Gruppen wurden erfolgreich mittels Palladium-katalysierter Kreuzkupplung in die Strukturen von Cr-MIL-101-Br und Cr-MIL-101-NH_2 eingeführt. Phosphonsäure-Gruppen wurden durch nukleophile Substitution in das Cr-MIL-101-NH_2 implementiert.

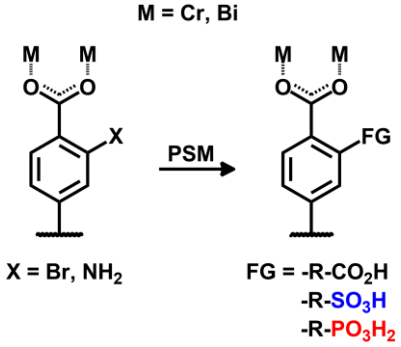

Abstract

The aim of this thesis was the development of pre- and post-synthetic modifications for the preparation of functionalized IRMOFs and proton-conductive MOFs.

For the presynthetic modification of functionalized IRMOFs, several amino, nitro, methoxy, and hydroxy functionalized triazine linkers were synthesized. Some were successfully used in the synthesis of new functionalized IRMOFs based on PCN-6, MIL-143 and CAU-7 topology.

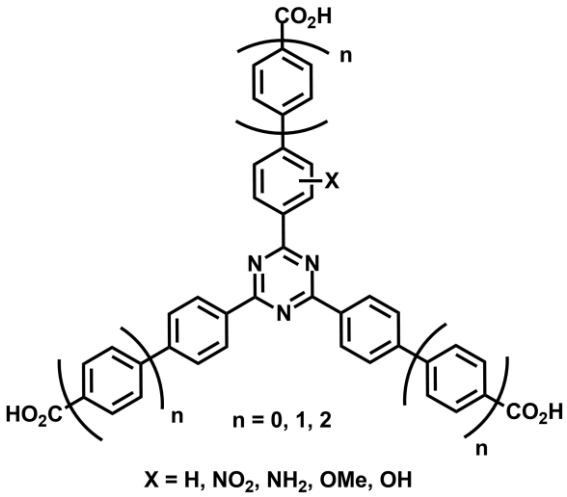

Post-synthetic modifications were developed for an amino functionalized bismuth IRMOF with CAU-7 topology. The amino groups were modified by reaction with aliphatic anhydrides, cyclic anhydrides and 1,3-propane sulton. Using this approach, carboxylic and sulfonic acid groups were introduced into the framework.

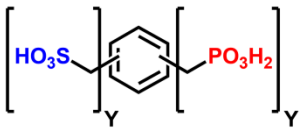

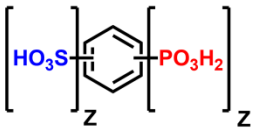

For the presynthetic modification of proton-conductive MOFs, several phosphonosulfonic acid linkers were synthesized. Some linkers were successfully used in the synthesis of lanthanum based MOFs.

Methods for the post-synthetic introduction of phosphonic acid groups into Cr-MIL-101 derivatives were developed to obtain proton-conductive MOFs. Cr-MIL-101-Br and Cr-MIL-101-NH_2 were successfully used in palladium-catalyzed cross coupling reactions to introduce phosphonic acid diethylester groups within the framework. Phosphonic acid groups were implemented into the framework of Cr-MIL-101-NH_2 by nucleophilic substitution.

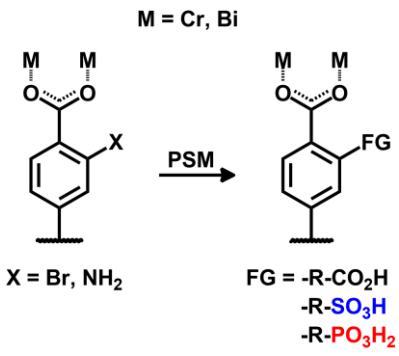

Abkürzungsverzeichnis

AK	Arbeitskreis
aliph.	aliphatisch
Ar	Aryl (NMR)
arom.	aromatisch
BBC	4,4′,4″-[benzene-1,3,5- triyl-tris(benzene-4,1-diyl)]-tribenzoate
BDC	benzenedicarboxylate
BET	Brunnauer-Emmet-Teller
BPDC	biphenyldicarboxylate
BTB	4,4′,4″-benzene-1,3,5-triyl-tribenzoate
BTC	benzenetricarboxylate
BTE	4,4′,4″-[benzene-1,3,5-triyl-tris(ethyne-2,1-diyl)]-tribenzoate
ber.	berechnet
br.	breit (NMR)
bzw.	beziehungsweise
CAU	Christian-Albrechts-Universität zu Kiel
COSY	correlated spectroscopy
CP	coordination polymer
d	Dublett (NMR)
DC	Dünnschichtchromatographie
DMF	*N*,*N*-Dimethylformamid
DOT	2,5-dioxidoterephthalate
dppf	1,1`-Bis(diphenylphosphin)ferrocen
EA	Elementaranalyse
EDXRD	energy dispersive X-ray diffraction
EI	Elektronen-Ionisation
ESI	Elektronenspray-Ionisation
gef.	gefunden
ges.	gesättigt
HKUST	Hongkong University of Science and Technology
HMBC	hetero nuclear multiple bond correlation
HPLC	high performance liquid chromatography
HRMS	high resolution mass spectrometry
HSQC	hetero single quantum coherence

i. Vak.	im Vakuum
IR	Infrarot
IRMOF	isoreticular metal-organic framework
IUPAC	International Union of Pure and Applied Chemistry
konz.	konzentriert
Lit.	Literatur
m	Multiplett (NMR)
m_c	zentriertes Multiplett (NMR)
MIL	Matérial Institut Lavoisier
MOF	metal-organic framework
MS	Massenspektrometrie
MW	Mikrowelle
NMR	nuclear magnetic resonance
org.	organisch
PCN	porous coordination network
PCP	porous coordination polymer
PSD	postsynthetic deprotection
PSE	postsynthetic exchange
PSI	postsynthetic insertion
PSM	postsynthetic modification
PSP	postsynthetic polymerization
pto	Pt_3O_4
PXRD	powder X-ray diffraction
q	Quartett (NMR)
quant.	quantitativ
Raumtemp.	Raumtemperatur
R_f	Retentionsfaktor
s	Singulett (NMR)
SBU	secondary building unit
SEM	scanning electron microscope
t	Triplett (NMR)
TAPB	4,4′,4″-(triazine-2,4,6-triyl-tris(benzene-4,1-diyl))tribenzoate
TATAB	4,4′,4″-[(1,3,5- triazine-2,4,6-triyl)tris(azanediyl)]tribenzoate
TATB	4,4′,4″-(1,3,5-triazine- 2,4,6-triyl)tribenzoate

tbo	twisted boracite
TCPT	2,4,6-tris-(4-carboxyphenoxy)-1,3,5-triazine
TDPAT	2,4,6-tris(3,5-dicarboxylphenylamino)-1,3,5-triazine
TMS	Trimethylsilyl
TPT	2,4,6-tris(4-pyridyl)-1,3,5-triazine
UiO	Universitetet i Oslo
Valenzschw.	Valenzschwingung
wässr.	wässrig
wasserfr.	wasserfrei
z. B.	zum Beispiel

Inhaltsverzeichnis

1 Einleitung

Ein in den letzten Jahrzehnten stetig wachsendes Forschungsgebiet beschäftigt sich mit der Untersuchung von Koordinationspolymeren (coordination polymers, CPs) oder auch Metall-organischen Gerüstverbindungen (metal-organic frameworks, MOFs).[1–7] Bis heute ist die Definition des Begriffes MOF bzw. eine genaue Abgrenzung zwischen CPs und MOFs umstritten.[8] Von 2009 bis 2013 befasste sich eine IUPAC-Arbeitsgruppe mit diesem Problem und empfahl die folgenden Terminologien. Als Überbegriff für sich wiederholende Koordinationsverbindungen in ein, zwei oder drei Dimensionen wird der Begriff Koordinationspolymer definiert. Dieser sehr allgemeine Begriff wird durch die Untergruppe des Koordinationsnetzwerkes genauer spezifiziert, indem auf Vernetzungen der Koordinationseinheiten eingegangen wird. MOFs wiederrum werden als Koordinations-netzwerke mit organischen Liganden und potenziellen Hohlräumen definiert.[9] Hierbei soll erwähnt werden, dass die Klassifizierung einiger Verbindungen, auf die im Rahmen dieser Arbeit verwiesen wird, nicht eindeutig ist und es sich eventuell nicht um MOFs handelt. Die Verbindungen werden trotzdem im Zusammenhang mit MOFs zitiert, da sie ähnliche Eigenschaften aufweisen oder ein auf MOFs übertragbares Prinzip verdeutlichen sollen.

MOFs sind Netzwerke, die aus organischen Liganden (sogenannte Linker) und anorganischen Baueinheiten (Metall-Ionen oder Metall-Oxo-Cluster) aufgebaut sind. Dabei koordinieren die Linker über funktionelle Gruppen an den anorganischen Baueinheiten und es können sich amorphe Strukturen oder kristalline 1D-, 2D- oder 3D-Netzwerke ausbilden. Diese Netzwerke besitzen Porensysteme (Mikro- bis Mesoporen) und können eine daraus resultierende hohe Oberfläche besitzen. Im Gegensatz zu anderen porösen Verbindungen wie Zeolithen oder Aktivkohle kann durch die Wahl der Metall-Ionen und Linker, sowohl die Porengröße als auch die Poreneigenschaft beeinflusst werden. Dies macht sie zu interessanten Materialien für Gasspeicherung[10–12]/-trennung[13,14], Katalyse[15–18], Wirkstofftransport[19,20] und Sensorik[21,22].

Obwohl Koordinationspolymere schon seit Anfang des 20. Jahrhunderts bekannt sind, wurden CPs erst zu Beginn der 1990er Jahre von HOSKINS und ROBSON genauer untersucht.[23,24] Der Begriff „MOF“ hingegen wurde erst 1995 von YAGHI für eine Schichtstruktur aus Kobalt-Ionen und Trimesinsäure (BTC, Abkürzungen für alle Linker werden im Abkürzungsverzeichnis erklärt) geprägt.[25] Ein paar Jahre später wurde die Synthese von

MOF-5[26] und HKUST-1[27] (Abkürzungen für alle MOFs werden im Abkürzungsverzeichnis erklärt) beschrieben. MOF-5 besteht aus Dianionen der Terephthalsäure (BDC), die über Zn_4O-Cluster verknüpft sind und zeichnet sich durch seine thermische Stabilität bis 300 °C und eine hohe Oberfläche (3800 m^2/g, BET[28,29]) aus.[30] HKUST-1 ist aus Kupfer-Kationen und BTC-Linkern aufgebaut und eignet sich trotz seiner recht kleinen Oberfläche (700 m^2/g, BET) gut zur Gasspeicherung[31]. Beide gehören bis heute zu den am besten untersuchten Verbindungen ihrer Klasse.

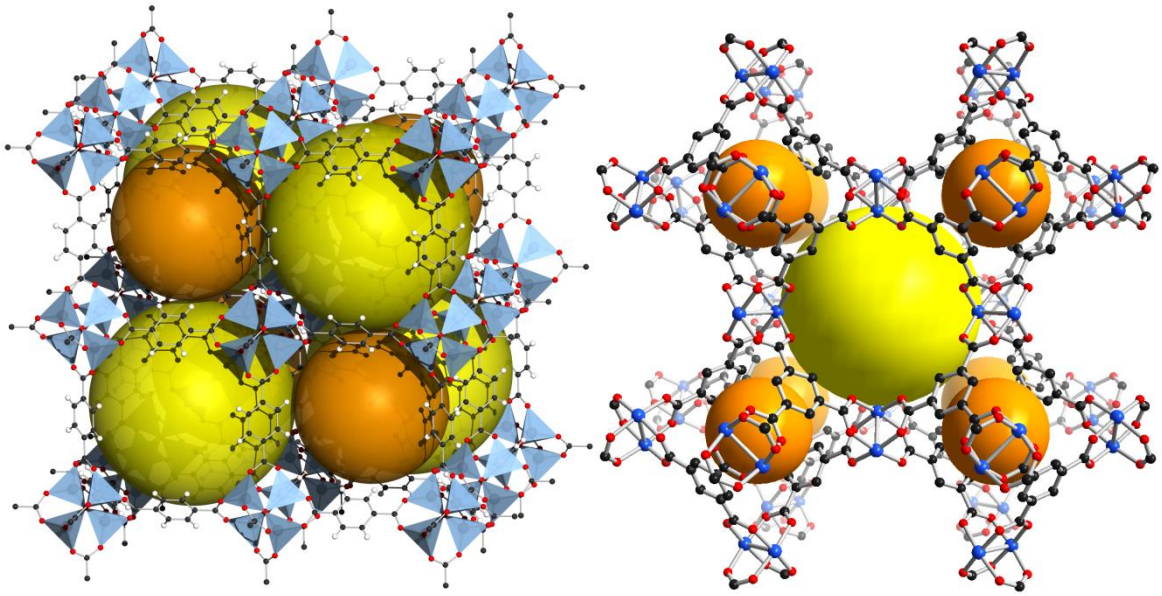

Abb. 1: Kristallstrukturen von MOF-5 (l.) und HKUST-1 (r.). Schwarz = Kohlenstoff, rot = Sauerstoff, blau = Kupfer, weiß = Wasserstoff, hellblaue Tetraeder = Zn_4O, gelbe und orange Sphären geben den größtmöglichen Platz in den Poren an. (Bilder: T. Boehle[32])

Der modulare Aufbau von MOFs ermöglicht eine nahezu unbegrenzte Kombinationsmöglichkeit von Linkern und Metall-Ionen. Trotzdem ist die gezielte Synthese von MOFs mit bestimmten Topologien und Eigenschaften oft schwierig, da die MOF-Synthese von vielen Faktoren abhängt. Die Koordinationseigenschaften von Linkern und Metall-Ionen müssen gut untersucht sein, mögliche Topologien sollten bekannt sein und die Synthesebedingungen müssen eine Kristallisation des MOFs ermöglichen. Dabei ist die Suche nach geeigneten Synthesebedingungen oft der entscheidende Faktor für eine gezielte MOF-Synthese. Je nach Synthesemethode und gewählten Syntheseparametern können sich unterschiedliche MOFs bilden.[33] Zu den gängigsten Synthesemethoden gehören konventionelles Heizen unter Normaldruck[34–36], Solvothermalsynthese[37], Mikrowellen-Synthese[38–40], Sonochemie[33,41], Mechanochemie[42] und Elektrochemie[43]. Außerdem können Parameter wie Reaktionszeit, Temperatur, Druck, Verhältnis der Ausgangsmaterialien, Lösungsmittel und pH-Wert variiert

werden.[44] Um die optimalen Parameter zu finden, können sogenannte Hochdurchsatz-methoden verwendet werden.[45,46] Vorteile dieser Methoden sind, dass mehrere MOF-Synthesen parallel durchgeführt werden können und viele Parameter variierbar sind. Um zusätzlich den Kristallisationsprozess zu verstehen, können z. B. in situ-Untersuchungen durch zeitaufgelöste EDXRD (energy-dispersive X-ray diffraction) durchgeführt werden.[47] Die Untersuchung dieser komplexen Zusammenhänge ist eine wichtige Voraussetzung für eine gezielte MOF-Synthese.

Bis heute gibt es nur wenige Strategien[48–51], die eine Kontrolle über die Struktur des MOFs und damit eine gezielte MOF-Synthese ermöglichen. Dies liegt unter anderem daran, dass die Ausgangsmaterialien ihre strukturelle Integrität während der MOF-Synthese oft nicht beibehalten und somit eine Vorhersage der Struktur, basierend auf den strukturellen Eigenschaften der Ausgangsmaterialien, schwierig ist. Das Konzept der „retikularen Synthese“[52,53] umgeht dieses Problem, indem es unveränderbare Baueinheiten (SBU = secondary building unit)[54,55] nutzt.

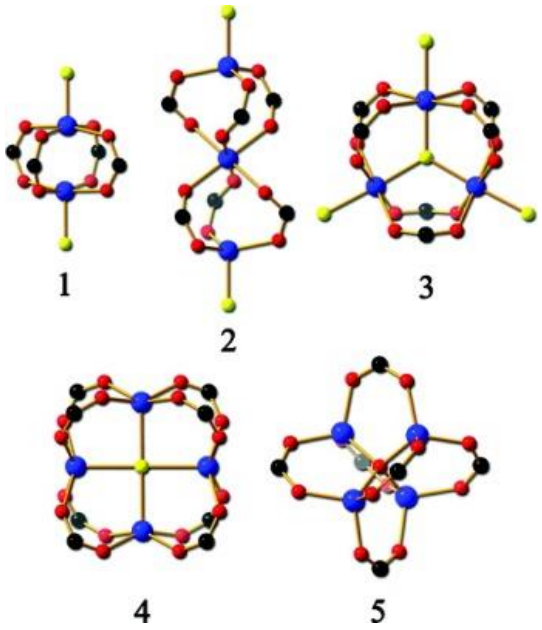

Abb. 2: Beispiele für typische SBUs. Schwarz = Kohlenstoff einer Carboxylat-Gruppe des Linkers, rot = Sauerstoff, blau = Metall, gelb = undefiniert). 1) dinuclear paddlewheel, 2) trinuclear hourglass, 3) trinuclear prism, 4) tetranuclear cuboid, 5) tetranuclear octahedron. (Bild[56])

Dabei handelt es sich um molekulare Komplexe oder Cluster bestehend aus Metall-Ionen und daran koordinierenden funktionellen Gruppen wie z.B. Carboxylate. Sind die geometrischen und chemischen Eigenschaften der SBUs und Linker bekannt, lässt sich die Topologie des MOFs vorhersagen. Entscheidend für erfolgreiche retikulare Synthese ist, dass sich entweder

die strukturelle Integrität der SBU während der Synthese nicht ändert oder die Synthesebedingungen zur *in situ*-Darstellung der SBU bekannt sind. Die ersten auf diese Weise synthetisierten MOFs sind MOF-2[57] und MOF-5[26].

Breite Anwendung findet die retikulare Synthese bei der Darstellung neuer IRMOFs (isoreticular MOF). Als IRMOFs wird eine Serie von MOFs mit unterschiedlichen Linkern aber gleicher SBU und gleicher Topologie bezeichnet. Ausgehend von einem MOF, dessen Synthesebedingungen bekannt sind, können durch die Verwendung verlängerter oder funktionalisierter Linker neue isoretikulare MOFs erhalten werden. Dabei kann der Linker Einfluss auf Größe, Form und Eigenschaft der Poren haben. Ein Beispiel ist der 2008 gleichzeitig von DIETZEL[58] und MATZGER[59] beschriebene Mg-MOF-74. Dieser MOF wird unter basischen Bedingungen aus dem DOT-Linker und Magnesiumnitrat synthetisiert. Sowohl die deprotonierten Carbonsäuregruppen als auch die deprotonierten Hydroxylgruppen koordinieren am Magnesium-Sauerstoff-Cluster und bilden einen zum Zn-MOF-74[60] isostrukturellen MOF.

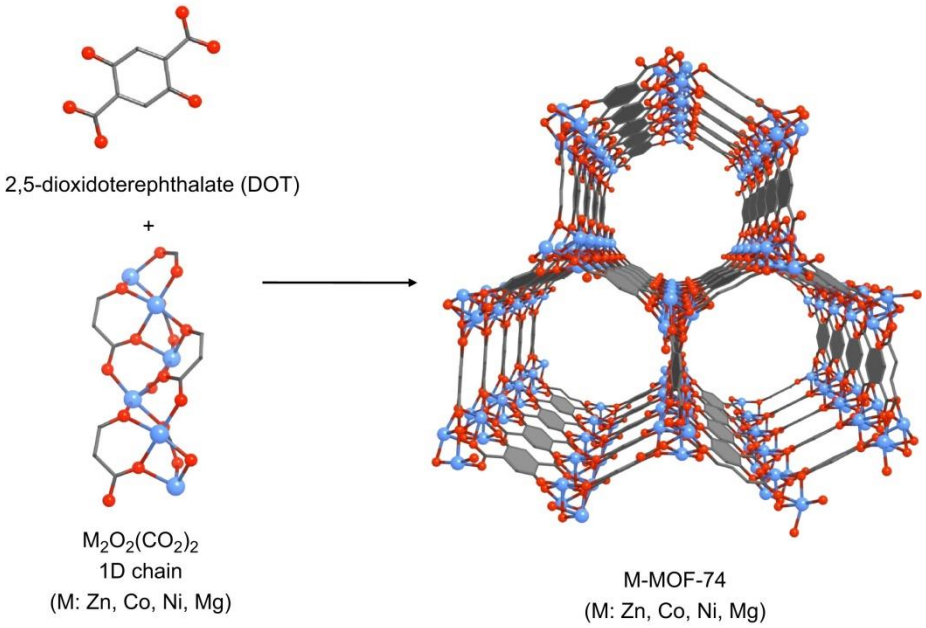

Abb. 3: Synthese und Struktur des MOF-74 mit unterschiedlichen Metall-Ionen. Grau = Kohlenstoff, rot = Sauerstoff, blau = Metall. (Bild[61])

YAGHI nutzte die retikulare Synthese zur Darstellung neuer IRMOFs (IRMOF-74-I bis -XI) basierend auf Mg-MOF-74.[62] Dazu wurde der DOT-Linker verlängert, indem der Abstand zwischen den koordinierenden Carboxylat/Phenolat-Paaren vergrößert wurde. Mit einer Größe von 98 Å besitzt der erhaltene IRMOF-74-XI einen der größten bisher beschriebenen Poreneingänge und gleichzeitig die niedrigste bekannte Dichte (0.195 g/cm^3) für einen

Kristall bei Raumtemperatur. Das Besondere der IRMOF-Serie des Mg-MOF-74 ist, dass keine interpenetrierenden Netzwerke entstehen können und alle IRMOFs permanent porös sowie stabil bis 300 °C sind. Ob interpenetrierende Netzwerke, also Netzwerke, die in einander verwoben, aber nicht über chemische Bedingungen verknüpft sind, entstehen können, hängt von der Struktur des MOFs ab.[51,54] Beispiele für Interpenetration zweier Netzwerke wurde bei einer anderen IRMOF-Serie basierend auf MOF-5 beobachtet.[63]

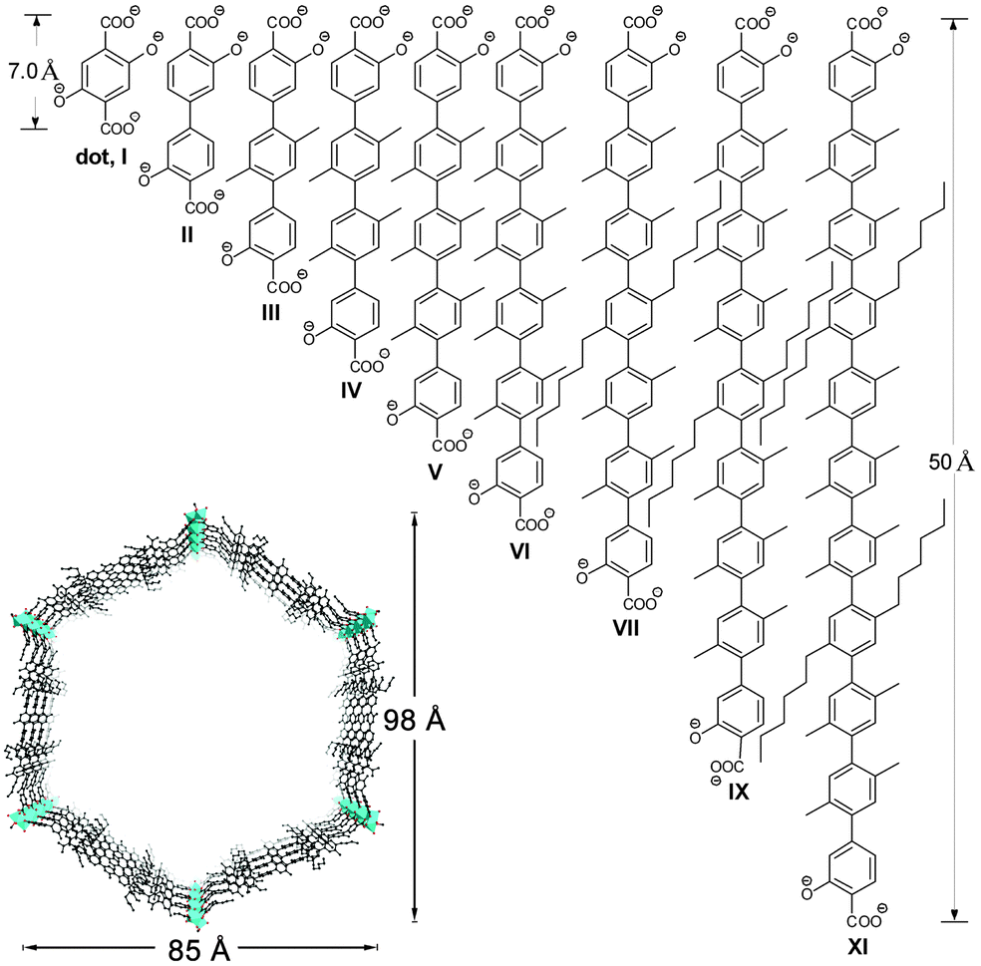

Abb. 4: Linker, die zur Darstellung von IRMOF-74-I bis XI verwendet wurden, und eine Ansicht der Poreneingänge des IRMOF-74-XI. Schwarz = Kohlenstoff, rot = Sauerstoff, türkis = Magnesium. (Bild[64])

Neben den gerade erwähnten Beispielen, basierend auf ditopen Linkern, gibt es auch IRMOF-Serien, die auf tritopen Linkern basieren. Ein Beispiel ist der aus H_3BTB-Linkern und Zn_4O-Clustern bestehende MOF-177.[65] Dieser zeichnet sich durch ein nicht-interpenetrierfähiges Netzwerk aus, eine wichtige Voraussetzung für die Synthese von hochporösen MOFs. Durch den Einsatz von verlängerten Linkern wie H_3BTE und H_3BBC konnten zwei isoretikulare MOFs (MOF-180 und MOF-200) erhalten werden.[66] Das Volumen der Elementarzelle ist 1.9-mal (MOF-180) bzw. 2.6-mal (MOF-200) größer als beim MOF-177. Ein anderes

Beispiel ist das MOF-399. Dabei handelt es sich um einen IRMOF, basierend auf HKUST-1 mit H_3BBC als Linker. MOF-399 besitzt eine 17.4-mal größere Elementarzelle als HKUST-1, eine extrem niedrige Dichte von 0.126 g/cm^3 und einen inneren Porendurchmesser von 43.2 Å.[67]

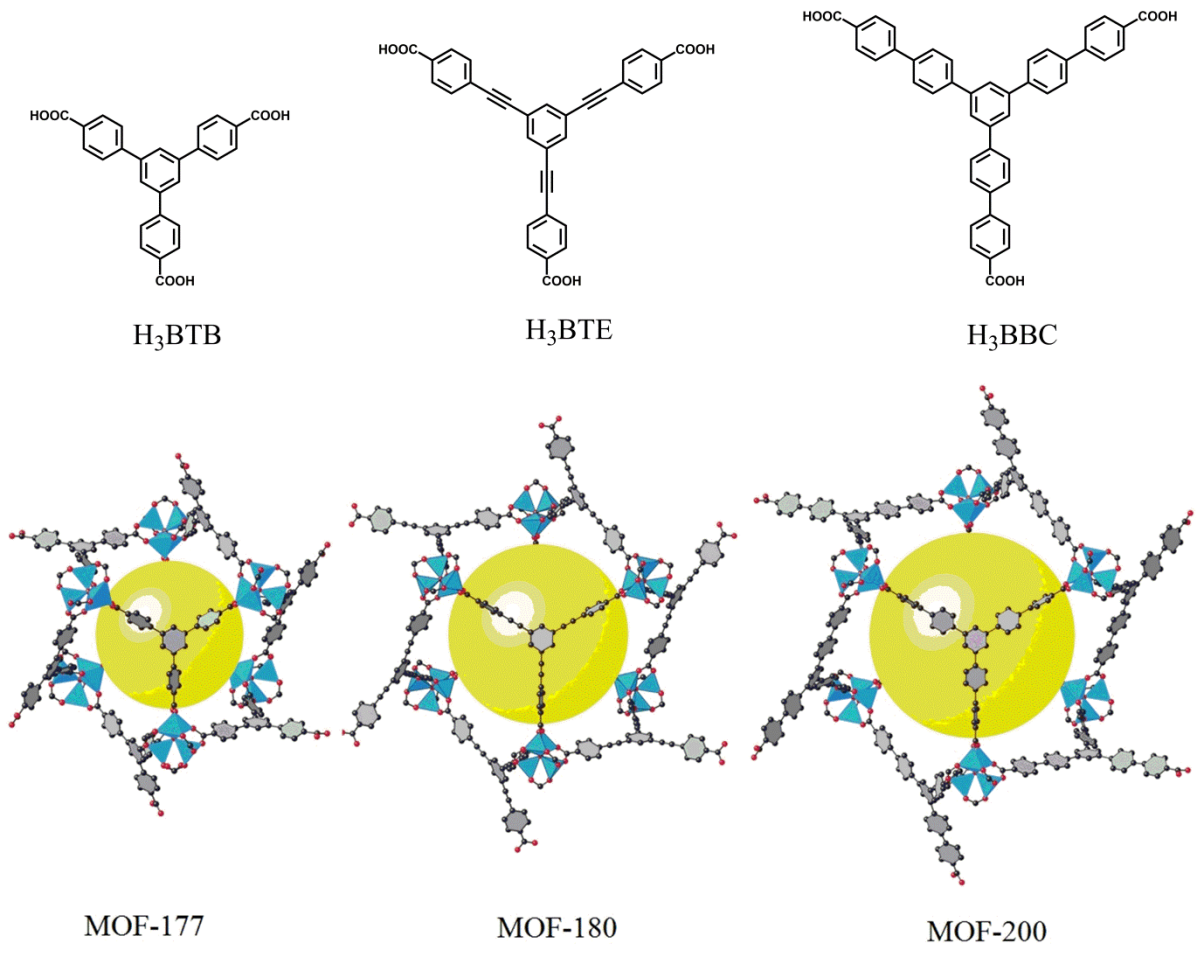

Abb. 5: Die Kristallstrukturen zeigen eine Vergrößerung der Poren von MOF-177 über MOF 180 bis MOF-200. Die zugehörigen Linker sind jeweils über der Kristallstruktur abgebildet. Schwarz = Kohlenstoff, rot = Sauerstoff, blaue Tetraeder = Zn_4O, gelbe Sphären geben den größtmöglichen Platz in den Poren an. (Bild[68])

Die beschriebenen Beispiele zeigen, wie die retikulare Synthese genutzt werden kann, um die Poren von MOFs zu vergrößern. Eine andere Möglichkeit, die Eigenschaften von MOF-Poren zu verändern, wäre der Einsatz von funktionalisierten Linkern (siehe Kapitel 1.2). Doch die Synthese und Untersuchung von erweiterten oder funktionalisierten IRMOFs ist oft durch die Verfügbarkeit der entsprechenden Linker limitiert. Ein Beispiel sind tritope Carbonsäure-Linker mit einem Triazinkern. Obwohl der bekannteste Vertreter H_3TATB schon erfolgreich in diversen MOF-Synthesen eingesetzt wurde, sind erweiterte Vertreter nur selten und funktionalisierte gar nicht beschrieben.

1.1 Triazin-basierte Linker

Obwohl bereits eine Vielzahl an MOFs mit Triazin-basierten Linkern bekannt sind, ist das Potential dieser Linker noch längst nicht erschöpft. Dies zeigt sich vor allem daran, dass der Großteil dieser MOFs auf gerade einmal fünf Linkern basiert. Dabei handelt es sich, bis auf den hexadentaten H_6TDPAT-Linker[69–72], grundsätzlich um tritope Linker. Eine Besonderheit ist der Pyridin-substituierte TPT-Linker[73–76], da dieser über seine Pyridin-Stickstoff-Atome an Metallzentren koordinieren kann. Während der Melamin-basierte H_3TATAB-Linker[77–80] bereits in einer Vielzahl von MOFs Anwendung findet, wurde der Cyanursäure-basierte H_3TCPT-Linker[81–83] bis jetzt nur selten eingesetzt. Trotz des offensichtlichen Potentials aller genannten Linker soll im Folgenden der Fokus auf den H_3TATB-Linker gelegt werden.

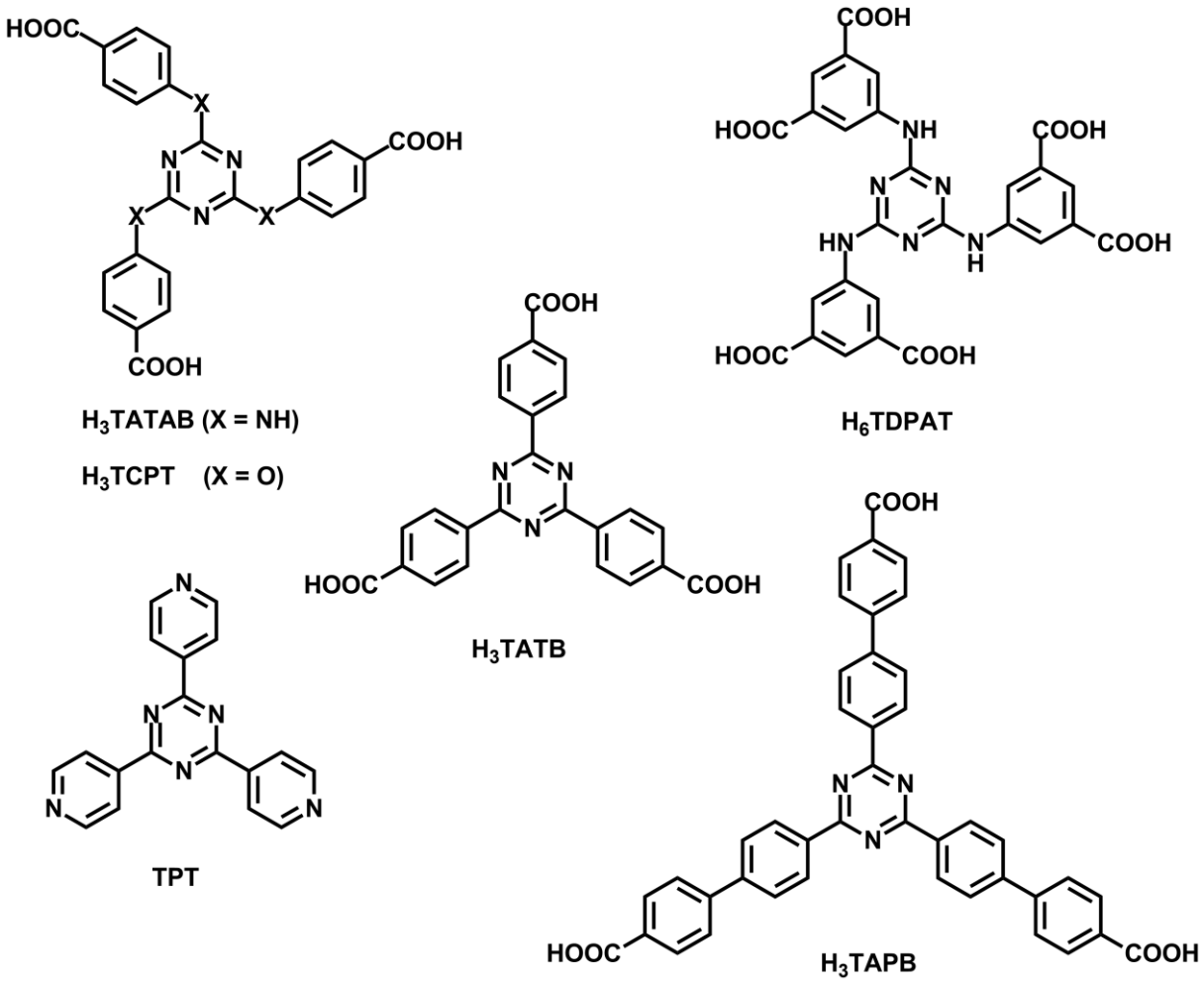

Abb. 6: Übersicht der am häufigsten eingesetzten Triazin-basierten Linker.

Der H_3TATB-Linker wurde bereits in einer Vielzahl von MOF-Synthesen erfolgreich eingesetzt. Je nach eingesetztem Metall-Ion (Al[84], Sc[84], Mn[85,86], Fe[84], Co[86–88], Ni[89], Cu[90,91], Zn[85,86,92–94], Cd[85,93], Lanthanoide[95–100]) konnten unterschiedliche Strukturen

beobachtet werden. Vergleicht man diese Triazin-basierten MOFs mit ähnlichen benzol-basierten MOFs, beobachtet man teilweise erhebliche Unterschiede in den Eigenschaften. Ein Beispiel sind die starken π-π-Wechselwirkungen, die sich zwischen den Triazin-Ringen ausbilden können. Diese sorgen für eine erhöhte thermische Stabilität von Triazin-basierten MOFs.[85,86] Gleichzeitig begünstigen die starken Wechselwirkungen die Bildung von interpenetrierenden Netzwerken. Die kleinen Poren dieser Netzwerke können bei der Adsorption von Gasen im Vorteil sein, da die Wechselwirkungen der meist kleinen Gasmoleküle mit der Porenoberfläche größer sind als bei MOFs mit großen Poren.[90,99] Aber auch die Stickstoffatome des Triazin-Kerns können einen direkten Einfluss auf die Menge und Selektivität bei der Adsorption von Gasen haben. Dies zeigte der Vergleich von zwei isoretikularen Dysprosium-MOFs mit H_3TATB und H_3BTB als Linker. Für den Triazin-basierten MOF wurde eine wesentlich höhere CO_2-Kapazität beobachtet.[95]

Hierbei sollte man erwähnen, dass dies ein seltenes Beispiel für isoretikulare MOFs basierend auf H_3TATB und H_3BTB ist. In den meisten Fällen werden trotz gleicher Synthesebedingungen völlig unterschiedliche Topologien erhalten. Dies ist hauptsächlich auf die fehlenden Wasserstoffatome am Triazin-Kern des H_3TATB-Linkers (im Gegensatz zum H_3BTB-Linker) und die daraus resultierende Planarität zurückzuführen.[67] Berechnungen in der Gasphase liefern für den Triazin-Linker einen Winkel von 0.006° zwischen den Ebenen der peripheren Aromaten bzw. den Carboxylat-Gruppen und dem Triazin-Ring. Der H_3BTB-Linker besitzt hingegen einen Winkel von 38.5°, da sich die Wasserstoffatome des Benzol-Kerns und die *ortho*-Wasserstoffatome der peripheren Aromaten abstoßen[101] (siehe Kapitel 3.1). Die Planarität des H_3TATB-Linkers sorgt außerdem für eine wesentlich stärkere Delokalisierung der π-Elektronen und trägt so wesentlich zu der beschriebenen thermischen Stabilität von Triazin-basierten MOFs bei (s.o.).

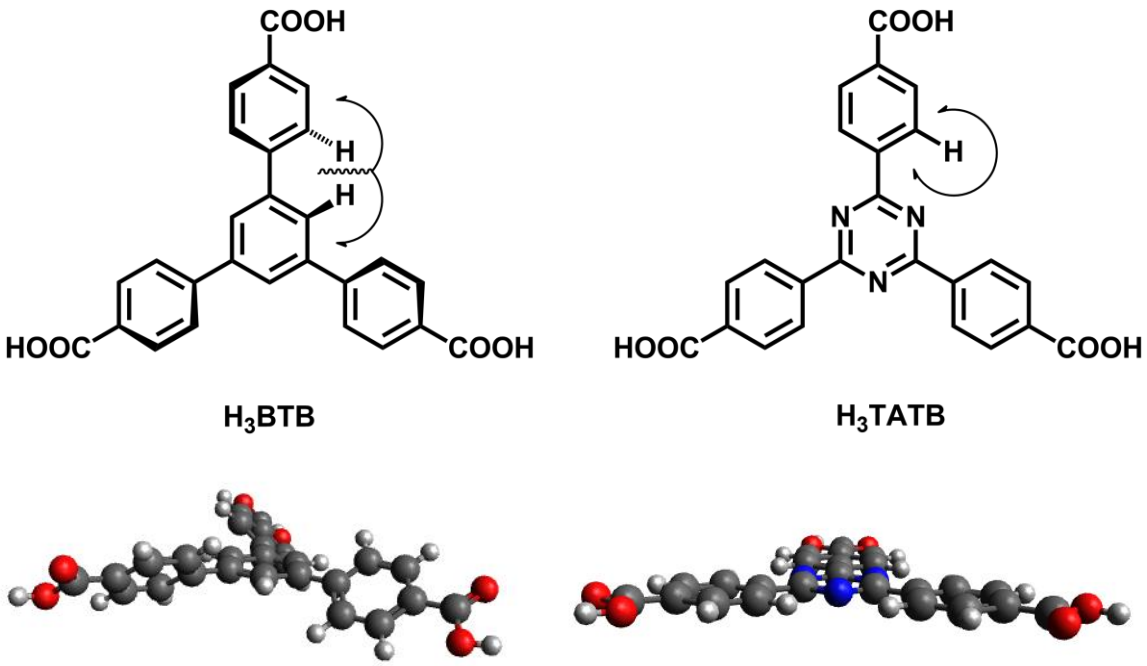

Abb. 7: Strukturelle Unterschiede der Linker H_3BTB und H_3TATB. Die unteren beiden Strukturen wurden mit B3LYP//6-31G* berechnet.[101]

Inwiefern der Triazin-Kern die Topologie eines MOFs beeinflusst, kann gut anhand zweier Beispiele gezeigt werden. Der 2001 von YAGHI beschriebene MOF-14[102] besitzt eine dinuclear paddle-wheel SBU aus Cu^{2+}-Ionen und den Carboxylat-Gruppen des H_3BTB-Linkers. Mit der gleichen SBU bildet sich unter Verwendung des H_3TATB-Linkers der sogenannte PCN-6[90] MOF. Aufgrund der strukturellen Unterschiede der Linker besitzt MOF-14 eine **pto**-Topologie und PCN-6 eine **tbo**-Topologie. (Topologie-Abkürzungen aus „Reticular Chemistry Structure Resource“[103]) Auch die um einen Phenyl-Ring erweiterten Linker H_3BBC und H_3TAPB bilden mit Cu^{2+}-Ionen stabile MOFs. In diesem Fall ändert sich die Topologie und der Triazin-basierte MOF-388 besitzt eine **pto**-Topologie und der benzol-basierte MOF-399 besitzt eine **tbo**-Topologie.[67]

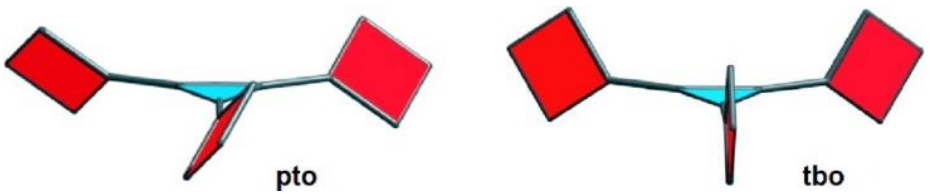

Abb. 8: Vereinfachte Darstellung der **pto**- und **tbo**-Topologie. Hellblaue Dreiecke = Linker, rote Quadrate = SBU. (Bild[104])

Wann welche Topologie bevorzugt wird, hängt davon ab, wie groß der Winkel zwischen der Ebene der Carboxylat-Gruppe und der Ebene des Kerns (Benzol oder Triazin) ist. Wenn beide

Ebenen koplanar zueinander sind, wird die **tbo**-Topologie bevorzugt. Sind sie zueinander verdreht, wird die **pto**-Topologie bevorzugt.

Die genannten Beispiele zeigen, dass schon kleine Änderungen am Linker große Auswirkungen auf die Struktur und Eigenschaft eines MOFs haben können. Da bereits eine Vielzahl an MOFs basierend auf dem H_3TATB-Linker bekannt sind, würden sich erweiterte und vor allem funktionalisierte Triazin-Linker für eine retikulare Synthese anbieten. Durch das prä- oder postsynthetische Einführen funktioneller Gruppen könnten IRMOFs mit definierten Eigenschaften dargestellt werden.

1.2 Prä- und postsynthetische Modifikation von MOFs

Die Entwicklung von postsynthetischen Methoden zur Modifizierung der physikalischen und chemischen Eigenschaften eines MOFs hat in den letzten Jahren stetig zugenommen. Methoden wie postsynthetische Entschützung (PSD), postsynthetischer Austausch (PSE), postsynthetische Insertion (PSI) und postsynthetische Polymerisation (PSP) sind mittlerweile etablierte Methoden, um nach der MOF-Synthese eine Funktionalität einzufügen.[105] Zu den am besten untersuchten und am häufigsten verwendeten Methoden gehören jedoch die präsynthetische Modifikation mittels funktionalisierter Linker und die postsynthetische Modifikation[105–108] (PSM) von MOFs. Beide Methoden haben Vor- und Nachteile.

Als präsynthetische Modifikation wird der Einsatz funktionalisierter Linker in der MOF-Synthese bezeichnet. Dabei geht man meistens von Linkern aus, die bereits erfolgreich zur Synthese von MOFs verwendet wurden. Diese werden mit funktionellen Gruppen versehen und im Idealfall zur Synthese von IRMOFs verwendet.[63] Entscheidend dabei ist, dass die funktionelle Gruppe die Löslichkeit möglichst nicht beeinflusst, nicht an Metall-Ionen koordinieren kann und während der MOF-Synthese stabil bleibt. Da viele interessante funktionelle Gruppen mindestens eine der genannten Voraussetzungen nicht erfüllen, ist die Synthese von funktionalisierten IRMOFs oft schwierig. Die Vorteile einer retikularen Synthese (gleiche Synthesebedingungen) fallen weg und für jeden funktionalisierten Linker muss das Ausprobieren neuer Synthesebedingungen in Kauf genommen werden. Trotzdem konnte bis heute eine Vielzahl an präsynthetisch funktionalisierten MOFs erfolgreich dargestellt werden.

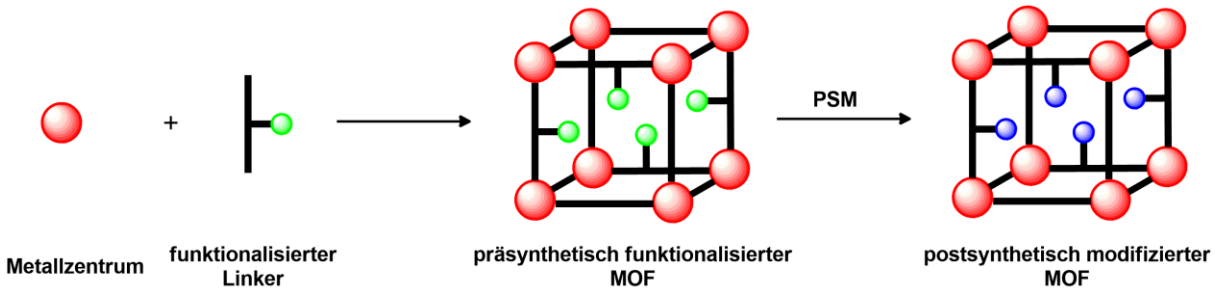

Abb. 9: Schematische Darstellung der Synthese eines präsynthetisch funktionalisierten MOFs und anschließender postsynthetischer Modifikation.

Bei der postsynthetischen Modifikation werden die eingesetzten Linker erst nach der Synthese des MOFs modifiziert. Damit eine PSM erfolgreich durchgeführt werden kann, müssen folgende Voraussetzungen erfüllt sein. Die Poren müssen ausreichend groß sein, damit die entsprechenden Reagenzien ins Netzwerk eindringen können. Außerdem muss das MOF stabil gegenüber den postsynthetischen Bedingungen sein und darf seine kristalline Struktur nicht verlieren. Die wohl wichtigste Voraussetzung ist, dass bereits funktionelle Gruppen im Netzwerk vorliegen, an denen die Modifikationen durchgeführt werden können. Es sind zwar auch „unfunktionalisierte“ bzw. aromatische MOFs mittels elektrophiler Substitutions-reaktionen modifiziert worden, aber dies ist auf Grund der sehr drastischen Reaktionsbedingungen nur bei extrem stabilen MOFs möglich.[109] Die Darstellung von präsynthetisch funktionalisierten MOFs ist also eine wichtige Grundlage, um postsynthetische Modifikationen durchführen zu können. Im Folgenden sollen einige Beispiele von kovalenter PSM erläutert werden. Für Beispiele von dativer PSM (PSM durch Metallionen-Koordination) sei auf Reviews verwiesen.[106,108]

Eines der ersten Beispiele für eine erfolgreiche PSM war die von COHEN beschriebene Acetylierung von IRMOF-3.[110] IRMOF-3 ist isoretikulär zu MOF-5, besitzt im Gegensatz zu MOF-5 aber nicht Terephthalsäure (BDC) als Linker sondern 2-Aminoterephthalsäure (NH_2-BDC). Die Aminogruppe des Linkers koordiniert nicht an die SBU (Zn_4O) und ist damit frei zugänglich für eine PSM. Die Umsetzung der Aminogruppe mit Essigsäureanhydrid verlief nach Optimierung der Reaktionsbedingungen quantitativ und lieferte den IRMOF-3-AM1. Der Einsatz von Anhydriden mit unterschiedlichen Kettenlängen lieferte zehn weitere modifizierte MOFs (IRMOF-3-AM2 - 7, -AM9, -AM13, -AM16, -AM19), wobei die Umsetzung zwischen 99 % (-AM2) und 7 % (-AM19) lag.[111] Kristallinität und Porosität wurden für alle MOFs durch Pulver-Röntgendiffraktometrie und Sorptionsmessungen bestätigt. Die Sorptionsmessungen zeigten außerdem, dass sich mit zunehmender Kettenlänge die Oberfläche des modifizierten MOFs verringerte.

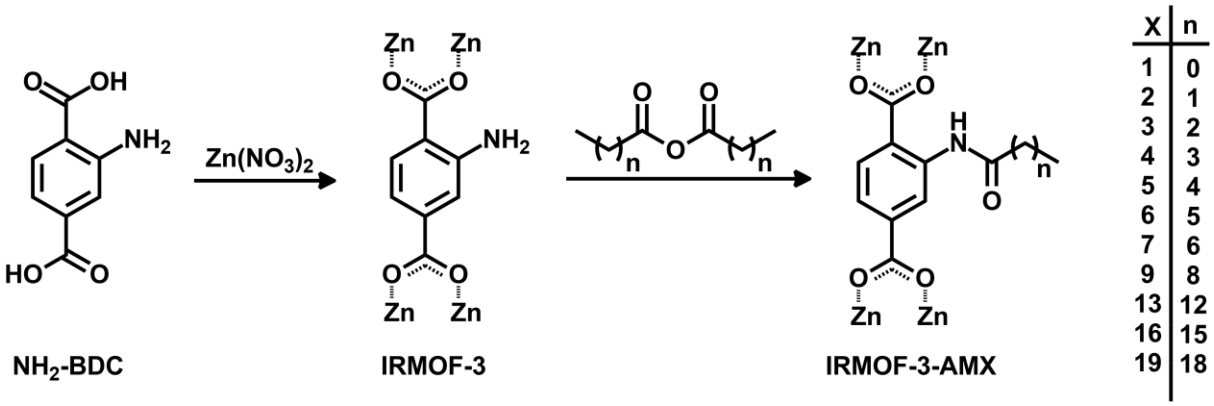

Abb. 10: Synthese von IRMOF-3 und postsynthetische Modifikation mit unterschiedlichen Anhydriden.

In den folgenden Jahren konnte eine Vielzahl postsynthetischer Modifikationen an funktionalisierten MOFs durchgeführt werden. Mehrere Azid-funktionalisierte MOFs wurden in 1,3-dipolaren Cycloadditionen mit Alkinen zu den jeweiligen Triazolen umgesetzt.[112–115] Aldehyd-funktionalisierte MOFs wurden mit Aminen zu den jeweiligen Iminen[116,117] umgesetzt oder mit Natriumborhydrid zum Alkohol[117] reduziert. Außerdem konnten Alken-funktionalisierte MOFs mittels Bromierung, Oxidation, Hydroborierung und Epoxidierung modifiziert werden.[118,119]

Trotzdem wird der Großteil der kovalenten PSM ausgehend von Amino-MOFs durchgeführt. Dies liegt zum einen daran, dass viele Amino-MOFs zur Verfügung stehen, und zum anderen daran, dass die Aminogruppe in einem breiten Spektrum an chemischen Reaktionen eingesetzt werden kann. Neben Acetylierungen mit Anhydriden[120–124], cyclischen Anhydriden[125–128] und Carbonsäurechloriden[129–131] sind auch Umsetzungen mit Isocyanaten[109,131–133], Diphosgen[134], Thiophosgen[134], Aldehyden[135–137] und Alkylbromiden[138] bekannt.

Eine besondere Herausforderung bei der Funktionalisierung von MOFs ist die Implementierung von organischen Säuren wie z.B. Carbon-, Sulfon-, oder Phosphonsäuren.[139] Während eine präsynthetische Modifikation[140–144] aufgrund der koordinativen Eigenschaften von organischen Säuren oft anspruchsvoll ist, muss das MOF für eine PSM neben den üblichen Voraussetzungen auch eine gewisse Stabilität gegenüber Säuren aufweisen. Je nach Stabilität des MOFs können die organischen Säuregruppen auf unterschiedliche Wege implementiert werden. Eine Möglichkeit, unter relativ milden Synthesebedingungen Carbon- und Sulfonsäure-Gruppen einzuführen, ist die Umsetzung von Amino-MOFs mit Sultonen[145–148] oder cyclischen Anhydriden[125–127]. Im Fall der sehr stabilen MOFs Cr-MIL-101 und Al-MIL-53 gelang sogar eine direkte Sulfonierung der

aromatischen Linker mit einer Mischung aus Schwefelsäure und Trifluormethan-sulfonsäure.[149] Nur ein Beispiel für eine postsynthetische Modifikation zur Implementierung von Phosphonsäuren-Gruppen ist bis heute bekannt.[150]

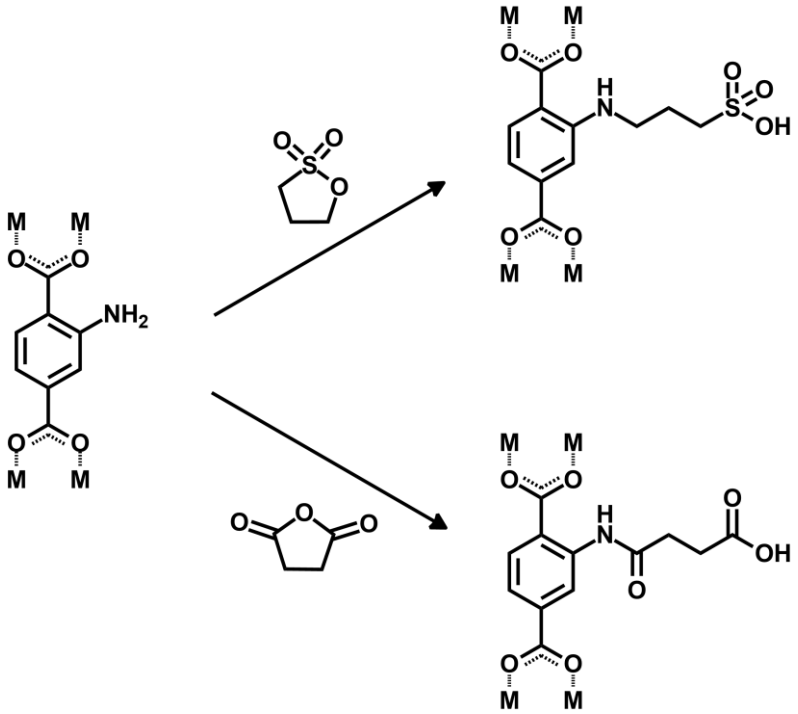

Abb. 11: Beispiele für die Umsetzung eines aminofunktionalisierten MOF mit Sultonen oder cyclischen Anhydriden.

Anwendung finden Brønsted-acide MOFs heutzutage hauptsächlich in der heterogenen Katalyse[16,139] und als protonenleitfähige Materialien[151–153]. Vor allem bei MOFs mit unkoordinierten Sulfon- oder Phosphonsäure-Gruppen wurde bereits eine hohe Protonenleitfähigkeit beobachtet.[144,154–157] Die Synthese solcher MOFs ist noch immer eine große Herausforderung und könnte durch das Entwickeln neuer postsynthetischer Methoden zur Implementierung von Sulfon- und Phosphonsäure-Gruppen erleichtert werden. Auch die Verfügbarkeit eines größeren Pools an präsynthetisch modifizierten Linkern könnte die Darstellung protonenleitfähiger MOFs (PCMOF, proton conducting MOF) erleichtern.

1.3 Linker für protonenleitfähige MOFs

In den letzten Jahren zeigten vor allem MOFs basierend auf Phosphonsäure-Linkern vielversprechende Ergebnisse in Bezug auf Protonenleitfähigkeit.[155,158–160] Die Phosphonsäure-Gruppen besitzen jeweils drei Sauerstoffatome und können mit diesen auf unterschiedliche Weise an ein Metall-Ion koordinieren. Viele protonenleitfähige MOFs

profitieren davon, dass ein Sauerstoffatom oder eine Hydroxylgruppe der Phosphonsäure nicht am Metall-Ion koordiniert und in der Pore frei zugänglich vorliegt. Diese können dann als Wasserstoffbrückenakzeptor oder -donor zur Protonenleitfähigkeit beitragen. Unter bestimmten Reaktionsbedingungen kann sogar ein MOF mit unkoordinierten Phosphonsäure-Gruppen hergestellt werden. Der von SHIMIZU beschriebene PCMOF-5 besitzt freie Phosphonsäure-Gruppen innerhalb der Poren und weist eine dementsprechend hohe Protonenleitfähigkeit auf.[154] Andere Beispiele für MOFs mit hoher Protonenleitfähigkeit basieren auf Linkern mit zwei verschiedenen organischen Säuregruppen. Durch Kombination von Carbonsäure-Gruppen und Phosphonsäure-Gruppen an einem Linker können stabile MOFs mit einer hohen Protonenleitfähigkeit erhalten werden.[161,162] Dabei bilden die Carboxylate eine koordinative Bindung zu den Metall-Ionen aus und die Phosphonsäure-Gruppen liegen im Idealfall frei oder nur teilweise koordiniert vor. Nach dem gleichen Prinzip wurden Linker mit Carbonsäure- und Sulfonsäure-Gruppen erfolgreich eingesetzt.[144,156,157,163] Die Sulfonsäure-Gruppe kann ebenfalls als Wasserstoffbrücken-akzeptor oder, wenn sie frei vorliegt, auch als Wasserstoffbrückendonor agieren.

Auf Grund der guten Eigenschaften von Sulfonsäure- und Phosphonsäure-Gruppen hinsichtlich der Protonenleitfähigkeit bietet sich eine Kombination beider Gruppen in einem Linker an. Obwohl bereits eine Vielzahl an Koordinationspolymeren und MOFs basierend auf solchen Linkern bekannt sind[164–169], gibt es nur wenige Untersuchungen bezüglich der Protonenleitfähigkeit[170,171]. Hinzu kommt, dass alle bekannten Netzwerke auf einen Pool aus gerade einmal vier Linkern zurückgreifen. Dies liegt vermutlich daran, dass die Synthese von Linkern, die sowohl Phosphonsäure-Gruppen als auch Sulfonsäure-Gruppen enthalten, oft schwierig ist (s. Kapitel. 4.1). Deshalb müssen neue Synthesestrategien gefunden werden, um den Pool dieser Linker (im Rahmen dieser Arbeit als Phosphosulfonsäure-Linker bezeichnet) zu erweitern und somit auch die Synthese neuer, protonenleitfähiger Koordinationspolymere oder MOFs zu erleichtern.

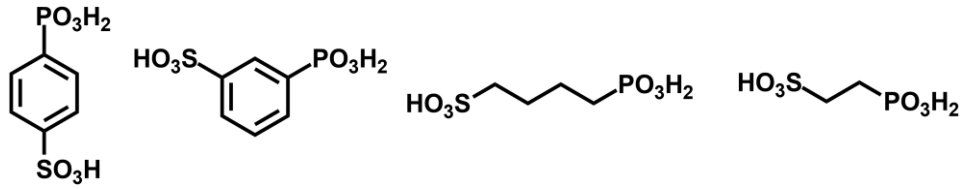

Abb. 12: Linker mit Phosphonsäure- und Sulfonsäure-Gruppe, die bereits erfolgreich zur Synthese von Koordinationspolymeren eingesetzt wurden.

2 Aufgabenstellung

Im Rahmen dieser Arbeit sollten funktionalisierte IRMOFs und protonenleitfähige MOFs durch prä- oder postsynthetischen Modifikation dargestellt werden. Für die präsynthetische Modifikation sollten funktionalisierte Triazin-Linker bzw. Phosphosulfonsäure-Linker synthetisiert und zur Verfügung gestellt werden. Ausgehend von präsynthetisch funktionalisierten MOFs sollten außerdem Methoden zur postsynthetischen Modifikation entwickelt werden, um die Eigenschaften eines MOFs, z. B. in Bezug auf Protonenleitfähigkeit, zu verändern.

Für die präsynthetische Darstellung von funktionalisierten IRMOFs sollten im Rahmen dieser Arbeit funktionalisierte Triazin-Linker synthetisiert und zur Verfügung gestellt werden. Dafür sollten die erstmals von KLINKEBIEL[172] beschriebenen nitro- und aminofunktionalisierten H_3TATB-Linker in einem möglichst großen Maßstab synthetisiert werden.

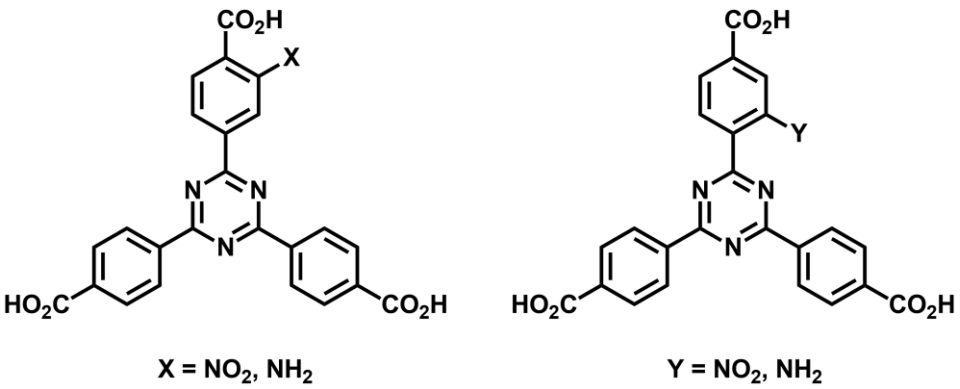

Abb. 13: Nitro- und aminofunktionalisierte H_3TATB-Linker.

Zur Vergrößerung des Pools an funktionalisierten Triazin-Linkern sollten außerdem Möglichkeiten zur Darstellung von hydroxyfunktionalisierten Triazin-Linkern untersucht werden. Dafür sollte ausgehend vom TAPB-OMe-Linker Synthesebedingungen zur Spaltung des Methylethers gefunden werden.

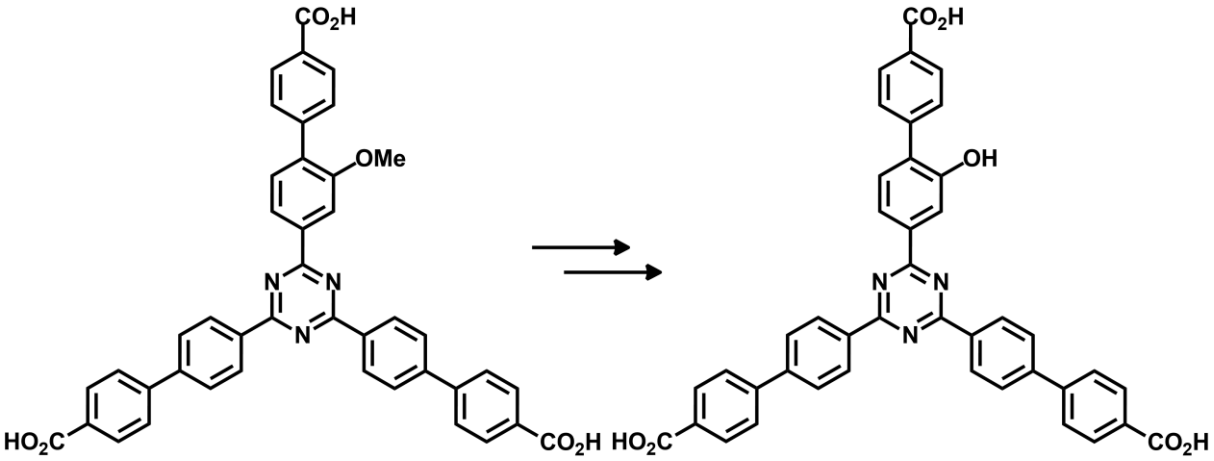

Abb. 14: Geplante Spaltung eines Methylethers zur Darstellung des hydroxyfunktionalisierten TAPB-OH-Linkers.

Die Erweiterung der funktionalisierten H_3TATB-Linker um einen zusätzlichen Benzol-Ring wurde bereits von KLINKEBIEL[172] beschrieben. Ausgehend von den funktionalisierten Tribromtriazinen wurden mittels dreifacher Suzuki-Kupplung funktionalisierte H_3TAPB-Linker dargestellt. Ein Ziel dieser Arbeit war die Erweiterung der H_3TATB-Linkern um zwei zusätzliche Benzol-Ringe.

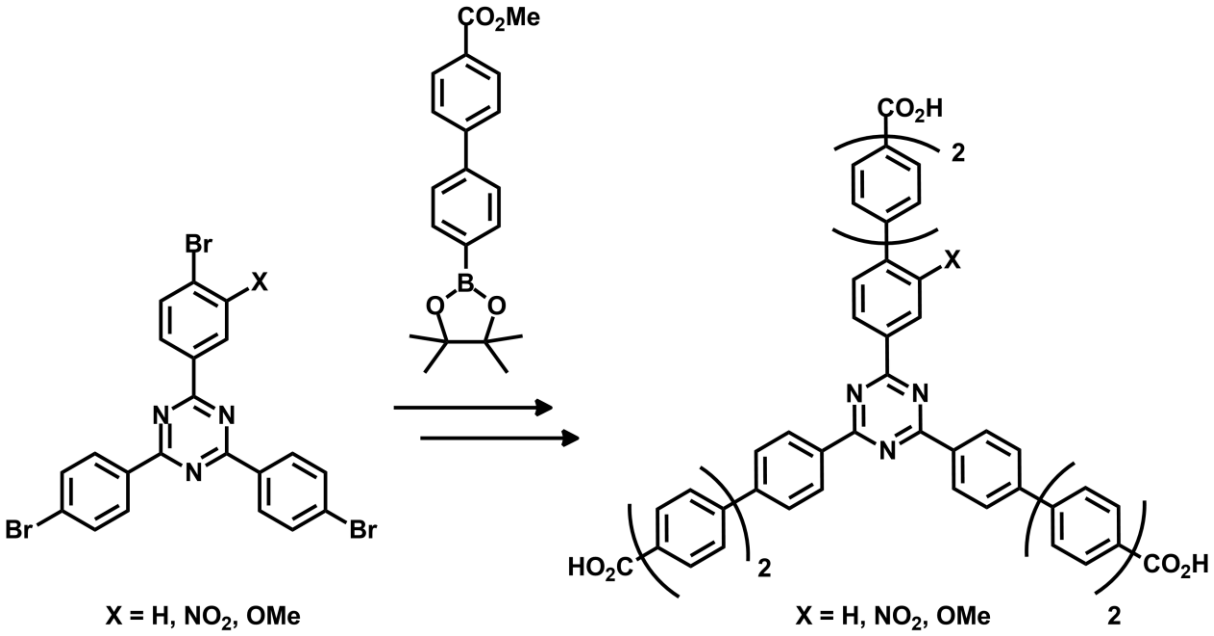

Abb. 15: Geplante Synthese für erweiterte Triazin-Linker.

Die funktionalisierten Triazin-Linker sollten nach erfolgreicher Synthese in Kooperationen mit MILAN KÖPPEN (AK STOCK) und ERIKA VIRMANI (geb. MÜHLBAUER, AK WUTTKE) zur Darstellung von funktionalisierten MOFs eingesetzt werden. Sollte die Darstellung eines

funktionalisierten MOFs erfolgreich sein, sollten im Rahmen dieser Arbeit postsynthetischer Modifikationen an dem jeweiligen MOF vorgenommen werden.

Ein weiteres Ziel dieser Arbeit war die Darstellung von protonenleitfähigen MOFs. Während die Synthese der MOFs von THOMAS HOMBURG (AK STOCK) durchgeführt werden sollte, war das Ziel dieser Arbeit die Synthese von geeigneten Linkern. Wie in Kapitel 1.3 bereits erwähnt, ist nur eine geringe Anzahl an potentiellen Linker-Molekülen bekannt, die sowohl Phosphonsäure- als auch Sulfonsäure-Gruppen besitzen (Phosphosulfonsäure-Linker). Um den verfügbaren Pool dieser Linker zu erweitern, sollten neue Synthesewege entwickelt werden.

Ein möglicher Syntheseweg basiert auf der Umsetzung von 1,2,4,5-Tetrakis(brommethyl)benzol mit Triethylphosphit oder Natriumsulfit. Während mit vier Äquivalenten Triethylphosphit der jeweilige Tetraphosphonsäurediethylester erhalten wird[154], entsteht bei der Umsetzung mit vier Äquivalenten Natriumsulfit das jeweilige Natriumsalz der Tetrasulfonsäure[173]. Durch die Verwendung von zwei Äquivalenten Triethylphosphit könnte zunächst ein Diphosphonsäurediethylester dargestellt werden, welcher anschließend mit zwei Äquivalenten Natriumsulfit umgesetzt werden würde. Nach Hydrolyse der Phosphonsäureethylester-Gruppen könnte ein Linker isoliert werden, der sowohl Phosphonsäure- als auch Sulfonsäure-Gruppen besitzt.

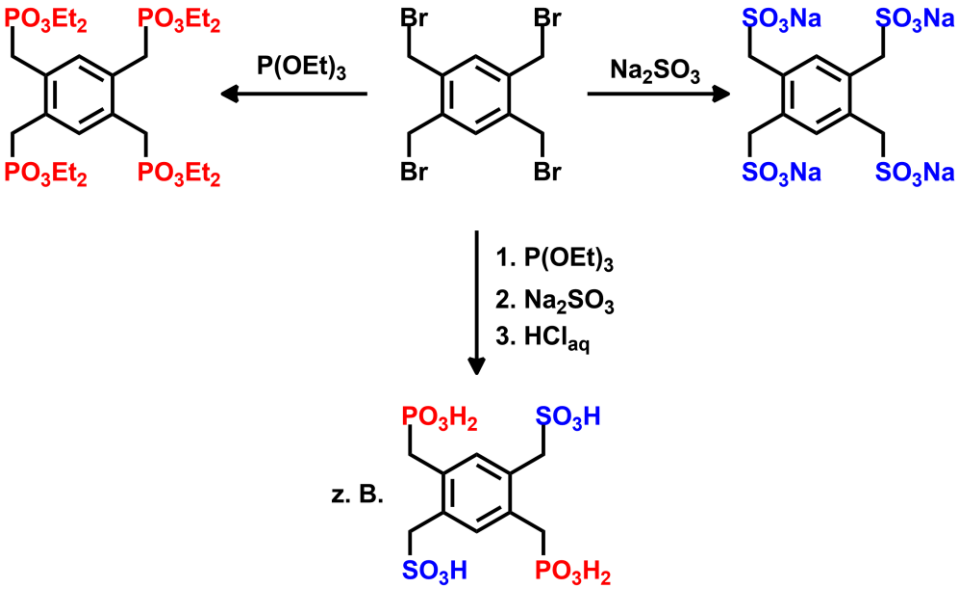

Abb. 16: Nucleophile Substitution von Tetrakis(brommethyl)benzol mit Triethylphosphit (links)[154] bzw. Natriumsulfit (rechts)[173] und die geplante Synthese eines Phosphosulfonsäure-Linkers (unten).

Mit der oben beschriebenen Methode können Phosphonsäure- und Sulfonsäure-Gruppen über Methylen-Einheiten mit einem Benzol-Ring verknüpft werden. Ein anderer Ansatz zur Darstellung von Phosphosulfonsäure-Linkern ist die direkte Verknüpfung von Phosphonsäure- und Sulfonsäure-Gruppen mit einem Benzol-Ring. Im Rahmen dieser Arbeit sollten Synthesewege zur Darstellung von tri- und tetrasubstituierten Phosphobenzolsulfonsäure-Linkern entwickelt werden.

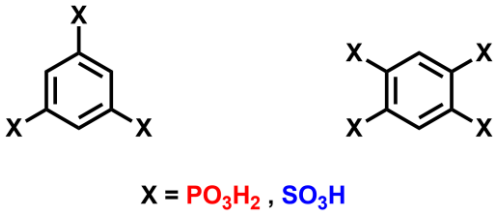

Abb. 17: Tri- und tetrasubstituierte Phosphobenzolsulfonsäure-Linker mit unterschiedlicher Anzahl und Position von Phosphon- und Sulfonsäure-Gruppen.

Eine weitere Möglichkeit, die Protonenleitfähigkeit eines MOFs zu verbessern, ist die postsynthetische Implementierung von organischen Säuregruppen. Im Rahmen dieser Arbeit sollten Methoden zur postsynthetischen Implementierung von Phosphonsäure-Gruppen in Cr-MIL-101-Derivate (Cr-MIL-101, Cr-MIL-101-Br, Cr-MIL-101-NH_2) entwickelt werden. Cr-MIL-101 wurde ausgewählt, da sich dieser MOF sowohl durch hohe thermische und chemische Stabilität auszeichnet als auch mit einer großen Variation an funktionellen Gruppen ausgestattet werden kann. Diese Eigenschaften sollten ein breites Spektrum an postsynthetischen Reaktionen zur Implementierung von Phosphonsäure-Gruppen ermöglichen.

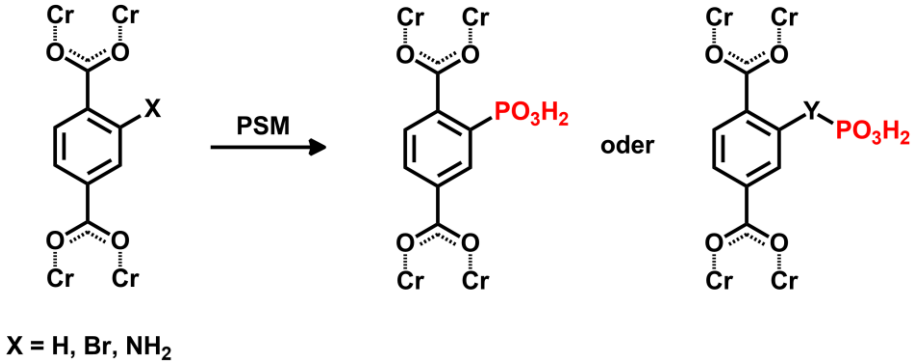

Abb. 18: Postsynthetische Implementierung von Phosphonsäure-Gruppen direkt am Benzol-Ring oder über eine funktionelle Gruppe (Y = z. B. NH, CH_2).

3 Triazin-basierte MOFs: Prä- und postsynthetische Modifikation

In diesem Kapitel wird die Synthese funktionalisierter Triazin-Linker und deren Einbau in MOFs besprochen. Zunächst wird in Kapitel 3.1 auf die Synthese und Erweiterung von funktionalisierten H_3TATB-Linkern eingegangen. In Kapitel 3.2 werden MOFs basierend auf funktionalisierten H_3TATB-Linkern vorgestellt. Postsynthetischen Modifikationen eines funktionalisierten Bismut-MOF werden in Kapitel 3.2.3 besprochen.

Anmerkung: Verbindungen, die in einer Veröffentlichung oder in einem Manuskript beschrieben sind, werden wie folgt benannt: **VX-Y** oder **MX-Y**. Mit dem Muster **VX-Y** werden Verbindungen aus einer Veröffentlichung und mit **MX-Y** Verbindungen aus einem Manuskript bezeichnet. **X** steht für eine Zahl, die sich auf eine bestimmte Veröffentlichung bzw. Manuskript bezieht. Für die erstgenannte Veröffentlichung bzw. das erstgenannte Manuskript wird das **X** durch eine **1** ersetzt (für das zweitgenannte mit einer **2** usw.). **Y** steht für die Zahl, die die jeweilige Verbindung in der Veröffentlichung oder dem Manuskript hat. **V2-10** beispielsweise bezeichnet Verbindung **10** aus der zweiten in dieser Arbeit genannten Veröffentlichung.

3.1 Synthese von funktionalisierten Triazin-Linkern

Die Erweiterung oder Funktionalisierung von bekannten Linkern konnte schon mehrfach zur Darstellung neuer MOFs genutzt werden. Ein Beispiel ist die Erweiterung des H_3TATB-Linkers zum H_3TAPB-Linker durch Einführen eines weiteren Benzol-Rings zwischen dem Triazin-Kern und der jeweiligen Carbonsäure-Gruppe.[67] In der folgenden Veröffentlichung wird die Synthese von funktionalisierten und erweiterten H_3TAPB-Linkern beschrieben.

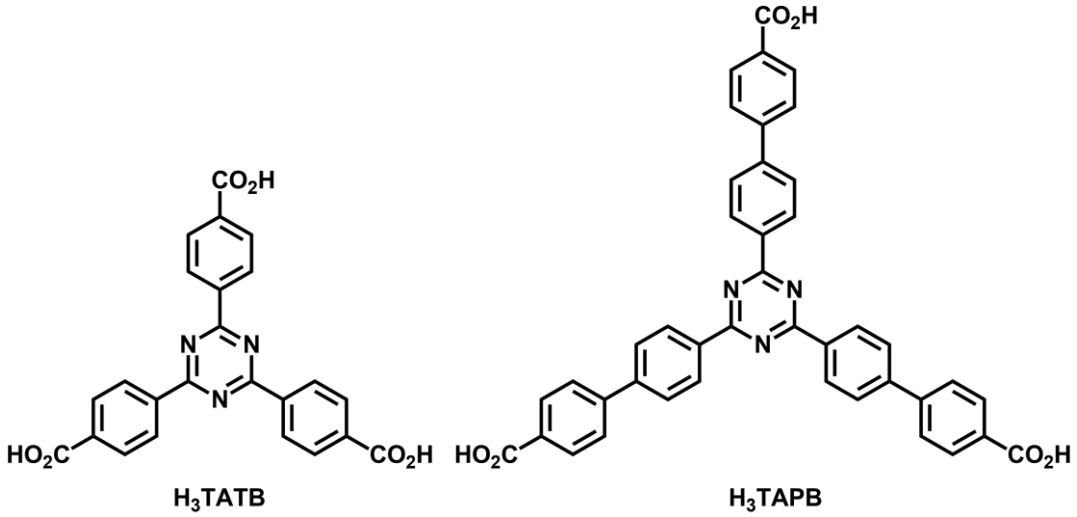

Abb. 19: Triazin-basierte Linker H_3TATB und H_3TAPB.

Die Darstellung der funktionalisierten H_3TAPB-Linker **V1-17b**, **V1-17c**, **V1-17d** und **V1-17e** erfolgte ausgehend von den funktionalisierten Tribromtriazinen **V1-3b** und **V1-3c**.

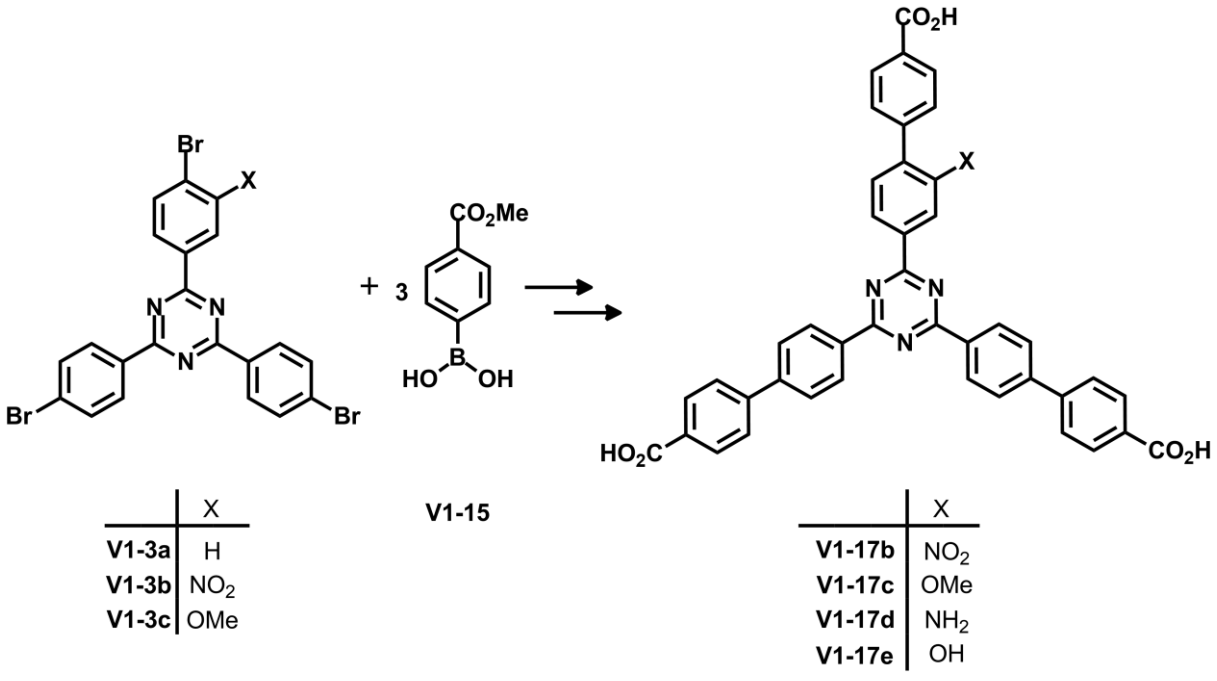

	X
V1-3a	H
V1-3b	NO_2
V1-3c	OMe

	X
V1-17b	NO_2
V1-17c	OMe
V1-17d	NH_2
V1-17e	OH

Abb. 20: Syntheseübersicht zur Darstellung der funktionalisierten H_3TAPB-Linker **V1-17b**, **V1-17c**, **V1-17d** und **V1-17e**.

Diese wurden jeweils in einer Suzuki-Kupplung mit drei Äquivalenten der Boronsäure **V1-15** umgesetzt. Nach anschließender Hydrolyse der Methylester-Gruppen konnten der nitrofunktionalisierte H_3TAPB-Linker **V1-17b** und der methoxyfunktionalisierte H_3TAPB-Linker **V1-17c** isoliert werden. Zur Darstellung des aminofunktionalisierten H_3TAPB-Linker **V1-17d** wurde die Nitrogruppe vor der Hydrolyse reduziert. Die Spaltung des Methylethers zur Darstellung des hydroxyfunktionalisierten H_3TAPB-Linker **V1-17e** erfolgte mit Pyridinhydrochlorid.

In Anlehnung an dieses Vorgehen wurden drei erweitertere H_3TAPB Linker **V1-20a**, **V1-20b** und **V1-20c** mit drei Benzol-Ringen zwischen dem Triazin-Kern und der jeweiligen Carbonsäure-Gruppe synthetisiert. Die Darstellung erfolgte über eine Suzuki-Kupplung der Tribromtriazine **V1-3a**, **V1-3b** und **V1-3c** mit jeweils drei Äquivalenten des Biphenylboronsäureester **V1-18**. Nach anschließender Hydrolyse der Methylester-Gruppen bzw. Spaltung des Methylethers mit Pyridinhydrochlorid konnten die jeweiligen Triazin-Linker **V1-20a**, **V1-20b** und **V1-20c** isoliert werden.

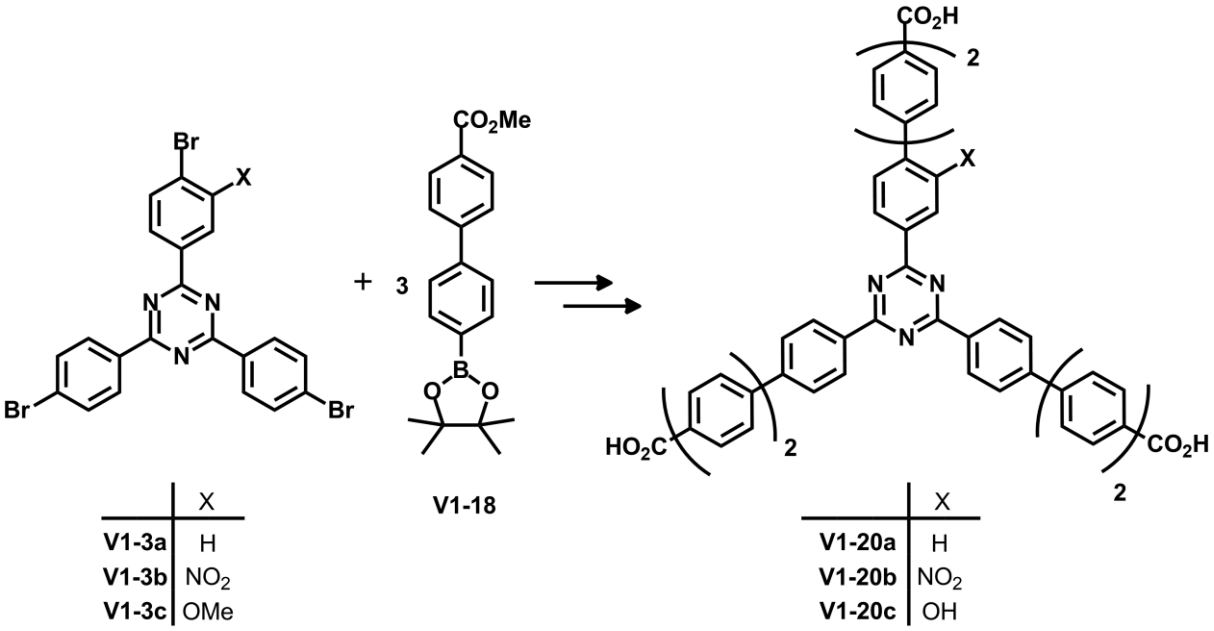

	X
V1-3a	H
V1-3b	NO_2
V1-3c	OMe

	X
V1-20a	H
V1-20b	NO_2
V1-20c	OH

Abb. 21: Syntheseübersicht zur Darstellung der Triazin-Linker **V1-20a**, **V1-20b** und **V1-20c**.

Die Ergebnisse wurden veröffentlicht:

A. Klinkebiel, O. Beyer, B. Malawko, U. Lüning, *Beilstein J. Org. Chem.* **2016**, *12*, 2267-2273.

Bis auf die Synthesen der Moleküle **V1-16d**, **V1-17b** und **V1-17d** wurden alle in der Veröffentlichung beschriebenen Synthesen im Rahmen dieser Dissertation durchgeführt.

Zusätzlich ist die erstmalige Charakterisierung der Moleküle **V1-17e**, **V1-19a-c** und **V1-20a-c** Bestandteil dieser Dissertation. Die erstmalige Synthese und Charakterisierung der Moleküle **V1-3a**, **V1-3b**, **V1-16b-d** und **V1-17b-d** wurde von ARNE KLINKEBIEL im Rahmen seiner Dissertation durchgeführt.

Anmerkung: Die Daten der B3LYP//6-31G*-Rechnungen aus der Supporting Information wurden dieser Arbeit aus Übersichtsgründen nicht beigefügt. Außerdem wurde die Formatierung der Supporting Information geringfügig verändert, um sie auf die Formatierung dieser Arbeit anzupassen. Dabei wurden keine Inhalte verändert.

BEILSTEIN JOURNAL OF ORGANIC CHEMISTRY

Elongated and substituted triazine-based tricarboxylic acid linkers for MOFs

Arne Klinkebiel, Ole Beyer, Barbara Malawko and Ulrich Lüning*

Full Research Paper

Open Access

Address:
Otto-Diels-Institut für Organische Chemie,
Christian-Albrechts-Universität zu Kiel, Olshausenstr. 40, D-24098
Kiel, Germany

Email:
Ulrich Lüning* - luening@oc.uni-kiel.de

* Corresponding author

Keywords:
isoreticular; linker; MOF; Suzuki coupling; triazine

Beilstein J. Org. Chem. **2016,** *12,* 2267–2273.
doi:10.3762/bjoc.12.219

Received: 15 June 2016
Accepted: 13 October 2016
Published: 27 October 2016

Associate Editor: P. J. Skabara

Abstract

New triazine-based tricarboxylic acid linkers were prepared as elongated relatives of triazinetribenzoic acid (TATB). Additionally, functional groups (NO_2, NH_2, OMe, OH) were introduced for potential post-synthetic modification (PSM) of MOFs. Functionalized tris(4-bromoaryl)triazine "cores" (**3a**,**3b**) were obtained by unsymmetric trimerization mixing one equivalent of an acid chloride (OMe or NO_2 substituted) with two equivalents of an unsubstituted nitrile. Triple Suzuki coupling of the cores **3** with suitable phenyl- and biphenylboronic acid derivatives provided elongated tricarboxylic acid linkers as carboxylic acids **17** and **20** or their esters **16** and **19**. Reduction of the nitro group and cleavage of the methoxy group gave the respective amino and hydroxy-substituted triazine linkers.

Introduction

A typical building block for many metal–organic frameworks (MOFs) [1-4] carries two functional groups such as carboxylic acids or heterocycles resulting in a bridging ligand for the metal-containing „edges" of the porous structures. Linkers with more than two ligating sites (carboxylic acids or heterocycles) have also been used successfully. Tri- to hexatopic linkers are also known. The prototype for a trivalent linker is 1,3,5-benzenetricarboxylic acid. By elongating the „arms" of the linkers, larger pores can be achieved, and often the MOF structures containing extended linkers resemble those obtained with the smaller parent linker (isoreticular structures, see for instance [5]).

In the case of the tritopic linker 1,3,5-benzenetricarboxylic acid (BTC, forming HKUST-1 [6] in the presence of copper ions), an obvious elongated building block is BTB (1,3,5-benzenetribenzoate, Figure 1, left) forming for instance MOF-14 [7]. But this type of elongation has a drawback: the direct vicinity of the aryl groups does not allow planarity due to the repulsion of the *ortho*-hydrogen atoms in the biphenyl subunits. An exchange of the central benzene ring by a 1,3,5-triazine (1,3,5-triazine-2,4,6-tribenzoate, TATB, Figure 1, right), however, permits planarity. The respective MOF from TATB and copper is PCN-6 [8]. While the orientation of the carboxylate plane relative to the central six-membered ring is in the same plane in the TATB

Beilstein J. Org. Chem. **2016,** *12,* 2267–2273.

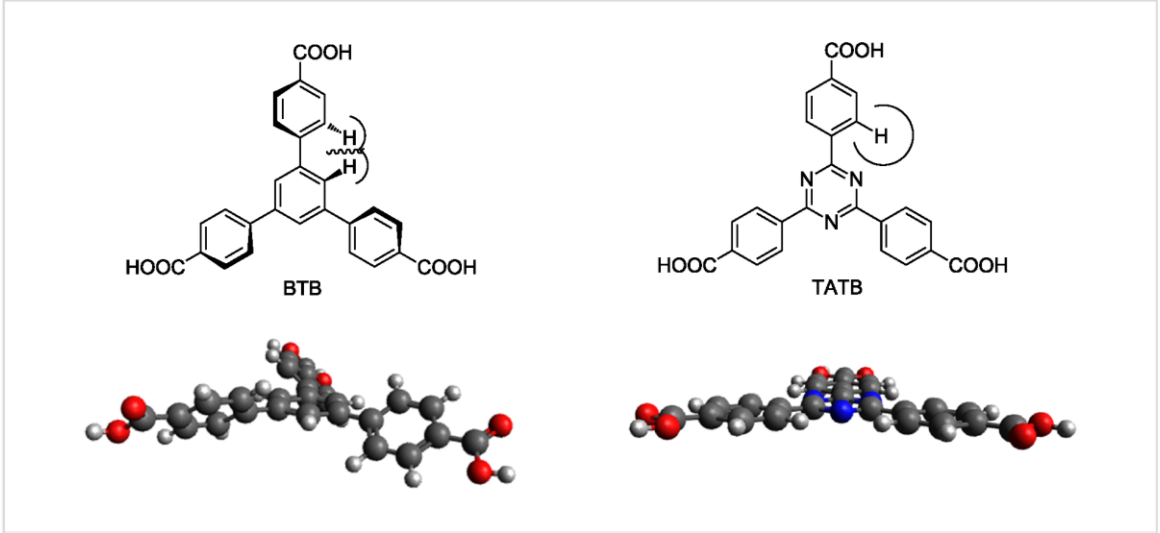

Figure 1: Steric repulsion between *ortho*-hydrogen atoms in benzene-1,3,5-tribenzoic acid (BTB) leads to a non-planar structure (left). The exchange of CH units by nitrogen atoms in the central six-membered ring allows a planar structure: 1,3,5-triazine-2,4,6-tribenzoic acid (TATB, right). The two structures in the lower half have been calculated with B3LYP//6-31G*.

based MOF PCN-6, the BTB analogue MOF-14 shows a tilt angle of ca. 35°. B3LYP//6-31G* calculations of the isolated linkers in the gas phase result in dihedral angles of 38.5° for BTB and 0.006° for TATB, respectively (for further information see Supporting Information File 1). A detailed comparison of triarylbenzene and triaryl-1,3,5-triazine based MOFs and a discussion on the differences in sterical hindrance in benzene and 1,3,5-triazine based structures has been undertaken for tetrazol terminated linkers [9].

The properties of MOFs are determined by the nature of the linker, the nature of the metal-containing secondary building unit (SBU) and of course by the pore size. Additional properties are expected if other functional groups were present in the pores. There are two general strategies to introduce additional functional groups into a MOF: (i) by post-synthetic modification, i.e., a reaction of an assembled MOF with some added reagent, or (ii) by the use of modified linkers in the synthesis of the MOF hoping that functionalized linkers lead to isoreticular structures.

It is obvious that the chance for isoreticular structures decreases with the extend with which the linker is altered. Therefore, in the case of tritopic linkers, it makes a difference whether one additional functional group is introduced per linker or one per „arm“. Also the issue of planarity discussed above is related to the amount of additional substituents in the linker.

Indeed, when TATB **1a** was substituted with only one substituent per linker, syntheses of isoreticular analogues of MOFs were possible. Structures which are isoreticular to PCN-6 could be synthesized with nitro and amino-substituted TATBs **1b–d** [10] (Figure 2).

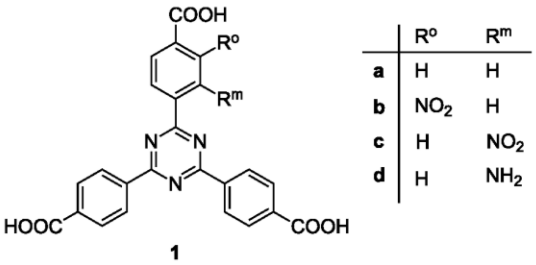

Figure 2: Mono-substituted TATB linkers **1b–d** were successfully employed in the isoreticular syntheses of PCN-6 MOFs [10].

How can this strategy be extended to even larger monofunctionalized triazine linkers? Obviously by the introduction of an additional benzene ring into each arm. Since some decades, palladium-catalyzed cross coupling is the method of choice when aryl–aryl bonds should be constructed, for instance by applying the Suzuki–Miyaura coupling [11]. A retrosynthetic analysis (Figure 3) of extended mono-functionalized triazinetricarboxylic acids **2** calls for tris(4-bromoaryl)-1,3,5-triazines **3** and boronic acids **4** with an additional carboxylic acid functionality. The respective methyl carboxylate of boronic acid **4** with $n = 1$, i.e. **15** (see below, Figure 7), is commercially available. In case of the elongated methyl carboxylate of **4** with $n = 2$, the pinacol boronate **18** (Figure 8) has been described in the literature [12].

Beilstein J. Org. Chem. **2016,** *12,* 2267–2273.

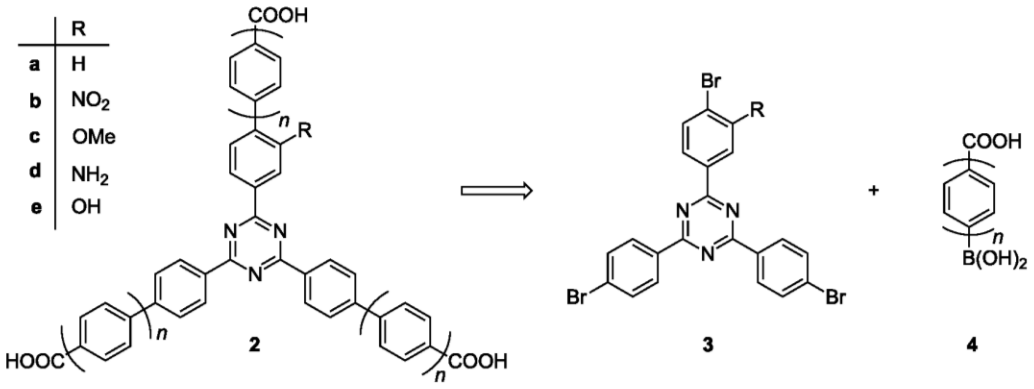

Figure 3: Retrosynthetic analysis for extended TATBs **2**: triple Suzuki coupling between tribromotriazines **3** and boronic acids **4**.

Results and Discussion

Symmetric 1,3,5-triazines such as **3a** are usually synthesized by trimerization of respective nitriles [13]. Unsymmetric 1,3,5-triazines **3** can be made by combining one equivalent of an acid chloride with two equivalents of a nitrile [14-16] (for a recently described alternative access to unsymmetrical 1,3,5-triazines; see [17]). In the presence of a suitable Lewis acid such as antimony(V) chloride, the acid chloride condenses with the nitriles to form an oxadiazinium salt from which the triazine can be obtained by reaction with ammonia (Figure 4).

The respective syntheses have successfully been carried out with nitro and methoxy-substituted benzoyl chlorides **5b** and **5c**. The resulting triazines **3b** and **3c** can then be coupled to boronic acids or boronates to give substituted and elongated triazine-based linkers. Furthermore, the reduction of the nitro group or cleavage of the methoxy group will give additional substituted linkers, amino and hydroxy-substituted ones (see below).

The syntheses of larger linkers **2** therefore need: (i) substituted 4-bromobenzoic acid chlorides **5**, 4-bromobenzonitrile (**6**) and the methoxycarbonyl-substituted phenylboronic acid **15** (n = 1) or pinacol biphenylboronate **18** (n = 2).

Syntheses

Four functional groups were chosen as additional substituents in the extended triazine linkers **2**: nitro, methoxy, amino and hydroxy groups. An amino group can be obtained from a nitro group by reduction, and a hydroxy group by cleavage of a methoxy group. Therefore, it was sufficient to synthesize the nitro and methoxy-substituted acid chlorides **5** for the unsymmetric trimerization of the desired tribromotriazines **3**.

The synthesis of 4-bromo-3-nitrobenzoyl chloride (**5b**) was straightforward. Commercially available 4-bromobenzoic acid (**8**) was nitrated according to a known procedure [18]. The reaction with thionyl chloride provided then acid chloride **5b** (Figure 5).

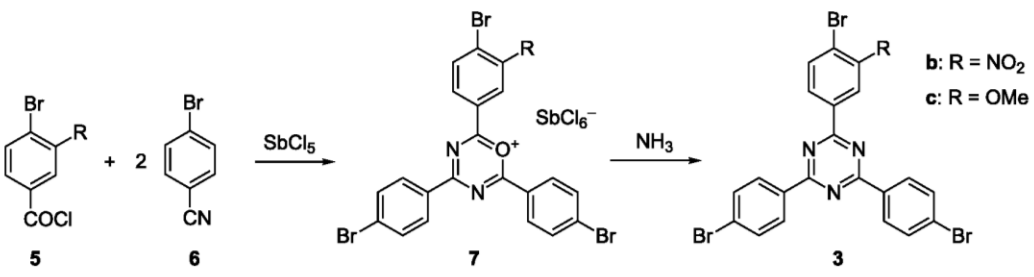

Figure 4: Synthesis of unsymmetrically substituted 2,4,6-tris(bromoaryl)-1,3,5-triazines **3** from one equivalent of a substituted benzoyl chloride **5** and two equivalents of benzonitrile **6**. As intermediates, oxadiazinium salts **7** are formed. The reaction with ammonia yields the desired triazines **3** (overall yields: 53% (**3b**), 61% (**3c**).

Beilstein J. Org. Chem. 2016, 12, 2267–2273.

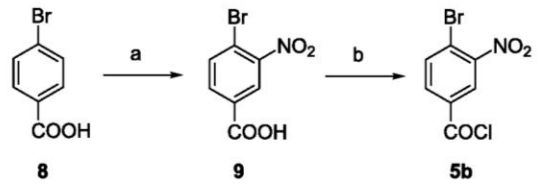

Figure 5: Synthesis of 4-bromo-3-nitrobenzoyl chloride (**5b**). Conditions: a) HNO_3/H_2SO_4, 3 h 0 °C, 2 h, room temperature, 98%, b) $SOCl_2$, 2 h reflux, not isolated.

In order to synthesize the respective methoxy compound **5c**, commercially available 3-hydroxybenzoic acid (**10**) was used as starting material (Figure 6). Bromination introduced a bromine atom into the 4 position (**11**) [19], then the phenol was turned into its methyl ether. This methylation can be performed with the free carboxylic acid **11** [20] or with ester **12** [21,22]. In order to generate the methoxy-substituted benzoyl chloride **5c**, methoxy ester **13** was cleaved first [23] and the resulting acid **14** was reacted with thionyl chloride. All steps were known from the literature and have been carried out on a multigram scale.

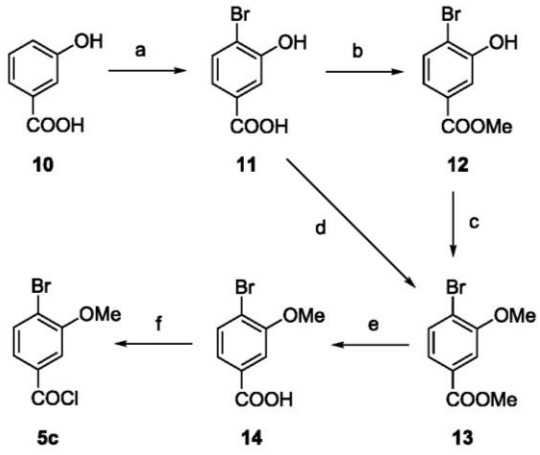

Figure 6: Syntheses of 4-bromo-3-methoxybenzoyl chloride (**5c**). Conditions: a) Br_2, EtOH/HOAc, 30 min, room temperature, 52%, b) $MeOH/H_2SO_4$, MeOH, 16 h, reflux, 94%, c) Me_2SO_4, K_2CO_3, acetone, 3 h, reflux, quant., d) MeI, K_2CO_3, DMF, 16 h, room temperature, 83%, e) NaOH, H_2O, MeOH, 6 h, room temperature, 66%, f) $SOCl_2$, DMF (cat.), 2 h, reflux, not isolated.

Cyclotrimerization of one equivalent of an acid chloride **5b** or **5c** with two equivalents of 4-bromobenzonitrile (**6**) was achieved using the Lewis acid antimony(V) chloride as depicted in Figure 4. The resulting colourful oxadiazinium salts **7** were mixed with aqueous ammonia solution resulting in the formation of the desired triazines **3b** and **3c** in 53 and 61% yield, respectively.

Following the synthetic plan of Figure 3, the tribromides **3b** and **3c** were used in the Suzuki couplings. In this and respective following synthetic steps, optimization of the reaction conditions was very important because each of the reactions had to be performed three times with each triazine. Thus the total yield of the final product depends on the yield of the single step to the power of three. In a triple Suzuki coupling, 4-(methoxycarbonyl)phenylboronic acid (**15**) as the coupling partner yielded elongated and monofunctionalized 1,3,5-triazines **16b** and **16c** carrying methyl ester groups at the end of each „arm" (Figure 7). The yields of 90% (**16b**) and 73% (**16c**) correspond to 97% and 90% yield per coupling step, respectively.

By selective reduction, the nitro-substituted triester **16b** could be transferred into its amino derivative. The reaction time and the hydrogen pressure had to be optimized. By heterogeneous catalytic hydrogenation at 5 bar with a Pd/C catalyst, aminotriazine **16d** was obtained in 77% yield after 5 days. Hydrolyses of all three methyl esters **16b–d** provided the tricarboxylic acids **17b–d** in 96% to quantitative yields. Also the methoxy group could be cleaved to yield a hydroxy-substituted elongated triazine. In this case, four methoxy, three ester and one ether group had to be cleaved leading to increasingly less soluble products (carboxylic acids are less soluble than the respective esters). In order to improve the yield, a methoxy cleaving procedure which has been found to be effective in other demanding demethylations [24] was used. In liquid pyridinium chloride (which melts at 144 °C), apparently all intermediates were sufficiently soluble and consequently all four methoxy groups of **16c** could be cleaved in a one-pot reaction. The tetrafold cleavage yielded hydroxytriazine **17e** in 52% yield. All tricarboxylic acids **17** are considerably less soluble in most solvents when compared to the respective methyl esters **16**. Nevertheless, they are sufficiently soluble in, for instance, DMSO or in base to allow proper analyses and future use in solvothermal syntheses of MOFs.

Tribromotriazines **3** are not only good starting materials for the syntheses of biphenyl-substituted triazine linkers **16** and **17**. Also longer terphenyl-substituted linkers can be obtained if the same approach is chosen but a biphenylboronic acid derivative such as boronate **18** [12] is used instead of the phenyl compound **15**.

As in the case of the biphenyl derivatives **16** and **17**, the nitro and the methoxy-substituted triazines **3b** and **3c** were used to obtain the terphenyl-based nitro and methoxy-substituted triesters **19b** and **19c** (Figure 8). But also the non-substituted

Beilstein J. Org. Chem. 2016, 12, 2267–2273.

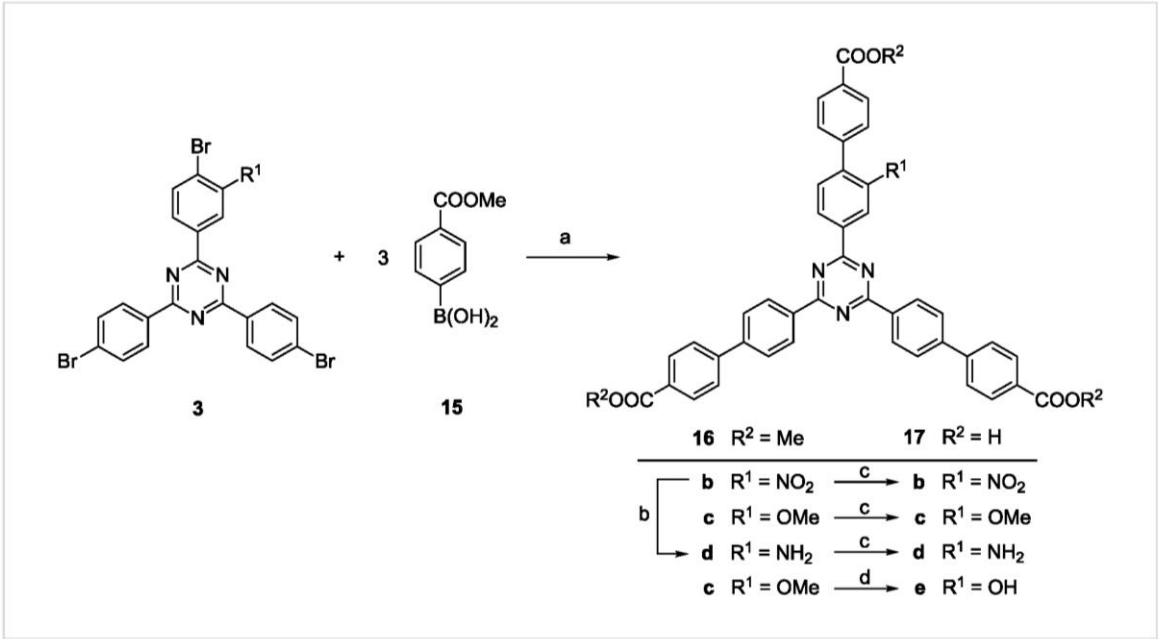

Figure 7: Triple Suzuki–Miyaura coupling between tribromotriazines **3** and boronic acid **15** and subsequent hydrolyses of the esters **16**. Conditions: a) $Pd(PPh_3)_4$, K_3PO_4, dioxane, H_2O, 48 h, reflux, **16b**: 90%, **16c**: 73%, b) Pd/C, H_2, 5 bar, CH_2Cl_2, 5 d, room temperature, **16d**: 77%. c) **17b**: LiOH/H_2O/dioxane, 48 h, room temp, 96%; **17c**: LiOH/H_2O/THF, 24 h, 60 °C, quant.; **17d**: H_2O/THF, 24 h, 60 °C, quant., d) pyridinium hydrochloride, 12 h, 200 °C, **17e**: 52%.

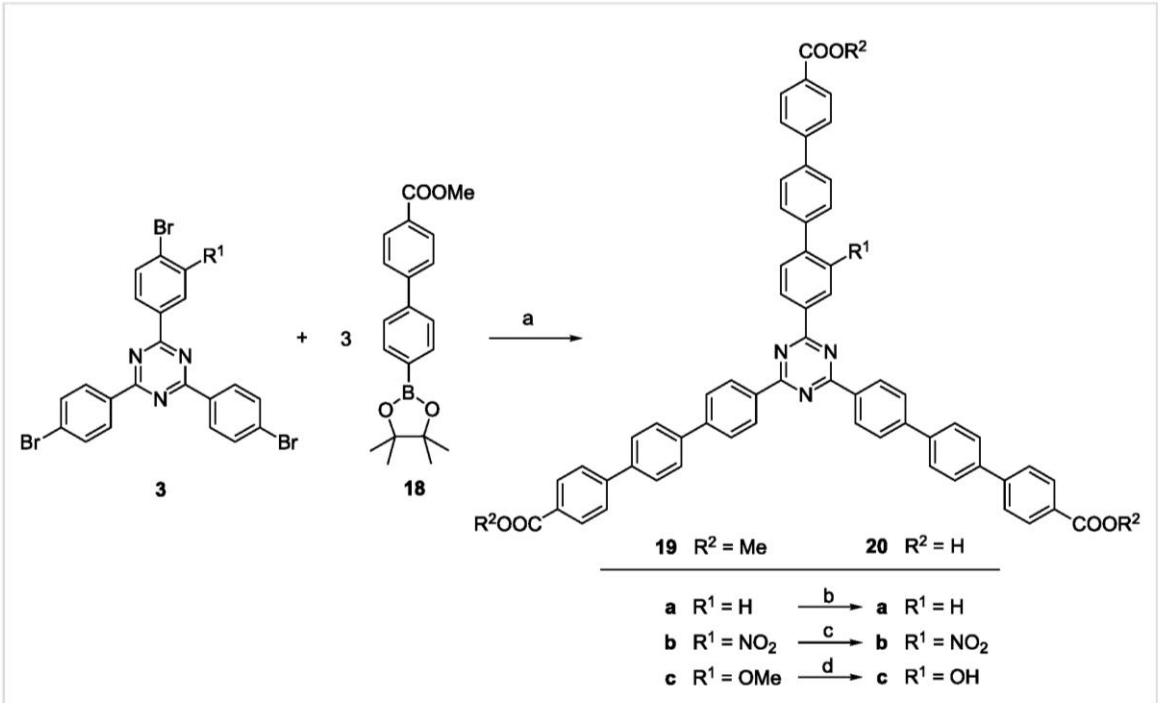

Figure 8: Triple Suzuki coupling between tribromotriazines **3** and boronate **18**. Conditions: a) **19a**: $Pd(PPh_3)_4$, K_3PO_4, dioxane/H_2O, 2 d, 120 °C, 24%; **19b**: $Pd(dppf)Cl_2$, K_3PO_4, dioxane/H_2O, 3 d, 120 °C, 16%; **19c**: $Pd(PPh_3)_4$, K_3PO_4, dioxane/H_2O, 2 d, 100 °C, 81%; b) LiOH/H_2O/THF, 24 h, 120 °C, **20a**: 99%; c) NaOH/H_2O/dioxane, 24 h, 120 °C, **20b**: 79%; d) pyridinium hydrochloride, 12 h, 200 °C, **20e**: 62%.

precursor **3a** was coupled leading to the unsubstituted parent compound **19a**, a triester which has not been described yet. Direct hydrolyses of triesters **19a** and **19b** gave the carboxylic acids **20a** and **20b**.

Finally, a hydroxy-functionalized terphenyl-based linker was synthesized from the methoxy-substituted triester **19c**. As successfully applied for **16c**, molten pyridinium chloride was used as the cleaving reagent and all four methoxy groups of **19c** could be cleaved leading to the hydroxy-substituted triacid **20e** in 62% yield.

All three triacids **20a, b** and **e** precipitate from water with decreasing pH. In DMSO, they are soluble and consequently, NMR analytics have been carried out in DMSO-d_6.

Conclusion

In conclusion, 13 new elongated relatives of TATB **16**, **17**, **19** and **20** have been synthesized in batch sizes up to several grams, of which 11 were mono-substituted. Syntheses, purifications and solubilities are satisfying in the case of the biphenyl derivatives **16** and **17**. The handling of the terphenyl derivatives **19**, and especially **20**, becomes more difficult due to a lower solubility. If the solublities were not sufficient for the solvothermal syntheses of MOFs, "discrete" methylation [25] could find a remedy.

Supporting Information

Supporting Information File 1

Experimental details.
[http://www.beilstein-journals.org/bjoc/content/supplementary/1860-5397-12-219-S1.pdf]

Acknowledgements

This work was supported by the Deutsche Forschungsgemeinschaft (Lu 378/24) as part of the priority program SPP 1362 (porous metal–organic frameworks). We thank Dr. Torsten Winkler for carrying out the calculations.

References

1. Zhou, H.-C. J.; Kitagawa, S., Eds. Metal–Organic Frameworks (MOFs). *Chem. Soc. Rev.* **2014,** *43,* 5415–6176. doi:10.1039/C4CS90059F
2. Furukawa, H.; Cordova, K. E.; O'Keeffe, M.; Yaghi, O. M. *Science* **2013,** *341,* 1230444. doi:10.1126/science.1230444
3. Farusseng, D. *Metal-Organic Frameworks;* Wiley-VCH: Weinheim, Germany, 2011. doi:10.1002/9783527635856
4. Férey, G. *Chem. Soc. Rev.* **2008,** *37,* 191–214. doi:10.1039/B618320B
5. Furukawa, H.; Go, Y. B.; Ko, N.; Park, Y. K.; Uribe-Romo, F. J.; Kim, J.; O'Keeffe, M.; Yaghi, O. M. *Inorg. Chem.* **2011,** *50,* 9147–9152. doi:10.1021/ic201376t
6. Chui, S. S.-Y.; Lo, S. M.-F.; Charmant, J. P. H.; Orpen, A. G.; Williams, I. D. *Science* **1999,** *283,* 1148–1150. doi:10.1126/science.283.5405.1148
7. Chen, B.; Eddaoudi, M.; Hyde, S. T.; O'Keeffe, M.; Yaghi, O. M. *Science* **2001,** *291,* 1021–1023. doi:10.1126/science.1056598
8. Ma, S.; Sun, D.; Ambrogio, M.; Fillinger, J. A.; Parkin, S.; Zhou, H.-C. *J. Am. Chem. Soc.* **2007,** *129,* 1858–1859. doi:10.1021/ja067435s
9. Dincă, M.; Dailly, A.; Tsay, C.; Long, J. R. *Inorg. Chem.* **2008,** *47,* 11–13. doi:10.1021/ic701917w
10. Mühlbauer, E.; Klinkebiel, A.; Beyer, O.; Auras, F.; Wuttke, S.; Lüning, U.; Bein, T. *Microporous Mesoporous Mater.* **2015,** *216,* 51–55. doi:10.1016/j.micromeso.2015.06.007
11. Miyaura, N.; Suzuki, A. *J. Chem. Soc., Chem. Commun.* **1979,** 866–867. doi:10.1039/c39790000866
12. Barnard, R. A.; Dutta, A.; Schnobrich, J. K.; Morrison, C. N.; Ahn, S.; Matzger, A. J. *Chem. – Eur. J.* **2015,** *21,* 5954–5961. doi:10.1002/chem.201406332
13. Cook, A. H.; Jones, D. G. *J. Chem. Soc.* **1941,** 278–282. doi:10.1039/jr9410000278
14. Eitner, P.; Krafft, F. *Ber. Dtsch. Chem. Ges.* **1892,** *25,* 2263–2269. doi:10.1002/cber.18920250218
15. Meerwein, H.; Laasch, P.; Mersch, R.; Spille, J. *Chem. Ber.* **1956,** *89,* 209–224. doi:10.1002/cber.19560890207
16. Schmidt, R. R. *Chem. Ber.* **1965,** *98,* 334–345. doi:10.1002/cber.19650980203
17. Tiwari, A. R.; Akash, T.; Bhanage, B. M. *Org. Biomol. Chem.* **2015,** *13,* 10973–10976. doi:10.1039/C5OB01835H
18. Bhat, L.; Mohapatra, P. P.; Bhat, S. R. Compositions, Synthesis, and Methods of Using Quinolinone Based Atypical Antipsychotic Agents. U.S. Pat. Appl. US20080293736 A1, Nov 27, 2008.
19. Li, X.; Longenecker, K. L.; Pei, Z.; Sham, H. L.; Wiedeman, P. E. Pyrrolidine-2-carbonitrile derivatives and their use as inhibitors of dipeptidyl peptidase-iv (dpp-iv). WO Pat. Appl. WO2005023762 A1, March 17, 2005.
20. Burrows, A. D.; Frost, C. G.; Mahon, M. F.; Richardson, C. *Angew. Chem., Int. Ed.* **2008,** *47,* 8482–8486. doi:10.1002/anie.200802908
Angew. Chem. **2008,** *120,* 8610–8614. doi:10.1002/ange.200802908
21. Govindachari, T. R.; Viswanathan, N.; Ravindranath, K. R.; Anjaneyulu, B. *Indian J. Chem.* **1973,** *11,* 1081–1083.
22. Failli, A.; Quagliato, D.; Andrae, P.; Heffernan, G.; Coghlan, R.; Shen, E. Pyrrolobenzodiazepine arylcarboxamides and derivatives thereof as follicle-stimulating hormone receptor antagonists. U.S. Pat. Appl. US20060199806 A1, Sept 7, 2006.
23. Fukaya, Y.; Mihara, Y.; Morizono, D.; Ohtake, Y.; Oishi, T.; Shoji, T.; Takashima, Y. 2,3,4,5-tetrahydro-1*H*-1,5-benzodiazepine derivative and medicinal composition. WO Pat. Appl. WO2006051851 A1, May 18, 2006.
24. Dawson, C. R.; Kurtz, A. P. *J. Med. Chem.* **1971,** *14,* 729–732. doi:10.1021/jm00290a015
25. Köhl, I.; Lüning, U. *Synthesis* **2014,** *46,* 2376–2382. doi:10.1055/s-0033-1339028

Supporting information

for

Elongated and substituted triazine based tricarboxylic acid linkers for MOFs

Arne Klinkebiel, Ole Beyer, Barbara Malawko, Ulrich Lüning*

Address: Otto-Diels-Institut für Organische Chemie, Christian-Albrechts-Universität zu Kiel, Olshausenstr. 40, D-24098 Kiel, Germany

*Corresponding author

Email: Ulrich Lüning – luening@oc.uni-kiel.de

Experimental details

General Remarks: Antimony(V) chloride (99 %, Alfa Aesar), [1,1′-bis(diphenylphosphino)ferrocene]dichloro palladium(II) (99.9 %, ABCR), 4-bromobenzoic acid (98 %, Sigma-Aldrich), 4-bromobenzonitrile (99%, Sigma-Aldrich), 3-hydroxybenzoic acid (97%, Sigma-Aldrich), 4-(methoxycarbonyl)phenylboronic acid (97 %, ABCR), palladium on charcoal (10%, Alfa Aesar) and tetrakis(triphenylphosphine)palladium(0) (99 %, ABCR) were purchased and used without further purification. Methyl 4'-(4,4,5,5-tetramethyl-1,3,2-dioxaborolan-2-yl)-1,1'-biphenyl-4-carboxylate (**18**) was synthesized as described.[1] Dry solvents were obtained with suitable desiccants. Other solvents were distilled before use. Column chromatography was carried out with silica gel (Macherey-Nagel, particle size 0.04–

0.063 mm). Melting points were measured with a Gallenkamp MPD350.BM2.5 instrument. NMR spectra were recorded with a Bruker AC 200, DRX 500 or Avance 600 instrument at 300 K. Assignments are supported by COSY, HSQC, and HMBC. In some cases, not all ^{13}C signals could be found in the 1D ^{13}C NMR spectra. In these cases, the listed chemical shifts have been extracted from the 2D spectra. Even when obtained by DEPT, the type of ^{13}C signal is always listed as singlet, doublet, etc. All chemical shifts are referenced to tetramethylsilane or the residual proton or carbon of the solvent. The NMR signals of atoms in the different arms of the triazines are assigned by using for instance Ar2 for atoms which are part of an benzene ring in the substituent at C-2 of the triazine. Aromatic rings within a biphenyl or terphenyl carry ’ or ’’ according to the biphenyl or terphenyl nomenclature. EI/CI mass spectra were recorded with a Finnigan MAT 8200, MAT 8230 or JEOL AccuTOF GCV 4G the latter one being used for HRMS as well. ESI mass spectra were recorded with an Applied Biosystems Mariner 5280. MALDI-TOF mass spectra were recorded with a Bruker-Daltronics Biflex III with Cl-CCA (4-chloro-α-cyano-cinnamic acid) as matrix. IR spectra were recorded with a Perkin-Elmer Spectrum 100 spectrometer equipped with a Golden Gate Diamond ATR unit A-531-G. Elemental analyses were carried out with a Euro EA 3000 Elemental Analyzer from Euro Vector.

2-(4-Bromo-3-nitrophenyl)-4,6-bis(4-bromophenyl)-1,3,5-triazine (3b)

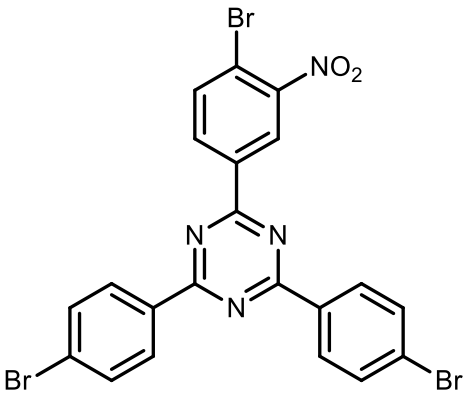

Under nitrogen and at 0 °C, antimony(V) chloride (5.23 mL, 40.8 mmol) was added to a solution of crude 4-bromo-3-nitrobenzoyl chloride (**5b**, 8.86 g, max. 33.5 mmol) and *p*-bromobenzonitrile (**6,** 12.5 g, 68.7 mmol) in dry chloroform (120 mL). The mixture was stirred for 1 h at room temp. and for 16 h at reflux. A yellow solid formed which was filtered off and washed with chloroform. At 0 °C, aq. ammonia (390 mL, 28 %) was added in portions to the residue and the suspension was stirred for 2 h at room temp. The solid changed its color from yellow to white. After filtration, the product was separated from insoluble side products by a Soxhlet extraction (chloroform, 48 h). Yield: 10.3 g (17.6 mmol, 53%). M. p.: >300 °C. ^{1}H NMR (500 MHz, $CDCl_3$, 323 K): δ = 9.11 (d, 1H, ^{4}J = 1.8 Hz, 2-Ar-*H*-2), 8.74 (dd, 1H, ^{3}J = 8.4 Hz, ^{4}J = 1.8 Hz, 2-Ar-*H*-6), 8.58 (d, 4H, ^{3}J = 8.5 Hz, 4,6-Ar-*H*-2,6), 7.98 (d, 1H, ^{3}J = 8.4 Hz, 2-Ar-*H*-5), 7.72 (d, 4H, ^{3}J = 8.5 Hz, 4,6-Ar-*H*-3,5) ppm. ^{13}C NMR (125 MHz, $CDCl_3$, 323 K): δ = 171.7 (s, triazine-*C*-4,6), 169.4 (s, triazine-*C*-2), 150.5 (s, 2-Ar-*C*-3), 136.7 (s, 2-Ar-*C*-4), 135.3 (d, 2-Ar-*C*-5), 134.4 (s, 4,6-Ar-*C*-4), 132.6 (d, 2-Ar-*C*-6), 132.3 (d, 4,6-Ar-*C*-3,5), 130.6 (d, 4,6-Ar-*C*-2,6), 128.4 (s, 4,6-Ar-*C*-1), 125.6 (d, 2-Ar-*C*-2), 118.8 (s, 2-Ar-*C*-1) ppm. MS (EI, 70 eV): *m/z* = 588/590/592/594 (34/100/90/33) $[M]^{+\cdot}$. MS (CI, isobutane): *m/z* = 589/591/593/595 (34/100/87/43) $[M + H]^{+}$. IR (ATR): $\tilde{\nu}$ = 3082 (aryl-H), 1592, 1509, 1486 (arom. C=C, arom. C=N), 1578 (NO_2), 1350 (C-N-val.), 806 (1,4-disubst. aryl, 1,2,4-trisubst. aryl) cm^{-1}. HRMS (EI): *m/z* = calcd. 589.8411; found 589.8391 (Δ 3.43 ppm). Elemental analysis ($C_{21}H_{11}Br_3N_4O_2$) (591.05): calcd. C 42.67 H 1.88 N 9.48; found C 42.67 H 1.77 N 9.07.

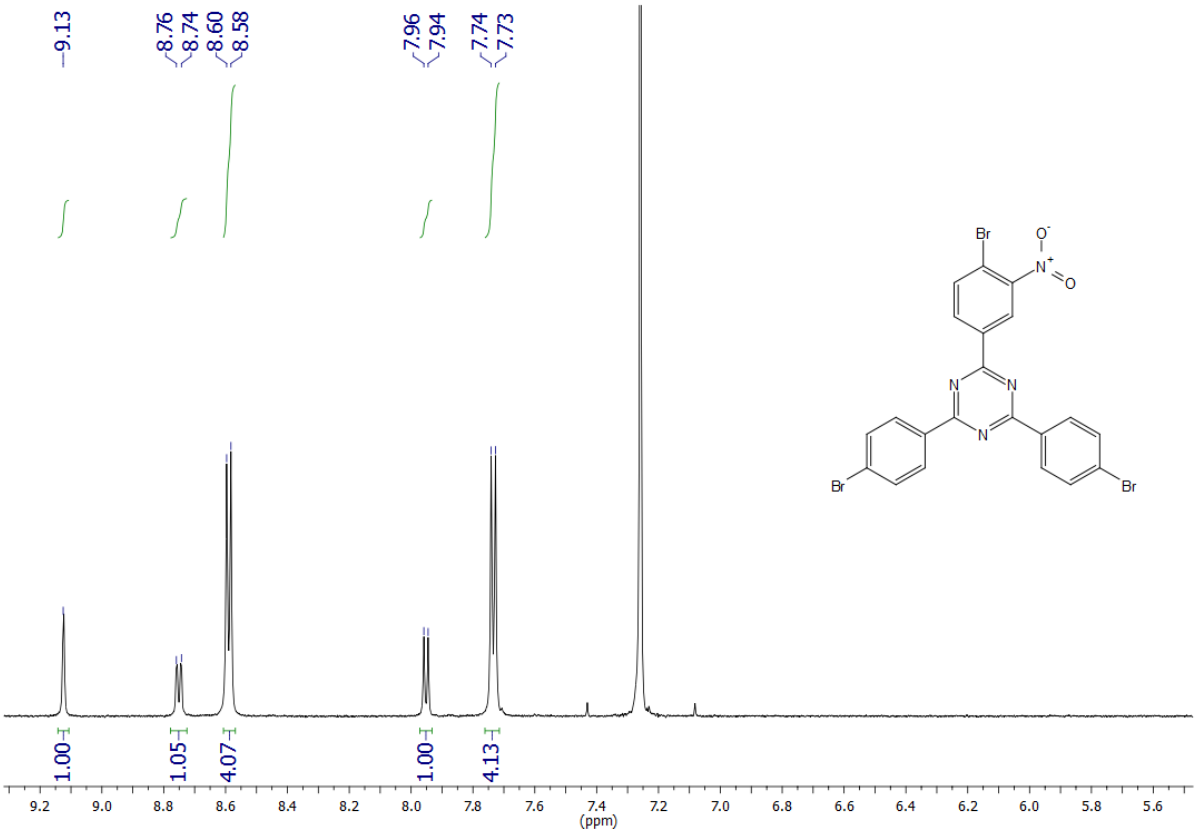
9.13
8.76
8.74
8.60
8.58
7.96
7.94
7.74
7.73
1.00
1.05
4.07
1.00
4.13
Br
O
N
O
N
N
N
Br
Br
9.2
9.0
8.8
8.6
8.4
8.2
8.0
7.8
7.6
7.4
7.2
7.0
6.8
6.6
6.4
6.2
6.0
5.8
5.6
(ppm)

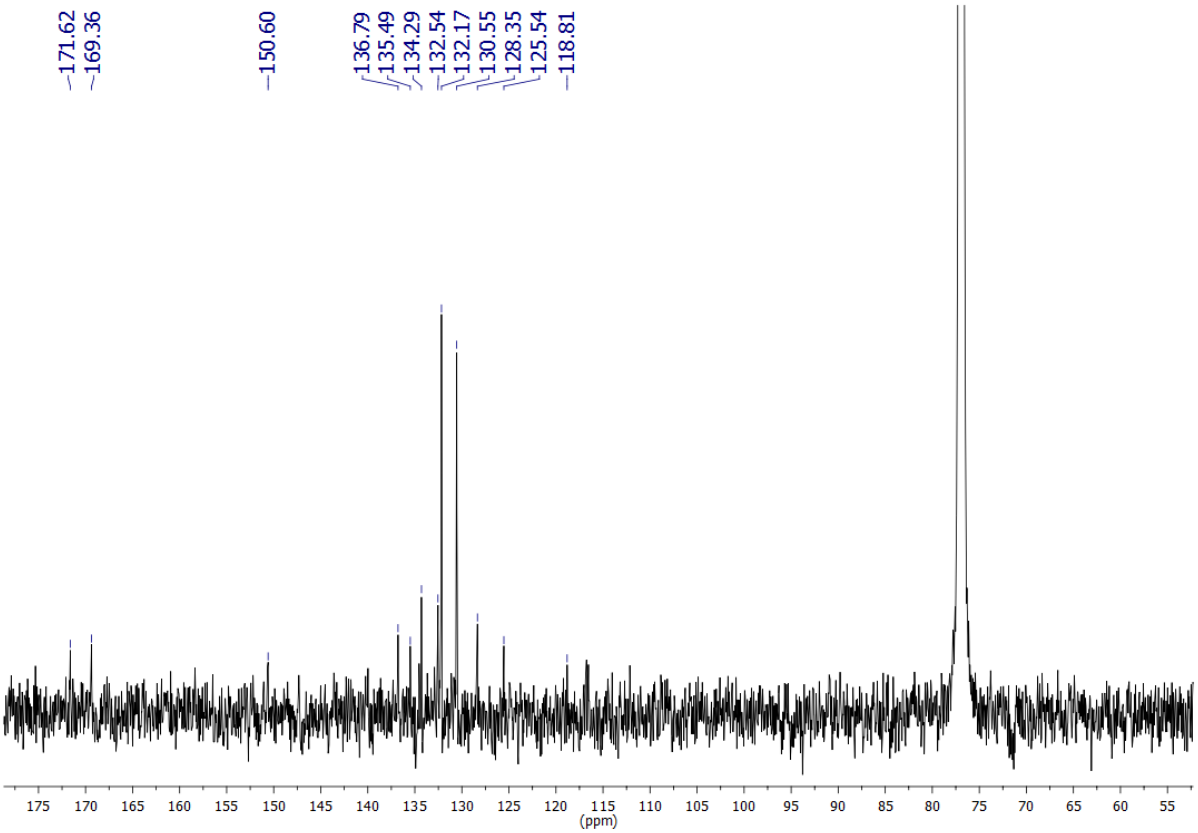
171.62
169.36
150.60
136.79
135.49
134.29
132.54
132.17
130.55
128.35
125.54
118.81
175
170
165
160
155
150
145
140
135
130
125
120
115
110
105
100
95
90
85
80
75
70
65
60
55
(ppm)

2-(4-Bromo-3-methoxyphenyl)-4,6-bis(4-bromophenyl)-1,3,5-triazine (3c)

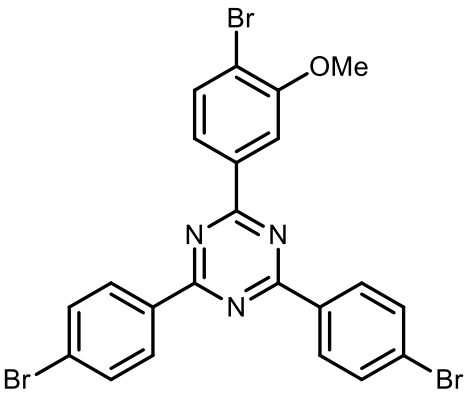

Under nitrogen, 4-bromo-3-methoxy-benzoyl chloride [**5c**, crude, from 1.00 g (4.01 mmol) of **14**] and *p*-bromobenzonitrile (**6**, 1.46 g, 8.02 mmol) were dissolved in dry chloroform (25 mL). At 0 °C, antimony(V) chloride (616 µL, 4.81 mmol) was added and the mixture was stirred for 1 h at room temp. followed by 16 h of reflux. The resulting red oxonium salt was filtered off and washed with chloroform. At 0 °C, aq. ammonia (50 mL, 28 %) was added to the residue and the suspension was stirred for 2 h at room temp. The solid changed its color from yellow to white. After filtration, the product was filtered off and was extracted for 24 h with chloroform (Soxhlet). After evaporation of the solvent, the residue was recrystallized from a boiling mixture of chloroform and petrol ether (30 - 60 °C) yielding a colourless solid. Yield: 1.41 g (2.45 mmol, 61 %). M. p.: 203 °C. ^{1}H NMR (500 MHz, $CDCl_3$): δ = 8.57 (m_c (d), 4H, ^{3}J = 8.7 Hz, 4,6-Ar-*H*-2,6), 8.23 (d, 1H, ^{4}J = 1.8 Hz, 2-Ar-*H*-2), 8.21 (dd, 1H, ^{3}J = 8.2 Hz, ^{4}J = 1.8 Hz, 2-Ar-*H*-6), 7.72 (d, 1H, ^{3}J = 8.2 Hz, 2-Ar-*H*-5), 7.70 (m_c (d), 4H, ^{3}J = 8.7 Hz, 4,6-Ar-*H*-3,5), 4.09 (s, 3H, O*C*H_3) ppm. ^{13}C NMR (125 MHz, $CDCl_3$): δ = 171.1 (s, triazine-*C*-4,6), 171.0 (s, triazine-*C*-2), 156.3 (s, 2-Ar-*C*-3), 136.4 (s, 2-Ar-*C*-1), 134.7 (s, 4,6-Ar-*C*-1), 133.6 (d, 2-Ar-*C*-5), 132.0 (d, 4,6-Ar-*C*-3,5), 130.4 (d, 4,6-Ar-*C*-2,6), 127.8 (s, 4,6-Ar-*C*-4), 122.5 (d, 2-Ar-*C*-6), 117.3 (s, 2-Ar-*C*-4), 111.6 (d, 2-Ar-*C*-2), 56.4 (q, O*C*H_3) ppm. MS (EI, 70 eV): *m/z* = 572/574/576/578 (34/100/96/34) $[M]^{+\cdot}$, 180 (85) $[M - C_{15}H_{10}Br_2N_2O]^{+}$. IR (ATR): $\tilde{\nu}$ = 3033 (aryl-H), 1598, 1505, 1485 (arom. C=C, arom. C=N), 1414 (C-N-val.), 1251 (aryl-OCH_3), 831 (1,4-disubst. aryl, 1,2,4-trisubst. aryl) cm^{-1}. HRMS (EI): *m/z* = calcd. 578.8625; found 578.8608 (Δ 3.12 ppm).

Elemental analysis ($C_{22}H_{14}Br_3N_3O$) (576.08): calcd. C 45.87 H 2.45 N 7.29; found C 46.09 H 2.46 N 6.94.

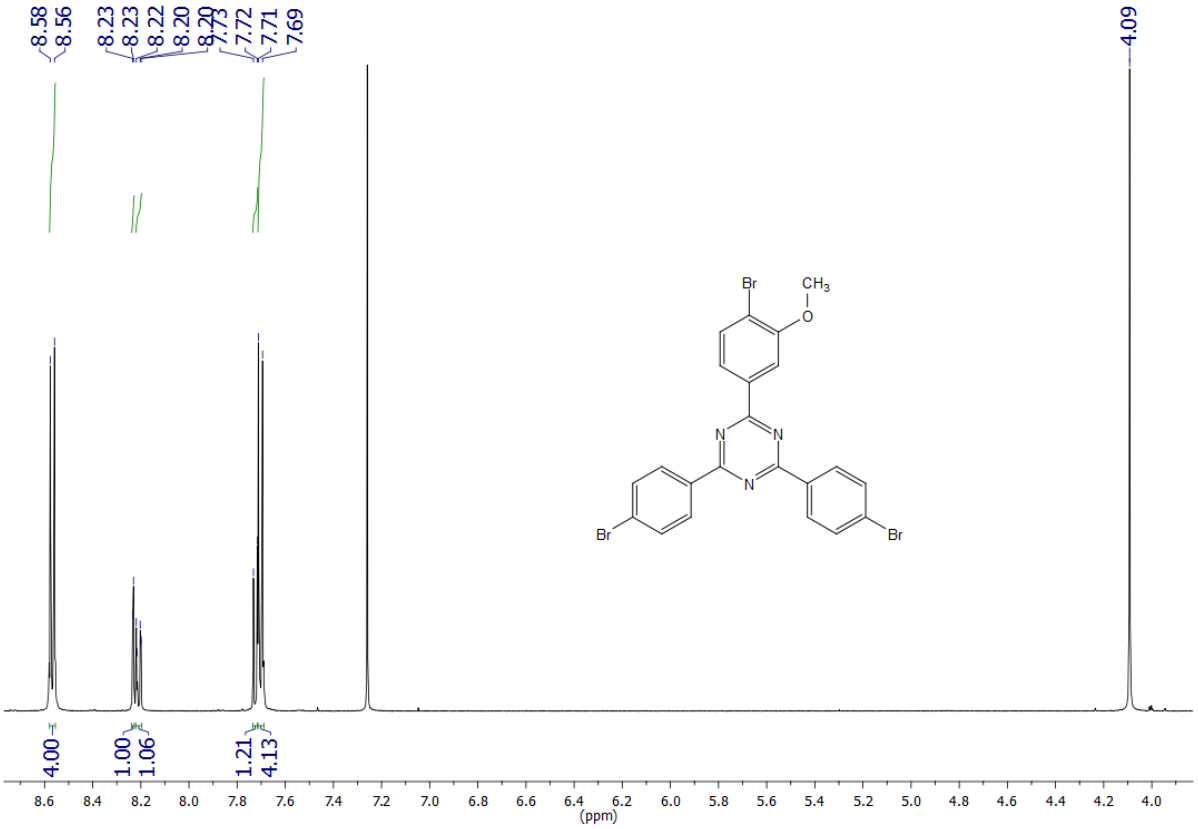

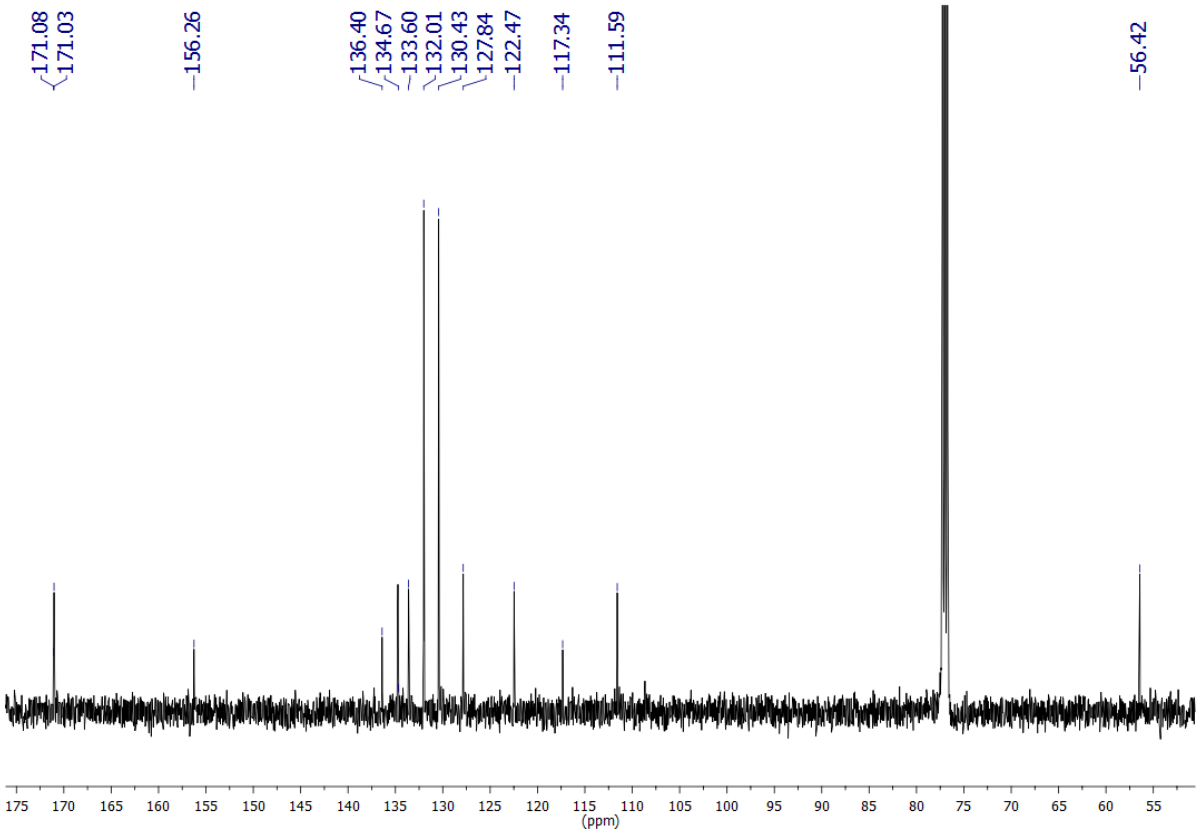
171.08
171.03
156.26
136.40
134.67
133.60
132.01
130.43
127.84
122.47
117.34
111.59
56.42
175 170 165 160 155 150 145 140 135 130 125 120 115 110 105 100 95 90 85 80 75 70 65 60 55
(ppm)

4-Bromo-3-nitrobenzoyl chloride (5b)

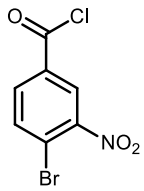

A solution of 4-bromo-3-nitrobenzoic acid (**9**, 4.00 g, 80.0 mmol) in thionyl chloride (24 mL) was heated to reflux for 2 h. Removal of excess thionyl chloride in vacuo yielded a yellow oil which was used without futher purification. ^{1}H NMR (500 MHz, $CDCl_3$): δ = 8.54 (d, 1H, ^{4}J = 2.2 Hz, Ar-*H*-2), 8.13 (dd, 1H, ^{3}J = 8.5 Hz, ^{4}J = 2.2 Hz, Ar-*H*-6), 7.94 (d, 1H, ^{3}J = 8.5 Hz, Ar-*H*-5) ppm. ^{13}C NMR (125 MHz, $CDCl_3$): δ = 166.0 (s, *C*OCl), 150.2 (s, Ar-*C*-3), 136.2 (d, Ar-*C*-6), 134.2 (d, Ar-*C*-5), 133.6 (s, Ar-*C*-1), 127.7 (d, Ar-*C*-2), 122.6 (s, Ar-*C*-4) ppm. MS (EI, 70 eV): *m/z* = 264/262 (14/11) $[M]^{+\cdot}$, 229/227 (96/100) $[M - Cl]^{+}$. MS (CI, isobutane): *m/z* = 265/263 (100/94) $[M + H]^{+}$, 229/227 (45/40) $[M - Cl]^{+}$.

4-Bromo-3-methoxy-benzoyl chloride (5c)

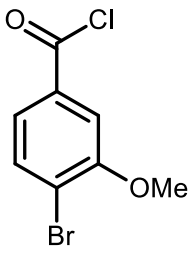

N,*N*-Dimethylformamide (10 µL) was added to a mixture of 4-bromo-3-methoxy-benzoic acid (**14**, 1.00 g, 4.01 mmol) and thionyl chloride (5 mL). After heating to reflux for 2 h, excess thionyl chloride was distilled off and the crude colourless solid was used without further purification. ^{1}H NMR (500 MHz, $CDCl_3$): δ = 7.70 (d, 1H, ^{3}J = 8.3 Hz, Ar-*H*-5), 7.63 (dd, 1H, ^{3}J = 8.3 Hz, ^{4}J = 2.0 Hz, Ar-*H*-6), 7.54 (d, 1H, ^{4}J = 2.0 Hz, Ar-*H*-2), 3.97 (s, 3H, O*C*H_3) ppm. ^{13}C NMR (125 MHz, $CDCl_3$): δ = 167.7 (s, *C*OCl), 156.3 (s, Ar-*C*-3), 133.8 (d, Ar-*C*-5), 133.5 (s, Ar-*C*-1), 125.0 (d, Ar-*C*-6), 120.9 (s, Ar-*C*-4), 113.0 (d, Ar-*C*-2), 56.5 (q, O*C*H_3) ppm.

4-Bromo-3-nitrobenzoic acid (9)

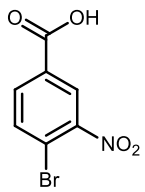

p-Brombenzoic acid (**8**, 5.00 g, 24.9 mmol) was slowly added in portions to a cold mixture (0 °C) of conc. nitric acid (6.2 mL, 0.15 mmol) and conc. sulfuric acid (15.2 mL, 300 mmol). The addition was performed in such a way that the temperature did not exceed 5 °C. After stirring for 3 h at 0 °C and 2 h at room temp., the mixture was poured on ice-containing water. The resulting colourless solid was filtered off and washed extensively with water. Yield: 6.00 g (24.4 mmol, 98%) (ref.[2]: 96 %), m. p. 202 °C. ^{1}H NMR (200 MHz, DMSO-d_6): δ = 8.46 – 8.42 (m, 1H, Ar-*H*-2), 8.09–8.05 (m, 2H, Ar-*H*-5,6) ppm. ^{13}C NMR (50 MHz, DMSO-d_6): δ = 165.0 (s, *C*O_2H), 149.7 (s, Ar-*C*-3), 135.4 (d, Ar-*C*-6), 132.4 (d, Ar-*C*-5), 131.7 (s, Ar-*C*-1), 125.9 (d, Ar-*C*-2), 118.0 (Ar-*C*-4) ppm. MS (EI, 70 eV): *m/z* = 245/247 (95/100) $[M]^{+\cdot}$. MS (CI, isobutane): *m/z* = 246/248 (100/99) $[M + H]^+$. IR (ATR): $\tilde{\nu}$= 3082 (aryl-H), 2820 (br., OH), 1684 (C=O), 1595 (arom. C=C), 1530, 1303 (NO_2), 1034 (aryl-Br), 907, 809 (1,2,4-trisubst. aryl) cm^{-1}.

4-Bromo-3-hydroxybenzoic acid (11)

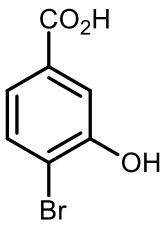

To a solution of 3-hydroxybenzoic acid (**10**, 15.0 g, 109 mmol) in a mixture of ethanol (60 mL) and acetic acid (30 mL), bromine (11.2 mL, 218 mmol) was added slowly and dropwise. After stirring for 30 min at room temp., aq. sodium thiosulfate solution (90 mL) was added and ethanol was removed in vacuo. The remaining aq. layer was extracted with ethyl acetate (5 x 200 mL) and the combined organic layer was dried with magnesium sulfate. After removal of the solvent, the crude product was recrystallized from boiling water and a colourless solid was obtained. Yield: 12.19 g (56.2 mmol, 52 %) (ref.[3]:

40 %). M. p.: 225 – 227 °C. ^{1}H NMR (500 MHz, DMSO-d_6): δ = 13.04 (br. s, 1H, CO_2H), 10.62 (s, 1H, O*H*), 7.59 (d, 1H, ^{3}J = 8.3 Hz, Ar-*H*-5), 7.51 (d, 1H, ^{4}J = 2.0 Hz, Ar-*H*-2), 7.28 (dd, 1H, ^{3}J = 8.3 Hz, ^{4}J = 2.0 Hz, Ar-*H*-6) ppm. ^{13}C NMR (125 MHz, DMSO-d_6): δ = 167.2 (s, *C*O_2H), 154.6 (s, Ar-*C*-3), 133.5 (d, Ar-*C*-5), 131.8 (s, Ar-*C*-1), 121.6 (d, Ar-*C*-6), 117.1 (d, Ar-*C*-2), 115.0 (s, Ar-*C*-4) ppm. MS (EI, 70 eV): *m/z* = 216/218 (100/97) $[M]^{+\cdot}$, 199, 201 (73, 70) $[M - OH]^{+}$.

Methyl 4-bromo-3-hydroxybenzoate (12)

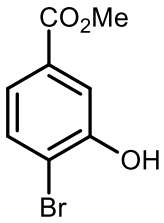

Conc. sulfuric acid (12 mL) was added to a suspension of 4-bromo-3-hydroxybenzoic acid (**11**, 12.2 g, 56.2 mmol) in methanol (120 mL). After heating to reflux for 16 h, the solution was neutralized with sat. aq. sodium bicarbonate solution and methanol was distilled off in vacuo. The remaining aq. phase was extracted with ethyl acetate (3 x 100 mL) and the combined organic layer was dried with magnesium sulfate. Filtration and removal of the solvent in vacuo yielded a colourless solid. Yield: 12.2 g (52.7 mmol, 94%) (ref.[4]: no yield given). M. p.: 124 °C (ref.[4]: 120 – 122 °C). ^{1}H NMR (500 MHz, $CDCl_3$): δ = 7.68 (d, 1H, ^{4}J = 2.0 Hz, Ar-*H*-2), 7.54 (d, 1H, ^{3}J = 8.3 Hz, Ar-*H*-5), 7.48 (dd, 1H, ^{3}J = 8.3 Hz, ^{4}J = 2.0, Ar-*H*-6), 5.75 (br. s, 1H, O*H*), 3.91 (s, 3H, CO_2CH_3) ppm. ^{13}C NMR (125 MHz, $CDCl_3$): δ = 166.2 (s, *C*O_2CH_3), 152.4 (s, Ar-*C*-3), 132.2 (d, Ar-*C*-5), 131.3 (s, Ar-*C*-1), 122.7 (d, Ar-*C*-6), 117.1 (d, Ar-*C*-2), 115.6 (s, Ar-*C*-4), 52.4 (q, CO_2CH_3) ppm. MS (EI, 70 eV): *m/z* = 230, 232 (63, 60) $[M]^{+\cdot}$.

Methyl 4-bromo-3-methoxy-benzoate (13)

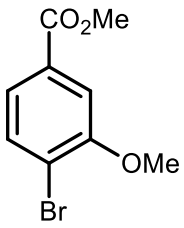

Method A: Potassium carbonate (4.56 g, 33.0 mmol) was added to a solution of methyl 4-bromo-3-hydroxybenzoate (**12**, 6.24 g, 27.0 mmol) in acetone (40 mL). Dimethyl sulfate (3.03 mL, 32.0 mmol) was added and the mixture was heated to reflux for 3 h. At room temp., deionized water was added (5 mL) and acetone was distilled off in vacuo. The remaining aq. phase was extracted with dichloromethane (3 x 100 mL), the combined organic layer was dried with magnesium sulfate, filtered and the solvent was removed in vacuo yielding a colourless solid. Yield: 6.59 g (26.9 mmol, >99 %) (ref.[5]: 99 %).

Method B: Potassium carbonate (2.54 g, 18.4 mmol) was added to a solution of 4-bromo-3-hydroxybenzoic acid (**11**, 1.00 g, 4.61 mmol) in *N*,*N*-dimethylformamide (10 mL). Methyl iodide (863 µL, 13.8 mmol) was added and the mixture was stirred for 16 h at room temp. Deionized water (50 mL) was added and the aq. phase was extracted with *tert*-butyl methyl ether (3 x 100 mL). The combined organic layer was washed with brine (100 mL) and dried with magnesium sulfate. After filtration, the solvent was evaporated in vacuo yielding a colourless solid. Yield: 938 mg (3.83 mmol, 83 %) (ref.[5]: 91 %).

M. p. 53 °C. ^{1}H NMR (500 MHz, $CDCl_3$): δ = 7.61 (d, 1H, ^{3}J = 8.2 Hz, Ar-*H*-5), 7.55 (d, 1H, ^{4}J = 1.8 Hz, Ar-*H*-2), 7.51 (dd, 1H, ^{3}J = 8.2 Hz, ^{4}J = 1.8 Hz, Ar-*H*-6), 3.95 (s, 3H, OCH_3), 3.92 (s, 3H, CO_2CH_3) ppm. ^{13}C NMR (125 MHz, $CDCl_3$): δ = 166.4 (s, CO_2Me), 155.9 (s, Ar-*C*-3), 133.3 (d, Ar-*C*-5), 130.6 (s, Ar-*C*-1), 122.9 (d, Ar-*C*-6), 117.5 (s, Ar-*C*-4), 112.4 (d, Ar-*C*-2), 56.4 (q, OCH_3), 52.4 (q, CO_2CH_3) ppm. HRMS (EI): *m/z* = calcd. 243.9735; found 243.9744 (Δ 4.01 ppm).

4-Bromo-3-methoxy-benzoic acid (14)

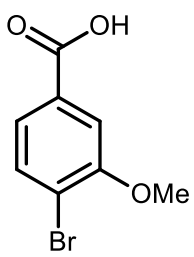

Aq. sodium hydroxide (2 M, 40 mL) was added to a solution of methyl 4-bromo-3-methoxy-benzoate (**13**, 6.52 g, 27.1 mmol) in methanol (200 mL) and the mixture was stirred for 6 h at room temp. Deionized water (100 mL) was added and methanol was distilled off in vacuo. The remaining aq. phase was washed with dichloromethane (3 x 100 mL) and acidified with hydrochloric acid (6 M). The precipitate was filtered off and was washed thoroughly with water yielding a colourless solid. Yield: 4.10 g (17.8 mmol, 66 %) (ref.[5]: 89 %). M. p.: 220 °C. ^{1}H NMR (500 MHz, DMSO-d_6): δ = 13.21 (br. s, 1H, CO_2H), 7.71 (d, 1H, ^{3}J = 8.2 Hz, Ar-*H*-5), 7.54 (d, 1H, ^{4}J = 1.8 Hz, Ar-*H*-2), 7.46 (dd, 1H, ^{3}J = 8.2 Hz, ^{4}J = 1.8 Hz, Ar-*H*-6), 3.91 (s, 3H, OCH_3) ppm. ^{13}C NMR (125 MHz, DMSO-d_6): δ = 167.1 (s, CO_2H), 155.9 (s, Ar-*C*-3), 133.6 (d, Ar-*C*-5), 132.1 (s, Ar-*C*-1), 123.2 (d, Ar-*C*-6), 116.5 (s, Ar-*C*-4), 113.0 (d, Ar-*C*-2), 56.8 (q, OCH_3) ppm. MS (EI, 70 eV): *m/z* = 230/232 (100/98) $[M]^{+\cdot}$.

2,4-Bis[4'-(methoxycarbonyl)-biphenyl-4-yl]-6-[4'-(methoxycarbonyl)-2-nitro-biphenyl-4-yl)-1,3,5-triazine (16b)

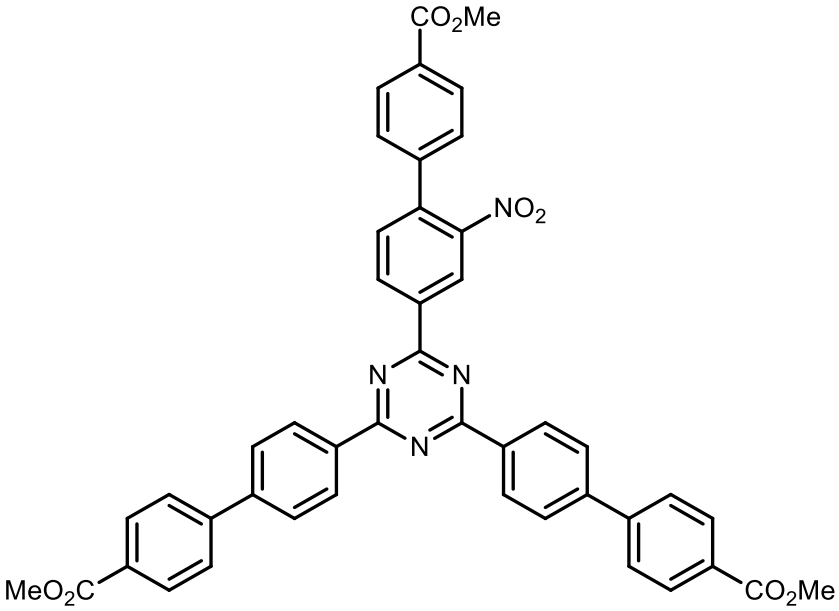

Under nitrogen, 2-(4-bromo-3-nitrophenyl)-4,6-bis(4-bromophenyl)-1,3,5-triazine (**3b**, 3.00 g, 5.08 mmol), 4-methoxycarbonyl-phenylboronic acid (**15**, 4.10 g, 22.8 mmol), potassium phosphate (7.00 g, 33.0 mmol) and tetrakis(triphenylphosphine) palladium(0) (300 mg, 260 µmol) in a mixture of 1,4-dioxane (300 mL) and deionized water (20 mL) were heated to reflux for 48 h. Conversion was checked by TLC (silica gel, cyclohexane/ethyl acetate, 1:1, R_f = 0.69). After evaporation of the 1,4-dioxane in vacuo, chloroform (150 mL) was added and the organic layer was washed with deionized water (2 x 100 mL) and brine (50 mL). The organic layer was dried with magnesium sulfate. After filtration and evaporation of the solvent in vacuo, the crude product was dissolved in chloroform, activated charcoal was added, and after filtration, the product was recrystallized from chloroform yielding a colourless solid. Yield: 3.46 g (4.57 mmol, 90 %). M. p.: 174 °C. ^{1}H NMR (500 MHz, $CDCl_3$,): δ = 9.22 (d, 1H, ^4J = 1.7 Hz, 6-Ar-*H*-3), 8.96 (dd, 1H, ^3J = 8.0 Hz, ^4J = 1.7 Hz, 6-Ar-*H*-5), 8.81 (m_c (d), 4H, ^3J = 8.6 Hz, 2,4-Ar-*H*-2,6), 8.15 (m_c (d), 4H, ^3J = 8.6 Hz, 2,4-Ar'-*H*-3,5), 8.13 (m_c (d), 2H, ^3J = 8.6 Hz, 6-Ar'-*H*-3,5), 7.81 (m_c (d), 4H, ^3J = 8.6 Hz, 2,4-Ar-*H*-3,5), 7.74 (m_c (d), 4H, ^3J = 8.6 Hz, 2,4-Ar'-*H*-2,6), 7.61 (d, 1H, ^3J = 8.0 Hz, 6-Ar-*H*-6), 7.44 (m_c (d), 2H, ^3J = 8.6 Hz, 6-Ar'-*H*-2,6), 3.97 (s, 9H, OCH_3) ppm. ^{13}C

NMR (125 MHz, $CDCl_3$): δ = 171.6 (s, triazine-*C*-2,4), 169.3 (s, triazine-*C*-6), 166.8 (s, 2,4-Ar'-*C*O_2Me), 166.5 (s, 6-Ar'-*C*O_2Me), 149.6 (s, 6-Ar-*C*-2), 144.4 (s, 2,4-Ar'-*C*-1), 144.3 (s, 2,4-Ar-*C*-4), 141.4 (s, 6-Ar'-*C*-1), 138.8 (s, 6-Ar-*C*-1), 137.3 (s, 6-Ar-*C*-4), 135.2 (s, 2,4-Ar-*C*-1), 132.2 (d, 6-Ar-*C*-5), 132.1 (d, 6-Ar-*C*-6), 130.4 (s, 6-Ar'-*C*-4), 130.3 (d, 2,4-Ar'-*C*-3,5), 130.1 (d, 2,4-Ar-*C*-3,5), 129.7 (s, 2,4-Ar'-*C*-4), 129.7 (d, 6-Ar'-*C*-2,6), 128.0 (d, 2,4-Ar'-*C*-2,6), 127.6 (6-Ar'-*C*-3,5), 127.2 (d, 2,4-Ar-*C*-2,6), 124.6 (d, 6-Ar-*C*-3), 52.3 (q, 6-Ar'-CO_2CH_3), 52.2 (q, 2,4-Ar'-CO_2CH_3) ppm. MS (MALDI, Cl-CCA): *m/z* = 757 $[M + H]^+$, 767 $[M + Na]^+$, 776 $[M + K]^+$. IR (ATR): $\tilde{\nu}$ = 3076, 3006 (aryl-H), 2951, 2895 (CH-val.), 2844 (OCH_3), 1717 (C=O), 1607, 1580, 1563, 1506 (arom. C=C, arom. C=N), 1535, 1314 (NO2), 1434 (CH-Def.), 1357 (C-N-val.), 1257, 1105 (CO_2Me), 813 (1,4-disubst. aryl, 1,2,4-trisubst. aryl) cm^{-1}. MS (EI, 70 eV): *m/z* (%) = 756 (65) $[M]^{+\cdot}$, 726 (100) $[M - CH_3O + H]^{+\cdot}$, 238 (61) $[(M - C_{15}H_{10}N_2O_4)/2]^+$, 206 (70) $[(M - C_{15}H_{10}N_2O_4)/2 - CH_3O]^+$, 178 (63) $[(M - C_{15}H_{10}N_2O_4)/2 - C_2H_3O]^+$. HRMS (EI): *m/z* = calcd. 756.2219; found 756.2191 (Δ 3.9 ppm). Elemental analysis ($C_{45}H_{32}N_4O_8$) (756.76): calcd. C 71.42 H 4.26 N 7.40; found C 71.54 H 4.16 N 7.32.

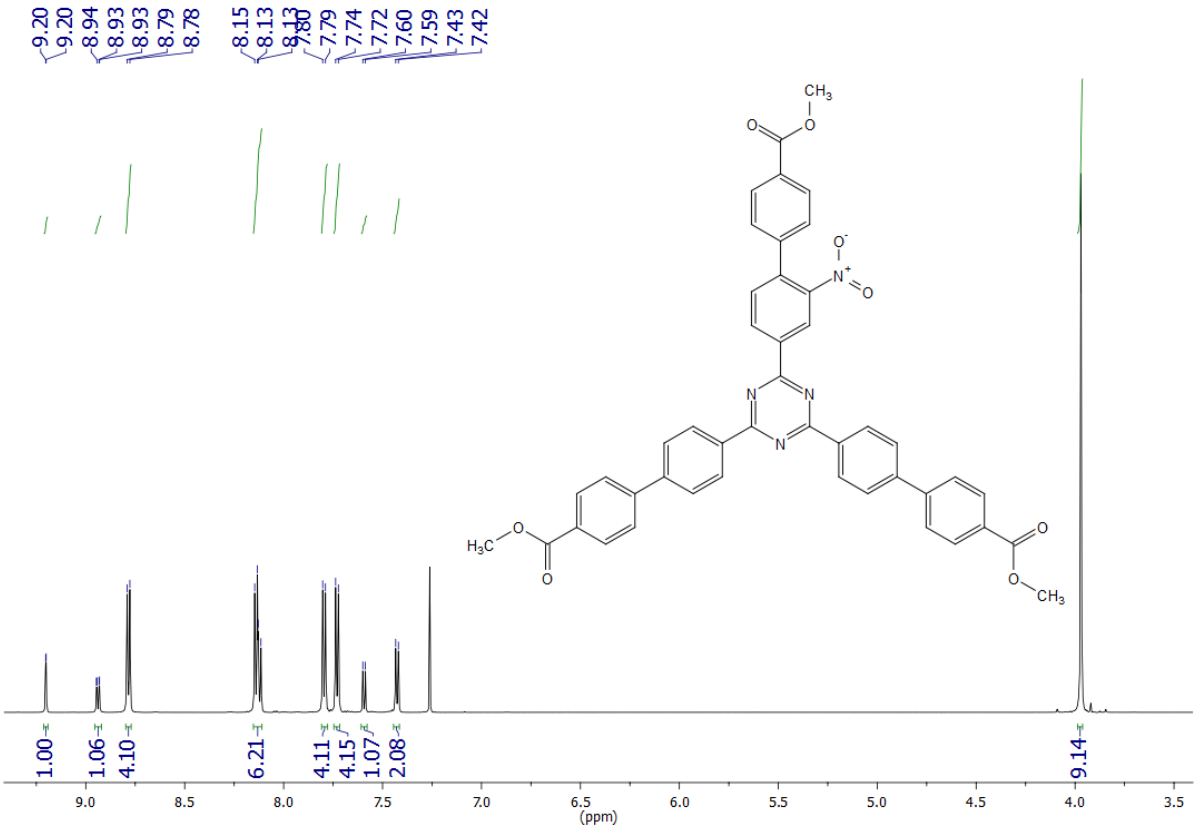
9.20
9.20
8.94
8.93
8.93
8.79
8.78
8.15
8.13
8.13
7.80
7.79
7.74
7.72
7.60
7.59
7.43
7.42
1.00
1.06
4.10
6.21
4.11
4.15
1.07
2.08
9.14
(ppm)

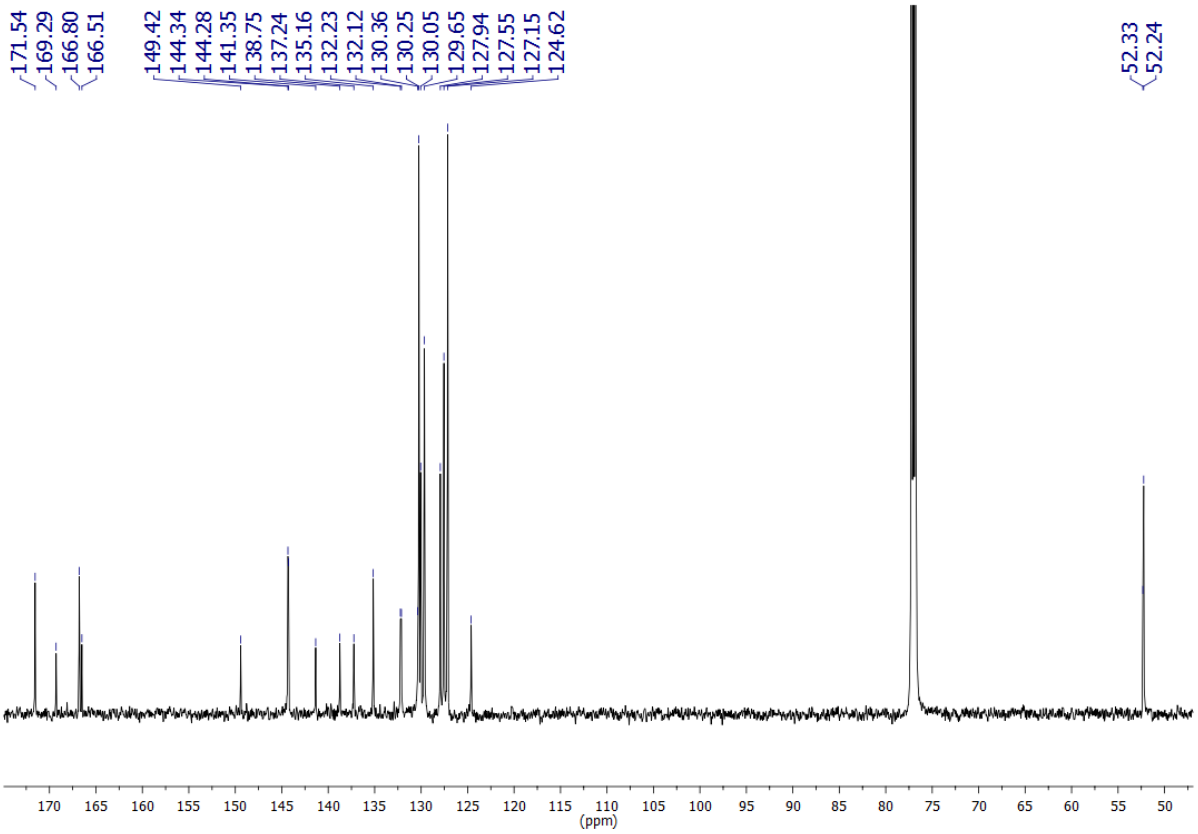
171.54
169.29
166.80
166.51
149.42
144.34
144.28
141.35
138.75
137.24
135.16
132.23
132.12
130.36
130.25
130.05
129.65
127.94
127.55
127.15
124.62
52.33
52.24
(ppm)

2,4-Bis[4'-(methoxycarbonyl)-biphenyl-4-yl]-6-[2-methoxy-4'-(methoxycarbonyl)-biphenyl-4-yl]-1,3,5-triazine (16c)

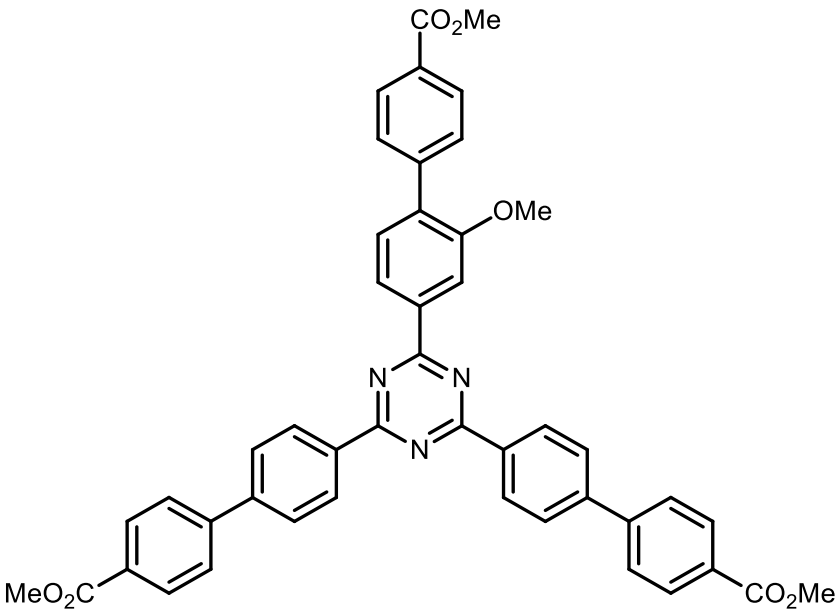

To a mixture of 2-(4-bromo-3-methoxyphenyl)-4,6-bis(4-bromophenyl)-1,3,5-triazine (**3c**, 100 mg, 174 µmol), 4-methoxycarbonyl-phenylboronic acid (**15**, 130 mg, 783 µmol) and potassium phosphate (250 mg, 1.18 mmol) in 1,4-dioxane (10 mL) and deionized water (1 mL) under nitrogen, tetrakis(triphenylphosphine)palladium(0) (19 mg, 16 µmol) was added. The mixture was stirred for 48 h at 100 °C, the solvent was evaporated in vacuo, the residue was dissolved in chloroform (50 ml) and washed with deionized water (3 x 25 mL) and brine (25 mL). The organic layer was dried with magnesium sulfate and heated after activated charcoal had been added. After filtration through celite, the solvent was evaporated in vacuo and the crude product was recrystallized from a boiling mixture of toluene and *n*-heptane. A colourless solid was obtained. Yield: 94 mg (127 µmol, 73 %). M. p.: 203 °C. ^{1}H NMR (500 MHz, $CDCl_{3,}$): δ = 8.85 (d, 4H, ^{3}J = 8.5 Hz, 2,4-Ar-*H*-2,6), 8.47 (dd, 1H, ^{3}J = 7.9 Hz, ^{4}J = 1.5 Hz, 6-Ar-*H*-5), 8.40 (d, 1H, ^{3}J = 1.5 Hz, 6-Ar-*H*-3), 8.16 (d, 4H, ^{3}J = 8.5 Hz, 2,4-Ar'-*H*-3,5), 8.12 (d, 2H, ^{3}J = 8.5 Hz, 6-Ar'-*H*-3,5), 7.83 (d, 4H, ^{3}J = 8.5 Hz, 2,4-Ar-*H*-3,5), 7.76 (d, 4H, ^{3}J = 8.5 Hz, 2,4-Ar'-*H*-2,6), 7.70 (d, 2H, ^{3}J = 8.5 Hz, 6-Ar'-*H*-2,6), 7.54 (d, 1H, ^{3}J = 7.9 Hz, 6-Ar-*H*-6), 4.04 (s, 3H, OCH_3), 3.97 (s, 6H, 2,4-Ar'-CO_2CH_3), 3.96 (s,

3H, 6-Ar'-CO_2CH_3) ppm. ^{13}C NMR (125 MHz, $CDCl_3$): δ = 171.2 (s, triazine-*C*-2,4), 171.2 (s, triazine-*C*-6), 167.0 (s, 2,4-Ar'-*C*O_2Me), 166.9 (s, 6-Ar'-*C*O_2Me), 156.8 (s, 6-Ar-*C*-2), 144.6 (s, 2,4-Ar'-*C*-1), 144.0 (s, 2,4-Ar-*C*-4), 142.6 (s, 6-Ar'-*C*-1), 137.2 (s, 6-Ar-*C*-4), 135.8 (s, 2,4-Ar-*C*-1), 133.8 (s, 6-Ar-*C*-1), 131.0 (s, 6-Ar-*C*-6), 130.2 (d, 2,4-Ar'-*C*-3,5), 129.6 (d, 2,4-Ar-*C*-2,6), 129.6 (d, 6-Ar'-*C*-2,6), 129.5 (s, 2,4-Ar'-*C*-4), 129.4 (d, 6-Ar'-*C*-3,5), 129.0 (s, 6-Ar'-*C*-4), 127.5 (d, 2,4-Ar-*C*-3,5), 127.2 (d, 2,4-Ar'-*C*-2,6), 121.9 (d, 6-Ar-*C*-5), 111.4 (d, 6-Ar-*C*-3), 55.8 (q, OCH_3), 52.2 (q, 2,4-Ar'-CO_2CH_3), 52.1 (q, 6-Ar'-CO_2CH_3) ppm. MS (EI, 70 eV): *m/z* = 741 (100) $[M]^{+\cdot}$, 238 (69) $[M - C_{31}H_{23}N_2O_5]^+$. IR (ATR): $\tilde{\nu}$ = 3005 (aryl-H), 2954, 2878, 2840 (CH-val.), 1715 (C=O), 1607, 1582, 1508, 1419 (arom. C=C, arom. C=N), 1434 (CH-Def.), 1360 (C-N-val.), 1273 (aryl-OCH_3), 812 (1,4-disubst. aryl, 1,3,4-trisubst. aryl) cm^{-1}. HRMS (EI): *m/z* = calcd. 741.2475; found 741.2465 (Δ 1.42 ppm). Elemental analysis ($C_{46}H_{35}N_3O_7$) (741.79): calcd. C 74.48 H 4.76 N 5.66; found C 74.59 H 4.93 N 5.69.

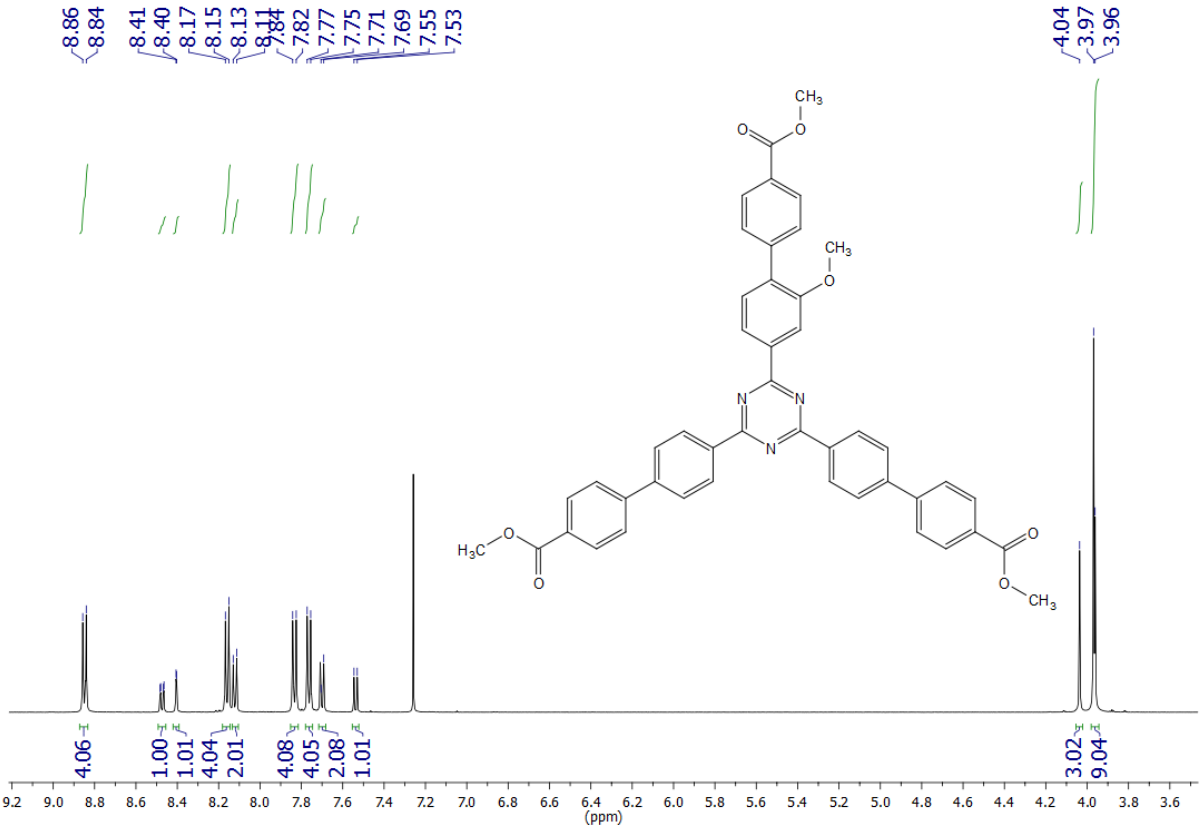
8.86
8.84
8.41
8.40
8.17
8.15
8.13
7.82
7.77
7.75
7.71
7.69
7.55
7.53
4.04
3.97
3.96
CH3
O
N
H3C
4.06
1.00
1.01
4.04
2.01
4.08
4.05
2.08
1.01
3.02
9.04
(ppm)

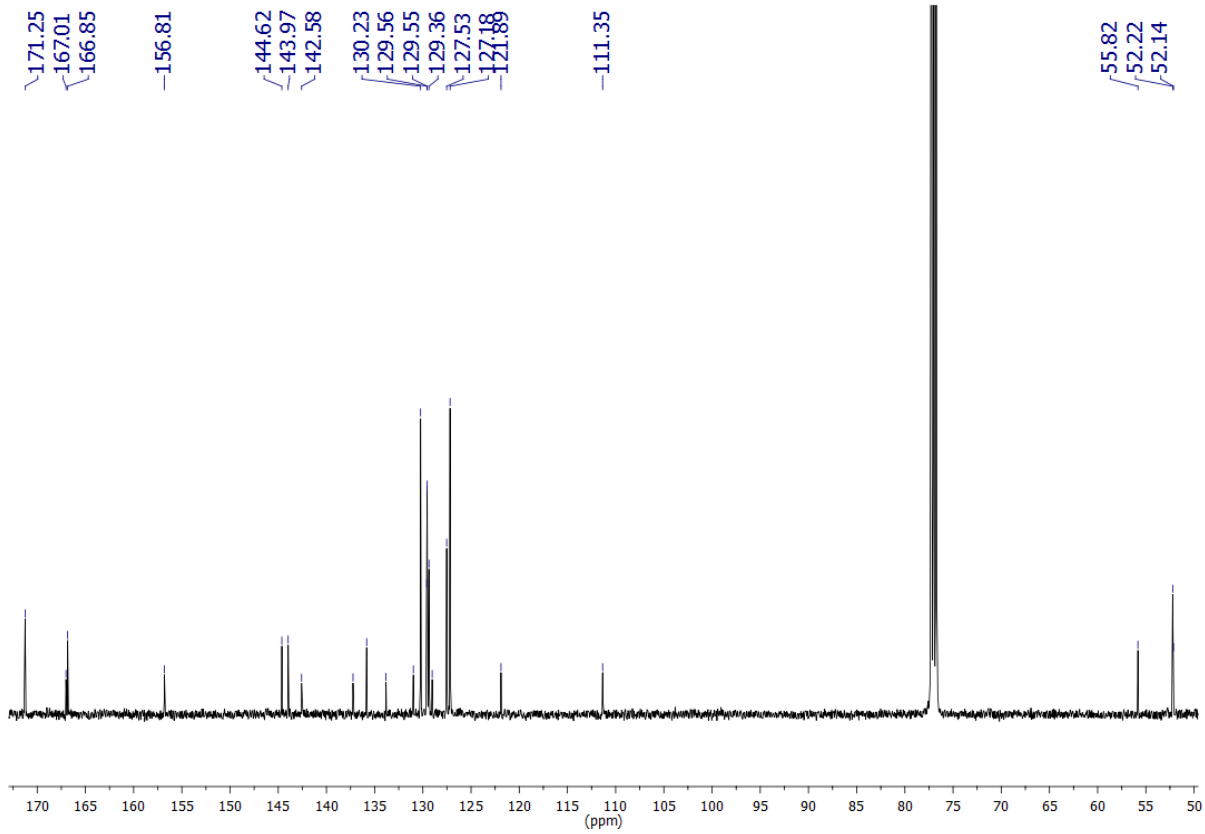
171.25
167.01
166.85
156.81
144.62
143.97
142.58
130.23
129.56
129.55
129.36
127.53
111.35
55.82
52.22
52.14
(ppm)

2-[2-Amino-4'-(methoxycarbonyl)-biphenyl-4-yl]-4,6-bis[4'-(methoxycarbonyl)-biphenyl-4-yl]-1,3,5-triazine (16d)

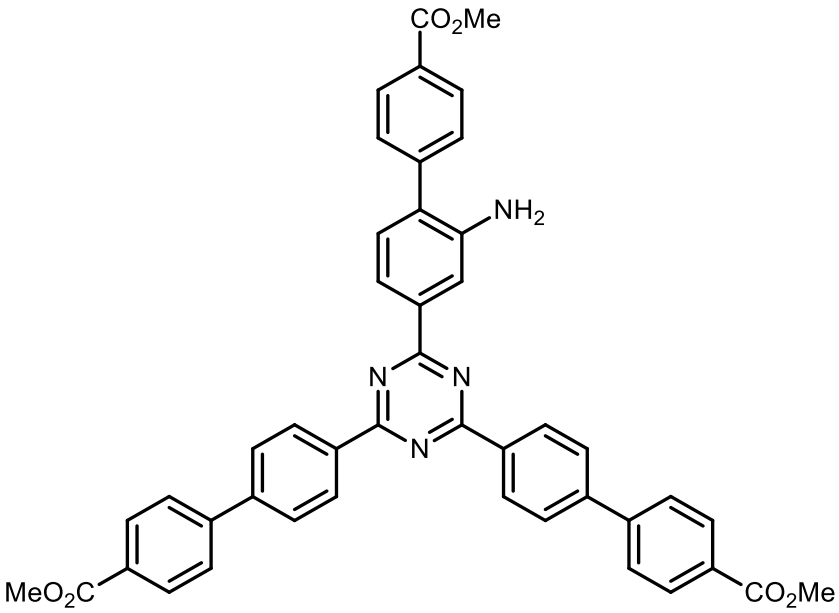

An autoclave was filled with 2-[4'-(methoxycarbonyl)-2-nitro-biphenyl-4-yl]-4,6-bis[4'-(methoxycarbonyl)-biphenyl-4-yl]-1,3,5-triazine (**16b**, 100 mg, 132 µmol) and palladium on charcoal (45 mg, 10 %) in dichloromethane (5 mL). The apparatus was evacuated five times and refilled with hydrogen (5 bar). After stirring under a 5 bar hydrogen atmosphere for 5 d at room temp., the mixture was filtered through celite and the solvent was evaporated in vacuo. The crude product was recrystallized from a boiling mixture of toluene and *n*-heptane yielding a yellow solid. Yield: 77 mg (0.11 mmol, 77 %). M. p.: 225 °C. ^{1}H NMR (600 MHz, $CDCl_3$): δ = 8.85 (d, 4H, ^{3}J = 8.3 Hz, 4,6-Ar-*H*-3,5), 8.25 (dd, 1H, ^{3}J = 8.0 Hz, ^{4}J = 1.3 Hz, 2-Ar-*H*-5), 8.20 (br. s, 1H, 2-Ar-*H*-3), 8.17 (d, 2H, ^{3}J = 8.2 Hz, 2-Ar'-*H*-3,5), 8.16 (d, 4H, ^{3}J = 8.4 Hz, 4,6-Ar'-*H*-3,5), 7.83 (d, 4H, ^{3}J = 8.4 Hz, 4,6-Ar'-*H*-2,6), 7.70 (d, 4H, ^{3}J = 8.3 Hz, 4,6-Ar-*H*-2,6), 7.64 (d, 2H, ^{3}J = 8.2 Hz, 2-Ar-*H*-2,6), 7.34 (d, 1H, ^{3}J = 8.0 Hz, 2-Ar-*H*-6), 3.97 (s, 3H, 2-Ar'-CO_2CH_3), 3.96 (s, 6H, 4,6-Ar'-CO_2CH_3) ppm. ^{13}C NMR (150 MHz, $CDCl_3$): δ = 171.4 (s, triazine-*C*-2), 171.1 (s, triazine-*C*-4,6), 166.9 (s, 4,6-Ar'-*C*O_2Me), 166.8 (s, 2-Ar'-*C*O_2Me), 144.6 (s, 2-Ar-*C*-2), 143.8 (s, 2-Ar'-*C*-1), 143.7 (s, 4,6-Ar-*C*-1), 143.7 (s, 4,6-Ar'-*C*-1), 136.8 (s, 2-Ar-*C*-4), 135.9 (s, 4,6-Ar-*C*-4),

130.9 (d, 2-Ar-*C*-6), 130.7 (d, 4,6-Ar'-*C*-3,5), 130.5 (s, 4,6-Ar'-*C*-4), 130.2 (d, 2-Ar'-*C*-3,5), 130.0 (s, 2-Ar-*C*-1), 129.5 (d, 4,6-Ar-*C*-3,5), 129.3 (s, 2-Ar-*C*-4), 128.9 (d, 2-Ar'-*C*-2,6), 127.4 (d, 4,6-Ar-*C*-2,6), 127.2 (d, 4,6-Ar'-*C*-2,6), 119.6 (d, 2-Ar-*C*-5), 116.1 (d, 2-Ar-*C*-3), 52.2 (q, 2-Ar'-CO_2CH_3), 52.2 (q, 4,6-Ar'-CO_2CH_3) ppm. MS (EI, 70 eV): *m/z* = 726 (100) $[M]^{+\cdot}$. IR (ATR): $\tilde{\nu}$ = 3350 (NH_2), 3001 (aryl-H), 2954, 2846 (CH–val.), 1715 (C=O), 1607, 1582, 1507, 1419 (arom. C=C, arom. C=N), 1434 (CH-Def.) 1360 (C-N-val.), 812 (1,4-disubst. aryl, 1,3,4-trisubst. aryl) cm^{-1}. HRMS (EI): *m/z* = calcd. 726.2478; found 726.2465 (Δ 1.78 ppm). Elemental analysis ($C_{45}H_{34}N_4O_6$) (726.77): calcd. C 74.73 H 7.71 N 4.72; ($C_{45}H_{34}N_4O_6 \cdot 1.3H_2O \cdot 0.5C_7H_8$) (796.26): calcd. C 73.16 H 5.14 N 7.04; found C 73.27 H 5.46 N 7.35.

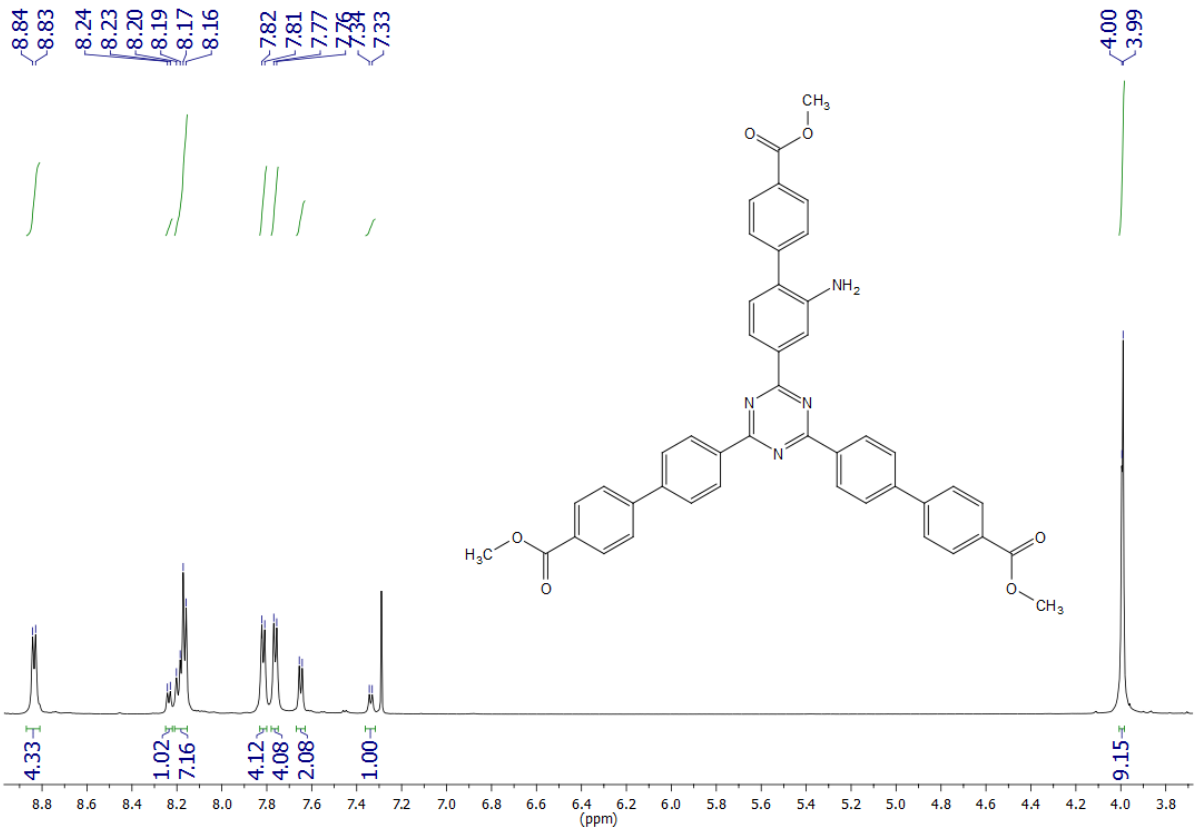
8.84
8.83
8.24
8.23
8.20
8.19
8.17
8.16
7.82
7.81
7.77
7.34
7.33
4.00
3.99
CH3
O
O
NH2
N
N
N
H3C
O
O
O
O
CH3
4.33
1.02
7.16
4.12
4.08
2.08
1.00
9.15
(ppm)

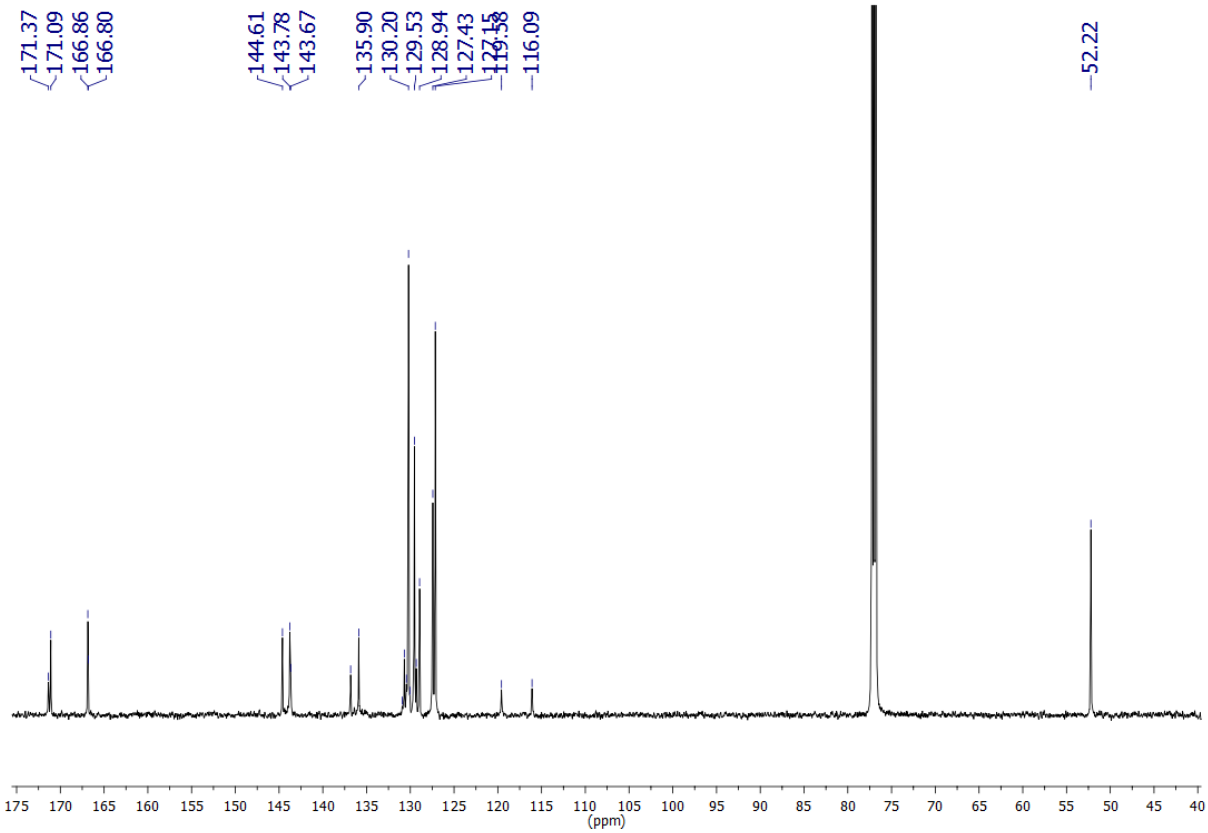
171.37
171.09
166.86
166.80
144.61
143.78
143.67
135.90
130.20
129.53
128.94
127.43
116.09
52.22
(ppm)

2,4-Bis(4'-carboxy-biphenyl-4-yl)-6-(4'-carboxy-2-nitro-biphenyl-4-yl)-1,3,5-triazine (17b)

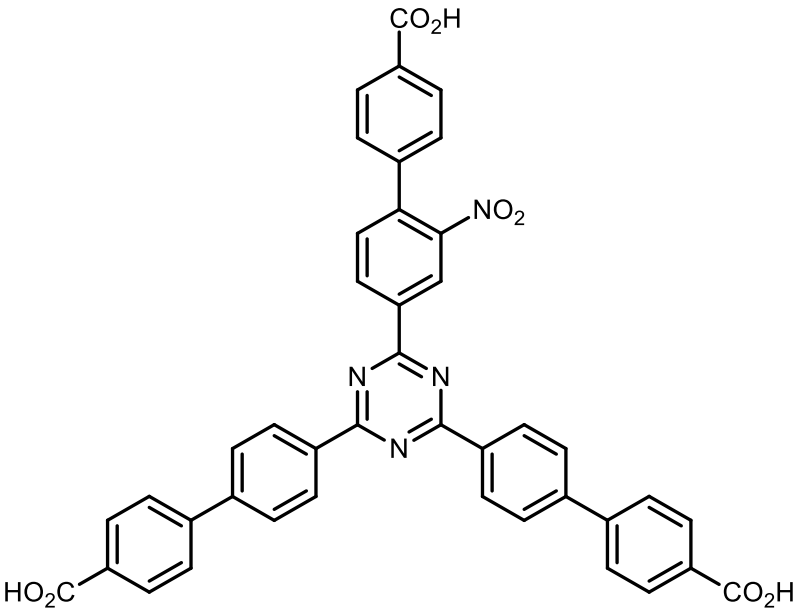

Lithium hydroxide monohydrate (5.12 g, 122 mol) was added to 2-[4'-(methoxycarbonyl)-2-nitro-biphenyl-4-yl]-4,6-bis[4'-(methoxycarbonyl)-biphenyl-4-yl]-1,3,5-triazine (**16b**, 3.30 g, 4.36 mmol) in a mixture of tetrahydrofuran (430 mL) and deionized water (45 mL). After stirring for 48 h at room temp., the solvent was evaporated in vacuo, the yellow residue was dissolved in water and acidified with hydrochloric acid (3 M). The yellow precipitate was filtered off and washed with deionized water and chloroform. Yield: 2.99 g (4.18 mmol, 96%). M. p.: >300 °C. ^{1}H NMR (500 MHz, DMSO-d_6): δ = 8.99 (d, 1H, ^{4}J = 1.4 Hz, 6-Ar-*H*-2), 8.77 (dd, 1H, ^{3}J = 7.9 Hz, ^{4}J = 1.4 Hz, 6-Ar-*H*-6), 8.58 (d, 4H, ^{3}J = 8.3 Hz, 2,4-Ar-*H*-2,6), 8.00 (d, 4H, ^{3}J = 8.3 Hz, 2,4-Ar'-*H*-3,5), 7.98 (d, 2H, ^{3}J = 8.3 Hz, 6-Ar'-*H*-3,5), 7.82 (d, 4H, ^{3}J = 8.3 Hz, 2,4-Ar-*H*-3,5), 7.77 (d, 4H, ^{3}J = 8.3 Hz, 2,4-Ar'-*H*-2,6), 7.64 (d, 1H, ^{3}J = 7.9 Hz, 6-Ar-*H*-5), 7.38 (d, 2H, ^{3}J = 8.3 Hz, 6-Ar'-*H*-2,6) ppm. ^{13}C NMR (125 MHz, DMSO-d_6): δ = 171.1 (s, triazine-*C*-2,4), 169.1 (s, triazine-*C*-6), 167.4 (s, 2,4-Ar-*C*O_2H), 167.2 (s, 6-Ar-*C*O_2H), 149.2 (d, 6-Ar-*C*-3), 143.7 (s, 2,4-Ar'-*C*-1), 143.4 (s, 2,4-Ar-*C*-4), 141.1 (s, 6-Ar'-*C*-1), 138.4 (s, 6-Ar-*C*-4), 136.7 (s, 6-Ar-*C*-1), 134.9 (s, 2,4-Ar-*C*-1), 132.9 (s, 6-Ar'-*C*-4), 132.7 (d, 6-Ar-*C*-6), 131.3 (s, 2,4-Ar'-*C*-4), 130.8 (d, 6-Ar-*C*-5), 130.4 (d, 2,4-Ar'-*C*-3,5), 130.0 (d, 2,4-Ar-*C*-3,5), 129.7 (d, 6-Ar'-

C-2,6), 129.0 (d, 2,4-Ar-*C*-2,6), 127.7 (6-Ar'-*C*-3,5), 127.4 (d, 2,4-Ar'-*C*-2,6), 124.3 (s, 6-Ar-*C*-2) ppm. MS (MALDI, Cl-CCA): *m/z* = 715 $[M + H]^+$. IR (ATR): $\tilde{\nu}$ = 3400 (br., OH), 3005 (aryl-H), 1714 (C=O), 1607, 1582, 1506, 1419 (arom. C=C, arom. C=N), 1510, 1316 (NO_2), 1359 (C-N–val.), 813 (1,4-disubst. aryl, 1,3,4-trisubst. aryl) cm^{-1}. Elemental analysis ($C_{42}H_{26}N_4O_8$) (714.69): calcd. C 70.58 H 3.67 N 7.84; ($C_{42}H_{26}N_4O_8 \cdot 1.35H_2O$) (738.99): calcd. C 68.69 H 3.91 N 7.58; found C 68.69 H 4.35 N 7.36.

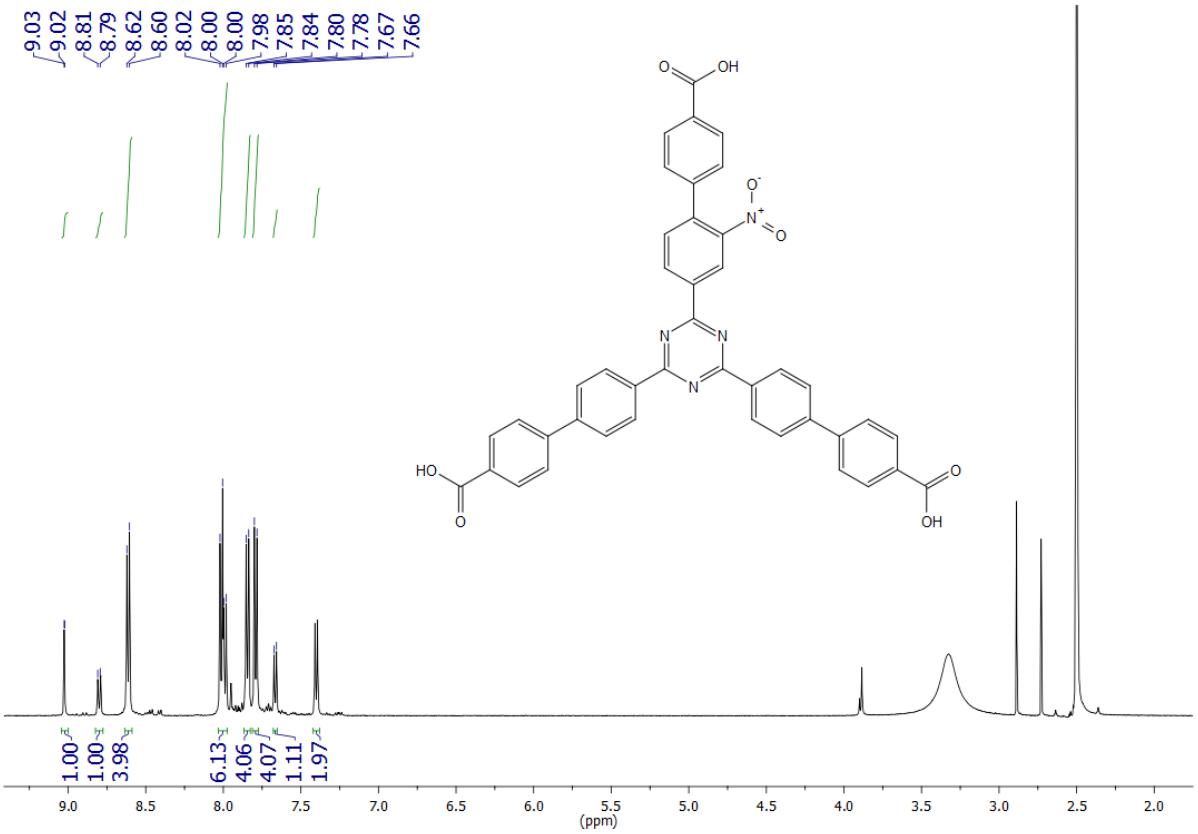
9.03
9.02
8.81
8.79
8.62
8.60
8.02
8.00
8.00
7.98
7.85
7.84
7.80
7.78
7.67
7.66
1.00
1.00
3.98
6.13
4.06
4.07
1.11
1.97
(ppm)

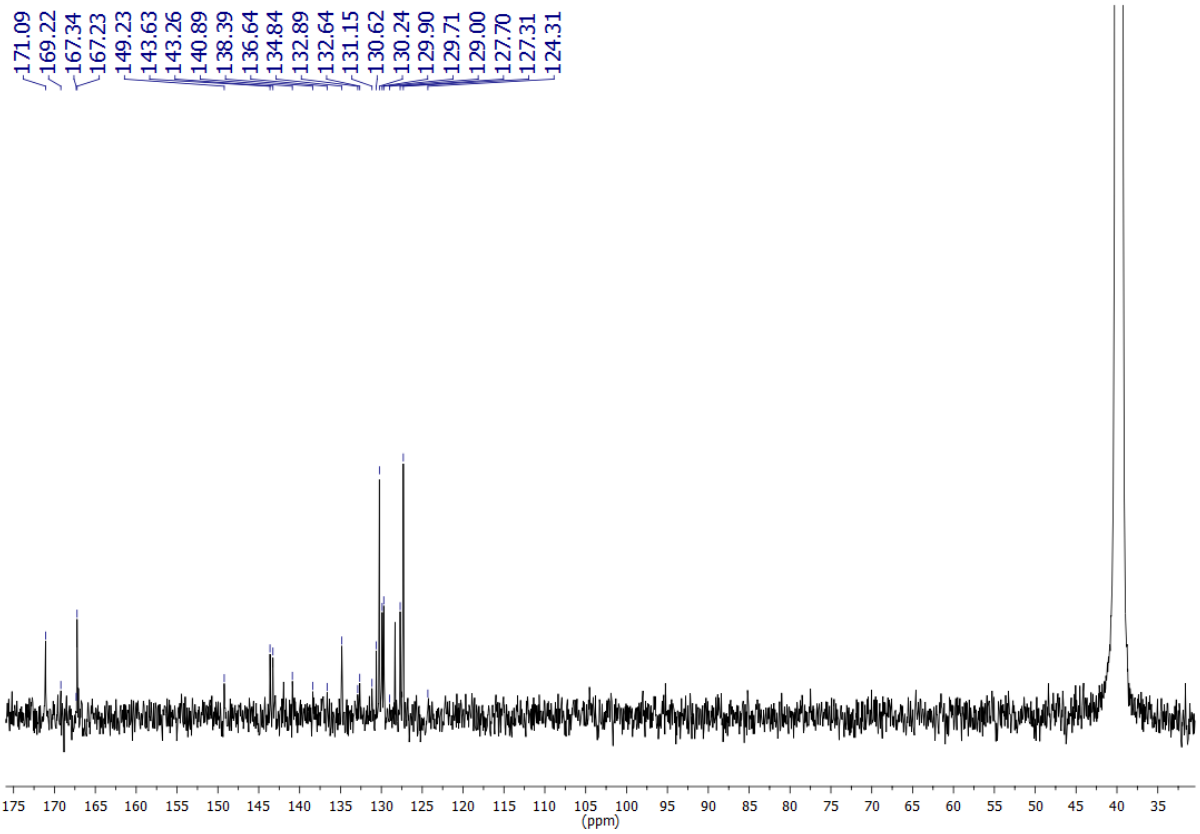
171.09
169.22
167.34
167.23
149.23
143.63
143.26
140.89
138.39
136.64
134.84
132.89
132.64
131.15
130.62
130.24
129.90
129.71
129.00
127.70
127.31
124.31
(ppm)

2,4-Bis(4'-carboxy-biphenyl-4-yl)-6-(4'-carboxy-2-methoxy-biphenyl-4-yl]-1,3,5-triazine (17c)

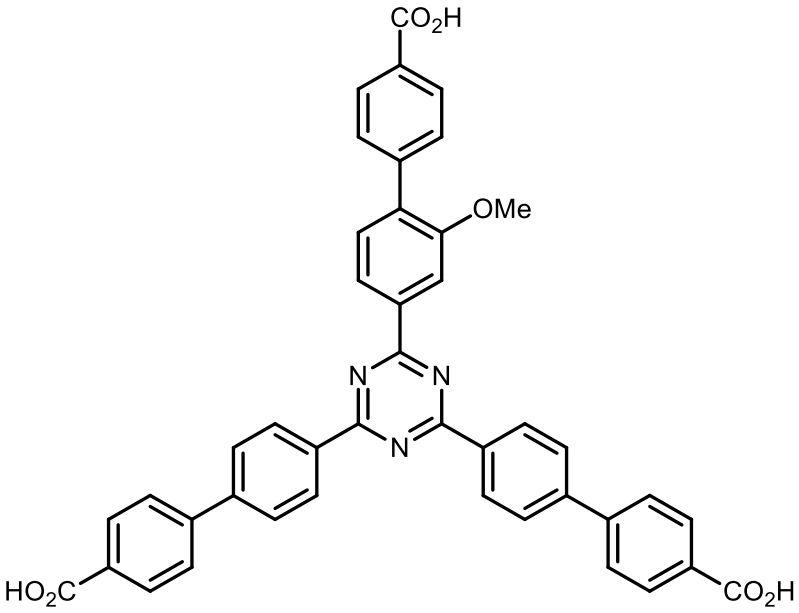

A suspension of 2,4-bis[4'-(methoxy-carbonyl)biphenyl-4-yl]-6-[2-methoxy-4'-(methoxycarbonyl)-biphenyl-4-yl]-1,3,5-triazine (**16c**, 50 mg, 67.5 µmol) and lithium hydroxide mono-hydrate (101 mg, 2.41 mmol) in a mixture of tetrahydrofuran (10 mL) and deionized water (1.5 mL) was stirred at 60 °C for 24 h. After removal of the tetrahydrofuran in vacuo, the aq. layer was diluted slightly and acidified with hydrochloric acid (3 M). The precipitate was filtered off and washed thoroughly with deionized water and chloroform. Yield: 47 mg (67 µmol, >99 %). M. p.: >300 mg. ^{1}H NMR (500 MHz, DMSO-d_6): δ = 13.01 (br. s, 3H, CO_2H), 8.74 (d, 4H, ^{3}J = 8.4 Hz, 2,4-Ar-*H*-3,5), 8.36 (m_c (dd), 1H, J = 7.9 Hz, ^{4}J = 1.2 Hz, 6-Ar-*H*-5), 8.29 (m_c (d), 1H, ^{4}J = 1.2 Hz, 6-Ar-*H*-3), 8.05 (d, 4H, ^{3}J = 8.4 Hz, 2,4-Ar'-*H*-3,5), 8.00 (d, 2H, ^{3}J = 8.4 Hz, 6-Ar'-*H*-3,5), 7.94 (d, 4H, ^{3}J = 8.4 Hz, 2,4-Ar-*H*-2,6), 7.86 (d, 4H, ^{3}J = 8.4 Hz, 2,4-Ar'-*H*-2,6), 7.67 (d, 2H, ^{3}J = 8.4 Hz, 6-Ar'-*H*-2,6), 7.56 (d, 1H, ^{3}J = 7.9 Hz, 6-Ar-*H*-6), 3.95 (s, 3H, OCH_3) ppm. ^{13}C NMR (125 MHz, DMSO-d_6): δ = 171.0 (s, triazine-*C*-2,4), 170.9 (s, triazine-*C*-6), 167.6 (s, 6-Ar'-*C*O_2H), 167.5 (s, 2,4-Ar'-*C*O_2H), 156.9 (s, 6-Ar-*C*-2), 143.6 (br. s, 2,4-Ar-*C*-1, 2,4-Ar'-*C*-1), 142.1 (s, 6-Ar'-*C*-1), 136.9 (s, 6-Ar-*C*-4), 135.4 (s, 2,4-Ar-*C*-4), 133.6 (s, 6-Ar-*C*-1), 131.7 (d, 6-Ar-*C*-6), 130.8 (s, 2,4-Ar'-*C*-4), 130.5 (d, 2,4-Ar'-*C*-

3,5), 130.1 (s, 6-Ar'-*C*-4), 129.9 (d, 6-Ar'-*C*-2,6), 129.8 (d, 2,4-Ar-*C*-3,5), 129.5 (d, 6-Ar'-*C*-3,5), 127.9 (d, 2,4-Ar-*C*-2,6), 127.5 (d, 2,4-Ar'-*C*-2,6), 121.9 (d, 6-Ar-*C*-5), 111.5 (d, 6-Ar-*C*-3), 56.1 (q, O*C*H_3) ppm. MS (MALDI, Cl-CCA): *m/z* = 700 $[M + H]^+$. IR (ATR): $\tilde{\nu}$ = 3100 (br., OH), 1684 (C=O), 1605, 1581, 1505, 1417 (arom. C=C, arom. C=N), 1357 (C-N-val.), 1231 (aryl-OCH_3), 813 (1,4-disubst. aryl, 1,3,4-trisubst. aryl) cm^{-1}. Elemental analysis ($C_{43}H_{29}N_3O_7$) (699.70): calcd. C 73.81 H 4.18 N 6.01; ($C_{43}H_{29}N_3O_7 \cdot 0.4H_2O \cdot 0.25CHCl_3$) (738.99): calcd. C 70.51 H 4.11 N 5.70; found C 70.47 H 4.11 N 5.73.

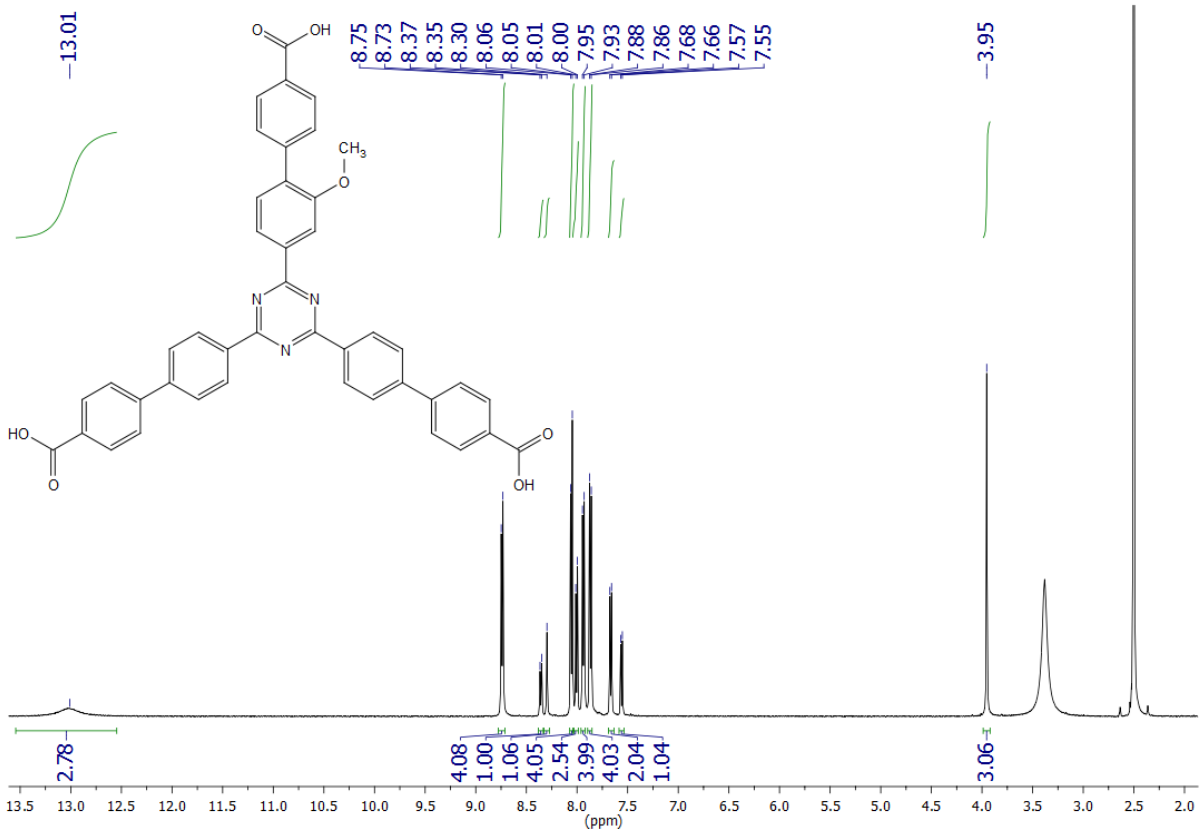
13.01
8.75
8.73
8.37
8.35
8.30
8.06
8.05
8.01
8.00
7.95
7.93
7.88
7.86
7.68
7.66
7.57
7.55
3.95
2.78
4.08
1.00
1.06
4.05
2.54
3.99
4.03
2.04
1.04
3.06
(ppm)

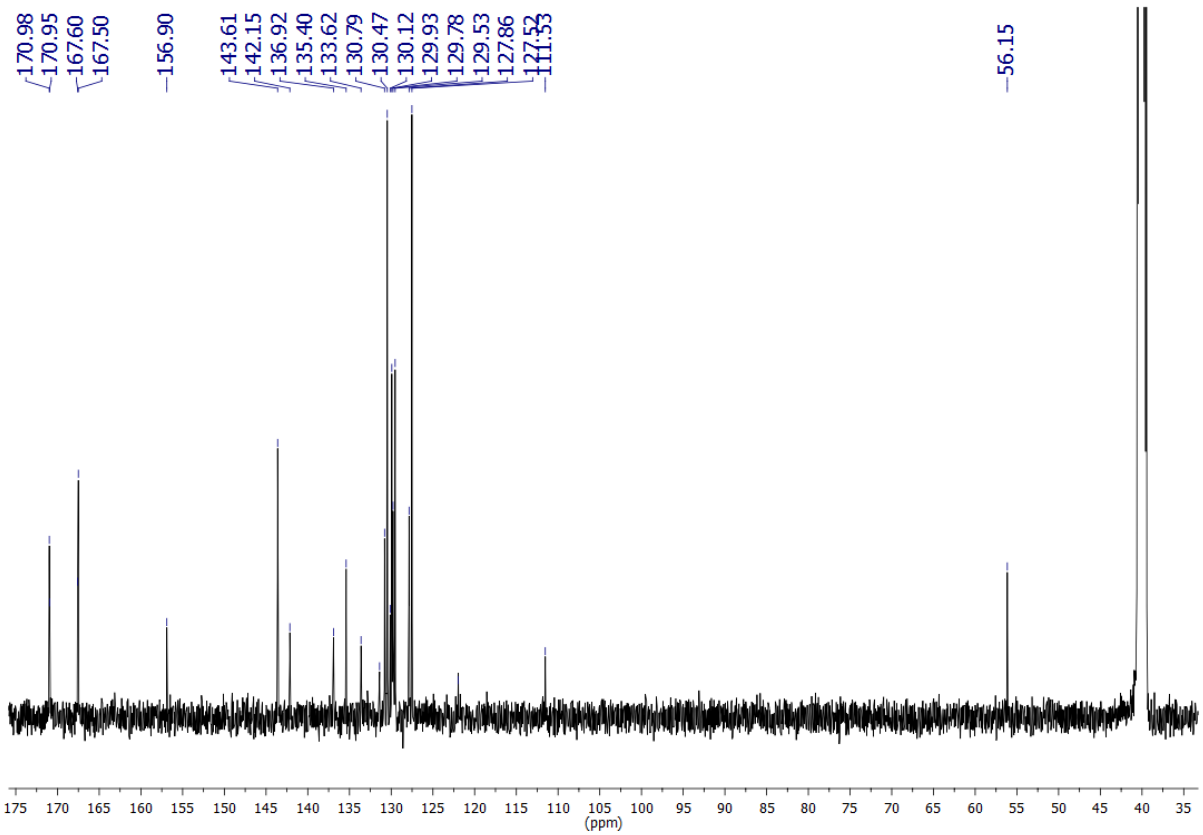
170.98
170.95
167.60
167.50
156.90
143.61
142.15
136.92
135.40
133.62
130.79
130.47
130.12
129.93
129.78
129.53
127.86
127.52
111.53
56.15
(ppm)

2-(2-Amino-4'-carboxy-biphenyl-4-yl)-4,6-bis(4'-carboxy-biphenyl-4-yl)-1,3,5-triazine (17d)

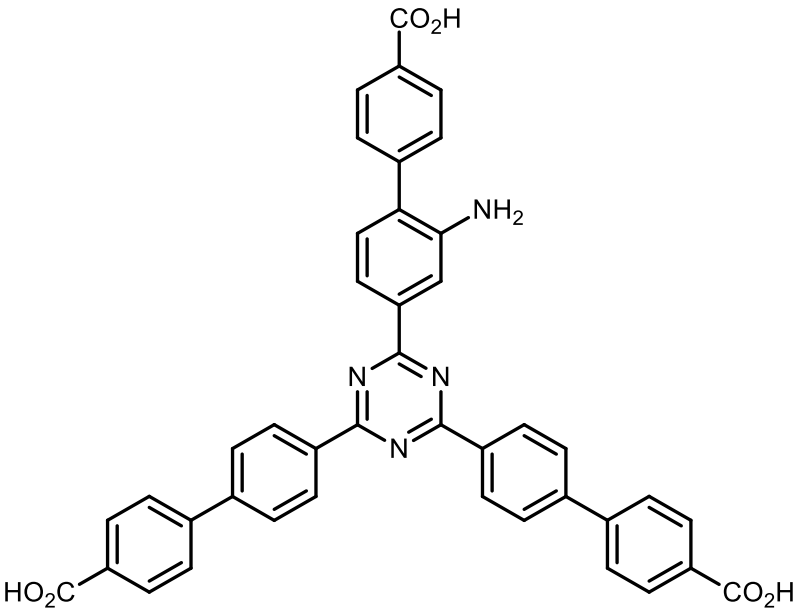

Lithium hydroxide mono hydrate (101 mg, 2.41 mmol) and 2-[2-amino-4'-carboxy-biphenyl-4-yl]-4,6-bis[4'-carboxy-biphenyl-4-yl]-1,3,5-triazine (**16d**, 50 mg, 69 µmol) in a mixture of tetrahydrofuran (430 mL) and deionized water (45 mL) were stirred at 60 °C for 48 h. After evaporation of the solvent in vacuo, the yellow residue was dissolved in deionized water and acidified with hydrochloric acid (3 M). The yellow precipitate was filtered off and washed with deionized water and chloroform. Yield: 47 mg (68 µmol, >99 %). M. p.: >300 °C. ^{1}H NMR (500 MHz, DMSO-d_6): δ = 13.02 (br. s, 3H, CO_2H), 8.81 (d, 4H, ^{3}J = 8.5 Hz, 4,6-Ar-*H*-3,5), 8.25 (d, 1H, ^{4}J = 1.6 Hz, 2-Ar-*H*-3), 8.08 (d, 4H, ^{3}J = 8.5 Hz, 4,6-Ar'-*H*-3,5), 8.05 (d, 2H, ^{3}J = 8.4 Hz, 2-Ar'-*H*-3,5), 8.03* (dd, 1H, ^{4}J = 1.6 Hz, 2-Ar-*H*-5), 8.01 (d, 4H, ^{3}J = 8.5 Hz, 4,6-Ar'-*H*-2,6), 7.93 (d, 4H, ^{3}J = 8.5 Hz, 4,6-Ar-*H*-2,6), 7.66 (d, 2H, ^{3}J = 8.4 Hz, 2-Ar'-*H*-2,6), 7.29 (d, 1H, ^{3}J = 8.0 Hz, 2-Ar-*H*-6) ppm. *signal overlaps with adjacent one unabling the determination of all coupling constants. ^{13}C NMR (125 MHz, DMSO-d_6): δ = 171.1 (s, triazine-*C*-2), 171.0 (s, triazine-*C*-4,6), 167.6 (s, 2-Ar'-CO_2H), 167.5 (s, 4,6-Ar'-CO_2H), 146.2 (s, 2-Ar-*C*-2), 144.0 (s, 2-Ar'-*C*-1), 143.7 (s, 4,6-Ar-*C*-1), 143.7 (s, 4,6-Ar'-*C*-1), 136.1 (s, 2-Ar-*C*-4), 135.7 (s, 4,6-Ar-*C*-4), 131.2 (d, 2-Ar-*C*-6), 130.8 (s, 4,6-Ar'-*C*-4), 130.5 (d, 4,6-Ar'-*C*-3,5), 130.3 (d, 2-

Ar'-*C*-3,5), 129.9 (s, 2-Ar'-*C*-4), 129.8 (d, 4,6-Ar-*C*-3,5), 129.4 (s, 2-Ar-*C*-1), 129.2 (d, 2-Ar'-*C*-2,6), 127.9 (d, 4,6-Ar-*C*-2,6), 127.6 (d, 4,6-Ar'-*C*-2,6), 117.7 (d, 2-Ar-*C*-5), 116.2 (d, 2-Ar-*C*-3) ppm. MS (MALDI, Cl-CCA): *m/z* = 686 $[M + H]^+$. IR (ATR): $\tilde{\nu}$ = 3100 (br., OH, NH_2), 1684 (C=O), 1606, 1581, 1507, 1419 (arom. C=C, arom. C=N), 1561 (NH_2), 1434 (CH-Def.) 1360 (C-N-val.), 810 (1,4-disubst. aryl, 1,3,4-trisubst. aryl) cm^{-1}. Elemental analysis ($C_{42}H_{18}N_4O_6$) (684.69): calcd. C 73.68 H 4.12 N 8.18; ($C_{42}H_{18}N_4O_6 \cdot 0.4CHCl_3 \cdot 0.2H_2O$) (753.89): calcd. C 69.19 H 3.94 N 7.61; found C 69.41 H 3.91 N 7.31.

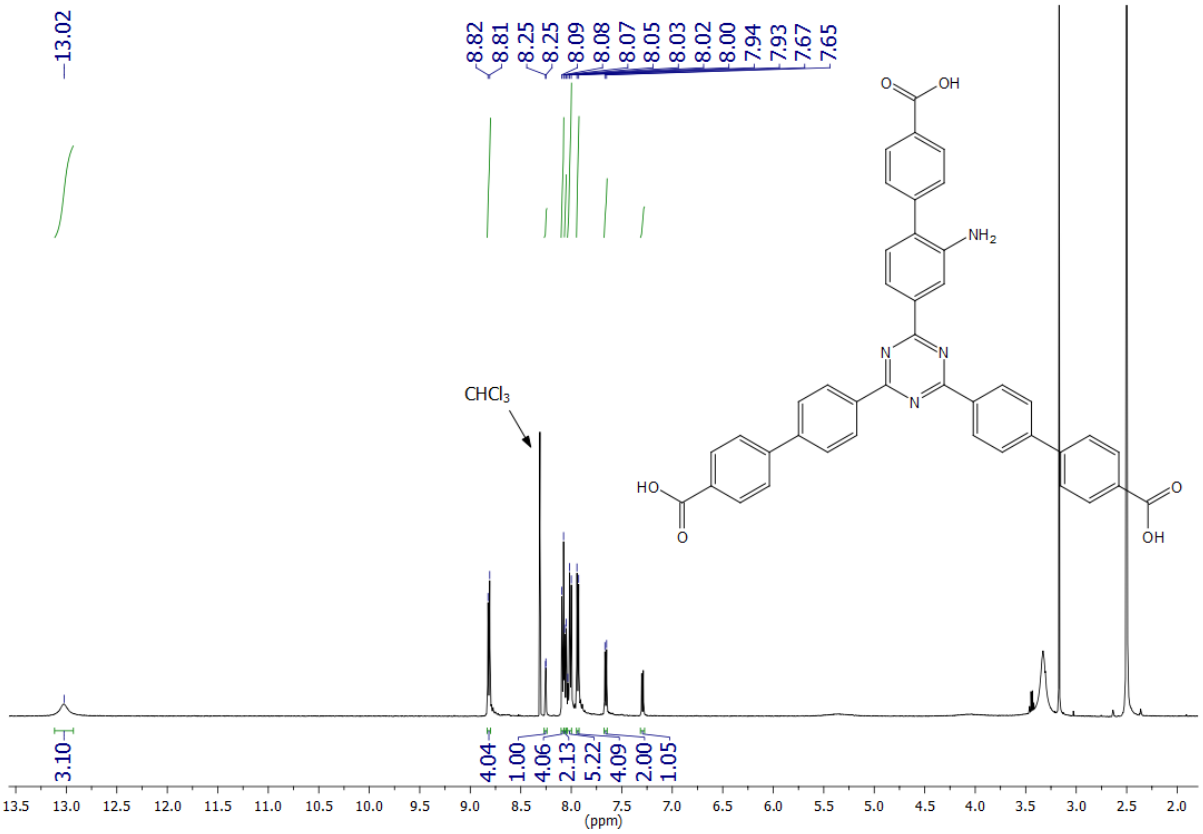
13.02
8.82
8.81
8.25
8.25
8.09
8.08
8.07
8.05
8.03
8.02
8.00
7.94
7.93
7.67
7.65
CHCl3
O
OH
NH2
N
N
N
HO
O
O
OH
3.10
4.04
1.00
4.06
2.13
5.22
4.09
2.00
1.05
(ppm)

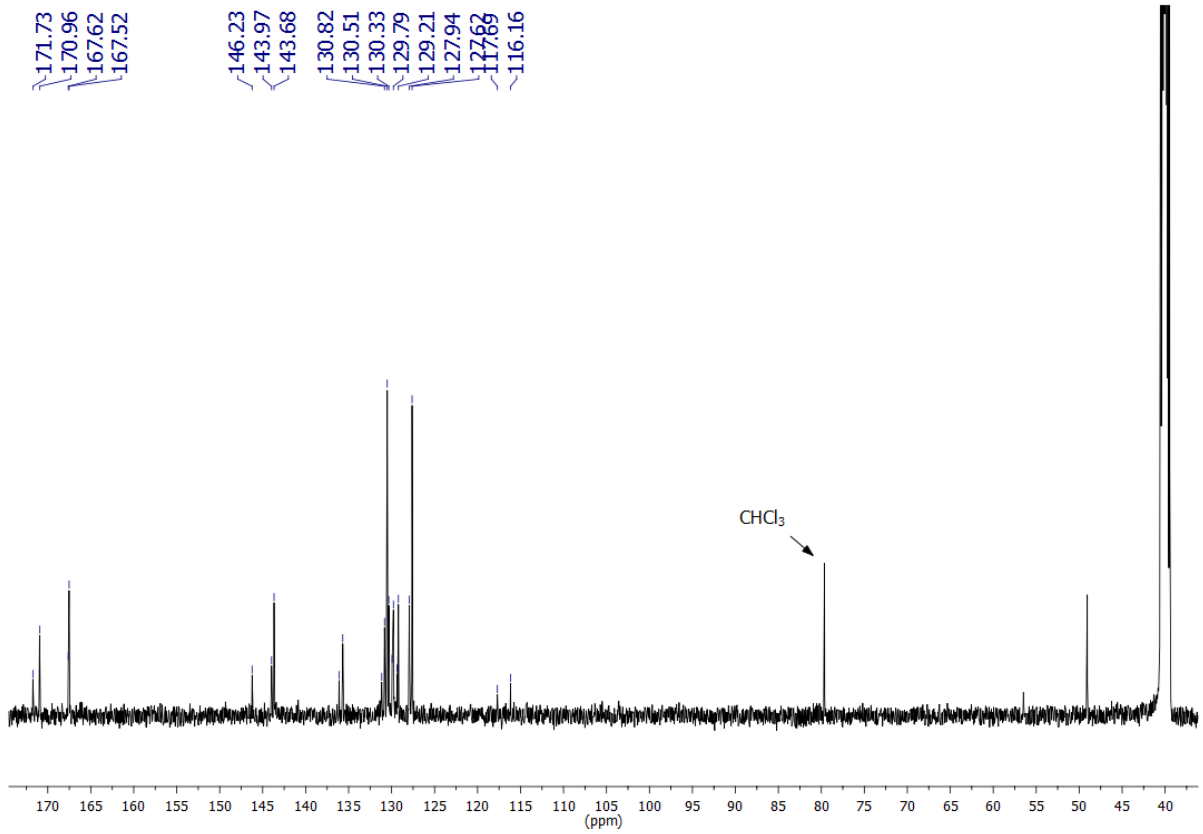
171.73
170.96
167.62
167.52
146.23
143.97
143.68
130.82
130.51
130.33
129.79
129.21
127.94
127.62
127.59
116.16
CHCl3
(ppm)

2,4-Bis(4'-carboxy-biphenyl-4-yl)-6-(4'-carboxy-2-hydroxy-biphenyl-4-yl)-1,3,5-triazine (17e)

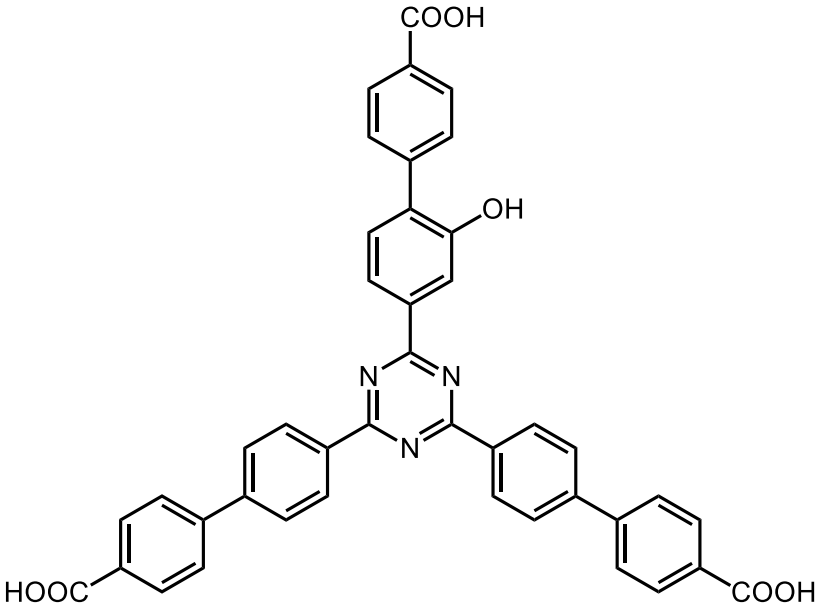

2,4-Bis[4'-(methoxycarbonyl)-biphenyl-4-yl]-6-[2-methoxy-4'-(methoxycarbonyl)-biphenyl-4-yl]-1,3,5-triazine (**16c**, 300 mg, 400 µmol) and pyridine hydrochloride (3.60 g, 31.2 mmol) were mixed and stirred for 12 h at 200 °C. After cooling to room temp., sodium hydroxide (2 M) was added to the solution until pH = 14 was reached. After stirring for 12 h at 120 °C, the reaction mixture was acidified with conc. hydrochloric acid and the precipitate was filtered off. Washing with water and drying gave a dark brown solid. Yield: 143 mg (209 µmol, 52%). M. p.: > 300 °C. ^{1}H NMR (500 MHz, DMSO-d$_6$): δ = 12.99 (br. s, 3H, COO*H*), 10.18 (s, 1H, O*H*), 8.70 (d, 4H, ^{3}J = 7.6 Hz, 2,4-Ar-*H*-3,5), 8.33 (s, 1H, 6-Ar-*H*-3), 8.18 (d, ^{3}J = 7.8 Hz, 1H, 6-Ar-*H*-5), 8.05 (d, ^{3}J = 8.0 Hz, 4H, 2,4-Ar'-*H*-3,5), 8.00 (d, ^{3}J = 8.2 Hz, 2H, 6-Ar'-*H*-3,5), 7.92 (d, ^{3}J = 7.6 Hz, 4H, 2,4-Ar-*H*-2,6), 7.86 (d, ^{3}J = 8.0 Hz, 4H, 2,4-Ar'-*H*-2,6), 7.74 (d, ^{3}J = 8.2 Hz, 2H, 6-Ar'-*H*-2,6), 7.50 (d, ^{3}J = 7.8 Hz, 1H, 6-Ar-*H*-6) ppm. ^{13}C NMR (125 MHz, DMSO-d$_6$): δ = 171.1 (s, triazine-*C*-6), 170.9 (s, triazine-*C*-2,4), 167.7 (s, 6-Ar'-*C*OOH), 167.5 (s, 2,4-Ar'-*C*OOH), 155.3 (s, 6-Ar-*C*-2), 143.6 (s, 2,4-Ar-*C*-1, 2,4-Ar'-*C*-1), 142.6 (s, 6-Ar'-*C*-1), 136.6 (s, 6-Ar-*C*-4), 135.5 (s, 2,4-Ar-*C*-4), 131.4 (s, 6-Ar-*C*-1), 131.2 (d, 6-Ar-*C*-6), 130.8 (s, 2,4-Ar'-*C*-4), 130.4 (d, 2,4-Ar'-*C*-3,5), 129.8 (d, 6-Ar'-*C*-2,6), 129.7 (d, 2,4-

Ar-*C*-3,5), 129.7 (s, 6-Ar'-*C*-4), 129.5 (d, 6-Ar'-*C*-3,5), 127.8 (d, 2,4-Ar-*C*-2,6), 127.5 (d, 2,4-Ar'-*C*-2,6), 120.5 (d, 6-Ar-*C*-5), 116.5 (d, 6-Ar-*C*-3) ppm. MS (MALDI, Cl-CCA): *m/z* = 686 $[M + H]^+$. IR (ATR): $\tilde{\nu}$ = 3050 (OH), 1681 (C=O), 1606, 1580, 1562, 1504 (arom. C=C, arom. C=N), 1418 (CH-Def.), 1360 (O-H-Def.), 1238, 1175, 1101 (C-O), 852, 813, 772 (1,4-disubst. aryl, 1,2,4-trisubst. aryl) cm^{-1}. Elemental analysis ($C_{42}H_{27}N_3O_7$) (685.18): calcd. C 73.57 H 3.97 N 6.13; ($C_{42}H_{27}N_3O_7 \cdot H_2O$) (703.20): calcd. C 71.69 H 4.15 N 5.97; found C 71.47 H 3.95 N 5.91.

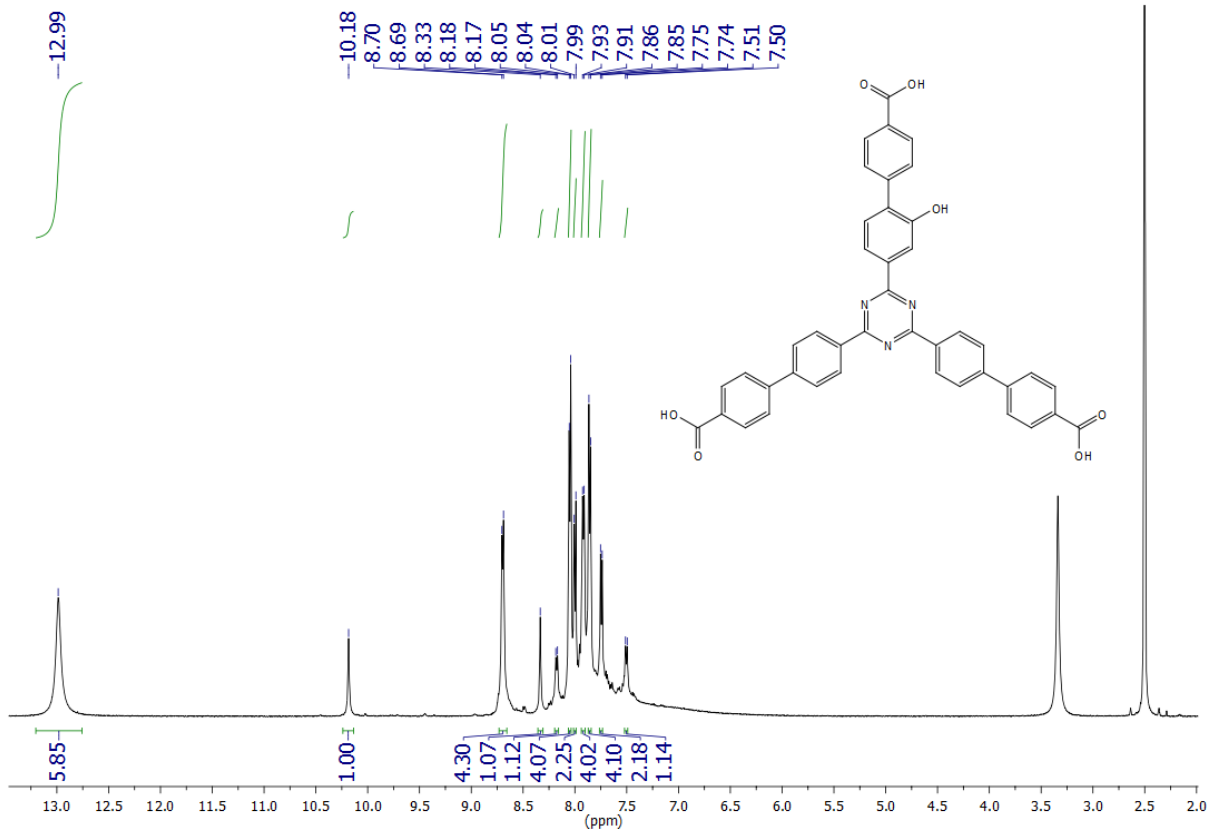
12.99
10.18
8.70
8.69
8.33
8.18
8.17
8.05
8.04
8.01
7.99
7.93
7.91
7.86
7.85
7.75
7.74
7.51
7.50
5.85
1.00
4.30
1.07
1.12
4.07
2.25
4.02
4.10
2.18
1.14
(ppm)

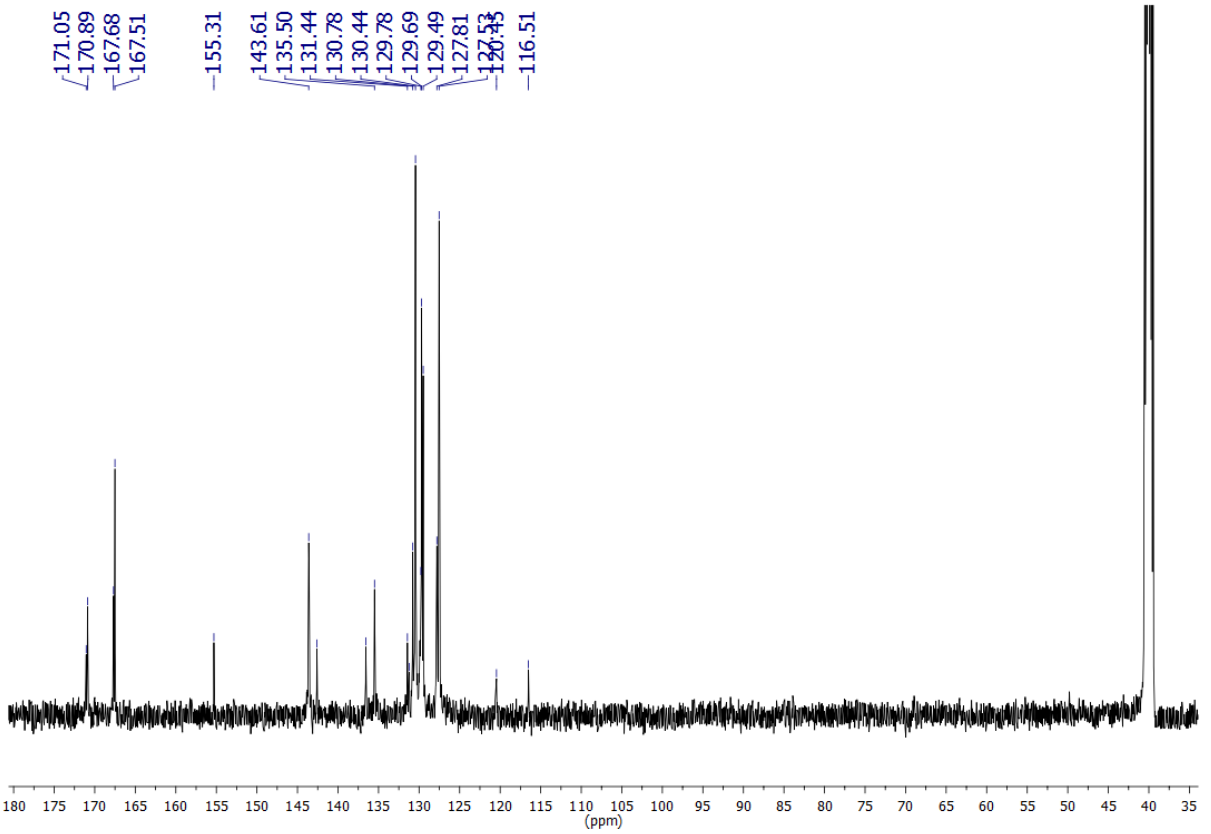
171.05
170.89
167.68
167.51
155.31
143.61
135.50
131.44
130.78
130.44
129.78
129.69
129.49
127.81
116.51
(ppm)

2,4,6-Tris[4''-(methoxycarbonyl)-1,1':4',1''-terphenyl-4-yl]-1,3,5-triazine (19a)

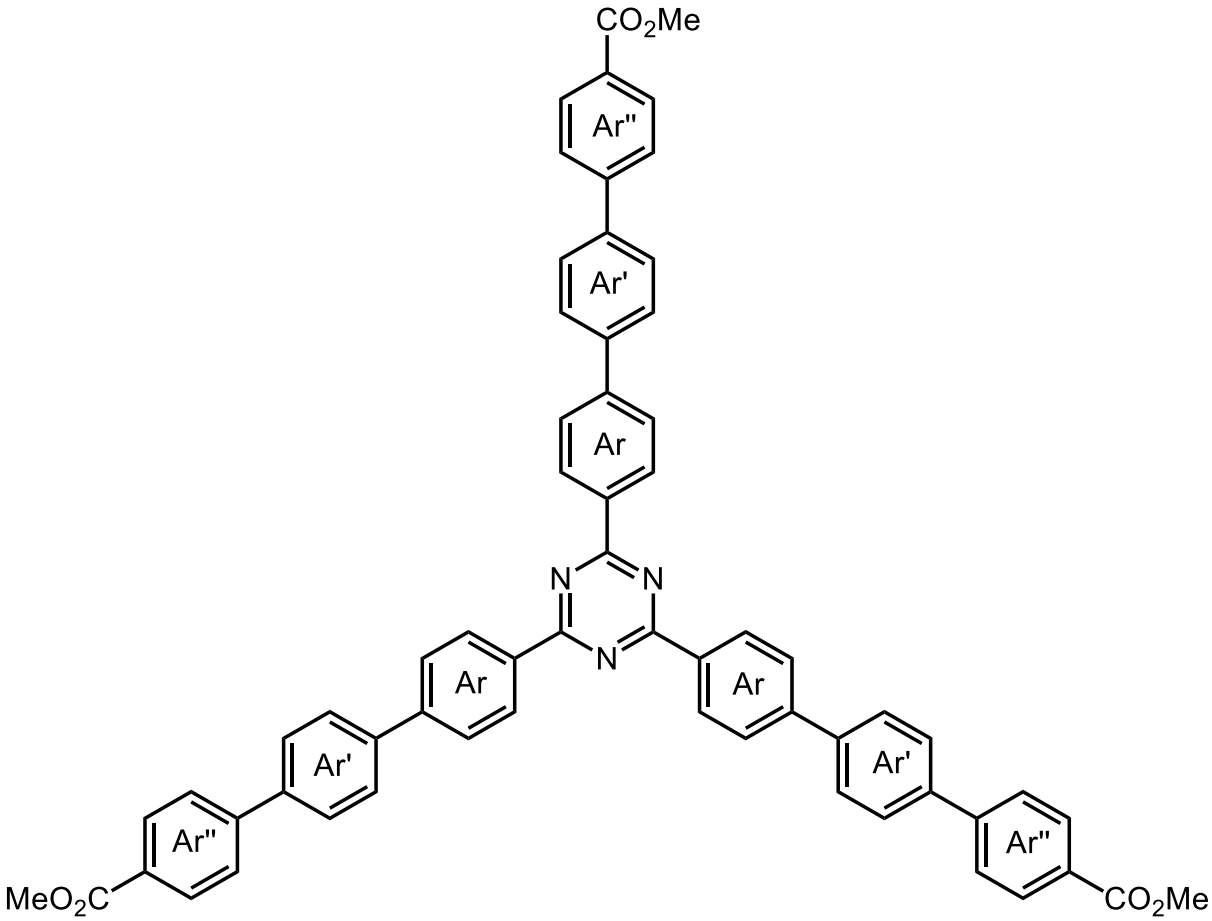

A suspension of 2,4,6-tris(4-bromophenyl)-1,3,5-triazine (**3a**, 413 mg, 758 µmol), methyl 4'-(4,4,5,5-tetramethyl-1,3,2-dioxaborolan-2-yl)-1,1'-biphenyl-4-carboxylate (**18**, 1.00 g, 2.96 mmol), potassium phosphate (1.44 g, 6.82 mmol) and tetrakis(triphenylphosphine)palladium(0) (79 mg, 68 µmol) in a mixture of 1,4-dioxane (70 mL) and deionized water (15 mL) was stirred under nitrogen for 2 d at 120 °C. Deionized water (50 mL) was added to the reaction mixture. The precipitate was filtered off and washed with water. The crude product was recrystallized from chloroform. A colourless solid was obtained. Yield: 174 mg (185 µmol, 24 %). M. p.: > 300 °C. ^{1}H NMR (600 MHz, $CDCl_3$,): δ = 8.90 (d, ^{3}J = 8.3 Hz, 6H, Ar-*H*-3,5), 8.15 (d, ^{3}J = 8.3 Hz, 6H, Ar''-*H*-3,5), 7.88 (d, ^{3}J = 8.3 Hz, 6H, Ar-*H*-2,6), 7.83 (d, ^{3}J = 8.3 Hz,

6H, Ar'-*H*-2,6), 7.78 (d, ^{3}J = 8.3 Hz, 6H, Ar'-*H*-3,5), 7.74 (d, ^{3}J = 8.3 Hz, 6H, Ar''-*H*-2,6), 3.97 (s, 9H, CO_2CH_3) ppm. ^{13}C NMR (150 MHz, $CDCl_3$): δ = 171.4 (s, triazine-*C*-2,4,6), 167.0 (s, CO_2CH_3), 145.0 (s, Ar''-*C*-1), 144.4 (s, Ar-*C*-1), 140.1 (s, Ar'-*C*-1), 139.6 (s, Ar'-*C*-4), 135.5 (s, Ar-*C*-4), 130.2 (d, Ar''-*C*-3,5), 129.6 (d, Ar-*C*-3,5), 129.1 (s, Ar''-*C*-4), 127.8 (d, Ar'-*C*-2,3,5,6), 127.3 (d, Ar-*C*-2,6), 127.0 (s, Ar''-*C*-2,6), 52.2 (q, CH_3) ppm. MS (MALDI, Cl-CCA): *m/z* = 940 $[M + H]^+$. IR (ATR): $\tilde{\nu}$ = 2950 (CH-val.), 1716 (C=O), 1606, 1581, 1552, 1505 (arom. C=C, arom. C=N), 1434 (CH-Def.), 1361 (C-N-val.), 1272, 1184, 1108 (C-O), 808, 773 (1,4-disubst. aryl) cm^{-1}. Elemental analysis ($C_{63}H_{45}N_3O_6$) (939.33): calcd. C 80.49 H 4.82 N 4.47; found C 80.15 H 4.74 N 4.27.

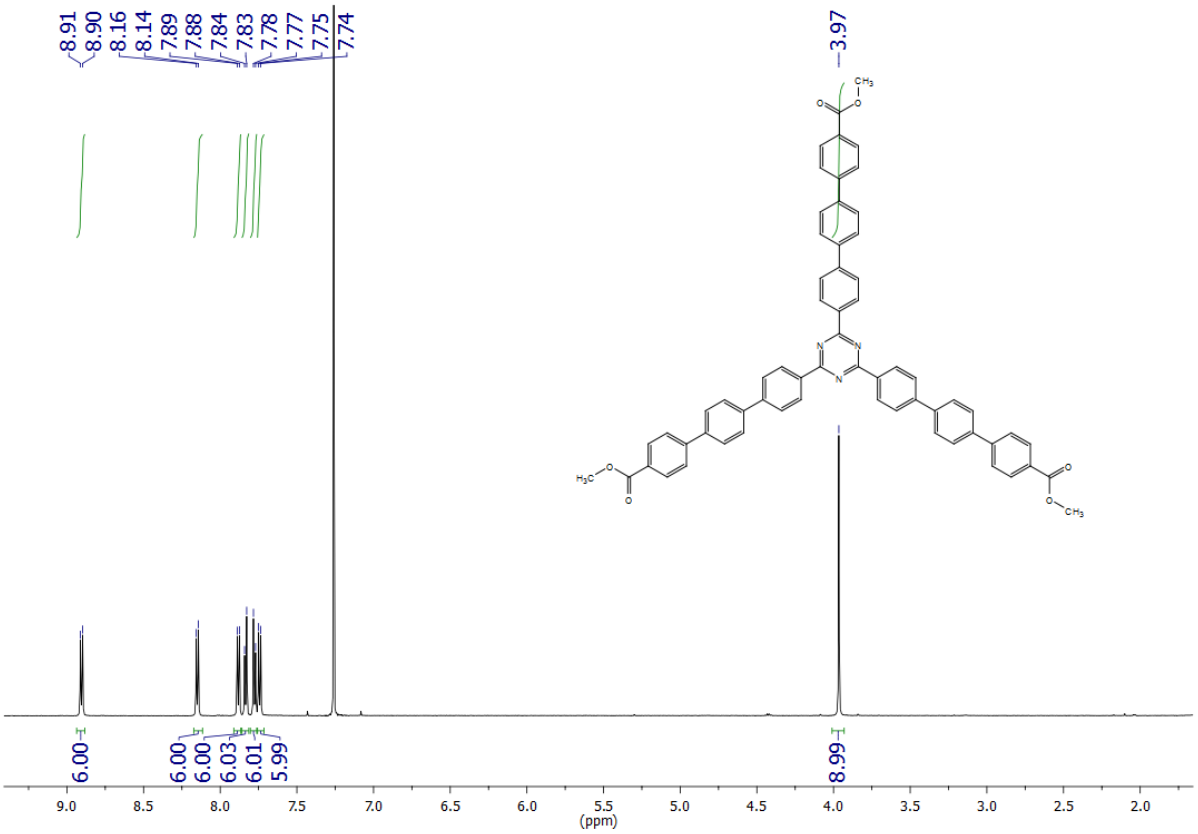
8.91
8.90
8.16
8.14
7.89
7.88
7.84
7.83
7.78
7.77
7.75
7.74
3.97
6.00
6.00
6.00
6.03
6.01
5.99
8.99
(ppm)

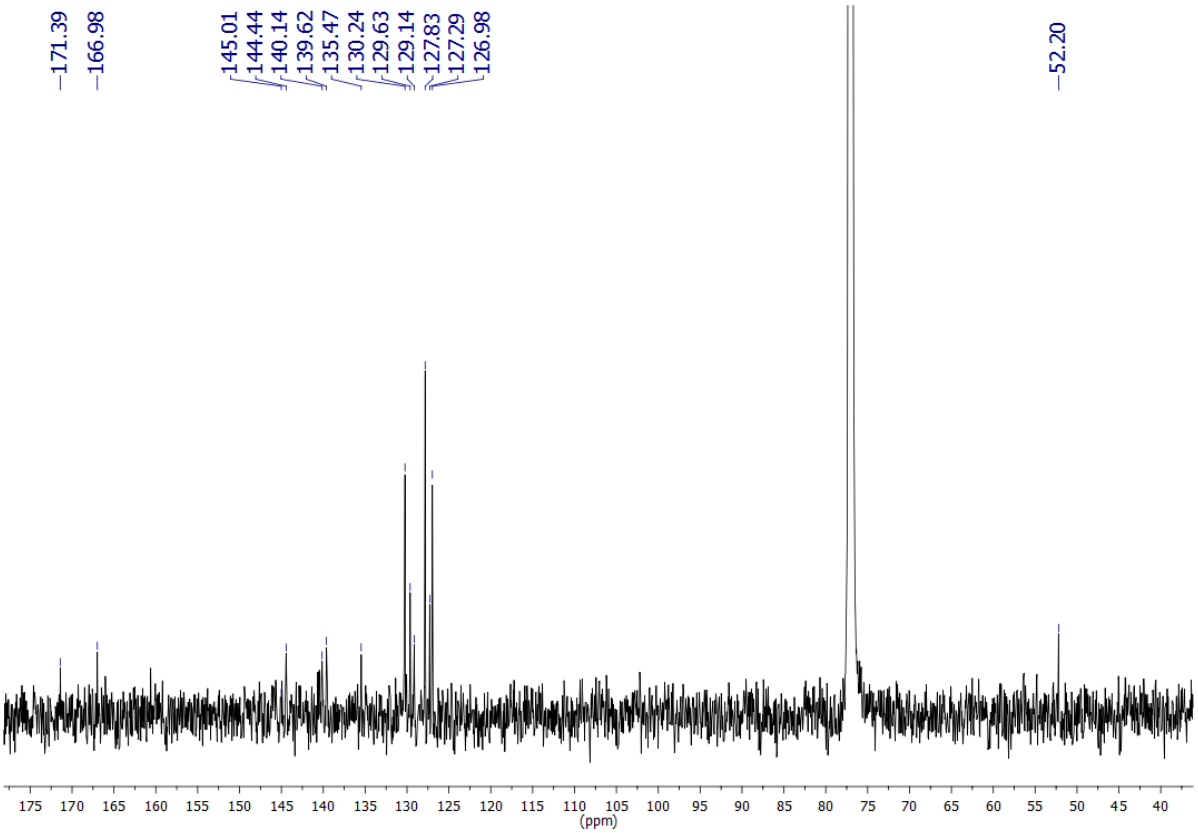
171.39
166.98
145.01
144.44
140.14
139.62
135.47
130.24
129.63
129.14
127.83
127.29
126.98
52.20
(ppm)

2-[4''-(Methoxycarbonyl)-2-nitro-1,1':4',1''-terphenyl-4-yl]-4,6-bis[4''-(methoxycarbonyl)-1,1':4',1''-terphenyl-4-yl]-1,3,5-triazine (19b)

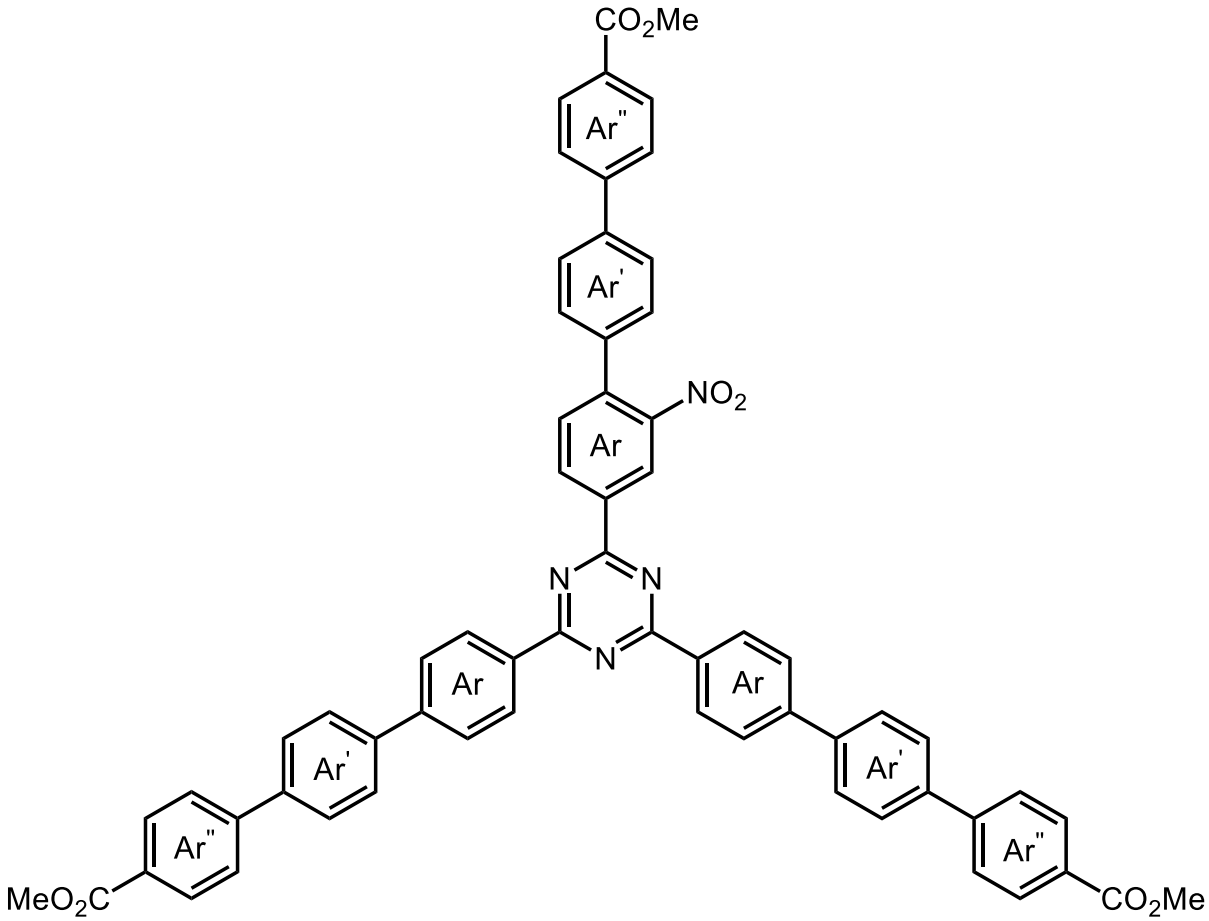

A mixture of 2-(4-bromo-3-nitrophenyl)-4,6-bis(4-bromophenyl)-1,3,5-triazine (**3b**, 500 mg, 846 µmol), methyl 4'-(4,4,5,5-tetramethyl-1,3,2-dioxaborolan-2-yl)-1,1'-biphenyl-4-carboxylate (**18**, 1.12 g, 3.30 mmol), potassium phosphate (1.62 g, 7.61 mmol) and [1,1′-bis(diphenylphosphino)ferrocene]dichloropalladium(II) (62.0 mg, 84.6 µmol) in a mixture of 1,4-dioxane (100 mL) and deionized water (10 mL) was stirred under nitrogen for 3 d at 120 °C. The solvent was evaporated in vacuo, the residue was dissolved in chloroform (2 L) and washed with deionized water (3 x 250 mL) and brine (250 mL). The organic layer was evaporated in vacuo until 1 L was left. Charcoal (5 g) was added and the solution was heated to 80 °C. The hot suspension was filtered through celite and the colourless filtrate was evaporated in vacuo. After

the addition ethyl acetate (50 mL), the undissolved solid was filtrated and dried to obtain the slightly yellow product. Yield: 132 mg (134 µmol, 16 %). M. p.: > 300 °C. ^{1}H NMR (500 MHz, $CDCl_3$): δ = 9.28 (d, ^{4}J = 1.4 Hz, 1H, 2-Ar-*H*-3), 9.06 (dd, ^{3}J = 8.1 Hz, ^{4}J = 1.4 Hz, 1H, 2-Ar-*H*-5), 8.90 (d, ^{3}J = 8.5 Hz, 4H, 4,6-Ar-*H*-3,5), 8.15 (d, ^{3}J = 8.5 Hz, 6H, 2,4,6-Ar''-*H*-3,5), 7.90 (d, ^{3}J = 8.5 Hz, 4H, 4,6-Ar-*H*-2,6), 7.84 (d, ^{3}J = 8.5 Hz, 4H, 4,6-Ar'-*H*-2,6), 7.78 (d, ^{3}J = 8.5 Hz, 4H, 4,6-Ar'-*H*-3,5), 7.77 – 7.70 (m, 9H, 2,4,6-Ar''-*H*-2,6, 2-Ar-*H*-6, 2-Ar'-*H*-3,5), 7.53 (d, ^{3}J = 8.3 Hz, 2H, 2-Ar'-*H*-2,6), 3.97 (s, 9H, CO_2CH_3) ppm. ^{13}C NMR (125 MHz, $CDCl_3$): δ = 171.5 (s, triazine-*C*-4,6), 169.5 (s, triazine-*C*-2), 166.9 (s, CO_2CH_3), 149.9 (s, 2-Ar-*C*-2), 144.9 (s, 4,6-Ar-*C*-1), 144.8 (s, 2,4,6-Ar''-*C*-1), 140.5 (s, 2-Ar'-*C*-4), 139.8 (s, 4,6-Ar'-*C*-1), 139.7 (s, 4,6-Ar'-*C*-4), 139.1 (s, 2-Ar-*C*-1), 137.6 (s, 2-Ar-*C*-4), 136.5 (s, 2-Ar'-*C*-1), 134.9 (s, 4,6-Ar-*C*-4), 132.4 (d, 2-Ar-*C*-6), 132.0 (d, 2-Ar-*C*-5), 130.2 (d, 2,4,6-Ar''-*C*-3,5), 129.7 (d, 4,6-Ar-*C*-3,5), 129.1 (s, 2,4,6-Ar''-*C*-4), 128.4 (d, 2-Ar'-*C*-2,6), 127.9 (d, 4,6-Ar'-*C*-3,5), 127.8 (d, 4,6-Ar'-*C*-2,6), 127.4 (d, 4,6-Ar-*C*-2,6), 127.1 (d, 2-Ar'-*C*-3,5), 126.9 (d, 2,4,6-Ar''-*C*-2,6), 124.6 (d, 2-Ar-*C*-3), 52.1 (q, CO_2CH_3) ppm. MS (MALDI, Cl-CCA): *m/z* = 986 $[M + H]^+$. IR (ATR): $\tilde{\nu}$ = 2952 (CH-val.), 1718 (C=O), 1606, 1572 (arom. C=C, arom. C=N), 1508 (asymm. N=O), 1400, 1433 (CH-def.), 1357 (symm. N=O), 1274, 1184, 1108 (C-O), 810, 771 (1,4-disubst. aryl, 1,2,4-trisubst. aryl) cm^{-1}. Elemental analysis ($C_{63}H_{44}N_4O_8$) (985.05): calcd. C 76.82 H 4.50 N 5.69; found C 77.04 H 4.83 N 5.38.

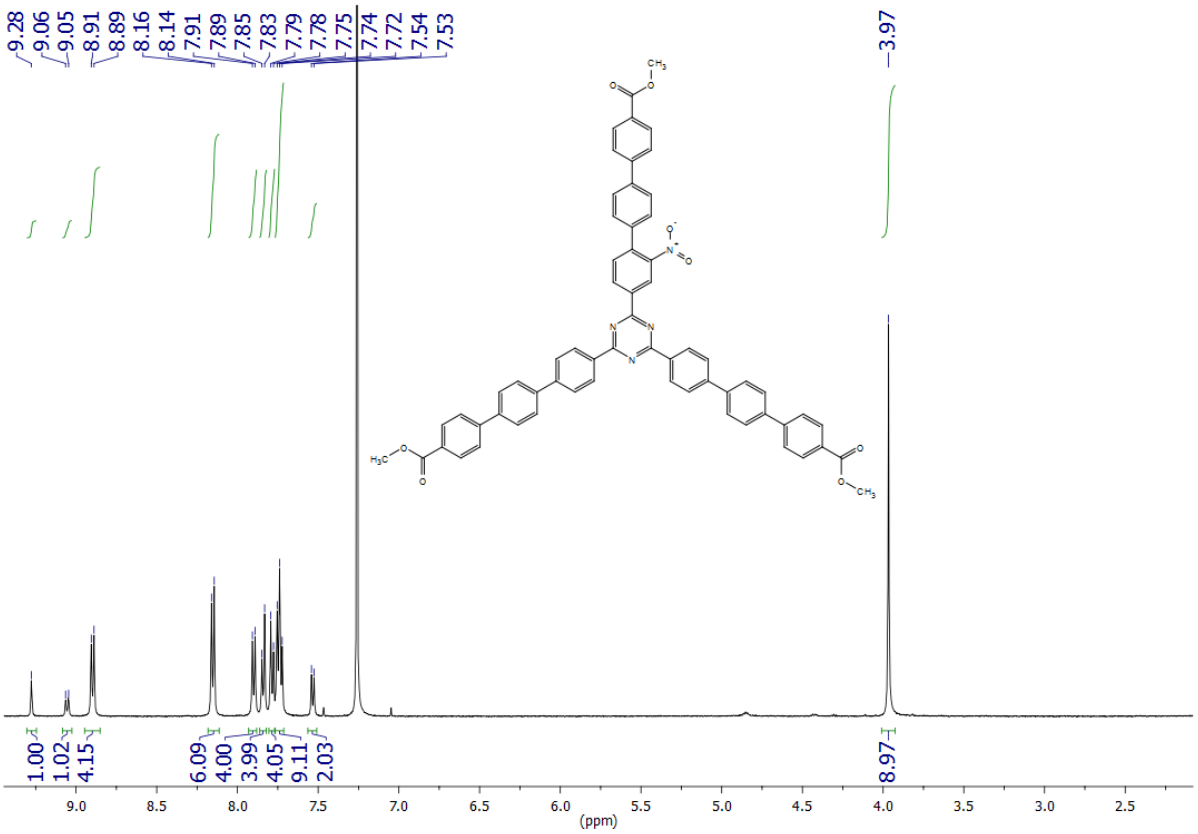
9.28
9.06
9.05
8.91
8.89
8.16
8.14
7.91
7.89
7.85
7.83
7.79
7.78
7.75
7.74
7.72
7.54
7.53
3.97
1.00
1.02
4.15
6.09
4.00
3.99
4.05
9.11
2.03
8.97
(ppm)

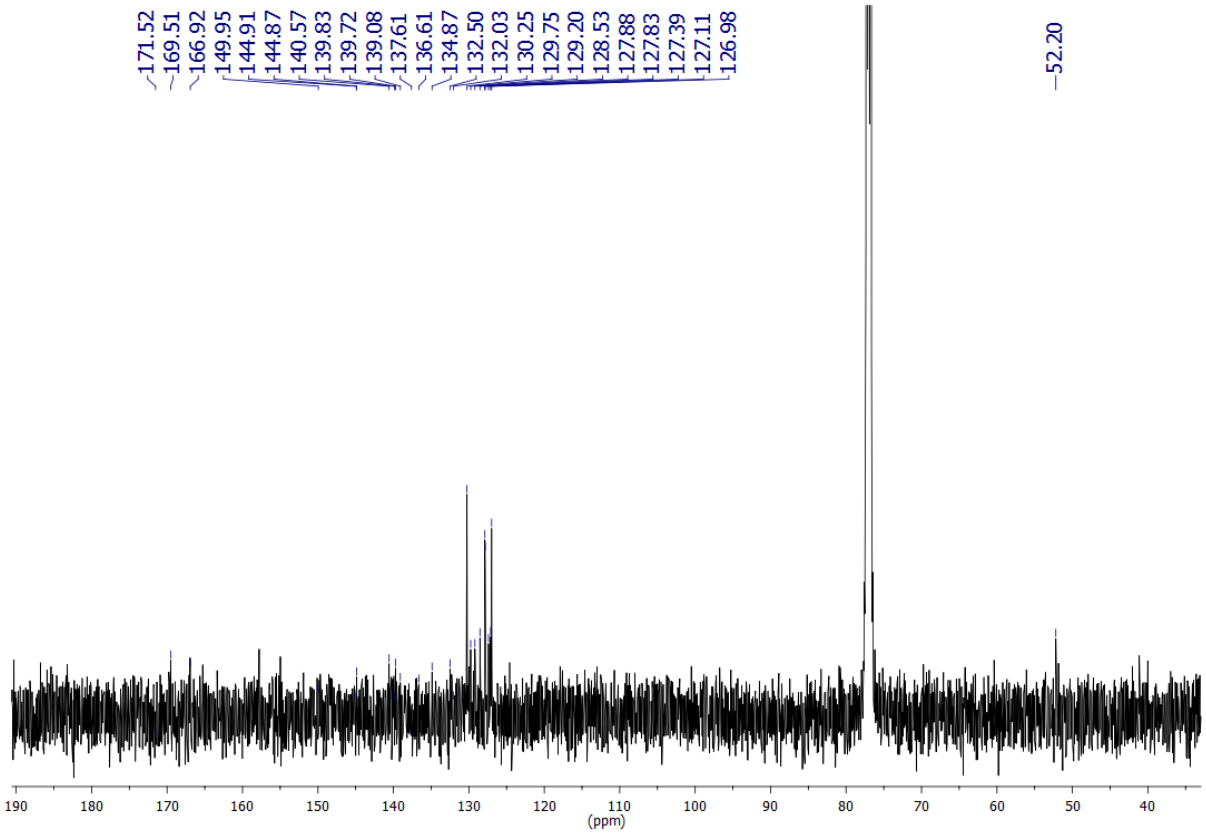
171.52
169.51
166.92
149.95
144.91
144.87
140.57
139.83
139.72
139.08
137.61
136.61
134.87
132.50
132.03
130.25
129.75
129.20
128.53
127.88
127.83
127.39
127.11
126.98
52.20
(ppm)

2,4-Bis[4''-(methoxycarbonyl)-1,1':4',1''-terphenyl-4-yl]-6-[2-methoxy-4''-(methoxycarbonyl)-1,1':4',1''-terphenyl-4-yl]-1,3,5-triazine (19c)

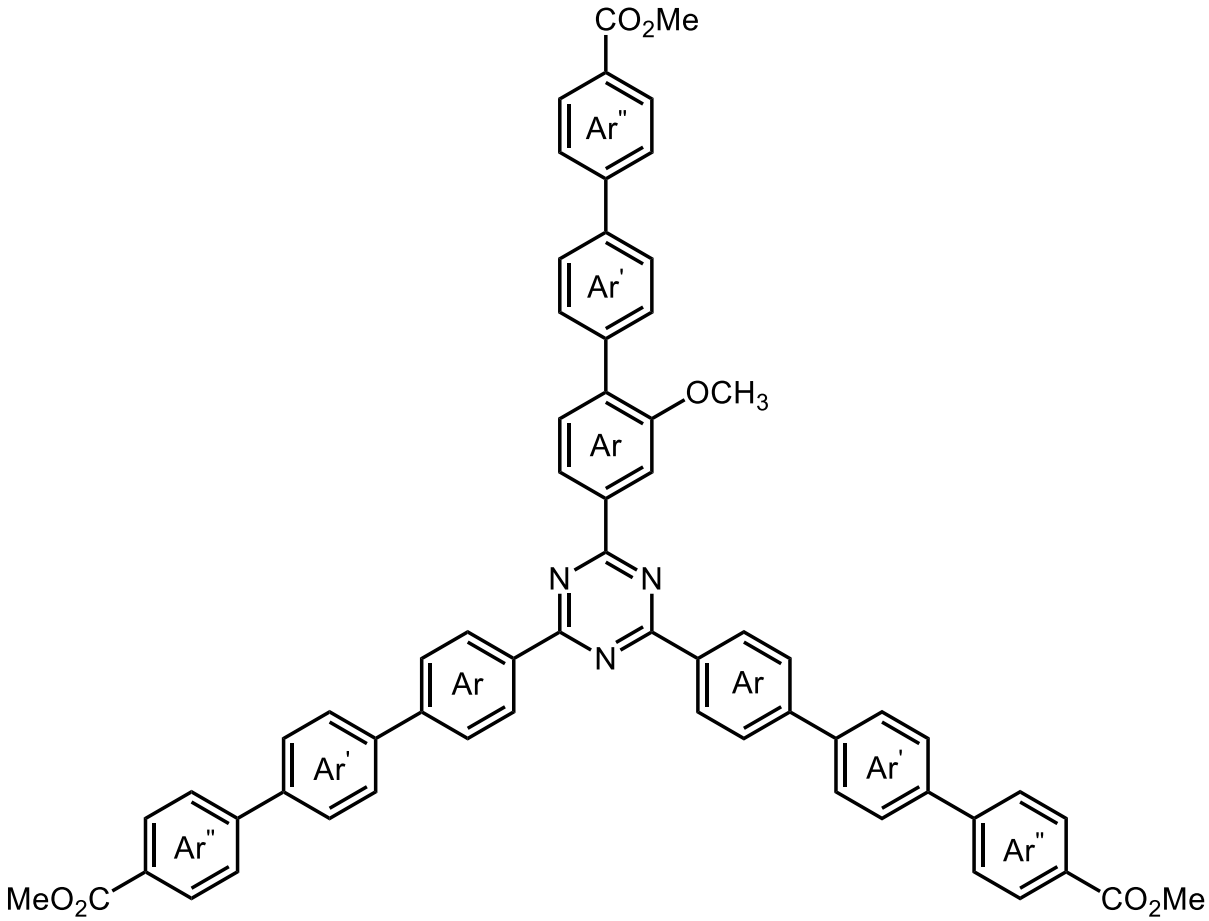

A mixture of 2-(4-bromo-3-methoxyphenyl)-4,6-bis(4-bromophenyl)-1,3,5-triazine (**3c**, 102 mg, 180 µmol), methyl 4'-(4,4,5,5-tetramethyl-1,3,2-dioxaborolan-2-yl)-1,1'-biphenyl-4-carboxylate (**18**, 269 mg, 796 µmol), potassium phosphate (259 mg, 1.22 mmol) and tetrakis(triphenylphosphine)palladium(0) (19.4 mg, 17.0 µmol) in a mixture of 1,4-dioxane (15 mL) and deionized water (1 mL) was stirred under nitrogen for 3 d at 100 °C. The solvent was evaporated in vacuo, the residue was dissolved in chloroform (50 mL) and washed with deionized water (3 x 25 mL) and brine (25 mL). The organic layer was dried with magnesium sulfate and the solvent was evaporated in vacuo. The crude product was recrystallized from a mixture of toluene and *n*-heptane. A colourless solid was obtained. Yield: 140 mg (144 µmol,

81 %). M. p.: > 300 °C. ^{1}H NMR (500 MHz, $CDCl_3$): δ = 8.87 (d, ^{3}J = 8.4 Hz, 4H, 2,4-Ar-*H*-3,5), 8.51 (dd, ^{3}J = 7.9 Hz, ^{4}J = 1.5 Hz, 1H, 6-Ar-*H*-5), 8.44 (d, ^{4}J = 1.5 Hz, 1H, *6*-Ar-*H*-3), 8.14 (d, ^{3}J = 8.4 Hz, 4H, 2,4-Ar''-*H*-3,5), 8.13 (d, ^{3}J = 8.4 Hz, 2H, 6-Ar''-*H*-3,5), 7.87 (d, ^{3}J = 8.4 Hz, 4H, 2,4-Ar-*H*-2,6), 7.82 (d, ^{3}J = 8.4 Hz, 4H, 2,4-Ar'-*H*-2,6), 7.78 – 7.71 (m, 14H, 2,4,6-Ar'-*H*-3,5, 6-Ar'-*H*-2,6, 2,4,6-Ar''-*H*-2,6), 7.59 (d, ^{3}J = 7.9 Hz, 1H, 6-Ar-*H*-6), 4.08 (s, 3H, O*CH*$_3$), 3.962 (s, 6H, 2,4-Ar''-CO_2*CH*$_3$), 3.960 (s, 3H, 6-Ar''-CO_2*CH*$_3$) ppm. ^{13}C NMR (125 MHz, $CDCl_3$): δ = 171.32 (s, triazine-*C*-2,4), 171.29 (s, triazine-*C*-6), 167.0 (s, 6-Ar''-*C*O_2CH_3), 166.9 (s, 2,4-Ar''-*C*O_2CH_3), 156.9 (s, 6-Ar-*C*-2), 145.3 (s, 6-Ar''-*C*-1), 144.9 (s, 2,4-Ar''-*C*-1), 144.4 (s, 2,4-Ar''-*C*-4), 140.1 (s, 2,4-Ar-*C*-1), 139.6 (s, 2,4-Ar'-*C*-4), 139.0 (s, 2,4-Ar'-*C*-1), 136.9 (s, 6-Ar'-*C*-1), 135.8 (s, 6-Ar-*C*-4), 135.3 (s, 2,4-Ar-*C*-4), 134.2 (s, 6-Ar-*C*-1), 130.9 (d, 6-Ar-*C*-6), 130.21 (d, 2,4-Ar''-*C*-3,5), 130.16 (d, 6-Ar''-*C*-3,5), 130.1 (d, 2,4-Ar-*C*-3,5), 129.0 (s, 6-Ar''-*C*-4), 128.2 (d, 6-Ar'-*C*-2,6), 127.8 (d, 2,4-Ar'-*C*-3,5), 127.76 (d, 2,4-Ar'-*C*-2,6), 127.2 (d, 2,4-Ar-*C*-2,6), 127.0 (d, 6-Ar'-*C*-3,5), 126.9 (d, 2,4,6-Ar''-*C*-2,6, 6-Ar'-*C*-4), 122.0 (d, 6-Ar-*C*-5), 111.3 (d, 6-Ar-*C*-3), 55.9 (q, O*CH*$_3$), 52.2 (q, 2,4-Ar''-CO_2*CH*$_3$), 52.1 (q, 6-Ar''-CO_2*CH*$_3$) ppm. MS (MALDI, Cl-CCA): *m/z* = 971 $[M + H]^+$. IR (ATR): $\tilde{\nu}$ = 3030, 3001 (aryl-H), 2949, 2842 (CH-val.), 1715 (C=O), 1605, 1582, 1505, 1403 (arom. C=C, arom. C=N), 1434 (CH-Def.), 1360 (C-N-val.), 1272 (Aryl-OCH_3), 807 (1,4-disubst. aryl, 1,2,4-trisubst. aryl) cm^{-1}. Elemental analysis ($C_{64}H_{47}N_3O_7$) (970.07): calcd. C 79.24 H 4.88 N 4.33; found C 79.10 H 5.11 N 4.02.

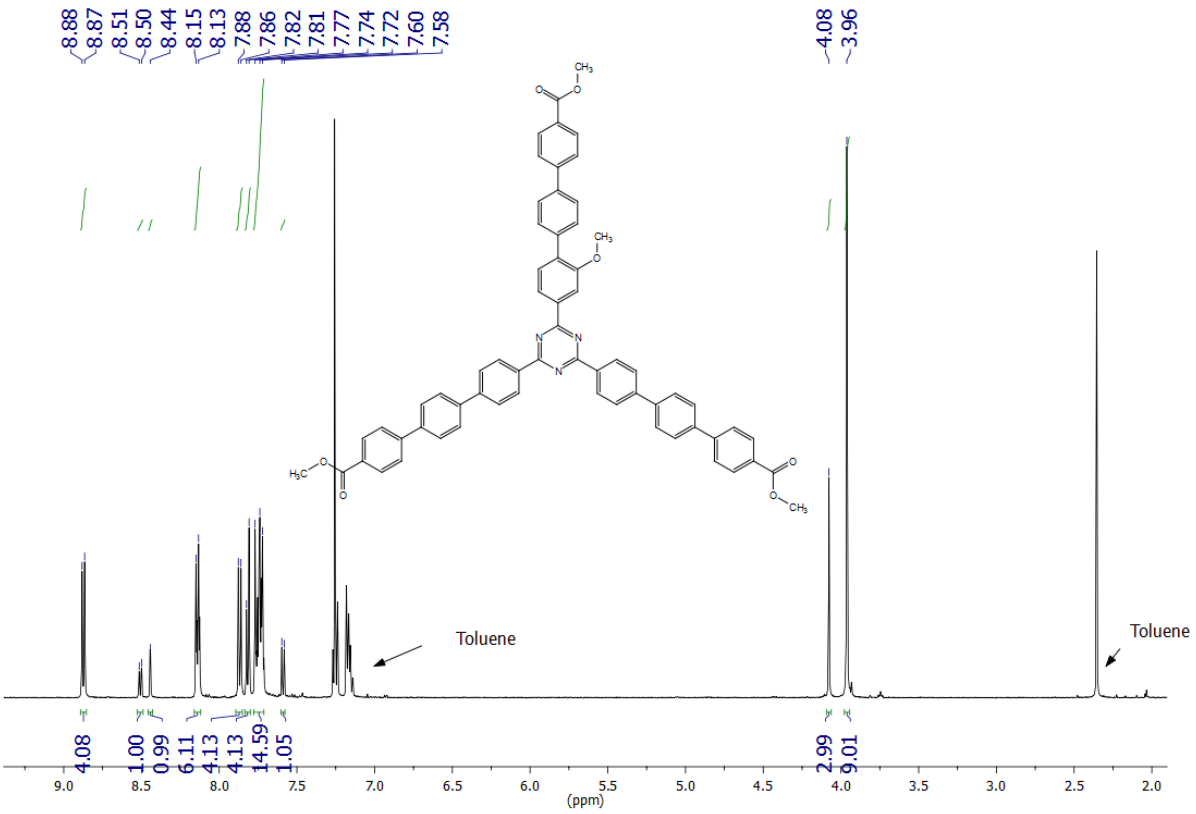
8.88
8.87
8.51
8.50
8.44
8.15
8.13
7.88
7.86
7.82
7.81
7.77
7.74
7.72
7.60
7.58
4.08
3.96
Toluene
Toluene
4.08
1.00
0.99
6.11
4.13
4.13
14.59
1.05
2.99
9.01
(ppm)

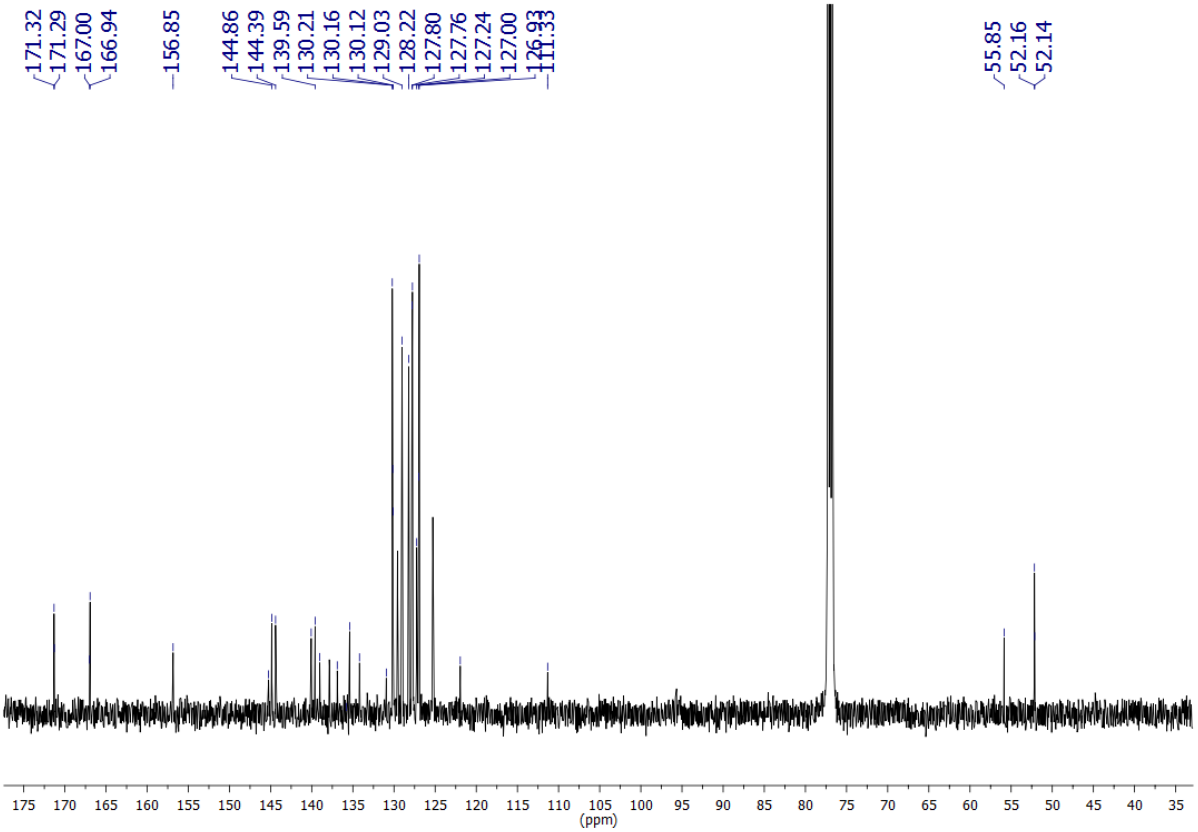
171.32
171.29
167.00
166.94
156.85
144.86
144.39
139.59
130.21
130.16
130.12
129.03
128.22
127.80
127.76
127.24
127.00
126.93
111.33
55.85
52.16
52.14
(ppm)

2,4,6-Tris(4''-carboxy-1,1':4',1''-terphenyl-4-yl)-1,3,5-triazine (20a)

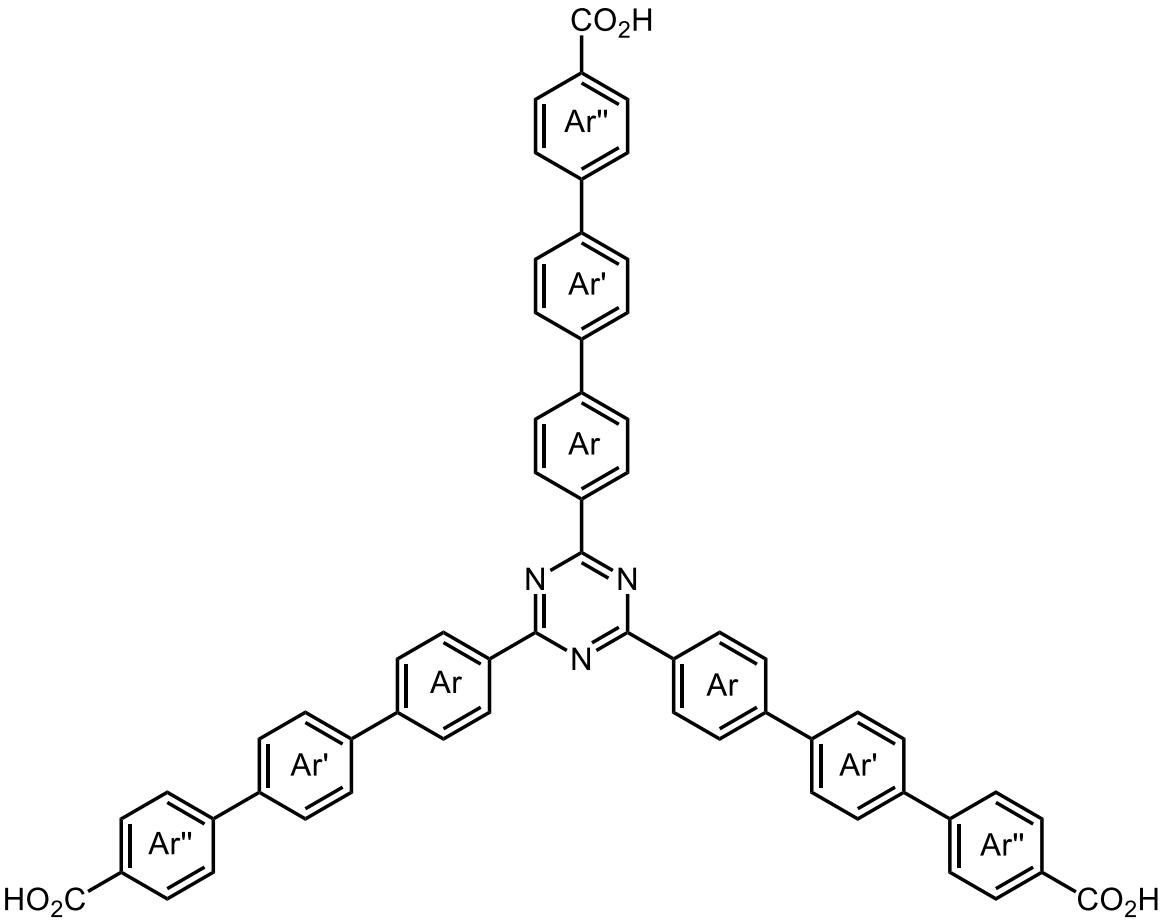

Lithium hydroxide monohydrate (733 mg, 17.5 mmol) was added to 2,4,6-tris[4''-(methoxycarbonyl)-1,1':4',1''-terphenyl-4-yl]-1,3,5-triazine (**19a**, 587 mg, 624 µmol) in a mixture of tetrahydrofuran (100 mL) and deionized water (10 mL). After stirring for 24 h at 120°C, the solvent was evaporated in vacuo and enough sodium hydroxide (2 M) was added to the residue to dissolved it. Then it was acidified with conc. hydrochloric acid. The precipitate was filtered off and washed with deionized water and chloroform. A white solid was obtained. Yield: 555 mg (618 µmol, 99 %). M. p.: > 300 °C. ^{1}H NMR (600 MHz, DMSO-d_6): δ = 8.89 (d, 6H, ^{3}J = 8.1 Hz, Ar-*H*-3,5), 8.10 – 8.05 (m, 12H, Ar''-*H*-3,5, Ar-*H*-2,6), 7.99 (d, ^{3}J = 8.3 Hz, 6H, Ar'-*H*-2,6), 7.94 (d, ^{3}J = 8.3 Hz, 6H, Ar'-*H*-3,5), 7.91 (d, ^{3}J = 7.9 Hz, 6H, Ar''-*H*-2,6) ppm. ^{13}C NMR (150 MHz, DMSO-d_6): δ = 171.2 (s, triazine-*C*-2,4,6), 167.6 (s, *C*OOH), 144.1 (s, Ar-*C*-1),

143.8 (s, Ar''-*C*-1), 139.3 (s, 6-Ar'-*C*-4), 139.2 (s, Ar'-*C*-1), 135.0 (s, Ar-*C*-4), 130.6 (s, Ar''-*C*-4),130.5 (d, Ar''-*C*-3,5), 129.9 (d, Ar-*C*-3,5), 128.1 (d, Ar'-*C*-2,3,5,6), 127.6 (d, Ar-*C*-2,6), 127.2 (s, Ar''-*C*-2,6) ppm. MS (MALDI, Cl-CCA): *m/z* = 898 $[M + H]^+$. IR (ATR): $\tilde{\nu}$= 1683 (C=O), 1605, 1580, 1504 (arom. C=C, arom. C=N), 1404 (CH-Def.), 1359 (C-N-val.), 1283, 1182 (C-O), 808, 773 (1,4-disubst. aryl) cm^{-1}. Elemental analysis ($C_{60}H_{39}N_3O_6$) (897.28): calcd. C 80.25 H 4.38 N 4.68; ($C_{60}H_{39}N_3O_6 \cdot 0.66$ H_2O) (909.29): calcd. C 79.19 H 4.47 N 4.62; found C 78.97 H 4.57 N 4.66.

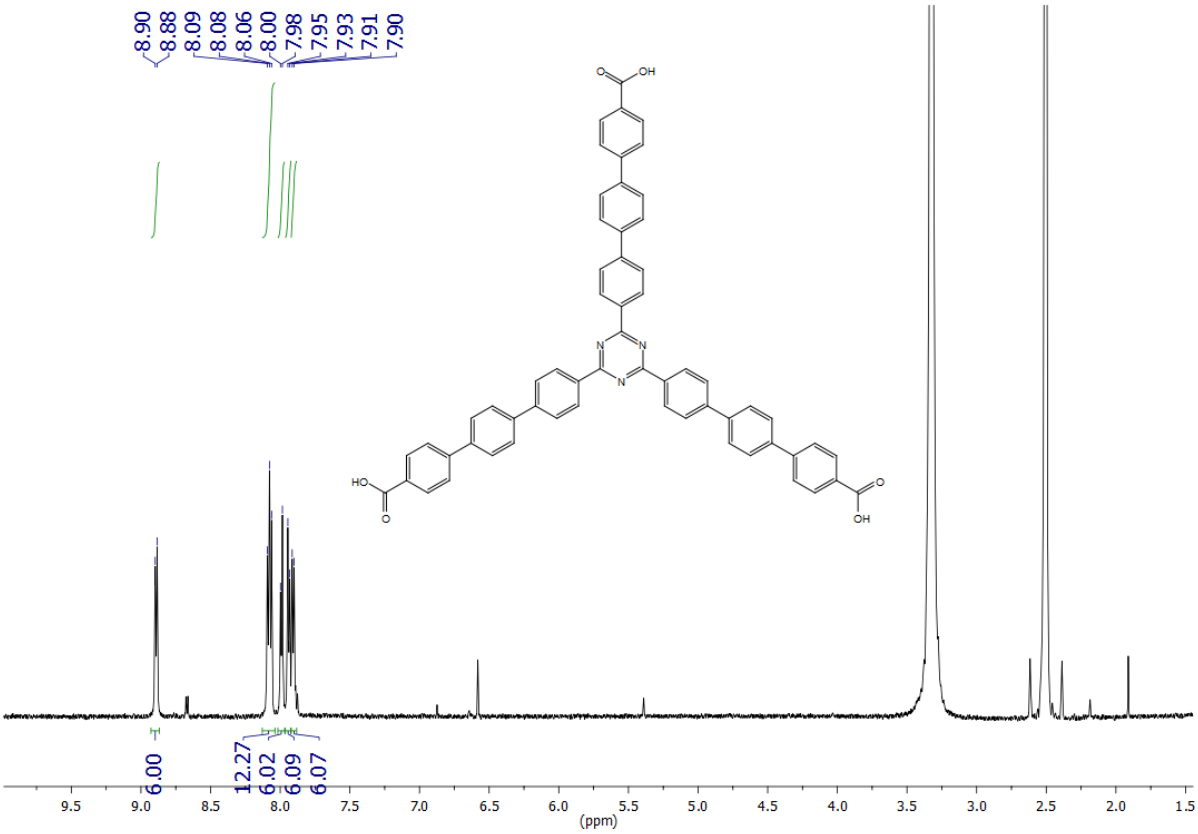
8.90
8.88
8.09
8.08
8.06
8.00
7.98
7.95
7.93
7.91
7.90
6.00
12.27
6.02
6.09
6.07
(ppm)

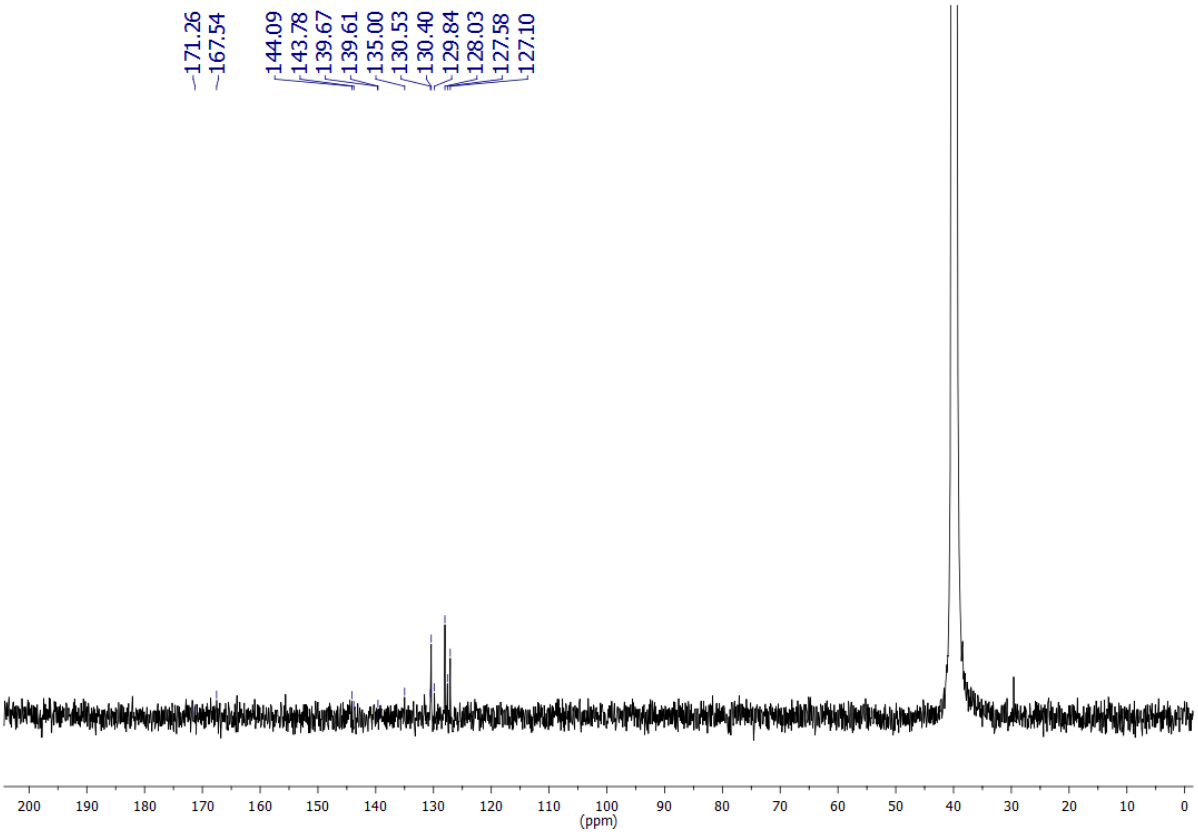
171.26
167.54
144.09
143.78
139.67
139.61
135.00
130.53
130.40
129.84
128.03
127.58
127.10
(ppm)

2-(4''-Carboxy-2-nitro-1,1',4',1''-terphenyl-4-yl)-4,6-bis(4''-carboxy-1,1':4',1''-terphenyl-4-yl)-1,3,5-triazine (20b)

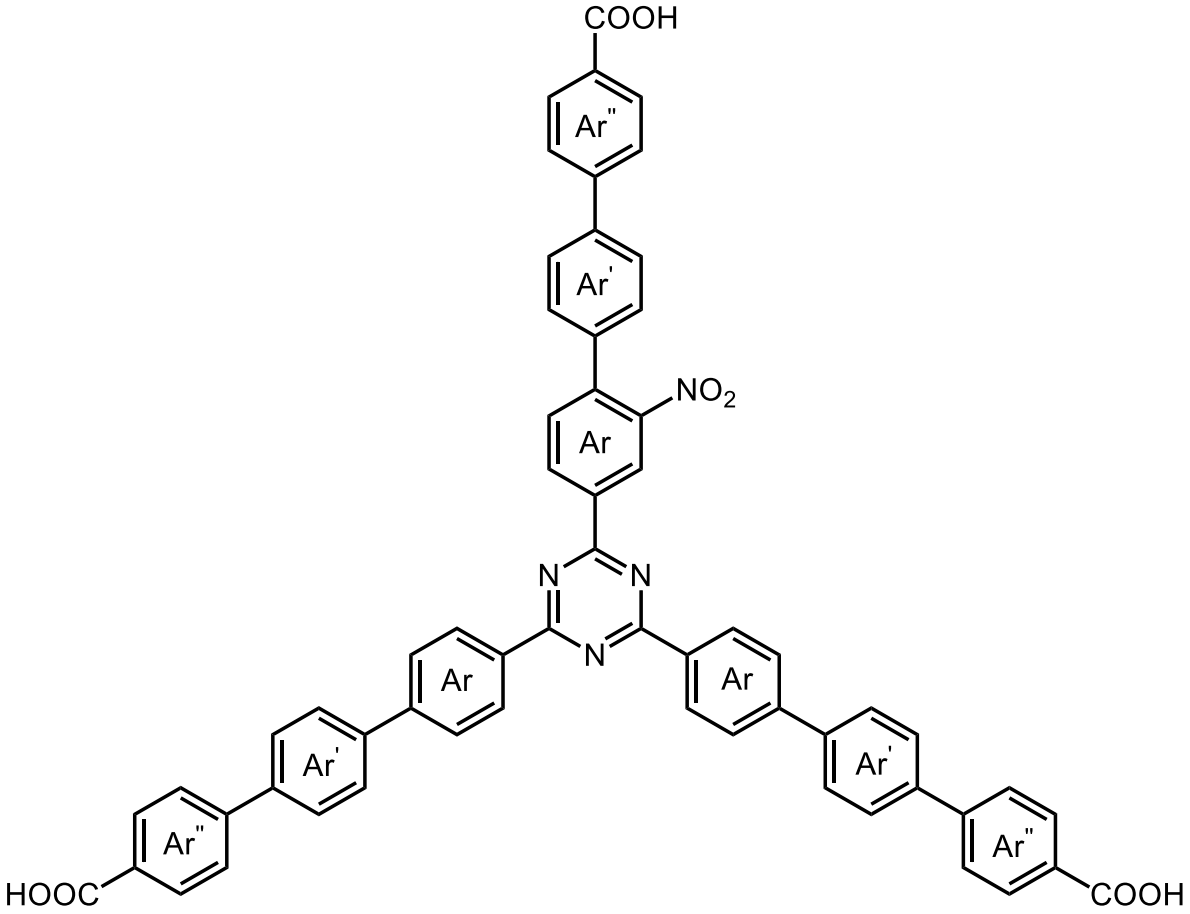

To a mixture of 1,4-dioxane (10 mL) and sodium hydroxide (6 M, 50 mL) was added 2-[4''-(methoxycarbonyl)-2-nitro-1,1':4',1''-terphenyl-4-yl]-4,6-bis[4''-(methoxycarbonyl)-1,1':4',1''-terphenyl-4-yl]-1,3,5-triazine (**19b**, 93 mg, 94 µmol). After stirring for 24 h at 120 °C the solvent was evaporated in vacuo. The residue was dissolved in 10 mL water and acidified with conc. hydrochloric acid. The precipitate was filtered off and washed with deionized water. A yellow solid was obtained. Yield: 70 mg (74 µmol, 79 %). M. p.: > 300 °C. ^{1}H NMR (600 MHz, DMSO-d_6): δ = 13.0 (br.s, 3H, COO*H*), 9.27 (d, ^{4}J = 1.3 Hz, 1H, 2-Ar-*H*-2), 9.10 (d, ^{3}J = 8.0 Hz, 1H, 2-Ar-*H*-5), 8.90 (d, ^{3}J = 8.3 Hz, 4H, 4,6-Ar-*H*-3,5), 8.12 – 8.04 (m, 10H, 2,4,6-Ar''-*H*-3,5, 4,6-Ar-*H*-2,6), 7.98 (d, ^{3}J = 8.3 Hz, 4H, 4,6-Ar'-*H*-2,6), 7.96 –

7.88 (m, 13H, 4,6-Ar'-*H*-3,5, 2,4,6-Ar''-*H*-2,6, 2-Ar-*H*-6, 2-Ar'-*H*-3,5), 7.60 (d, ^{3}J = 8.1 Hz, 2H, 2-Ar'-*H*-2,6) ppm. ^{13}C NMR (150 MHz, DMSO-d_6): δ = 170.9 (s, triazine-*C*-4,6), 169.0 (s, triazine-*C*-2), 167.2 (s, *C*O_2H), 149.5 (s, 2-Ar-*C*-2), 143.9 (s, 4,6-Ar-*C*-1), 143.3 (s, 2,4,6-Ar''-*C*-1), 139.3 (s, 2-Ar'-*C*-4), 138.8 (s, 4,6-Ar'-*C*-1), 138.7 (s, 4,6-Ar'-*C*-4), 138.0 (s, 2-Ar-*C*-1), 137.5 (s, 2-Ar-*C*-4), 136.3 (s, 2-Ar'-*C*-1), 134.1 (s, 4,6-Ar-*C*-4), 133.7 (d, 2-Ar-*C*-6), 132.6 (d, 2-Ar-*C*-5), 130.4 (d, 2,4,6-Ar''-*C*-3,5), 130.0 (d, 4,6-Ar-*C*-3,5), 129.8 (s, 2,4,6-Ar''-*C*-4), 129.0 (d, 2-Ar'-*C*-2,6), 128.0 (d, 4,6-Ar'-*C*-2,6), 127.9 (d, 4,6-Ar'-*C*-3,5), 127.6 (d, 4,6-Ar-*C*-2,6), 127.3 (d, 2-Ar'-*C*-3,5), 127.3 (d, 2,4,6-Ar''-*C*-2,6), 124.4 (d, 2-Ar-*C*-3) ppm. MS (MALDI, Cl-CCA): *m/z* = 944 $[M + H]^+$. IR (ATR): $\tilde{\nu}$ = 3031 (aryl-H), 1684 (C=O), 1605, 1571 (arom. C=C, arom. C=N), 1506 (asymm. N=O), 1424, 1401 (CH-Def.), 1356 (symm. N=O), 1272, 1182, 1110 (C-O), 811, 773 (1,4-disubst. aryl, 1,2,4-trisubst. aryl) cm^{-1}. Elemental analysis ($C_{60}H_{38}N_4O_8$) (942.97): calcd. C 76.42 H 4.06 N 5.94; ($C_{60}H_{38}N_4O_8 \cdot 0.5\ H_2O$) (951.96): calcd. C 75.70 H 4.13 N 5.89; found C 75.43 H 4.06 N 5.87.

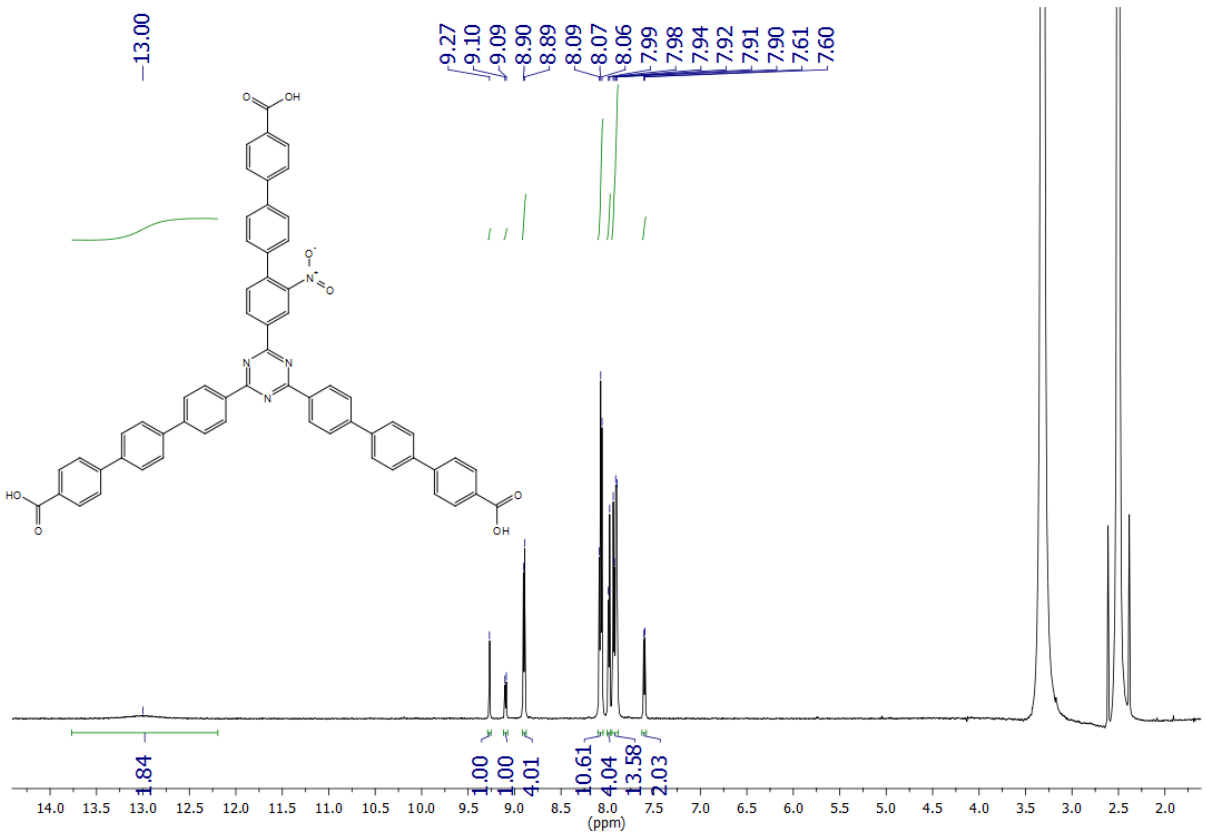
13.00
9.27
9.10
9.09
8.90
8.89
8.09
8.07
8.06
7.99
7.98
7.94
7.92
7.91
7.90
7.61
7.60
1.84
1.00
1.00
4.01
10.61
4.04
13.58
2.03
(ppm)

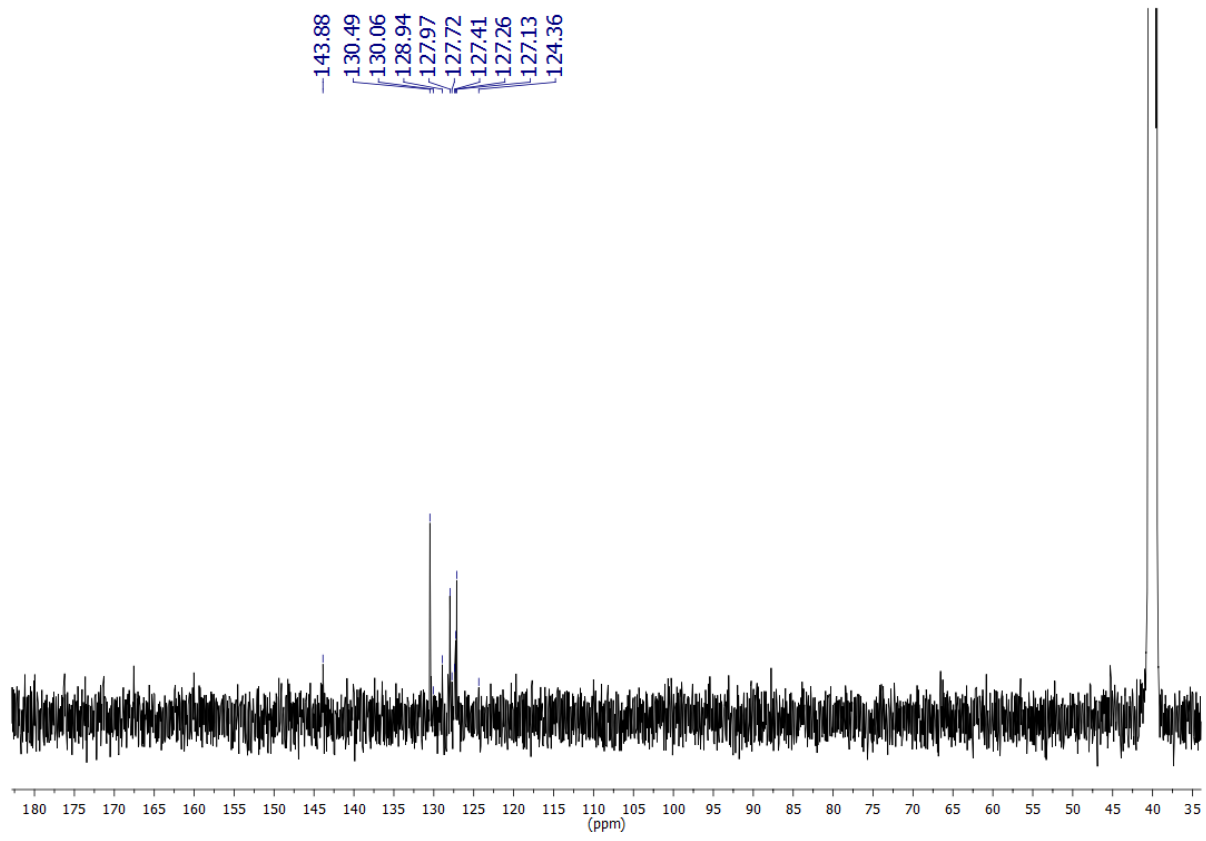
143.88
130.49
130.06
128.94
127.97
127.72
127.41
127.26
127.13
124.36
(ppm)

2-(4''-Carboxy-2-hydroxy-1,1':4',1''-terphenyl-4-yl)-4,6-bis(4''-carboxy-1,1':4',1''-terphenyl-4-yl)-1,3,5-triazine (20e)

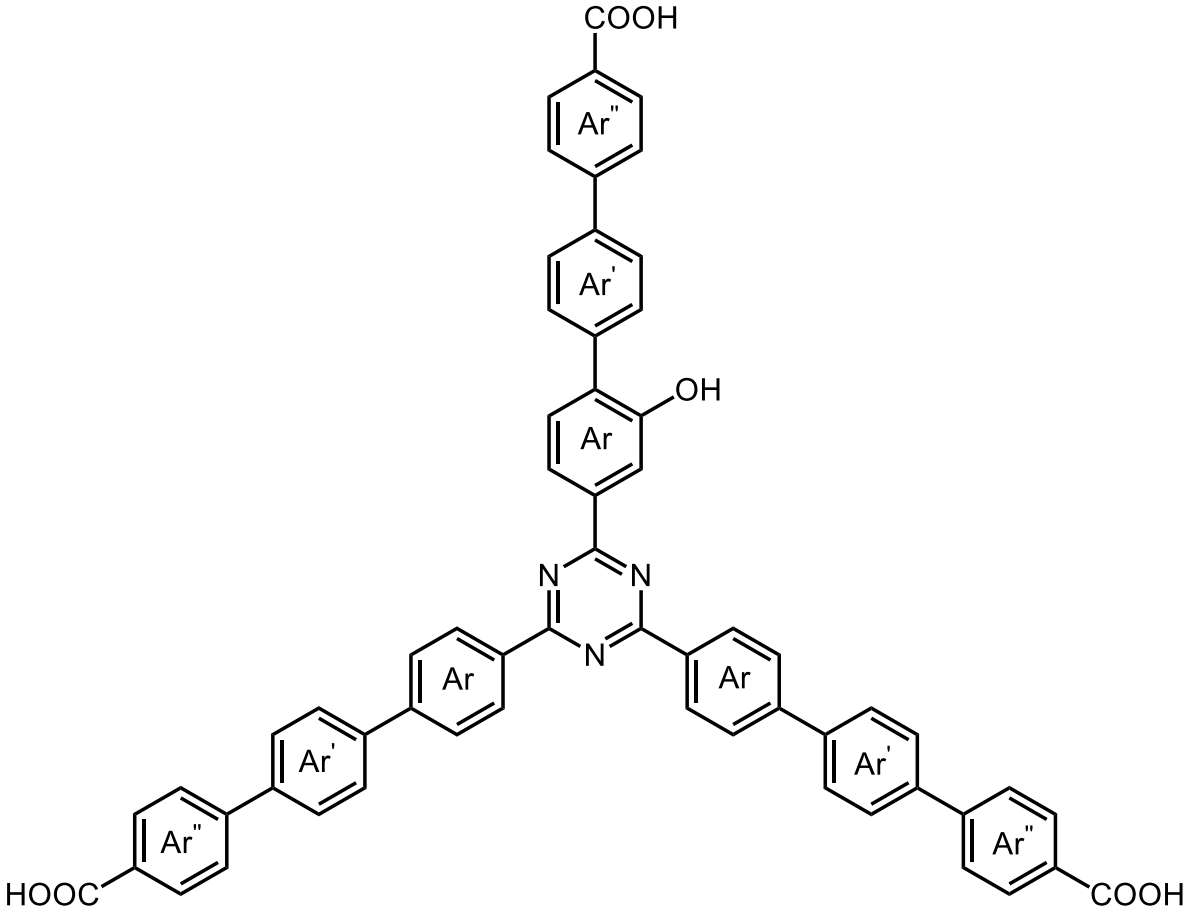

2,4-Bis[4''-(methoxycarbonyl)-(1,1':4',1''-terphenyl)-4-yl]-6-[2-methoxy-4''-(methoxycarbonyl)-(1,1':4',1''-terphenyl)-4-yl]-1,3,5-triazine (**19c**, 109 mg, 113 µmol) and pyridine hydrochloride (1.80 g, 15.6 mmol) were mixed and stirred for 12 h at 200 °C. After cooling to room temp., sodium hydroxide (2 M) was added to the solution until pH = 14 was reached. The reaction mixture was stirred for 12 h at 120 °C before it was acidified with conc. hydrochloric acid and the resulting precipitate was filtered off. Washing with water and drying gave a dark red solid. Yield: 64 mg (70.0 µmol, 62 %). M. p.: > 300 °C. ^{1}H NMR (600 MHz, DMSO-d_6): δ = 12.99 (br.s, 3H, COO*H*), 10.09 (s, 1H, O*H*), 8.63 (d, ^{3}J = 7.7 Hz, 4H, 4,6-Ar-*H*-3,5), 8.31 (s, 1H, *2*-Ar-*H*-3), 8.11 (d, ^{3}J = 7.6 Hz, 1H, 2-Ar-*H*-5), 8.06 - 7.99 (m, 6H, 4,6-

Ar''-*H*-3,5, 2-Ar''-*H*-3,5), 7.86 (d, ^{3}J = 7.7 Hz, 4H, 4,6-Ar-*H*-2,6), 7.82 - 7.75 (m, 14H, 2-Ar''-*H*-2,6, 4,6-Ar'-2,3,5,6, 4,6-Ar''-2,6), 7.74 – 7.68 (m, 4H, 2-Ar'-*H*-2,3,5,6), 7.44 (d, ^{3}J = 7.6 Hz, 1H, 2-Ar-*H*-6) ppm. ^{13}C NMR (150 MHz, DMSO-d_6): δ = 170.5 (s, triazine-*C*-2), 170.4 (s, triazine-*C*-4,6), 167.2 (s, 2-Ar''-*C*OOH), 167.1 (s, 4,6-Ar''-*C*OOH), 154.8 (s, 2-Ar-*C*-2), 143.9 (s, 2-Ar''-*C*-1), 143.4 (s, 4,6-Ar-*C*-1), 143.3 (s, 4,6-Ar''-*C*-1), 138.8 (s, 4,6-Ar'-*C*-1), 138.6 (s, 4,6-Ar'-*C*-4), 137.6 (s, 2-Ar'-*C*-4), 137.5 (s, 2-Ar'-*C*-1), 135.7 (s, 2-Ar-*C*-4), 134.6 (s, 4,6-Ar-*C*-4), 131.4 (s, 2-Ar''-*C*-4), 131.2 (s, 2-Ar-*C*-1), 130.4 (d, 2-Ar-*C*-6), 130.0 (d, 2-Ar''-*C*-3,5, 4,6-Ar''-*C*-3,5), 129.8 (d, 2-Ar'-*C*-2,6), 129.6 (s, 4,6-Ar''-*C*-4), 129.1 (d, 4,6-Ar-*C*-3,5), 127.5 (d, 2-Ar''-*C*-2,6, 4,6-Ar''-*C*-2,6), 126.8 (d, 4,6-Ar-*C*-2,6), 126.6 (d, 4,6-Ar'-*C*-2,3,5,6), 126.4 (d, 2-Ar'-*C*-3,5), 120.0 (d, 2-Ar-*C*-5), 115.9 (d, 2-Ar-*C*-3) ppm. MS (MALDI, Cl-CCA): *m/z* = 914 $[M + H]^+$. IR (ATR): $\tilde{\nu}$ = 2925 (O-H), 1682 (C=O), 1605, 1572, 1504 (arom. C=C, arom. C=N), 1407 (CH-Def.), 1361 (O-H-Def.), 1251, 1180, 1100 (C-O), 808, 773 (1,4-disubst. aryl, 1,2,4-trisubst. aryl) cm^{-1}. Elemental analysis ($C_{60}H_{39}N_3O_7$) (913.28): calcd. C 78.35 H 4.30 N 4.60; ($C_{60}H_{39}N_3O_7 \cdot 2.5\ H_2O$) (958.31): calcd. C 75.14 H 4.62 N 4.38; found C 75.23 H 4.29 N 4.35.

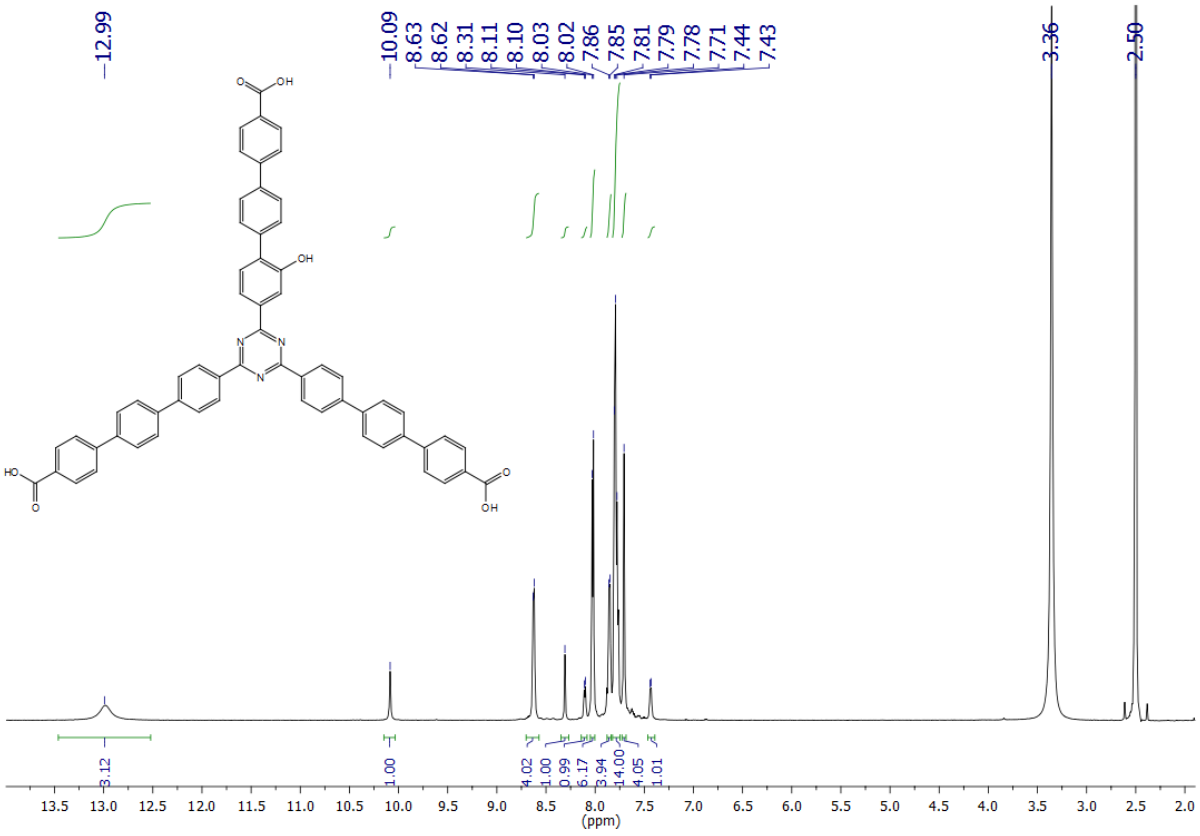
12.99
10.09
8.63
8.62
8.31
8.11
8.10
8.03
8.02
7.86
7.85
7.81
7.79
7.78
7.71
7.44
7.43
3.36
2.50
3.12
1.00
4.02
1.00
0.99
6.17
3.94
14.00
4.05
1.01
(ppm)

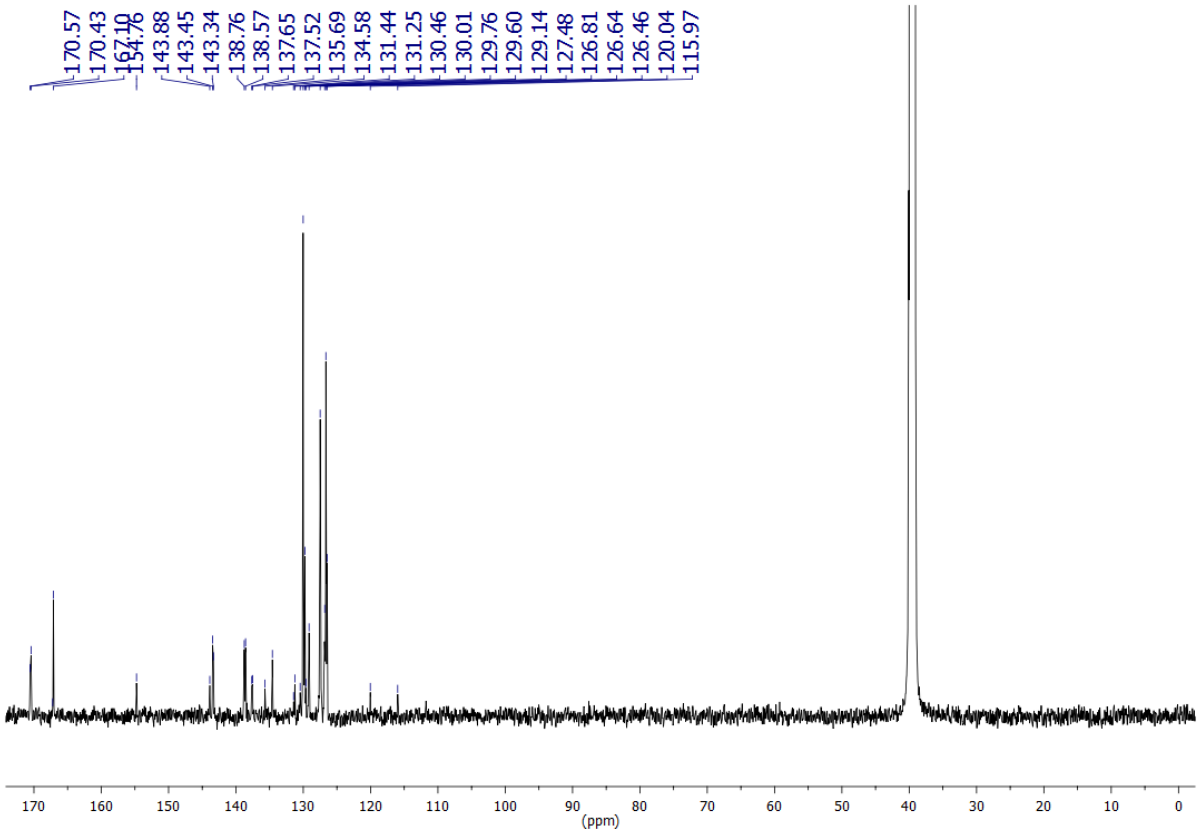
170.57
170.43
167.10
154.76
143.88
143.45
143.34
138.76
138.57
137.65
137.52
135.69
134.58
131.44
131.25
130.46
130.01
129.76
129.60
129.14
127.48
126.81
126.64
126.46
120.04
115.97
(ppm)

[1] Fukaya, Y.; Mihara, Y.; Morizono, D.; Ohtake, Y.; Oishi, T.; Shoji, T.; Takashima Y. (Wakamoto Pharma), *patent application*, **2006**, WO2006051851 A1.

[2] Bhat, L.; Mohapatra, P. P.; Bhat S. R. (Reviva Pharmaceuticals), *patent application*, **2008**, US20080293736 A1.

[3] Li, X.; Longenecker, K. L.; Pei, Z.; Sham, H. L.; Wiedeman P. E. (Abbott Laboratories), *patent application*, **2005**, WO2005023762 A1.

[4] Burrows, A. D.; Frost, C. G.; Mahon, M. F.; Richardson, C. *Angew. Chem.* **2008**, *120*, 8610-8614; *Angew. Chem. Int. Ed.* **2008**, *47*, 8482–8416.

[5] Failli, A.; Quagliato, D.; Andrae, P.; Heffernan, G.; Coghlan, R.; Shen, E. (Wyeth), *patent application*, **2006**, US20060199806 A1.

[6] Gaussian 09, Revision D.01, M. J. Frisch, G. W. Trucks, H. B. Schlegel, G. E. Scuseria, M. A. Robb, J. R. Cheeseman, G. Scalmani, V. Barone, B. Mennucci, G. A. Petersson, H. Nakatsuji, M. Caricato, X. Li, H. P. Hratchian, A. F. Izmaylov, J. Bloino, G. Zheng, J. L. Sonnenberg, M. Hada, M. Ehara, K. Toyota, R. Fukuda, J. Hasegawa, M. Ishida, T. Nakajima, Y. Honda, O. Kitao, H. Nakai, T. Vreven, J. A. Montgomery, Jr., J. E. Peralta, F. Ogliaro, M. Bearpark, J. J. Heyd, E. Brothers, K. N. Kudin, V. N. Staroverov, T. Keith, R. Kobayashi, J. Normand, K. Raghavachari, A. Rendell, J. C. Burant, S. S. Iyengar, J. Tomasi, M. Cossi, N. Rega, J. M. Millam, M. Klene, J. E. Knox, J. B. Cross, V. Bakken, C. Adamo, J. Jaramillo, R. Gomperts, R. E. Stratmann, O. Yazyev, A. J. Austin, R. Cammi, C. Pomelli, J. W. Ochterski, R. L. Martin, K. Morokuma, V. G. Zakrzewski, G. A. Voth, P. Salvador, J. J. Dannenberg, S. Dapprich, A. D. Daniels, O. Farkas, J. B. Foresman, J. V. Ortiz, J. Cioslowski, D. J. Fox, Gaussian, Inc., Wallingford CT, 2013.

[7] Gaussian 09, Revision D.01, M. J. Frisch, G. W. Trucks, H. B. Schlegel, G. E. Scuseria, M. A. Robb, J. R. Cheeseman, G. Scalmani, V. Barone, B. Mennucci, G. A. Petersson, H. Nakatsuji, M. Caricato, X. Li, H. P. Hratchian, A. F. Izmaylov, J. Bloino, G. Zheng, J. L. Sonnenberg, M. Hada, M. Ehara, K. Toyota, R. Fukuda, J. Hasegawa, M. Ishida, T. Nakajima, Y. Honda, O. Kitao, H. Nakai, T. Vreven, J. A. Montgomery, Jr., J. E. Peralta, F. Ogliaro, M. Bearpark, J. J. Heyd, E. Brothers, K. N. Kudin, V. N. Staroverov, T. Keith, R. Kobayashi, J. Normand, K. Raghavachari, A. Rendell, J. C. Burant, S. S. Iyengar, J. Tomasi, M. Cossi, N. Rega, J. M. Millam, M.

Klene, J. E. Knox, J. B. Cross, V. Bakken, C. Adamo, J. Jaramillo, R. Gomperts, R. E. Stratmann, O. Yazyev, A. J. Austin, R. Cammi, C. Pomelli, J. W. Ochterski, R. L. Martin, K. Morokuma, V. G. Zakrzewski, G. A. Voth, P. Salvador, J. J. Dannenberg, S. Dapprich, A. D. Daniels, O. Farkas, J. B. Foresman, J. V. Ortiz, J. Cioslowski, D. J. Fox, Gaussian, Inc., Wallingford CT, 2013.

3.2 MOF-Synthese und postsynthetische Modifikation

Das Konzept der „retikularen Synthese“ nutzt das Wissen über die Eigenschaften von SBUs und Linkern zur gezielten Synthese eines MOFs mit ausgewählter Topologie. Sind die Eigenschaften für einen bestimmten Linker bekannt, kann dieses Konzept genutzt werden, um funktionelle Gruppen in ein MOF-Gerüst einzuführen. Dafür wird an Stelle des bekannten Linkers eine funktionalisierte Variante in der MOF-Synthese eingesetzt. Hat die funktionelle Gruppe nur einen geringen Einfluss auf die koordinativen Eigenschaften des Linkers, kann im Idealfall ein MOF mit der gewünschten Topologie erhalten werden. Durch die Implementierung von funktionellen Gruppen in einen MOF können dessen chemische und physikalische Eigenschaften verändert werden. Zusätzlich können die funktionellen Gruppen eine postsynthetische Modifikation des MOFs ermöglichen.

In den folgenden Kapiteln wird die Synthese, Charakterisierung und postsynthetische Modifikation von MOFs basierend auf funktionalisierten H_3TATB-Linkern beschrieben.

3.2.1 Funktionalisierte PCN-6-MOFs

Zur Darstellung von isoretikularen PCN-6-MOFs wurden drei funktionalisierte H_3TATB-Linker synthetisiert. Da die Anzahl an funktionellen Gruppen am H_3TATB-Linker einen Einfluss auf die MOF-Synthese haben kann, wurde ein Syntheseweg gewählt, der das Einführen nur einer funktionellen Gruppe pro Triazin-Linker ermöglicht.

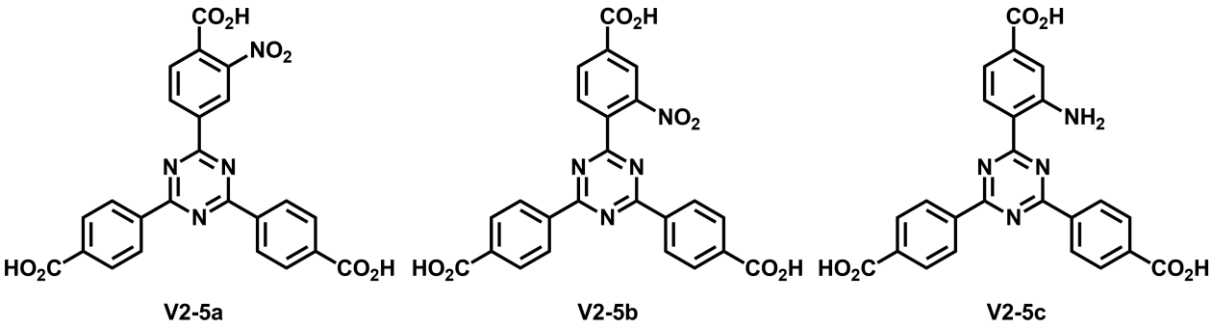

Abb. 22: Funktionalisierte H_3TATB-Linker.

Zwei Nitro-H_3TATB-Linker (*ortho* **V2-5a** und *meta* **V2-5b**) und ein Amino-H_3TATB-Linker (*meta* **V2-5c**) wurden analog einer Synthese von ZHOU[90] mit $Cu(NO_3)_2 \bullet 3H_2O$ umgesetzt. Die erhaltenen PCN-6-R-MOFs (R = *o*-NO_2, *m*-NO_2, *m*-NH_2) zeigen große Unterschiede in ihren Eigenschaften. Während PCN-6-NO_2 (*meta*) und PCN-6-NO_2 (*ortho*) bis 175 °C stabil sind, zersetzt sich PCN-6-NH_2 schon beim Aufheizprozess. Außerdem hat die Position der Nitrogruppe einen Einfluss auf die Oberfläche und die Farbe des jeweiligen MOFs.

Die Ergebnisse wurden veröffentlicht:

E. Mühlbauer, A. Klinkebiel, O. Beyer, S. Wuttke, U. Lüning, T. Bein, *Microporous Mesoporous Mater.* **2015**, *216*, 51-55.

Die Reduktion des Nitro-H_3TATB-Linker **V2-5b** zum Amino-H_3TATB-Linker **V2-5c** unter Verwendung von Natriumdithionit ist Bestandteil dieser Dissertation. Die Synthese und Charakterisierung der H_3TATB-Linker **V2-5a-d** wurde von ARNE KLINKEBIEL im Rahmen seiner Dissertation durchgeführt. Die Darstellung und Charakterisierung der PCN-6-MOFs wurde von ERIKA VIRMANI (geb. MÜHLBAUER) und STEFAN WUTTKE an der Ludwigs-Maximilian-Universität München durchgeführt.

Anmerkung: Die Formatierung der Supporting Information wurde geringfügig verändert, um sie auf die Formatierung dieser Arbeit anzupassen. Dabei wurden keine Inhalte verändert.

Microporous and Mesoporous Materials 216 (2015) 51–55

Contents lists available at ScienceDirect

Microporous and Mesoporous Materials

journal homepage: www.elsevier.com/locate/micromeso

Functionalized PCN-6 metal-organic frameworks

Erika Mühlbauer [a, 1], Arne Klinkebiel [b, 1], Ole Beyer [b], Florian Auras [a], Stefan Wuttke [a], Ulrich Lüning [b, *], Thomas Bein [a, *]

[a] University of Munich (LMU) and Center for NanoScience (CeNS), Department of Chemistry, Butenandtstraße 5-11, 81377 Munich, Germany
[b] Christian-Albrechts-Universität zu Kiel, Otto Diels-Institut für Organische Chemie, Olshausenstr. 40, 24098 Kiel, Germany

ARTICLE INFO

Article history:
Received 13 February 2015
Received in revised form
25 May 2015
Accepted 7 June 2015
Available online 16 June 2015

Keywords:
Metal organic frameworks – MOFs

ABSTRACT

Mono-substituted triangular linker molecules for metal-organic frameworks (MOFs) based on triazine-2,4,6-triyl-tribenzoate (TATB) were successfully synthesized with a nitro group in *ortho* (**5a**) and in *meta* (**5b**) position, as well as with an amino group (**5c**) in *meta* positon to the carboxylic acid. The synthetic route starts from substituted benzoyl chlorides **2** and the corresponding unsubstituted nitriles **1**. Furthermore, the novel functionalized TATB-R linkers **5a-c** were successfully used for the synthesis of microporous metal-organic frameworks based on the PCN-6 structure. Powder X-ray diffraction revealed identical high crystallinity of the PCN-6-R [R = –H, $-NO_2$ (*ortho* or *meta*), $-NH_2$ (*meta*)] structures. These MOF structures were found to exhibit different porosity, stability and color depending on the substitution of the linker.

1. Introduction

Metal-organic frameworks (MOFs) have shown to be promising candidates for gas storage and separation [1], catalysis [2], chemical sensing [3], and drug delivery [4]. MOFs are crystalline materials constructed of metal ions or metal clusters joined by organic linkers. On the one hand, the compositional and structural variety of MOFs is due to the great diversity of possible secondary building units (SBU) of different metals ranging from three up to twenty-two points of extensions [5]. On the other hand, there is a wide variety of possible organic linker molecules that can be incorporated into MOFs, ranging from ditopic to hexatopic with different lengths and geometries [1]. A common concept for tuning the pore size of MOFs is the isoreticular expansion of known topologies by using elongated and/or modified organic linker molecules [6]. The isoreticular chemistry of MOFs has been shown for HKUST-1 (HKUST stands for Hong Kong University of Science and Technology), which is one of the benchmark MOFs and is already being produced on an industrial scale [7]. The SBU of this structure is a dicopper tetracarboxylate paddlewheel with axial aqua ligands. In HKUST-1 the organic linker is the trivalent benzene-1,3,5-tricarboxylic acid. This linker can be elongated to BTB (BTB stands for 1,3,5-benzenetribenzoate) containing aryl–aryl subunits. This leads to 120° angles between the arms, but due to the repulsion of the *ortho* hydrogen atoms in a biphenyl moiety, the BTB building block is not entirely planar, resulting in a topology that is different from the one found in HKUST-1 [6]. We note that by changing the synthesis conditions *Klein* et al. [8] were able to obtain a similar topology as HKUST-1 with the BTB linker.

Planarity can be enhanced through substituting the central benzene ring of BTB by a 1,3,5-triazine [9]. The synthesis of MOFs with the triazine-2,4,6-triyl-tribenzoate (TATB) linker and copper ions results in an isoreticular structure of HKUST-1, named PCN-6 [9,10]. This material exhibits a permanent high porosity and a remarkable volumetric storage capacity for hydrogen [10]. To further functionalize this MOF structure and possibly enhance its gas storage capacity, the design of linkers with different functional groups would be desirable. Despite the richness of different structures using tritopic carboxylate linkers, examples for functionalized versions of such linkers are surprisingly rare [11–13]. Additional functional groups at the linker molecules can be used as anchoring points for the covalent attachment of further moieties. In this context, amino groups are particularly suitable for post-synthetic modifications (PSM), and a multitude of such reactions with amino groups have been reported so far [14–16]. Therefore, trivalent linkers with additional reactive substituents would be attractive synthetic targets.

* Corresponding authors.
E-mail addresses: luening@oc.uni-kiel.de (U. Lüning), bein@lmu.de (T. Bein).
[1] These authors contributed equally.

http://dx.doi.org/10.1016/j.micromeso.2015.06.007
1387-1811/

Here we report on the synthesis of novel MOFs having the PCN-6 topology with functionalized TATB linkers. As mentioned above, TATB is more planar than BTB. However, additional substituents on TATB will start to disturb planarity. We therefore decided to only introduce one additional functional group per TATB linker. In the case of mono-substituted TATBs **5a-c**, two regioisomers are conceivable: substitution *ortho* or *meta* to one of the carboxylates. Neither of these molecules has been prepared yet. The novel TATB linkers were used to synthesize the corresponding PCN-6 structures. Furthermore, the influence of the functional substituents on the material properties was studied.

2. Experimental

2.1. Linker synthesis

Three mono-substituted TATB linkers **5a-c** were synthesized. A nitro group was introduced by using nitrosubstituted benzoyl chlorides **2a** or **2b** in the synthesis of an unsymmetric TATB precursor **3**, while amino substituted TATB **5c** was obtained by reduction of nitro-TATB **5b** (see Scheme 1). For further synthesis details see Supplementary Information.

2.2. MOF synthesis

The PCN-6-R [R = −H, -NO_2 (*ortho* or *meta*) or−NH_2 (*meta*)] materials were synthesized in a 100 mL Schott-Duran glass bottle with a PBT cap equipped with a Teflon seal. $Cu(NO_3)_2 \cdot 3H_2O$ and the functionalized TATB-R linkers [R = −H, −NO_2 (*ortho* or *meta*) or−NH_2 (*meta*)] were dissolved in 15 mL of DMF by ultrasonic treatment. The reaction mixture was heated within 1 h−75 °C, held at this temperature for 48 h, and was afterwards cooled to room temperature within 24 h. The resulting colored powder was collected by centrifugation (10 min, 20 000 rpm), washed three times with DMF and dried under reduced pressure at room temperature. For further synthetic details see Supplementary Information.

2.3. Characterization

Wide-angle X-ray diffraction (XRD) data were recorded in transmission mode on a STOE Stadi MP diffractometer with a Cu $K_{\alpha 1}$ radiation source (λ = 1.54060 Å) operating at 40 kV and 40 mA. The diffractometer was equipped with a DECTRIS MYTHEN 1K solid-state strip detector. Nitrogen sorption isotherms were measured at 77 K with a Quantachrome AUTOSORB-1 instrument. Prior to measurement, the sample was degassed at 120 °C for 12 h in vacuum. BET surface areas were calculated from the relative pressure range of p/p_0 0.005 to 0.01, and Langmuir surface areas were calculated in the range of p/p_0 $1 \cdot 10^{-6}$ to 0.05. Pore size distributions were calculated by employing a quenched solid state functional theory (QSDFT) model supplied by Quantachrome. UV–Vis spectra were recorded using a Perkin Elmer Lambda 1050 spectrometer equipped with a 150 mm integrating sphere. Measurements of powder samples were carried out in reflection geometry using a Praying Mantis (Harrick) accessory and were referenced to barium sulfate serving as white standard. For further characterization of the materials see Supplementary Information.

3. Results and discussion

Scheme 1 shows the syntheses of mono-substituted TATBs **5a-c** containing the substituent *ortho* or *meta* to the carboxylic acid. Two substituents R with considerably different electronic effects were selected: nitro (Hammett value: $\sigma_m = 0.71$) and amino (Hammett value: $\sigma_m = -0.16$). While symmetrical 1,3,5-triazines can be synthesized by trimerization of nitriles [17–21], a modified synthetic route must be chosen for mono-substituted triazines [22,23]. The substituted arm is introduced as an acid chloride (**2**), while the two unsubstituted ones are derived from the respective nitrile (**1**). Trimerization syntheses of triazines use rather acidic reaction conditions, thus requiring robust protecting groups. In the case of TATBs, methyl groups are unaffected by the reaction conditions, nevertheless they allow subsequent oxidation to the respective carboxylic acids. Another advantage of introducing the carboxylic acid groups later in the synthesis is the improved solubility, an important feature in handling and purification of polycarboxylates. Using a 2:1 mixture of nitrile **1** and nitro substituted acid chloride **2a** or **2b** together with antimony(V) chloride as a Lewis acid, the yellow oxonium salt **3a** or **3b** was generated, which was converted to the nitro-triazine **4a** or **4b** with 59% or 54% total yield, respectively. Oxidation of all three methyl groups generates nitro-substituted TATBs **5a** or **5b**. Initially, chromium(VI) oxide was used as oxidant, yielding 86% of nitrotriazine **5b**. The less toxic permanganate can also be used as the oxidant if pyridine-soluble tetrabutylammonium permanganate (Bu_4N MnO_4) is used instead of $KMnO_4$ [24]. This synthetic alternative produces triacid **5b** in 91% isolated yield, which relates to 97% yield per oxidized methyl group of **4b**. In case of the *ortho* variant **5a**, the triple oxidation of **4a** could be performed in 85% isolated yield.

Although numerous reagents exist that are able to reduce nitro groups to amino groups, many of them cannot be employed for the reduction in these systems. First, triacids **5** contain free carboxylic acids (not allowing hydrides as reducing agents). Second, their solubility is low even in polar solvents. Tin(II) chloride in acetic acid/ethanol proved to be the first successful reagent for the reduction of *meta*-nitrotriazine **5b**, and **5c** could be isolated in gram quantities with 64% yield. Alternatively, sodium dithionite can be used for the reduction (79% yield, half gram scale).

The crystalline PCN-6 structure with the composition $Cu_3(TATB)_2(H_2O)_3$ was synthesized according to *Zhou* et al. [10] in a solvothermal reaction of $Cu(NO_3)_2 \cdot 3H_2O$ with TATB (**5d**) in DMF at 75 °C. The high crystallinity of the structure was confirmed by PXRD measurements and compared to the theoretical diffractogram (Fig. 1A). In a similar solvothermal reaction of $Cu(NO_3)_2 \cdot 3H_2O$ with nitro or amino functionalized TATBs **5a-c** in DMF at 75 °C, highly crystalline PCN-6-NO_2 (*ortho* or *meta*) and PCN-6-NH_2 (*meta*) structures were obtained (Fig. 1A). The PXRD patterns of all four PCN-6-R structures [R = −H, −NO_2 (*ortho* or *meta*), -NH_2 (*meta*)] are very similar and match the theoretical structure of PCN-6. Pawley refinement of the obtained XRD patterns (Fig. S11) revealed virtually identical cell parameters *a* and *b* (3.32 nm), but a slight variation in the length of the crystallographic *c*-axis. Both NO_2-functionalized MOFs exhibit a slightly longer *c*-axis (8.23 nm and 8.24 nm for the *ortho* and *meta* variants, respectively) than their unfunctionalized and amino-functionalized counterparts. Temperature-dependent PXRD measurements confirmed that the PCN-6-R frameworks are stable up to temperatures of 175 °C for PCN-6-NO_2 (*ortho* or *meta*) and of 250 °C for PCN-6 (Fig. S5 – S7). The PCN-6-NH_2 (*meta*) framework (Fig. S8) was found to be significantly less temperature-stable; i.e., decomposition starts by heating the sample. These temperature stabilities were also confirmed in TGA measurements (Fig. S1). Due to the low thermal stability of PCN-6-NH_2 (*meta*), nitrogen sorption measurements were not possible, but the other three PCN-6-R MOFs exhibit high permanent porosities as confirmed by nitrogen sorption at 77 K (Fig. 1B). For the three PCN-6-R [R = −H and −NO_2 (*ortho* or *meta*)] structures, the nitrogen sorption isotherms exhibit a type I shape that is characteristic for microporous materials. PCN-6 has a Langmuir surface area of 3758 m^2/g, in agreement to the reported

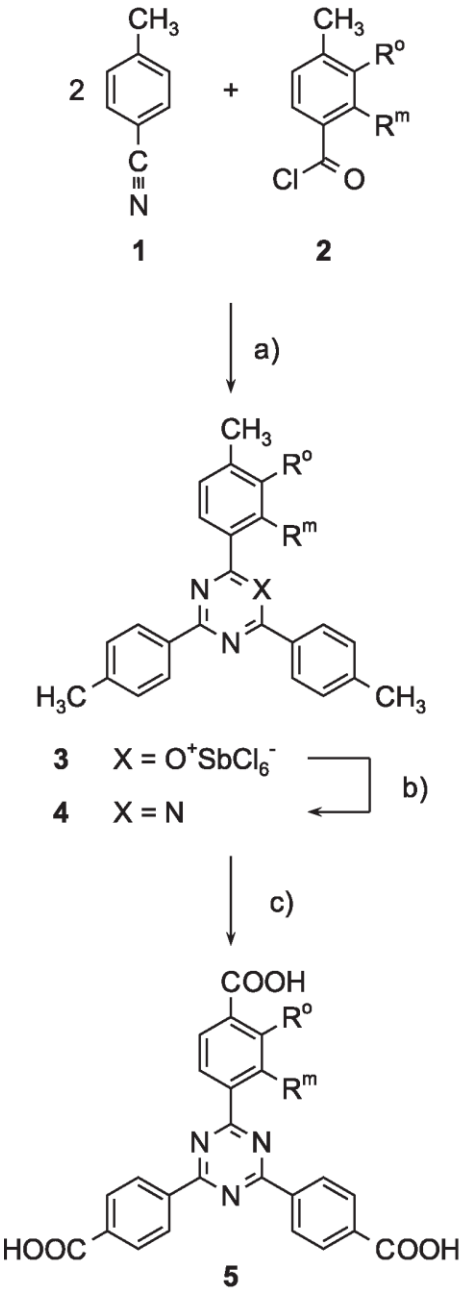

one [10] for PCN-6 (3800 m^2/g), and a BET surface area of 3231 m^2/g, in reasonable agreement with the Connolly surface area of 3670 m^2/g derived from the theoretical PCN-6 structure. For PCN-6-NO_2 (*meta*) and PCN-6-NO_2 (*ortho*), Langmuir surface areas of 3892 m^2/g and 2036 m^2/g and BET surface areas of 3354 m^2/g and 1797 m^2/g were obtained, respectively. The BET surface area of the NO_2 (*meta*)-functionalized MOF is in excellent agreement with the Connolly surface of 3350 m^2/g. The NO_2 (*ortho*)-functionalization, however, leads to a lower surface area than expected (Connolly surface 3390 m^2/g).

The values for the total pore volumes obtained from N_2 sorption are 1.31 cm^3/g (PCN-6), 1.36 cm^3/g [PCN-6-NO_2 (*meta*)] and 0.71 cm^3/g [PCN-6-NO_2 (*ortho*)] and are consistent with the pore volume of 1.45 cm^3/g reported by *Zhou* et al. [10] Hence, the surface area of the PCN-6 framework is strongly affected by the position of the functional group on the triangular linker molecule. The nitro functional group in *meta* position has no noticable effect, while the nitro group in *ortho* position drastically decreases the resulting surface area. The pore size distributions (Fig. 1C) for these three materials were evaluated from nitrogen sorption isotherms using the QSDTF method based on slit-like and cylindrical pores, showing one sharp single pore size of 1.0 nm. These micropores of 1.0 nm represent the triangular channels of the framework, which occur due to the interpenetration of two identical networks as reported in the literature for PCN-6 [10].

One important aspect of our functionalized TATB linkers is the influence of the position of the functional group on the material properties. To investigate this aspect, the PCN−NO_2 (*ortho* or *meta*) structures were exposed to 60% humidity at room temperature. XRD patterns recorded after different duration of exposure confirm that both frameworks are stable under these conditions for up to 8 h (Fig. S9 and S10). The stability towards moist air thus seems unaffected by the position of the nitro group.

Notably, the synthesized PCN-6-R structures are powders of different colors, depending on the functionality of the organic linker molecule used. In comparison, the colors of the linker molecules themselves range from white [TATB (**5d**)] to yellow [TATB-NO_2 (*ortho* or *meta*) (**5a-b**) and TATB-NH_2 (*meta*) (**5c**)] (Fig. S12). The colors of the MOFs are turquoise for unfunctionalized PCN-6, turquoise-green in the case of the nitro functionalization in the *meta* position [PCN-6-NO_2 (*meta*)], green-blue for the nitro functionalization in the *ortho* position [PCN-6-NO_2 (*ortho*)] and green for the amino functionalized [PCN-6-NH_2 (*meta*)] sample (Fig. 2A). The corresponding diffuse reflectance spectra of the MOFs follow the absorption spectra of the triazine linkers in the UV and blue spectral region and feature an additional absorption band extending from 600 to 1200 nm, which we attribute to metal-to-ligand charge transfer (Fig. 2B and Fig. S13). The maximum of this charge transfer absorption varies only slightly depending on the position of the functional group, indicating a relatively similar coordination environment of the copper SBU in all four MOFs (Fig. S14).

4. Conclusion

We have successfully synthesized mono-substituted TATB linkers bearing a nitro group in *ortho* or *meta* position to the carboxylic acid (**5a-b**), as well as with an amino group in *meta* positon (**5c**). The chosen synthetic route starts from a substituted benzoyl

Scheme 1. Syntheses of substituted TATBs **5** (R^o, R^m = $-NO_2$ and $-NH_2$ (*meta*)): a) $SbCl_5$, $CHCl_3$; b) NH_4OH, 59% (**4a**), 54% (**4b**) (two steps); c) CrO_3, Ac_2O, H_2SO_4, 86% (**5b**); or: Bu_4NMnO_4, pyridine, 85% (**5a**), 91% (**5b**); d) $SnCl_2$, 2 M HOAc, EtOH, 63%; or: $Na_2S_2O_4$, $EtOH/H_2O$, 79%.

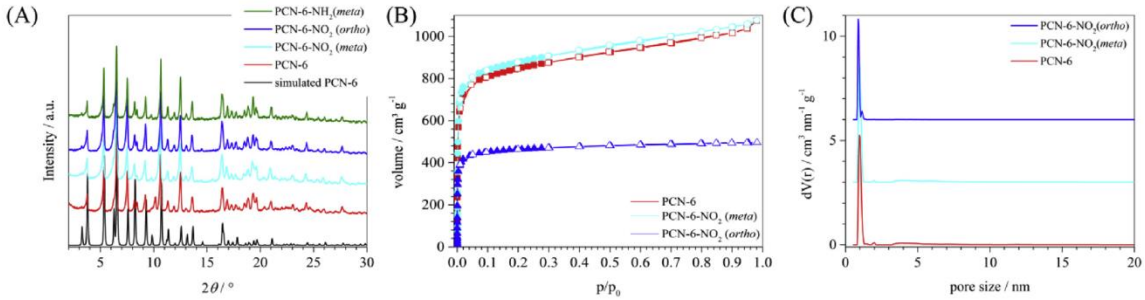

Fig. 1. (A) PXRD patterns of the different functionalized PCN-6 structures (black: theoretical PCN-6 [10]; red: PCN-6; cyan: PCN-6-NO_2 (*meta*); blue: PCN-6-NO_2 (*ortho*) and green: PCN-6-NH_2 (*meta*)). (B) N_2 sorption isotherms of PCN-6 (red), PCN-6-NO_2 (*meta*) (cyan) and PCN-6-NO_2 (*ortho*) (blue) at 77 K. Adsorption is denoted by filled symbols and desorption by empty symbols. (C) Pore size distributions calculated with the QSDFT model using slit-like and cylindrical pores (red: PCN-6; cyan: PCN-6-NO_2 (*meta*) and blue: PCN-6-NO_2 (*ortho*)). (For interpretation of the references to colour in this figure legend, the reader is referred to the web version of this article.)

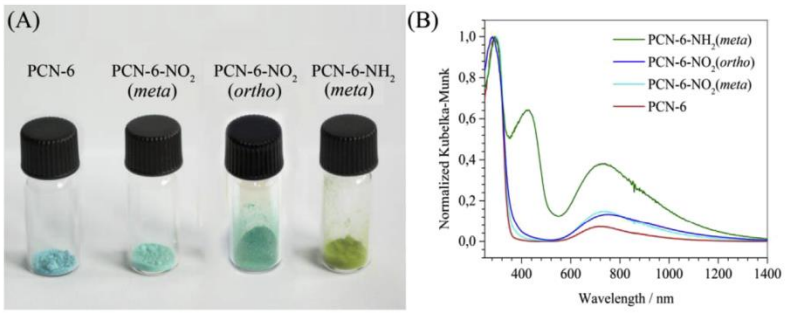

Fig. 2. Differently colored powders (A) of the functionalized PCN-6-R structures and corresponding powder UV–Vis spectra (B) (red: PCN-6; cyan: PCN-6-NO_2 (*meta*); blue: PCN-6-NO_2 (*ortho*) and green: PCN-6-NH_2 (*meta*)). (For interpretation of the references to colour in this figure legend, the reader is referred to the web version of this article.)

chloride **2** and by choosing substituents other than nitro, additional mono-functionalized TATBs are anticipated to be accessible (for example halogeno or alkoxy substituted ones). Furthermore, we successfully used the novel functionalized TATB-R linkers **5a-c** for the synthesis of microporous metal-organic frameworks based on the PCN-6 structure. Powder X-ray diffraction confirmed the successful synthesis of the PCN-6-R [R = –H, -NO_2 (*ortho* or *meta*), -NH_2 (*meta*)] structures. These MOF structures exhibit different temperature stabilities depending on the nature of the functional group. The position of the functional group also has a strong influence on the resulting surface area. While a *meta* nitro substitution has no impact on the surface area, *ortho* nitro substitution strongly decreases it. The PCN-6-NH_2 (*meta*) structure is not very stable and further post-synthetic modification of this framework was not possible. Depending on the substitution of the linker, the powders show different colors. The absorption that is responsible for the copper SBU (600–850 nm) is slightly affected by the position of the functional group, rather than by its nature. All in all, this work illustrates the strong influence of functional groups on linker molecules on the resulting material properties of MOFs.

Acknowledgement

This work was supported by the Deutsche Forschungsgemeinschaft (Be1042/4 and Lu 378/24) as part of the priority program SPP 1362 (Porous metal–organic frameworks).

We also thank the students Thomas Saal, Bernhard Illes and Michael Betz for their help with the synthesis of PCN-6-R structures, and Tina Reuther for nitrogen sorption and TG measurements.

Appendix A. Supplementary data

Supplementary data related to this article can be found at http://dx.doi.org/10.1016/j.micromeso.2015.06.007.

References

[1] D. Zhao, D.J. Timmons, D. Yuan, H.C. Zhou, Acc. Chem. Res. 44 (2011) 123–133.
[2] O.K. Farha, I. Eryazici, N.C. Jeong, B.G. Hauser, C.E. Wilmer, A.A. Sarjeant, R.Q. Snurr, S.T. Nguyen, A.O. Yazaydin, J.T. Hupp, J. Am. Chem. Soc. 134 (2012) 15016–15021.
[3] A.K. Cheetham, C.N. Rao, R.K. Feller, Chem. Commun. 46 (2006) 4780–4795.
[4] T.R. Cook, Y.R. Zheng, P.J. Stang, Chem. Rev. 113 (2013) 734–777.
[5] D.J. Tranchemontagne, J.L. Mendoza-Cortes, M. O'Keeffe, O.M. Yaghi, Chem. Soc. Rev. 38 (2009) 1257–1283.
[6] Q. Yao, J. Su, X. Zou, Z. Krist. – Cryst. Mat. 228 (2013) 323–329.
[7] S.S. Chui, Science 283 (1999) 1148–1150.
[8] N. Klein, I. Senkovska, I.A. Baburin, R. Grünker, U. Stoeck, M. Schlichtenmayer, B. Streppel, U. Mueller, S. Leoni, M. Hirscher, S. Kaskel, Chem. Eur. J. 17 (2011) 13007–13016.
[9] D. Sun, S. Ma, Y. Ke, D.J. Collins, H.C. Zhou, J. Am. Chem. Soc. 128 (2006) 3896–3897.
[10] S. Ma, D. Sun, M. Ambrogio, J.A. Fillinger, S. Parkin, H.C. Zhou, J. Am. Chem. Soc. 129 (2007) 1858–1859.
[11] K. Peikert, F. Hoffmann, M. Fröba, Chem. Commun. 48 (2012) 11196–11198.
[12] O. Shekhah, H.K. Arslan, K. Chen, M. Schmittel, R. Maul, W. Wenzel, C. Wöll, Chem. Commun. 47 (2011) 11210–11212.
[13] Y. Liu, J.-R. Li, W.M. Verdegaal, T.-F. Liu, H.-C. Zhou, Chem. Eur. J. 19 (2013) 5637–5643.
[14] S.M. Cohen, Chem. Rev. 112 (2012) 970–1000.
[15] H. Hintz, S. Wuttke, Chem. Mater. 26 (2014) 6722–6728.

[16] A. Klinkebiel, N. Reimer, M. Lammert, N. Stock, U. Lüning, Chem. Commun. 50 (2014) 9306–9308.
[17] A.H. Cook, D.G. Jones, J. Chem. Soc. (1941) 278–282.
[18] D. Martin, M. Bauer, V.A. Pankratov, Russ. Chem. Rev. 47 (1978) 975–990.
[19] S. Yanagida, M. Yokoe, I. Katagiri, M. Ohoka, S. Komori, Bull. Chem. Soc. Jpn. 46 (1973) 306–310.
[20] I.S. Bengelsdorf, J. Am. Chem. Soc. 80 (1958) 1442–1444.
[21] K. Matsumoto, A. Sera, T. Uchida, Synthesis 1985 (1985) 1–26.
[22] R.R. Schmidt, Chem. Ber. 98 (1965) 334–345.
[23] P. Eitner, F. Krafft, Ber. Dtsch. Chem. Ges. 25 (1892) 2263–2269.
[24] T. Sala, M.V. Sargent, J. Chem. Soc. Chem. Commun. (1978) 253–254.

Supplementary information

Functionalized PCN-6 metal-organic frameworks

Erika Mühlbauer,[a]† Arne Klinkebiel,[b]† Ole Beyer,[b] Florian Auras,[a] Stefan Wuttke,[a] Ulrich Lüning,[b]* and Thomas Bein[a]*

[a] *University of Munich (LMU) and Center for NanoScience (CeNS), Department of Chemistry, Butenandtstraße 5-11, 81377 Munich, Germany*

[b] *Christian-Albrechts-Universität zu Kiel, Otto Diels-Institut für Organische Chemie, Olshausenstr. 40, 24098 Kiel, Germany*

†Both authors contributed equally

**Correspondence authors (e-mail: luening@oc.uni-kiel.de and bein@lmu.de)*

1. Materials

4-Methyl-2-nitrobenzoic acid (**2b**, 97 %, Aldrich), 4-methylbenzonitrile (**1**, 98 %, Aldrich), acetic acid (p.a.), acetic anhydride (≥ 99 %, Carl Roth), acetone (99 %, in-house chemical supply), ammonia solution (2 M, in-house chemical supply), barium sulfate (99.99 %, Aldrich), chromium(VI)-oxide (99.5 %, Acros), copper (II) nitrate trihydrate (99 %, Fluka), hydrochloric acid (2 M, in-house chemical supply), *N*,*N*-dimethylformamide (anhydrous, synthesis grade, Fischer Scientific), palladium on activated charcoal (Alfa Aesar), sodium hydroxide solution (2 M, in-house chemical supply), sulfuric acid (96 %, in-house chemical supply), tetrabutylammonium bromide (98 %, Aldrich), toluene (technical, in-house chemical supply), trifluoromethanesulfonic acid (99 %, Apollo Scientific) were used without further purification.

2. Characterization

X-ray diffraction (XRD): Wide-angle X-ray diffraction data were recorded in transmission geometry using a STOE Stadi MP diffractometer with a Cu $K_{\alpha 1}$ radiation (λ = 1.54060 Å) source operating at 40 KV and 40 mA and a Ge(111) single crystal monochromator. The diffractometer was equipped with a DECTRIS MYTHEN 1K strip solid-state detector. Diffraction patterns were collected with an omega–2-theta scan using a step size of 4.71° and a counting time of 60 s or 180 s per step. Temperature stability measurements were performed using a Bruker D8 Discover with Ni-filtered Cu $K_{\alpha 1}$ radiation and a LynxEye position-sensitive detector. The sample was heated from 25 °C to 300 °C in steps of 25 °C and equilibrated for 10 min prior to measurement. Pawley refinements of the powder patterns were performed using the Reflex module of the Accelrys Materials Studio software package.

Nitrogen sorption: Nitrogen sorption isotherms were measured at 77 K with a Quantachrome AUTOSORB-1. About 35 mg of sample material was degassed at 120 °C in high vacuum for at least 12 h prior to measurement. Evaluation of sorption data was carried out using the ASiQwin^{TM} software suite (Version 3.0, Quantachrome Instruments). BET surface areas were calculated employing the linearized form of the BET equation with 10 data points (p/p_0 = 0.005, 0.008, 0.010, 0.015, 0.02, 0.03, 0.04, 0.05, 0.07 and 0.01) in the range from p/p_0 = 0.005 to 0.01, according to Quantachrome recommendations for microporous materials.[1] For all samples the correlation coefficient was higher than 0.999. Langmuir surface areas were calculated employing data points in the range form p/p_0 1 10^{-6} to 0.05. Adsorption isotherms were used to calculate the pore size distribution by employing quenched solid state functional theory (QSDFT, N_2 at 77 K on carbon, slit/cylindrical pore equilibrium model). Total pore volumes were calculated at p/p_0 0.20. The Connolly surface areas were simulated using the Accelrys Materials Studio software package and applying modified and Pawley-refined models of the PCN-6 crystal structure.

UV-Vis spectroscopy: UV-Vis measurements were carried out using a Perkin Elmer Lambda 1050 UV-Vis-NIR spectrometer equipped with a 150 mm InGaAs integrating sphere. Diffuse reflectance spectra were collected with a Praying Mantis (Harrick) accessory and were referenced to barium sulfate.

Infrared (IR) spectroscopy: Infrared spectroscopy was performed on a Perkin Elmer Spectrum BX II FT-IR system equipped with a diamond total reflection (ATR) unit in a scan range from 650 cm^{-1} to 4000 cm^{-1}or a Perkin-Elmer Paragon 1000/Perkin-Elmer Spectrum 100 fitted with an MKII Golden Gate™ Single Reflection ATR unit.

Nuclear magnetic resonance (NMR) spectroscopy: NMR data were recorded on JEOL ECX-400, Bruker DRX 500 and AV 600 spectrometers. All chemical shifts are referenced to the residual proton or carbon signal of the solvent. Assignments are supported by COSY, HSQC, and HMBC. Even when obtained by DEPT, the type of ^{13}C signal is always listed as singlet, doublet, etc.

Mass spectrometry (MS): Electronspray ionization (ESI) mass spectroscopy was carried out with a Therom Finnigan LTQ FT with Finnigan IonMax ion source. Electron ionization (EI) mass spectra were recorded with a Finnigan MAT 8200 or MAT 8230. High-resolution mass spectra were recorded in the EI mode using a Jeol Accu TOF GCV 4G instrument.

Elemental analysis: The elemental composition (C, H and N) was measured by combustion analysis with an Elementar Vario Micro Cube or an Euro EA 3000 Elemental Analyzer from Euro Vector.

Thermogravimetric (TG) analysis: TG measurements were carried out using a Netzsch Jupiter ST 449 C instrument equipped with a Netsch TASC 414/4 controller. The samples (10 mg to 15 mg) were heated in an aluminum oxide crucible between 25 °C and 900 °C with a heating rate of 10 K/min.

3. Experimental section

3.1. Linker synthesis

Tetrabutylammonium permanganate was prepared from tetrabutylammonium bromide according to literature procedures.[2]

4-Methyl-3-nitro-benzoyl chloride (2a)

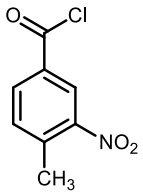

N,*N*-Dimethylformamide (1 µl, ca. 15 µmol) was added to a suspension of 4-methyl-3-nitro-benzoic acid (1.00 g, 5.52 mmol) in thionyl chloride (5 mL) and the mixture was heated to reflux for 2 h. Excess thionyl chloride was distilled off and the resulting yellow oil was used without further purification.

^{1}H-NMR (500 MHz, $CDCl_3$): δ = 8.69 (d, 1H, *J* = 1.9 Hz, Ar-*H*-2), 8.22 (dd, 1H, *J* = 8.1 Hz, *J* = 1.9 Hz, Ar-*H*-6), 7.55 (d, 1H, *J* = 8.1 Hz, Ar-*H*-5), 2.71 (s, 3H, C*H*$_3$) ppm.

^{13}C-NMR (125 MHz, $CDCl_3$): δ = 166.45 (s, *C*OCl), 149.42 (s, Ar-*C*-3), 141.20 (s, Ar-*C*-4), 134.35 (d, Ar-*C*-6), 133.71 (d, Ar-*C*-5), 132.43 (s, Ar-*C*-1), 127.42 (d, Ar-*C*-2), 20.75 (q, *C*H_3) ppm.

MS (EI, 70 eV): *m/z* (%) = 199 (100) $[M]^{+\cdot}$, 164 (52) $[M - Cl]^{+}$.

MS (Cl, isobutane): *m/z* (%) = 200 (11) $[M + H]^{+}$, 183 (58) $[M - O]^{+\cdot}$, 164 (100) $[M - Cl]^{+\cdot}$.

4-Methyl-2-nitrobenzoyl chloride (2b)

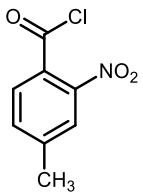

4-Methyl-2-nitrobenzoyl chloride (**2b**) is commercially available, but has been prepared from the respective acid by reaction with thionyl chloride. *N*,*N*-Dimethylformamide (1 µl, ca. 15 µmol) was added to a suspension of 4-methyl-2-nitrobenzoic acid (5.00 g, 27.6 mmol) in thionyl chloride (20 mL) and the mixture was heated to reflux for 2 h. Excess thionyl chloride was distilled off and the resulting oil was used without further purification.

^{1}H-NMR (500 MHz, $CDCl_3$): δ = 7.81 (m_c (d), 1H, *J* = 0.7 Hz, Ar-*H*-3), 7.69 (d, 1H, *J* = 7.9 Hz, Ar-*H*-6), 7.55 (m_c (d), 1H, *J* = 7.9 Hz, *J* = 0.7 Hz, Ar-*H*-5), 2.53 (s, 3H, C*H*$_3$) ppm.

^{13}C-NMR (125 MHz, $CDCl_3$): δ = 165.46 (s, *C*OCl), 146.24 (s, Ar-*C*-1), 144.91 (s, Ar-*C*-2), 133.89 (d, Ar-*C*-5), 129.24 (d, Ar-*C*-6), 128.81 (s, Ar-*C*-4), 124.86 (d, Ar-*C*-3), 21.42 (q, *C*H_3) ppm.

2-(4-Methyl-3-nitrophenyl)-4,6-bis(4-methylphenyl)-1,3,5-triazine (4a)

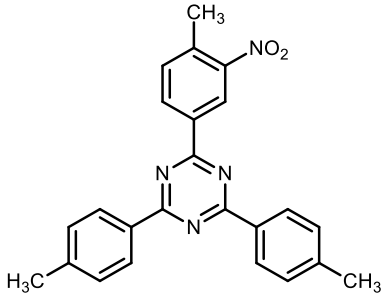

At 0 °C, antimony(V) chloride (8.48 mL, 66.1 mmol) was carefully added to a solution of crude 4-methyl-3-nitrobenzoic chloride (**2a,** 11.0 g, 55.0 mmol) and *p*-methylbenzonitrile (**1**, 12.9 g, 110 mmol) in chloroform (100 mL). The mixture was heated to reflux for 16 h and the resulting yellow oxonium salt was filtered off. At 0 °C, it was added to 28 % aqueous ammonia (500 mL) in small batches. After 2 h of stirring at room temperature, the colorless solid was filtered off and extracted with boiling chloroform (3 x 250 mL). The solvent was evaporated in vacuo yielding 12.9 g (32.5 mmol, 59 %) of a colorless solid, m. p. 254 °C.

^{1}H-NMR (500 MHz, $CDCl_3$): δ = 9.24 (d, 1H, *J* = 1.7 Hz, Ar-*H*-2), 8.80 (dd, 1H, *J* = 8.0 Hz, *J* = 1.7 Hz, Ar-*H*-6), 8.59 (m_c (d), 4H, *J* = 8.1 Hz, Ar'-*H*-2,6), 7.49 (d, 1H, *J* = 8.0 Hz, Ar-*H*-5), 7.35 (m_c (d), 4H, *J* = 8.1 Hz, Ar'-*H*-3,5), 2.69 (s, 3H, Ar-CH_3), 2.47 (s, 6H, Ar'-CH_3) ppm.

^{13}C-NMR (125 MHz, $CDCl_3$): δ = 171.70 (s, Tri-*C*-1), 169.33 (s, Tri-*C*-3,5), 149.86 (s, Ar-*C*-3), 143.39 (Ar'-*C*-4), 137.33 (s, Ar-*C*-4), 135.93 (s, Ar-*C*-1), 133.11 (s, Ar'-*C*-1), 133.01 (d, Ar-*C*-5), 132.62 (d, Ar-*C*-6), 129.42 (d, Ar'-*C*-3,5), 128.99 (d, Ar'-*C*-2,6), 124.90 (d, Ar-*C*-2), 21.75 (q, Ar'-*C*H_3), 20.61 (q, Ar-*C*H_3) ppm.

IR (ATR): $\tilde{\nu}$ = 3036, 3014 (aryl-H), 2982, 2922, 2852 (CH-val.), 1609, 1581, 1506, 1408 (arom. C=C, arom. C=N), 1350 (C-N-val.), 1267 (aryl-NO_2), 802 (1,4-disubst. aryl, 1,3,4-trisubst. aryl) cm^{-1}.

HRMS (EI): *m/z* = calcd. 396.1586; found 396.1577 (Δ 2.1 ppm).

Elemental analysis ($C_{24}H_{20}N_4O_2$) (396.44): calcd. C 72.71 H 5.08 N 14.13; found C 72.62 H 5.04 N 13.97.

2-(4-Methyl-2-nitrophenyl)-4,6-bis(4-methylphenyl)-1,3,5-triazine (4b)

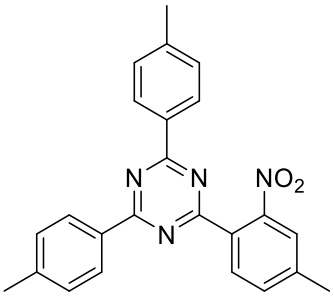

At 0 °C, antimony(V) chloride (4.26 mL, 33.2 mmol) was carefully added to a solution of 4-methyl-2-nitrobenzoic chloride (**2b**, 5.51 g, 27.6 mmol) and 4-methylbenzonitrile (**1**, 6.46 g, 55.2 mmol) in chloroform (80 mL). After heating to reflux for 16 h, the resulting yellow oxonium salt was filtered off, added in portions to aqueous ammonia (28 %, 250 mL) at 0 °C, and stirred for 16 h at room temperature. The colorless solid was filtered off and separated from antimon oxide by Soxhlet extraction with chloroform for 15 h. Removal of the solvent yielded 6.00 g (54 %) of a colorless solid, m.p. 160 °C.

FTIR (ATR): $\tilde{\nu}$ = 3034, 3015 (aryl-C-H), 2917 (C-H), 1610, 1581, 1508, 1408 (arom. C=C, arom. C=N), 1362 (C-N), 1301 (CH), 1179 (aryl-NO_2), 800 (1,4-disubst. aryl, 1,2,4-trisubst. aryl) cm^{-1}.

^{1}H-NMR (500 MHz, $CDCl_3$): δ = 8.52 (m_c (d), 4H, *J* = 8.1 Hz, Ar'-*H*-2,6), 8.32 (d, 1H, *J* = 8.0 Hz, Ar-*H*-6), 7.54 (s, 1H, Ar-*H*-3), 7.49 (m_c (d), 1H, *J* = 8.0 Hz, Ar-*H*-5), 7.33 (m_c (d), 4H, *J* = 8.1 Hz, Ar'-*H*-3,5), 2.50 (s, 3H, Ar-CH_3), 2.44 (s, 6H, Ar'-CH_3) ppm.

^{13}C-NMR (125 MHz, $CDCl_3$): δ = 171.61 (s, Tri-*C*-4,6), 169.70 (s, Tri-*C*-2), 150.84 (s, Ar-*C*-2), 143.41 (s, Ar'-*C*-4), 143.03 (s, Ar-*C*-4), 133.02 (s, Ar'-*C*-1), 132.08 (d, Ar-*C*-5), 131.50 (d, Ar-*C*-6), 129.47 (d, Ar'-*C*-3,5), 129.09 (d, Ar'-*C*-2,6), 127.86 (s, Ar-*C*-1), 124.18 (d, Ar-*C*-3), 21.74 (q, Ar'-*C*H_3), 21.32 (q, Ar-*C*H_3) ppm.

MS (EI, 70 eV): *m/z* (%) = 396 (50) $[M]^{+\cdot}$. **HRMS** (EI): *m/z* = calcd. 396.1586; found 396.1579 (Δ 2.0 ppm).

Elemental analysis $C_{24}H_{20}N_4O_2$ (396.44): calcd. C 72.71, H 5.08, N 14.13; found C 72.84, H 5.07, N 14.04.

2-(4-Carboxy-3-nitrophenyl)-4,6-bis(4-carboxyphenyl)-1,3,5-triazine (5a)

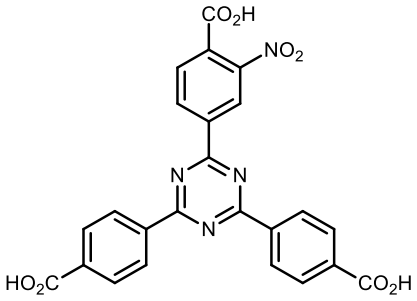

Tetrabutylammonium permanganate (1.38 g, 3.81 mmol) was added to a solution of 2-(4-methyl-3-nitrophenyl)-4,6-bis(4-methylphenyl)-1,3,5-triazine (**4a,** 250 mg, 635 umol) in pyridine (10 mL). The mixture was stirred for 24 h at 50 °C. Aqueous sodium hydroxide (2 M, 10 mL) was added to the resulting brown reaction mixture followed by filtration. The filtrate was washed with *tert*-butyl methyl ether (3 x 25 mL) and acidified with conc. hydrochloric acid. Filtration yielded 261 mg (540 µmol, 85 %) of a slightly yellow solid, m. p. >300 °C.

^{1}H-NMR (600 MHz, DMSO-d_6): δ = 9.06 (m_c (d), 1H, *J* = 0.9 Hz, Ar-*H*-2), 8.96 (m_c (dd), 1H, *J* = 8.0 Hz, *J* = 0.9 Hz, Ar-*H*-6), 8.74 (d, 4H, *J* = 8.3 Hz, Ar'-*H*-3,5), 8.13 (d, 4H, *J* = 8.3 Hz, Ar'-*H*-2,6), 8.06 (d, 1H, *J* = 8.0 Hz, Ar-*H*-5) ppm.

^{13}C-NMR (150 MHz, DMSO-d_6): δ = 170.69 (s, Ar'-*C*O_2H), 168.89 (s, Tri-*C*-2), 166.72 (s, Tri-*C*-4,6), 165.43 (s, Ar-*C*O_2H), 148.80 (s, Ar-*C*-3), 138.60 (s, Ar-*C*-1), 138.46 (d, Ar-*C*-4), 138.36 (s, Ar'-*C*-4), 134.84 (s, Ar'-*C*-1), 132.56 (d, Ar-*C*-6), 130.75 (d, Ar-*C*-5), 129.76 (d, Ar'-*C*-2,6), 128.94 (d, Ar'-*C*-3,5), 123.27 (d, Ar-*C*-2) ppm.

IR (ATR): $\tilde{\nu}$ = 3072 (br., OH), 1697 (C=O), 1582, 1513, 1408 (arom. C=C, arom. C=N), 1356 (C-N-Val.), 1277 (aryl-NO_2), 827 (1,4-disubst. aryl, 1,2,4-trisubst. aryl) cm^{-1}.

MS (EI, 70 eV): *m/z* (%) = 486 (5) $[M]^{+\cdot}$, 442 (97) $[M - CO_2]^{+\cdot}$. **HRMS** (EI): *m/z* = calcd. 486.0811; found. 486.0796 (Δ 3.3 ppm).

Elemental analysis ($C_{24}H_{14}N_4O_8$) (486.39): calcd. C 59.26 H 2.90 N 11.52; ($C_{24}H_{14}N_4O_8 \cdot H_2O$) (504.42): calcd. C 56.95 H 3.25 N 11.07; found C 56.71 H 3.23 N 11.03.

2-(4-Carboxy-2-nitrophenyl)-4,6-bis(4-carboxyphenyl)-1,3,5-triazine (5b)

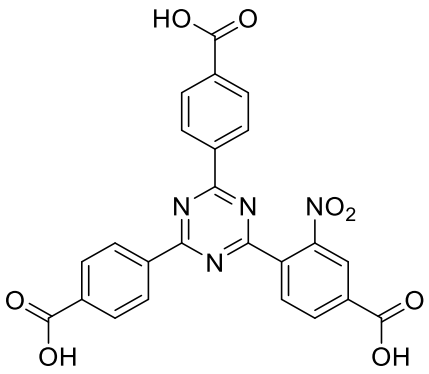

Method A: A solution of chromium(VI) oxide (7.39 g, 73.9 mmol) in acetic anhydride (24 mL) was added to a solution of 2-(4-methyl-2-nitrophenyl)-4,6-bis(4-methylphenyl)-1,3,5-triazine (**4b,** 2.20 g, 5.55 mmol) in 24 mL of acetic acid and 5.2 mL of conc. sulfuric acid in such a way that the temperature did not exceed 50 °C. After stirring for 16 h at room temperature, the brown reaction mixture was carefully poured on ice water. The resulting precipitate was filtered off and washed intensively with water. After dissolution with aqueous sodium hydroxide (2 M, 25 mL) and filtration, the filtrate was acidified with half conc. hydrochloric acid. The resulting solid was recrystallized from *N*,*N*-dimethylformamide/water (2:1) yielding 2.31 g (4.75 mmol, 86 %) of a slightly yellow solid.

Method B: Tetrabutylammonium permanganate[3] (12.9 g, 25.6 mmol) was added to a solution of 2-(4-methyl-2-nitro)-4,6-bis(4-methylphenyl)-1,3,5-triazine (**4b,** 2.35 g, 5.93 mmol) in pyridine (50 mL). After stirring for 24 h at 50 °C, aqueous sodium hydroxide (2 M, 50 mL) was added and the mixture was filtered. The filtrate was acidified with conc. hydrochloric acid, the resulting solid was filtered off and washed thoroughly with water. 2.63 g (5.41 mmol, 91 %) of **5** was obtained as a slightly yellow solid, m.p. >300°C.

IR (ATR): $\tilde{\nu}$ = 3069 (br., OH), 1692 (C=O), 1580, 1513, 1408 (arom. C=C, arom. C=N), 1358 (C-N), 1238 (aryl-NO_2), 828 (1,4-disubst. aryl, 1,2,4-trisubst. aryl) cm^{-1}.

^{1}H-NMR (500 MHz, DMSO-d_6): δ = 8.67 (m_c (d), 4H, *J* = 8.4 Hz, Ar'-*H*-3,5), 8.52 (d, 1H, *J* = 8.0 Hz, Ar-*H*-6), 8.43 – 8.42 (m, 1H, Ar-*H*-3), 8.41 – 8.38 (m, 1H, Ar-*H*-5), 8.17 (m_c (d), 4H, J = 8.4 Hz, Ar'-*H*-2,6) ppm.

^{13}C-NMR (125 MHz, DMSO-d_6): δ = 171.10 (s, Ar'-*C*O_2H), 170.49 (s, Tri-*C*-2), 167.31 (s, Tri-*C*-4,6), 165.99 (s, Ar-*C*O_2H), 150.27 (s, Ar-*C*-2), 139.40 (s, Ar-*C*-4), 138.50 (s, Ar'-*C*-1), 136.07 (s, Ar'-*C*-4), 133.14 (d, Ar-*C*-5), 132.43 (d, Ar-*C*-6), 131.55 (s, Ar-*C*-1), 130.32 (d, Ar'-*C*-2,6), 139.34 (d, Ar'-*C*-3,5), 124.87 (d, Ar-*C*-3) ppm.

MS (EI, 70 eV): *m/z* (%) = 486 (18) $[M]^{+\cdot}$. **HRMS** (EI): *m/z* = calcd. 486.0811; found 486.0797 (Δ 2.9 ppm).

Elemental analysis $C_{24}H_{14}N_4O_8$ (486.39): calcd. C 59.26, H 2.90, N 11.52; $C_{24}H_{14}N_4O_8 \cdot 1.8H_2O$ (518.76): calcd. C 55.57, H 3.42, N 10.80; found C 55.18, H 3.72, N 10.55.

2-(2-Amino-4-carboxyphenyl)-4,6-bis(4-carboxyphenyl)-1,3,5-triazine (5c)

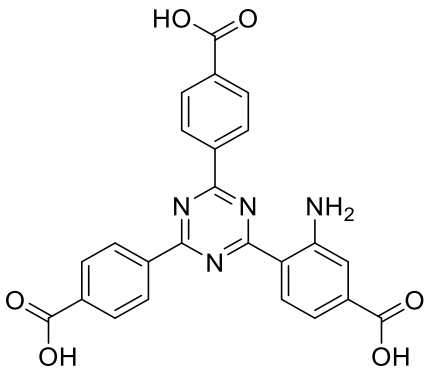

Method A: A mixture of 2-(4-carboxy-2-nitrophenyl)-4,6-bis(carboxy-phenyl)-1,3,5-triazine (**5b**, 2.50 g, 5.18 mmol) and tin(II) chloride-hydrate (11.7 g, 51.8 mmol) in aqueous acetic acid (2 M, 32.5 mL, 65.0 mmol) and ethanol (250 mL) was heated to reflux for 48 h. After removal of the solvents in vacuo, distilled water was added and aqueous sodium hydroxide (2 M) was added until pH = 9.5 - 10.0 was reached. A yellow solid was filtered off through Celite. The filtrate was acidified with conc. hydrochloric acid until pH = 3.5 - 4.0 was reached. The resulting solid was filtered off and washed thoroughly with water resulting in 1.49 g (3.27 mmol, 63 %) of a yellow solid, m.p. >300 °C.

Method B: 2-(4-Carboxy-2-nitrophenyl)-4,6-bis(4-carboxyphenyl)-1,3,5-triazine (**5b**, 590 mg, 1.21 mmol) was suspended in water (15 mL), and potassium carbonate was added until the entire solid was dissolved. Sodium dithionite (1.05 g, 6.07 mmol) and ethanol (15 mL) were added and the mixture was stirred for 1 h at room temperature Ethanol was removed under reduced pressure and the residue was poured into conc. hydrochloric acid. The precipitate was washed with water and dried, to yield 440 mg (964 µmol, 79 %) of a yellow solid.

IR (ATR): $\tilde{\nu}$ = 3300 (br., OH, NH), 1691 (C=O), 1619, 1581, 1499 (arom. C=C, arom. C=N), 1355 (C-N), 760 (1,4-disubst. aryl, 1,2,4-trisubst. aryl) cm^{-1}.

^{1}H-NMR (600 MHz, DMSO-d_6): δ = 8.72 (m_c (d)*, 1H, Ar-*H*-6), 8.71 (m_c (d), 4H, *J* = 8.2 Hz, Ar'-*H*-2,6), 8.19 (m_c (d), 4H, *J* = 8.2 Hz, Ar'-*H*-3,5), 7.66 (br. s, 2H, NH_2), 7.58 (d, 1H, *J* = 1.3 Hz, Ar-*H*-3), 7.22 (dd, 1H, *J* = 8.4 Hz, *J* = 1.3 Hz, Ar-*H*-5) ppm. *overlapping signals, determination of *J* was not possible.

^{13}C-NMR (150 MHz, DMSO-d_6): δ = 171.97 (s, Tri-*C*-2), 169.86 (s, Tri-*C*-4,6), 167.39 (s, Ar-*C*O_2H), 167.21 (s, Ar'-*C*O_2H), 151.32 (s, Ar-*C*-2), 138.41 (s, Ar'-*C*-1), 136.57 (s, Ar'-*C*-4), 136.22 (s, Ar-*C*-4), 131.06 (d, Ar-*C*-6), 129.81 (d, Ar'-*C*-3,5), 128.59 (d, Ar'-*C*-2,6), 118.55 (d, Ar-*C*-3), 116.93 (s, Ar-*C*-1), 115.38 (d, Ar-*C*-5) ppm.

HRMS (EI): *m/z* = calcd. 456.1070; found 456.1070 (Δ 0.0 ppm). $C_{24}H_{16}N_4O_6$ (456.11): calcd. C 63.16, H 3.53, N 12.28.

Elemental analysis $C_{24}H_{16}N_4O_6 \cdot H_2O$ (474.42): calcd. C 60.77, H 3.82, N 11.82; found C 60.65, H 3.65, N 11.73.

2,4,6-Tris(4-methylphenyl)-1,3,5-triazine

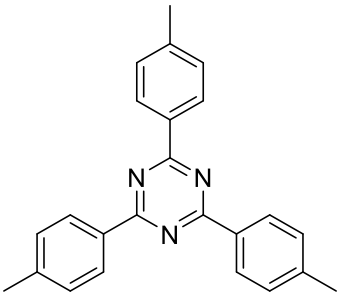

4-Methylbenzonitrile (**1**, 10.0 g, 86.0 mmol) was slowly added to trifluoromethanesulfonic acid (20.9 mL, 236 mmol). After stirring at room temperature for 17 h, the yellow reaction mixture was poured on ice and neutralized with aqueous ammonia solution (2 M). The white precipitate was filtered by suction filtration and washed with water and acetone. Recrystallization from toluene gave 8.1 g of 2,4,6-tris(4-methylphenyl)-1,3,5-triazine (23.0 mmol, 80 %) in form of white crystals.

IR (ATR): $\tilde{\nu}$ = 1610 (*m*), 1583 (*m*), 1510 (*vs*), 1406 (*m*), 1370 (*s*), 1298 (*w*), 1178 (*m*), 1149 (*w*), 1111 (*w*), 1036 (*w*), 1018 (*w*), 963 (*w*), 852 (*w*), 833 (w), 797 (*s*), 772 (*w*), 712 (w), 642 (*w*).

^{1}H-NMR (400 MHz, $CDCl_3$): δ = 8.63 (d, *J* = 8.0 Hz, 6 H), 7.34 (d, *J* = 8.0 Hz, 6 H), 2.46 (s, 9 H).

^{13}C-NMR (100 MHz, $CDCl_3$):δ = 171.6, 143.1, 134.0, 129.1, 21.9 (3 x CH_3).

HRMS (ESI^+, $[M+H]^+$: calc. for $[C_{24}H_{21}N_3 + H^+]^+$: 352.1808, found: 352.18055.

4,4',4''-(1,3,5-Triazine-2,4,6-triyl)-tribenzoic acid (5d, TATB)

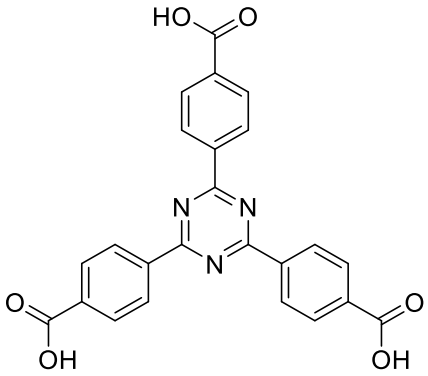

A solution of 2,4,6-tris(4-methylphenyl)-1,3,5-triazine (7.92 g, 22.5 mmol), acetic acid (217 mL, 3.79 mol) and sulfuric acid (12.5 mL, 234 mmol) was stirred, while chromium (VI)-oxide (20.5 g, 205 mmol) and acetic anhydride (13.7 mL, 145 mmol) were added. The green slurry was stirred at room temperature for 72 h, then poured into water (900 mL) under ice cooling, well mixed and filtered by suction filtration. The green solid was washed with water and dissolved in aqueous sodium hydroxide solution (2 M, 500 mL). After filtration, the solution was acidified with hydrochloric acid (2 M) obtaining a slightly green crude product. After recrystallization from *N*,*N*-dimethylformamide, 7.37 g (16.7 mmol, 74 %) of as a white crystalline product was obtained.

IR (ATR): $\tilde{\nu}$ = 1703 (*vs*), 1678 (*w*), 1626 (*s*), 1583 (*s*), 1516 (*vs*), 1437 (*m*), 1408 (*m*), 1379 (*s*), 1360 (*s*), 1303 (*w*), 1271 (*vs*), 1250 (*w*), 1175 (*w*), 1150 (*w*), 1117 (*m*), 1106 (*m*), 1066 (*w*), 1016 (*m*), 879 (*m*), 852 (*w*), 829 (*m*), 793 (w), 781 (*s*), 766 (*vs*), 691 (*m*), 670 (*m*).

^{1}H-NMR (400 MHz, DMSO-d_6): δ = 13.31 (s, 3 H), 8.74 (d, J = 8.3 Hz, 6 H), 8.14 (d, J = 8.4 Hz, 6 H).

^{13}C-NMR (100 MHz, DMSO-d_6): δ = 170.5, 166.8, 138.7, 134.6, 129.8, 128.8.

HRMS (ESI^-, $[M+H]^-$: calc. for $[C_{24}H_{15}N_3O_6 - H^+]^-$: 440.0888, found: 440.0886.

3.2 MOF synthesis

PCN-6

PCN-6 was synthesized according to literature.[4] For the reaction, a 100 mL Schott-Duran glass bottle with a PBT cap equipped with a Teflon seal was used. $Cu(NO_3)_2 \cdot 3H_2O$ (271 mg, 1.12 mmol) and 4,4',4''-(1,3,5-triazine-2,4,6-triyl)-tribenzoic acid (**5d**, 100 mg, 0.227 mmol) were dissolved in 15 mL of *N*,*N*-dimethylformamide by ultrasonic treatment. The reaction mixture was heated within 1 h to 75 °C and held at this temperature for 48 h and afterwards cooled to room temperature within 24 h. The resulting turquoise powder was collected by centrifugation (10 min, 20 000 rpm) and washed three times with *N*,*N*-dimethylformamide and dried under reduced pressure at room temperature.

PCN-6-NO_2 (*meta*)

A 100 mL Schott-Duran glass bottle with a PBT cap equipped with a Teflon seal was used. $Cu(NO_3)_2 \cdot 3H_2O$ (217 mg, 1.12 mmol) and 2-(4-carboxy-2-nitrophenyl)-4,6-bis(4-carboxyphenyl)-1,3,5-triazine (**5b,** 110 mg, 0.226 mmol) were dissolved in 15 mL of *N*,*N*-dimethylformamide by ultrasonic treatment. The reaction mixture was heated within 1 h to 75 °C and held at this temperature for 48 h and afterwards cooled to room temperature within 24 h. The resulting turquoise-green powder was collected by centrifugation (10 min, 20 000 rpm) and washed three times with *N*,*N*-dimethylformamide and dried under reduced pressure at room temperature.

PCN-6-NO_2 (*ortho*)

A 100 mL Schott-Duran glass bottle with a PBT cap equipped with a Teflon seal was used. $Cu(NO_3)_2 \cdot 3H_2O$ (217 mg, 1.12 mmol) and 2-(4-carboxy-3-nitrophenyl)-4,6-bis(4-carboxyphenyl)-1,3,5-triazine (**5a,** 110 mg, 0.226 mmol) were dissolved in 15 mL of *N*,*N*-dimethylformamide by ultrasonic treatment. The reaction mixture was heated within 1 h to 75 °C and held at this temperature for 48 h and afterwards cooled to room temperature within 24 h. The resulting green-blue powder was collected by centrifugation (10 min, 20 000 rpm) and washed three times with *N*,*N*-dimethylformamide and dried under reduced pressure at room temperature.

PCN-6-NH_2 (*meta*)

A 100 mL Schott-Duran glass bottle with a PBT cap equipped with a Teflon seal was used. $Cu(NO_3)_2 \cdot 3H_2O$ (271 mg, 1.12 mmol) and 2-(2-amino-4-carboxyphenyl)-4,6-bis(4-carboxyphenyl)-1,3,5-triazine (**5c**, 102 mg, 0.225 mmol) were dissolved in 15 mL of *N*,*N*-dimethylformamide by ultrasonic treatment. The reaction mixture was heated within 1 h to 75 °C and held at this temperature for 48 h and afterwards cooled to room temperature within 24 h. The resulting green powder was collected by centrifugation (10 min, 20 000 rpm) and washed three times with *N*,*N*-dimethylformamide and dried under reduced pressure at room temperature.

4. Further Characterization of PCN-6-R (R = -H, -NO_2 (*meta* or *ortho*) and -NH_2 (*meta*))

TG measurements

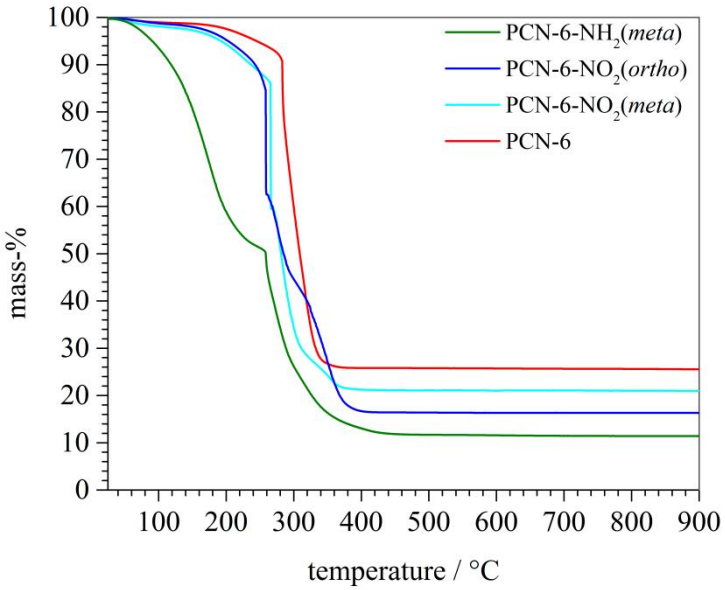

Figure S1: TGA curves of the synthesized PCN-6-R frameworks (red: PCN-6; cyan: PCN-6-NO_2 (*meta*); blue: PCN-6-NO_2 (*ortho*); green: PCN-6-NH_2 (*meta*)) showing a decomposition of the framework structure ranging from moderate temperatures (for PCN-6-NH_2 (*meta*)) and about 350 °C (for PCN-6-NO_2(*ortho*)).

Crystallinity and stability of the PCN-6-R frameworks after degassing of the sample at 120 °C and nitrogen sorption measurements

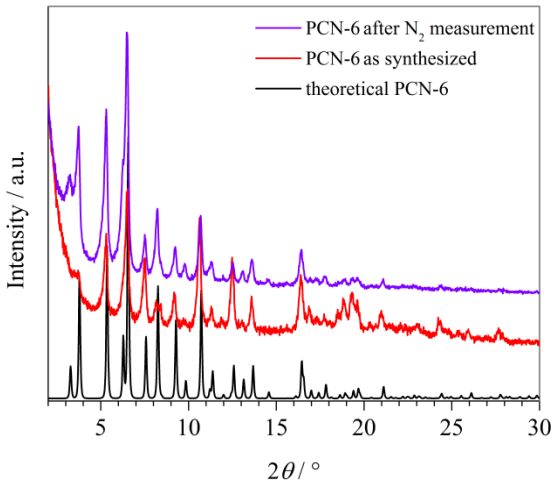

Figure S2: XRD measurements demonstrating the crystallinity and stability of the PCN-6 framework after degassing the sample at 120 °C over night and following nitrogen sorption measurement. (Black: theoretical PCN-6; red: PCN-6 as synthesized; violet: PCN-6 after N_2 measurement)

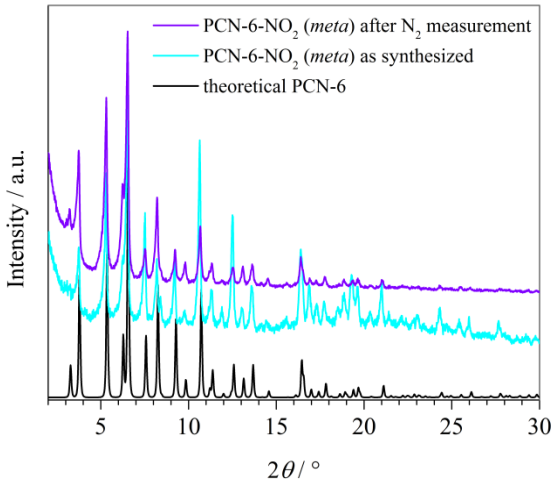

Figure S3: XRD measurement demonstrating the crystallinity and stability of the PCN-6-NO_2 (*meta*) framework after degassing the sample at 120 °C over night and following nitrogen sorption measurement. (Black: theoretical PCN-6; cyan: PCN-6-NO_2 (*meta*) as synthesized; violet: PCN-6-NO_2 (*meta*) after N_2 measurement)

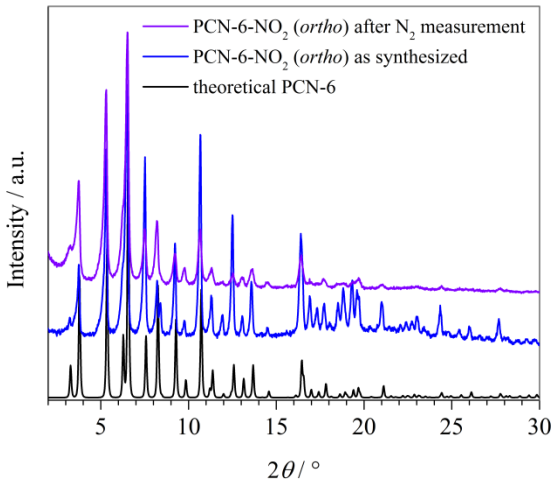

Figure S4: XRD measurement demonstrating the crystallinity and stability of the PCN-6-NO_2 (*ortho*) framework after degassing the sample at 120 °C over night and following nitrogen sorption measurement. (Black: theoretical PCN-6; blue: PCN-6-NO_2 (*ortho*) as synthesized; violet: PCN-6-NO_2 (*ortho*) after N_2 measurement)

Temperature stability measurements

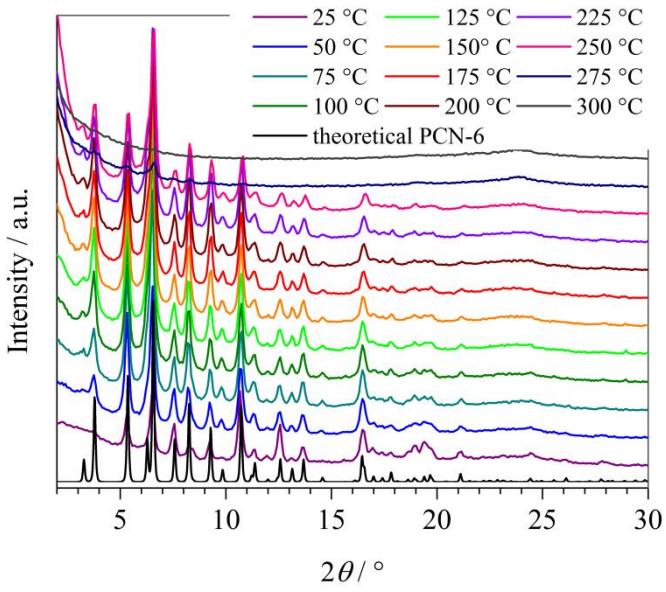

Figure S5: Temperature stability of the PCN-6 examined by heating the sample on a D8 Bruker instrument under air from 25 °C up to 300 °C. The framework is stable up to 250 °C before starting to decompose.

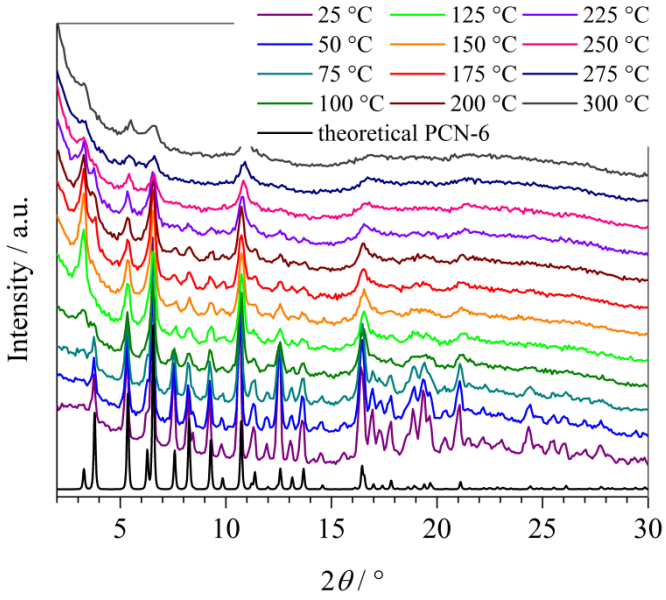

Figure S6: Temperature stability of the MOF PCN-6-NO_2 (*meta*) measured by heating the sample at a D8 Bruker instrument in air from 25 °C up to 300 °C. The framework is stable up to 175 °C before starting to decompose.

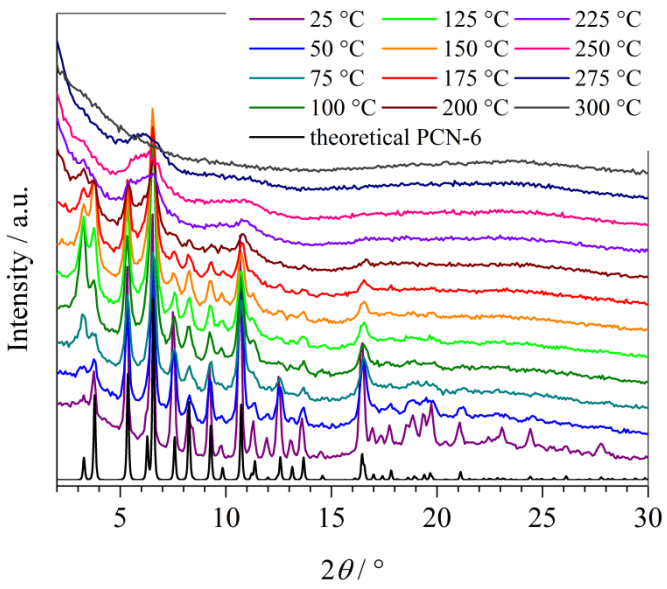

Figure S7: Temperature stability of the MOF PCN-6-NO_2 (or*tho*) measured by heating the sample at a D8 Bruker instrument in air from 25 °C up to 300 °C. The framework is stable up to 175 °C before starting to decompose.

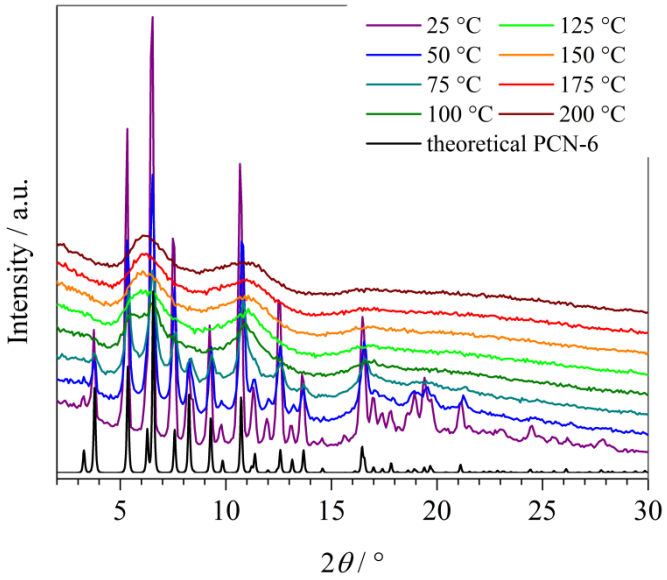

Figure S8: Temperature stability of the MOF PCN-6-NH_2 (*meta*) measured by heating the sample at a D8 Bruker instrument in air from 25 °C up to 200 °C. The framework is stable up to 75 °C before starting to decompose.

Humidity stability test of PCN-6-NO_2 (*meta* or *ortho*)

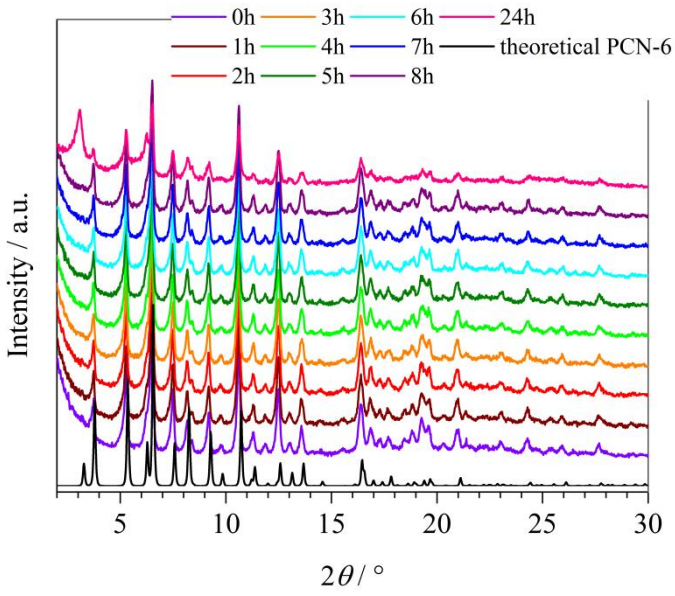

Figure S9: XRD measurements of the MOF PCN-6-NO_2 (*meta*) after different times of exposure to a humidity of 60 % at room temperature. The framework is stable under these conditions for up to about 8 h.

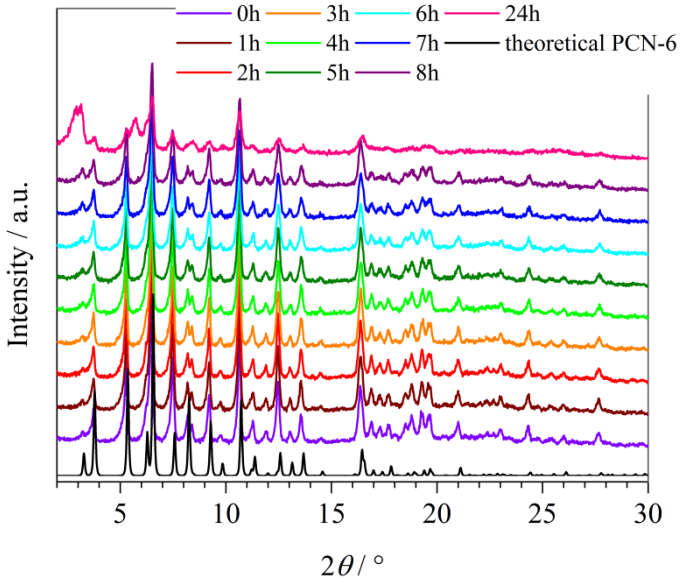

Figure S10: XRD measurements of the MOF PCN-6-NO_2 (*ortho*) after different times of exposure to a humidity of 60 % at room temperature. The framework is stable under these conditions for up to about 8 h.

Pawley refinement of the PXRD patterns

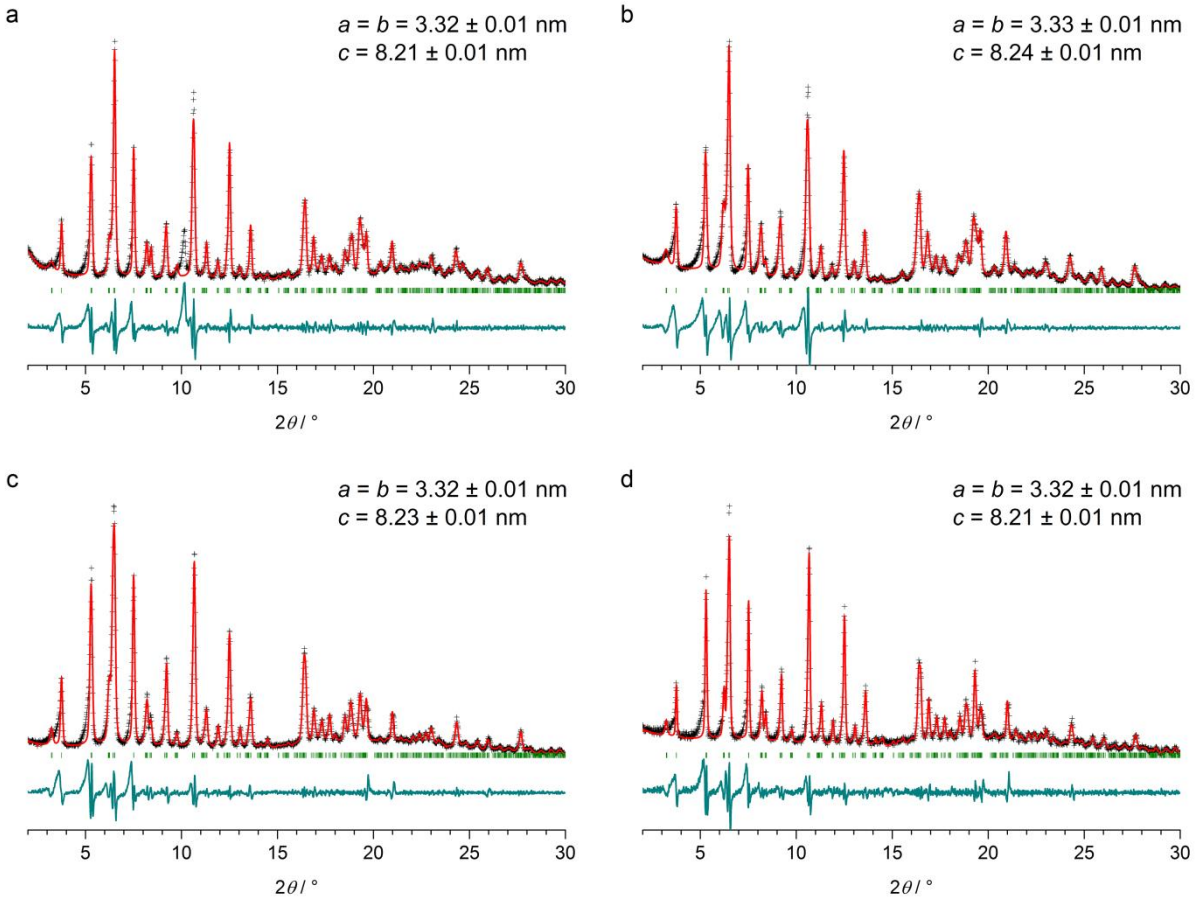

Figure S11: Experimental (black) and Pawley-refined (red) powder XRD patterns, difference (cyan) and observed reflections (green). (a) PCN-6, (b) PCN-6-NO_2 (*meta*), (c) PCN-6-NO_2 (*ortho*), and (d) PCN-6-NH_2 (*meta*).

Pawley refinements were carried out using a Pseudo-Voigt peak shape function and without accounting for the asymmetry at low 2θ values that is due to the experimental setup. Using an experimentally determined instrumental broadening of 0.10 ° 2θ, we refined the crystallite size along the *a*, *b* and *c* axis (Table S1).

Table S1. R-factors and refined crystallite sizes of the PCN-6 MOFs.

	wR_p / %	R_p / %	crystal size *a*, *b* / µm	crystal size *c* / µm
PCN-6	21.19	21.16	1.70	0.43
PCN-6-NO_2 (*meta*)	20.58	20.21	1.47	0.43
PCN-6-NO_2 (*ortho*)	16.17	17.58	1.45	0.66
PCN-6-NH_2 (*meta*)	20.51	23.66	2.76	0.88

Pictures

Figure S12: Differently colored triazine linkers (left: TATB-H (**5d**); middle left: TATB-NO_2 (*meta*) (**5b**) middle right: TATB-NO_2 (*ortho*) (**5a**) and right: TATB-NH_2 (*meta*) (**5c**)).

UV-Vis spectra of the triazine linkers

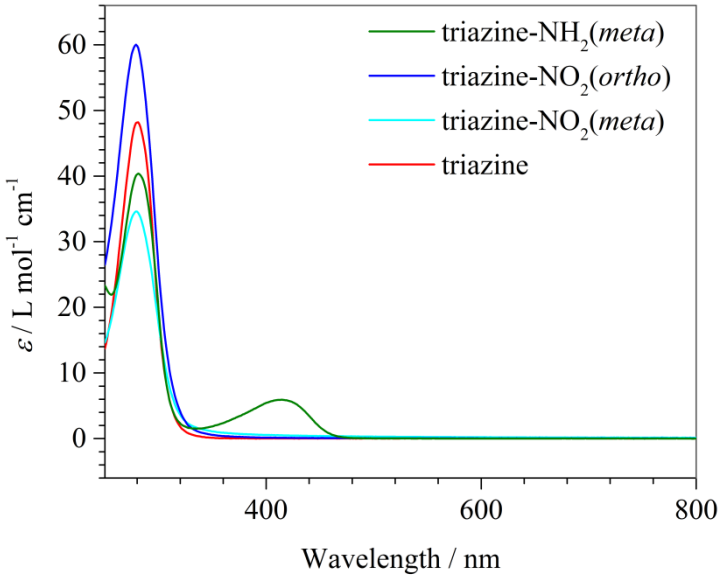

Figure S13: UV-Vis spectra of the TATB-R linkers as 25 µM dioxane solutions; red: TATB-H (**5d**); cyan: TATB-NO_2 (*meta*) (**5b**); blue: TATB-NO_2 (*ortho*) (**5a**); green: TATB-NH_2 (*meta*) (**5c**)).

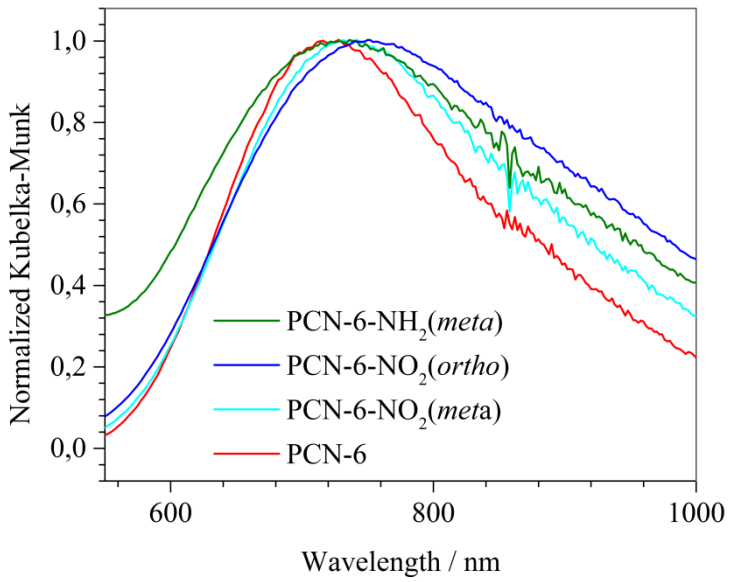

Figure S14: Selected region of the diffuse reflectance spectra of the unfunctionalized and functionalized MOFs normalized to their respective maximum at around 730 nm; red: PCN-6; cyan: PCN-6-NO_2 (*meta*); blue: PCN-6 -NO_2 (*ortho*); green: PCN-6-NH_2 (*meta*).

5. References

[1] D. Klank, Partikelwelt, 2 (2003) 6-7.

[2] T. Sala, M.V. Sargent, J. Chem. Soc., Chem. Commun., (1978) 253-254.

[3] D. Martin, M. Bauer, V.A. Pankratov, Russ. Chem. Rev., 47 (1978) 975-990.

[4] S. Ma, D. Sun, M. Ambrogio, J.A. Fillinger, S. Parkin, H.C. Zhou, J. Am. Chem. Soc., 129 (2007) 1858-1859.

3.2.2 Eisen(III)-basierte Misch-Linker-MOFs mit MIL-143-Topologie

Durch Kombination von linearen und triangulären Linkern konnten fünf Eisen(III)-MOFs mit MIL-143-Topologie dargestellt werden. Als trianguläre Linker wurden sowohl der unfunktionalisierte **H_3TATB**-Linker als auch die beiden nitrofunktionalisierten Linker **H_3TATB-NO_2(*meta*)** und **H_3TATB-NO_2(*ortho*)** verwendet. Diese wurden mit $FeCl_3$•$6H_2O$ und Terephthalsäure (**BDC**) bzw. 2-Aminoterephthalsäure (**BDC-NH_2**) zu sogenannten Mischlinker-MOFs umgesetzt. Diese unterscheiden sich voneinander dadurch, dass sie nicht funktionalisiert (**Fe-TATB-BDC-a**), aminofunktionalisiert (**Fe-TATB-BDC-b**), nitrofunktionalisiert (**Fe-TATB-BDC-c**, **Fe-TATB-BDC-d**) oder sogar nitro- und aminofunktionalisiert (**Fe-TATB-BDC-e**) vorliegen. Alle fünf MOFs wurden vollständig charakterisiert, sowie die Stabilität gegenüber Wasser, 1M Salzsäure und 1M Natronlauge getestet. Während sie in Wasser auch nach 14 Tagen noch stabil sind, wird sowohl unter sauren als auch unter basischen Bedingungen eine Zersetzung der MOFs beobachtet.

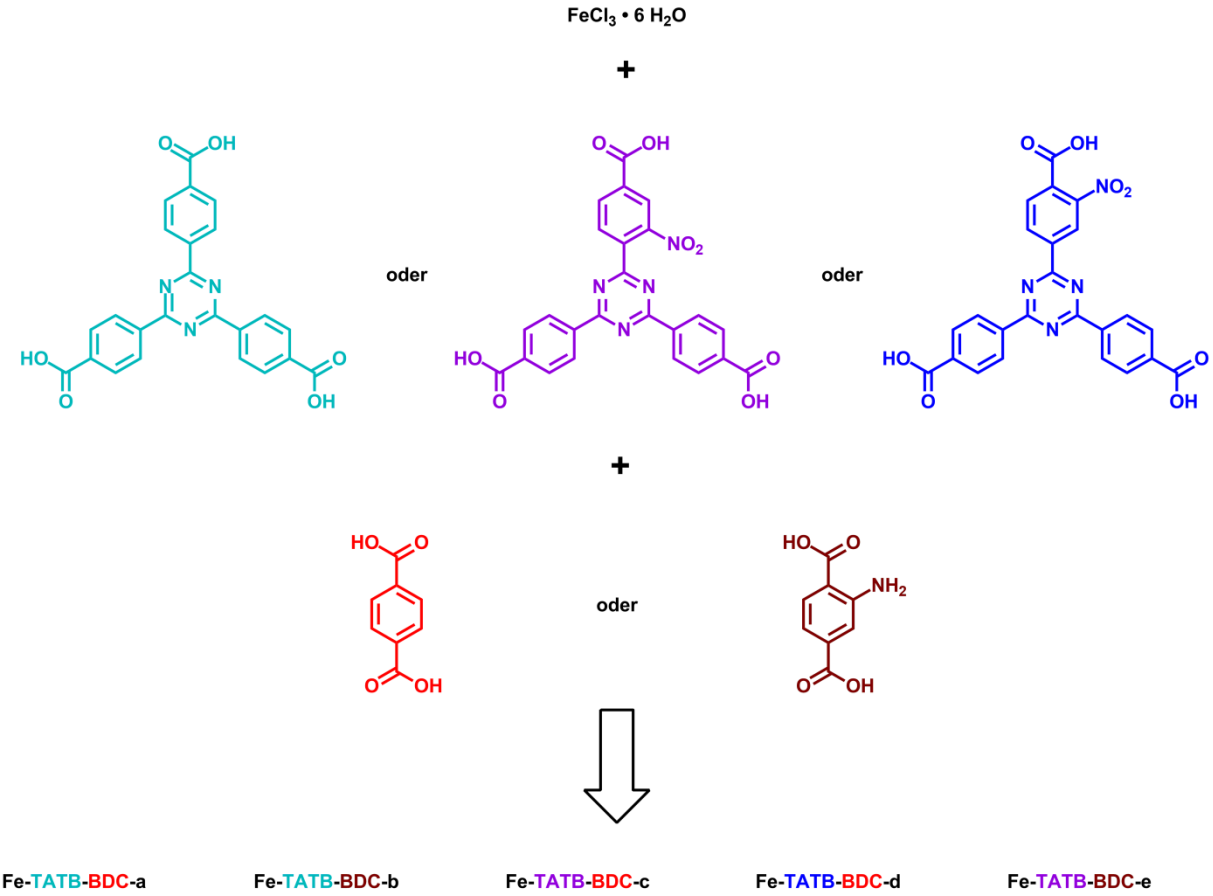

Abb. 23: Syntheseübersicht zur Darstellung der fünf Eisen(III)-MOFs.

Zusätzlich wurden Versuche zur Erweiterung der MOF-Struktur unternommen. Dafür wurden entweder die linearen Terephthalsäure-Linker durch den H_2BPDC-Linker ersetzt oder die

H_3TATB-Linker durch den erweiterten H_3TAPB-OMe-Linker. Auch die Darstellung eines MOFs durch die Verwendung der beiden erweiterten Linker H_2BPDC und H_3TAPB-OMe wurde versucht. Ausgehend vom H_3TAPB-OMe-Linker und Terephthalsäure konnte auf diese Weise der erweiterte MOF Fe-TAPB-BDC erhalten werden. Versuche mit dem H_2BPDC-Linker sowie mit beiden erweiterten Linkern H_2BPDC und H_3TAPB-OMe waren nicht erfolgreich.

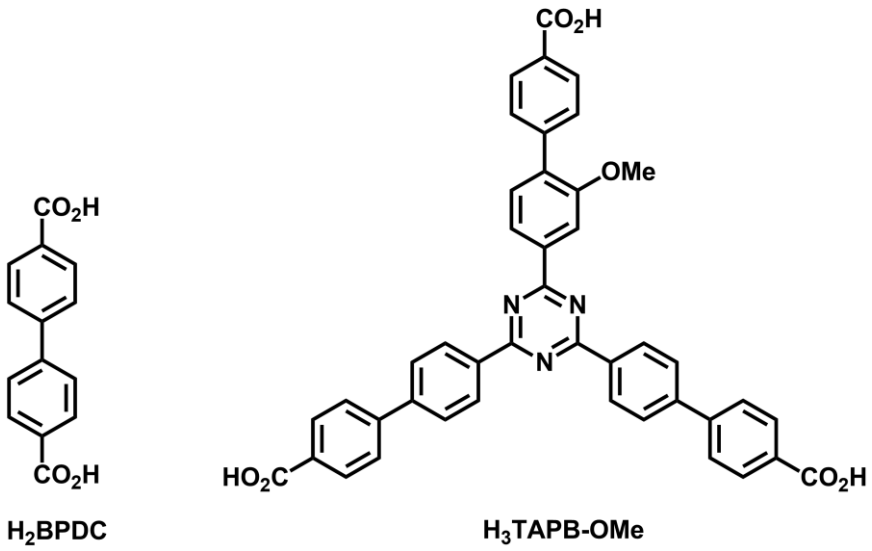

Abb. 24: Eingesetzte Linker zur Erweiterung der MIL-143-Struktur.

Die Ergebnisse sind zusammen gefasst:

E. Virmani, O. Beyer, T. Bein, U. Lüning, U. Ruschewitz, S. Wuttke, **2017**, *in Vorbereitung*.

Bestandteil dieser Dissertation ist die Synthese der nitrofunktionalisierten Linker **H_3TATB-NO_2(*meta*)** und **H_3TATB-NO_2(*ortho*)** sowie des H_3TAPB-OMe-Linkers. Die Darstellung und Charakterisierung der beschriebenen MOFs wurde von ERIKA VIRMANI an der Ludwigs-Maximilian-Universität München durchgeführt. Die Strukturaufklärung wurde von UWE RUSCHEWITZ durchgeführt.

Topology-guided functional multiplicity of iron(III)-based metal-organic frameworks

Erika Virmani,[a] Ole Beyer,[b] Thomas Bein,[a] Ulrich Lüning,[b] Uwe Ruschewitz[c] and Stefan Wuttke*[a]

Department für Chemie und Center for NanoScience (CeNS), Ludwig-Maximilians-Universität München, Butenandtstraße 11, D-81377 München, Germany

*Christian-Albrechts-Universität zu Kiel, Otto Diels-Institut für Organische Chemie, Otto-Hahn-Platz 4, D-*24118 *Kiel, Germany*

Universität zu Köln, Institut für Anorganische Chemie, Greinstr. 6, D-50939 Köln, Germany

**E-mail: stefan.wuttke@cup.uni-muenchen.de*

Abstract

We report here the synthesis and characterization of a new series of mixed-linker iron(III)-based metal-organic frameworks (MOFs) consisting of dicarboxylate linkers (1,4-benzendicarboxylic acid ≡ BDC or its amino functionalized derivative) and tricarboxylate linkers (4,4',4''-[1,3,5-triazine-2,4,6-triyl]tribenzoic acid ≡ TATB or its nitro functionalized derivative). The resulting mesoporous MOFs with MIL-143 topology are stable under ambient water conditions for 14 d regardless of the functionalization of the organic linkers. Powder X-ray diffractions reveal high crystallinity of the materials. This structure type is very tolerant to variation in the functional groups (e.g. nitro and/or amino) along the BDC and/or TATB linkers, but is less tolerant to changes in the size of the linkers themselves. It was attempted to replace linear BDC by biphenyl-4,4'-dicarboxylic acid (BPDC) and trigonal TATB by 2,4-bis(4’-carboxy-biphenyl-4-yl)-6-(4’-carboxy-2-methoxy-biphenyl-4-yl)-1,3,5-triazine (TAPB). Of the three additional structures made possible by combinations of these linkers (BDC/TAPB, BPDC/TATB, BPDC/TAPB), only one (BDC/TAPB) yields a crystalline product which, like the BDC/TATB crystal, exhibits MIL-143 topology. However, this material is not very stable and collapses upon guest removal. Our results suggest that the incorporation of diverse functional groups on linkers with different geometries in this new iron(III)-based MOF series offers a simple method of precisely tuning the chemical environment within the pores. More importantly, our work expands the scope of mixed-linker MOFs to include a subset of multivariate MOFs characterized by different functionalities in each type of linker.

1. Introduction

Metal–organic framework (MOF) crystal engineering is based on the study of periodically assembled metal ions or metal clusters (inorganic building units or IBUs, also known as secondary building units or SBUs) and organic linkers (organic building units or OBUs). This concept allows control over the structure of MOFs with respect to their topology. This ability to control structure, composition, porosity, and properties on the molecular level promises potential applications in gas storage[1-3] and gas separation,[4-6] catalysis,[7, 8] chemical sensing,[9, 10] and drug release[11-13]. However, all of these applications are dependent upon the presence of chemical functionality either at the IBU and/or OBU.

Multivariate MOFs (MTV-MOFs) are constructed from a parent MOF structural backbone along which different functionalities are distributed.[14, 15] The disordered spatial arrangement of the functionalities allows the MTV-MOFs to create unique synergistic effects.[14] The random arrangement of the functionalities makes it difficult to draw conclusions about the relationship between structure, spatial arrangement and performance of the MTV-MOFs. Determining the location of randomly dispersed functionalities within MTV-MOFs is a huge scientific challenge that has recently been addressed with a combination of multidimensional solid-state NMR and molecular simulations.[16] This challenge, however, can be circumvented by deliberately placing different functional linkers at specific, defined positions in the MOF scaffold.

By using the so-called mixed linker approach, two or more non-functionalized OBUs can be precisely incorporated into a MOF scaffold with predetermined structural topologies. Three approaches for synthesizing mixed linker MOFs are reported so far. The first approach creates a MOF composed of linkers with different binding sites (mostly carboxylic groups and electron donating nitrogen atoms), but the same linker topology.[17-19] The second approach creates a MOF that is built from different linker topologies but the same binding sites.[3, 20, 21] The third approach is a combination of the previous two by using linkers with different binding sites and different topologies.[22]

Interestingly, up to now only one functional group has been incorporated in MOFs using the mixed linker approach and the functionalization occurs so far only at linear dicarboxylic acid linkers. Therefore, the MOF is assembled by using one functionalized dicarboxylic acid linker and one non-functionalized linker. In this way, nitro, methyl, amino, fluoro, chloro, bromo, hydroxy, diacetoxy, sulfone, sulfonic

acidband dioxole groups[20, 23-33] or different alkyloxy or alkyl groups and even alkyl ether groups of the type –O-$(CH_2)_n$-O-CH_3[34-36] have been successfully incorporated into MOF scaffolds. The amino-functionalization of 1,4-benzendicarboxylic acid has already been addressed through post-synthetic modification with acetic anhydride and derivatives with different alkyl chain length.[37, 38] Recently the Zhou group[39] reported a mixed linker MOF where methyl and amino functional groups had been incorporated at two linker backbones. This MOF is constructed of three linear dicarboxylic acid linkers of varied length (2-amino-1,4-dicarboxylate, 2,2'-dimethylbiphenyl-4,4'-dicarboxylate and 2',5'-dimethoxyterphenyl), and can only be obtained through a multiple step synthesis protocol.

Herein we report the synthesis of new iron(III)-based mixed linker MOFs exhibiting OBUs with different geometries (i.e. linear and triangular) and functionalities (nitro and/or amino). Using different combinations of functionalized and non-functionalized 1,4-benzendicarboxylic acid (BDC) and 4,4',4''-(1,3,5-triazine-2,4,6-triyl)tribenzoic acid (TATB) linkers, it was possible to synthesize MOFs exhibiting the mesoporous MIL-143 topology. After the syntheses of the organic linkers and the corresponding iron(III)-based mixed linker MOFs, the materials were fully characterized in terms of their crystal structure, morphology, porosity, thermal and water stability. In addition, we describe the extension of either the linear BDC, by replacing it with biphenyl-4,4'-dicarboxylic acid (BPDC) or the trigonal TATB linker by replacing it with 2,4-bis(4'-carboxy-biphenyl-4-yl)-6-(4'-carboxy-2-methoxy-biphenyl-4-yl)-1,3,5-triazine (TAPB) which led to MOFs with reduced crystallinities and stabilities.

2. Experimental

2.1 Linker synthesis

4,4',4''-(1,3,5-triazine-2,4,6-triyl)tribenzoic acid (TATB) and two mono-substituted nitro-TATB linker versions were synthesized as described in the literature.[40] Figure 1 illustrates the synthesis in which the trimerization of one equivalent of a nitro-substituted benzoyl chloride **1a** or **1b** with two equivalents of 4-methylbenzonitrile (**2**) leads to nitro-triazines **3a** or **3b**. By oxidizing the methyl groups with tetra-*n*-butylammonium permanganate, the respective nitro-TATB linkers **4a** and **4b** were obtained.

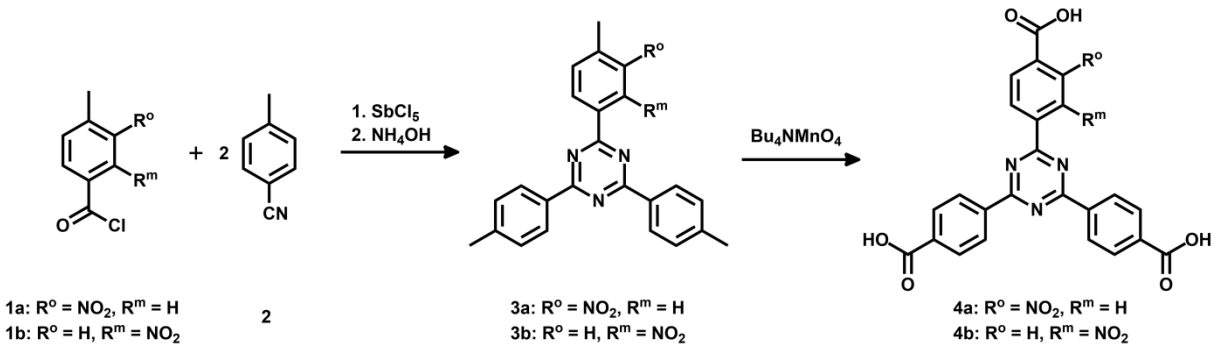

Figure 1: Illustration of the modified synthetic route to obtain mono-substituted nitro-functionalized triazine-based trigonal linkers for the synthesis of iron(III)-based MOFs exhibiting different linker topologies.

Precursor **5** for the mono-substituted methoxy-TAPB linker **8** was obtained in a similar way. 4-Bromo-3-methoxy-benzoyl chloride was synthesized and used in the trimerization with two equivalents of 4-bromobenzonitrile to obtain tribromo-triazine **5**[41] (for the synthetic route see supporting information Figure S1). Triple Suzuki coupling with 4-(methoxycarbonyl)-phenylboronic acid (**6**) and alkaline hydrolysis of the methyl ester groups in **7** led to the desired methoxy-TAPB linker **8** (Figure 2). In this paper, the synthesis was performed on a multigram scale with modifications in the last two steps (for further information see SI).

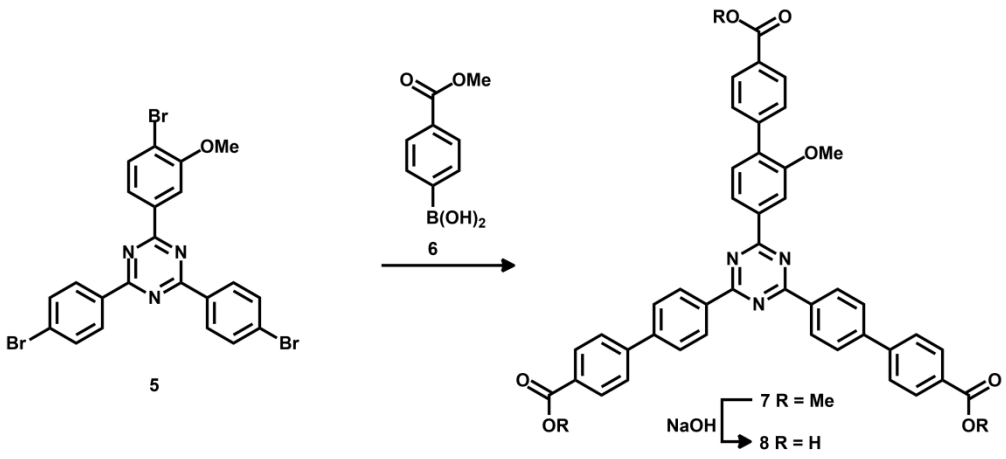

Figure 2 Illustration of the synthesis of the mono-subsituted methoxy-functionalized elongated triazine based linker (TAPB) for the synthesis of iron(III)-based MOFs exhibiting different linker topologies.

2.2 MOF synthesis

The Fe-TATB-BDC MOFs were synthesized in 5 mL Schott Duran culture tubes with a PBT cap equipped with a Teflon seal. $FeCl_3 \cdot 6H_2O$ (0.222 mmol) was dissolved in 1 mL DMF via ultrasonication. 4,4',4''-(1,3,5-triazine-2,4,6-triyl)tribenzoic acid (TATB, 0.110 mmol) and 1,4-benzenedicarboxylic acid (BDC, 0.220 mmol), or their functionalized derivatives, were added and dissolved by ultrasonication. The reaction

mixture was heated within 1 h to 150 °C, held at this temperature for 20 h and was afterwards cooled to room temperature within 1 h. The resulting powders were collected by centrifugation (5 min, 7830 rpm), washed three times with DMF and dried under reduced pressure at room temperature. The samples were afterwards extracted with methanol in a Soxhlet device for 72 h, dried again under reduced pressure and stored under nitrogen atmosphere at room temperature. For further synthetic details and the synthesis of the other iron(III)-based mixed linker MOF structures (Fe-TATB-BPDC, Fe-TAPB-BDC, Fe-TAPB-BPDC and Fe-BTB-BDC), see SI.

2.3 Characterization

Powder X-ray diffraction (PXRD) data were recorded on a STOE Stadi MP diffractometer in transmission mode. The Cu $K_{\alpha1}$ radiation source (λ = 1.54060 Å) was operating at 40 kV and 40 mA and the scattered X-rays were recorded on a DECTRIS MYTHEN 1K solid state detector. High-resolution synchrotron powder diffraction data were recorded at the Swiss Norwegian BeamLine (SNBL BM01B) at the European Synchrotron at Grenoble/France (ESRF).[42] The wavelength was calibrated with a Si standard NIST 640c to 0.504477 Å. The diffractometer is equipped with five counting channels, delivering five complete patterns collected simultaneously with a small 1.1° offset in 2θ. A Si(111) analyzer crystal was mounted in front of each NaI scintillator/photomultiplier detector. Data were collected at room temperature (Fe-TATB-BDC-a, -b, -c, -e) and 100 K (Fe-TATB-BDC-a, -e) between 0° and 20°/25° in 2θ with steps of 0.002° and 100 ms integration time per data point (approx. 20 min for one scan). This scanning procedure was repeated several times and the resulting data from all detectors and measurements were averaged into one pattern (Table S8, and Figure S33) with local software. Quantachrome AUTOSORB-1 or AUTOSOR-IQ instruments were used for measuring nitrogen sorption isotherms. The samples were degassed prior to the measurement at 120 °C for 12 h in vacuum. The calculation of the BET surface area was carried out in the p/p_0 range of 0.005 to 0.01. A quenched solid state functional theory (QSDFT) was employed for calculating the pore size distribution. Thermogravimetric analysis (TGA) and differential scanning calorimetry (DSC) measurements were determined in parallel using a Netzsch Jupiter ST 449 C instrument equipped with a Netsch TASC 414/4 controller. Scanning

electron microscopy (SEM) images were recorded with a FEI Helios G33 UC. For further characterization of the materials see SI.

3. Results and Discussion

3.1 Different functionalized Fe-TATB-BDC MOFs

In this work five different functionalized iron(III)-based MOF structures exhibiting two different linker geometries were synthesized. Figure 3A illustrates the different functionalized linkers and the five combinations tested. Either 1,4-benzendicarboxylic acid (BDC; red) or its amino-functionalized version (brown) were used as the linear linkers, and 4,4',4''-(1,3,5-triazine-2,4,6-triyl)tribenzoic acid (TATB; turquois) or its nitro-functionalized version (violet for *meta* position and blue for *ortho* position) were used as the trigonal linker.

While the BDC linkers are commercially available, the TATB ones had to be synthesized. The symmetrical functionalization of triazine-base materials can be easily achieved by a trimerization of nitriles. A modified synthetic route was chosen for the introduction of only one nitro group per linker molecule (Figure 1). The nitro group was placed at different positions to investigate the effect on the resulting MOF structure and its properties.

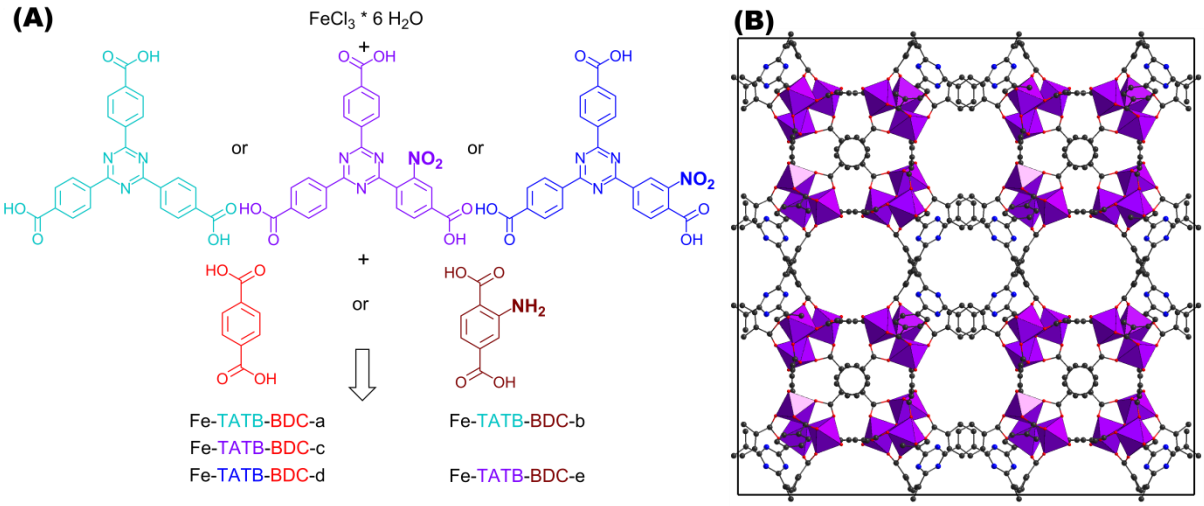

Figure 3: A) Schematic representation of triazine-based trigonal linker TATB (turquois) and its mono-substituted nitro-functionalized version, in *meta* (violet) or *ortho* (blue) position to the connecting carboxylic acid group. The reactions of iron chloride hexahydrate with one TATB linker in combination with one of the two linear BDC linkers used (1,4-benzendicarboxylic acid, illustrated in red and its amino-functionalized version illustrated in brown) result in different possible Fe-TATB-BDC MOF frameworks. Five different combinations were tested, resulting in the Fe-TATB-BDC structures indicated. B) Presentation of the MIL-143 framework of Fe-TATB-BDC-a along [001] with FeO_6 octahedra shown in purple, carbon as grey spheres, oxygen as red spheres, and nitrogen as blue spheres. Hydrogen atoms have been omitted for clarity. Note: the positional parameters have not been refined, but were taken from the literature.[43] The cubic lattice constant was taken from our *Le Bail* fits

and three carbon atoms of the benzene ring of the BTB linker were replaced by nitrogen atoms to obtain the TATB linker.

The key to success in the synthesis of the five new iron(III)-based mixed linker compounds was the adaption of the synthesis protocol reported by Chevreau *et al*.[43] In this report, they were able to synthesize MOFs with the MIL-142 and MIL-143 topologies for the first time. MOFs with the MIL-143 topology can be regarded as mesoporous zeolytic solids based on the β-christobalite topology, and the related MIL-142 topology is best described as a microporous interpenetrated structure similar to the ReO_3 topology. The MIL-142 and MIL-143 structures are built up by the same linkers (BDC and BTB and their respective derivatives), but with different linker ratios (BDC to BTB is 3:4 for MIL-142, while for MIL-143 the ratio is 3:2).*[43]* Our goal was to synthesize MOFs exhibiting only the mesoporous MIL-143 topology (pore diameters: 2.0 nm and 2.4 nm; window sizes: 1.6 nm and 1.8 nm) as the synthesis of robust mesoporous MOFs is still a great challenge.

For the successful synthesis, $FeCl_3 \cdot 6H_2O$, trigonal TATB and linear BDC linkers were dissolved in DMF and the reaction mixture was heated at 150 °C for 20 h. The reaction mixture was purified by centrifugation, washing with DMF, and Soxhlet-extraction with methanol, which has proven to be much more effective in removing guest molecules - such as DMF - than washing alone.[44] We also synthesized MIL-142 (hereafter called Fe-BTB-BDC with BTB = 4,4′,4″-benzene-1,3,5-triyl-tris(benzoic acid), see SI and Figure S2) according to our new synthesis protocol, to compare the chemical properties with the new Fe-TATB-BDC structures. The key difference between the Fe-BTB-BDC and the Fe-TATB-BDC structures is the trigonal linker, as the core of the trigonal linker in Fe-BTB-BDC is based on a benzene ring and not a triazine ring, as for Fe-TATB-BDC. Therefore, we were curious whether the enhancement of planarity through the substitution of the central benzene ring in BTB with a triazine core in the TATB linker would influence the properties (e.g. crystallinity, porosity, thermal and water stability) of the resulting MOF scaffold.

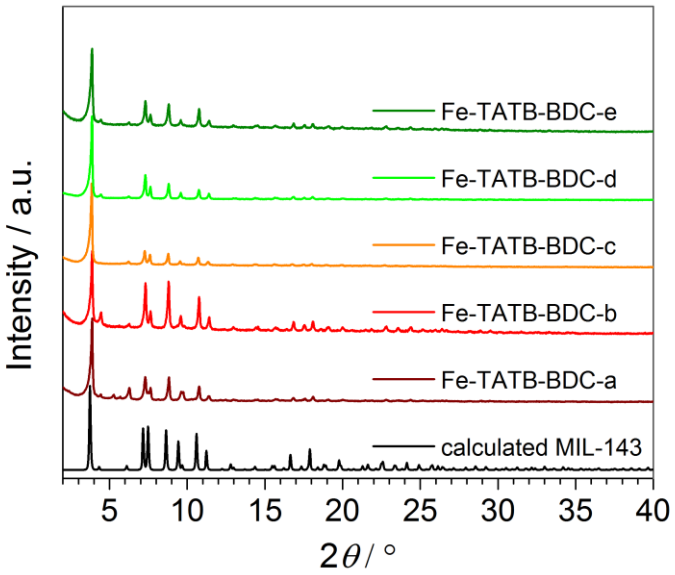

Figure 4: PXRD patterns of the five different functionalized Fe-TATB-BDC structures in comparison to the calculated pattern of the MIL-143 topology.[43]

The PXRD patterns (Figure 4) of the Fe-TATB-BDC structures indicate that the products are highly crystalline materials. The similarities between the PXRD patterns allow us to conclude that all five MOF samples crystallize in the same MOF topology. Comparison with calculated PXRD patterns based on the reported crystallographic data[43] clearly prove that the MIL-143 topology is formed in all Fe-TATB-BDC compounds. Chevreau *et al.*[43] were able to achieve the MIL-142 and MIL-143 topologies for combinations of BTB and BDC linkers by changing the relative amounts of starting materials as well as synthesis conditions. As we only obtained the MIL-143 topology, we assume that the trigonal linker based on a triazine core favors the formation of the non-interpenetrating MIL-143 topology, while the trigonal linker based on a benzene core favors the MIL-142 structure (Figure S27).

The PXRD patterns shown in Figure 4 were recorded on samples after Soxhlet-extraction, but exposure to air and moisture thereafter. To get more structural information high-resolution synchrotron powder diffraction data of selected compounds (Fe-TATB-a, -b, -c, and -e) were recorded at the European Synchrotron at Grenoble/France. Here the samples were activated (2 h at $5 \cdot 10^{-2}$ mbar, 100 °C) and sealed in glass capillaries (∅ = 1.0 mm) to prevent the uptake of any water from the atmosphere.

A visual inspection and comparison with calculated PXRD patterns again confirmed the MIL-143 topology of these four compounds. But even with these high quality data no stable Rietveld refinement was achieved. Therefore, *Le Bail* fits in space group

*F*23 using the GSAS software[45] were conducted to obtain the cubic lattice parameters *a* for all compounds. The results of these fits (synchrotron data and laboratory X-ray data) are summarized in Table S8 and depicted in Figures S32 and S33. The quality of the *Le Bail* fits of the synchrotron data is not as good as that of the STOE data. This is probably due to the fact that the synchrotron profiles cannot be accurately modelled with the functions implemented in GSAS. Nonetheless, these fits allow us to draw clear conclusions. All compounds Fe-TATB-BDC crystallize in the MIL-143 topology; the unit cell volume is not significantly influenced by changes in the functionalized linkers. Compounds Fe-TATB-BDC-b-d appear to be single-phase samples, whereas in the PXRD patterns of compounds Fe-TATB-BDC-a and -e small amounts of some MIL-142 impurity can be spotted. On the other hand, Fe-BTB-BDC gives a very good *Le Bail* fit in space group *R*3*c* with lattice parameters similar to those obtained in the original paper.[43] No additional reflections that would suggest a MIL-143 impurity are observed. Another remarkable finding is the shrinkage of the unit cell volume upon activation (Table S8). This shrinkage accounts for 1.5–2.7% of the original unit cell volume, indicating a remarkable degree of flexibility in the MIL-143 framework. Another noteworthy finding is the increase of the unit cell volume of the non-functionalized compound Fe-TATB-BDC-a upon cooling. Such a negative thermal expansion (NTE) of coordination polymers and MOFs is not rare and has already been reported before.[46-48]

In Figure 5, the PXRD pattern collected for Fe-TATB-BDC-b (STOE Stadi P data) is compared with a pattern calculated from the lattice parameter of the *Le Bail* fit (Table S8) and the positional parameters given for MIL-143 in the literature.[43] The agreement is reasonable thus confirming the MIL-143 topology of this compound. Differences in the intensities especially at higher 2θ angles can be attributed to the fact that the theoretical pattern was only calculated with framework atoms, while the measurement was recorded on an as-synthesized sample with guest molecules in its pores. In Figure 6, the recorded pattern of Fe-BTB-BDC is compared with a theoretical pattern of MIL-142 calculated as described above for MIL-143. Here, the similarity of both patterns is obvious thus confirming the MIL-142 topology of this compound.

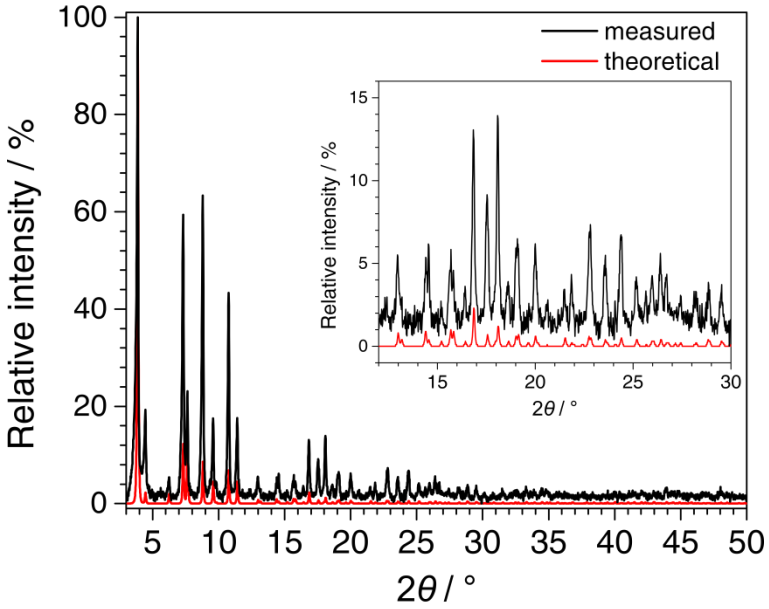

Figure 5: Comparison of the PXRD pattern recorded for Fe-TATB-BDC-b (STOE Stadi P, CuKα_1 radiation, MYTHEN detector, background subtracted and zero shift corrected) with the pattern calculated from the refined lattice parameters of Fe-TATB-BDC-b (*Le Bail* fit) and the atomic coordinates of MIL-143 taken from the literature.[43] The good agreement between the patterns confirms the MIL-143 topology of Fe-TATB-BDC-b.

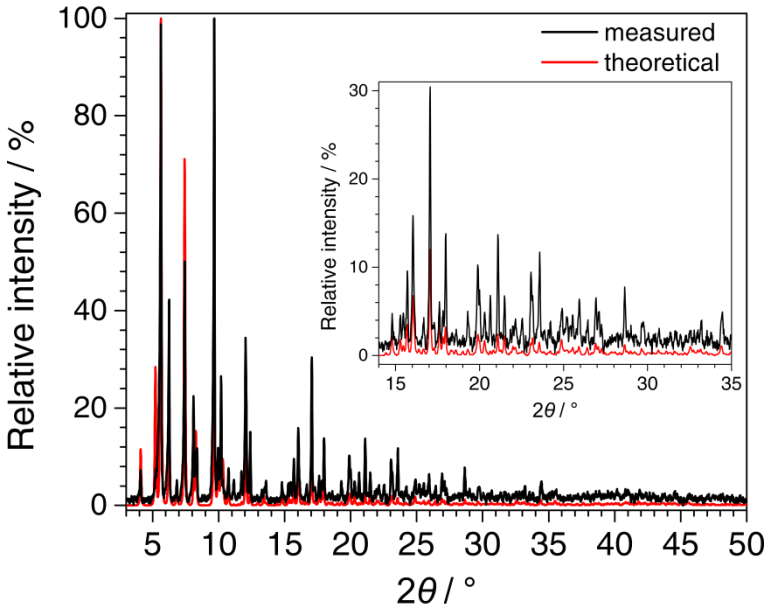

Figure 6: Comparison of the PXRD pattern recorded for Fe-BTB-BDC (STOE Stadi P, CuKα_1 radiation, MYTHEN detector, background subtracted and zero shift corrected) with the pattern calculated from the refined lattice parameters of Fe-BTB-BDC (Le Bail fit) and the atomic coordinates of MIL-142 taken from the literature.[43] The good agreement between the patterns confirms the MIL-142 topology of Fe-BTB-BDC.

The SEM images of the Fe-TATB-BDC samples (Figure S8, S11, S14, S17 and S20) show intergrown aggregates with undefined particle shapes. However, on some images crystallites are visible and the sizes of the individual particles range from less

than 100 nm to about 10 µm. Fe-BTB-BDC (Figure S30), in contrast, appears to be composed of plate-like hexagonal shaped crystals which is expected due to the rhombohedral space group *R3c*. The plates have similar sizes of approximately 400 nm thickness with edges lengths of 1.3-2.3 µm.

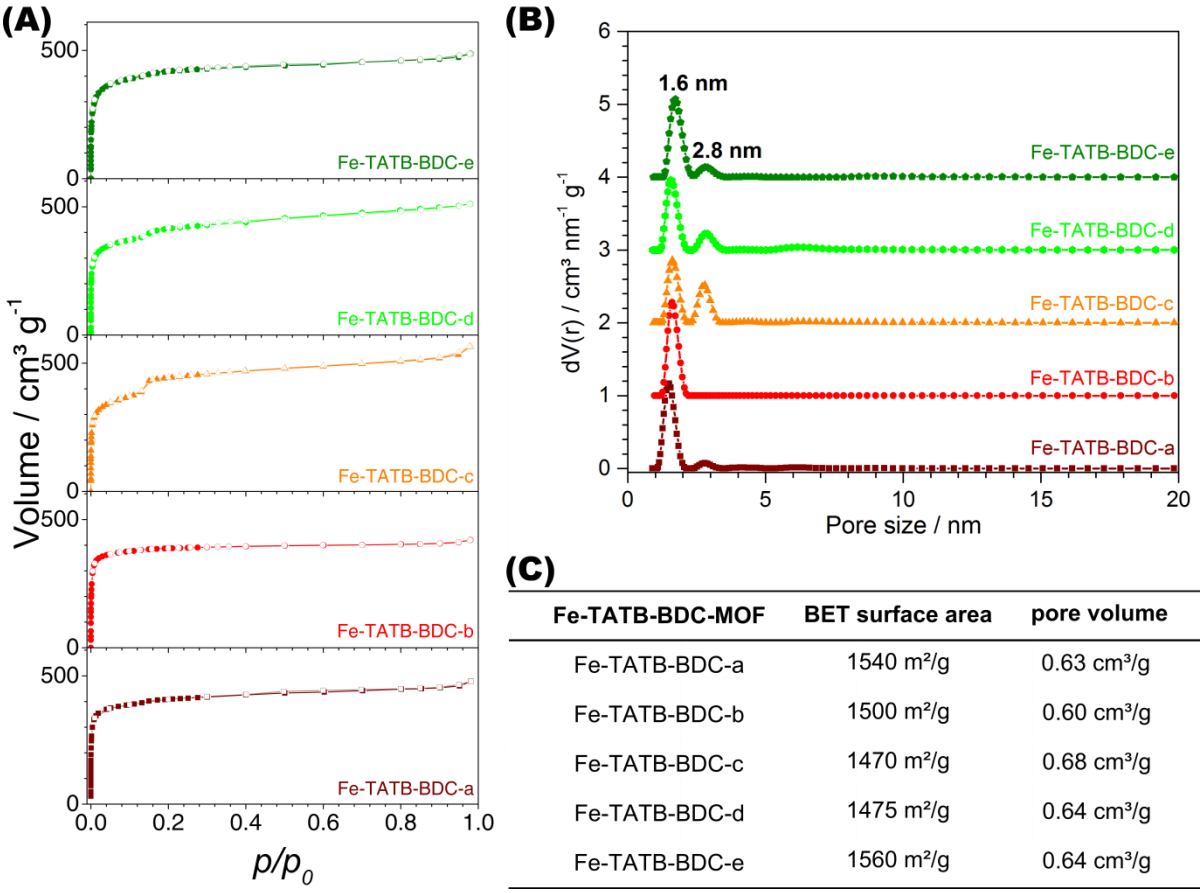

(C)

Fe-TATB-BDC-MOF	BET surface area	pore volume
Fe-TATB-BDC-a	1540 m²/g	0.63 cm³/g
Fe-TATB-BDC-b	1500 m²/g	0.60 cm³/g
Fe-TATB-BDC-c	1470 m²/g	0.68 cm³/g
Fe-TATB-BDC-d	1475 m²/g	0.64 cm³/g
Fe-TATB-BDC-e	1560 m²/g	0.64 cm³/g

Figure 7: A) Nitrogen isotherms of Fe-TATB-BDC measured at 77 K. The adsorption and desorption are shown with filled and empty symbols, respectively. B) Pore size distributions calculated using a QSDFT model with cylindrical and spherical pores in the adsorption branch. C) Table summarizing the calculated BET surface area in the range of p/p_0 from 0.005 to 0.01 and the pore volume, measured at p/p_0 0.19.

Figure 7A presents the nitrogen isotherms of the Fe-TATB-BDC materials, which exhibit a type IV(b) shape, except Fe-TATB-BDC-b which exhibits a type I shape, according to IUPAC.[49, 50] The type IV(b) isotherm, which had been recently added to the categorization of isotherms by IUPAC,[50] is typical for mesoporous materials with pores smaller than 4 nm, while the type I isotherm is typical for microporous materials. This type IV(b) shape is in good agreement with the MIL-143 structure type, as the network is mesoporous and exhibits two different pore sizes of 2.0 nm and 2.8 nm. The presence of these two different pore widths is observed in the calculated pore size distribution, which shows two defined peaks (Figure 7B). For all samples, except Fe-TATB-BDC-b, the pore size distribution indicates well-defined

dimensions of about 1.6 nm and 2.8 nm, while Fe-TATB-BDC-b shows only one prominent pore with a diameter of 1.6 nm. One drastic difference in the pore size distributions of the MOFs is the relative amplitude of the second peak, which corresponds to the larger pores. This peak is significantly larger in the samples containing a nitro-functionalization at the trigonal TATB linker (Fe-TATB-BDC-c, -d, and -e).

The BET surface areas of the five Fe-TATB-BDC materials fall within the same range: 1470 – 1560 $m^2\ g^{-1}$ (Figure 7C) regardless of which functional group is added or whether or not the linker is functionalized at all. Saturation of all isotherms was reached at p/p_0 of 0.19, therefore this data point was used for the calculation of the pore volume. The pore volumes of the five Fe-TATB-BDC frameworks are also very similar at approximately 0.64 $cm^3\ g^{-1}$. In comparison, for the Fe-BTB-BDC network, crystallizing in the MIL-142 topology, a BET surface area of 1585 $m^2\ g^{-1}$ was observed (Figure S28). This is in a good agreement with the reported value of 1580 $m^2\ g^{-1}$.[43] The pore volume (0.62 $cm^3\ g^{-1}$) was also calculated using a p/p_0 value of 0.19 and is also in accordance with the value in the literature of 0.70 $cm^3\ g^{-1}$.[43] The shape of the isotherm of Fe-BTB-BDC (Figure S28) is a type I, according to IUPAC,[49, 50] which is typical for microporous materials and consistent with the structure of MIL-142.[43] The pore size distribution (Figure S28) is narrow with a maximum at 1.4 nm, slightly above the theoretical pore size (0.8 nm) of the MIL-142 topology.

Thermogravimetric analysis (TGA) was applied to determine the thermal stability and composition of the Fe-TATB-BDC frameworks (Figure S7, S10, S13, S16 and S19). The TGA curve indicates that the frameworks with unmodified linear BDC linkers (Fe-TATB-BDC-a, -c and -d; Figure S7, S13 and S16) are stable up to approximately 300 °C, while the frameworks containing an amino-functionalization (Fe-TATB-BDC-b and -e; Figure S10 and S19) are only stable up to 270 °C. These thermal stability value fits well with the stability of MIL-143 and the Fe-BTB-BDC framework (Figure S29), which are stable up to 315 °C.[43] Hence, the triazine core of the trigonal linker has little influence on the resulting thermal stability of the framework. The main weight loss processes depicted in the TGA curves are more or less the same. The first main weight loss process is attributed to the removal of guest molecules. For Fe-TATB-BDC-a (Figure S7) the weight loss occurs until 315 °C and consists of two separated steps. These two steps of the curve indicate that the framework hosts two

species of guest molecules, in this case water and DMF. In comparison, the TGAs of Fe-TATB-BDC-b (Figure S10) and -e (Figure S19) show a single weight loss step for the guest molecules up to 270 °C. Similarly, Fe-TATB-BDC-c (Figure S13) and -d (Figure S16) have a single weight loss step up to 300 °C. All of the MOFs also experience a second weight loss at higher temperatures, which can be attributed to the combustion of the organic linker. For Fe-TATB-a (Figure S7), -c (Figure S13) and -d (Figure S16) the weight loss process occurs in a single step that is finished at 410 °C, 400 °C and 430 °C, respectively. The TGA curves of Fe-TATB-b (Figure S10) and -e (Figure S19) indicate that bimodal linker decomposition occurs until approximately 480 °C. This can be attributed to the presence of amino groups at the linear BDC linker. The position of the nitro-functionalization seems to have a small effect on the thermal stability of the network, while the amino-functionalization has only an impact on the linker decomposition, but not on the thermal stability of the networks. In comparison, Fe-BTB-BDC (Figure S29) exhibits a defined two-step weight loss process in agreement with reported values of MIL-142.[40] The first step (between 25 °C and 315 °C) can be attributed to the removal of guest molecules, while the second step (between 315 °C and 360 °C) can be attributed to the decomposition of the linkers. Assuming that at higher temperatures the residue only consisting of Fe_2O_3 and the molecular formula of MIL-143 to $[Fe_3O(Cl)(H_2O)_2(BDC)_{3/2}(TATB)]$, the compositions of the Fe-TATB-BDC materials can be calculated (Table S1-S5). Comparison of these calculated compositions of the Fe-TATB-BDC MOFs with the data obtained from the TGA measurements (where an ideal network without guest molecules is denoted as guest-free) shows that the theoretical and experimental values agree and discrepancies fall within the range of accuracy of TGA measurements (1%). The same is true for Fe-BTB-BDC if the molecular formula is assumed to be $[Fe_3O(Cl)(H_2O)_2(BDC)(BTB)_{4/3}]$ (Table S7).

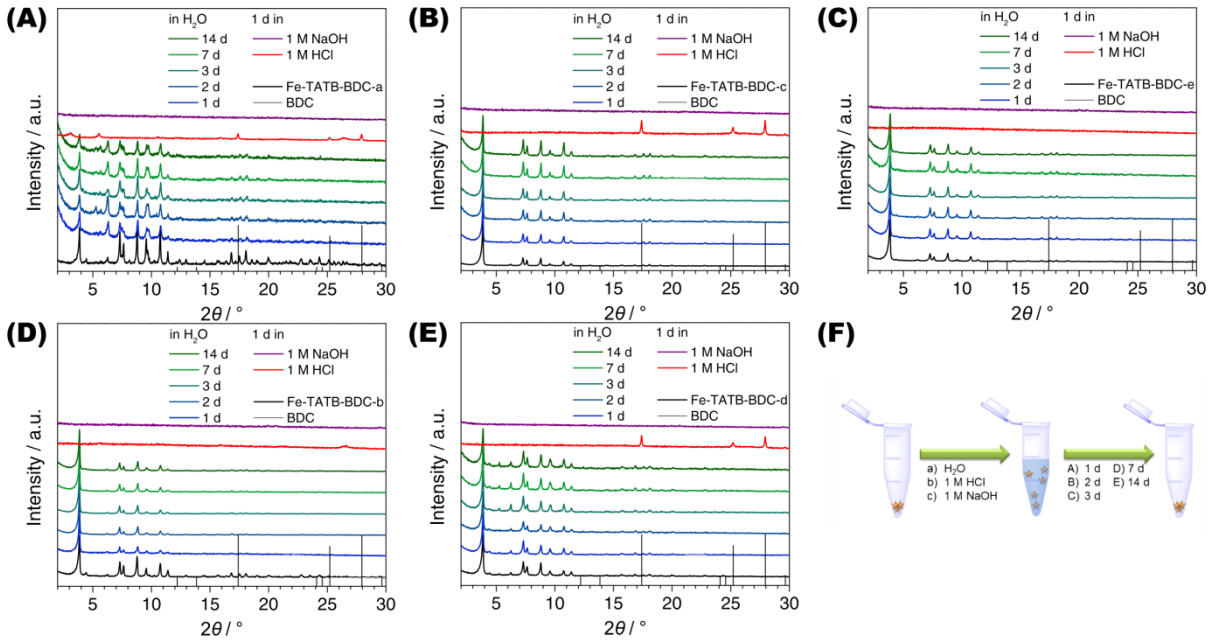

Figure 8: PXRD patterns of the different functionalized Fe-TATB-BDC MOFs after varied time periods of exposure to water, acid or base. (A: Fe-TATB-BDC-a, B: Fe-TATB-BDC-b, C: Fe-TATB-BDC-c, D: Fe-TATB-BDC-d and E: Fe-TATB-BDC-e). F: Schematic representation of the procedure for testing the stability of the iron(III)-based MOFs exhibiting two different linker topologies in water, 1 M hydrochloric acid, or 1 M sodium hydroxide. The sample was suspended in one of the solvents and shaken for different times. Afterwards, the samples were centrifuged and dried at 100 °C before PXRD measurement was recorded.

The stability of each MOF structure was tested in water and acidic or basic media. The samples were immersed in either Millipore water, 1 M hydrochloric acid, or 1 M sodium hydroxide. After different times of exposure, the MOF samples were then collected by centrifugation and dried at 100 °C before PXRD measurements were recorded. The PXRD data shown in Figure 8 indicate that all five Fe-TATB-BDC frameworks are stable in water up to 14 d (Figure 8, blue and green curves) but decompose under acidic (Figure 8, red curves) and basic (Figure 8, purple curves) conditions within one day. After the treatment under acidic conditions, BDC was detectable via PXRD for Fe-TATB-BDC-a, -c and -d (Figure 8A, 8C and 8D, respectively). BDC was identified by comparing the reflections with theoretical patterns of BDC, shown as black line diagram in the PRXD plots (Figure 8). This proves that the new synthesized iron(III)-based mix linker MOFs display similar chemical stability regardless of the functionalization of the organic linker. In most studies, iron(III)-based MOFs are members of the MIL (Matériaux de l'Institut Lavoisier) family and the framework stability in water increases from MIL-101(Fe),[51, 52] to MIL-88(Fe),[53, 54] further to MIL-53(Fe)[55, 56] and MIL-100(Fe).[55-58] The newly synthesized iron(III)-based mixed linker MOFs exhibit a stability comparable to MIL-53(Fe) and MIL-100(Fe). MIL-53(Fe)[55] is a flexible microporous material (with pores

whose diameters range from 0.4 nm and 0.85 nm in the closed and opened form, respectively), while MIL-100(Fe)[59] is a mesoporous material exhibiting pores of 2.5 nm and 2.9 nm. Compared to the newly synthesized iron(III)-based mixed linker materials, the surface and pores of MIL-100(Fe) are slightly larger. MIL-100(Fe) is constructed of benzene-1,3,5-tricarboxylic acid as the OBU and thus no functionalized MIL-100(Fe) network has been reported so far. In addition, the chemical stability of the Fe-TATB-BDC series is comparable to the Fe-BTB-BDC framework exhibiting a MIL-142 topology. The Fe-BTB-BDC framework (Figure S31) also decomposes under acidic and basic conditions, but is stable in water up to 14 d.

3.2 Elongation of the Fe-TATB-BDC network

In addition to the challenges associated with functionalizing the pore, developing a system to systematically expand the pore size of any given MOF structure is a daunting undertaking, but one that is crucial for making the MOF's surface accessible for large organic, inorganic, and biological molecules. Therefore, we tried to elongate the Fe-TATB-BDC framework by extending the length of both linkers (Figure S2). First, we extended the linear linker BDC by replacing it with biphenyl-4,4'-dicarboxylic acid (BPDC) to achieve a Fe-TATB-BPDC framework. All our attempts led to a less crystalline material (Figure S21), but the PXRD pattern may indicate some first reflections of the Fe-TATB-BPDC framework. We then turned our attention to the elongation of the trigonal TATB linker by replacing it with 2,4-bis(4'-carboxy-biphenyl-4-yl)-6-(4'-carboxy-2-methoxy-biphenyl-4-yl)-1,3,5-triazine (TAPB). The respective MOF (Fe-TAPB-BDC) was obtained as a crystalline material (Figure S22) that also exhibits the MIL-143 topology. This was verified by a *Le Bail* fit in space group *F23* leading to the cubic lattice parameter *a* = 50.910(8) Å. Attempts to obtain a structural model of Fe-TAPB-BDC failed due to the only modest data quality. It is remarkable that no interpenetration, that would stabilize the MOF structure, was observed. It seems that the triazine core of the TATB linker hinders interpenetration even when the networks are elongated, in contrast to the behavior of MOFs incorporating BTB linker.

To our knowledge, this is the first time that an elongation of a MIL-143 structure type has been reported. Unfortunately, Soxhlet extraction with methanol led to an amorphous material (Figure S22, dark cyan curve). Removing guest molecules in high vacuum at 120 °C or 50 °C for 12 h led to a collapse of the structure (Figure

S22, dark/light grey curves). Increasing the length of the organic linker is known to decrease the stability of a MOF structure.[60] TGA was also used to determine the thermal stability of the framework, therefore the as-synthesized material was used. The curve shown in Figure S23 indicates that multiple weight loss processes occurred. In comparison to the Fe-TATB-BDC networks, the first two weight loss steps (up to 315 °C) can be attributed to guest molecule removal. The third and fourth weight loss steps (up to 510 °C) can be attributed to the combustion of the linkers. The ideal composition of Fe-TAPB-BDC was calculated assuming the molecular formula to be $[Fe_3O(Cl)(H_2O)_2(BDC)_{3/2}(TAPB)]$ (Table S6). Based on these calculations the MOF framework seems to exhibit many defects (such as missing linkers), which could account for some of the observed reduced framework stability. SEM images (Figure S24) reveal intergrown octahedral shaped crystals with sizes of around 300 nm.

To complete our study, we also tried to elongate the network by extending both linkers at the same time. Instead of the desired Fe-TAPB-BPDC network, an amorphous material was obtained with only two broad reflections in the PXRD pattern (Figure S25).

4. Conclusion

In conclusion, five new mesoporous iron(III)-based mixed linker MOF materials exhibiting the non-interpenetrated MIL-143 topology were synthesized. Through the replacement of the central benzene ring of a BTB linker by a triazine core, the interpenetration of the network was avoided. As the MIL-143 topology is constructed from two different linker types, we were able to successfully synthesize MOFs that were functionalized by amino (linear BDC linker) or nitro groups (trigonal TATB linker). In the end, we were able to create a multivariate MOF with both amino and nitro groups by combining two differently functionalized linkers.

All mesoporous iron(III)-based MOFs exhibit high thermal stability up to 300 °C. The water-stability is remarkable and comparable to the mesoporous MIL-100(Fe) structure. The frameworks are very crystalline and defect free, and the porosity is not affected by the functionalization of the linker molecules. We also demonstrated that the framework can be elongated by substituting the trigonal linker, but elongation of the linear linker leads to a less crystalline material. The resulting elongated

framework of MIL-143, which has not been reported before, is unstable upon removal of guest molecules.

Apart from expanding the scope of mesoporous iron(III)-based MOFs, the strategy developed herein to synthesize multivariate mixed-linker MOFs, in which each linker can be functionalized separately, could lead to a better understanding of the relationship between functionality, arrangement, and performance of the MOF material.

Acknowledgement

We want to thank Tina Reuther (University of Munich) for nitrogen sorption and TGA/DSC measurements and Heidi Schwartz (University of Cologne) for preparing the samples for the investigations with synchrotron radiation as well as Dr. Hermann Emerich for support at the SNBL beamline.

Appendix A. Supplementary data

Detailed experimental procedures, additional material characterization for the linkers and the MOFs can be found in the Supplementary Information.

References

[1] O. K. Farha, A. Ö. Yazaydin, I. Eryazici, C. D. Malliakas, B. G. Hauser, M. G. Kanatzidis, S. T. Nguyen, R. Q. Snurr, J. T. Hupp, *Nat. Chem.* **2010**, *2*, 944-948.

[2] O. K. Farha, I. Eryazici, N. C. Jeong, B. G. Hauser, C. E. Wilmer, A. A. Sarjeant, R. Q. Snurr, S. T. Nguyen, A. Ö. Yazaydin, J. T. Hupp, *J. Am. Chem. Soc.* **2012**, *134*, 15016-15021.

[3] H. Furukawa, N. Ko, Y. B. Go, N. Aratani, S. B. Choi, E. Choi, A. Ö. Yazaydin, R. Q. Snurr, M. O'Keeffe, J. Kim, O. M. Yaghi, *Science* **2010**, *329*, 424-428.

[4] J.-R. Li, J. Sculley, H.-C. Zhou, *Chem. Rev.* **2012**, *112*, 869-932.

[5] L. J. Murray, M. Dincă, J. R. Long, *Chem. Soc. Rev.* **2009**, *38*, 1294-1314.

[6] J. B. DeCoste, G. W. Peterson, *Chem. Rev.* **2014**, *114*, 5695-5727.

[7] J. Lee, O. K. Farha, J. Roberts, K. A. Scheidt, S. T. Nguyen, J. T. Hupp, *Chem. Soc. Rev.* **2009**, *38*, 1450-1459.

[8] L. Ma, C. Abney, W. Lin, *Chem. Soc. Rev.* **2009**, *38*, 1248-1256.

[9] L. E. Kreno, K. Leong, O. K. Farha, M. Allendorf, R. P. Van Duyne, J. T. Hupp, *Chem. Rev.* **2012**, *112*, 1105-1125.

[10] M. Allendorf, A. Bétard, R. A. Fischer, in *Metal-Organic Frameworks*, Wiley-VCH Verlag GmbH & Co. KGaA, **2011**, pp. 309-335.

[11] J. An, S. J. Geib, N. L. Rosi, *J. Am. Chem. Soc.* **2009**, *131*, 8376-8377.

[12] M. Lismont, L. Dreesen, S. Wuttke, *Adv. Funct. Mater.* **2017**, *27*, 1606314.

[13] S. Wuttke, M. Lismont, A. Escudero, B. Rungtaweevoranit, W. J. Parak, *Biomaterials* **2017**, *123*, 172-183.

[14] H. Deng, C. J. Doonan, H. Furukawa, R. B. Ferreira, J. Towne, C. B. Knobler, B. Wang, O. M. Yaghi, *Science* **2010**, *327*, 846-850.

[15] H. Furukawa, U. Müller, O. M. Yaghi, *Angew. Chem. Int. Ed.* **2015**, *54*, 3417-3430.

[16] X. Kong, H. Deng, F. Yan, J. Kim, J. A. Swisher, B. Smit, O. M. Yaghi, J. A. Reimer, *Science* **2013**, *341*, 882-885.

[17] D. Senthil Raja, C.-C. Pan, C.-W. Chen, Y.-H. Kang, J.-J. Chen, C.-H. Lin, *Microporous Mesoporous Mater.* **2016**, *231*, 186-191.
[18] J. Tao, M.-L. Tong, X.-M. Chen, *J. Chem. Soc., Dalton Trans.* **2000**, 3669-3674.
[19] K. Seki, *Chem. Commun.* **2001**, 1496-1497.
[20] C. J. Doonan, W. Morris, H. Furukawa, O. M. Yaghi, *J. Am. Chem. Soc.* **2009**, *131*, 9492-9493.
[21] S. Yuan, J.-S. Qin, L. Zou, Y.-P. Chen, X. Wang, Q. Zhang, H.-C. Zhou, *J. Am. Chem. Soc.* **2016**, *138*, 6636-6642.
[22] T.-T. Zhou, Z.-H. Xuan, D.-S. Zhang, Z. Chang, Y.-H. Zhang, X.-H. Bu, *CrystEngComm* **2015**, *17*, 5884-5888.
[23] P. V. Dau, L. R. Polanco, S. M. Cohen, *Dalton Trans.* **2013**, *42*, 4013-4018.
[24] K. Uemura, F. Onishi, Y. Yamasaki, H. Kita, *J. Solid State Chem.* **2009**, *182*, 2852-2857.
[25] T. Fukushima, S. Horike, Y. Inubushi, K. Nakagawa, Y. Kubota, M. Takata, S. Kitagawa, *Angew. Chem. Int. Ed.* **2010**, *49*, 4820-4824.
[26] H. Chun, D. N. Dybtsev, H. Kim, K. Kim, *Chem. - Eur. J.* **2005**, *11*, 3521-3529.
[27] V. Safarifard, A. Morsali, *CrystEngComm* **2014**, *16*, 8660-8663.
[28] A. Schoedel, W. Boyette, L. Wojtas, M. Eddaoudi, M. J. Zaworotko, *J. Am. Chem. Soc.* **2013**, *135*, 14016-14019.
[29] T. Yamada, S. Iwakiri, T. Hara, K. Kanaizuka, M. Kurmoo, H. Kitagawa, *Cryst. Growth Des.* **2011**, *11*, 1798-1806.
[30] T. Yamada, H. Kitagawa, *J. Am. Chem. Soc.* **2009**, *131*, 6312-6313.
[31] K. Uemura, Y. Yamasaki, F. Onishi, H. Kita, M. Ebihara, *Inorg. Chem.* **2010**, *49*, 10133-10143.
[32] S. Henke, R. A. Fischer, *J. Am. Chem. Soc.* **2011**, *133*, 2064-2067.
[33] S. Horike, R. Matsuda, D. Tanaka, S. Matsubara, M. Mizuno, K. Endo, S. Kitagawa, *Angew. Chem. Int. Ed.* **2006**, *45*, 7226-7230.
[34] S. Henke, R. Schmid, J.-D. Grunwaldt, R. A. Fischer, *Chem. - Eur. J.* **2010**, *16*, 14296-14306.
[35] S. Henke, A. Schneemann, S. Kapoor, R. Winter, R. A. Fischer, *J. Mater. Chem.* **2012**, *22*, 909-918.
[36] S. Henke, A. Schneemann, A. Wutscher, R. A. Fischer, *J. Am. Chem. Soc.* **2012**, *134*, 9464-9474.
[37] Z. Wang, K. K. Tanabe, S. M. Cohen, *Inorg. Chem.* **2009**, *48*, 296-306.
[38] Z. Wang, S. M. Cohen, *J. Am. Chem. Soc.* **2009**, *131*, 16675-16677.
[39] S. Yuan, W. Lu, Y.-P. Chen, Q. Zhang, T.-F. Liu, D. Feng, X. Wang, J. Qin, H.-C. Zhou, *J. Am. Chem. Soc.* **2015**, *137*, 3177-3180.
[40] E. Mühlbauer, A. Klinkebiel, O. Beyer, F. Auras, S. Wuttke, U. Lüning, T. Bein, *Microporous Mesoporous Mater.* **2015**, *216*, 51-55.
[41] A. Klinkebiel, O. Beyer, B. Malawko, U. Lüning, *Beilstein J. Org. Chem.* **2016**, *12*, 2267-2273.
[42] W. van Beek, O. V. Safonova, G. Wiker, H. Emerich, *Phase Transitions* **2011**, *84*, 726-732.
[43] H. Chevreau, T. Devic, F. Salles, G. Maurin, N. Stock, C. Serre, *Angew. Chem. Int. Ed.* **2013**, *52*, 5056-5060.
[44] J. Lippke, B. Brosent, T. von Zons, E. Virmani, S. Lilienthal, T. Preuße, M. Hülsmann, A. M. Schneider, S. Wuttke, P. Behrens, A. Godt, *Inorg. Chem.* **2017**, *56*, 748-761.
[45] A. C. Larson, R. B. Von Dreele, *Los Alamos Laboratory, Rep. No. LA-UR* **1987**, *86*, 748.
[46] F. Hohn, I. Pantenburg, U. Ruschewitz, *Chem. - Eur. J.* **2002**, *8*, 4536-4541.
[47] S. R. G. Balestra, R. Bueno-Perez, S. Hamad, D. Dubbeldam, A. R. Ruiz-Salvador, S. Calero, *Chem. Mater.* **2016**, *28*, 8296-8304.
[48] S. S. Han, W. A. Goddard III, *J. Phys. Chem. C* **2007**, *111*, 15185-15191.
[49] K. S. W. Sing, D. H. Everett, R. A. W. Haul, L. Moscou, R. A. Pierotti, J. Rouquérol, T. Siemieniewska, *Pure Appl. Chem.* **1985**, *57*, 603-619.
[50] M. Thommes, K. Kaneko, A. V. Neimark, J. P. Olivier, F. Rodriguez-Reinoso, J. Rouquerol, K. S. W. Sing, *Pure Appl. Chem.* **2015**, *87*, 1051-1069.
[51] S. Liu, L. Zhai, C. Li, Y. Li, X. Guo, Y. Zhao, C. Wu, *ACS Appl. Mater. Interfaces* **2014**, *6*, 5404-5412.

[52] P. Küsgens, M. Rose, I. Senkovska, H. Fröde, A. Henschel, S. Siegle, S. Kaskel, *Microporous Mesoporous Mater.* **2009**, *120*, 325-330.
[53] C. Serre, S. Surblé, C. Mellot-Draznieks, Y. Filinchuk, G. Férey, *Dalton Trans.* **2008**, 5462-5464.
[54] P. Horcajada, F. Salles, S. Wuttke, T. Devic, D. Heurtaux, G. Maurin, A. Vimont, M. Daturi, O. David, E. Magnier, N. Stock, Y. Filinchuk, D. Popov, C. Riekel, G. Férey, C. Serre, *J. Am. Chem. Soc.* **2011**, *133*, 17839-17847.
[55] I. Bezverkhyy, G. Weber, J.-P. Bellat, *Microporous Mesoporous Mater.* **2016**, *219*, 117-124.
[56] X. Lan, H. Zhang, P. Bai, X. Guo, *Microporous Mesoporous Mater.* **2016**, *231*, 40-46.
[57] E. Soubeyrand-Lenoir, C. Vagner, J. W. Yoon, P. Bazin, F. Ragon, Y. K. Hwang, C. Serre, J.-S. Chang, P. L. Llewellyn, *J. Am. Chem. Soc.* **2012**, *134*, 10174-10181.
[58] Y.-K. Seo, J. W. Yoon, J. S. Lee, U.-H. Lee, Y. K. Hwang, C.-H. Jun, P. Horcajada, C. Serre, J.-S. Chang, *Microporous Mesoporous Mater.* **2012**, *157*, 137-145.
[59] P. Horcajada, T. Chalati, C. Serre, B. Gillet, C. Sebrie, T. Baati, J. F. Eubank, D. Heurtaux, P. Clayette, C. Kreuz, J.-S. Chang, Y. K. Hwang, V. Marsaud, P.-N. Bories, L. Cynober, S. Gil, G. Férey, P. Couvreur, R. Gref, *Nat. Mater.* **2010**, *9*, 172-178.
[60] I. Senkovska, S. Kaskel, *Chem. Commun.* **2014**, *50*, 7089-7098.

Supplementary information

Topology-guided functional multiplicity of iron-based metal-organic frameworks

Erika Virmani,[a] Ole Beyer,[b] Thomas Bein,[a] Ulrich Lüning,[b] Uwe Ruschewitz[c] and Stefan Wuttke*[a]

Department of Chemistry and Center for NanoScience (CeNS), LMU Munich, Butenandtstraße 11, D-81377 Munich, Germany

Christian-Albrechts-Universität zu Kiel, Otto Diels-Institut für Organische Chemie, Otto-Hahn-Platz 4, D-24118 Kiel, Germany

Universität zu Köln, Institut für Anorganische Chemie, Greinstr. 6, D-50939 Köln, Germany

*Correspondence to:
stefan.wuttke@cup.uni-muenchen.de

Table of Contents

Abbreviations

BDC	1,4-benzenedicarboxylic acid
BET	Brunauer-Emmett-Teller
BPDC	biphenyl-4,4'-dicarboxylic acid
BTB	4,4′,4″,-benzene-1,3,5-triyl-tris(benzoic acid)
DSC	differential scanning calorimetry
EA	elemental analysis
EDX	energy dispersive X-ray
M	molar
PXRD	powder X-ray diffractrogram
SEM	scanning electron microscopy
TAPB	2,4-bis(4’-carboxy-biphenyl-4-yl)-6-(4’-carboxy-2-methoxy-biphenyl-4-yl]-1,3,5-triazine
TATB	4,4',4''-(1,3,5-triazine-2,4,6-triyl)tribenzoic acid
TGA	thermogravimetric analysis

1. Characterization Techniques

Powder X-ray diffraction (PXRD): On a STOE Stadi MP diffractometer, the X-ray diffraction data were recorded using the transmission geometry mode. The X-ray was Ge-filtered Cu $K_{\alpha 1}$ (λ = 1.54060 Å) and generated at 40 kV and 40 mA. A DECTRIS MYTHEN 1K strip solid-state detector was used to detect the reflections. The sample was placed in the sample holder between two 0.014 mm thick acetate-foils (ultraphan) in the sample holder. In an omega-2-theta scanning mode, the diffraction patterns were collected using a step size of 4.71° and a counting time of 60 s per step between 2.00 – 44.375°. For the refinement, the diffraction pattern was also collected in an omega-2-theta scanning mode with a step size of 4.71° and a counting time of 60 s per step between 2.000 – 91.400°, 2.005 – 91.405° and 2.010 – 91.410°. Afterwards the patterns were merged together.

Synchrotron PXRD: High-resolution synchrotron powder diffraction data were recorded at the Swiss Norwegian BeamLine (SNBL BM01B) at the European Synchrotron at Grenoble/France (ESRF).[1] The wavelength was calibrated with a Si standard NIST 640c to 0.504477 Å. The diffractometer is equipped with five counting channels, delivering five complete patterns collected simultaneously with a small 1.1° offset in 2θ. A Si(111) analyzer crystal was mounted in front of each NaI scintillator/photomultiplier detector. Data were collected at room temperature (Fe-TATB-BDC-a, -b, -c, -e) and 100 K (Fe-TATB-BDC-a, -e) between 0° and 20°/25° in 2θ with steps of 0.002° and 100 ms integration time per data point (approx. 20 min for one scan). This scanning procedure was repeated several times and the resulting data from all detectors and measurements were averaged into one pattern (Table S8, and Figure S33) with local software. Samples were after activation sealed in glass capillaries (∅ 1.0 mm) in an argon atmosphere.

Analysis of PXRD data: *Rietveld* refinements of the resulting PXRD data with the published structural data of MIL-142 and MIL-143[2] as starting parameters turned out to be unstable. This is not surprising for the laboratory PXRD data, as the non-activated samples contain electron density within their pores, which is always difficult to be modelled. But also for the synchrotron data recorded on activated samples no stable refinements were obtained obviously due to the large unit cells and relatively low statistics of the measurements, which seems to be reasonably lower than that given by Chevreau *et al.*[2] for MIL-143. Therefore only *Le Bail* fits were performed in space group *F*23 (MIL-143 topology) or *R*3*c* (MIL-142 topology) using the GSAS software.[3] The published lattice parameters of MIL-142 and MIL-143 were used as starting values, the resulting lattice parameters are summarized in Table S8. The respective *Le Bail* fits are depicted in Figures S32 and S33. After these refinements

it was possible to look for possible impurity phases by visual inspection of the resulting fits. This is mainly the MOF of the other topology. This information has also been added to Table S8.

The pattern of as-synthesized Fe-TAPB-BDC (Figure S22) was indexed using the TREOR algorithm allowing only cubic unit cells.[4] The resulting lattice parameter *a* was used as starting value for a *Le Bail* fit in *F*23. The good agreement between the recorded and the calculated pattern confirms the MIL-143 topology also for this compound.

Nitrogen sorption: Prior to the measurement, the materials were degassed at 120 °C in high vacuum for at least 12 h. Nitrogen sorption isotherms were recorded at 77 K with a Quantachrome AUTOSORB-IQ or AUTOSORB-1 instrument. Evaluation of sorption data was carried out using ASiQwin^{TM} software suite (Version 3.0, Quantachrome Instruments). Brunauer-Emmett-Teller (BET) surface areas were calculated in the p/p_0 range from 0.005 to 0.01, according to Quantachrome recommendations,[5, 6] as in this region the linearized form of the BET equation is valid. The total pore volumes were calculated at p/p_0 0.19 and the pore size distributions were calculated from the adsorption isotherms by employing a quenched solid state functional theory (QSDFT, N_2 at 77 K on carbon, slit/cylindrical pore in the adsorption branch).

Scanning electron microscopy (SEM): First the samples were mounted onto an aluminum cylinder with a carbon sticky tape. Secondly the samples were coated with a thin carbon layer by carbon fiber flash evaporation under high vacuum. SEM images were recorded on a FEI Helios G33 UC. The acceleration voltage of 2 kV was produced by a field emission gun.

Thermal properties: Thermogravimetric analysis (TGA) and differential scanning calorimetry (DSC) measurements were determined in parallel using a Netzsch Jupiter ST 449 C instrument equipped with a Netsch TASC 414/4 controller. The samples were loaded into an aluminum oxide crucible and heated from 25 °C to 900 °C with a heating rate of 10 °C min^{-1} under a synthetic air flow (20.5% oxygen in nitrogen from Air Liquide supplier).

Nuclear magnetic resonance (NMR) spectroscopy: ^{1}H-NMR data were recorded on a Bruker DRX 500 spectrometer. The chemical shifts are referenced to the residual proton signal of the solvent.

2. Experimental

2.1 General

[1,1′-Bis(diphenylphosphino)ferrocene]dichloro palladium(II) (99.9 %, ABCR); 2-amino-1,4-benzenedicarboxylic acid (99%, Sigma Aldrich); 4-(methoxycarbonyl)phenylboronic acid (97 %, ABCR); biphenyl-4,4'-dicarboxylic acid (97%, Sigma Aldrich); iron(III) chloride hexahydrate ($FeCl_3$ • 8 H_2O, analysis grade, in-house supply); methanol (anhydrous, 99.8%, Sigma Aldrich); *N*,*N*-dimethylformamide (anhydrous, synthesis grade, Fischer Scientific); 1,4-benzendicarboxylic acid (98%, Sigma Aldrich).

2.2 Linker synthesis

2-(4-Bromo-3-methoxyphenyl)-4,6-bis(4-bromophenyl)-1,3,5-triazine: 2-(4-Bromo-3-methoxyphenyl)-4,6-bis(4-bromophenyl)-1,3,5-triazine was prepared according to the literature procedure.[7]

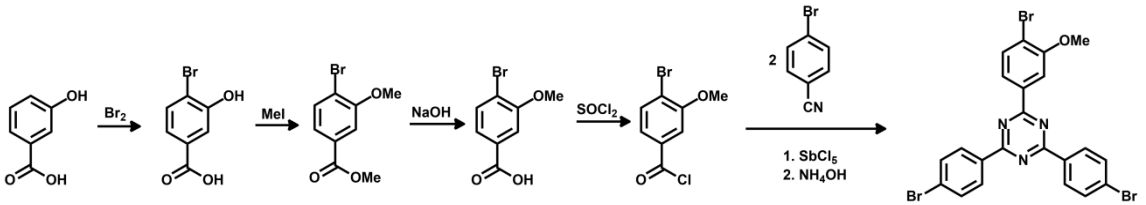

Figure S15: Illustration of the synthetic route to obtain mono-substituted methoxy-functionalized triazine-based trigonal linker for the synthesis of the elongated version of TATB.

2,4-Bis[4'-(methoxycarbonyl)-biphenyl-4-yl]-6-[2-methoxy-4'-(methoxycarbonyl)-biphenyl-4-yl]-1,3,5-triazine (7)

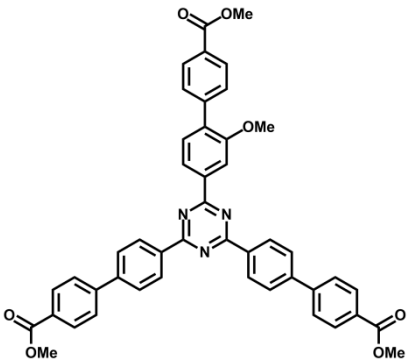

Under nitrogen atmosphere, 2-(4-bromo-3-methoxyphenyl)-4,6-bis(4-bromophenyl)-1,3,5-triazine (**5**, 5.00 g, 8.68 mmol), 4-methoxycarbonyl-phenylboronic acid (**6**, 6.10 g, 33.9 mmol), [1,1′-bis(diphenylphosphino) ferrocene] dichloro palladium(II) (635 mg, 868 µmol) and potassium phosphate (16.6 g, 78.1 mmol) were suspended in 1,4-dioxane (300 mL) and deionized water (30 mL). The mixture was stirred for 72 h at 120 °C and the solvent was evaporated in vacuo. Ethyl acetate (400 mL) and deionized water (100 mL) were added to

the residue. The organic layer was separated, washed with water (3 x 100 mL) and brine (1 x 100 mL) and dried with magnesium sulphate. The solvent was evaporated in vacuo and the residue was recrystallized from a mixture of toluene and *n*-heptane. A colourless solid was obtained. Yield: 4.1 g (4.94 mmol, 57 %).

^{1}H-NMR (500 MHz, 300 K, $CDCl_3$): δ = 8.88 (d, 4H, ^3J = 8.4 Hz, 2,4-Ar-*H*-2,6), 8.50 (dd, 1H, ^3J = 7.9 Hz, ^4J = 1.4 Hz, 6-Ar-*H*-5), 8.43 (d, 1H, ^4J = 1.4 Hz, 6-Ar-*H*-3), 8.17 (d, 4H, ^3J = 8.4 Hz, 2,4-Ar'-*H*-3,5), 8.13 (d, 2H, ^3J = 8.4 Hz, 6-Ar'-*H*-3,5), 7.86 (d, 4H, ^3J = 8.4 Hz, 2,4-Ar-*H*-3,5), 7.78 (d, 4H, ^3J = 8.4 Hz, 2,4-Ar'-*H*-2,6), 7.71 (d, 2H, ^3J = 8.4 Hz, 6-Ar'-*H*-2,6), 7.56 (d, 1H, ^3J = 7.9 Hz, 6-Ar-*H*-6), 4.04 (s, 3H, OCH_3), 3.97 (s, 6H, 2,4-Ar'-$CO_2C H_3$), 3.96 (s, 3H, 6-Ar'-$CO_2C H_3$) ppm.

2,4-Bis(4'-carboxy-biphenyl-4-yl)-6-(4'-carboxy-2-methoxy-biphenyl-4-yl)-1,3,5-triazine (8)

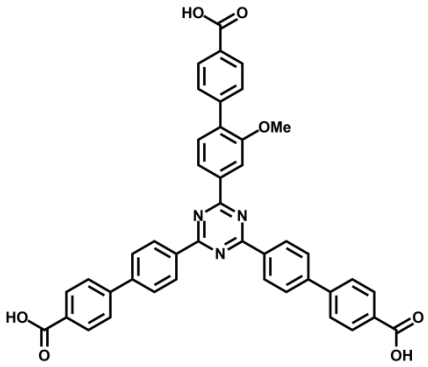

2,4-Bis[4'-(methoxycarbonyl)-biphenyl-4-yl)-6-[2-methoxy-4'-(methoxycarbonyl)-biphenyl-4-yl]-1,3,5-triazine (**7**, 3.00 g, 4.04 mmol) was mixed with 2 M aqueous sodium hydroxide (200 mL) and 1,4-dioxane (10 mL). The suspension was stirred for 12 h at 120 °C and became a clear solution. The reaction mixture was acidified with concentrated hydrochloric acid (200 mL) and the resulting precipitate was filtered off and washed with deionized water. A colorless solid was obtained. Yield: 2.74 g (3.92 mmol, 97 %).

^{1}H-NMR (500 MHz, 300K, DMSO-d_6): δ = 13.02 (br. s, 3H, CO_2H), 8.71 (d, 4H, ^3J = 8.4 Hz, 2,4-Ar-*H*-3,5), 8.33 (dd, 1H, *J* = 7.9 Hz, ^4J = 1.1 Hz, 6-Ar-*H*-5), 8.27 (d, 1H, ^4J = 1.1 Hz, 6-Ar-*H*-3), 8.04 (d, 4H, ^3J = 8.4 Hz, 2,4-Ar'-*H*-3,5), 8.00 (d, 2H, ^3J = 8.3 Hz, 6-Ar'-*H*-3,5), 7.91 (d, 4H, ^3J = 8.4 Hz, 2,4-Ar-*H*-2,6), 7.85 (d, 4H, ^3J = 8.4 Hz, 2,4-Ar'-*H*-2,6), 7.65 (d, 2H, ^3J = 8.3 Hz, 6-Ar'-*H*-2,6), 7.56 (d, 1H, ^3J = 7.9 Hz, 6-Ar-*H*-6), 3.95 (s, 3H, OCH_3) ppm.

2.3 Synthesis of iron(III) based MOFs exhibiting different linker topologies

Fe-TATB-BDC-a: A glass bottle (Schott Duran culture tube, Borosilicate, 5 mL) with a PBT cap equipped with a Teflon seal was used. $FeCl_3$ • 6 H_2O (60.0 mg, 0.222 mmol) was dissolved in DMF (1 mL) via ultrasonication. TATB acid (**4a**, 48.6 mg, 0.110 mmol) and 1,4-benzendicarboxylic acid (36.6 mg, 0.220 mmol) were added and dissolved via ultrasonication. The reaction mixture was placed in an oven and heated to 150 °C within 1 h, kept at this temperature for 20 h and afterwards slowly cooled down to room temperature within 1 h. The solid was isolated by centrifugation (Eppendorf centrifuge 5430, 7830 rpm, 5 min) and washed via suspension in DMF (10 mL) and subsequent centrifugation. Suspension and centrifugation were repeated three times. The isolated brick-red powdery solid was dried in vacuum ($2.4 \cdot 10^{-3}$ bar) for 6 h. The sample was extracted with methanol (4 Å molecular sieve was added to methanol phase) under nitrogen atmosphere using a Soxhlet device (5 mL) for 72 h. The powder (41.5 mg, 40%) was dried in vacuum ($2.4 \cdot 10^{-3}$ bar) for 6 h and afterwards the sample was stored under nitrogen atmosphere at room temperature.

Fe-TATB-BDC-b: A glass bottle (Schott Duran culture tube, Borosilicate, 5 mL) with a PBT cap equipped with a Teflon seal was used. $FeCl_3$ • 6 H_2O (60.0 mg, 0.222 mmol) was dissolved in DMF (1 mL) via ultrasonication. TATB acid (**4a**, 48.6 mg, 0.110 mmol) and 2-amino-1,4-benzenedicarboxylic acid (40.2 mg, 0.220 mmol) were added and dissolved via ultrasonication. The reaction mixture was placed in an oven and heated to 150 °C within 1 h, kept at this temperature for 20 h and afterwards slowly cooled down to room temperature within 1 h. The solid was isolated by centrifugation (Eppendorf centrifuge 5430, 7830 rpm, 5 min) and washed via suspension in DMF (10 mL) and subsequent centrifugation. Suspension and centrifugation were repeated three times. The isolated light brown powdery solid was dried under vacuum ($2.4 \cdot 10^{-3}$ bar) for 6 h. The sample was extracted with methanol (4 Å molecular sieve was added to methanol phase) under nitrogen atmosphere using a Soxhlet device (5 mL) for 72 h. The powder (46.5 mg, 44%) was dried in vacuum ($2.4 \cdot 10^{-3}$ bar) for 6 h and afterwards the sample was stored under nitrogen atmosphere at room temperature.

Fe-TATB-BDC-c: A glass bottle (Schott Duran culture tube, Borosilicate, 5 mL) with a PBT cap equipped with a Teflon seal was used. $FeCl_3$ • 6 H_2O (60.0 mg, 0.222 mmol) was dissolved in DMF (1 mL) via ultrasonication. TATB-NO_2(meta) acid (**4b**, 53.5 mg, 0.110 mmol) and 1,4-benzenedicarboxylic acid (36.6 mg, 0.220 mmol) were added and dissolved via ultrasonication. The reaction mixture was placed in an oven and heated to 150 °C within 1 h, kept at this temperature for 20 h and afterwards slowly cooled down to room temperature within 1 h. The solid was isolated by centrifugation (Eppendorf centrifuge 5430, 7830 rpm, 5 min) and washed via suspension in DMF (10 mL) and subsequent centrifugation. Suspension and centrifugation were repeated three times. The isolated

orange powdery solid was dried under vacuum ($2.4 \cdot 10^{-3}$ bar) for 6 h. The sample was extracted with methanol (4 Å molecular sieve was added to methanol phase) under nitrogen atmosphere using a Soxhlet device (5 mL) for 72 h. The powder (38.2 mg, 35%) was dried in vacuum ($2.4 \cdot 10^{-3}$ bar) for 6 h and afterwards the sample was stored under nitrogen atmosphere at room temperature.

Fe-TATB-BDC-d: A glass bottle (Schott Duran culture tube, Borosilicate, 5 mL) with a PBT cap equipped with a Teflon seal was used. $FeCl_3 \bullet 6\ H_2O$ (60.0 mg, 0.222 mmol) was dissolved in DMF (1 mL) via ultrasonication. TATB-NO_2(ortho) acid (**4c**, 53.5 mg, 0.110 mmol) and 1,4-benzenedicarboxylic acid (36.6 mg, 0.220 mmol) were added and dissolved via ultrasonication. The reaction mixture was placed in an oven and heated to 150 °C within 1 h, kept at this temperature for 20 h and afterwards slowly cooled down to room temperature within 1 h. The solid was isolated by centrifugation (Eppendorf centrifuge 5430, 7830 rpm, 5 min) and washed via suspension in DMF (10 mL) and subsequent centrifugation. Suspension and centrifugation were repeated three times. The isolated dark brown powdery solid was dried under vacuum ($2.4 \cdot 10^{-3}$ bar) for 6 h. The sample was extracted with methanol (4 Å molecular sieve was added to methanol phase) under nitrogen atmosphere using a Soxhlet device (5 mL) for 72 h. The powder (39.6 mg, 36%) was dried in vacuum ($2.4 \cdot 10^{-3}$ bar) for 6 h and afterwards the sample was stored under nitrogen atmosphere at room temperature.

Fe-TATB-BDC-e: A glass bottle (Schott Duran culture tube, Borosilicate, 5 mL) with a PBT cap equipped with a Teflon seal was used. FeCl3 • 6 H2O (60.0 mg, 0.222 mmol) was dissolved in DMF (1 mL) via ultrasonication. TATB-NO2(meta) acid (4b, 53.5 mg, 0.110 mmol) and 2-amino-1,4-benzenedicarboxylic acid (40.2 mg, 0.222 mmol) were added and dissolved via ultrasonication. The reaction mixture was placed in an oven and heated to 150 °C within 1 h, kept at this temperature for 20 h and afterwards slowly cooled down to room temperature within 1 h. The solid was isolated by centrifugation (Eppendorf centrifuge 5430, 7830 rpm, 5 min) and washed via suspension in DMF (10 mL) and subsequent centrifugation. Suspension and centrifugation were repeated three times. The isolated light brown powdery solid was dried under vacuum (2.4·10-3 bar) for 6 h. The sample was extracted with methanol (4 Å molecular sieve was added to methanol phase) under nitrogen atmosphere using a Soxhlet device (5 mL) for 72 h. The powder (63.1 mg, 57%) was dried in vacuum (2.4·10-3 bar) for 6 h and afterwards the sample was stored under nitrogen atmosphere at room temperature.

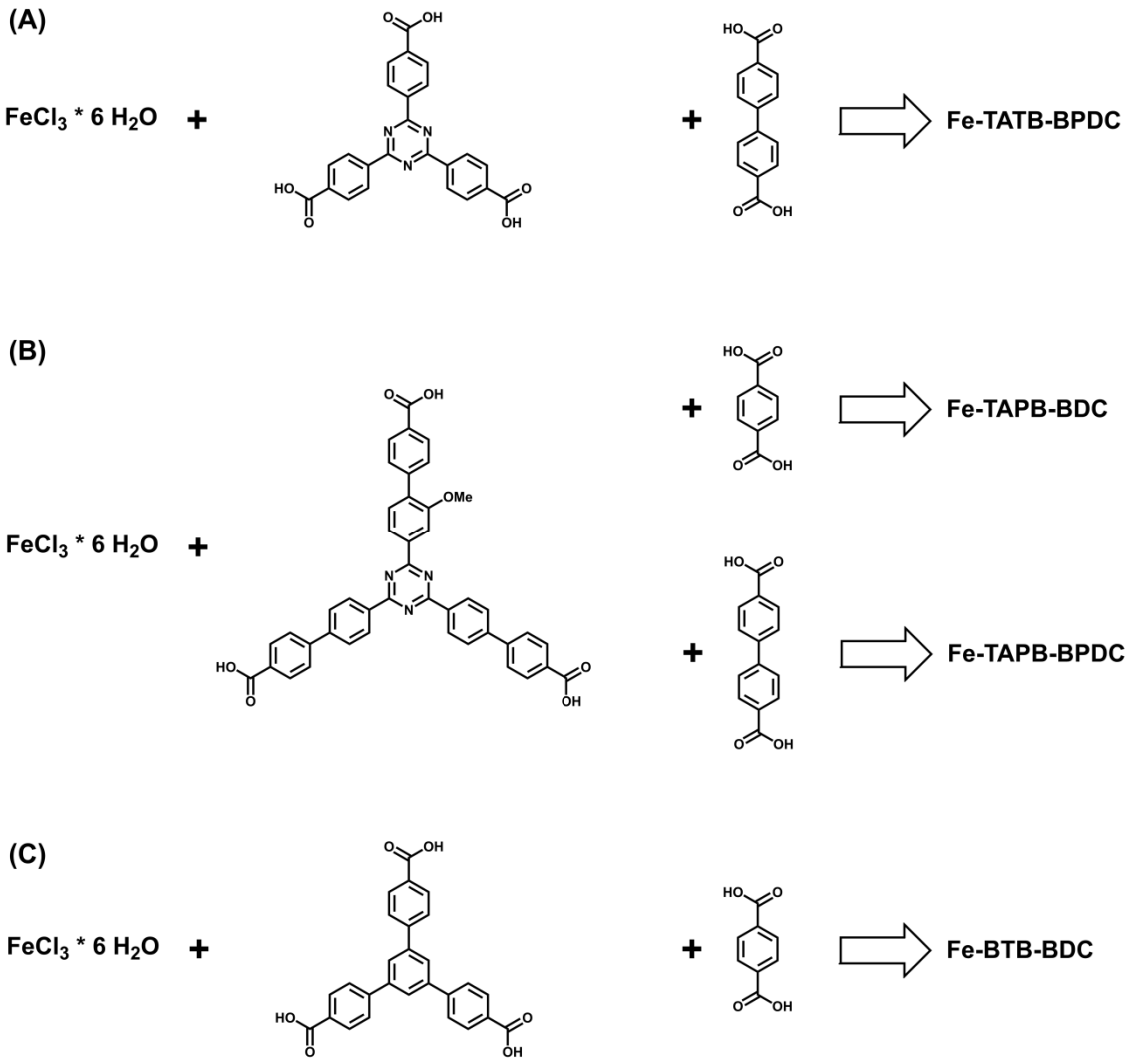

Figure S16: Scheme representing the additional tried combinations for the synthesis of iron(III)-based MOFs. a) The elongation of the 1,4-benzendicarboxylic acid was investigated, while b) an elongation of the TATB linker was examined in combination with the 1,4-benzenedicarboxylic acid and its elongated version, biphenyl-4,4'-dicarboxylic acid. c) Iron(III)-based MOF consisting of the trigonal linker BDC, this MOF is already known in the literature[2] as MIL-142 or MIL-143 – isomeric structures with different linker contents – and was synthesized for comparison reasons.

Fe-TATB-BPDC: A glass bottle (Schott Duran culture tube, Borosilicate, 5 mL) with a PBT cap equipped with a Teflon seal was used. $FeCl_3$ • 6 H_2O (60.0 mg, 0.222 mmol) was dissolved in DMF (1 mL) by ultrasonic treatment. TATB acid (**4a**, 48.6 mg, 0.110 mmol) and biphenyl-4,4'-dicarboxylic acid (53.3 mg, 0.220 mmol) were added and dissolved through ultrasonic treatment. The reaction mixture was placed in an oven and heated to 150 °C within 1 h, kept at this temperature for 20 h and afterwards slowly cooled down to room temperature within 1 h. The solid was isolated bycentrifugation (Eppendorf centrifuge 5430, 7830 rpm, 5 min) and washed via suspension in DMF (10 mL) and subsequent centrifugation. Suspension and centrifugation were repeated three times. The isolated red brown powdery solid (24.9 mg, 21%) was dried in vacuum ($2.4 \cdot 10^{-3}$ bar) for 6 h and stored under nitrogen atmosphere at room temperature.

Fe-TAPB-BDC: A glass bottle (Schott Duran culture tube, Borosilicate, 5 mL) with a PBT cap equipped with a Teflon seal was used. $FeCl_3 \cdot 6\ H_2O$ (60.0 mg, 0.222 mmol) was dissolved in DMF (1 mL) via ultrasonication. TAPB acid (**8**, 77.7 mg, 0.110 mmol) and 1,4-benzenedicarboxylic acid (36.6 mg, 0.220 mmol) were added and dissolved via ultrasonication. The reaction mixture was placed in an oven and heated to 150 °C within 1 h, kept at this temperature for 20 h and afterwards slowly cooled down to room temperature within 1 h. The solid was isolated by centrifugation (Eppendorf centrifuge 5430, 7830 rpm, 5 min) and washed via suspension in DMF (10 mL) and subsequent centrifugation. Suspension and centrifugation were repeated three times. The isolated ochre powdery solid (59.6 mg, 45%) was dried in vacuum ($2.4 \cdot 10^{-3}$ bar) for 6 h and stored under nitrogen atmosphere at room temperature.

Fe-TAPB-BPDC: A glass bottle (Schott Duran culture tube, Borosilicate, 5 mL) with a PBT cap equipped with a Teflon seal was used. $FeCl_3 \cdot 6\ H_2O$ (60.0 mg, 0.222 mmol) was dissolved in DMF (1 mL) via ultrasonication. TAPB acid (**8**, 77.7 mg, 0.110 mmol) and biphenyl-4,4'-dicarboxylic acid (53.3 mg, 0.220 mmol) were added and dissolved via ultrasonication. The reaction mixture was placed in an oven and heated to 150 °C within 1 h, kept at this temperature for 20 h and afterwards slowly cooled down to room temperature within 1 h. The solid was isolated by centrifugation (Eppendorf centrifuge 5430, 7830 rpm, 5 min) and washed via suspension in DMF (10 mL) and subsequent centrifugation. Suspension and centrifugation were repeated three times. The isolated yellow powdery solid (26.9 mg, 19%) was dried in vacuum ($2.4 \cdot 10^{-3}$ bar) for 6 h and stored under nitrogen atmosphere at room temperature.

Fe-BTB-BDC: A glass bottle (Schott Duran culture tube, Borosilicate, 5 mL) with a PBT cap equipped with a Teflon seal was used. $FeCl_3 \cdot 6\ H_2O$ (405 mg, 1.50 mmol) was dissolved in DMF (3 mL) via ultrasonication. 4,4′,4″,-benzene-1,3,5-triyl-tris(benzoic acid) (292 mg, 0.660 mmol) and 1,4-benzenedicarboxylic acid (83.0 mg, 0.500 mmol) were added and dissolved via ultrasonication. The reaction mixture was placed in an oven and heated to 150 °C within 1 h, kept at this temperature for 20 h and afterwards slowly cooled down to room temperature within 1 h. The solid was isolated by centrifugation (Eppendorf centrifuge 5430, 7830 rpm, 5 min) and washed via suspension in DMF (10 mL) and subsequent centrifugation. Suspension and centrifugation were repeated three times. The isolated orange-yellow powdery solid was dried under vacuum ($2.4 \cdot 10^{-3}$ bar) for 6 h. The sample was extracted with methanol (4 Å molecular sieve was added to methanol phase) under nitrogen atmosphere using a Soxhlet device (5 mL) for 72 h. The powder (280 mg, 56%) was dried in

vacuum ($2.4 \cdot 10^{-3}$ bar) for 6 h and afterwards the sample was stored under nitrogen atmosphere at room temperature.

2.4 Stability tests

The sample was tested against water, 1 M hydrochloric acid, and 1 M sodium hydroxide. An Eppendorf tube was filled with 5 mg of the MOF sample and 500 µL of either Millipore water, 1 M hydrochloric acid or 1 M sodium hydroxide were added. The tubes were placed into a Thermo-Shaker (Peglab, TS-100) at 25 °C for a defined period of time, either 1 d, 2 d, 3 d, 7 d or 14 d. Afterwards the samples were centrifuged (Eppendorf centrifuge 5418 R, 14000 rpm, 10 min), the supernatant was pipetted off, and the MOF material was dried in an oven at 100 °C for 3 h before PXRD investigations were carried out.

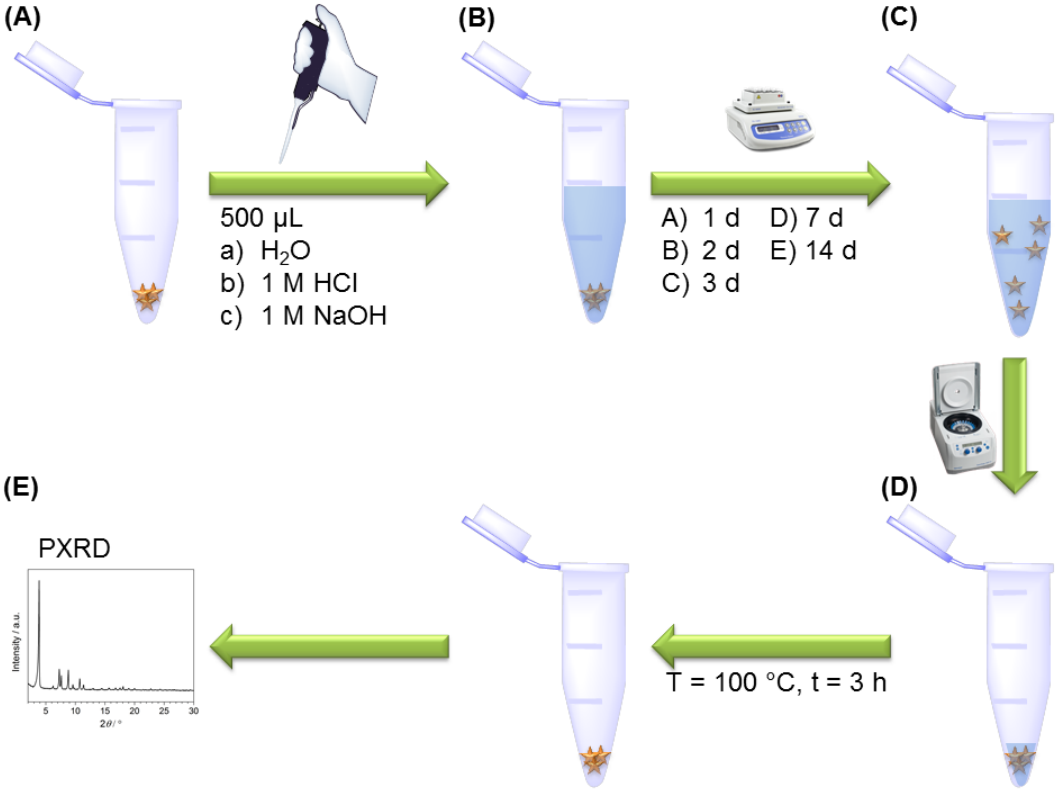

Figure S17: Schematic representation of the strategy for investigating the stability of the MOF samples. The procedure was the following: A) An Eppendorf tube is loaded with 5 mg of the MOF sample and 500 µL either of Millipore water, 1 M hydrochloric acid or 1 M sodium hydroxide were added. B) The mixture was placed on a Thermo-Shaker and shaked at T = 25 °C for either 1 d, 2 d, 3 d, 7 d or 14 d. C) The suspension was centrifuged and the supernatant was pipetted off. D) The resulting wet MOF powder was dried in a preheated oven at T = 100 °C for 3 h. E) The MOF sample was investigated with a PXRD measurement.

3. Figures

2-(4-Bromo-3-methoxyphenyl)-4,6-bis(4-bromophenyl)-1,3,5-triazine (5)

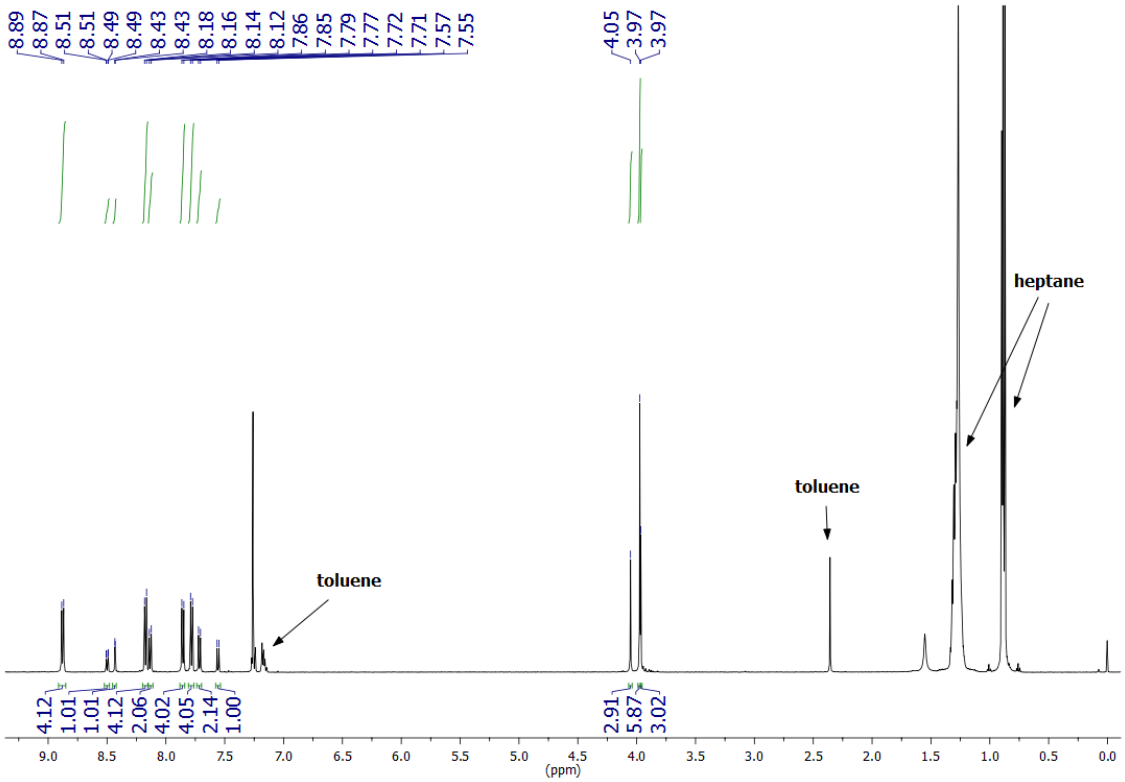

Figure S18: ^{1}H-NMR spectrum (500 MHz, 300 K, $CDCl_3$) of 2-(4-bromo-3-methoxyphenyl)-4,6-bis(4-bromophenyl)-1,3,5-triazine (**5**).

2,4-Bis(4'-carboxy-biphenyl-4-yl)-6-(4'-carboxy-2-methoxy-biphenyl-4-yl)-1,3,5-triazine (8)

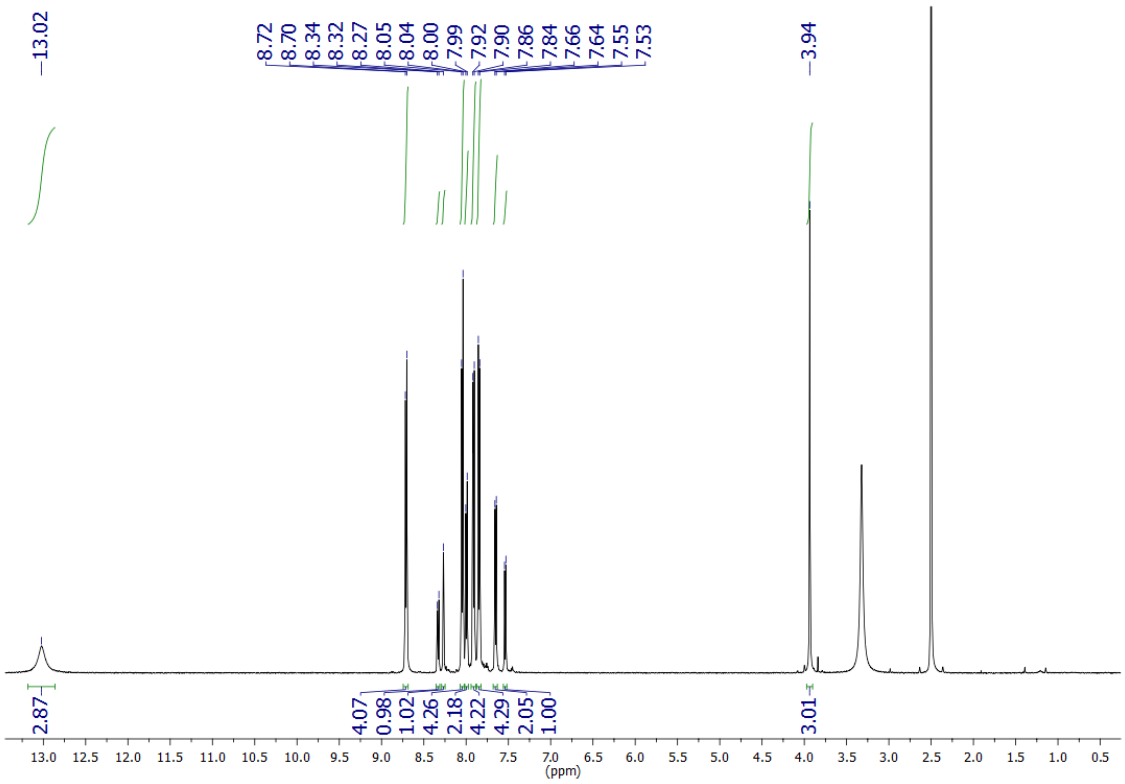

Figure S19: ^{1}H-NMR spectrum (500 MHz, 300 K, DMSO-d_6) of 2,4-bis(4'-carboxy-biphenyl-4-yl)-6-(4'-carboxy-2-methoxy-biphenyl-4-yl]-1,3,5-triazine (**8**).

Fe-TATB-BDC-a

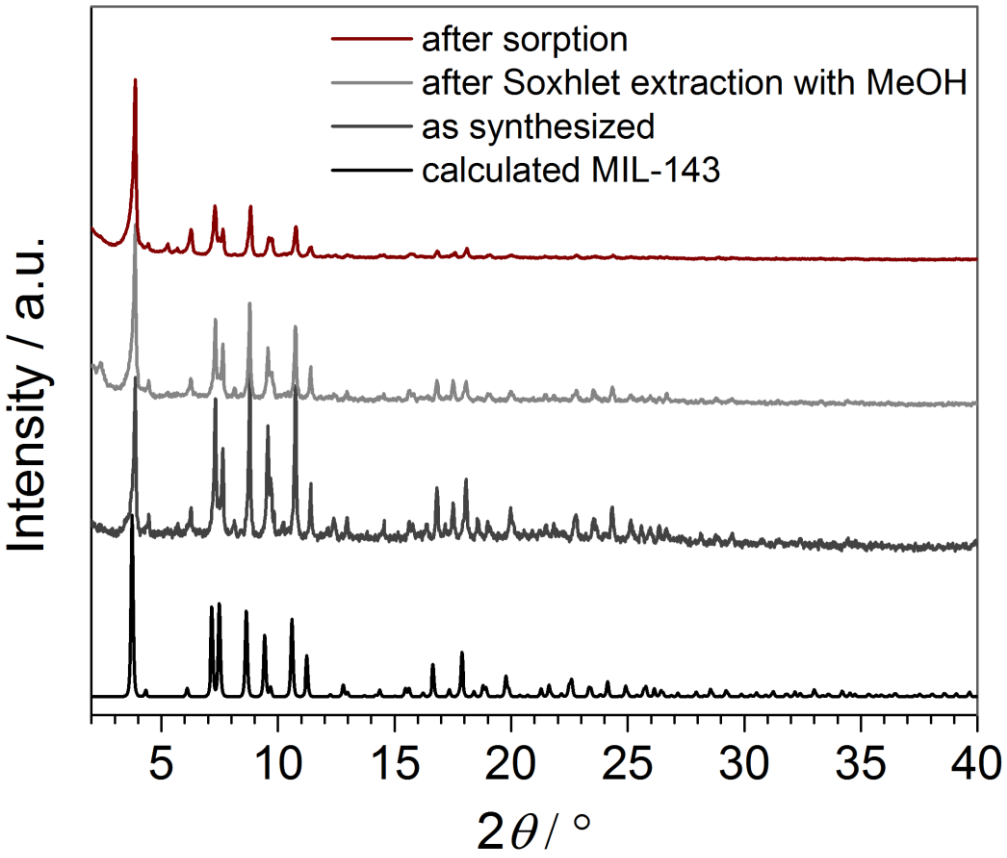

Figure S20: PXRD patterns of Fe-TATB-BDC-a as synthesized (dark gray), after Soxhlet extraction with methanol (light gray), and after sorption isotherm measurement (dark red) are compared to the calculated pattern of MIL-143 (black). All data are from the same synthesis batch.

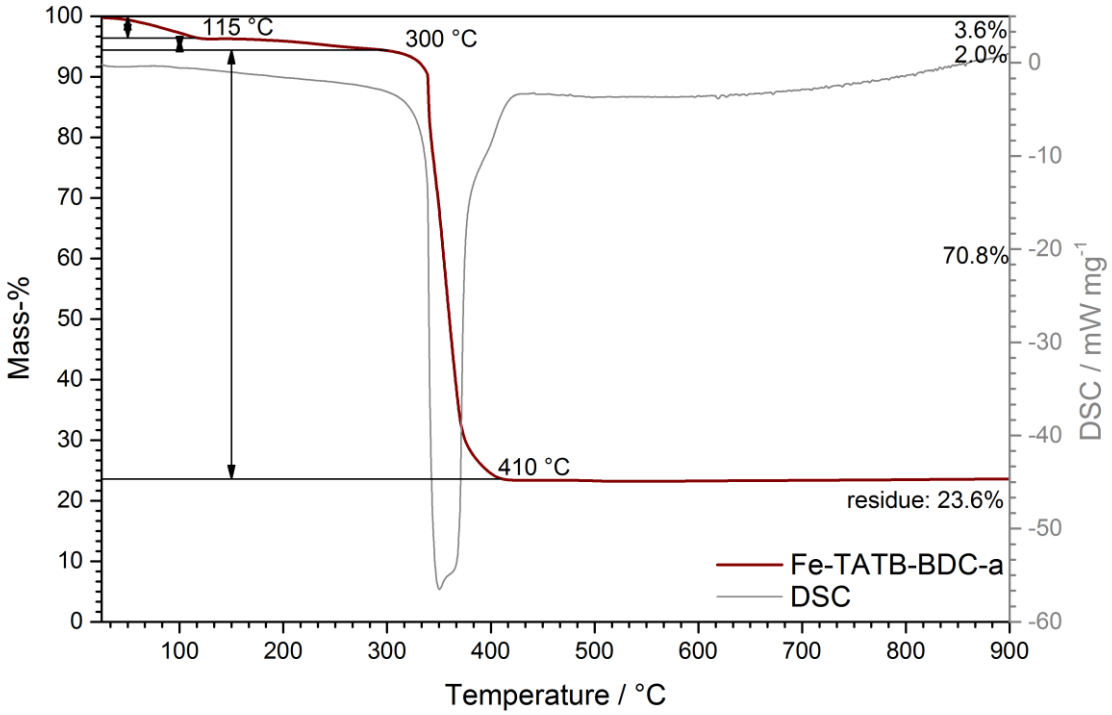

Figure S21: Results of thermogravimetric analysis (dark red curve) and differential scanning calorimetry (light gray curve) of Fe-TATB-BDC-a in flowing air with a heating rate of 10 ^{o}C min^{-1}. Prior to the TGA/DSC measurement, the material had been used for the nitrogen sorption experiments. The start temperature of the decomposition and the mass loss of individual steps are indicated.

Table S1: Mass-losses of Fe-TATB-BDC-a during thermogravimetric analysis: experimentally determined data (Figure S7), experimentally determined data taking the content of guests into account, and calculated data based on the ideal composition of Fe-TATB-BDC-a [$Fe_3O(Cl)(H_2O)_2(BDC)_{3/2}(TATB)$].

	experimental	**guest free**	**calculated**
guest	5.6%		
linker	70.8%	75.0%	74.5%
residue	23.6%	25.0%	25.5%

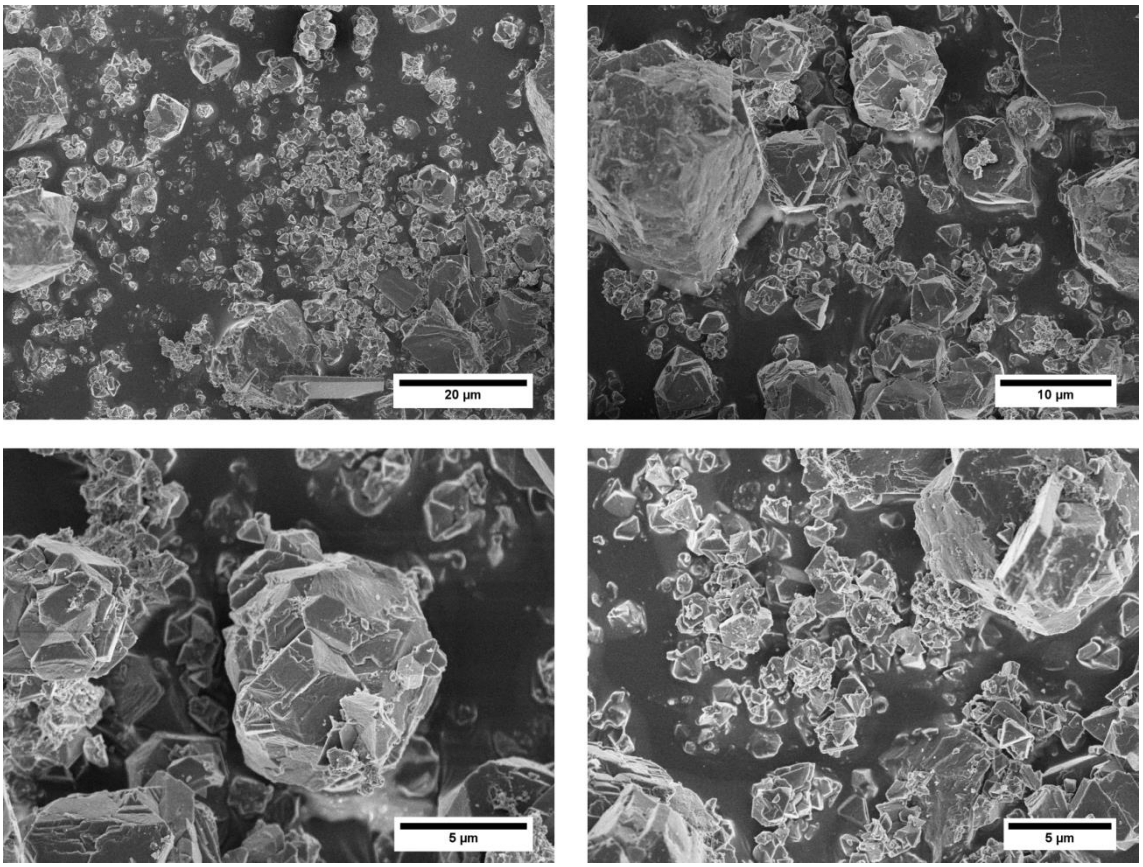

Figure S22: SEM images of the Fe-TATB-BDC-a recorded at different magnifications, showing randomly shaped particles with small and large crystallite sizes.

Fe-TATB-BDC-b

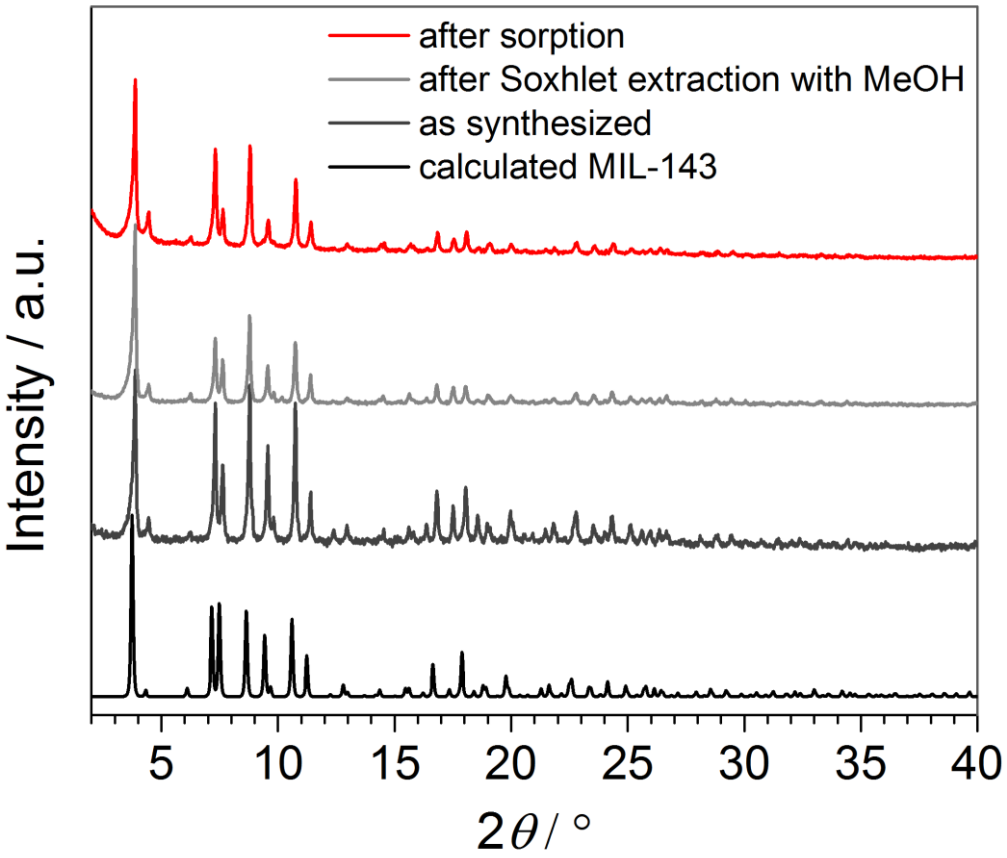

Figure S23: PXRD patterns of Fe-TATB-BDC-b as synthesized (dark gray), after Soxhlet extraction with methanol (light gray), and after sorption isotherm measurement (red) are compared to the calculated pattern of MIL-143 (black). All data are from the same synthesis batch.

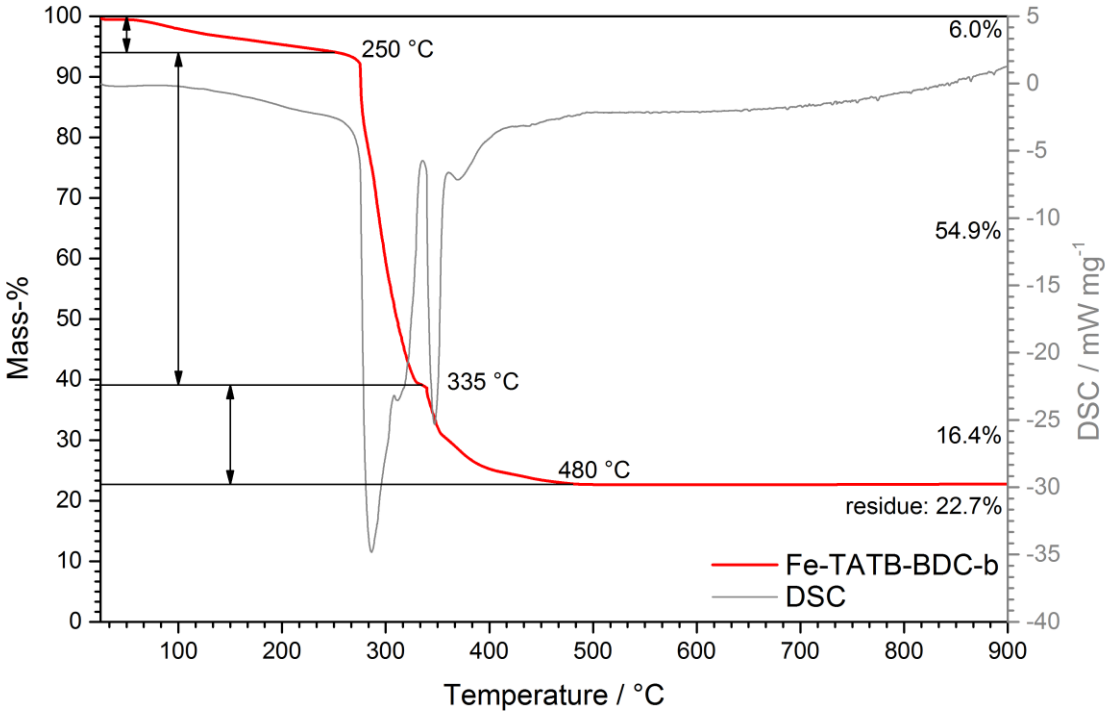

Figure S24: Results of thermogravimetric analysis (red curve) and differential scanning calorimetry (light gray curve) of Fe-TATB-BDC-b in flowing air with a heating rate of 10 ^{o}C min^{-1}. Prior to the TGA/DSC measurement, the material had been used for the nitrogen sorption experiments. The start temperature of the decomposition and the mass loss of individual steps are indicated.

Table S2: Mass-losses of Fe-TATB-BDC-b during thermogravimetric analysis: experimentally determined data (Figure S10), experimentally determined data taking the content of guests into account, and calculated data based on the ideal composition of Fe-TATB-BDC-b [$Fe_3O(Cl)(H_2O)_2(BDC\text{-}NH_2)_{3/2}(TATB)$].

	experimental	**guest free**	**calculated**
guest	6.0%		
linker	71.3%	75.8%	75.1%
residue	22.7%	24.2%	24.9%

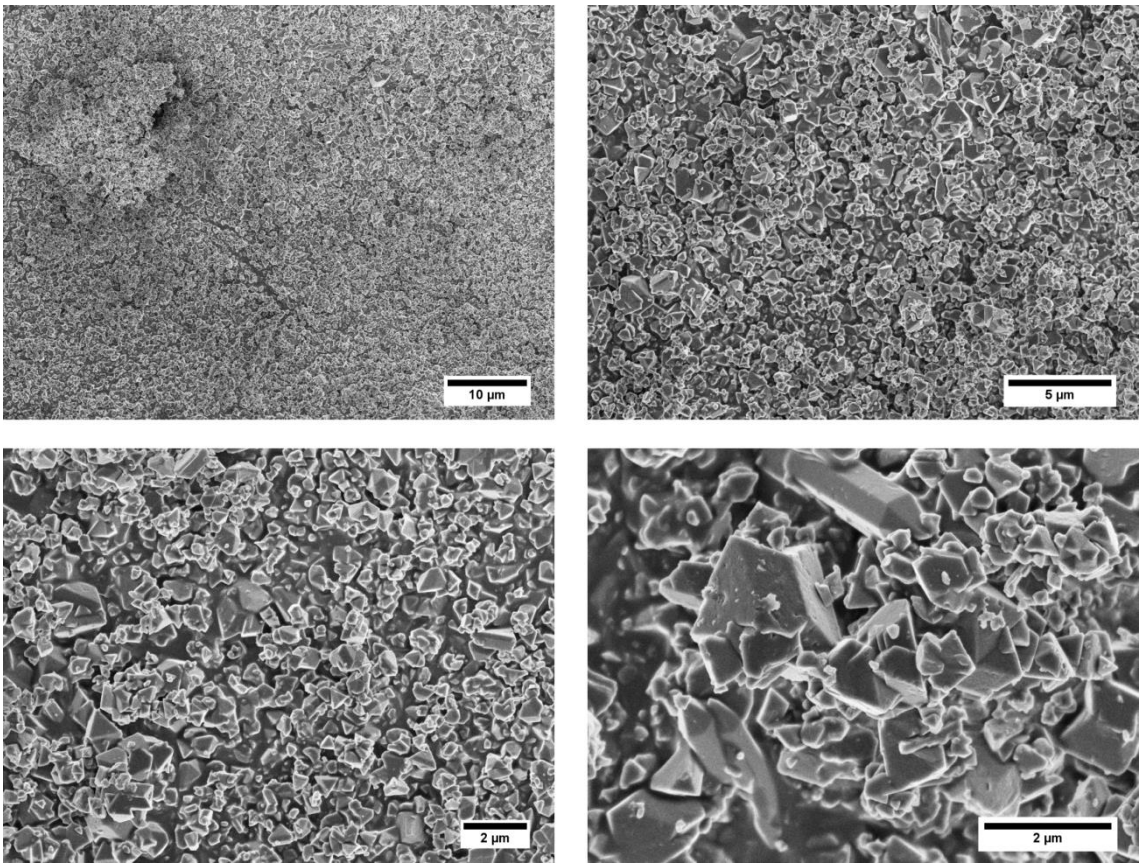

Figure S25: SEM images of the Fe-TATB-BDC-b recorded at different magnifications, showing randomly shaped particles with similar crystallite sizes.

Fe-TATB-BDC-c

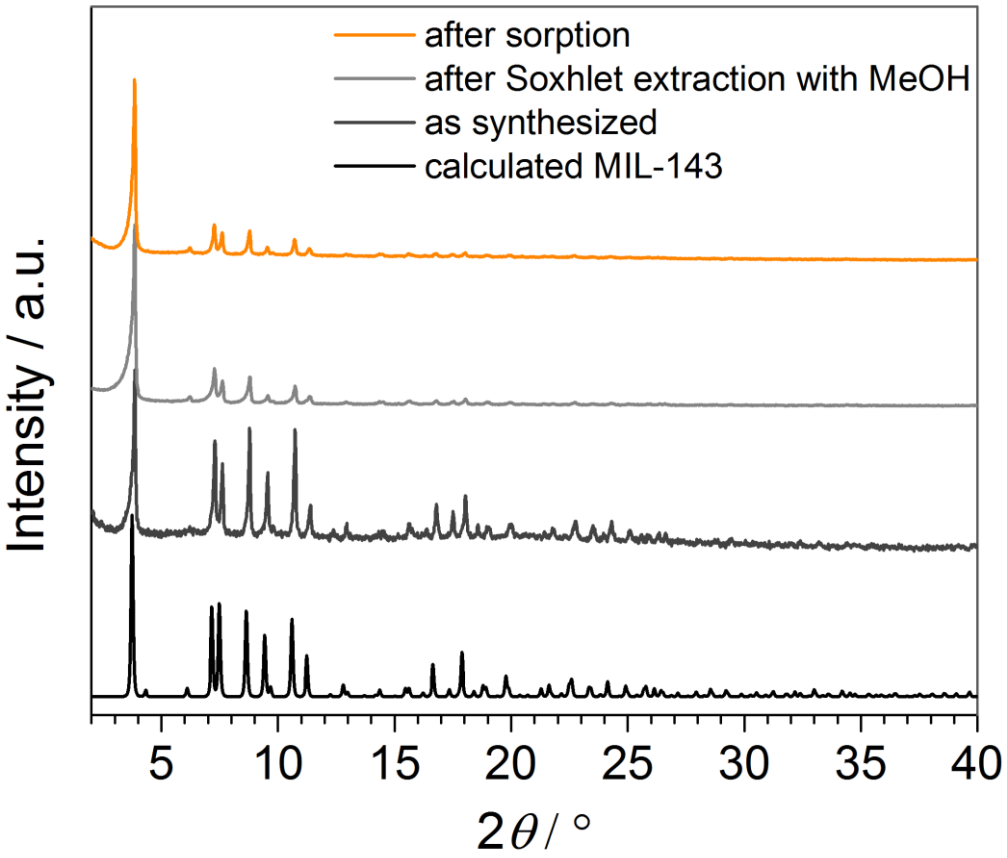

Figure S26: PXRD patterns of Fe-TATB-BDC-c as synthesized (dark gray), after Soxhlet extraction with methanol (light gray), and after sorption isotherm measurement (orange) are compared to the calculated pattern of MIL-143 (black). All data are from the same synthesis batch.

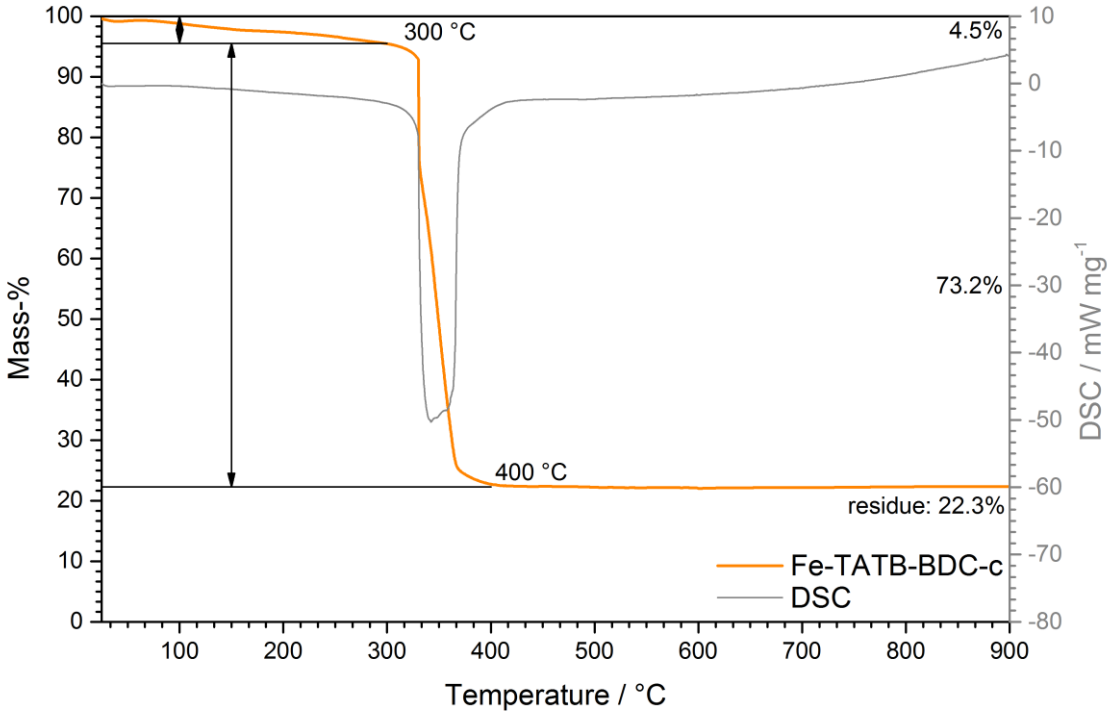

Figure S27: Results of thermogravimetric analysis (orange curve) and differential scanning calorimetry (light gray curve) of Fe-TATB-BDC-c in flowing air with a heating rate of 10 ^{o}C min^{-1}. Prior to the TGA/DSC measurement, the material had been used for the nitrogen sorption experiments. The start temperature of the decomposition and the mass loss of individual steps are indicated.

Table S3: Mass-losses of Fe-TATB-BDC-c during thermogravimetric analysis: experimentally determined data (Figure S13), experimentally determined data taking the content of guests into account, and calculated data based on the ideal composition of Fe-TATB-BDC-c [$Fe_3O(Cl)(H_2O)_2(BDC)_{3/2}$(TATB-$NO_2$(*meta*))].

	experimental	**guest free**	**calculated**
guest	4.5%		
linker	73.2%	76.6%	75.7%
residue	22.3%	23.4%	24.3%

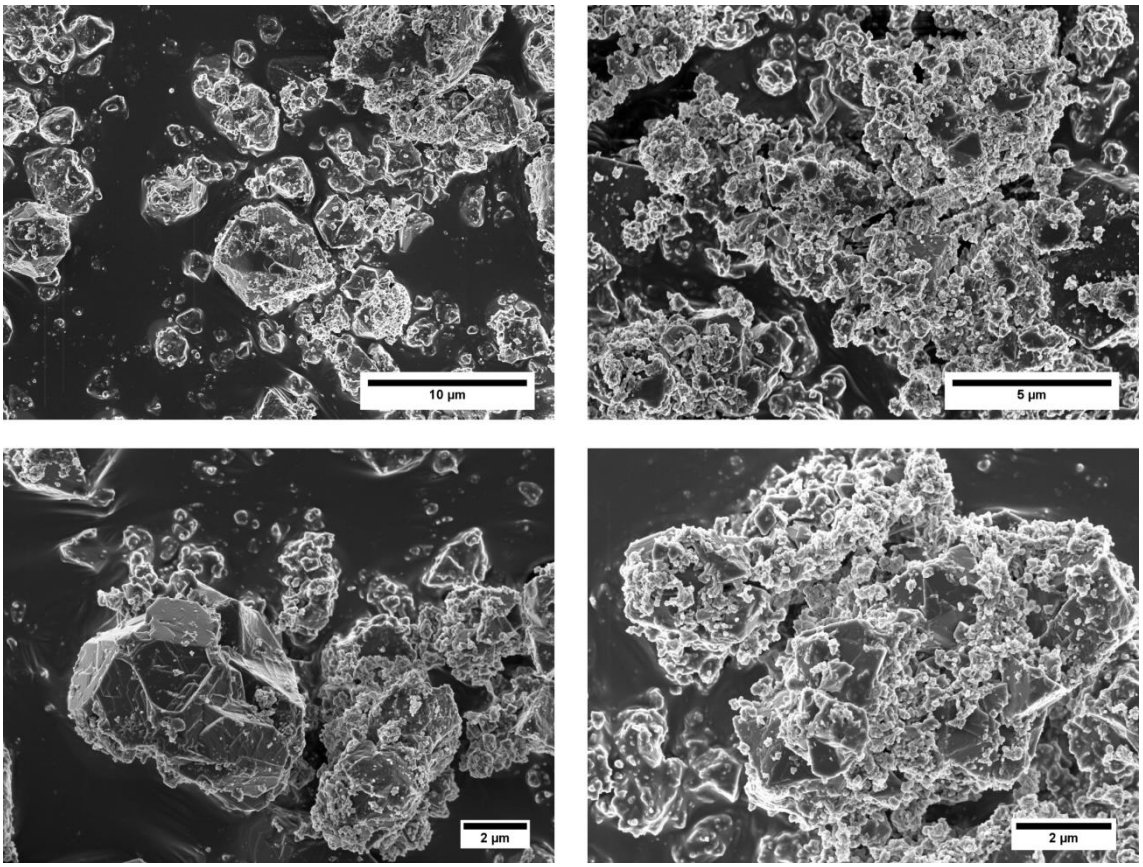

Figure S28: SEM images of the Fe-TATB-BDC-c recorded at different magnifications, showing randomly shaped particles with small and large crystallite sizes.

Fe-TATB-BDC-d

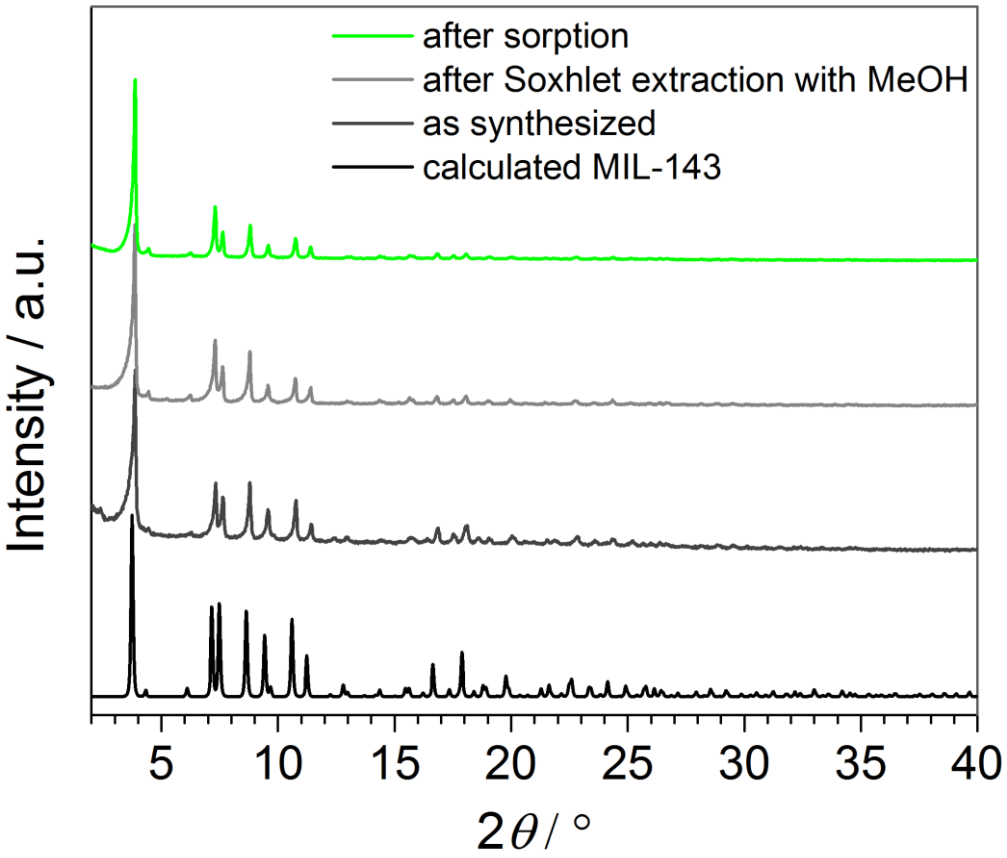

Figure S29: PXRD patterns of Fe-TATB-BDC-d as synthesized (dark gray), after Soxhlet extraction with methanol (light gray), and after sorption isotherm measurement (light green) are compared to the calculated pattern of MIL-143 (black). All data are from the same synthesis batch.

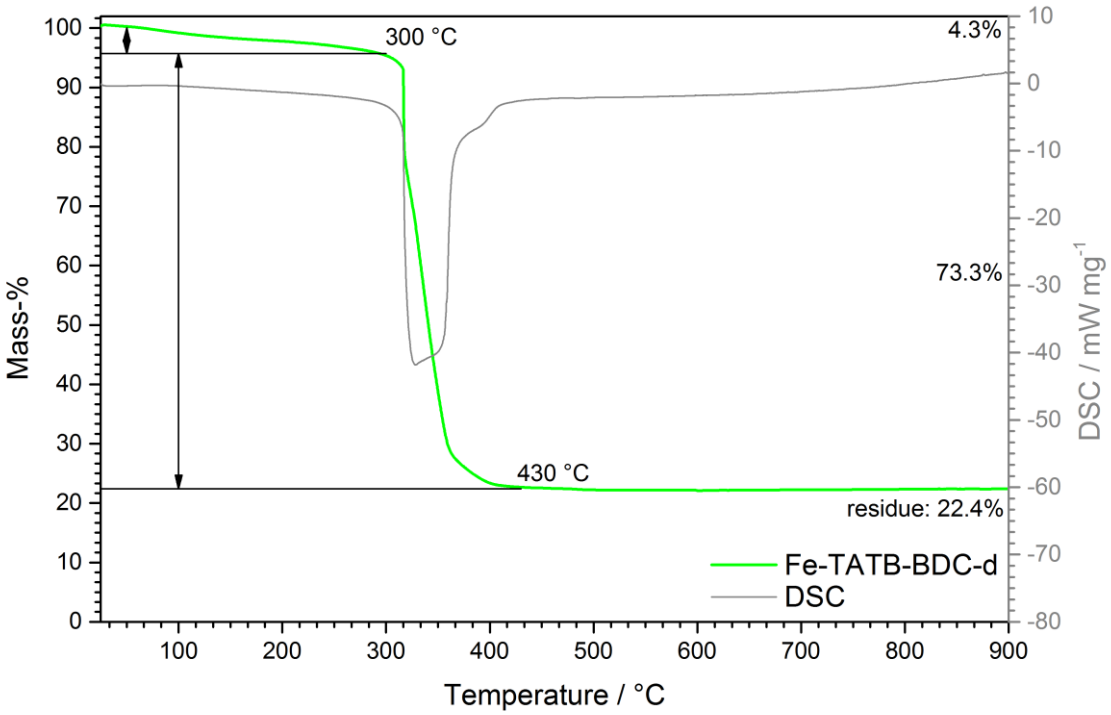

Figure S30: Results of thermogravimetric analysis (light green curve) and differential scanning calorimetry (light gray curve) of Fe-TATB-BDC-d in flowing air with a heating rate of 10 ^{o}C min^{-1}. Prior to the TGA/DSC measurement, the material had been used for the nitrogen sorption experiments. The start temperature of the decomposition and the mass loss of individual steps are indicated.

Table S4: Mass-losses of Fe-TATB-BDC-d during thermogravimetric analysis: experimentally determined data (Figure S16), experimentally determined data taking the content of guests into account, and calculated data based on the ideal composition of Fe-TATB-BDC-d [$Fe_3O(Cl)(H_2O)_2(BDC)_{3/2}$(TATB-$NO_2$(*ortho*))].

	experimental	**guest free**	**calculated**
guest	4.3%		
linker	73.3%	76.6%	75.7%
residue	22.4%	23.4%	24.3%

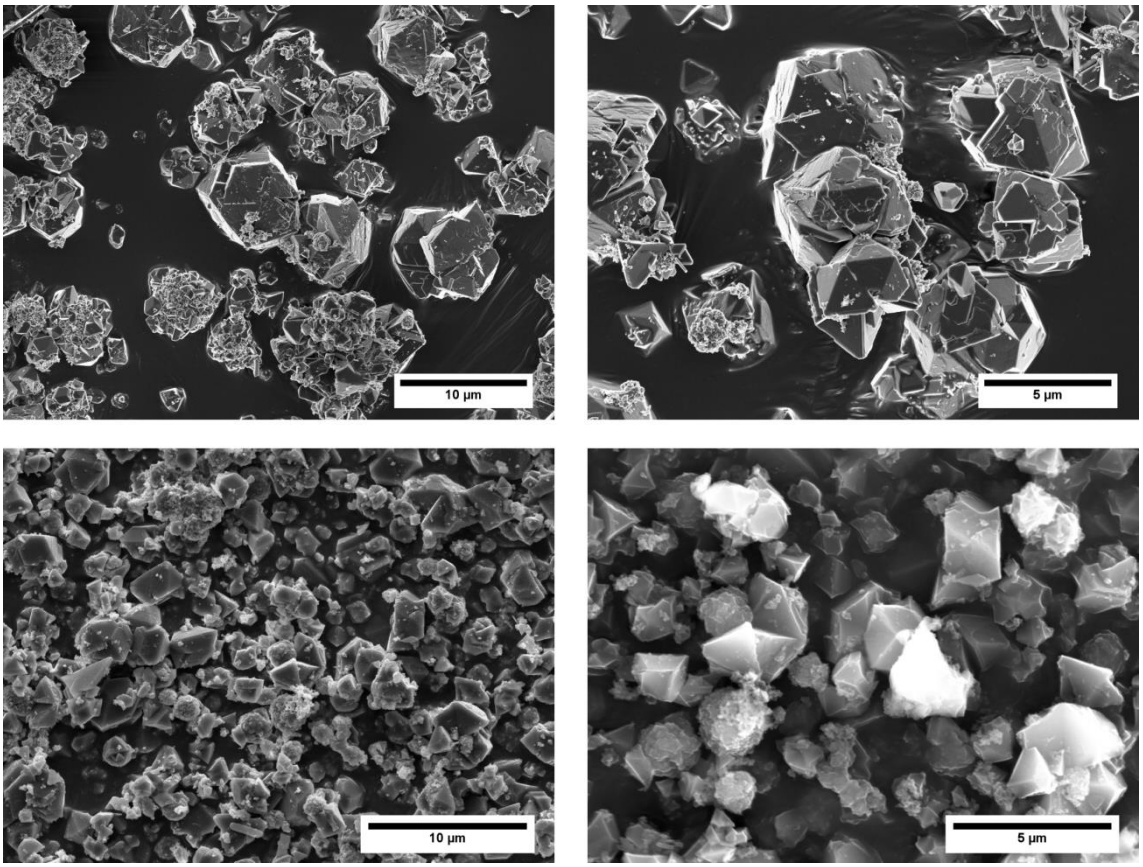

Figure S31: SEM images of the Fe-TATB-BDC-d recorded at different magnifications, showing randomly shaped particles with small and large crystallite sizes.

Fe-TATB-BDC-e

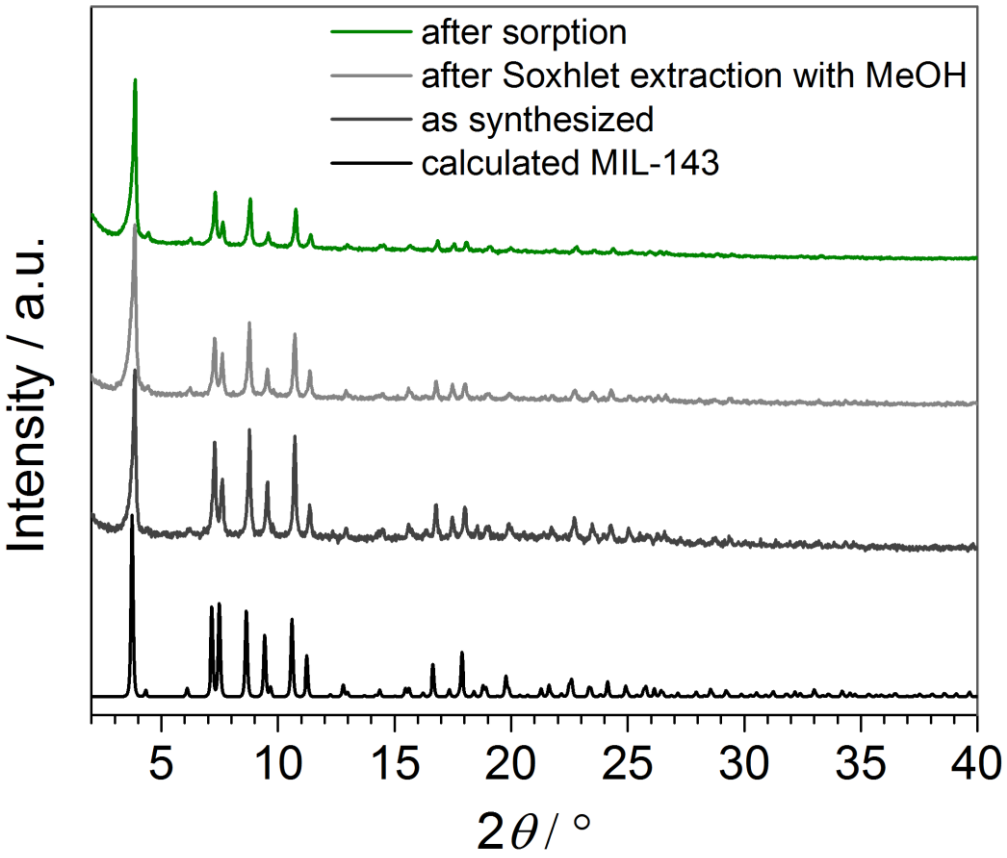

Figure S32: PXRD patterns of Fe-TATB-BDC-e as synthesized (dark gray), after Soxhlet extraction with methanol (light gray), and after sorption isotherm measurement (dark green) are compared to the calculated pattern of MIL-143 (black). All data are from the same synthesis batch.

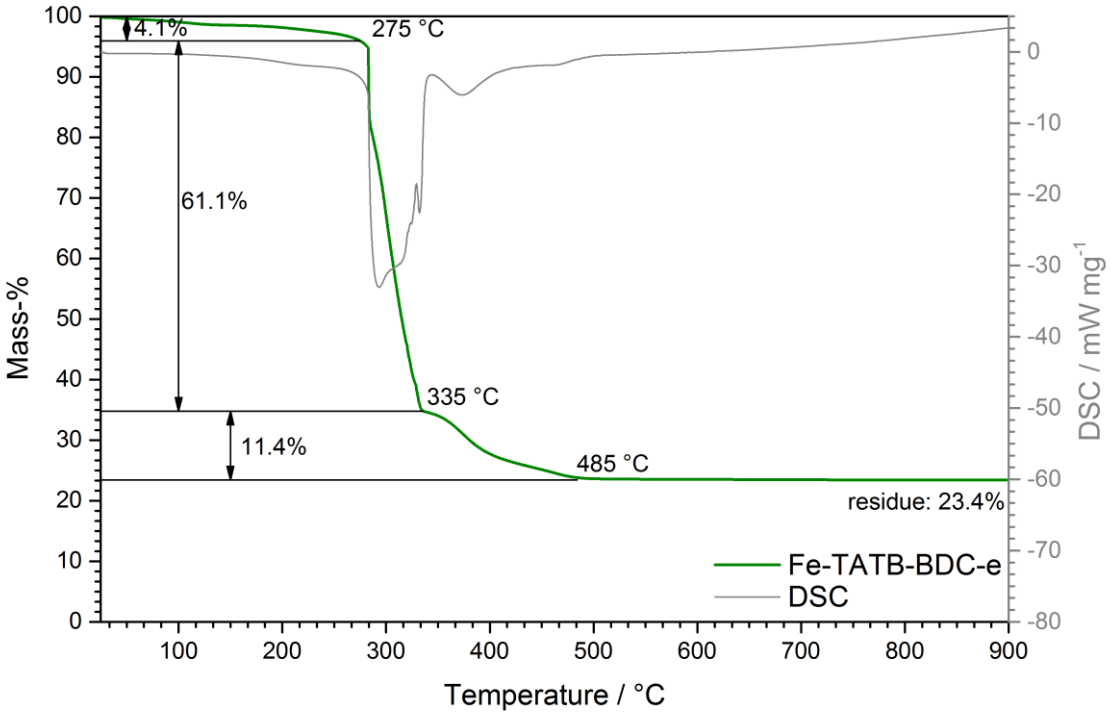

Figure S33: Results of thermogravimetric analysis (dark green curve) and differential scanning calorimetry (light gray curve) of Fe-TATB-BDC-e in flowing air with a heating rate of 10 ^{o}C min^{-1}. Prior to the TGA/DSC measurement, the material had been used for the nitrogen sorption experiments. The start temperature of the decomposition and the mass loss of individual steps are indicated.

Table S5: Mass-losses of Fe-TATB-BDC-e during thermogravimetric analysis: experimentally determined data (Figure S19), experimentally determined data taking the content of guests into account, and calculated data based on the ideal composition of Fe-TATB-BDC-e [$Fe_3O(Cl)(H_2O)_2(BDC\text{-}NH_2)_{3/2}(TATB\text{-}NO_2(\textit{meta}))$].

	experimental	**guest free**	**calculated**
guest	4.1%		
linker	72.5%	75.6%	76.2%
residue	23.4%	24.4%	23.8%

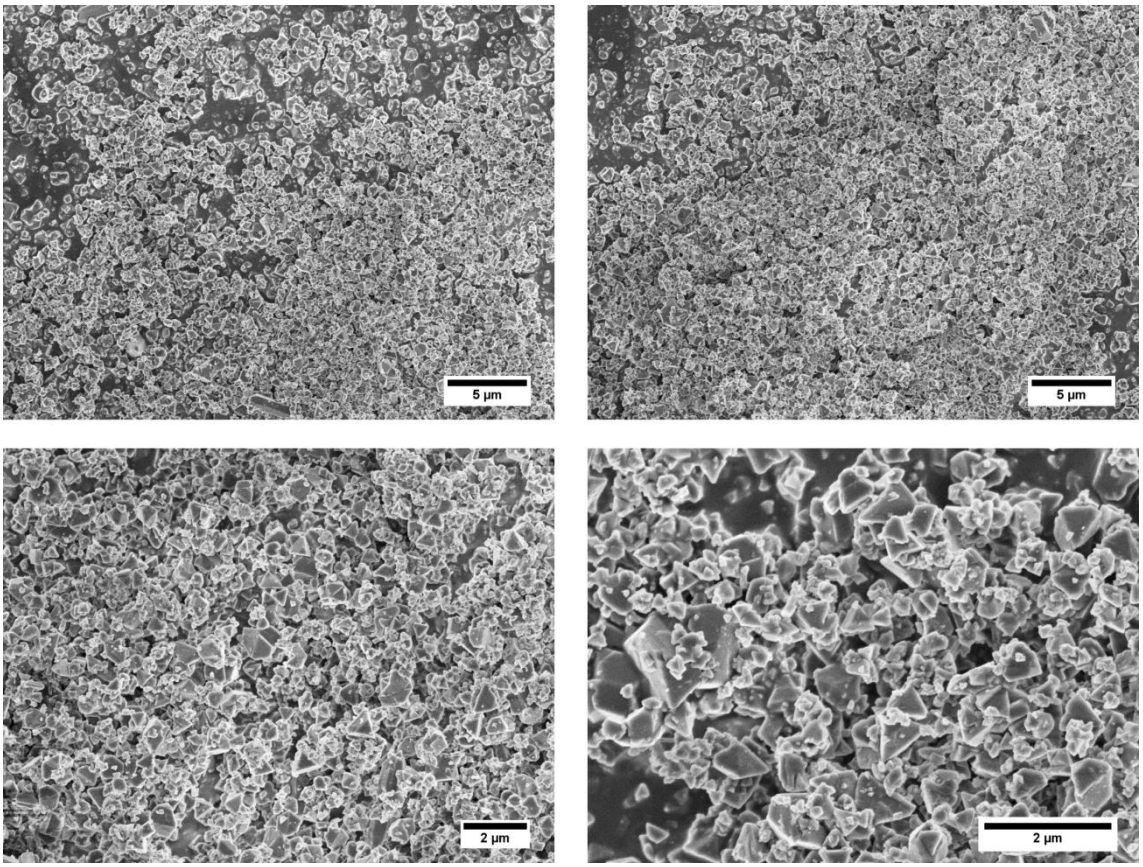

Figure S34: SEM images of the Fe-TATB-BDC-e recorded at different magnifications, showing randomly shaped particles with similar crystallite sizes.

Fe-TATB-BPDC

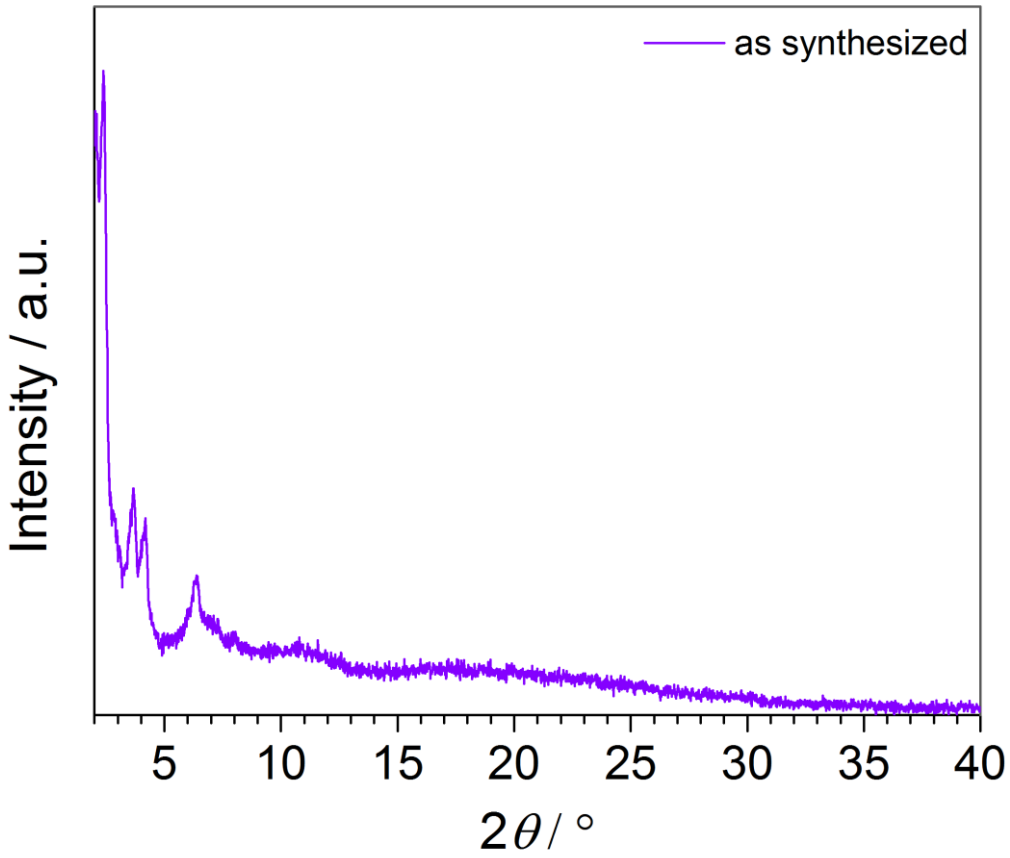

Figure S35: PXRD pattern of Fe-TATB-BPDC as synthesized (purple).

Fe-TAPB-BDC

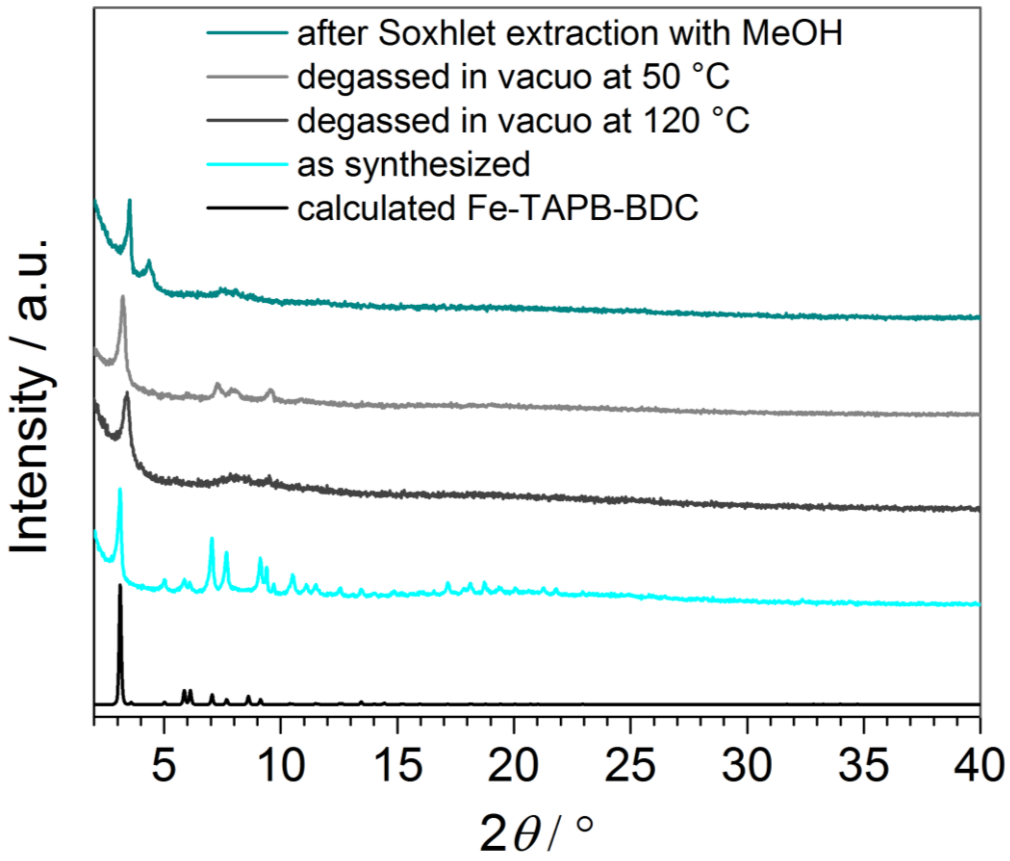

Figure S36: PXRD patterns of Fe-TAPB-BDC as synthesized (cyan), after at 120 °C in vacuo (dark gray), after degassing the sample at only 50 °C in vacuo (light gray) and after Soxhlet extraction with methanol (dark cyan) are compared to a calculated pattern with MIL-143 topology (black; for details see page 4). For testing the different activation conditions only a few mg of the samples were used. And all tested conditions can be referred to the as synthesized sample.

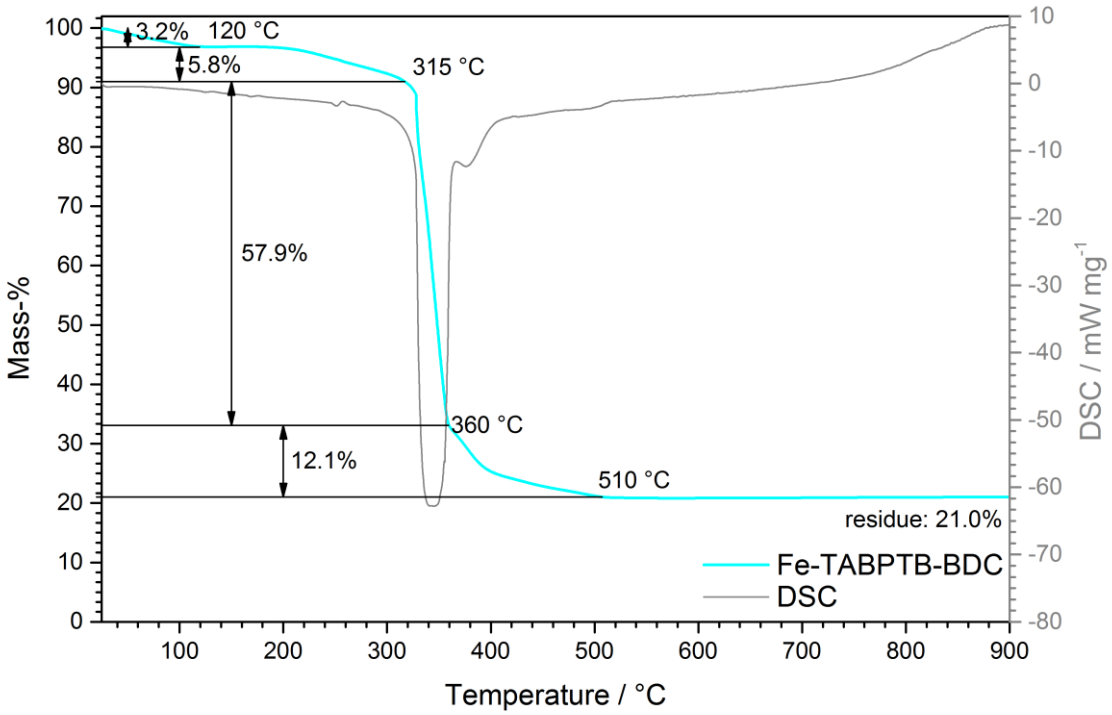

Figure S37: Results of thermogravimetric analysis (cyan curve) and differential scanning calorimetry (light gray curve) of Fe-TAPB-BDC in flowing air with a heating rate of 10 ^{o}C min^{-1}. The start temperature of the decomposition and the mass loss of individual steps are indicated.

Table S6: Mass-losses of Fe-TAPB-BDC during thermogravimetric analysis: experimentally determined data (Figure S23), experimentally determined data taking the content of guests into account, and calculated data based on the ideal composition of Fe-TAPB-BDC [$Fe_3O(Cl)(H_2O)_2(BDC)_{3/2}(TAPB)$].

	experimental	**guest free**	**calculated**
guest	9.0%		
linker	70.0%	76.9%	80.0%
residue	21.0%	23.1%	20.0%

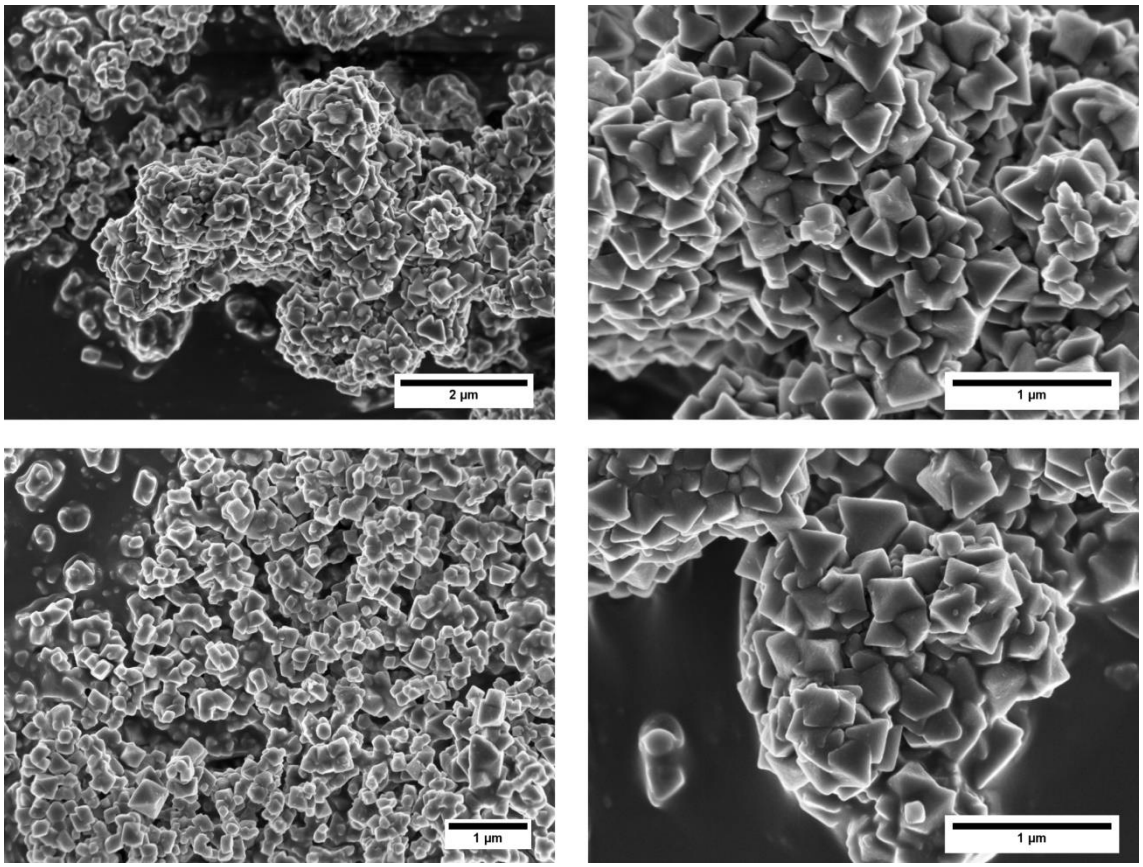

Figure S38: SEM images of the Fe-TAPB-BDC recorded at different magnifications, showing randomly shaped particles with similar crystallite sizes.

Fe-TAPB-BPDC

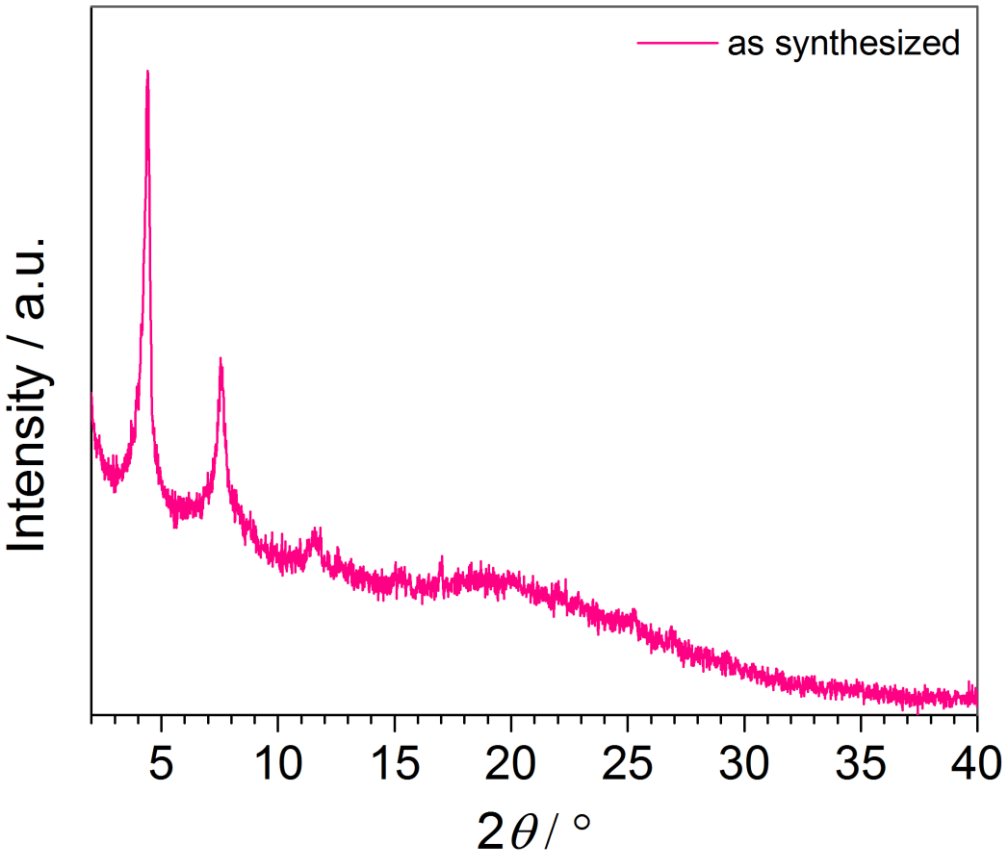

Figure S39: PXRD patterns of Fe-TAPB-BPDC as synthesized (pink).

Fe-BTB-BDC

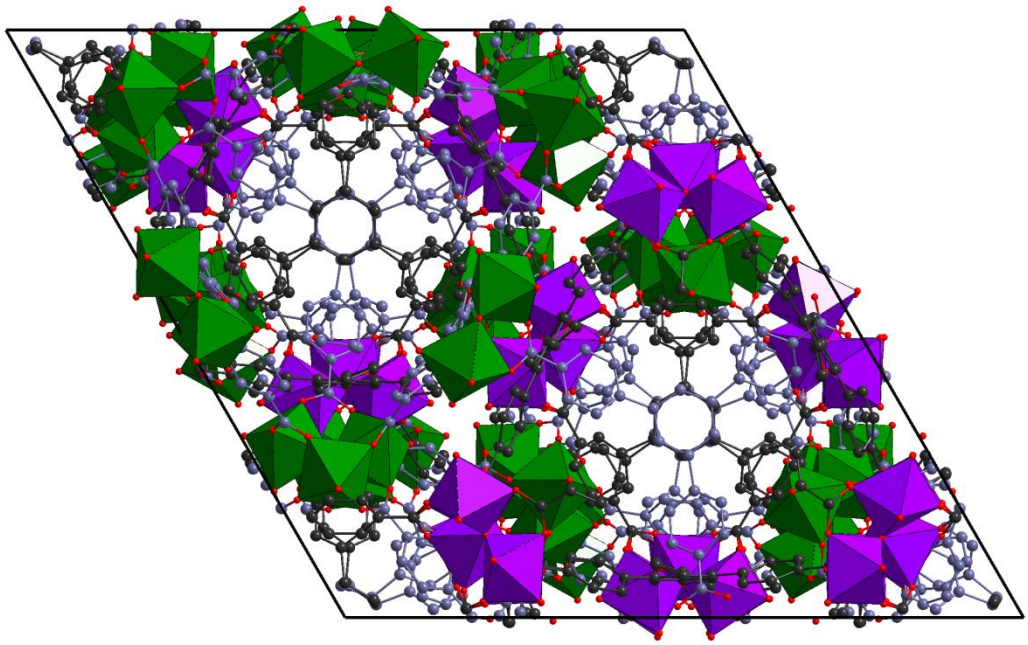

Figure S40: View of the MIL-142 framework along [001]. The interpenetration in MIL-142 by two individual networks is represented by the two different colours of the FeO_6 octahedra (purple and green) and carbon atoms (grey and grey blue); carbon (grey and blue grey spheres), oxygen (red spheres), hydrogen atoms have been omitted for clarity.

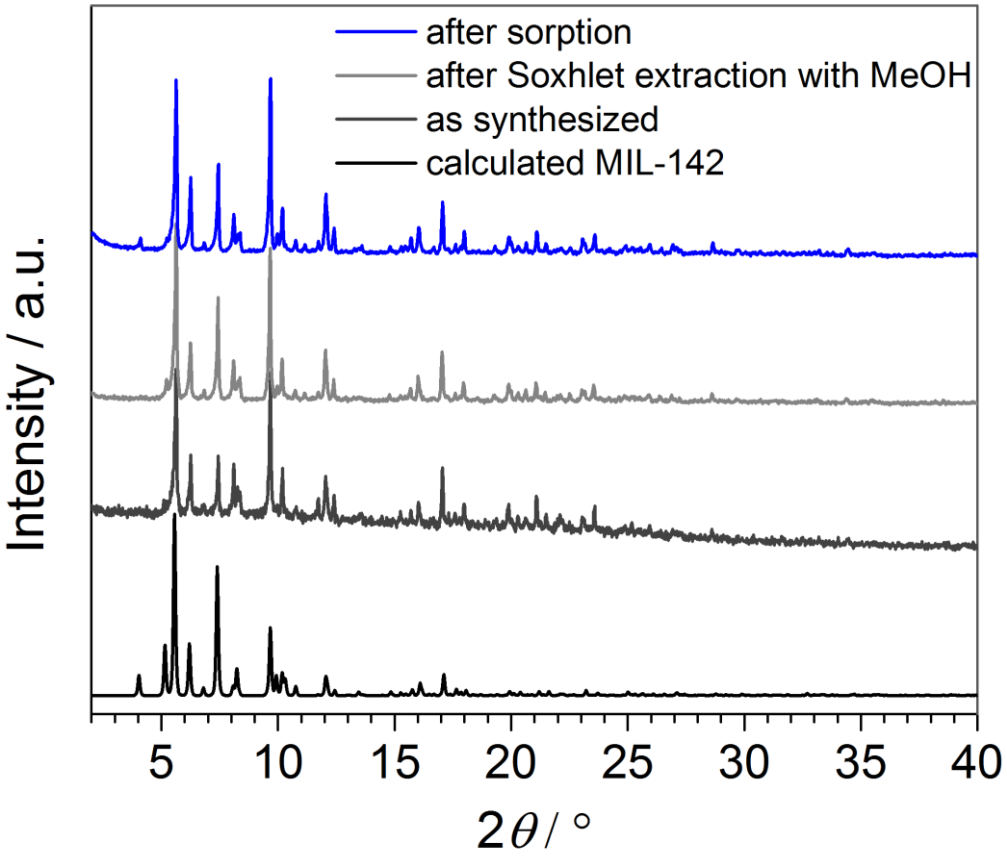

Figure S41: PXRD patterns of Fe-BTB-BDC as synthesized (dark gray), after Soxhlet extraction with methanol (light gray), and after sorption isotherm measurement (blue) are compared to the calculated pattern of MIL-142 (black). All data are from the same synthesis batch.

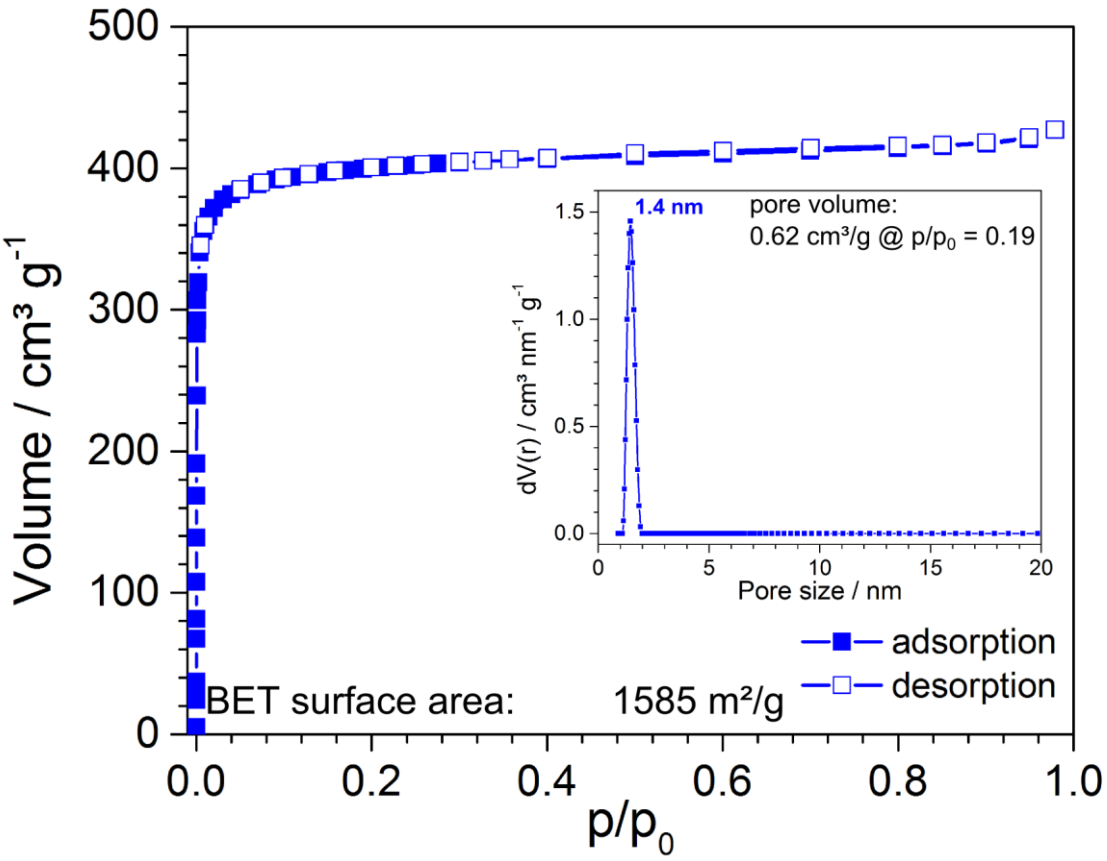

Figure S42: N_2 sorption isotherm of Fe-BTB-BDC at 77 K with the adsorption denoted by filled symbols and desorption by empty symbols. The insert shows the pore size distribution and was calculated with the QSDFT model using cylindrical and sphere pores at the adsorption branch. Also the BET surface area as well as the pore volume are reported.

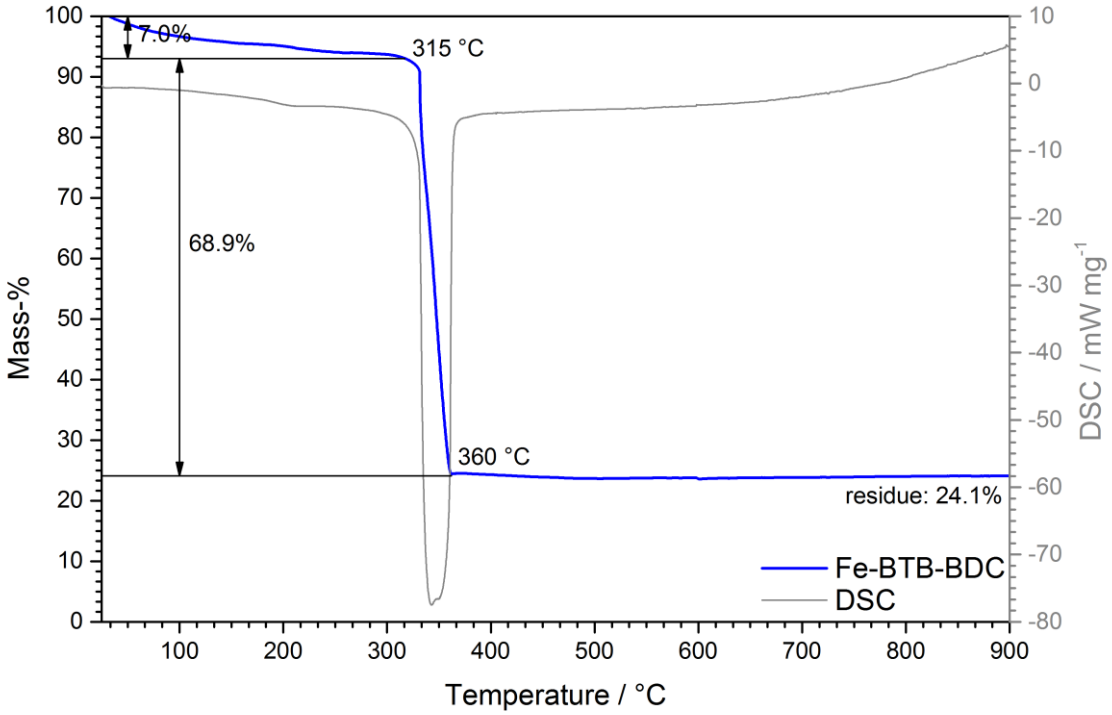

Figure S43: Results of thermogravimetric analysis (blue curve) and differential scanning calorimetry (light gray curve) of Fe-BTB-BDC in flowing air with a heating rate of 10 ^{o}C min^{-1}. Prior to the TGA/DSC measurement, the material had been used for the nitrogen sorption experiments. The start temperature of the decomposition and the mass loss of individual steps are indicated.

Table S7: Mass-losses of Fe-BTB-BDC during thermogravimetric analysis: experimentally determined data (Figure S29), experimentally determined data taking the content of guests into account, and calculated data based on the ideal composition of Fe-BTB-BDC [$Fe_3O(Cl)(H_2O)_2(BDC)(BTB)_{4/3}$].

	experimental	guest free	calculated
guest	7.0%		
linker	68.9%	74.1%	75.8%
residue	24.1%	25.9%	24.2%

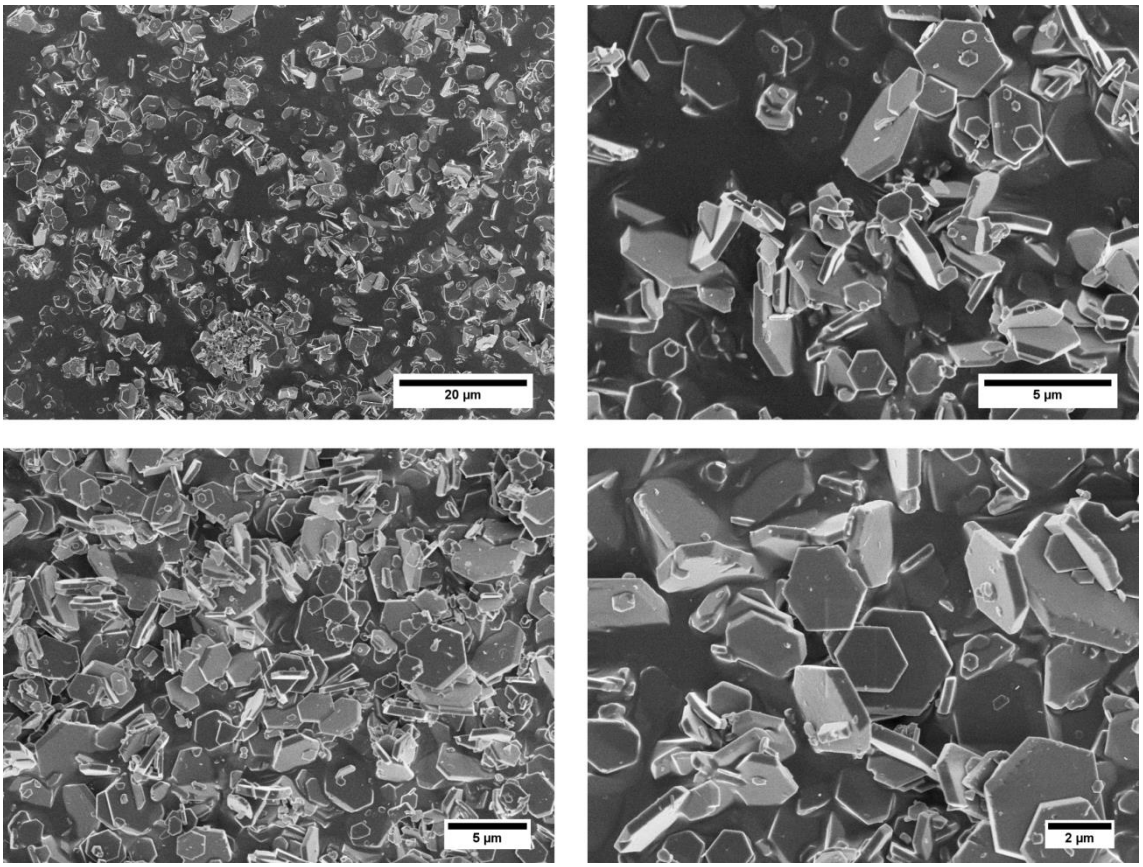

Figure S44: SEM images of the Fe-BTB-BDC recorded at different magnifications, showing hexagonal shaped plate-like-particles with different crystallite sizes.

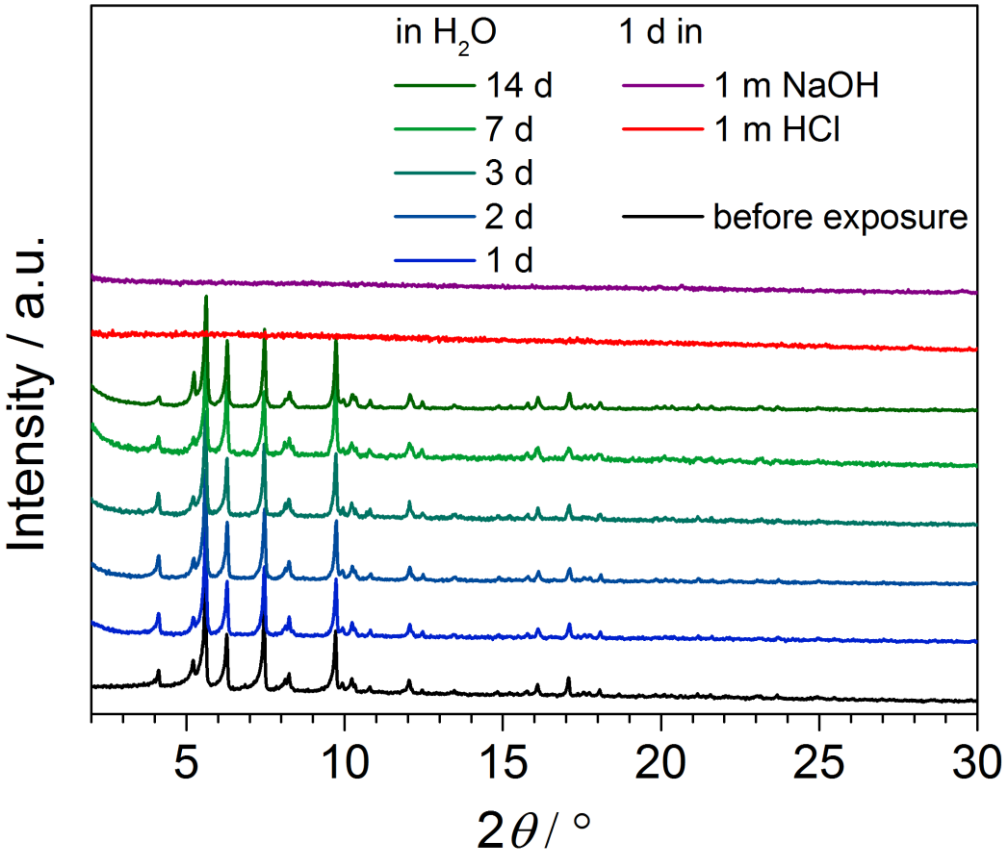

Figure S45: PXRD measurement of Fe-BTB-BDC before exposure (black curve) is compared to the PXRD plots after the exposure to Millipore water with different times of exposure (1 d, 2d, 3 d, 7d, 14 d; blue and green curve, respectively). Also the exposure to a 1 M hydrochloric acid (red curve) and to a 1 M sodium hydroxide (purple curve) solution for 1 d are presented here. The framework is stable up to 7 d in water, while the framework decomposes under acidic and basic conditions.

Table S8: Summary of *Le Bail* fits of PXRD data.

	Instrument	MIL-142 (*R*3*c*, no. 161)	MIL-143 (*F*23, no. 196)
Fe-TATB-BDC-a	Stoe data (RT)	Minor amounts	a = 40.623(3) Å V = 67039(14) Å^3
	ESRF data (RT, 3 scans)	Minor amounts	a = 40.254(8) Å V = 65230(40) Å^3
	ESRF data (100 K, 5 scans)	Minor amounts	a = 40.308(8) Å V = 65490(40) Å^3
Fe-TATB-BDC-b	Stoe data (RT)	None	a = 40.606(2) Å V = 66955(12) Å^3
	ESRF data (RT, 7 scans)	None	a = 40.332(4) Å V = 65610(20) Å^3
Fe-TATB-BDC-c	Stoe data (RT)	None	a = 40.770(2) Å V = 67768(8) Å^3
Fe-TATB-BDC-d	Stoe data (RT)	None	a = 40.649(2) Å V = 67165(8) Å^3
	ESRF data (RT, 4 scans)	None	a = 40.369(10) Å V = 65790(50) Å^3
Fe-TATB-BDC-e	Stoe data (RT)	Minor amounts	a = 40.603(3) Å V = 66936(15) Å^3
	ESRF data (RT, 1 scan)	Minor amounts	a = 40.392(6) Å V = 65900(30) Å^3
	ESRF data (100 K, 5 scans)	Minor amounts	a = 40.388(9) Å V = 65880(40) Å^3
Fe-BTB-BDC	Stoe data (RT)	a = 28.801(1) Å c = 96.040(6) Å V = 68993(7) Å^3	None

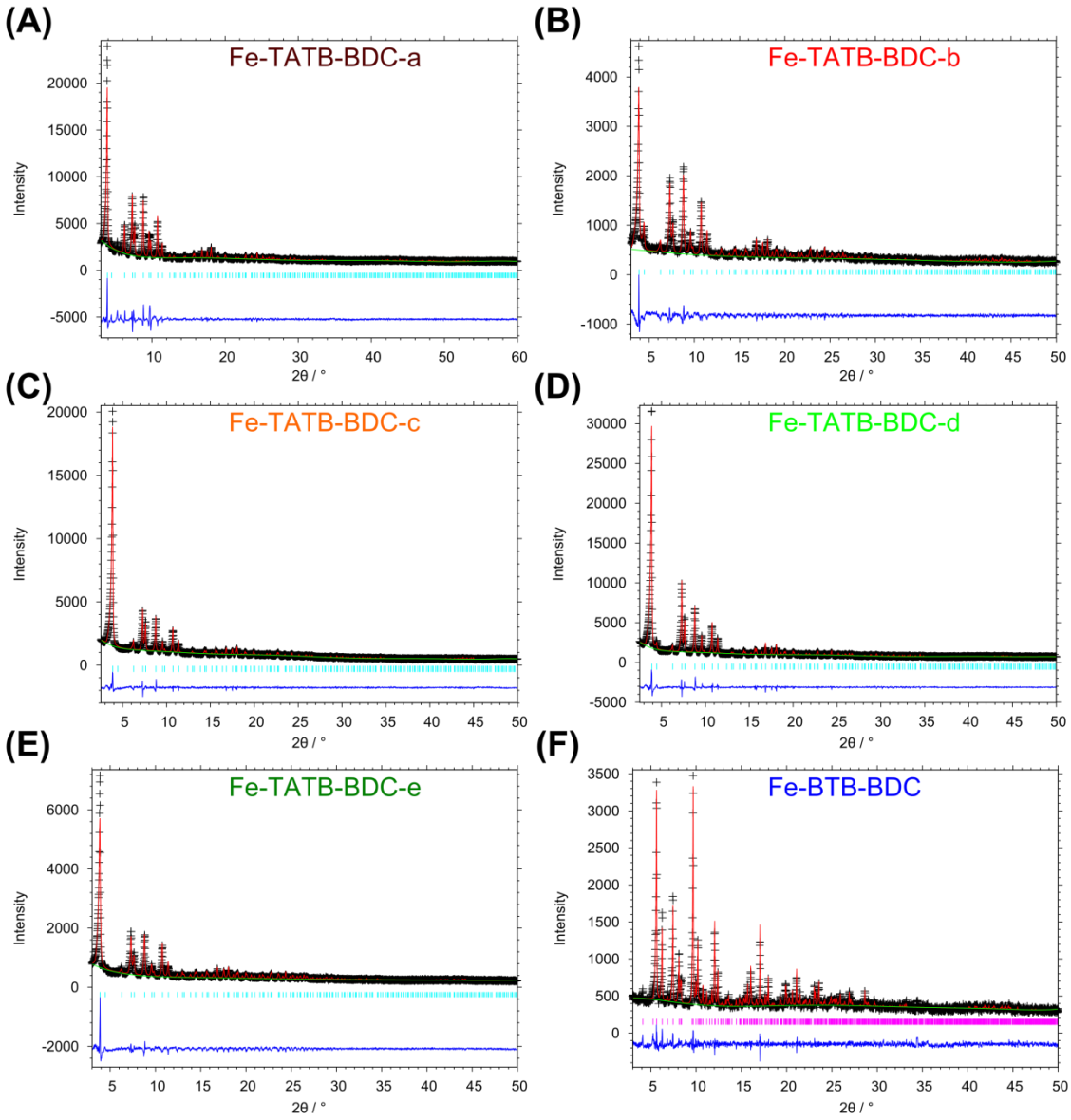

Figure S46: Plots of *Le Bail* fits of PXRD data recorded with a Stoe Stadi P diffractometer (RT, CuKα_1 radiation, flat sample). a) Fe-TATB-BDC-a, b) Fe-TATB-BDC-b, c) Fe-TATB-BDC-c, d) Fe-TATB-BDC-d, e) Fe-TATB-BDC-e and f) Fe-BTB-BDC.

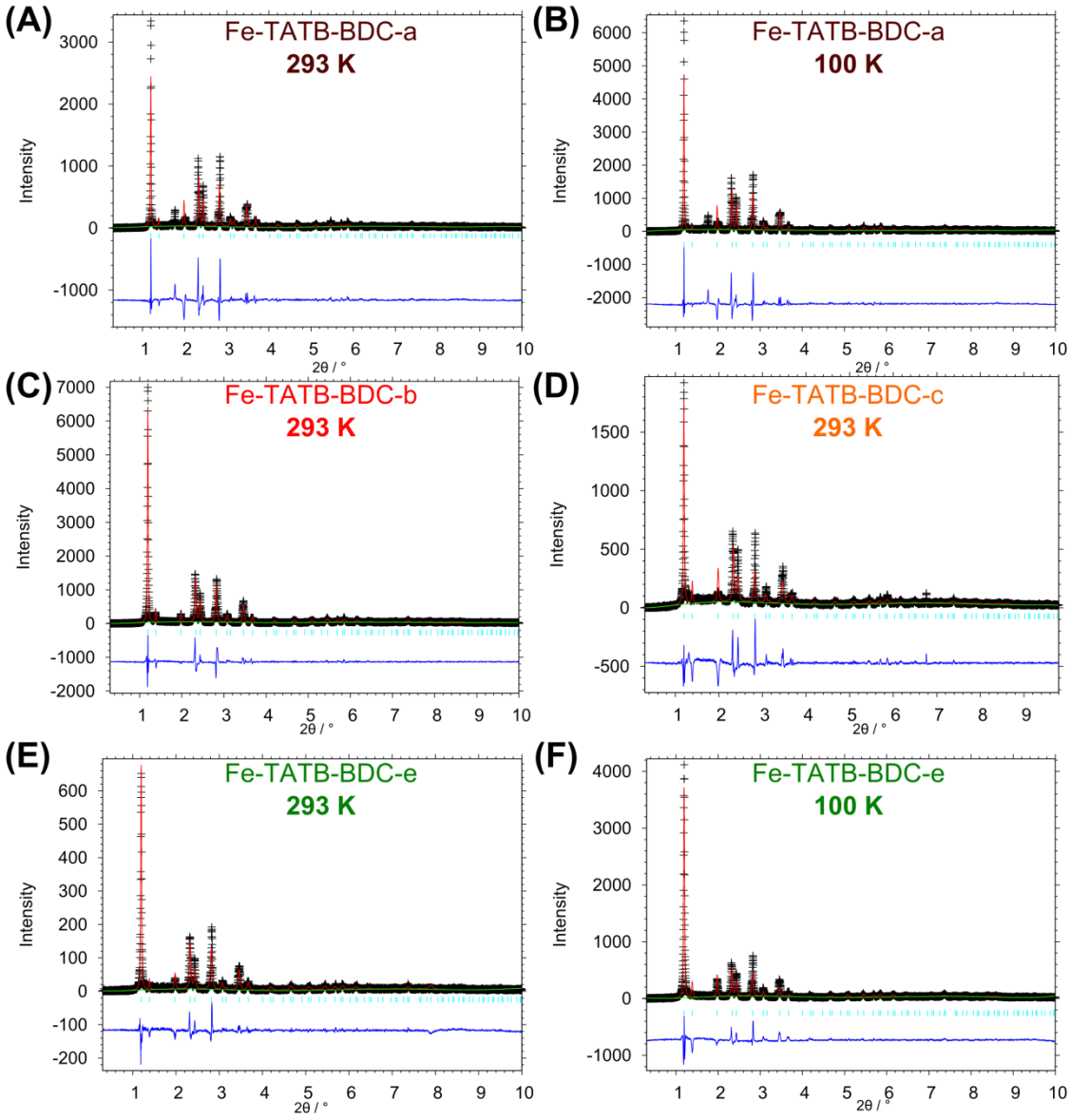

Figure S47: Plots of *Le Bail* fits of synchrotron PXRD data recorded at beamline SNBL BM01b / ESRF (λ = 0.504477 Å, capillary with ∅ = 1.0 mm), either at 298 K or 100 K. a) Fe-TATB-BDC-a at 298 K, b) Fe-TATB-BDC-a at 100 K, c) Fe-TATB-BDC-b at 298 K, d) Fe-TATB-BDC-c at 298 K, e) Fe-TATB-BDC-e at 298 K and f) Fe-TATB-BDC-e at 100 K.

4. References

[1] W. van Beek, O. V. Safonova, G. Wiker, H. Emerich, *Phase Transitions* **2011**, *84*, 726-732.
[2] H. Chevreau, T. Devic, F. Salles, G. Maurin, N. Stock, C. Serre, *Angew. Chem. Int. Ed.* **2013**, *52*, 5056-5060.
[3] A. C. Larson, R. B. Von Dreele, *Los Alamos Laboratory, Rep. No. LA-UR* **1987**, *86*, 748.
[4] P.-E. Werner, L. Eriksson, M. Westdahl, *J. Appl. Crystallogr.* **1985**, *18*, 367-370.
[5] D. Klank, *Partikelwelt* **2003**, *2*, 6-7.
[6] K. S. Walton, R. Q. Snurr, *J. Am. Chem. Soc.* **2007**, *129*, 8552-8556.
[7] A. Klinkebiel, O. Beyer, B. Malawko, U. Lüning, *Beilstein J. Org. Chem.* **2016**, *12*, 2267-2273.

3.2.3 Synthese und postsynthetische Modifikation von Bismut-MOFs

Unter Verwendung von H_3TATB und H_3TATB-NH_2 als Linker konnten neue Bismut-MOFs, analog der Struktur des CAU-7, erhalten werden. Für die Darstellung der als CAU-7-TATB und CAU-7-TATB-NH_2 bezeichneten MOFs wurde der jeweilige Linker mit $Bi(NO_3)_3 \bullet 5H_2O$ umgesetzt. Durch Variation der Reaktionsbedingungen konnte mit H_3TATB als Linker zusätzlich ein bisher unbekannter Bismut-MOF dargestellt werden. Die Struktur des als CAU-35 bezeichneten MOFs wurde aus PXRD-Daten gelöst.

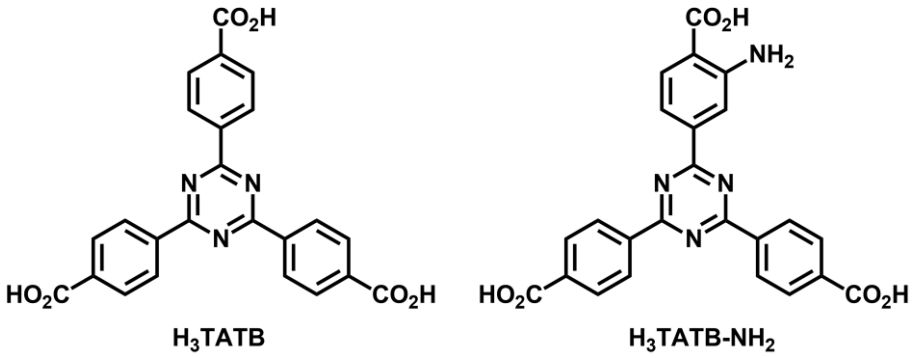

Abb. 25: Erfolgreich eingesetzte H_3TATB-Linker zur Darstellung neuer Bismut-MOFs.

Da es sich bei CAU-7-TATB-NH_2 um das erste Beispiel eines funktionalisierten Bismut-MOFs handelt, wurden verschiedene Methoden zur postsynthetischen Modifikationen ausprobiert. Die Aminogruppen des CAU-7-TATB-NH_2 konnten erfolgreich mit Anhydriden unterschiedlicher Kettenlänge zu den jeweiligen Amiden umgesetzt werden. Zusätzlich konnten Carbonsäure- und Sulfonsäure-Gruppen postsynthetisch in den MOF implementiert werden. Dafür wurden die Aminogruppen mit cyclischen Anhydriden oder 1,3-Propansulton umgesetzt. Der Umsatz einer postsynthetischen Modifikation wurde mit Hilfe von NMR-spektroskopischen Untersuchungen bestimmt und lag je nach Reaktionspartner zwischen 33 % und 79 %.

Die Ergebnisse wurden veröffentlicht:

M. Köppen, O. Beyer, S. Wuttke, T. Bein, U. Lüning, N. Stock, *Dalton Trans.* **2017**, *submitted.*

Bestandteil dieser Dissertation ist die Synthese und Charakterisierung des H_3TATB-NH_2-Linkers sowie Durchführung und NMR-spektroskopische Analyse der postsynthetischen Modifikationen. Die Darstellung und Charakterisierung von CAU-7-TATB, CAU-7-TATB-NH_2 und CAU-35 sowie die Charakterisierung der postsynthetisch modifizierten MOFs wurde

von MILAN KÖPPEN im Rahmen seiner Dissertation durchgeführt. SEM-Bilder des CAU-7-H_3TATB-NH_2 wurden von STEFAN WUTTKE mit einem Rasterelektronenmikroskop aufgenommen.

Anmerkung: Die Formatierung der Supporting Information wurde geringfügig verändert, um sie auf die Formatierung dieser Arbeit anzupassen. Dabei wurden keine Inhalte verändert.

Dalton Transactions

ARTICLE

Synthesis, functionalisation and post-synthetic modification of bismuth metal-organic frameworks

Received 00th January 20xx,
Accepted 00th January 20xx

DOI: 10.1039/x0xx00000x

www.rsc.org/

M. Köppen,†[a] O. Beyer,†[b] S. Wuttke,[c] T. Bein,[c] U. Lüning[b,*] and N. Stock[a,*]

Two new bismuth metal-organic frameworks (Bi-MOFs) have been discovered using high throughput experiments employing bismuth(III) nitrate pentahydrate and triazine-2,4,6-triyl-trisbenzoic acid (H_3TATB). Long reaction times (~ 5 d) in a water/DMF-mixture resulted in the formation of $[Bi_2(O)(OH)(TATB)]\cdot H_2O$ (denoted as CAU-35). By switching to short reaction times and a methanol/DMF-mixture as the solvent, an analogue of CAU-7-BTB with the composition $[Bi(TATB)]\cdot DMF\cdot 6H_2O$ (denoted as CAU-7-TATB) was obtained. The use of the amino-functionalised H_3TATB linker (H_3TATB-NH_2) resulted in the formation of a functionalised porous Bi-MOF with the composition $[Bi(TATB\text{-}NH_2)]\cdot 5H_2O\cdot 0.5DMF$ (CAU-7-TATB-NH_2). The structure of CAU-35 and CAU-7-TATB were successfully solved and refined from PXRD data. CAU-7-TATB-NH_2 was post-synthetically modified using anhydrides (acetic anhydride, valeric anhydride), cyclic anhydrides (succinic anhydride, phthalic anhydride) and 1,3-propane sultone. The degree of conversion ranges from 33 % to 79 %.

Introduction

Tuneable properties and high specific surface areas made metal-organic frameworks (MOFs) one of the main focussed compounds in chemistry over the last decade.[1] Many different metal ions have been incorporated into MOF structures, but for future applications most often abundant and non-toxic metal ions are the elements of choice.[2] Bismuth compounds are generally known to be non-toxic, even though bismuth is the heaviest stable element in nature.[3] So far, only three Bi-MOFs have been published which possess permanent porosity, i.e. CAU-7,[4] NOTT-220[5] and CAU-17[6]. Among these, CAU-7-BTB ([Bi(BTB)], BTB^{3-} = 1,3,5-benzenetrisbenzoate, Scheme 1) has been proven to be catalytically active in the hydroxymethylation of furane derivatives.[4] In addition, Bi-MOFs have also been studied for application in gas storage,[5] photocatalysis[7] and photoluminescence.[8]

The introduction of functional groups into the MOF scaffold is a common way to adjust their chemical and physical properties and thereby extend their possible field of applications. This can be achieved either by directly using a functionalised linker in the MOF synthesis or via post-synthetic modification (PSM).[9,10] An isoreticular MOF can sometimes be synthesised under the same reaction conditions using a functionalised linker,[11] but very often the conditions must be optimised again. An additional functional group in the linker can also lead to a different reaction product due to changes in the solubility and/or coordination properties. Nevertheless, the tedious optimisation is often worthwhile because a functionalised MOF facilitates PSM. Especially amino-functionalised MOFs and their usage for PSM have resulted in many modified framework compounds.[9,12,13] Besides acetylation with anhydrides,[13,14] cyclic anhydrides[15] and carboxylic acid chlorides,[16] there are also known modification reactions with isocyanates,[17] aldehydes,[18] alkylbromides[19] and peptide coupling reagent.[20] The large pool of potential PSM reactions for amino-functionalised MOFs allows many possibilities to generate new, functionalised frameworks.

In this work, we present the results of the systematic investigation of the system $Bi^{3+}/TATB^{3-}/H_2O/DMF/CH_3OH$, which led to two different Bi-MOFs of the composition $[Bi_2(O)(OH)(TATB)]$ (CAU-35, $TATB^{3-}$ = 1,3,5-triazine-2,4,6-trisbenzoate, Scheme 1) and [Bi(TATB)] (CAU-7-TATB). The latter was also obtained using a functionalised linker with one amino group per linker molecule (CAU-7-TATB-NH_2), and this Bi-MOF was investigated in several PSM reactions.

[a] *Institut für Anorganische Chemie, Christian-Albrechts-Universität zu Kiel, Max-Eyth-Str. 2, 24118 Kiel, Germany.*
[b] *Otto-Diels-Institut für Organische Chemie, Christian-Albrechts-Universität zu Kiel, Otto-Hahn-Platz 4, 24118 Kiel, Germany.*
[c] *Department of Chemistry and Center for NanoScience (CeNS), LMU München, Butenandtstraße 11, 81377 München, Germany*
† These authors contributed equally to this work.
* correspondence to: luening@oc.uni-kiel.de, stock@ac.uni-kiel.de
Electronic Supplementary Information (ESI) available: [details of any supplementary information available should be included here]. See DOI: 10.1039/x0xx00000x

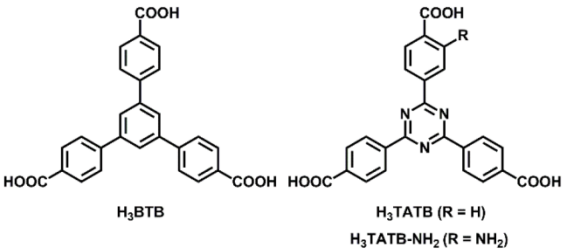

Scheme 1 Molecular structure of the organic linkers H_3BTB, H_3TATB and $H_3TATB\text{-}NH_2$.

Results and discussion

The systematic investigation of the system $Bi^{3+}/TATB^{3-}/H_2O/DMF/CH_3OH$ was carried out using our high-throughput set-up.[21] To study the influence of different reaction parameters on the product formation the molar ratio and concentration of starting materials, the solvent (-mixtures) and reaction temperatures/times were varied.

Depending on the reaction conditions, two different products were obtained using $Bi(NO_3)_3 \cdot 5H_2O$ and H_3TATB. CAU-35 is formed when water/DMF-mixtures and long reaction times are used. On the other hand, short reaction times and methanol/DMF-mixtures led to CAU-7-TATB. The conditions for the synthesis of CAU-7-TATB-NH_2 are very similar.

CAU-35

During the high-throughput experiments with H_3TATB and bismuth(III) nitrate pentahydrate, a product with the composition $[Bi_2(O)(OH)(TATB)]$, denoted as CAU-35, was discovered. The crystal structure of this compound was successfully solved and refined from PXRD data. Details about the solution and refinement are given in the Supporting Information (page S20), the Rietveld plot is shown in Fig. 1.

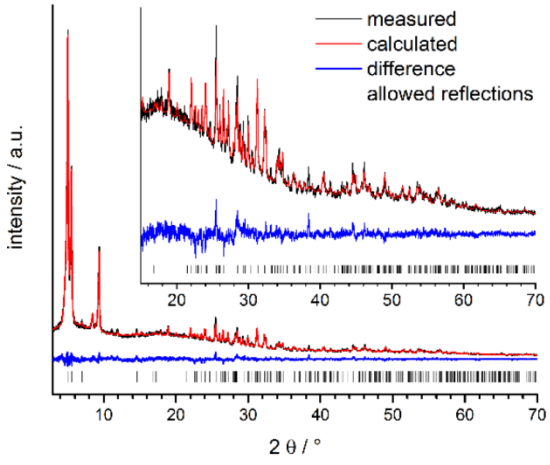

Fig. 1 Rietveld plot of the refinement of CAU-35. Measured and calculated PXRD data, the difference of both and the allowed reflections are shown in black, red, blue and as black bars, respectively.

The structure is reminiscent to the one of CAU-7-TATB, with one additional linker inside the distorted hexagonal pore (Fig. 2 and 3). The different connectivities are only possible with different inorganic building units (IBUs). While in CAU-7-TATB, the linear chain of face sharing BiO_{10}-polyhedra with composition $\{BiO_5\}$ is observed, in CAU-35 the IBU contains BiO_7-polyhedra, which are connected to a chain of composition $\{Bi_2O_{6.5}\}$ (Fig. S22). According to the Rietveld analysis, two oxygen atoms are observed in the IBU of CAU-35. One is coordinating to four Bi^{3+} ions (μ_4-O^{2-} ion) and the other oxygen atom is bridging three Bi^{3+} ions (μ_3-OH^- ion). Since the structure is solved and refined from PXRD data, we were not able to unequivocally locate the position of the proton. Charge balance by dimethylammonium ions in the pores, which can be formed by hydrolysis of DMF during the synthesis, can be excluded based on the characterisation data (IR spectroscopy as well as TG and elemental analysis). CAU-35 exhibits moderate sorption properties, with a specific BET surface area of 77 m^2/g and a micropore volume of 0.06 cm^3/g (Fig. S23). A detailed characterisation of this compound, including N_2 sorption, IR, TG and elemental analysis data, is given in the Supporting Information (page S26-S28).

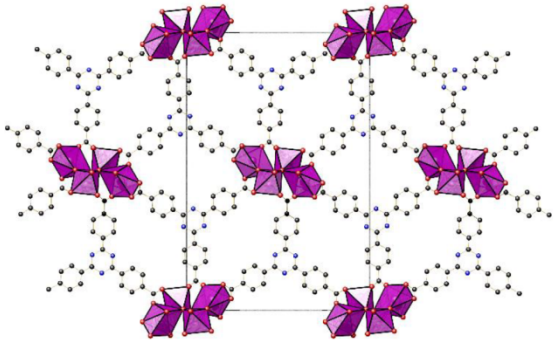

Fig. 2 Crystal structure of CAU-35 (view along [001]). The unit cell dimension is represented by the box.

CAU-7-TATB

$[Bi(TATB)] \cdot DMF \cdot 6H_2O$ (CAU-7-TATB (*as*), *as* = as synthesised) was obtained employing H_3TATB and bismuth(III) nitrate pentahydrate using short reaction times (20 min) and a mixture of methanol and DMF as the solvent. In contrast to CAU-7-BTB, which was first obtained using H_3BTB as the linker (Scheme 1),[4] structural transformation upon activation of CAU-7-TATB (*as*) is observed. The PXRD pattern of CAU-7-TATB (*as*) is very similar to the one of CAU-7-BTB. Indexing of the PXRD pattern led to a monoclinic unit cell, which was confirmed by a LeBail fit (Table S1, Fig. S1). When the as synthesised sample is treated at 120 °C for 1 d, the crystal structure changes to the orthorhombic high temperature (*ht*) phase of CAU-7-TATB. High resolution PXRD data of CAU-7-TATB (*ht*) allowed a Rietveld refinement of the structure (Tab.

S1, Fig. S3). To obtain a guest free sample of CAU-7-TATB (*ht*) activation was carried out in a glass capillary, which was heated at 120 °C under reduced pressure for 1 h. In comparison to the structure of CAU-7-BTB, in CAU-7-TATB (*ht*) (Fig. 3) less rotation of the benzoate groups is observed with respect to the central aromatic ring, and thus the rings are more co-planar. This observation is typical for triazine based linkers, due to the missing steric hindrance of the hydrogen atoms.[22] The analysis of the nitrogen sorption isotherm of CAU-7-TATB led to a specific BET surface area of 813 m^2/g and a micropore volume of 0.31 cm^3/g (Fig. S7). These are lower than the published values for CAU-7-BTB (A_{BET} = 1150 m^2/g, V_{mic} = 0.43 cm^3/g),[4] but correlate well with the theoretical values (A_{BET} = 867 m^2/g, V_{mic} = 0.32 cm^3/g), which are calculated using the program Materials Studio.[23]

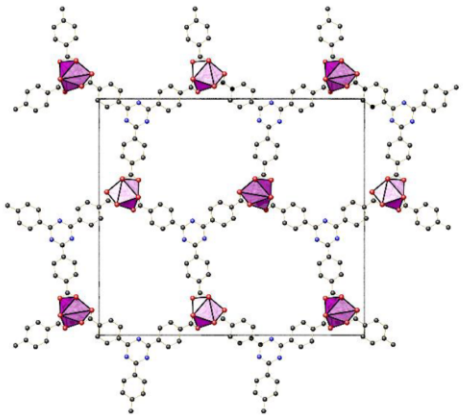

Fig. 3 Crystal structure of CAU-7-TATB (view along [001]). The unit cell dimension is represented by the box.

CAU-7-TATB-NH_2

Reactions carried out under very similar synthesis conditions to those of CAU-7-TATB with H_3TATB-NH_2 as the linker resulted in successful formation of the CAU-7 analogue [Bi(TATB-NH_2)] $\cdot 5H_2O \cdot 0.5$DMF (CAU-7-TATB-NH_2), which is, to the best of our knowledge, the first example of a functionalised Bi-MOF. Whereas for CAU-7-TATB two different phases (*as* and *ht*) were discovered, for CAU-7-TATB-NH_2 only one phase with an orthorhombic crystal structure was observed (Table S4, Fig. S10). Since synthesis scale-up could not be carried out, several batches of CAU-7-TATB-NH_2 were synthesised under identical reaction conditions. In order to get sufficiently large amounts of the compound for a systematic PSM study, the exact same starting materials were used in every synthesis.

Although the characterisation of the different batches by PXRD, elemental- and thermogravimetric analysis, as well as the infrared spectroscopy did not indicate any impurity (Supporting Information, page S16-S17 and page S36-S38) large variation in the nitrogen adsorption properties (A_{BET} in a range of 104-627 m^2/g) were observed. To get insight into this effect, high resolution scanning electron microscope (SEM) micrographs were taken of two samples with significantly different BET surface areas. Surprisingly, no differences could be detected (Fig. S13-S16).

Post-synthetic modification of CAU-7-TATB-NH_2

The possibility of PSM reactions using CAU-7-TATB-NH_2 was explored using some typical literature procedures.[9] For this purpose eight synthesis batches of CAU-7-TATB-NH_2 were combined to ensure data consistency and all PSM reactions were performed using this mixture. CAU-7-TATB-NH_2 was treated with methanesulfonyl chloride, acetyl chloride, ethyl isocyanate, several anhydrides and two different sultones. After treatment with methanesulfonyl chloride and acetyl chloride, a clear solution was obtained. Since CAU-7-TATB-NH_2 is not stable against HCl, the reaction was performed in the presence of pyridine or triethyl amine to capture the HCl which is formed during the acetylation of the amino group. Nevertheless, dissolution of the material was observed. Different observations were made for the treatment of CAU-7-TATB-NH_2 with ethyl isocyanate. In this case, a degradation of the structure was observed (Fig. S33). In all three cases, it remains unclear why the degradation takes place.

In contrast, the treatment with anhydrides like acetic anhydride and valeric anhydride was successful and resulted in the formation of CAU-7-TATB-NH_2-AA and CAU-7-TATB-NH_2-VA, respectively (Scheme 2). Both MOFs maintain their structure according to PXRD data (Fig. S32). The degree of conversion was determined by comparing the relative integrals in the ^{1}H-NMR-spectra after digestion of the MOF (Fig. S26 and S27). The degree of conversion drops from 79 % for CAU-7-TATB-NH_2-AA to 47 % for CAU-7-TATB-NH_2-VA, which may be attributed to the longer alkyl chain of valeric anhydride.

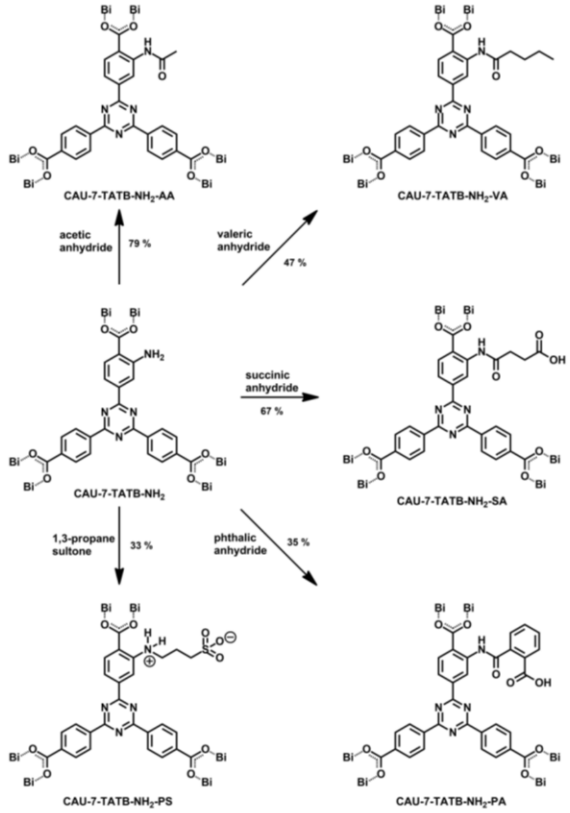

Scheme 2 Post-synthetic modification of CAU-7-TATB-NH_2 with the respective anhydrides and 1,3-propane sultone. Degree of conversion in %.

Despite the limited stability of CAU-7-TATB-NH_2 towards acids, four reactions were carried out to introduce pendant carboxylic and sulfonic acid groups into the framework. By treating CAU-7-TATB-NH_2 with cyclic anhydrides such as succinic and phthalic anhydride, two functionalised MOFs with free carboxylic acid groups were obtained (Scheme 2). Succinic anhydride resulted in the formation of CAU-7-TATB-NH_2-SA with 67 % conversion and phthalic anhydride gave CAU-7-TATB-NH_2-PA with 35 % conversion (Fig. S28 and S29). To introduce pendant sulfonic acid groups into the framework, ring-opening reactions using 1,3-propane sultone or 1,4-butane sultone were performed. In both cases, the MOF maintained its structure after the reaction but only the treatment with 1,3-propane sultone led to a conversion of the amino groups. The respective CAU-7-TATB-NH_2-PS was obtained with a conversion of 33 % (Fig. S30). It should be mentioned that the sulfonic acid group within the framework most likely might be deprotonated due to internal neutralisation. The investigation of the same PSM reaction on a different MOF proved that a zwitterionic form is preferred and the acidity is attributed to the ammonium group.[24] Nevertheless, these results show that CAU-7-TATB-NH_2 is capable of bearing acidic groups within the pores. Analytical data (^{1}H-NMR, PXRD, TGA, elemental analysis, IR) for all modified MOFs are available in the Supporting Information (page S29-S38).

Experimental

Chemicals and experimental details

The chemicals were purchased from Aldrich, Alfa Aesar or Walter CMP and used without further purification. Syntheses were carried out under solvothermal conditions in a Biotage Initiator microwave oven or in self-made high-throughput autoclaves with in PTFE inserts of 2 mL volume.[21]

Powder X-ray diffraction (PXRD) was performed on a STOE Stadi P Combi (λ = 1.5406 Å) equipped with a MYTHEN detector. FOX[25] was used for structure solution from PXRD data and TOPAS Academic 4.1[26] for LeBail fits and Rietveld refinement.

Sorption measurements were performed on a BELsorp max or BELsorp mini, infrared spectroscopy on a Bruker Alpha-P spectrometer and elemental analyses on a HEKAtech Euro Elemental Analyzer. The scanning electron microscopy (SEM) experimentswere performed on a *Jeol JSM-6500F* with EDX-Detector and *Inca*-software (*Oxford Instruments*).

NMR spectra were recorded on Bruker DRX 500 or AV 600 instruments and assignments were supported by COSY, HSQC and HMBC. Even when spectra were obtained as broad-band decoupled ^{13}C-NMR, the type of ^{13}C signal is always listed as singlet, doublet, etc. Degree of conversion by post-synthetic modification reaction was determined by comparing the relative integrals in ^{1}H-NMR-spectra of digested material. Digestion was achieved by adding a mixture of DMSO-d_6 and DCl (37 %) to the MOF.

Syntheses of the organic linkers

The synthesis of H_3TATB[27] and functionalised H_3TATB-NO_2[28] were performed according to literature procedures. The nitro-group of H_3TATB-NO_2 was reduced by sodium dithionite to obtain H_3TATB-NH_2. For synthetic details and characterisation see Supporting Information.

Syntheses of the metal-organic frameworks

Synthesis of [Bi(TATB)] (CAU-7-TATB): H_3TATB (30.0 mg, 68.0 µmol) and ground $Bi(NO_3)_3{\cdot}5\ H_2O$ (28.7 mg, 59.2 µmol) were mixed in a 30 mL glass vial and MeOH (6 mL) and DMF (6 mL) were added. The sealed vial was shaken and heated in a microwave-assisted synthesis at 120 °C for 20 min while stirring with 600 rpm. The solid product was filtered off and washed with DMF (5 mL) and MeOH (5 mL). A white powder was obtained in a yield of 30.8 mg (55% based on H_3TATB). Phase purity was confirmed by PXRD (Fig. S1) and elemental analysis (calc. (%) for $BiC_{24}H_{12}N_3O_6{\cdot}C_3H_7NO{\cdot}6H_2O$: C 39.14, H 3.77, N 6.76; meas. (%): C 37.29, H 2.93, N 7.84).

Synthesis of [Bi(TATB-NH_2)] (CAU-7-TATB-NH_2): H_3TATB-NH_2 (100 mg, 219 µmol) and ground $Bi(NO_3)_3{\cdot}5\ H_2O$ (76.8 mg, 158 µmol) were mixed in a 30 mL glass vial and MeOH (10 mL) and DMF (10 mL) were added. The sealed vial was shaken and

heated in a microwave-assisted synthesis at 120 °C for 20 min while stirring with 600 rpm. The solid product was filtered off and washed with DMF (5 mL) and MeOH (5 mL). A yellow powder was obtained in a yield of 118 mg (68% based on H_3TATB-NH_2). Phase purity was confirmed by PXRD (Fig. S10) and elemental analysis (calc. (%) for $BiC_{24}H_{13}N_4O_6 \cdot 0.5C_3H_7NO \cdot 5H_2O$: C 38.82, H 3.39, N 7.99; meas. (%): C 39.74, H 1.85, N 7.99).

Synthesis of [Bi_2(O)(OH)(TATB)] (CAU-35):

H_3TATB (5.0 mg, 11.3 µmol) and ground $Bi(NO_3)_3 \cdot 5\ H_2O$ (5.5 mg, 11.3 µmol) were mixed in a 2 mL PTFE inserts and H_2O (800 µL) and DMF (200 µL) were added. The autoclave was sealed and heated to 120 °C in 12 h. The temperature was kept for 36 h and subsequently the reactor was slowly cooled to room temperature in 60 h. The solid product was filtered off and washed with DMF (1 mL) and H_2O (1 mL). A white powder was obtained. Phase purity was confirmed by PXRD (Fig. S17) and elemental analysis (calc. (%) for $Bi_2C_{24}H_{13}N_3O_8 \cdot H_2O$: C 31.77, H 1.67, N 4.63; meas. (%): C 32.77, H 1.41, N 4.97).

Post-synthetic modification procedure

Prior to the modification reactions, CAU-7-TATB-NH_2 was dried for 12 h at 60 °C in a vacuum oven. 15 equivalents of the respective anhydride or sultone were added to a suspension of CAU-7-TATB-NH_2 (130 mg, 195 µmol) in dichloromethane (6 mL). The reaction mixture was stirred under reflux for 72 h. The solid was separated by centrifugation and washed with dichloromethane (2 x 10 mL), ethanol (2 x 10 mL) and water (2 x 10 mL). After drying for 4 d at 60 °C in a vacuum oven, 10 mg of the solid was digested with a mixture of DMSO-d_6 (595 µL) and DCl (37 %, 5 µL). The conversion was determined by ^{1}H-NMR spectroscopy (see Supporting Information).

Conclusions

In summary, we used the triazine-based H_3TATB linker for the synthesis of two new Bi-MOFs. Depending on the solvent mixture and the reaction time, either a MOF with CAU-7 structure (CAU-7-TATB) or a new MOF (CAU-35) was obtained. The structure of CAU-35 was successfully solved and refined from PXRD data, the structure of CAU-7-TATB was confirmed by a Rietveld analysis of the PXRD data. Additionally, a new amino-substituted H_3TATB linker (H_3TATB-NH_2) was synthesised and used for the synthesis of the first functionalised Bi-MOF, denoted CAU-7-TATB-NH_2. This MOF was successfully treated with acetic anhydride, valeric anhydride, succinic anhydride, phthalic anhydride and 1,3-propane sultone to give the respective modified Bi-MOFs with degrees of conversion varying from 33 to 79 %.

Acknowledgements

We thank A. Ken Inge and Helge Reinsch for helpful discussions.

Notes and references

1 H. Furukawa, K. E. Cordova, M. O'Keeffe and O. M. Yaghi, *Science*, 2013, **341**, 1230444.

2 A. C. McKinlay, R. E. Morris, P. Horcajada, G. Férey, R. Gref, P. Couvreur and C. Serre, *Angew. Chem.*, 2010, **122**, 6400–6406, *Angew. Chem. Int. Ed.*, **49**, 6260–6266.

3 Y. Yang, R. Ouyang, L. Xu, N. Guo, W. Li, K. Feng, L. Ouyang, Z. Yang, S. Zhou and Y. Miao, *J. Coord. Chem.*, 2014, **68**, 379–397.

4 M. Feyand, E. Mugnaioli, F. Vermoortele, B. Bueken, J. M. Dieterich, T. Reimer, U. Kolb, D. de Vos and N. Stock, *Angew. Chem.*, 2012, **124**, 10519–10522, *Angew. Chem. Int. Ed.*, 2012, **51**, 10373–10376.

5 M. Savage, S. Yang, M. Suyetin, E. Bichoutskaia, W. Lewis, A. J. Blake, S. A. Barnett and M. Schröder, *Chem. - Eur. J.*, 2014, **20**, 8024–8029.

6 A. K. Inge, M. Köppen, J. Su, M. Feyand, H. Xu, X. Zou, M. O'Keeffe and N. Stock, *J. Am. Chem. Soc.*, 2016, **138**, 1970–1976.

7 a) G. Wang, Y. Liu, B. Huang, X. Qin, X. Zhang and Y. Dai, *Dalton Trans.*, 2015, **44**, 16238–16241; b) G. Wang, Q. Sun, Y. Liu, B. Huang, Y. Dai, X. Zhang and X. Qin, *Chem. - Eur. J.*, 2015, **21**, 2364–2367.

8 M. Feyand, M. Köppen, G. Friedrichs and N. Stock, *Chem. - Eur. J.*, 2013, **19**, 12537–12546.

9 S. M. Cohen, *Chem. Rev.*, 2012, **112**, 970–1000.

10 a) S. M. Cohen, *J. Am. Chem. Soc.*, 2017, **139**, 2855–2863; b) K. K. Tanabe and S. M. Cohen, *Chem. Soc. Rev.*, 2011, **40**, 498–519.

11 M. Eddaoudi, J. Kim, N. Rosi, D. Vodak, J. Wachter, M. O'Keeffe and O. M. Yaghi, *Science*, 2002, **295**, 469–472.

12 A. Klinkebiel, N. Reimer, M. Lammert, N. Stock and U. Lüning, *Chem. Commun.*, 2014, **50**, 9306–9308.

13 H. Hintz and S. Wuttke, *Chem. Mater.*, 2014, **26**, 6722–6728.

14 a) S. J. Garibay and S. M. Cohen, *Chem. Commun.*, 2010, **46**, 7700–7702; b) K. K. Tanabe, Z. Wang and S. M. Cohen, *J. Am. Chem. Soc.*, 2008, **130**, 8508–8517; c) Z. Wang, K. K. Tanabe and S. M. Cohen, *Inorg. Chem.*, 2009, **48**, 296–306.

15 a) S. J. Garibay, Z. Wang and S. M. Cohen, *Inorg. Chem.*, 2010, **49**, 8086–8091; b) K. K. Tanabe and S. M. Cohen, *Angew. Chem.*, 2009, **121**, 7560–7563, *Angew. Chem. Int. Ed.*, **48**, 7424–7427.

16 a) A. Modrow, D. Zargarani, R. Herges and N. Stock, *Dalton Trans.*, 2012, **41**, 8690–8696; b) M. Savonnet, S. Aguado, U. Ravon, D. Bazer-Bachi, V. Lecocq, N. Bats, C. Pinel and D. Farrusseng, *Green Chem.*, 2009, **11**, 1729.

17 a) S. Bernt, V. Guillerm, C. Serre and N. Stock, *Chem. Commun.*, 2011, **47**, 2838–2840; b) E. Dugan, Z. Wang, M. Okamura, A. Medina and S. M. Cohen, *Chem. Commun.*, 2008, 3366–3368.

18 a) A. D. Burrows and L. L. Keenan, *CrystEngComm*, 2012, **14**, 4112; b) C. J. Doonan, W. Morris, H. Furukawa and O. M. Yaghi, *J. Am. Chem. Soc.*, 2009, **131**, 9492–9493; c) M.

J. Ingleson, J. P. Barrio, J.-B. Guilbaud, Y. Z. Khimyak and M. J. Rosseinsky, *Chem. Commun.*, 2008, 2680–2682.
19 K. M. L. Taylor-Pashow, J. Della Rocca, Z. Xie, S. Tran and W. Lin, *J. Am. Chem. Soc.*, 2009, **131**, 14261–14263.
20 H. Hintz and S. Wuttke, *Chem. Commun.*, 2014, **50**, 11472–11475.
21 N. Stock and S. Biswas, *Chem. Rev.*, 2012, **112**, 933–969.
22 A. Klinkebiel, O. Beyer, B. Malawko and U. Lüning, *Beilstein J. Org. Chem.*, 2016, **12**, 2267–2273.
23 a) *Materials Studio 5.5.3*, Accelrys Software Inc., 2010; b) T. Düren, F. Millange, G. Férey, K. S. Walton and R. Q. Snurr, *J. Phys. Chem. C*, 2007, **111**, 15350–15356.
24 H. Liu, F.-G. Xi, W. Sun, N.-N. Yang and E.-Q. Gao, *Inorg. Chem.*, 2016, **55**, 5753–5755.
25 V. Favre-Nicolin and R. Černý, *J. Appl. Crystallogr.*, 2002, **35**, 734–743.
26 A. Coelho, *TOPAS Academic 4.1*, Coelho Software, 2007.
27 M. Krüger, H. Reinsch, A. K. Inge and N. Stock, *Microporous Mesoporous Mater.*, 2017, **249**, 128-136.
28 E. Mühlbauer, A. Klinkebiel, O. Beyer, F. Auras, S. Wuttke, U. Lüning and T. Bein, *Microporous Mesoporous Mater.*, 2015, **216**, 51–55.

Supporting Information

Synthesis, functionalisation and post-synthetic modification of bismuth metal-organic frameworks

M. Köppen,[a] O. Beyer,[b] S. Wuttke,[c] T. Bein,[c] U. Lüning,[b,*] and N. Stock[a,*]

[a]Institut für Anorganische Chemie, Christian-Albrechts-Universität zu Kiel, Max-Eyth-Str. 2, 24118 Kiel, Germany

[b]Otto Diels-Institut für Organische Chemie, Christian-Albrechts-Universität zu Kiel, Otto-Hahn-Platz 4, 24118 Kiel, Germany

[c]Department of Chemistry and Center for NanoScience (CeNS), LMU München, Butenandtstraße 11, 81377 München, Germany

* correspondence to:

stock@ac.uni-kiel.de

luening@oc.uni-kiel.de

Table of contents

Organic linker synthesis

Synthesis of H_3TATB

The precursor 2,4,6-tris(4-methylphenyl)-1,3,5-triazine was synthesised by trimerization of 4-methylbenzonitrile. H_3TATB was obtained by oxidation of the methyl groups according to a literature procedure.[174]

Synthesis of H_3TATB-NH_2

H_3TATB-NO_2 was synthesized according to the literature procedure by Mühlbauer et al.[175]

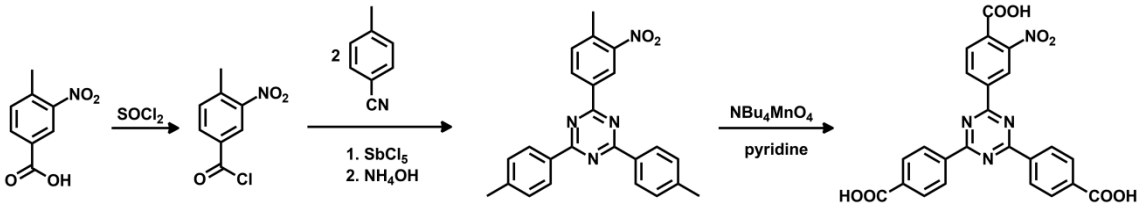

Reduction of the nitro group gave H_3TATB-NH_2 by using the following procedure:

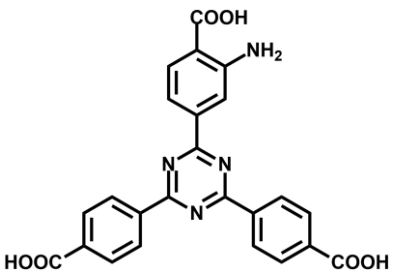

2-(4-Carboxy-3-nitrophenyl)-4,6-bis(4-carboxyphenyl)-1,3,5-triazine (H_3TATB-NO_2, 2.50 g, 5.14 mmol) and potassium carbonate (4.47 g, 25.7 mmol) were suspended in water (80 mL) and stirred until the entire solid was dissolved. Ethanol (30 mL) was added to the solution followed by sodium dithionite (3.55 g, 25.7 mmol). The reaction mixture was stirred for 1 h at room temperature. Ethanol was removed under reduced pressure and the residue was poured into conc. hydrochloric acid (200 mL). The precipitate was filtered off and the residue was washed thoroughly with water. The resulting solid was recrystallized from DMSO/water to yield 1.72 g (3.77 mmol, 73 %) of a yellow solid.

M. p.: >300 °C

^{1}H-NMR (500 MHz, DMSO-d_6): δ = 8.82 (d, ^3J = 8.6 Hz, 4H, Ar'-*H*-2,6), 8.23 (d, ^4J = 1.6 Hz, 1H, Ar-*H*-2), 8.20 (d, ^3J = 8.6 Hz, 4H, Ar'-*H*-3,5), 7.94 (d, ^3J = 8.3 Hz, 1H, Ar-*H*-5), 7.83 (dd, ^3J = 8.3 Hz, ^4J = 1.6 Hz, 1H, Ar-*H*-6) ppm.

^{13}C-NMR (125 MHz, DMSO-d_6): δ = 171.1 (s, Tri-*C*-2), 170.5 (s, Tri-*C*-4,6), 169.2 (s, Ar-*C*O_2H), 166.8 (s, Ar'-*C*O_2H), 151.6 (s, Ar-*C*-3), 139.4 (s, Ar-*C*-1), 139.0 (s, Ar'-*C*-1), 134.7 (s, Ar'-*C*-4), 131.8 (d, Ar-*C*-5), 129.8 (d, Ar'-*C*-3,5), 128.8 (d, Ar'-*C*-2,6), 117.1 (d, Ar-*C*-2), 114.3 (d, Ar-*C*-6), 113.0 (s, Ar-*C*-4) ppm.

IR (ATR): $\tilde{\nu}$ = 2982 (br., OH), 1685 (C=O), 1579, 1505 (arom. C=C, arom. C=N), 1358 (C-N), 766 (1,4-disubst. aryl, 1,2,4-trisubst. aryl) cm^{-1}.

HRMS (EI): *m/z* = $C_{24}H_{16}N_4O_6$ calcd. 456.1069; meas. 456.1056 (Δ 2.9 ppm).

EA: $C_{24}H_{16}N_4O_6$ (456.41): calcd. C 63.16 H 3.53 N 12.28;

$C_{24}H_{16}N_4O_6 \cdot 1.5\ H_2O$ (483.43): calcd. C 59.63 H 3.96 N 11.59;

meas. C 59.48 H 3.95 N 11.68.

CAU-7-TATB [Bi(TATB)]

LeBail fit and Rietveld refinement

Refinement details

The Rietveld refinement was performed with TOPAS Academic 4.1[176] using one individual bismuth atom and one linker molecule as rigid body with z-matrix. Torsion angles of phenyl rings and carboxylate oxygen atoms were refined individually, bond lengths in groups ($C_{triazine}$-$N_{triazine}$, C_{phenyl}-C_{phenyl}).

Table S1: Cell parameters of CAU-7 (from Rietveld refinement),[177] of CAU-7-TATB (*as*, from LeBail fit) and of CAU-7-TATB (*ht*, from Rietveld refinement).

	CAU-7	**CAU-7-TATB (*as*)**	**CAU-7-TATB (*ht*)**
Space group	*Pb*2_1a	*Pc* (one poss.)	*Pb*2_1a
a	32.36(1) Å	27.357(3) Å	31.001(6) Å
b	28.084(7) Å	4.4766(6) Å	27.623(5) Å
c	3.9132(9) Å	30.598(3) Å	3.913(1) Å
α	90°	90°	90°
β	90°	90.910(5)°	90°
γ	90°	90°	90°
R_{wp}	9.43	4.269	3.303
GOF	2.85	1.463	5.371

LeBail plot of CAU-7-TATB (*as*)

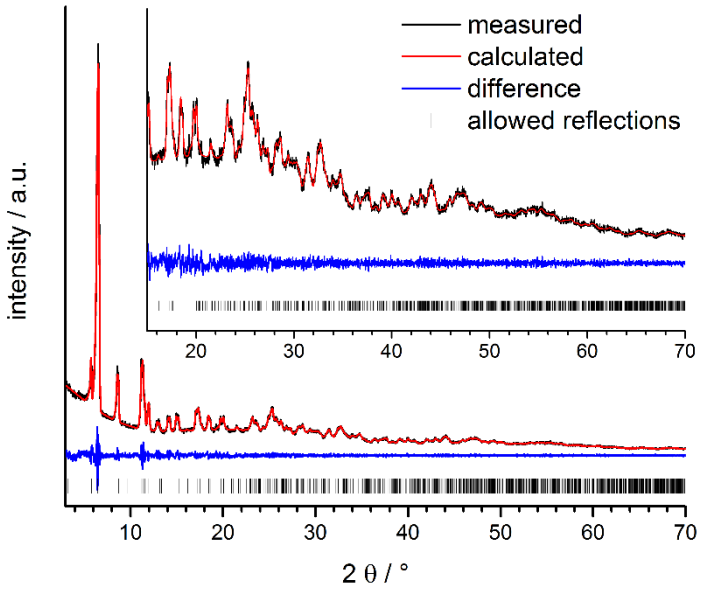

Figure S9: LeBail plot of the refinement of CAU-7-TATB (*as*). Measured and calculated PXRD data, the difference of both and the allowed reflections are shown in black, red, blue and as black bars, respectively.

PXRD patterns of CAU-7-TATB (*as*) and CAU-7-TATB (*ht*)

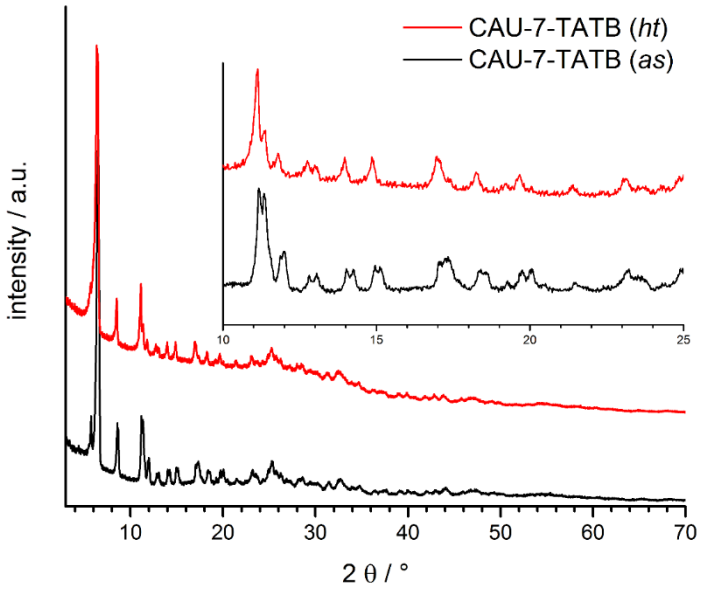

Figure S10: PXRD patterns of CAU-7-TATB (*as*) and CAU-7-TATB (*ht*) in comparison.

Rietveld plot of CAU-7-TATB (*ht*)

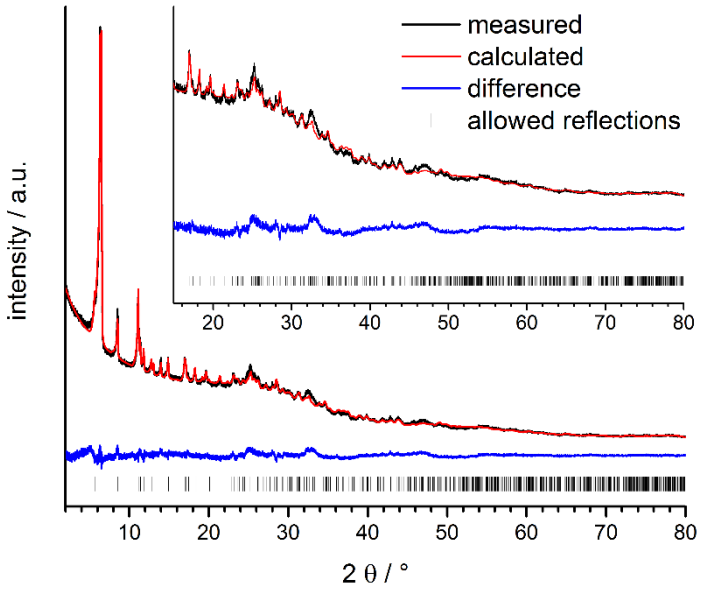

Figure S11: Rietveld plot of the refinement of CAU-7-TATB (*ht*). Measured and calculated PXRD data, the difference of both and the allowed reflections are shown in black, red, blue and as black bars, respectively.

Selected bond lengths

Table S2: Selected bond lengths in CAU-7-TATB (*ht*).

Atom 1	Symmetry 1	Atom 2	Symmetry 2	Distance / Å
Bi1	x, y, z	O1	x, y, -1+z	2.465(17)
Bi1	x, y, z	O2	x, y, z	2.762(11)
Bi1	x, y, z	O2	x, y, -1+z	2.690(11)
Bi1	x, y, z	O3	0.5+x, y, 1-z	2.982(10)
Bi1	x, y, z	O3	0.5+x, y, -z	2.444(10)
Bi1	x, y, z	O4	0.5+x, y, 1-z	2.489(14)
Bi1	x, y, z	O4	0.5+x, y, -z	2.487(14)
Bi1	x, y, z	O5	1.5-x, 0.5+y, z	2.881(14)
Bi1	x, y, z	O5	1.5-x, 0.5+y, -1+z	2.231(16)
Bi1	x, y, z	O6	1.5-x, 0.5+y, -1+z	2.678(14)
C1/C9/C17		C2/C10/C18		1.4064(2)
C5/C13/C21		C8/C16/C24		1.4064(2)
N		C		1.4474(2)
C (phenyl)		C (phenyl)		1.4474(2)

Structure of CAU-7-TATB (*ht*)

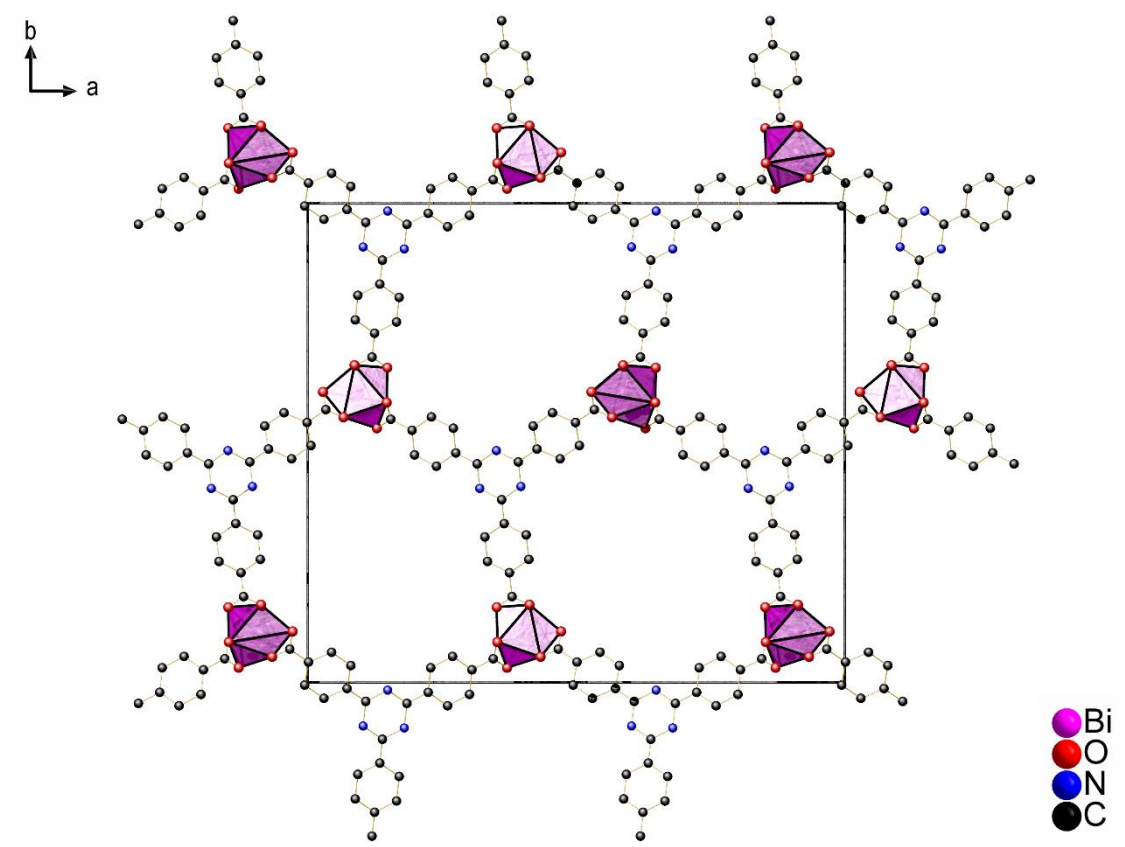

Figure S12: Crystal structure of CAU-7-TATB (*ht*), view along [001]. The unit cell dimension is represented by the box.

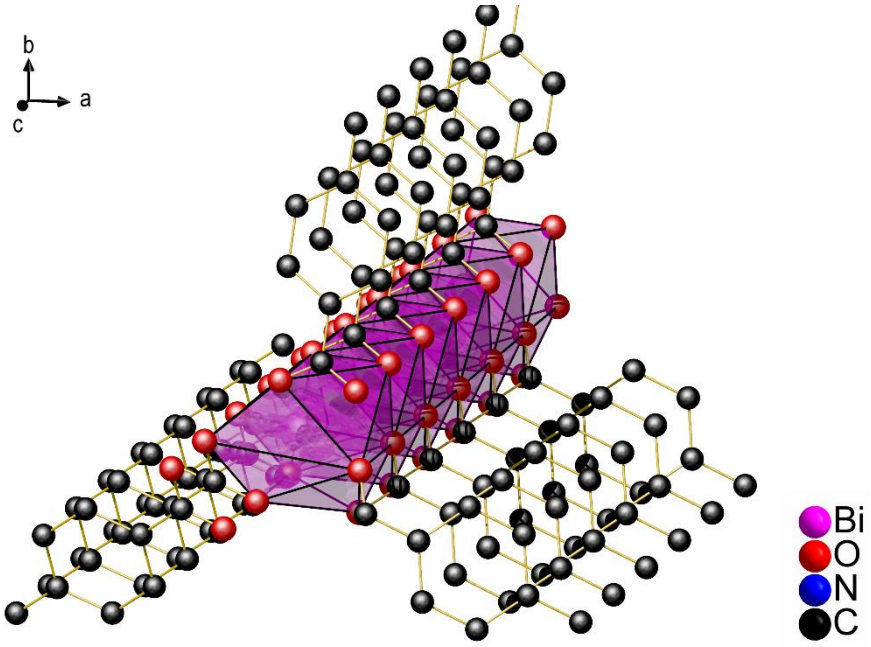

Figure S13: Linear chain in crystal structure of CAU-7-TATB (*ht*). See also Fig. S22.

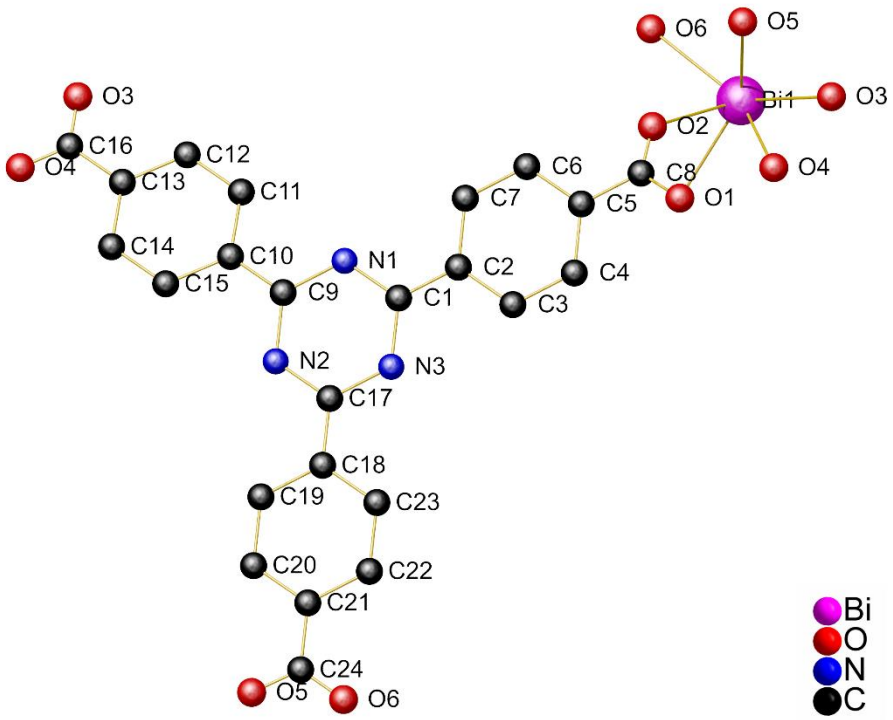

Figure S14: Extended asymmetric unit of the crystal structure of CAU-7-TATB (*ht*).

Characterisation of CAU-7-TATB

Sorption

The N_2 sorption measurement leads to a specific BET surface area of A_{BET} = 813 m²/g and a micropore volume of V_{mic} = 0.31 cm^3/g. These values correlate well with the theoretical maximum values of $A_{BET,theo}$ = 867 m²/g and $V_{mic,theo}$ = 0.32 cm^3/g, calculated with accessible solvent surface module in Materials Studio 5.5 using a probe molecule radius of 1.82 Å for simulated N_2.[178,179]

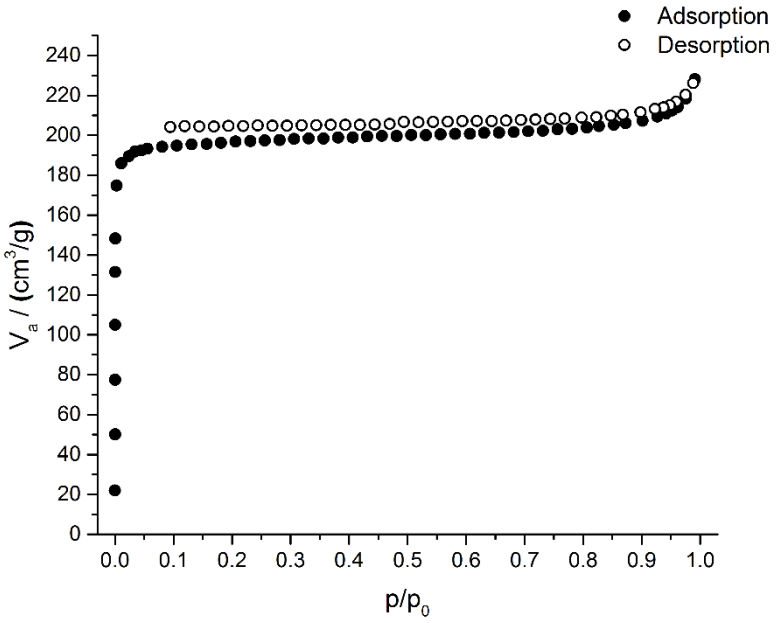

Figure S15: N_2 sorption isotherm of CAU-7-TATB (*ht*), measured at 77 K. Activation of the sample at 150 °C for 12 h in vacuum.

Infrared spectroscopy

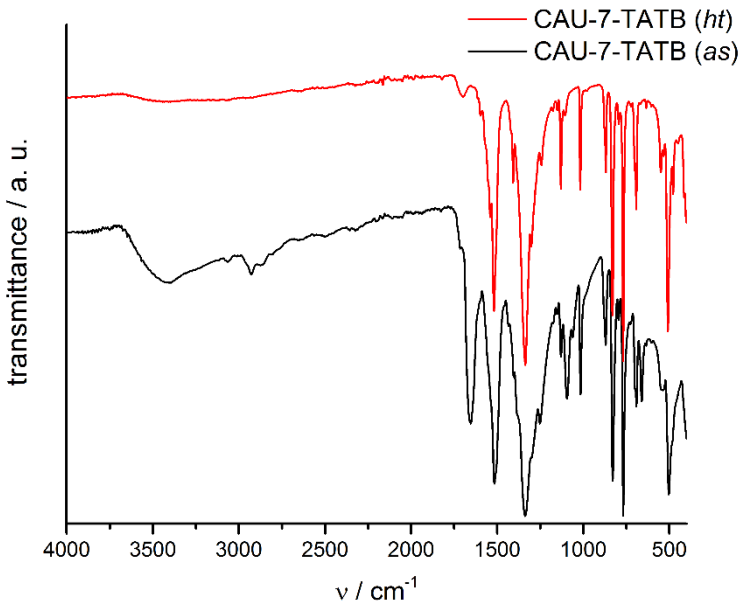

Figure S16: IR spectra of CAU-7-TATB. Characteristic frequencies: 1518 cm^{-1} (asymm. carboxylate), 1410-1240 cm^{-1} (symm. carboxylate), 1017 cm^{-1}, 880-692 cm^{-1} (aryl-H). The only significant differences for CAU-7-TATB (*as*) are the bands at 3700-2150 cm^{-1} (OH, water) and all bands that are attributed to DMF molecules inside the pores (2927 cm^{-1}, 2871 cm^{-1}, 1654 cm^{-1}).

Thermogravimetric and elemental analysis

The chemical formulas of the *as*- and *ht*-phase were determined by combining the results from TG and elemental analyses and are summarized in the following table. The results of the thermogravimetric analysis are in agreement with the theoretical weight losses (meas.: 19.5 %, 50.7 %; theo.: 21.9 %, 50.0 %; first step: pore content, second step: decomposition of the framework). TG and elemental analyses were performed under ambient conditions, which might have led to water adsorption from the air.

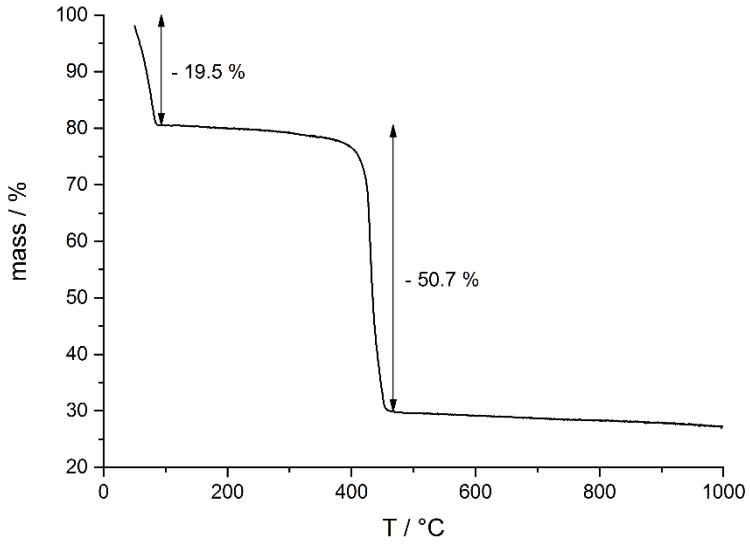

Figure S17: Thermogravimetric analysis of CAU-7-TATB (*ht*).

Table S3: Results of the elemental analyses of CAU-7-TATB (*as*, top) and CAU-7-TATB (*ht*, bottom).

Chemical formula		**C / %**	**H / %**	**N / %**	**S / %**
[Bi(TATB)]·DMF·6H_2O	meas.	37.29	2.93	7.84	0.00
	theo.	39.14	3.77	6.76	0.00
[Bi(TATB)]·9H_2O	meas.	35.96	1.52	5.57	0.00
	theo.	35.61	3.74	5.19	0.00

CAU-7-TATB-NH_2 [Bi(TATB-NH_2)]

LeBail fit

Table S4: Results of the LeBail fit of [Bi(TATB-NH_2)].

	CAU-7-TATB-NH_2
Space group	*Pb*2_1*a*
a	30.861(3) Å
b	27.521(2) Å
b	3.8907(5) Å
α	90°
β	90°
γ	90°
R_{wp}	3.32
GOF	1.72

LeBail plot

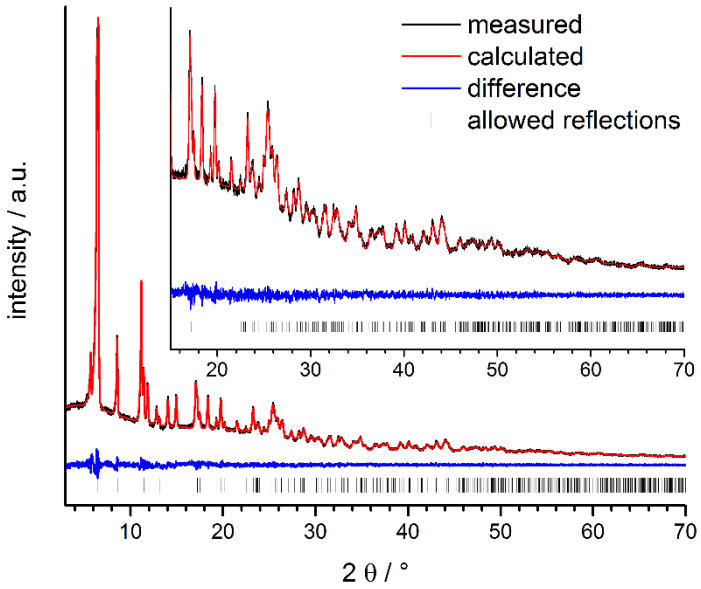

Figure S18: LeBail plot of the refinement of CAU-7-TATB-NH_2. Measured and calculated PXRD data, the difference of both and the allowed reflections are shown in black, red, blue and as black bars, respectively.

Characterisation of CAU-7-TATB-NH_2

Sorption

The N_2 sorption measurements of the CAU-7-TATB-NH_2 samples, obtained from different synthesis batches, vary strongly. Fig. S11 shows the adsorption curves of eight exemplary reaction products. The results of the BET analyses are summarized in the following table.

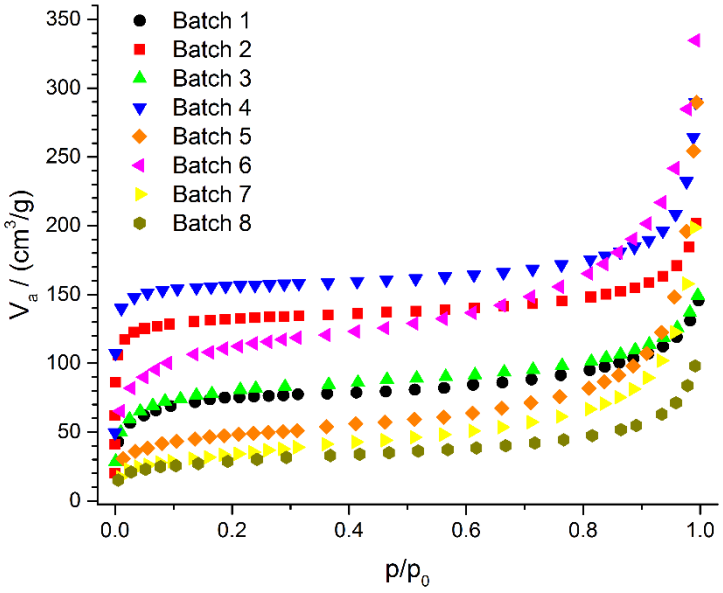

Figure S19: N_2 adsorption isotherms of eight different batches of CAU-7-TATB-NH_2, measured at 77 K. All batches were obtained under identical reaction conditions using the same batches of starting materials. Activation of the samples at 190 °C for 12 h in vacuum. Only the adsorption curves are shown for more clarity.

Table S5: Specific BET surface areas and micropore volumes of eight different batches of CAU-7-TATB-NH_2.

Sample	A_{BET} / (m^2/g)	V_{mic} / (cm^3/g)
Batch 1	279	0.12
Batch 2	519	0.21
Batch 3	295	0.14
Batch 4	627	0.25
Batch 5	176	0.09
Batch 6	415	0.20
Batch 7	120	0.07
Batch 8	104	0.06

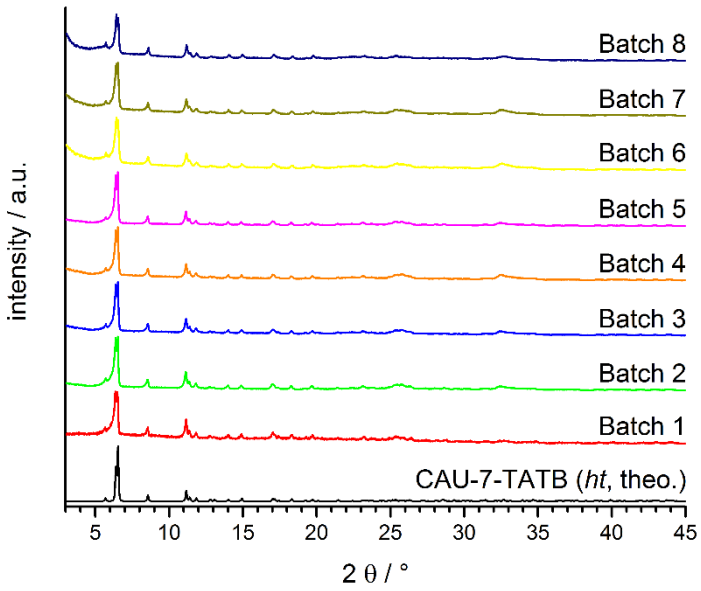

Figure S20: PXRD patterns of eight different batches of CAU-7-TATB-NH_2. For all patterns there is no significant difference in the PXRD patterns of these batches.

Scanning Electron Microscopy

The SEM experiments, which are presented here, were performed on a *Jeol JSM-6500F* with EDX-Detektor and *Inca*-software (*Oxford Instruments*). For sample preparation, an ethanolic dispersion of the MOF sample was dried and subsequently sputtered with carbon.

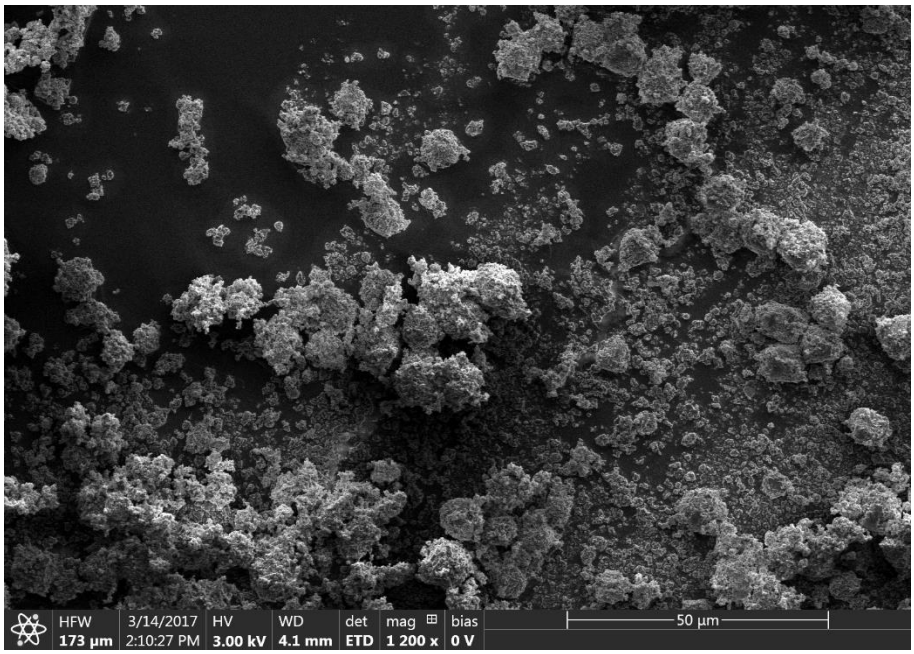

Figure S21: SEM micrograph of CAU-7-NH_2 with 50 µm scale bar (*Batch 8*, A_{BET} = 104 m^2/g).

Figure S22: SEM micrograph of CAU-7-NH_2 with 5 µm scale bar (*Batch 8*, A_{BET} = 104 m^2/g).

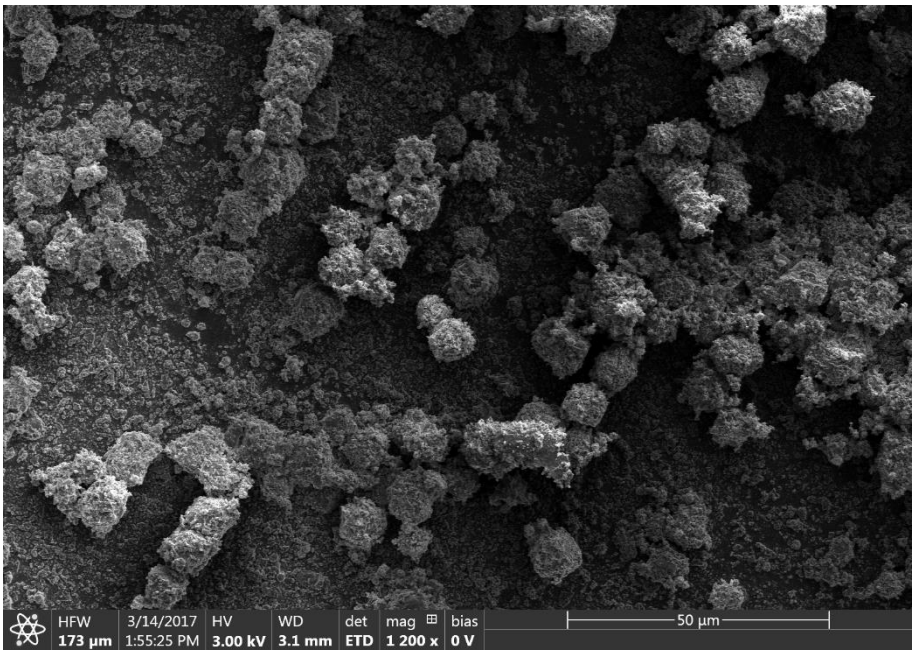

Figure S23: SEM micrograph of CAU-7-NH_2 with 50 µm scale bar (*Batch 4*, A_{BET} = 627 m^2/g).

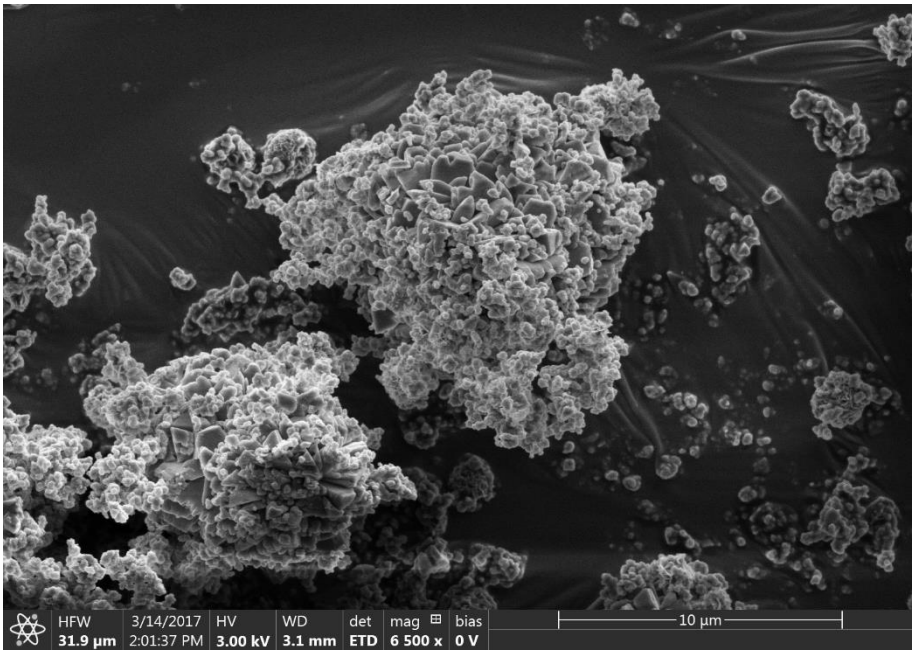

Figure S24: SEM micrograph of CAU-7-NH_2 with 5 µm scale bar (*Batch 4*, A_{BET} = 627 m^2/g).

Infrared spectroscopy, thermogravimetric and elemental analysis

Further characterisation of CAU-7-TATB-NH_2 is summarized in the post-synthetic modification part of this document for better comparison.

CAU-35 $[Bi_2(O)(OH)(TATB)]\cdot H_2O$

Structure solution and Rietveld refinement of CAU-35

Refinement details

After indexing the powder pattern with TOPAS Academic 4.1,[176] the structure was solved using the software FOX,[180] starting from two Bi atoms and one $TATB^{3-}$ molecule, which was introduced as a rigid body. Bi-positions were located first and fixed afterwards, since bismuth is the most dominant scatterer in the structure. The *parallel tempering function* was used for the solution of the structure.

The Rietveld refinement was performed with TOPAS Academic 4.1[176] using two individual bismuth atoms and one linker molecule as rigid body with z-matrix. Torsion angles of phenyl rings and carboxylate oxygen atoms were refined individually, bond lengths in groups ($C_{triazine}$-$N_{triazine}$, C_{phenyl}-C_{phenyl}, $C_{carboxy}$-$O_{carboxy}$). The two separate oxygen atoms in the inorganic building unit were added from Fourier difference analysis.

Table S6: Results of the structure refinement of $[Bi_2(O)(OH)(TATB)]\cdot H_2O$.

	CAU-35
Space group	$Pna2_1$
a	20.868(2) Å
b	31.658(3) Å
b	3.9596(3) Å
α	90°
β	90°
γ	90°
R_{wp}	4.94
GOF	1.74

Rietveld plot

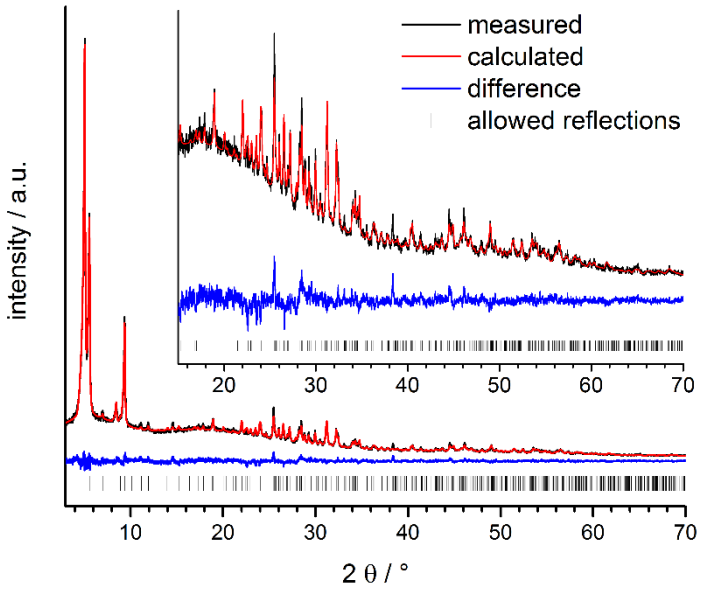

Figure S25: Rietveld plot of the refinement of CAU-35. Measured and calculated PXRD data, the difference of both and the allowed reflections are shown in black, red, blue and as black bars, respectively.

Selected bond lengths

Table S7: Selected bond lengths in CAU-35.

Atom 1	Symmetry 1	Atom 2	Symmetry 2	Distance / Å
Bi1	x, y, z	O7	0.5+x, 0.5-y, z	2.141(53)
Bi1	x, y, z	O3	1.5-x, 0.5+y, -0.5+z	2.287(12)
Bi1	x, y, z	O3	1.5-x, 0.5+y, -1.5+z	3.003(14)
Bi1	x, y, z	O7	1.5-x, -0.5+y, -0.5+z	2.53(48)
Bi1	x, y, z	O7	1.5-x, -0.5+y, 0.5+z	2.44(47)
Bi1	x, y, z	O8	1.5-x, -0.5+y, 0.5+z	2.115(52)
Bi1	x, y, z	O1	1-x, -y, -0.5+z	2.3236(97)
Bi2	x, y, z	O6	x, 1+y, z	2.455(12)
Bi2	x, y, z	O8	1.5-x, 0.5+y, 1.5+z	2.29(16)
Bi2	x, y, z	O8	1.5-x, 0.5+y, 0.5+z	2.36(16)
Bi2	x, y, z	O7	1.5-x, 0.5+y, 0.5+z	2.853(50)
Bi2	x, y, z	O2	1-x, 1-y, -0.5+z	2.1691(88)
Bi2	x, y, z	O5	x, 1+y, z	2.1706(87)
Bi2	x, y, z	O4	0.5+x, 0.5-y, -1+z	2.362(13)
C1/C2/C3		C4/C11/C18		1.3175(1)
C7/C14/C21		C10/C17/C24		1.4926(1)
N		C		1.3500(1)
C (phenyl)		C (phenyl)		1.3809(1)

Structure of CAU-35

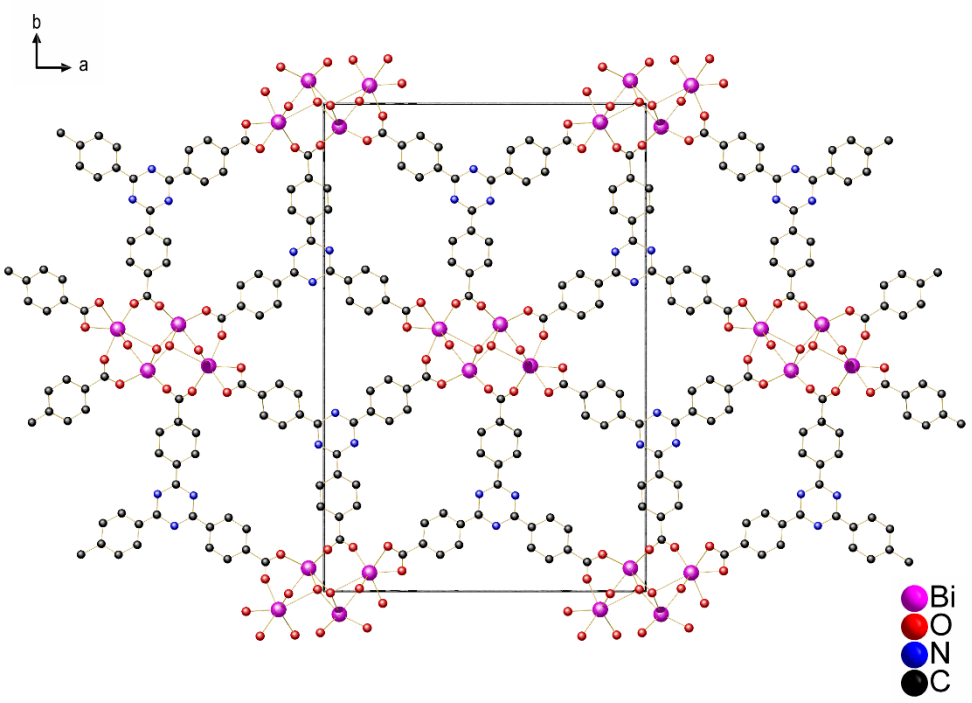

Figure S26: Crystal structure of CAU-35, view along [001]. The unit cell dimension is represented by the box.

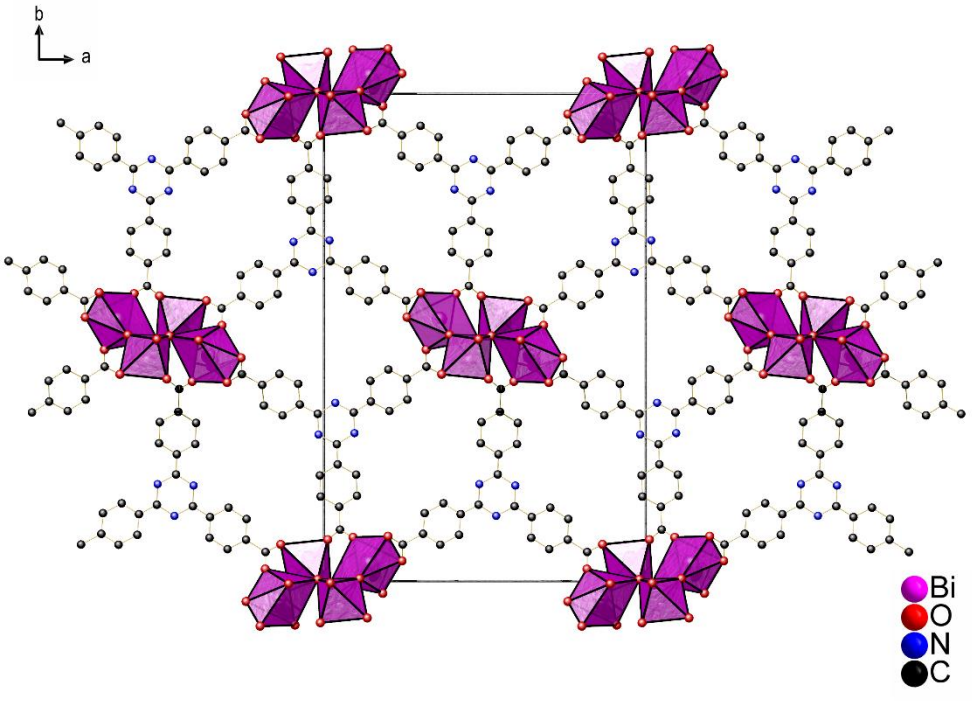

Figure S27: Crystal structure of CAU-35, view along [001]. The unit cell dimension is represented by the box.

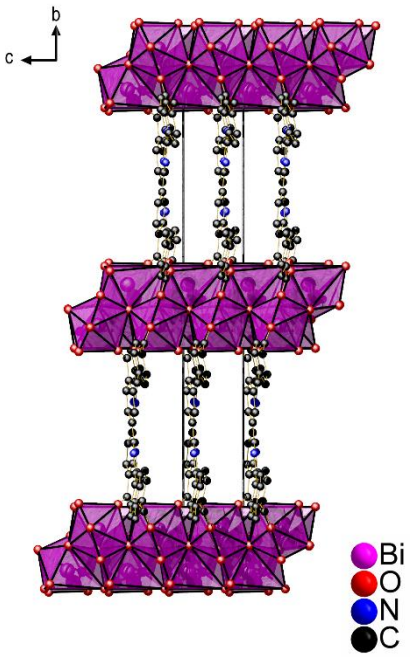

Figure S28: Crystal structure of CAU-35, view along [100]. The unit cell dimension is represented by the box.

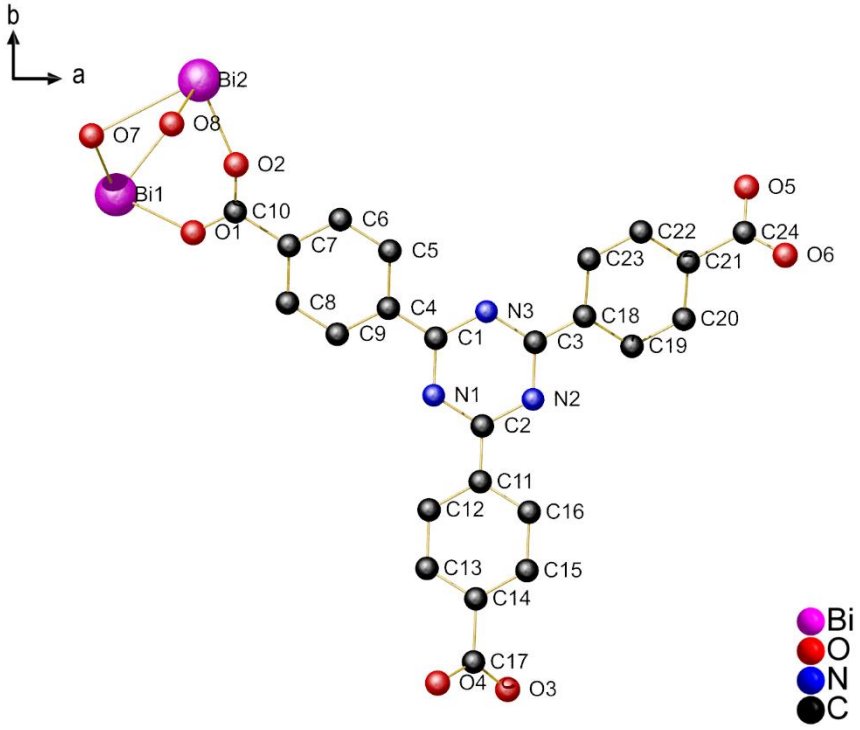

Figure S29: Asymmetric unit of the crystal structure of CAU-35.

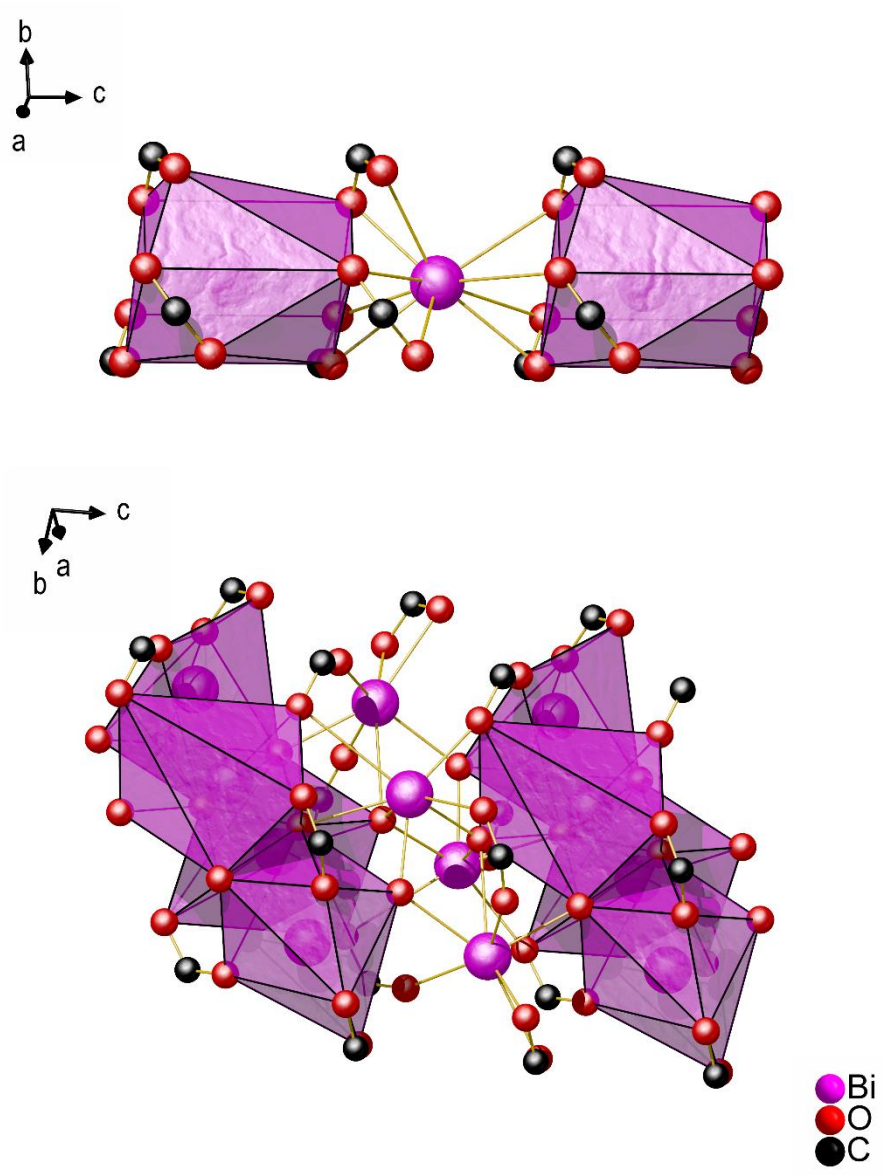

Figure S30: IBUs in CAU-7-TATB and CAU-35, on top and bottom, respectively.

Characterisation of CAU-35

Sorption

The N_2 sorption measurement leads to a specific BET surface area of A_{BET} = 77 m²/g and a micropore volume of V_{mic} = 0.05 cm^3/g. This value correlates well with the theoretical maximum value of $V_{mic,theo}$ = 0.06 cm^3/g, calculated with accessible solvent surface module in Materials Studio 5.5 using a probe molecule radius of 1.82 Å for simulated N_2.[179,178]

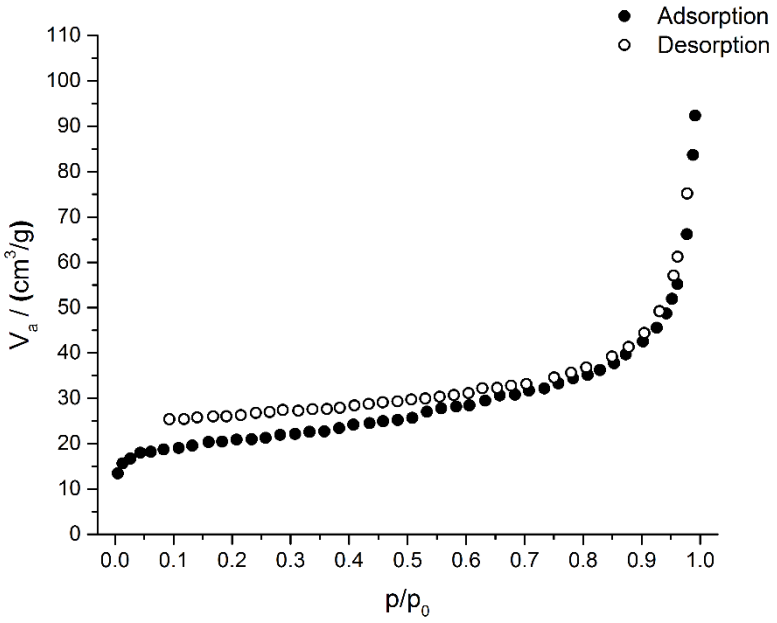

Figure S31: N_2 sorption isotherm of CAU-35, measured at 77 K. Activation of the sample at 150 °C for 12 h in vacuum.

Infrared spectroscopy

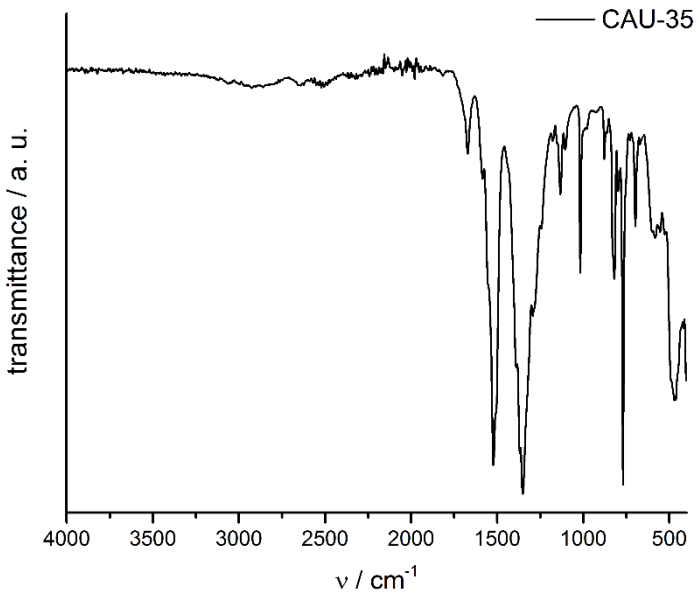

Figure S32: IR spectrum of CAU-35. Characteristic frequencies: 1671 cm^{-1}, 1585 cm^{-1} (C-N, triazine), 1522 cm^{-1} (asymm. carboxylate), 1351 cm^{-1} (symm. carboxylate), 1018 cm^{-1}, 820-697 cm^{-1} (aryl-H).

Thermogravimetric and elemental analysis

The chemical formula of CAU-35 was also determined by combining TG and elemental analysis and is shown in the following table. The results of the thermogravimetric analysis agree reasonably well with this data (meas.: 2.6 %, 41.4 %; theo.: 2.0 %, 45.8 %; first step: pore content, second step: decomposition of the framework). TG and elemental analyses were performed under ambient conditions, which might have led to water adsorption from the air.

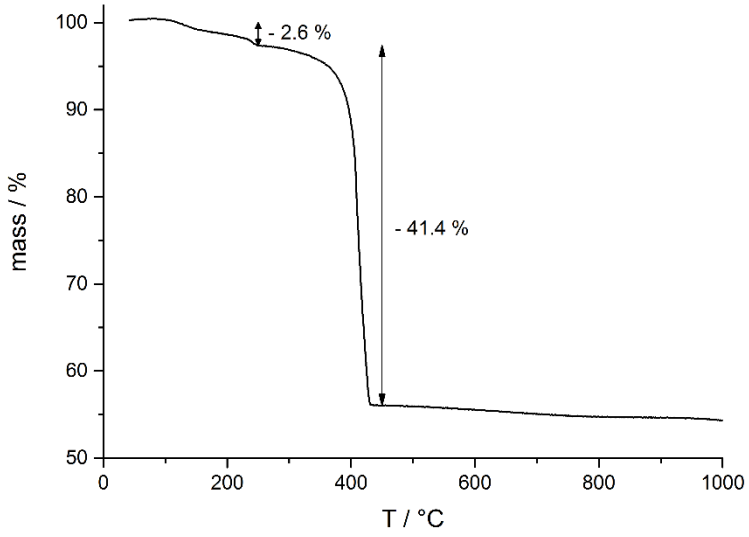

Figure S33: Thermogravimetric analysis of CAU-35.

Table S8: Results of the elemental analysis of CAU-35.

Chemical formula		C / %	H / %	N / %	S / %
$[Bi_2(O)(OH)(TATB)]\cdot H_2O$	meas.	32.77	1.41	4.97	0.00
	theo.	31.77	1.67	4.63	0.00

Post-synthetic modification

For the characterisation of CAU-7-TATB-NH_2 and the five products of the PSM reactions, eight synthesis batches of CAU-7-TATB-NH_2 were combined and mixed. All PSM reactions and characterisations were performed with this mixture to facilitate the highest data consistence.

The degree of conversion after post-synthetic modification was determined by comparing the relative integrals in ^{1}H-NMR-spectra of digested MOFs (digested with a mixture of DMSO-d_6 and DCl (37 %)).

Table 9: Degree of conversion after post-synthetic modification of CAU-7-TATB-NH_2.

Sample	Reagent	Conversion
CAU-7-TATB-NH_2-AA	acetic anhydride	79 %
CAU-7-TATB-NH_2-VA	valeric anhydride	47 %
CAU-7-TATB-NH_2-SA	succinic anhydride	67 %
CAU-7-TATB-NH_2-PA	phthalic anhydride	35 %
CAU-7-TATB-NH_2-PS	1,3-propane sultone	33 %

^{1}H-NMR spectra

The aromatic protons of unreacted H_3TATB-NH_2 are indicated by black numbers and the protons of modified H_3TATB-NH_2 by red letters. Protons within the residue (R) are indicated in red as well. The conversion after post-synthetic modification was determined by comparing the integrals of the aromatic protons **1**, **2** or **3** with **B**. The assignments of the respective protons are shown in the following scheme:

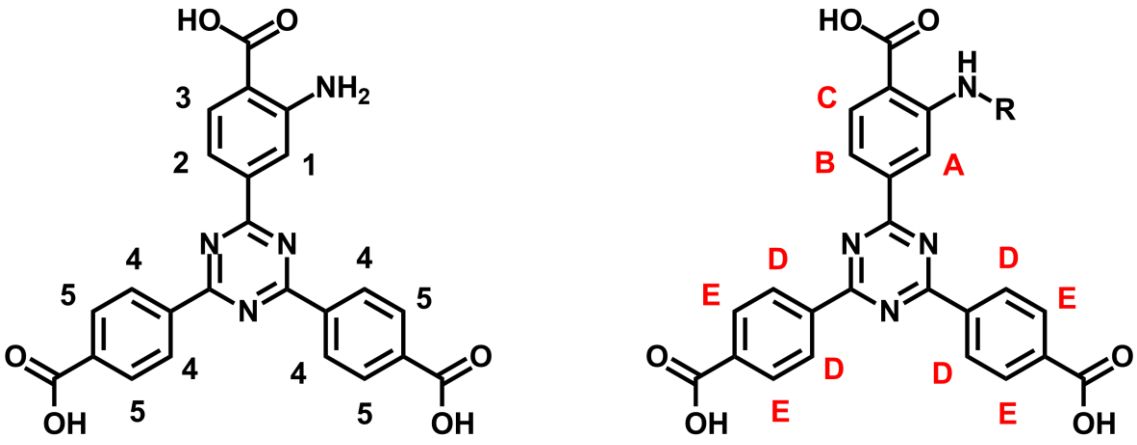

In the following Figures only an excerpt of the ^{1}H-NMR spectra with significant signals is shown.

CAU-7-TATB-NH_2-AA

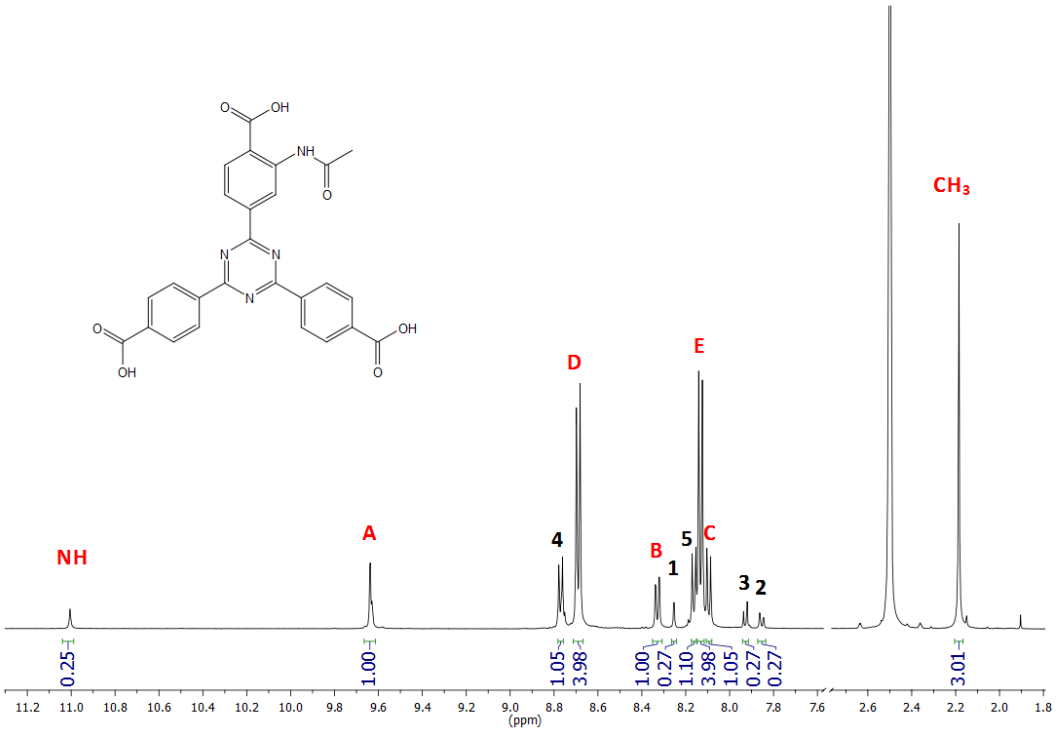

Figure S34: ^{1}H-NMR spectrum (500 MHz, 300 K, DMSO-d6/DCl) of digested CAU-7-TATB-NH_2 after post-synthetic modification with acetic anhydride.

CAU-7-TATB-NH_2-VA

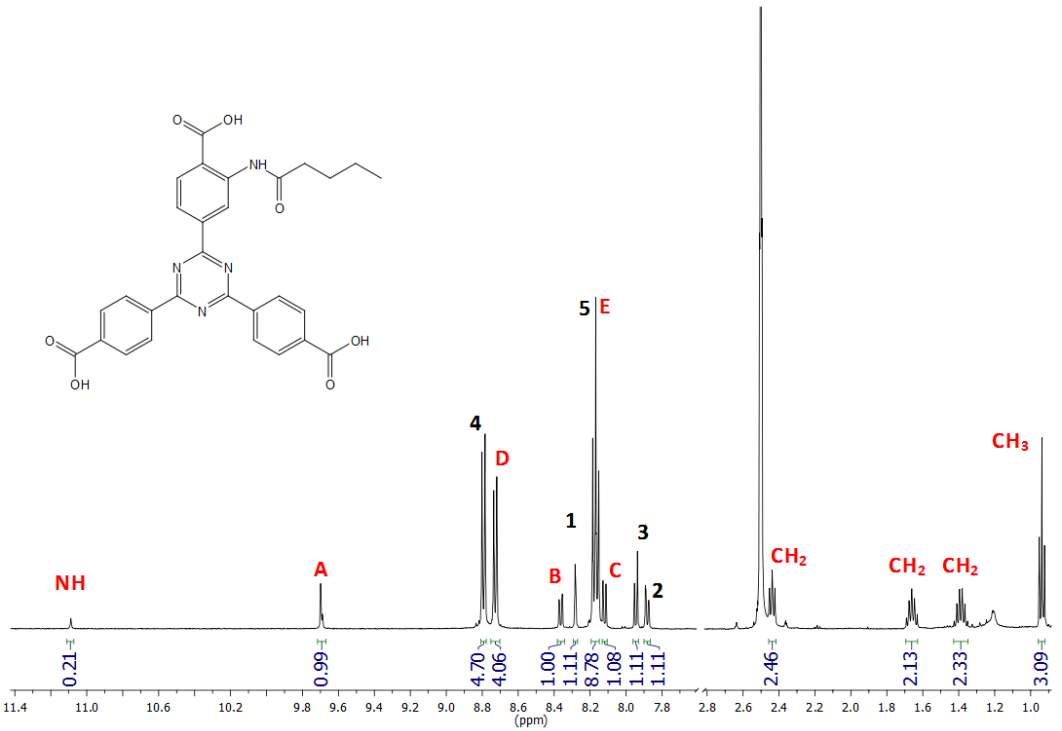

Figure S35: ^{1}H-NMR spectrum (500 MHz, 300 K, DMSO-d6/DCl) of digested CAU-7-TATB-NH_2 after post-synthetic modification with valeric anhydride.

CAU-7-TATB-NH_2-SA

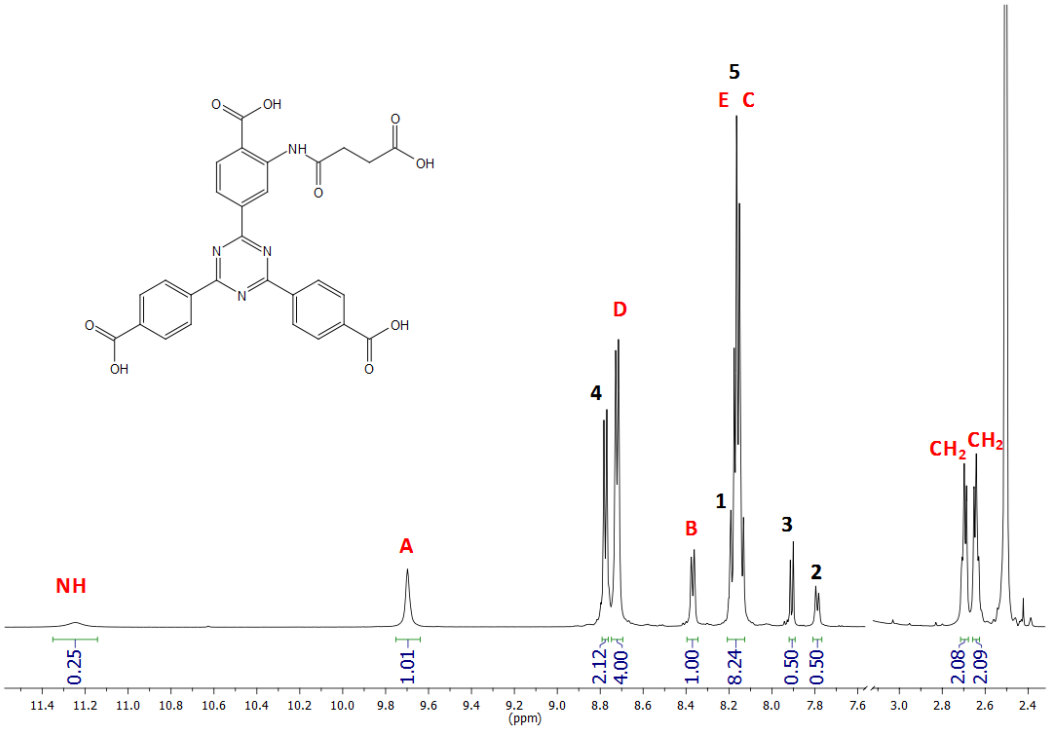

Figure S36: ^{1}H-NMR spectrum (500 MHz, 300 K, DMSO-d6/DCl) of digested CAU-7-TATB-NH_2 after post-synthetic modification with succinic anhydride.

CAU-7-TATB-NH_2-PA

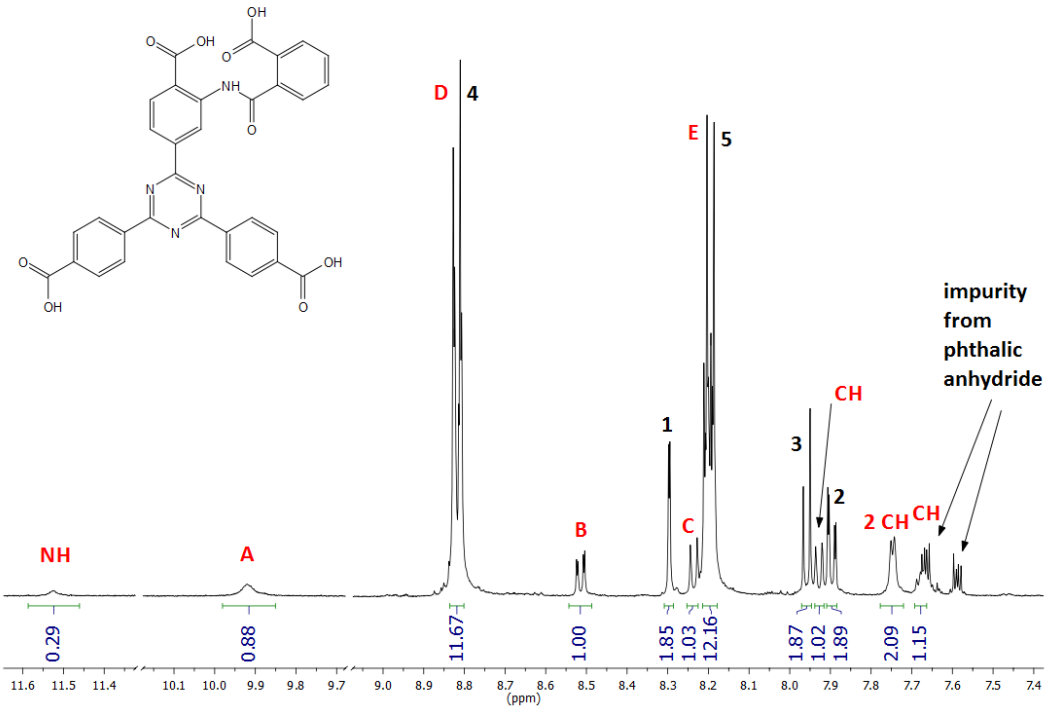

Figure S37: ^{1}H-NMR spectrum (500 MHz, 300 K, DMSO-d6/DCl) of digested CAU-7-TATB-NH_2 after post-synthetic modification with phthalic anhydride.

CAU-7-TATB-NH_2-PS

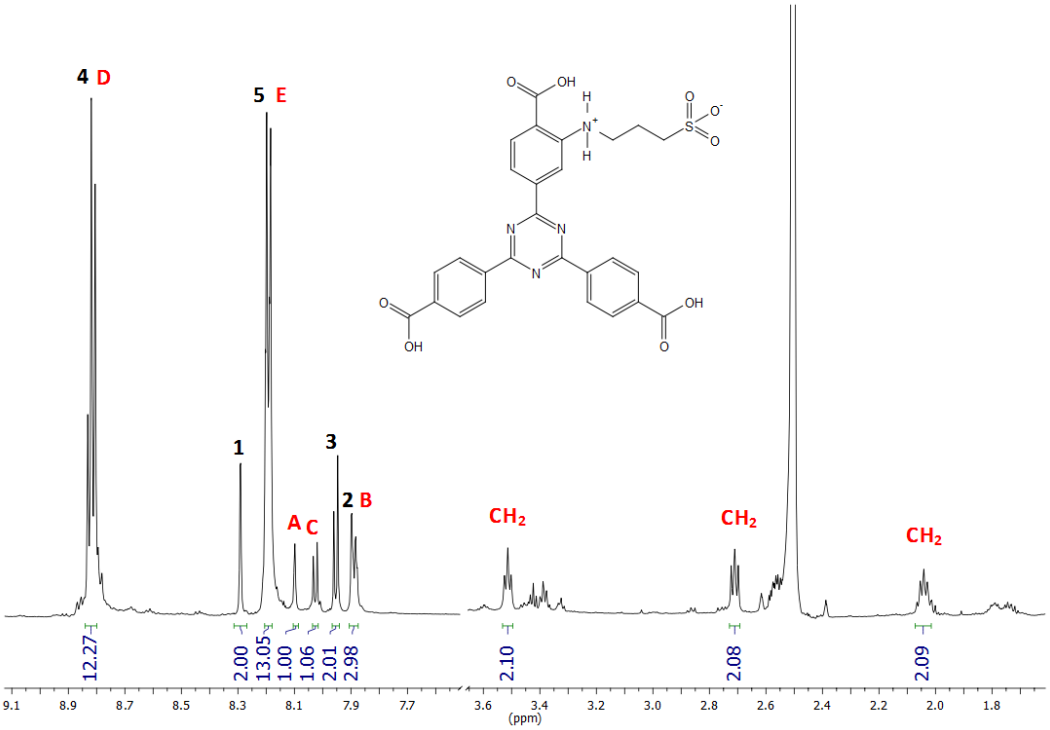

Figure S38: ^{1}H-NMR spectrum (500 MHz, 300 K, DMSO-d6/DCl) of digested CAU-7-TATB-NH_2 after post-synthetic modification with 1,3-propane sultone.

Comparison of PSM with valeric anhydride for two batches with different BET surface

Despite the fact that the unmodified CAU-7-TATB-NH_2 varied in its nitrogen adsorption behaviour, the respective surface area had no influence on the degree of conversion. Two batches of CAU-7-TATB-NH_2 with different surface areas (137 m^2/g and 627 m^2/g) were used for a PSM with valeric anhydride. For both MOFs a similar conversion was observed (Fig. S31). This points out that the inconsistent nitrogen sorption behaviour is not influencing the porosity in fluid media.

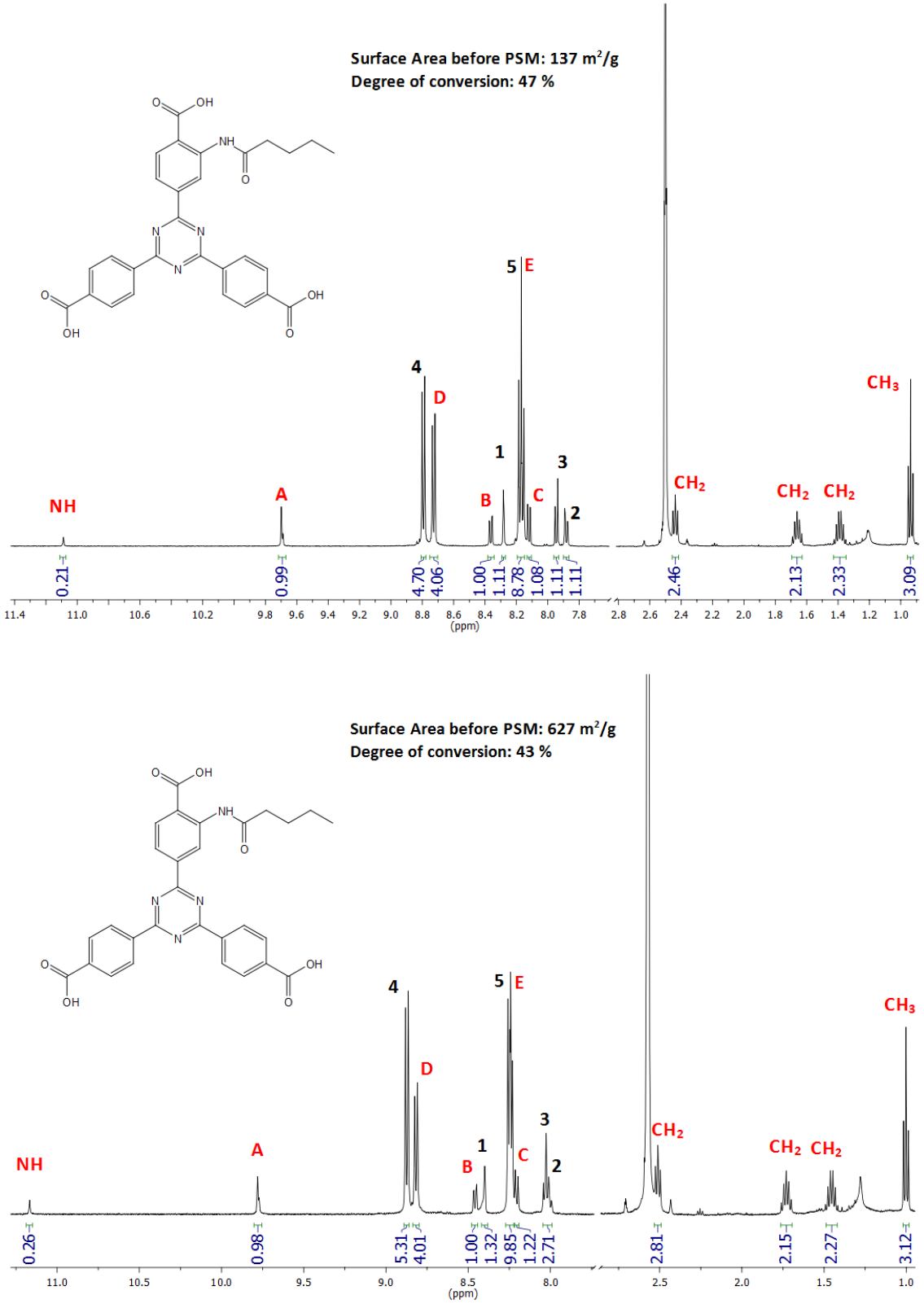

Figure S39: Comparison of ^{1}H-NMR spectra from PSM with valeric anhydride for two batches with different BET surface areas. The comparison of both ^{1}H-NMR spectra shows no significant difference in the degree of conversion.

X-ray powder diffraction

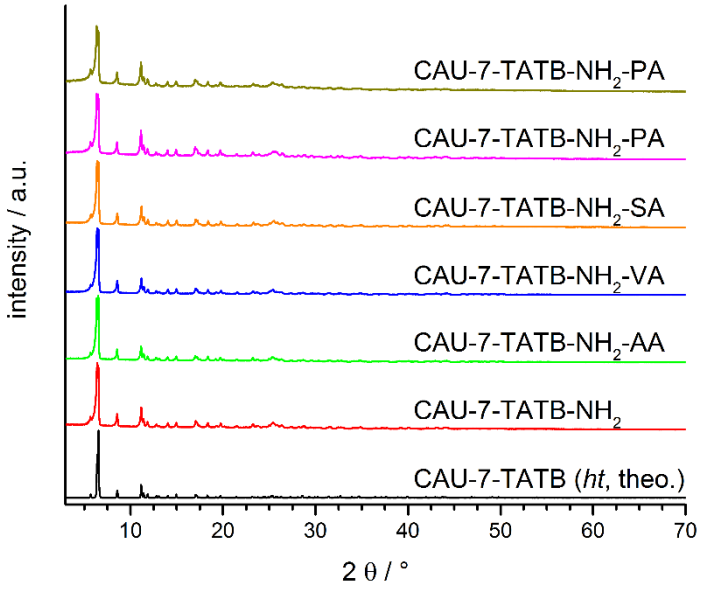

Figure S40: PXRD patterns of CAU-7-TATB-NH_2 (mixture of several batches) and the post-synthetically modified samples. For all patterns, there is no indication for loss of crystallinity due to the post-synthetic modification.

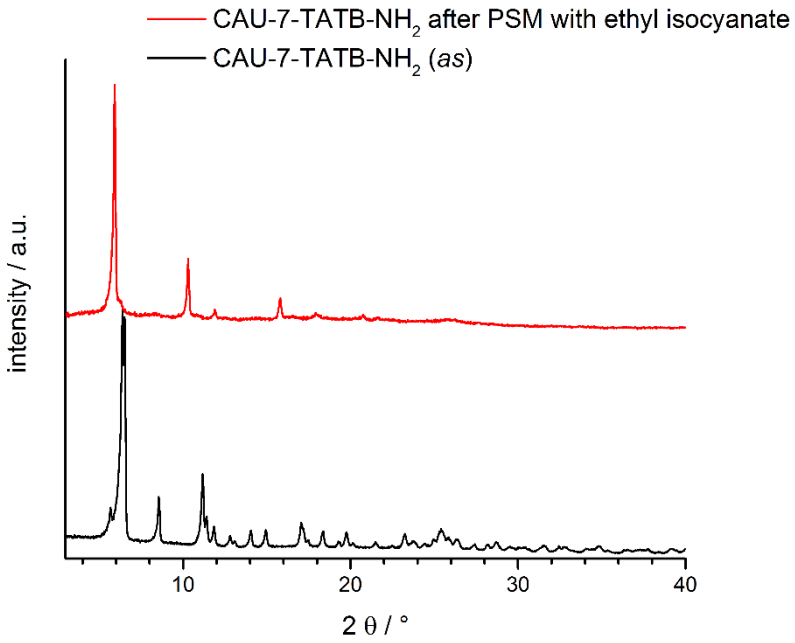

Figure S41: PXRD patterns of CAU-7-TATB-NH_2 (mixture of several batches) and the post-synthetically modified sample, which was treated with ethyl isocyanate. The reaction led to degradation of the crystal structure and formed a crystalline compound which has not identified yet.

Sorption

The N_2 sorption curves of CAU-7-TATB-NH_2 (mixture of several batches) and the post-synthetically modified samples are shown in Fig. S34. The results of the BET analysis are summarized in Table S10. It remains unclear why the post-synthetic modification reaction with acetic anhydride led to a higher specific BET surface area in the resulting product (CAU-7-TATB-NH_2-AA) when compared to the starting material CAU-7-TATB-NH_2.

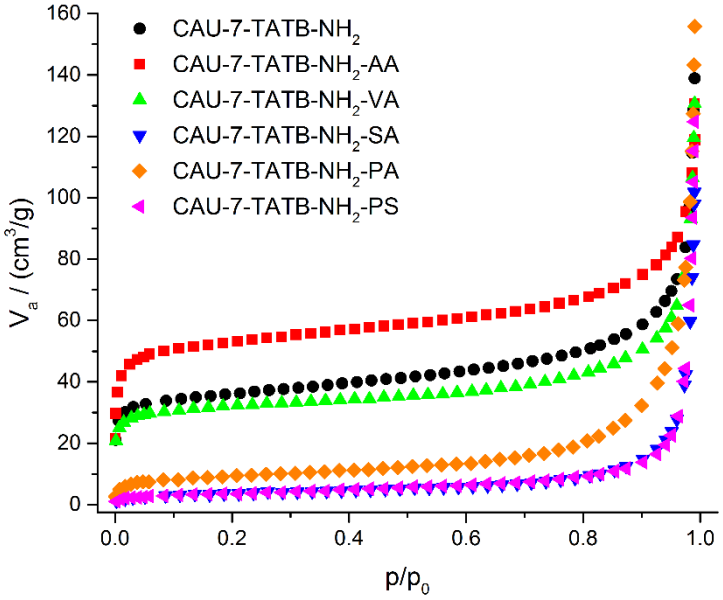

Figure S42: N_2 adsorption isotherms of CAU-7-TATB-NH_2 (mixture of several batches) and the post-synthetically modified samples, measured at 77 K. Activation of the samples at 100 °C for 12 h in vacuum. Only the adsorption curves are shown for more clarity.

Table S10: Specific BET surface areas and micropore volumes of CAU-7-TATB-NH_2 (mixture of several batches) and the post-synthetically modified samples.

Sample	A_{BET} / (m^2/g)	V_{mic} / (cm^3/g)
CAU-7-TATB-NH_2	137	0.06
CAU-7-TATB-NH_2-AA	203	0.09
CAU-7-TATB-NH_2-VA	123	0.05
CAU-7-TATB-NH_2-SA	13	0.01
CAU-7-TATB-NH_2-PA	33	0.02
CAU-7-TATB-NH_2-PS	13	0.01

Infrared spectroscopy

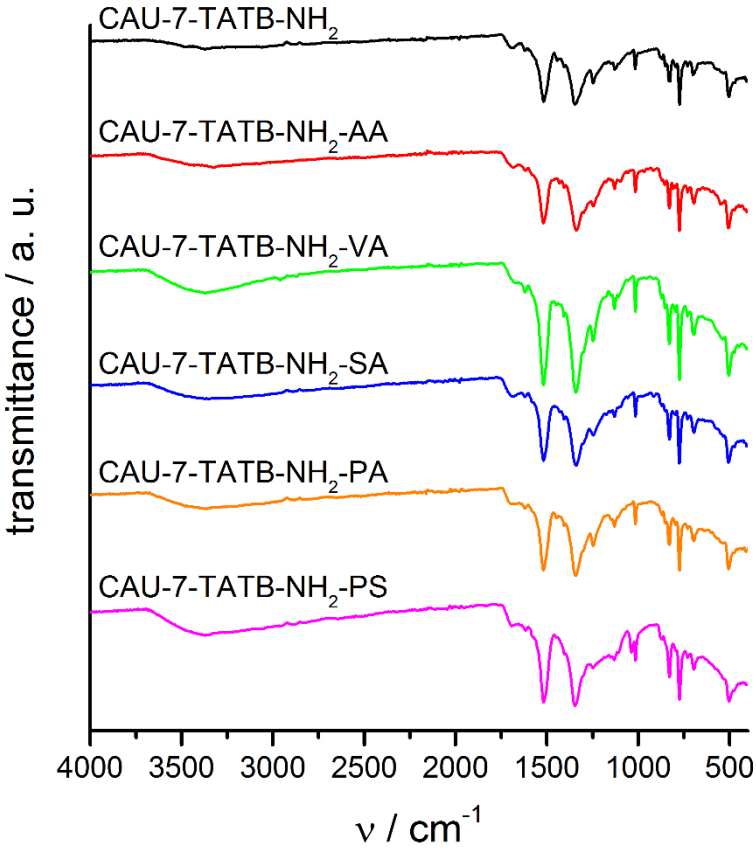

Figure S43: IR spectrum of CAU-7-TATB-NH_2 (mixture of several batches) in comparison with the spectra of the post-synthetically modified MOFs. All spectra have the same characteristic frequencies: 1518 cm^{-1} (asymm. carboxylate), 1344 cm^{-1} (symm. carboxylate), 829 cm^{-1}, 775 cm^{-1} (aryl-H). The only significant difference is an additional frequency at 1036 cm^{-1} (S=O) for CAU-7-TATB-NH_2-PS, which can be attributed to the sulfonate group.

Thermogravimetric and elemental analysis

For the analysis of CAU-7-TATB-NH_2, the same mixture of several batches was used, as it has been used for the post-synthetic modification (A_{BET} = 137 m^2/g). The thermogravimetric and elemental analyses (Fig. S36, Table S11-S12) do not indicate any impurity, neither for CAU-7-TATB-NH_2, nor for the post-synthetically modified samples. The results are in agreement with the theoretical values (Table S11-S12).

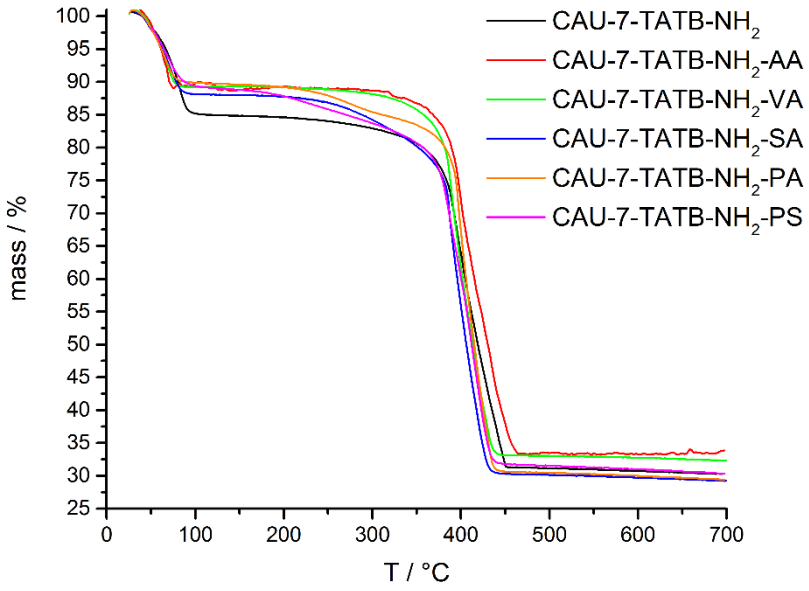

Figure S44: TG curves of CAU-7-TATB-NH_2 (mixture of several batches) and the post-synthetically modified samples.

Table S11: Combined results of the TG and elemental analysis of CAU-7-TATB-NH_2 (mixture of several batches) and the post-synthetically modified samples.

Sample		C / %	H / %	N / %	S / %	TGA 1. step / %	TGA 2. step / %
CAU-7-TATB-NH_2	meas.	39.74	1.85	7.99	0.00	15.61	53.64
	theo.	38.82	3.39	7.99	0.00	16.05	54.42
CAU-7-TATB-NH_2-AA	meas.	39.55	2.04	7.27	0.00	12.38	55.31
	theo.	39.11	3.15	7.13	0.00	11.46	58.88
CAU-7-TATB-NH_2-VA	meas.	38.84	2.36	7.01	0.00	11.12	56.21
	theo.	39.96	3.41	7.07	0.00	11.37	59.21
CAU-7-TATB-NH_2-SA	meas.	38.50	2.16	6.90	0.00	12.43	57.89
	theo.	38.26	3.33	6.69	0.00	12.91	59.28
CAU-7-TATB-NH_2-PA	meas.	39.68	1.90	6.91	0.00	10.71	59.29
	theo.	38.45	3.23	6.97	0.00	11.20	59.83
CAU-7-TATB-NH_2-PS	meas.	36.73	2.51	6.79	1.66	9.44	57.39
	theo.	38.74	2.99	7.23	1.37	9.30	60.63

Table S12: Chemical formulas obtained from combined results of NMR, TG and elemental analysis of CAU-7-TATB-NH_2 (mixture of several batches) and the post-synthetically modified samples. The degree of conversion has been determined by the ^{1}H-NMR analyses.

Sample	Chemical formula
CAU-7-TATB-NH_2	[Bi(TATB-NH_2)]·5 H_2O·0.5 DMF
CAU-7-TATB-NH_2-AA	[Bi(TATB-NH_2)$_{0.21}$(TATB-NHR)$_{0.79}$]·5 H_2O
CAU-7-TATB-NH_2-VA	[Bi(TATB-NH_2)$_{0.53}$(TATB-NHR)$_{0.47}$]·5 H_2O
CAU-7-TATB-NH_2-SA	[Bi(TATB-NH_2)$_{0.33}$(TATB-NHR)$_{0.67}$]·6 H_2O
CAU-7-TATB-NH_2-PA	[Bi(TATB-NH_2)$_{0.65}$(TATB-NHR)$_{0.35}$]·5 H_2O
CAU-7-TATB-NH_2-PS	[Bi(TATB-NH_2)$_{0.67}$(TATB-NHR)$_{0.33}$]·4 H_2O

References

1 M. Krüger, H. Reinsch, A. K. Inge and N. Stock, *Microporous Mesoporous Mater.*, 2017, **249**, 128-136.

2 E. Mühlbauer, A. Klinkebiel, O. Beyer, F. Auras, S. Wuttke, U. Lüning and T. Bein, *Microporous Mesoporous Mater.*, 2015, **216**, 51–55.

3 A. Coelho, *TOPAS Academic 4.1*, Coelho Software, 2007.

4 M. Feyand, E. Mugnaioli, F. Vermoortele, B. Bueken, J. M. Dieterich, T. Reimer, U. Kolb, D. de Vos and N. Stock, *Angew. Chem.*, 2012, **124**, 10519–10522, *Angew. Chem. Int. Ed.*, 2012, **51**, 10373–10376.

5 T. Düren, F. Millange, G. Férey, K. S. Walton and R. Q. Snurr, *J. Phys. Chem. C*, 2007, **111**, 15350–15356.

6 *Materials Studio 5.5.3*, Accelrys Software Inc., 2010.

7 V. Favre-Nicolin and R. Černý, *J. Appl. Crystallogr.*, 2002, **35**, 734–743.

4 Linker-Synthese und PSM zur Darstellung von protonenleitfähigen MOFs

MOFs mit unkoordinierten Säuregruppen sind potentielle Kandidaten für den Einsatz als protonenleitfähige Materialien. Die Darstellung dieser MOFs kann sowohl durch postsynthetische Modifikation (s. Kapitel 3.2.3) als auch durch präsynthetische Modifikation erfolgen (s. Kapitel 1.2). Vor allem MOFs basierend auf Phosphonsäure- und Sulfonsäure-Linker zeigten bereits vielversprechende Ergebnisse in Bezug auf Protonenleitfähigkeit (s. Kapitel 1.3). Dies kann hauptsächlich auf zwei Eigenschaften zurückgeführt werden: hohe Acidität und das Ausbilden von Wasserstoffbrückenbindungen. Beide Gruppen besitzen, auch wenn sie koordiniert vorliegen, freie Sauerstoffatome, die als Wasserstoffbrückensakzeptoren fungieren können. Zusätzlich kann die Phosphonsäure-Gruppe, wenn sie nur einfach deprotoniert vorliegt, mit ihrer Hydroxylgruppe auch als Wasserstoffbrückendonator agieren. Um eine möglichst hohe Protonenleitfähigkeit zu erreichen, sollten die Phosphonsäure- und Sulfonsäure-Gruppen also möglichst unkoordiniert im MOF vorliegen. In den folgenden Kapiteln werden zwei Möglichkeiten zur Darstellung solcher MOFs vorgestellt.

Zunächst wird in Kapitel 4.1 die Synthese von Linkern beschrieben, die sowohl Phosphonsäure- als auch Sulfonsäure-Gruppen besitzen. Anschließend werden in Kapitel 4.2 postsynthetische Methoden zur Implementierung von Phosphonsäure-Gruppen in Cr-MIL-101-Derivate diskutiert.

4.1 Synthese von Phosphosulfonsäure-Linkern

Neun literaturunbekannte Phosphosulfonsäure-Linker (**M3-8** bis **M3-11**, **M3-24** bis **M3-28**) wurden für den Einsatz in protonenleitfähigen MOFs synthetisiert und vollständig charakterisiert. Zusätzlich wurde für die Darstellung des literaturbekannten Linkers **M3-23** ein neuer, zweistufiger Syntheseweg entwickelt und eine vollständige Charakterisierung vorgenommen. Die Synthese der Linker **M3-8** bis **M3-11** erfolgte ausgehend von 1,2,4,5-Tetrakis(brommethyl)benzol (**M3-1**) mittels zweier aufeinanderfolgender nucleophiler Substitutionen und anschließender Hydrolyse. Für die Darstellung der Linker **M3-23** bis **M3-28** wurden zunächst die jeweiligen Brombenzolsulfonsäuren synthetisiert, um anschließend eine Kreuzkupplung mit Triethylphosphit durchführen zu können. Die entstandenen Phosphonsäureethylester-Gruppen wurden mit konzentrierter Salzsäure hydrolysiert. Zusätzlich konnte der Linker **M3-9** erfolgreich zur Darstellung eines neuen Lanthan-basierten MOFs (im folgenden Manuskript als Koordinationspolymer bezeichnet, da keine Sorptionsdaten vorlagen) eingesetzt werden.

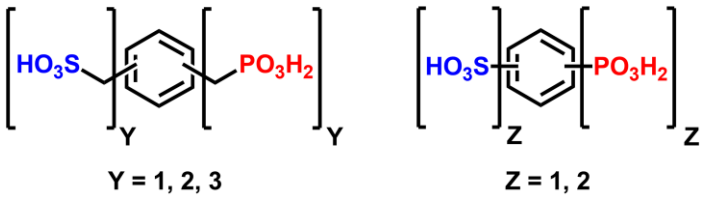

Abb. 26: Vereinfachte Darstellung der Phosphosulfonsäure-Linker **M3-8** bis **M3-11** und **M3-23** bis **M3-28**.

Die Ergebnisse wurden veröffentlicht:

O. Beyer, T. Homburg, M. Albat, N. Stock, U. Lüning, *New J. Chem.* **2017**, *submitted.*

Die Synthese und Charakterisierung der zehn Phosphosulfonsäure-Linker (**M3-8** bis **M3-11**, **M3-23** bis **M3-28**) war Bestandteil dieser Dissertation. Die Synthese des La-MOF $[La_4(H_2L)_3(H_2O)_8]$ wurde von THOMAS HOMBURG im Rahmen seiner Dissertation durchgeführt. Die Kristallstruktur des MOFs wurde von MARTIN ALBAT gelöst.

Anmerkung: Die Formatierung der Supporting Information wurde geringfügig verändert, um sie auf die Formatierung dieser Arbeit anzupassen. Dabei wurden keine Inhalte verändert.

NJC

PAPER

Synthesis of phosphonosulfonic acid building blocks as linkers for coordination polymers

Received 00th January 20xx,
Accepted 00th January 20xx

DOI: 10.1039/x0xx00000x

www.rsc.org/

O. Beyer,[a] T. Homburg,[b] M. Albat,[b] N. Stock[b] and U. Lüning[a]

Ten aromatic building blocks (**8-11**, **23-28**) containing phosphonic and sulfonic acid groups within one molecule were synthesized. Twofold nucleophilic substitution starting from 1,2,4,5-tetrakis(bromomethyl)benzene (**1**) followed by hydrolysis gave building blocks **8-11**. To obtain building blocks **23-28**, the respective bromobenzenesulfonic acids **13**, **16**, **18-20** and **22** had to be synthesized first. Palladium-catalysed cross coupling with triethylphosphite followed by hydrolysis gave the desired building blocks with phosphonic and sulfonic acid groups. Building block **9** was successfully used as a linker for the synthesis of a new La-based CP with the composition $[La_4(H_2L)_3(H_2O)_8]$.

Introduction

Coordination polymers (CP)[1] and metal-organic frameworks (MOF)[2] are intensively studied compounds with possible application in gas storage, gas separation, catalysis, drug delivery and ion conduction.[3,4]

The most investigated frameworks are based on carboxylates as organic building blocks.[5] Considerably less studied are organic phoshonates and sulfonates. This might be because single crystal growth and the prediction of the coordination chemistry of metal phosphonates is more difficult and since they mostly form non-porous dense layered materials. In case of metal sulfonates, the relatively weak coordination of the anions to the metal nodes facilitates the formation of crystalline products, but often these networks are less robust. Nevertheless, there is a broad spectrum of phosphonate and sulfonate frameworks described to date.[6]

Especially in the field of ion conduction, the use of organic building blocks with phosphonic or sulfonic acid groups showed promising results. While metal phosphonates are able to build stable frameworks with high proton conductivity[7,8], metal sulfonates seem to be more promising in sulfonate-carboxylate frameworks.[9] In the latter case, the carboxylates coordinate to metal nodes and the sulfonate remains free. But also phosphonate-carboxylate frameworks are known for very high proton conduction.[4,10]

Examples[11,12,13] of organic building blocks containing a phosphonic and a sulfonic acid group are rare, which limits the investigation of metal phosphonate-sulfonate frameworks.[14,15–18] In case of the known frameworks, very little is known in terms of proton conduction.[19,20] To the best of our knowledge, only four organic building blocks have been successfully used until today. In case of flexible building blocks, only 2-phosphonoethanesulfonic acid[18,21] and 4-phosphonobutanesulfonic acid[17,22] have been investigated. The majority of known metal phosphonate-sulfonate frameworks have been obtained using rigid *m*- or *p*-phosphonobenzenesulfonic acid.[15,16,19,23]

Our research focuses on the synthesis of new rigid and flexible benzene-based building blocks containing at least one sulfonic acid and one phosphonic acid group.

Results and discussion

The synthesis of aromatic building blocks containing both sulfonic and phosphonic acid groups (herein called phosphonosulfonic acids) can be divided into two approaches. Either these groups are connected directly to the aromatic ring or via a flexible spacer unit.

To obtain flexible phosphonosulfonic acids, 1,2,4,5-tetrakis(bromomethyl)benzene (**1**) was chosen as starting material. Nucleophilic substitution of the bromides with triethyl phosphite[7] or sodium sulfite[24] at the benzyl positions has proven to be an efficient tool to introduce $-PO_3H_2$ and $-SO_3H$ groups.

The synthesis of new rigid phosphonosulfonic acids is based on combining different synthetic approaches. Previously sulfonation of benzenephosphonic acid has been reported to give 3-phosphonobenzenesulfonic acid and

[a] *Otto-Diels-Institut für Organische Chemie, Christian-Albrechts-Universität zu Kiel, Otto-Hahn-Platz 4, 24118 Kiel, Germany*
[b] *Institut für Anorganische Chemie, Christian-Albrechts-Universität zu Kiel, Max-Eyth-Str. 2, 24118 Kiel, Germany*

Electronic Supplementary Information (ESI) available: linker synthesis and characterization, $[La_4(H_2L)_3(H_2O)_8]$ synthesis and characterization, PXRD data, and X-ray crystallographic files. CCDC 1547972. For ESI and crystallographic data (CIF) see DOI: 10.1039/x0xx00000x

5-phosphonobenzene-1,3-disulfonic acid (**23**).[13] But sulfonation of aromatic phosphonic acids has two major draw backs: long reaction times up to 35 d and only *meta*-substitution due to the electron withdrawing effect of the phosphonic acid group. Therefore Montoneri *et al.* synthesized 4-phosphonobenzenesulfonic acid using a different approach.[11] 4-Bromobenzenesulfonic acid ethyl ester was synthesized from the respective sulfonic acid chloride and sodium ethanolate. The obtained arylbromide was converted with triethyl phosphite and nickel(II) chloride to the respective arylphosphonic acid diethyl ester. This synthesis is known as Tavs reaction.[25] Hydrolysis of the diester yielded 4-phosphonobenzenesulfonic acid.

Sulfonation of arylbromides and bromination of arylsulfonic acids were chosen to obtain a large variety of different bromobenzenesulfonic acids. Compared to arylphosphonic acids, many different arylbromides are commercially available and the electron donating effect of the bromine allows *ortho*- and *para*-sulfonation in short reaction times. Followed by a modified Tavs reaction using microwave-assisted heating, the respective phosphonobenzenesulfonic acids were obtained.

Synthesis of flexible phosphonosulfonic acids

Although 1,2,4,5-tetrakis(bromomethyl)benzene (**1**) is commercially available, it was synthesized from durene (1,2,4,5-tetramethylbenzene) according to a literature procedure.[26] Nucleophilic substitution of **1** was performed with two equivalents of triethyl phosphite. Two equivalents were chosen to get di-substituted phosphonic acid ethyl esters. The remaining bromomethylene groups would allow nucleophilic substitution with sodium sulfite to introduce sulfonic acid groups.

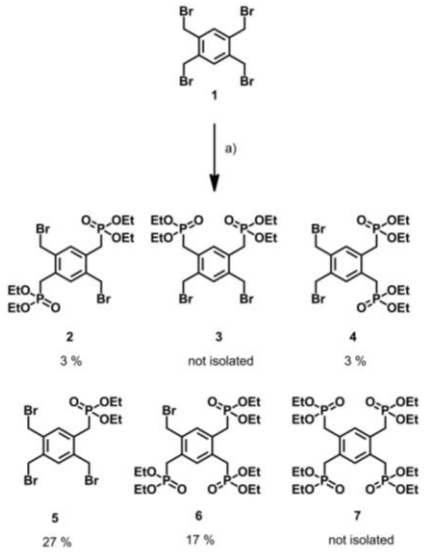

Scheme 1 Nucleophilic substitution of 1,2,4,5-tetrakis(bromomethyl)benzene (**1**) with two equivalents triethyl phosphite. a) $P(OEt)_3$, toluene, 12 h reflux.

Due to very similar reactivities of the bromomethylene groups in starting material and products, a mixture of the starting material and six different phosphonic acid ethyl esters (mono-, di-, tri- and tetra-phosphonic acid diethyl esters) was obtained. Column chromatography of the mixture yielded pure mono-substituted phosphonic acid diethyl ester **5** in the first fraction, a mixture of di-substituted **2**, **3** and **4** in the second fraction and pure tri-substituted phosphonic acid diethyl ester **6** in the third fraction. The tetra-substituted phosphonic acid diethyl ester **7** was not isolated. A mixture of the di-substituted esters **2** and **4** were obtained from the second fraction by crystallization. Column chromatography of this mixture yielded pure **2** and pure **4**. Fortunately **3** did not crystallize because separation of **2** from **3** or **4** via column chromatography is possible but separation of **3** from **4** was not successful even after several attempts. Nevertheless, these purification procedures reduced the yields, especially for the di-substituted phosphonic acid diethyl esters **2** and **4**.

The ^{1}H-NMR and ^{13}C-NMR spectra of **2** and **4** are very similar and differ only by the chemical shift of the signals. NOESY experiments of both isomers were performed for unequivocal assignment. In case of isomer **2** a NOE interaction was observed between the protons of the bromomethylene group and the phosphonic acid diethyl ester methylene group. Such a NOE interaction was not found for isomer **4**. Also, a doublet of a doublet is observed for the ^{13}C-NMR signal of the methylene carbon atom connected to the phosphorus atom for isomer **4**. The coupling constants could be assigned to ^{1}J and ^{4}J coupling with the respective phosphorus atom. For the respective carbon atom of isomer **2**, only a doublet with a ^{1}J coupling is observed. The ^{6}J coupling to the second phosphorus atom seems to be too small.

It is important to notice that tri-substituted phosphonic acid diethyl ester **6** should be used as fast as possible for further reactions. Ethanol impurities originating from column chromatography were difficult to remove and tended to react in a nucleophilic substitution of the bromide after some time. The respective ether was observed via ^{1}H-NMR spectroscopy and EI mass spectrometry.

The desired phosphonobenzenesulfonic acids **8**, **9**, **10** and **11** were obtained by introduction of sulfonic acid groups and hydrolysis of the phosphonic acid diethyl esters. Sulfonic acid groups were introduced by nucleophilic substitution of the bromides in **2**, **4**, **5** and **6** with sodium sulfite. The respective phosphonic acid diethyl esters was dissolved in acetone, added to a saturated sodium sulfite solution in water and heated for 12 h. A saturated solution was used to reduce nucleophilic side reaction with water. After removing acetone, conc. hydrochlorid acid was added to hydrolyze the phosphonic acid diethyl ester and to decompose sodium sulfite. After removing conc. hydrochloric acid, dimethylsulfoxide was added to dissolve the respective phosphonobenzenesulfonic acid. The majority of sodium chloride remained undissolved and was removed by filtration. The acids were precipitated by adding dichloromethane and filtered off. Since it is difficult to know whether the respective acids or sodium salts were obtained, ion exchange was used to remove sodium ions. The four

desired phosphonobenzenesulfonic acids **8**, **9**, **10** and **11** were obtained as colourless solids.

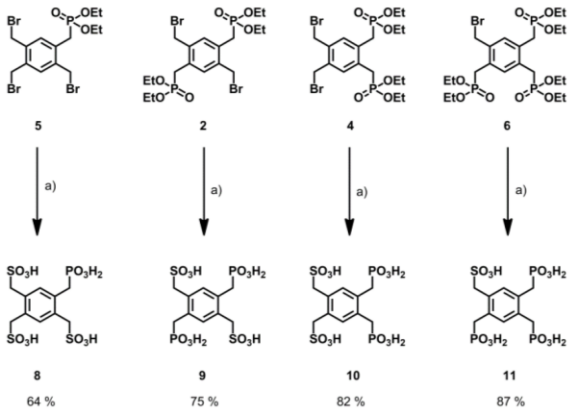

Scheme 2 Nucleophilic substitution of the bromides with sodium sulfite followed by hydrolysis of the phosphonic acid diethyl esters. a) 1. $Na_2SO_{3(aq)}$, acetone, 12 h, 100 °C; 2. $HCl_{(aq)}$, 2 d, 120 °C; 3. ion exchange.

Synthesis of rigid phosphonosulfonic acids

The general procedure for the preparation of different phosphonobenzenesulfonic acids can be divided into two steps: synthesis of bromobenzenesulfonic acids and Tavs reaction to introduce the phosphonic acid groups. Different approaches to obtain tri- and tetra-substituted bromobenzenesulfonic acids will be discussed.

5-Bromobenzene-1,3-disulfonic acid (**13**) was synthesized by bromination of benzenedisulfonic acid disodium salt (**12**). The starting material **12** was dissolved in conc. sulfuric acid and brominated with *N*-bromosuccinimide (NBS). Unbrominated starting material and dibrominated benzenedisulfonic acid were obtained as byproducts depending on the reaction time and the amount of NBS used. Starting material **12** could be separated by transferring product **13** into the organic layer with tetra-*n*-butylammonium cations. Surprisingly, starting material **12** stayed in the aqueous layer. Since this was not the case for the dibrominated byproduct, the reaction conditions were optimized to prevent double-bromination. Stirring starting material **12** with 1.1 equivalents NBS for 12 h at room temperature showed satisfying results. Cation-exchange after workup yielded the desired 5-bromobenzene-1,3-disulfonic acid (**13**).

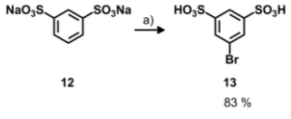

Scheme 3 Bromination of benzenedisulfonic acid disodium salt (**12**). a) 1. NBS, conc. sulfuric acid, 12 h, room temp.; 2. ion exchange.

In a similar approach, benzenesulfonic acid was reacted with NBS to obtain 3,5-dibromobenzenesulfonic acid (**16**). But only a mixture of different dibrominated benzenesulfonic acids was obtained due to the electron-donating effect of the first substituted bromine. Since separation was too difficult, another approach using *ipso*-sulfonation of a trimethylsilylbenzene was tried.[27] 3,5-Dibromo-1-(trimethylsilyl)benzene (**14**) was treated with trimethylsilyl chlorosulfonate to give 3,5-dibromobenzenesulfonic acid (**16**). The +I effect of the trimethylsilyl group surpasses the +M effect of the bromine atoms and enables an *ipso*-substitution. The addition of aqueous sodium hydroxide is necessary to hydrolyze the sulfonic acid trimethylsilyl ester intermediate **15**.

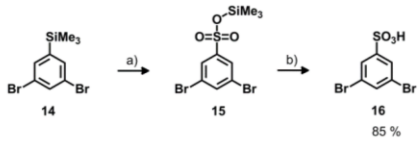

Scheme 4 *ipso*-Sulfonation of **14**. a) $ClSO_3SiMe_3$, 1,2-dichloroethane, 2 d, 90 °C; b) 1. $NaOH_{(aq)}$; 2. ion exchange.

Another tri-substituted bromobenzenesulfonic acid was obtained by using a modification of a published procedure.[28] 1,4-Dibromobenzene (**17**) was sulfonated with fuming sulfuric acid (20-30 % SO_3) to give 2,5-dibromobenzenesulfonic acid (**18**). After stirring for 2 h at 150 °C, the suspension became a clear solution. A mixture of mono- and disulfonated dibromobenzenes was obtained in a ratio of 3:2. Optimization of the reaction conditions in favor of the mono-sulfonated product **18** was not successful. Using a weaker sulfonation agent like conc. sulfuric acid led to unexplainable side reactions. Reducing the reaction time favored mono-sulfonation but at the same time not all starting material **17** was converted. Nevertheless, 2,5-dibromobenzenesulfonic acid (**18**) was obtained after separation from disulfonated byproducts **19** and **20**.

Scheme 5 Mono-sulfonation of 1,4-dibromobenzene (**17**). a) 1. Fuming sulfuric acid (20 - 30 % SO_3), 2 h, 150 °C; 2. ion exchange.

As described in the literature[29], double-sulfonation of 1,4-dibromobenzene (**17**) gives two isomers which are perfect precursor for the synthesis of tetra-substituted phosphonobenzenesulfonic acids.

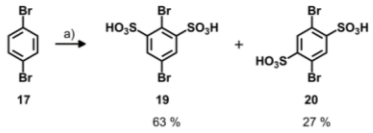

Scheme 6 Double-sulfonation of 1,4-dibromobenzene (**17**) to obtain isomers **19** and **20**. a) 1. Fuming sulfuric acid (20 - 30 % SO_3), 24 h, 200 °C; 2. ion exchange.

By increasing the reaction time to 24 h and raising the temperature to 200 °C, only the disulfonated isomers 2,5-dibromobenzene-1,3-disulfonic acid (**19**) and 2,5-

dibromobenzene-1,4-disulfonic acid (**20**) were obtained. Contrary to the literature, both isomers were characterized.
Double-sulfonation was also possible for 1,3-dibromobenzene (**21**). Treatment with fuming sulfuric acid (65 % SO_3) gave 4,6-dibromobenzene-1,3-disulfonic acid (**22**). No disulfonated isomer was observed as well as any mono- or triple-sulfonation.

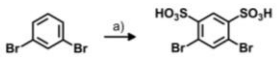

Scheme 7 Double-sulfonation of 1,3-dibromobenzene (**21**). a) 1. Fuming sulfuric acid (65 % SO_3), 5 h, 120 °C; 2. ion exchange.

The second step to obtain tri- and tetra-substituted phosphonobenzenesulfonic acids involves the introduction of phosphonic acid groups. Conversion of the described bromobenzenesulfonic acids in a modified Tavs reaction[25] gave the respective phosphonic acid diethyl esters. Most common reaction conditions for arylbromides and aryliodides in a Tavs reactions are: high temperature (up to 200 °C), nickel(II) chloride as catalyst and triethyl phosphite as reagent and solvent. But also changing the catalyst to palladium(II) chloride and using microwave-assisted heating showed promising results in literature.[30] Palladium(II) chloride gave better yields for bromoaryls in general and in the presence of a sterically demanding group in *ortho*-position. Microwave-assisted heating was chosen because the necessary high temperatures (≥ 200°C) are easier to accomplish and the reaction time is much shorter compared to ordinary heating.
These conditions were adapted for all Tavs reactions performed. Nevertheless, some optimizations had to be carried out to get satisfying results. Since acidity of the sulfonic acid might be problematic for the reaction and the workup, the respective tetra-*n*-butylammonium sulfonates were used. In contrast to sodium sulfonates, the organic sulfonates possess a better solubility and have a lower melting point. Both aspects ensure that the sulfonate mixes and reacts with triethyl phosphite. The synthesis of sulfonic acid esters, as described by Montoneri *et al.*[11], becomes irrelevant. The tetra-*n*-butylammonium sulfonates are easy and fast to obtain by treating the respective sulfonic acid with tetra-n-butylammonium hydroxide.
This procedure was successfully used for the conversion of tri-substituted bromobenzenesulfonic acids **13** and **16**. Subsequent hydrolysis of the respective phosphonic acid diethyl esters with conc. hydrochloric acid gave 5-phosphonobenzene-1,3-disulfonic acid (**23**) and 3,5-diphosphonobenzenesulfonic acid (**24**).

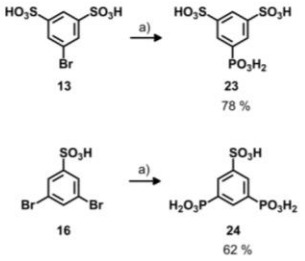

Scheme 8 Tavs reaction and hydrolysis to obtain **23** and **24**. a) 1.NBu_4OH; 2. $P(OEt)_3$, $PdCl_2$, MW; 3. $HCl_{(aq)}$; 4. ion exchange.

An unexpected side reaction reduced the yields of the three phosphonobenzenesulfonic acids **25**, **26** and **27** significantly. An ethylphosphinic acid ethylester group was partly introduced instead of the desired phosphonic acid diethyl ester group.

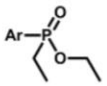

Scheme 9 The observed ethylphosphinic acid ethylester group.

^{1}H-NMR spectra showed characteristic signals for an ethyl group connected directly to a phosphorus atom and a second set of aromatic signals. For all three cases, integration of the signals showed that the byproduct possesses one ethylphosphinic acid ethylester group and one phosphonic acid diethyl ester group. It remains unclear why and how this side reaction takes place. But it was observed only when a sulfonate group was in *ortho* position to a bromine atom.
After ester hydrolysis, the phosphinic acid byproducts could be separated by recrystallization. Pure 2,5-diphosphonobenzenesulfonic acid (**25**), 2,5-diphosphonobenzene-1,4-disulfonic acid (**26**) and 4,6-diphosphonobenzene-1,3-disulfonic acid (**27**) were obtained.

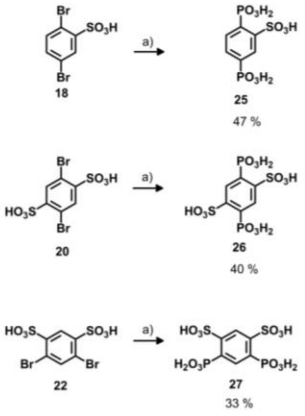

Scheme 10 Synthesis of phosphonobenzenesulfonic acids **25**, **26** and **27**. a) 1.NBu_4OH; 2. $P(OEt)_3$, $PdCl_2$, MW; 3. $HCl_{(aq)}$; 4. ion exchange.

Different side reactions were observed during the synthesis of 2,5-diphosphonobenzene-1,3-disulfonic acid (**28**). The Tavs reaction at the bromine in 5-position works very well but the conversion of the bromine in 2-positon is very slow. ^{1}H-NMR spectra suggested that either the bromine atom did not react at all or it was substituted by a hydrogen atom. The desired product **28** was obtained in a mixture which mainly contains byproducts **29** and **23**. 2,5-Diphosphonobenzene-1,3-disulfonic acid (**28**) could be obtained by recrystallization in low yield.

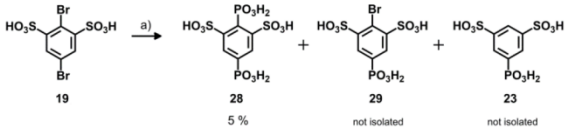

Scheme 11 Synthesis of 2,5-diphosphonobenzene-1,3-disulfonic acid (**28**) with non-isolated byproducts **29** and **23**. a) 1.NBu_4OH; 2. $P(OEt)_3$, $PdCl_2$, MW; 3. $HCl_{(aq)}$; 4. ion exchange.

Synthesis of a La-based coordination polymer

High-throughput experiments were performed using $La(NO_3)_3{\cdot}6H_2O$ and flexible linker **9**.[31] A new La-based CP with the composition $[La_4(H_2L)_3(H_2O)_8]$ was obtained. The crystal structure of this compound was determined from single-crystal X-ray diffraction data and phase purity was confirmed by powder X-ray diffraction (see Supporting Information Fig. S1). The compound $[La_4(H_2L)_3(H_2O)_8]$ crystallizes in the monoclinic space group *C*2/*m*. The asymmetric unit contains two La^{3+} ions, two linker molecules on special positions and four water molecules (see Figure 1).

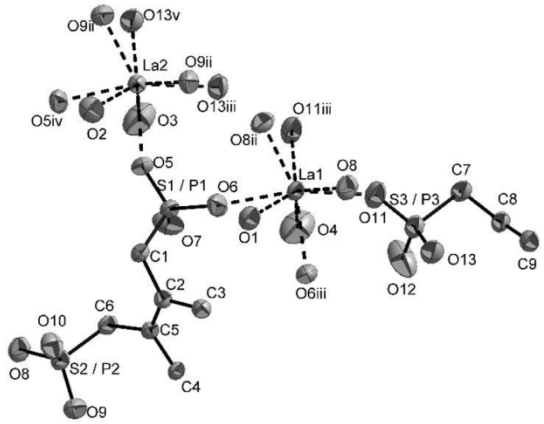

Figure 1 Extended asymmetric unit of compound $[La_4(H_2L)_3(H_2O)_8]$ with 50% thermal ellipsoids. La-O bonds are presented by dashed lines. H atoms are omitted for clarity. [Symmetry code: (i) x + 0.5, y + 0.5, z; (ii) x + 0.5, y - 0.5, z; (iii) x,1 - y, z; (iv) x, - y, z; (v) x, y - 1, z]

Both La^{3+} ions (La1 and La2) are eightfold coordinated by two water molecules and six oxygen atoms from five or four different linker molecules for La1 and La2, respectively. Due to statistical incorporation of phosphonate and sulfonate groups the structure was refined with an occupancy of 0.5 for sulfur and phosphorus atoms at each position. All sulfonate/phosphonate groups coordinate two La^{3+} ions in a [2, 1 1 0] fashion and connect the linker molecule to six La^{3+} ions (Fig. S2). Every La^{3+} ion is bound to two other La^{3+} ions by three sulfonic/phosphonic groups, forming chains along the *b* axis (Figure 2).

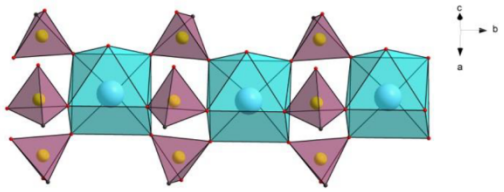

Figure 2 Excerpt of the structure of $[La_4(H_2L)_3(H_2O)_8]$. Chains are formed by interconnections of La^{3+} ions through sulfonate/phosphonate groups. LaO_8 polyhedra in light blue and sulfonate/phosphonate groups as purple tetrahedra.

Each chain is interconnected via the organic moieties to three other chains and a doublelayer in the *a*-*b* plane with diamond shaped pores is built (see Figure 3). Calculation of the Connolly surface results in one-dimensional pores (see SI Fig. S3).

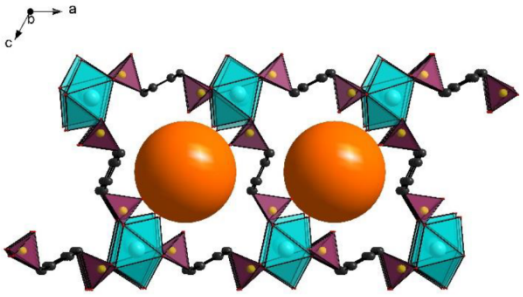

Figure 3 Excerpt of the structure of $[La_4(H_2L)_3(H_2O)_8]$. Doublelayer, in the *a*-*b* plane with diamond shaped pores along the *b* axis. The orange sphere with a diameter of 6.8 Å is used for easier visualisation. LaO_8 polyhedra in light blue and sulfonic/phosphonic groups as purple tetrahedra.

Taking the van der Waals radii into account, the diameter of the pores is 3.8 Å (see Fig. S4). Considering the IR-spectra as well as the synthesis condition the pores are filled with disordered water molecules. Based on the distances between oxygen atoms in the crystal structure, the presence of hydrogen bonds can be postulated. Thus, the doublelayers are connected by hydrogen bonds between the oxygen atoms O1 and O2 which are two coordinating water molecules connected to La1 and La2, respectively, and O10 (Tab. S2). The latter oxygen atom (O10) belongs to a sulfonate/phosphonate group. Due to charge balancing, two protons must be present in the structure. Since these could not be localised, we postulate that $-PO_3H$ groups are formed, which is supported by IR spectroscopy (Fig. S5). The presence of hydrogen

acceptor and donor groups in combination with the coordinating water molecules within the pores makes this CP a potential candidate for proton conduction.

Conclusions

In summary, ten aromatic building blocks (**8-11**, **23-28**) with phosphonic and sulfonic acid groups were synthesized in batch sizes and up to several grams. For the literature-known building block **23,** complete characterization and a new synthetic route was provided. Building blocks **8-11** possess a flexible methylene unit between each functional group and the benzene ring. The more rigid building blocks **23-28** have their functional groups directly connected to the benzene ring. Due to the coordinating ability of phosphonic and sulfonic acid groups, all ten building blocks might be used as linkers for CP or MOF synthesis. First attempts used flexible building block **9** as a linker in high-throughput experiments with $La(NO_3)_3{\cdot}6H_2O$. A new La-based CP with the composition $[La_4(H_2L)_3(H_2O)_8]$ was discovered. Single-crystal X-ray diffraction data showed free hydrogen acceptor and donor groups within the pores. These results indicate the potential of these new organic building blocks for the preparation of proton conducting materials.

Acknowledgement

This project was supported by the Deutsche Forschungsgemeinschaft (STO 643/10-1).

References

1 a) A. Y. Robin and K. M. Fromm, *Coord. Chem. Rev.*, 2006, **250**, 2127–2157; b) S. Kitagawa, R. Kitaura and S.-i. Noro, *Angew. Chem.*, 2004, **116**, 2388–2430, *Angew. Chem. Int. Ed.*, 2004, *43*, 2334–2375.

2 a) D. Farrusseng, ed., *Metal-organic frameworks. Applications from catalysis to gas storage*, Wiley-VCH-Verl., Weinheim, 2011; b) S. Kaskel, ed., *The chemistry of metal-organic frameworks. Synthesis, characterization, and applications*, Wiley-VCH Verlag GmbH & Co. KGaA, Weinheim, 2016; c) H.-C. Zhou, J. R. Long and O. M. Yaghi, *Chem. Rev.*, 2012, **112**, 673–674; d) H.-C. J. Zhou and S. Kitagawa, *Chem. Soc. Rev.*, 2014, **43**, 5415–5418.

3 a) U. Mueller, M. Schubert, F. Teich, H. Puetter, K. Schierle-Arndt and J. Pastré, *J. Mater. Chem.*, 2006, **16**, 626–636; b) P. Horcajada, C. Serre, M. Vallet-Regí, M. Sebban, F. Taulelle and G. Férey, *Angew. Chem.*, 2006, **118**, 6120–6124, *Angew. Chem. Int. Ed.*, 2006, **45**, 5974–5978.; c) J. Lee, O. K. Farha, J. Roberts, K. A. Scheidt, S. T. Nguyen and J. T. Hupp, *Chem. Soc. Rev.*, 2009, **38**, 1450–1459; d) J.-R. Li, J. Sculley and H.-C. Zhou, *Chem. Rev.*, 2012, **112**, 869–932; e) K. Sumida, D. L. Rogow, J. A. Mason, T. M. McDonald, E. D. Bloch, Z. R. Herm, T.-H. Bae and J. R. Long, *Chem. Rev.*, 2012, **112**, 724–781.

4 P. Ramaswamy, N. E. Wong and G. K. H. Shimizu, *Chem. Soc. Rev.*, 2014, **43**, 5913–5932.

5 a) O. M. Yaghi, H. Li, M. Eddaoudi and M. O'Keeffe, *Nature*, 1999, **402**, 276–279; b) Chui, Lo Charmant, Orpen and Williams, *Science*, 1999, **283**, 1148–1150; c) A. Klinkebiel, O. Beyer, B. Malawko and U. Lüning, *Beilstein J. Org. Chem.*, 2016, **12**, 2267–2273; d) M. Latroche, S. Surblé, C. Serre, C. Mellot-Draznieks, P. L. Llewellyn, J.-H. Lee, J.-S. Chang, S. H. Jhung and G. Férey, *Angew. Chem.*, 2006, **118**, 8407–8411, *Angew. Chem. Int. Ed.*, 2006, **45**, 8227–8231.

6 G. K. H. Shimizu, R. Vaidhyanathan and J. M. Taylor, *Chem. Soc. Rev.*, 2009, **38**, 1430–1449.

7 J. M. Taylor, K. W. Dawson and G. K. H. Shimizu, *J. Am. Chem. Soc.*, 2013, **135**, 1193–1196.

8 a) J. M. Taylor, R. K. Mah, I. L. Moudrakovski, C. I. Ratcliffe, R. Vaidhyanathan and G. K. H. Shimizu, *J. Am. Chem. Soc.*, 2010, **132**, 14055–14057; b) S. Pili, S. P. Argent, C. G. Morris, P. Rought, V. Garcia-Sakai, I. P. Silverwood, T. L. Easun, M. Li, M. R. Warren, C. A. Murray, C. C. Tang, S. Yang and M. Schroder, *J. Am. Chem. Soc.*, 2016, **138**, 6352–6355; c) S. Kim, K. W. Dawson, B. S. Gelfand, J. M. Taylor and G. K. H. Shimizu, *J. Am. Chem. Soc.*, 2013, **135**, 963–966; d) M. Feyand, C. F. Seidler, C. Deiter, A. Rothkirch, A. Lieb, M. Wark and N. Stock, *Dalton Trans.*, 2013, **42**, 8761–8770.

9 a) L.-J. Zhou, W.-H. Deng, Y.-L. Wang, G. Xu, S.-G. Yin and Q.-Y. Liu, *Inorg. Chem.*, 2016, **55**, 6271–6277; b) S.-N. Zhao, X.-Z. Song, M. Zhu, X. Meng, L.-L. Wu, S.-Y. Song, C. Wang and H.-J. Zhang, *Dalton Trans.*, 2015, **44**, 948–954; c) X.-Y. Dong, R. Wang, J.-B. Li, S.-Q. Zang, H.-W. Hou and T. C. W. Mak, *Chem. Commun.*, 2013, **49**, 10590–10592; d) W. J. Phang, H. Jo, W. R. Lee, J. H. Song, K. Yoo, B. Kim and C. S. Hong, *Angew. Chem.*, 2015, **127**, 5231–5235, *Angew. Chem. Int. Ed.*, 2015, **54**, 5142–5146; e) T. Kundu, S. C. Sahoo and R. Banerjee, *Chem. Commun.*, 2012, **48**, 4998–5000.

10 a) X. Meng, H.-N. Wang, S.-Y. Song and H.-J. Zhang, *Chem. Soc. Rev.*, 2017, **46**, 464–480; b) M. Bazaga-Garcia, R. M. P. Colodrero, M. Papadaki, P. Garczarek, J. Zon, P. Olivera-Pastor, E. R. Losilla, L. Leon-Reina, M. A. G. Aranda, D. Choquesillo-Lazarte, K. D. Demadis and A. Cabeza, *J. Am. Chem. Soc.*, 2014, **136**, 5731–5739; c) P. Ramaswamy, N. E. Wong, B. S. Gelfand and G. K. H. Shimizu, *J. Am. Chem. Soc.*, 2015, **137**, 7640–7643.

11 E. Montoneri, G. Viscardi, S. Bottigliengo, M. R. Chierotti, R. Buscaino and P. Quagliotto, *Chem. Mater.*, 2007, **19**, 2671–2678.

12 a) E. Montoneri and G. Ricca, *Phosphorus, Sulfur Silicon Relat. Elem.*, 1991, **55**, 111–115; b) E. Montoneri, P. Savarino, G. Viscardi and M. C. Gallazzi, *Phosphorus, Sulfur Silicon Relat. Elem.*, 1994, **86**, 145–155.

13 E. Montoneri, *Phosphorus, Sulfur Silicon Relat. Elem.*, 1991, **55**, 201–204.

14 a) F. Adani, M. Casciola, D. J. Jones, L. Massinelli, E. Montoneri, J. Rozière and R. Vivani, *J. Mater. Chem.*, 1998, **8**, 961–964; b) A. F. Benedetto, P. J. Squattrito, F. Adani and E. Montoneri, *Inorg. Chim. Acta*, 1997, **260**, 207–216.

15 P. Maniam, C. Näther and N. Stock, *Eur. J. Inorg. Chem.*, 2010, 3866–3874.

16 Z.-Y. Du, A. V. Prosvirin and J.-G. Mao, *Inorg. Chem.*, 2007, **46**, 9884–9894.

17 A. Sonnauer, M. Feyand and N. Stock, *Cryst. Growth Des.*, 2009, **9**, 586–592.

18 A. Sonnauer, C. Nather, H. A. Hoppe, J. Senker and N. Stock, *Inorg. Chem.*, 2007, **46**, 9968–9974.

19 V. Zima, J. Svoboda, K. Melánová, L. Beneš, M. Casciola, M. Sganappa, J. Brus and M. Trchová, *Solid State Ionics*, 2010, **181**, 705–713.

20 J. Pan, S. Wang, M. Xiao, M. Hickner and Y. Meng, *J. Membr. Sci.*, 2013, **443**, 19–27.

21 a) A. Sonnauer and N. Stock, *Eur. J. Inorg. Chem.*, 2008, 5038–5045; b) A. Sonnauer and N. Stock, *J. Solid State Chem.*, 2008, **181**, 3065–3070; c) A. Sonnauer and N. Stock, *J. Solid State Chem.*, 2008, **181**, 473–479; d) S.

Bauer, T. Bein and N. Stock, *Inorg. Chem.*, 2005, **44**, 5882–5889.
22 M. Feyand, C. Nather, A. Rothkirch and N. Stock, *Inorg. Chem.*, 2010, **49**, 11158–11163.
23 a) Z.-Y. Du, H.-B. Xu, X.-L. Li and J.-G. Mao, *Eur. J. Inorg. Chem.*, 2007, 4520–4529; b) Z.-Y. Du, H.-B. Xu and J.-G. Mao, *Inorg. Chem.*, 2006, **45**, 6424–6430; c) M. Curini, F. Montanari, O. Rosati, E. Lioy and R. Margarita, *Tetrahedron Lett.*, 2003, **44**, 3923–3925; d) P. Maniam and N. Stock, *Z. anorg. allg. Chem.*, 2011, **637**, 1145–1151; e) Z.-Y. Du, J.-J. Huang, Y.-R. Xie and H.-R. Wen, *J. Mol. Struct.*, 2009, **919**, 112–116.
24 D. J. Hoffart, S. A. Dalrymple and G. K. H. Shimizu, *Inorg. Chem.*, 2005, **44**, 8868–8875.
25 P. Tavs, *Chem. Ber.*, 1970, **103**, 2428–2436.
26 H. Kawai, T. Umehara, K. Fujiwara, T. Tsuji and T. Suzuki, *Angew. Chem.*, 2006, **118**, 4387–4392, *Angew. Chem. Int. Ed.*, 2006, **45**, 4281–4286.
27 B. Bennetau, F. Rajarison, J. Dunoguès and P. Babin, *Tetrahedron*, 1993, **49**, 10843–10854.
28 M. F. Teasley, *US Pat.*, 20120004387A1, 2012.
29 M. H. Litt and J. Kang, *US Pat.*, 20090259013A1, 2009.
30 D. Villemin, A. Elbilali, F. SimÉon, P.-A. Jaffrès, G. Maheut, M. Mosaddak and A. Hakiki, *J. Chem. Res. (S)*, 2003, 436–437.
31 N. Stock, *Microporous and Mesoporous Materials*, 2010, **129**, 287–295.

Supplementary information

Synthesis of phosphonosulfonic acid building block as linkers for coordination polymers

O. Beyer,[a] T. Homburg,[b] M. Albat,[b] N. Stock,[b] and U. Lüning*[a]

[a]Otto-Diels-Institut für Organische Chemie, Christian-Albrechts-Universität zu Kiel, Otto-Hahn-Platz 4, 24118 Kiel, Germany

[b]Institut für Anorganische Chemie, Christian-Albrechts-Universität zu Kiel, Max-Eyth-Str. 2, 24118 Kiel, Germany

*Correspondence to:

luening@oc.uni-kiel.de

Table of content

1. Linker Synthesis

General remarks: All commercially available reagents were used without further purification: benzene-1,3-disulfonic acid disodium salt (94 %, Alfa Aesar), *N*-bromosuccinimide (99 %, Alfa Aesar), 1,3-dibromobenzene (97 %, chemPUR), 1,4-dibromobenzene (98 %, Alfa Aesar), 3,5-dibromo-1-(trimethylsilyl)benzene (97 %, TCI), 1,2-dichloroethane (anhydrous 99.8 %, VWR), calcium hydroxide (95 %, Alfa Aesar), Dowex 50WX8 hydrogen form (200-400 mesh, Sigma Aldrich), fuming sulfuric acid 20 - 30 % SO_3 (abcr), fuming sulfuric acid 65 % SO_3 (VWR), palladium(II) chloride (99.9 %, Alfa Aesar), sodium iodide (99+%, Alfa Aesar), sodium sulfite (98 %, Sigma Aldrich), tetra-*n*-butylammonium bromide (99 %, Sigma Aldrich), tetra-*n*-butylammonium hydroxide 40 % in water (Sigma Aldrich), tetra-*n*-butylammonium iodide (98 %, Alfa Aesar), triethyl phosphite (98 %, Alfa Aesar), trimethylsilyl chlorosulfonate (99 %, Sigma Aldrich). 1,2,4,5-Tetrakis(bromomethyl)benzene (**1**) was prepared according to a literature procedure.[1] Solvents were distilled before use. Column chromatography was carried out with silica gel (Macherey-Nagel, particle size 0.04–0.063 mm). Melting points were measured with a Gallenkamp MPD350.BM2.5 instrument. NMR spectra were recorded with a Bruker DRX 500 instrument and assignments were supported by COSY, HSQC and HMBC. ^{1}H-NMR signals of acidic protons were listed with the expected number of protons, even if the integral was much larger due to moisture. Even when spectra were obtained as broad-band decoupled ^{13}C-NMR, the type of ^{13}C signal is always listed as singlet, doublet, etc. Additionally, the multiplicities for ^{31}P-coupled ^{1}H-decoupled ^{13}C signals are given in square brackets and the coupling constants were assigned if possible. All chemical shifts are referenced to the residual proton or carbon of the solvent. EI mass spectra and HRMS were recorded with a JEOL AccuTOF GCV 4G. ESI mass spectra were recorded with an Applied Biosystems Mariner 5280. IR spectra were recorded with a Perkin-Elmer Spectrum 100 spectrometer equipped with a Golden Gate Diamond ATR unit A-531-G. All IR spectra containing sulfonic acids were dominated by three typical broad bands besides the fingerpint section. Elemental analyses (EA) were carried out with a Euro EA 3000 Elemental Analyzer from Euro Vector. For Microwave synthesis, a CEM Discover SP was used.

Procedure for the syntheses of phosphonic acid diethyl esters 2, 4, 5 and 6

To a solution of 1,2,4,5-tetrakis(bromomethyl)benzene (**1**, 15.0 g. 33.33 mmol) in toluene (400 mL) was added triethyl phosphite (11.4 mL, 66.66 mmol) and the mixture was heated to reflux for 12 h. The solvent was evaporated in vacuo. To obtain the desired products, the residue was purified by column chromatography using a gradient of three different solvents. Starting with cyclohexane/ethyl acetate (2:1) as eluant, the unreacted starting material **1** was

separated. By slowly switching to cyclohexane/ethyl acetate (1:2), the mono-substituted product **5** was eluated. The gradient was changed to pure ethyl acetate and ethanol was gradually added to eluate the di-substituted products **2**, **3** and **4** with ethyl acetate/ethanol (95:5). Tri-substituted product **6** was obtained with ethyl acetate/ethanol (65:35) as eluant. Solvents were removed in vacuo and the residue of the di-substituted products **2**, **3** and **4** were dissolved with *tert*-butyl methyl ether (10 mL) and kept at 5°C for 7 d. Colourless crystals, a mixture of **2** and **4**, were obtained by filtration. The mixture was purified by column chromatography (ethyl acetate/ethanol 98:2). **2, 4** and **5** were obtained as colourless solids and **6** as a colourless oil.

[2,4,5-Tris(bromomethyl)phenyl]methylphosphonic acid diethyl ester (5)

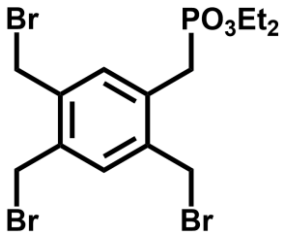

Yield: 4.61 g (9.09 mmol, 27 %)

M. p.: 76 °C

^{1}H-NMR (500 MHz, 300 K, $CDCl_3$): δ = 7.35 (s, 1H, Ar-3-*H*), 7.30 (d, $^{4}J_{H\text{-}P}$ = 2.8 Hz, 1H, Ar-6-*H*), 4.65 (s, 2H, Ar-2-CH_2), 4.61 (s, 2H, Ar-5-CH_2), 4.60 (s, 2H, Ar-4-CH_2), 4.04 (m_c, 4H, P-O-CH_2), 3.31 (d, $^{2}J_{H\text{-}P}$ = 22.0 Hz, 2H, Ar-1-CH_2), 1.27 (t, ^{3}J = 7.1 Hz, 6H, CH_3) ppm.

^{13}C-NMR (125 MHz, 300 K, $CDCl_3$): δ = 138.0 (s[d_P], $^{3}J_{C\text{-}P}$ = 6.3 Hz, Ar-2-*C*), 137.3 (s[d_P], $^{4}J_{C\text{-}P}$ = 3.8 Hz, Ar-5-*C*), 136.0 (s[d_P], $^{5}J_{C\text{-}P}$ = 4.0 Hz, Ar-4-*C*), 134.5 (d[d_P], $^{3}J_{C\text{-}P}$ = 5.6 Hz, Ar-6-*C*), 133.5 (d[d_P], $^{4}J_{C\text{-}P}$ = 3.2 Hz, Ar-3-*C*), 132.7 (s[d_P], $^{2}J_{C\text{-}P}$ = 9.5 Hz, Ar-1-*C*), 62.6 (t[d_P], $^{2}J_{C\text{-}P}$ = 6.8 Hz, P-O-*C*H_2), 31.1 (t, Ar-2-*C*H$_2$), 30.8 (t[d_P], $^{1}J_{C\text{-}P}$ = 137.6 Hz, Ar-1-*C*H$_2$), 29.2 (t, Ar-4,5-*C*H$_2$), 16.6 (q[d_P], $^{3}J_{C\text{-}P}$ = 6.0 Hz, *C*H$_3$) ppm.

^{31}P-NMR (202 MHz, 300 K, $CDCl_3$): 24.4 (s, 1P, *P*O_3Et_2) ppm.

MS (EI): *m/z* = 510, 508, 506, 504 (1.2, 3.6, 3.7, 1.3) $[M]^{+\cdot}$, 429, 427, 425 (27.5, 56.1, 28.6) $[M\text{ -Br}]^{+\cdot}$, 347, 345 (94.1, 77.9) $[M\text{ -H -2Br}]^{+\cdot}$, 267 (80.8) $[M\text{ -3Br}]^{+\cdot}$, 211 (100) $[M\text{ -3Br -}C_4H_8]^{+\cdot}$.

HRMS (EI): *m/z* = $C_{14}H_{20}{}^{79}Br_2{}^{81}BrO_3P$ calcd. 505.8680; found 505.8682 (Δ <0.4 ppm); $C_{14}H_{20}{}^{79}Br{}^{81}Br_2O_3P$ calcd. 507.8659; found 507.8664 (Δ 0.9 ppm).

IR (ATR): $\tilde{\nu}$ = 3044 (aryl-H val.), 2978, 2903 (CH_2-val.), 1508 (arom. C=C), 1439 (CH_2-def.) cm^{-1}.

EA ($C_{14}H_{20}Br_3O_3P$) (506.99): calcd. C 33.17 H 3.98;
($C_{14}H_{20}Br_3O_3P \cdot 0.166\ C_4H_8O_2$) (521.68): calcd. C 33.77 H 4.12;
found C 33.78 H 4.05.

^{1}H-NMR (500 MHz, 300 K, $CDCl_3$) of **5**

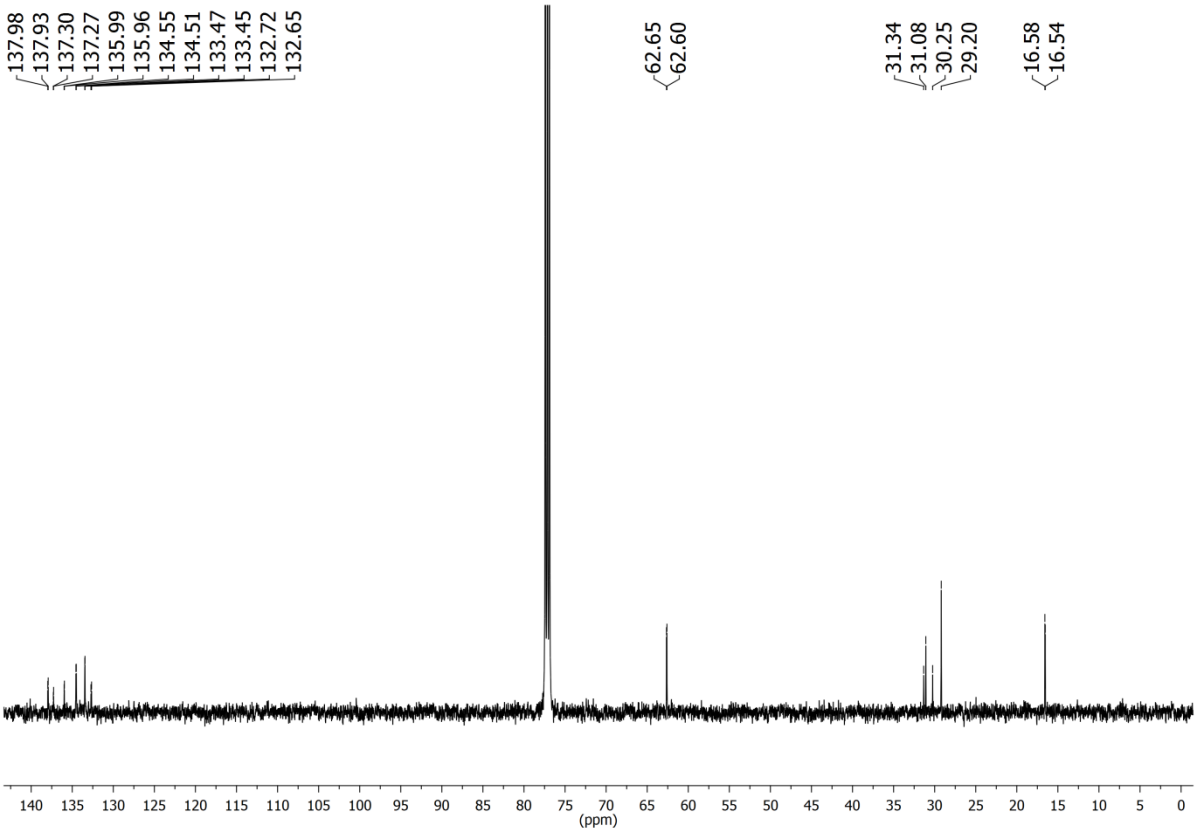

^{13}C-NMR (125 MHz, 300 K, $CDCl_3$) of **5**

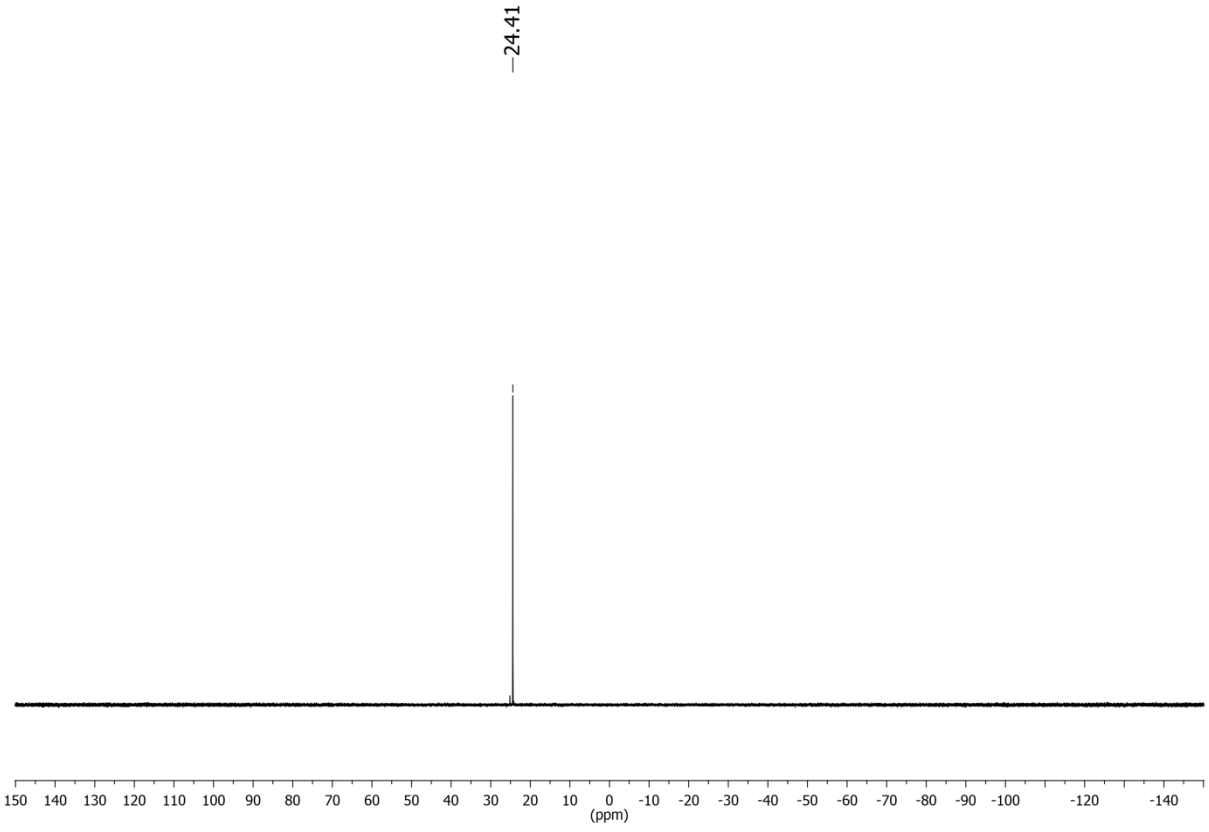

^{31}P-NMR (202 MHz, 300 K, $CDCl_3$) of **5**

[2,5-Bis(bromomethyl)-benzene-1,4-diyl]bis(methylphosphonic acid diethyl ester) (2)

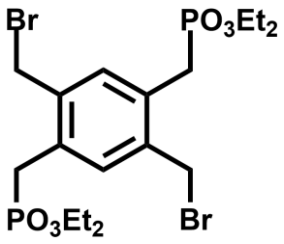

Yield: 602 mg (1.07 mmol, 3 %)

M. p.: 115 °C

^{1}H-NMR (500 MHz, 300 K, CD_2Cl_2): δ = 7.28 (d, $^{4}J_{H\text{-}P}$ = 1.8 Hz, 2H, Ar-3,6-*H*), 4.68 (s, 4H, Ar-2,5-C*H*$_2$), 4.00 (m_c, 8H, P-O-C*H*$_2$), 3.31 (d, $^{2}J_{H\text{-}P}$ = 20.4 Hz, 4H, Ar-1,4-C*H*$_2$), 1.24 (t, ^{3}J = 7.1 Hz, 12H, C*H*$_3$) ppm.

^{13}C-NMR (125 MHz, 300 K, CD_2Cl_2): δ = 138.0 (s, Ar-2,5-*C*), 134.5 (d, Ar-3,6-*C*), 131.3 (s, Ar-1,4-*C*), 62.9 (t[m_P], P-O-*C*H$_2$), 32.1 (t, Ar-2,5-*C*H$_2$), 31.0 (t[d_P], $^{1}J_{C\text{-}P}$ = 137.9 Hz, Ar-1,4-*C*H$_2$), 16.8 (q[m_P], *C*H$_3$) ppm.

^{31}P-NMR (202 MHz, 300 K, CD_2Cl_2): 24.4 (s, 2P, *P*O$_3$Et$_2$) ppm.

MS (EI): *m/z* = 566, 564, 562 (0.9, 1.9, 1.0) $[M]^{+\cdot}$, 485, 483 (21.0, 21.4) $[M\text{ -Br}]^{+\cdot}$, 403 (86.7) $[M\text{ -H -2Br}]^{+\cdot}$, 375 (100) $[M\text{ -2Br -}C_2H_5]^{+\cdot}$.

HRMS (EI): *m/z* = $C_{18}H_{30}{}^{79}Br^{81}BrO_6P_2$ calcd. 563.9864; found 553.9838 (Δ 4.6 ppm).

IR (ATR): $\tilde{\nu}$ = 2980, 2905 (CH_2-val.), 1508 (arom. C=C), 1440 (CH_2-def.) cm^{-1}.

EA ($C_{18}H_{30}Br_2O_6P_2$) (564.18): calcd. C 38.32 H 5.36;
found C 38.71 H 5.52.

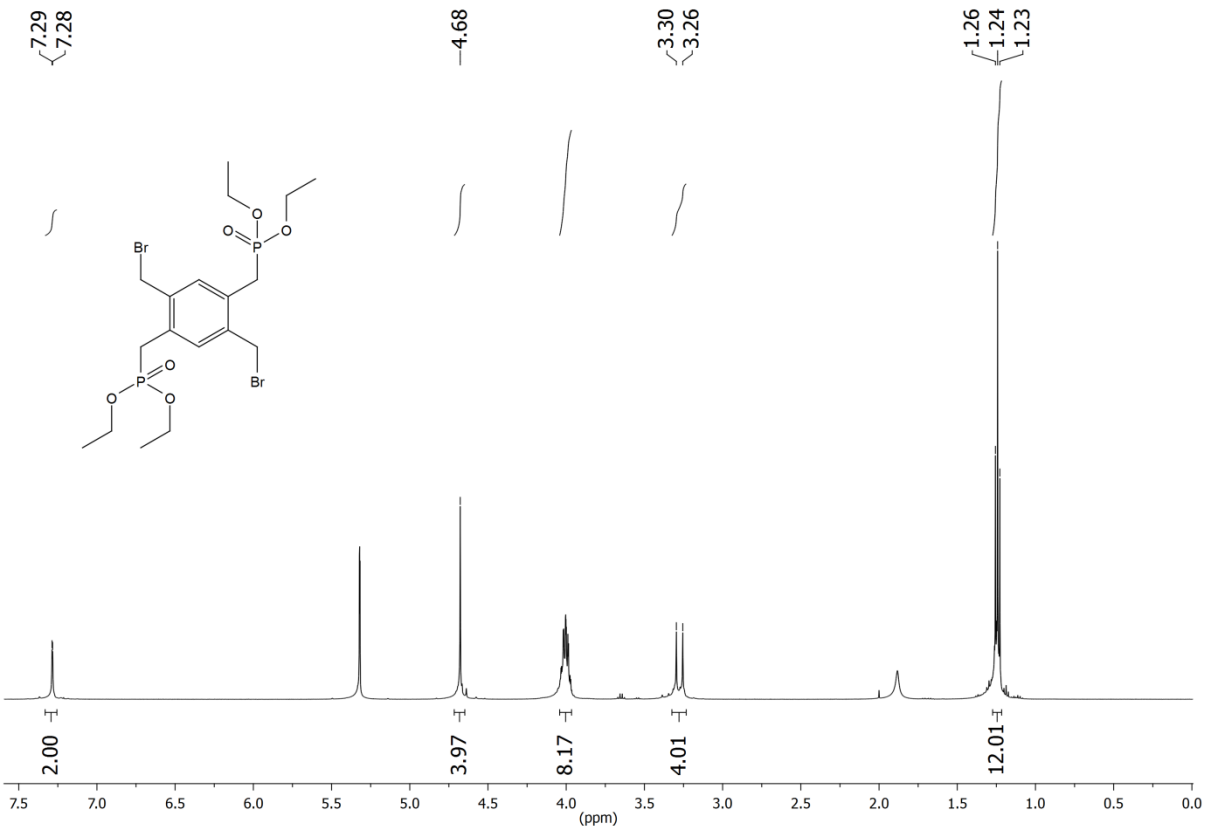

^{1}H-NMR (500 MHz, 300 K, CD_2Cl_2) of **2**

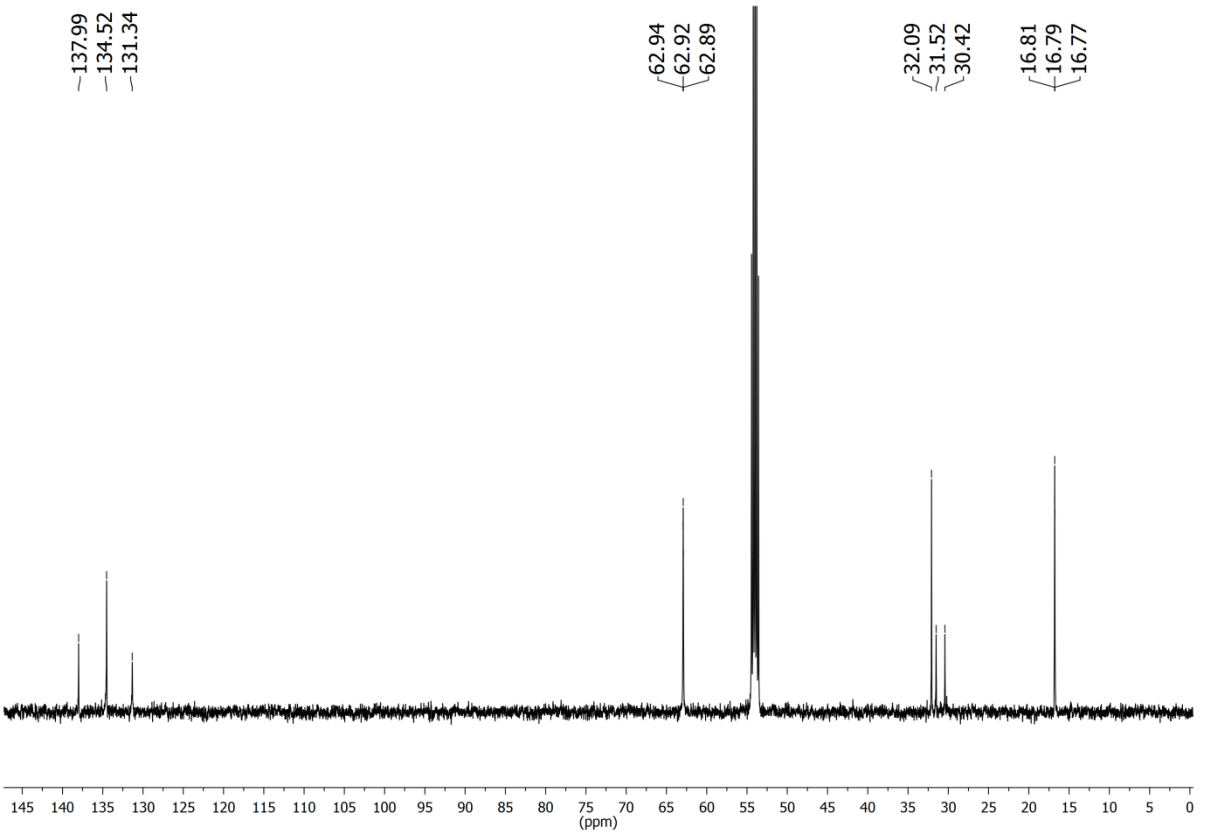

^{13}C-NMR (125 MHz, 300 K, CD_2Cl_2) of **2**

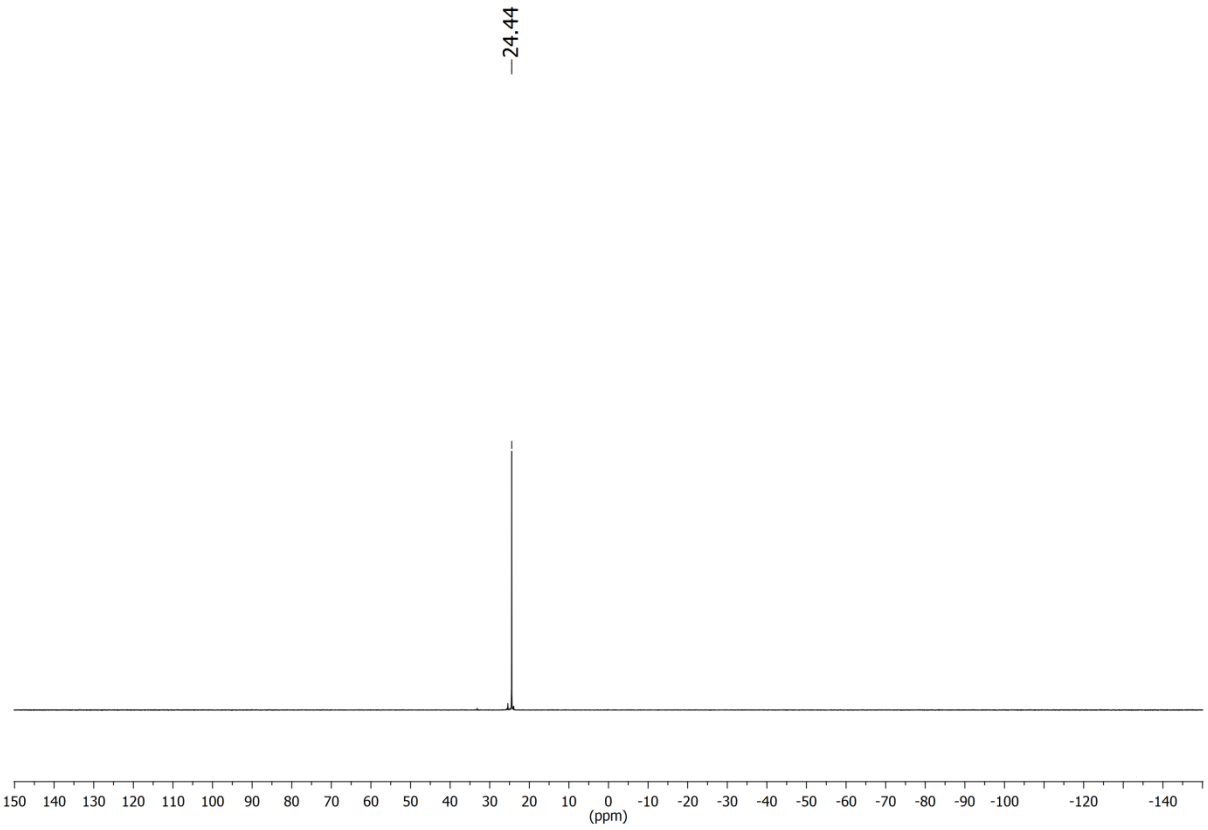

^{31}P-NMR (202 MHz, 300 K, CD_2Cl_2) of **2**

[4,5-Bis(bromomethyl)-benzene-1,2-diyl]bis(methylphosphonic acid diethyl ester) (4)

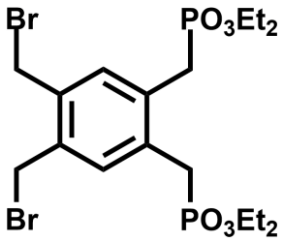

Yield: 584 mg (1.04 mmol, 3 %)

M. p.: 107 °C

^{1}H-NMR (500 MHz, 300 K, CD_2Cl_2): δ = 7.27 (d, $^{4}J_{H\text{-}P}$ = 1.9 Hz, 2H, Ar-3,6-*H*), 4.64 (s, 4H, Ar-4,5-C*H*$_2$), 4.00 (m$_c$, 8H, P-O-C*H*$_2$), 3.37 (d, $^{2}J_{H\text{-}P}$ = 20.4 Hz, 4H, Ar-1,2-C*H*$_2$), 1.24 (t, ^{3}J = 7.1 Hz, 12H, C*H*$_3$) ppm.

^{13}C-NMR (125 MHz, 300 K, CD_2Cl_2): δ = 135.9 (s, Ar-4,5-*C*), 134.7 (d, Ar-3,6-*C*), 133.6 (s[m$_P$], Ar-1,2-*C*), 62.8 (t[m$_P$], P-O-*C*H$_2$), 32.5 (t[d$_P$d$_P$], $^{1}J_{C\text{-}P}$ = 137.1 Hz, $^{4}J_{C\text{-}P}$ = 1.5 Hz, Ar-1,2-*C*H$_2$), 30.2 (t, Ar-4,5-*C*H$_2$), 16.8 (q[m$_P$], *C*H$_3$) ppm.

^{31}P-NMR (202 MHz, 300 K, CD_2Cl_2): 25.4 (s, 2P, PO_3Et_2) ppm.

MS (EI): *m/z* = 566, 564, 562 (3.4, 7.0, 3.6) $[M]^{+\cdot}$, 485, 483 (100, 99.3) $[M\text{ -Br}]^{+\cdot}$.

HRMS (EI): *m/z* = $C_{18}H_{30}{}^{79}Br_2O_6P_2$ calcd. 561.9884; found 561.9882 (Δ 0.5 ppm);
$C_{18}H_{30}{}^{79}Br^{81}BrO_6P_2$ calcd. 563.9864; found 563.9864 (Δ <0.1 ppm);
$C_{18}H_{30}{}^{81}Br_2O_6P_2$ calcd. 565.9843; found 565.9849 (Δ 1.0 ppm).

IR (ATR): $\tilde{\nu}$ = 2979, 2926 (CH_2-val.), 1508 (arom. C=C), 1474, 1441 (CH_2-def.) cm^{-1}.

EA ($C_{18}H_{30}Br_2O_6P_2$) (564.18): calcd. C 38.32 H 5.36;
found C 38.51 H 5.58.

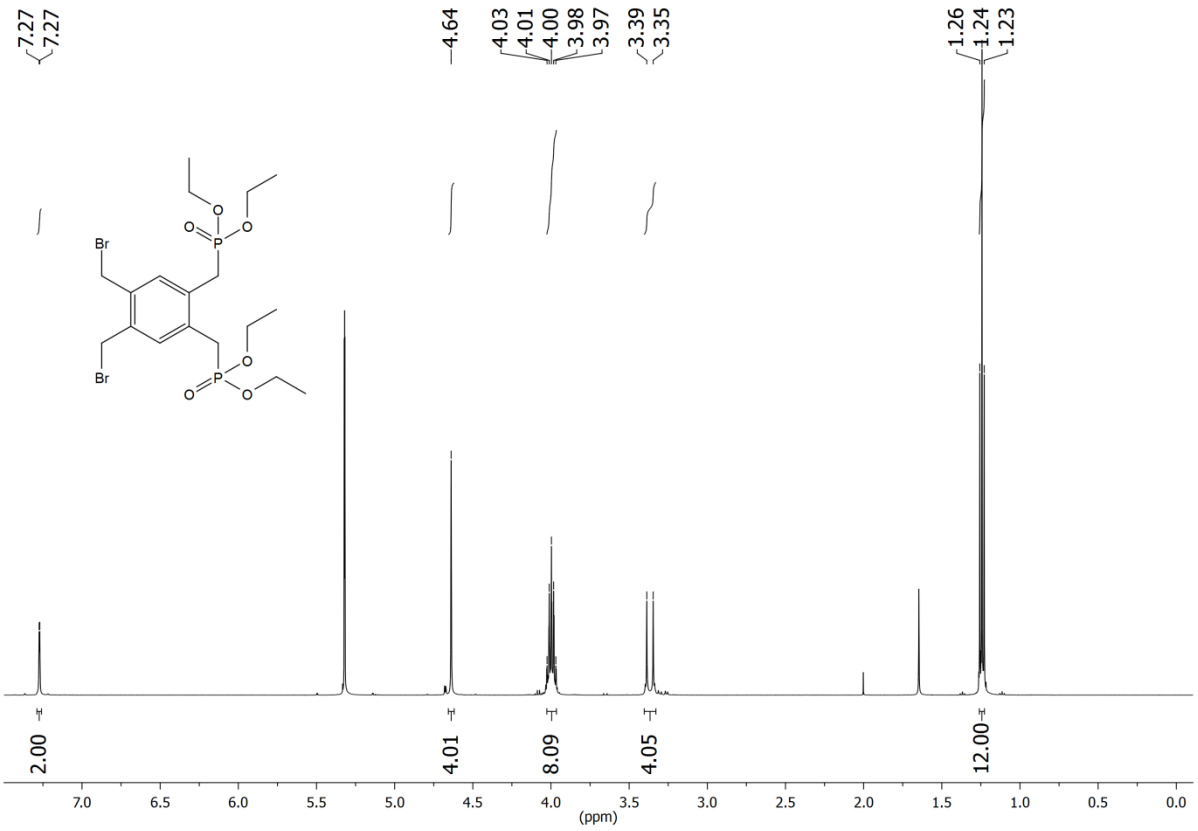

^{1}H-NMR (500 MHz, 300 K, CD_2Cl_2) of **4**

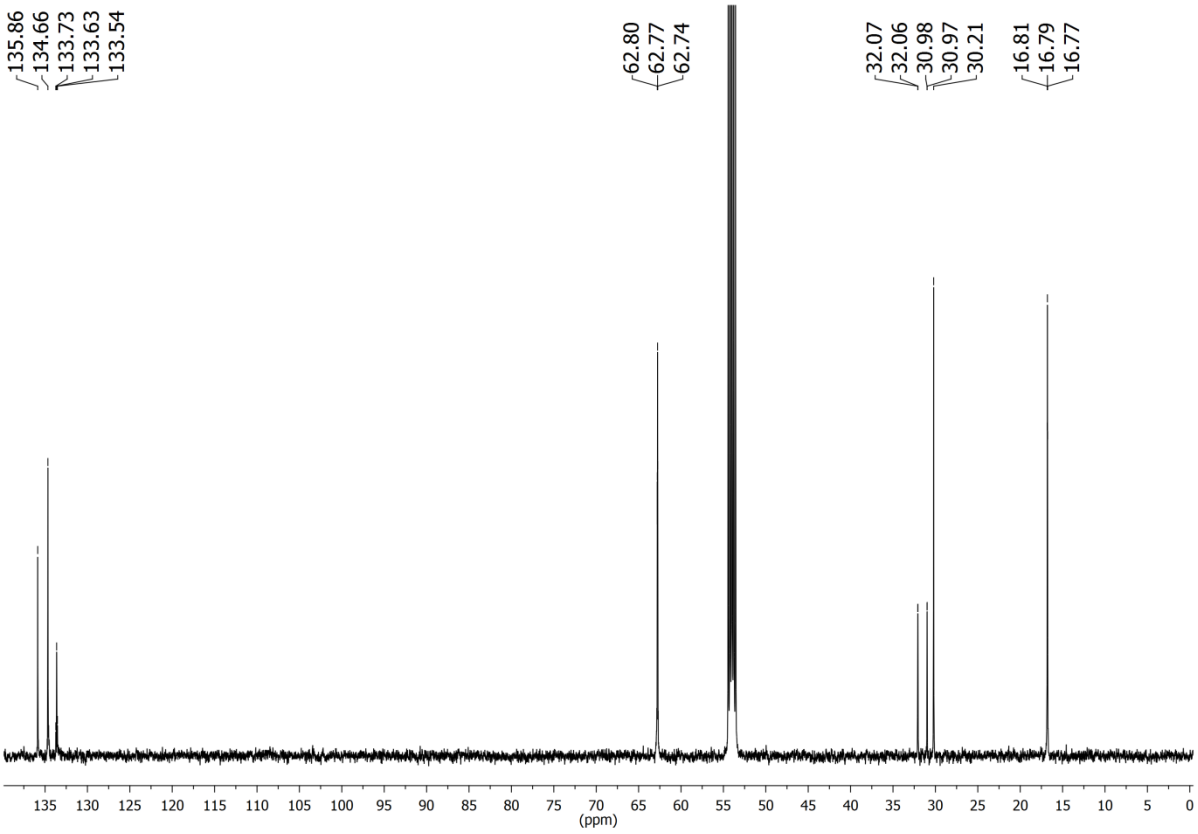

^{13}C-NMR (125 MHz, 300 K, CD_2Cl_2) of **4**

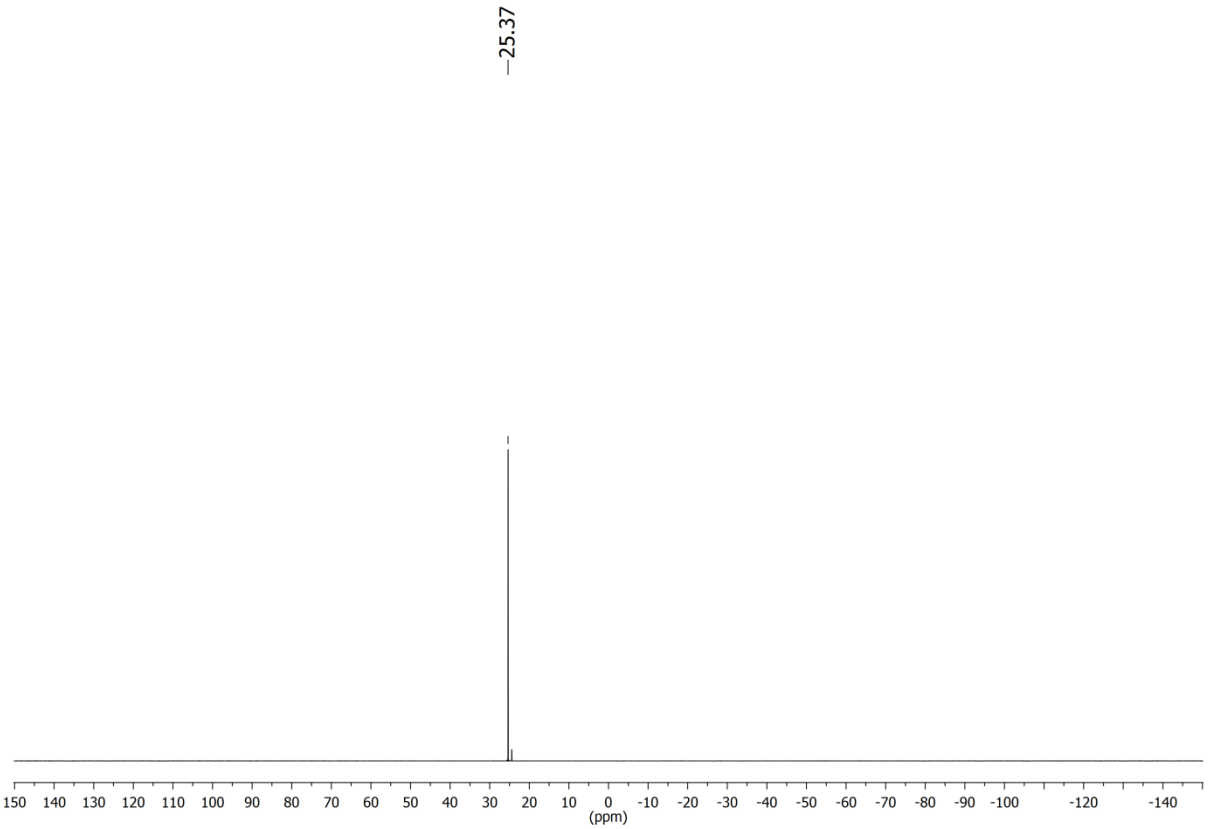

^{31}P-NMR (202 MHz, 300 K, CD_2Cl_2) of **4**

[5-(Bromomethyl)-benzene-1,2,4-triyl]tris(methylphosphonic acid diethyl ester) (6)

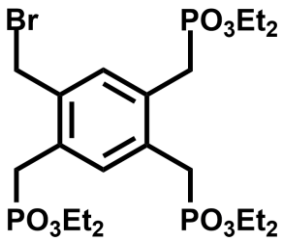

Yield: 3.52 g (5.66 mmol, 17 %)

M. p.: Oil

^{1}H-NMR (500 MHz, 300 K, CD_2Cl_2): δ = 7.25 (m_c, 1H, Ar-6-*H*), 7.18 (m_c, 1H, Ar-3-*H*), 4.67 (s, 2H, Ar-5-C*H*$_2$), 4.00 (m_c, 12H, P-O-C*H*$_2$), 3.36 (d, $^{2}J_{H\text{-}P}$ = 20.7 Hz, 2H, Ar-2-C*H*$_2$), 3.34 (d, $^{2}J_{H\text{-}P}$ = 20.2 Hz, 2H, Ar-1-C*H*$_2$), 3.27 (d, $^{2}J_{H\text{-}P}$ = 21.7 Hz, 2H, Ar-4-C*H*$_2$), 1.26-1.21 (m, 18H, C*H*$_3$) ppm.

^{13}C-NMR (125 MHz, 300 K, CD_2Cl_2): δ = 136.1 (s[m_P], Ar-5-*C*), 135.2 (d[m_P], Ar-3-*C*), 134.3 (d[m_P], Ar-6-*C*), 133.0 (s[m_P], Ar-2-*C*), 131.5 (s[m_P], Ar-1-*C*), 130.7 (s[m_P], Ar-4-*C*), 63.0-62.7 (t[m_P], P-O-*C*H$_2$), 32.5 (t, Ar-5-*C*H$_2$), 31.5 (t[d_P], $^{1}J_{C\text{-}P}$ = 135.9 Hz, Ar-1-*C*H$_2$), 31.3 (t[d_P], $^{1}J_{C\text{-}P}$ = 136.7 Hz, Ar-2-*C*H$_2$), 30.9 (t[d_P], $^{1}J_{C\text{-}P}$ = 137.3 Hz, Ar-4-*C*H$_2$), 16.8 (q[m_P], *C*H$_3$) ppm.

^{31}P-NMR (202 MHz, 300 K, CD_2Cl_2): 25.9 (dd, ^{5}J = 9.0 Hz, ^{7}J = 2.7 Hz, 1P, Ar-1-CH$_2$-*P*), 25.9 (dd, ^{5}J = 9.0 Hz, ^{6}J = 8.5 Hz, 1P, Ar-2-CH$_2$-*P*), 24.9 (dd, ^{6}J = 8.5 Hz, ^{7}J = 2.7 Hz, 1P, Ar-4-CH$_2$-*P*) ppm.

MS (EI): *m/z* = 622, 620 (0.1, 0.1) $[M]^{+\cdot}$, 586 (5.5) $[M - Br + C_2H_5O]^{+\cdot}$, 557 (100) $[(M - Br + C_2H_5O) - C_2H_5]^{+\cdot}$, 529 (79.3) $[(M - Br + C_2H_5O) - C_4H_9]^{+\cdot}$.

IR (ATR): $\tilde{\nu}$ = 2980, 2930 (CH$_2$-val.), 1507 (arom. C=C), 1478, 1443 (CH$_2$-def.) cm^{-1}.

EA ($C_{22}H_{40}BrO_9P_3$) (621.37): calcd. C 42.52 H 6.49;
($C_{22}H_{40}BrO_9P_3 \cdot 2\ C_2H_6O$) (713.51): calcd. C 43.77 H 7.35;
found C 44.00 H 7.45.

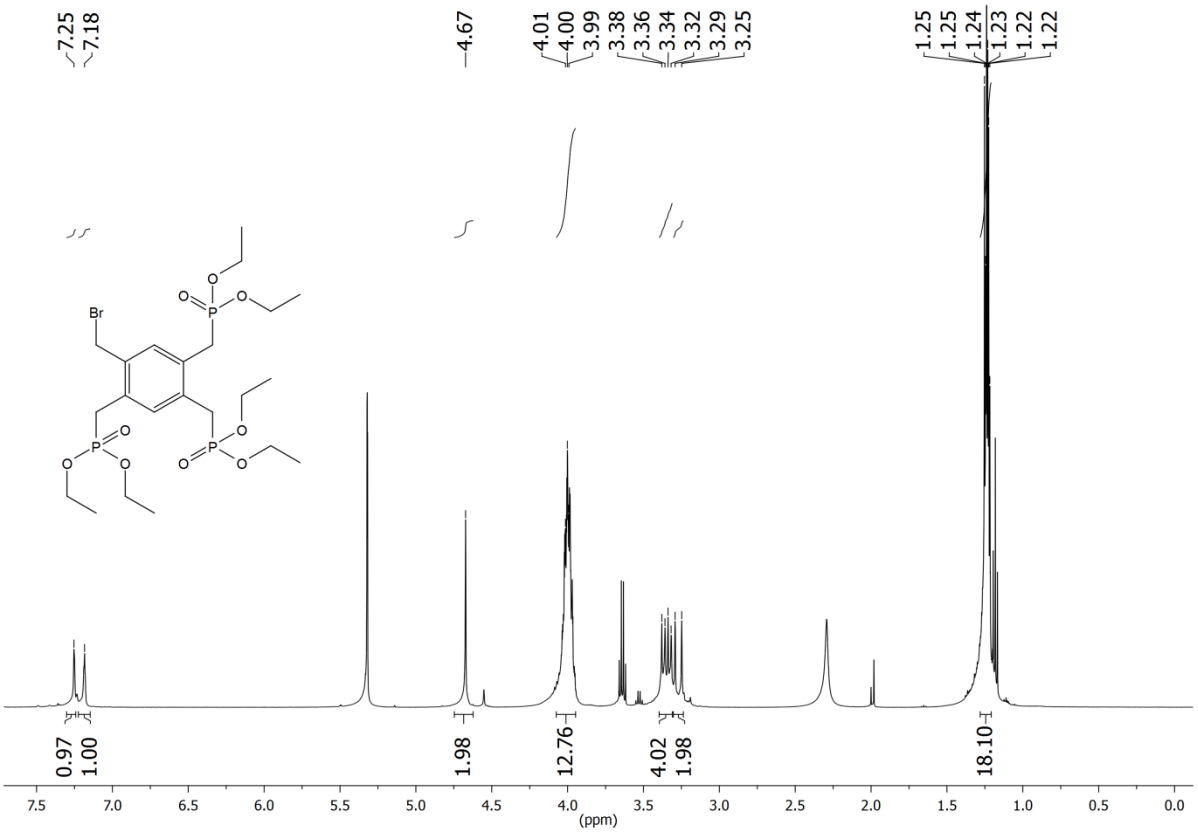

^{1}H-NMR (500 MHz, 300 K, CD_2Cl_2) of **6**

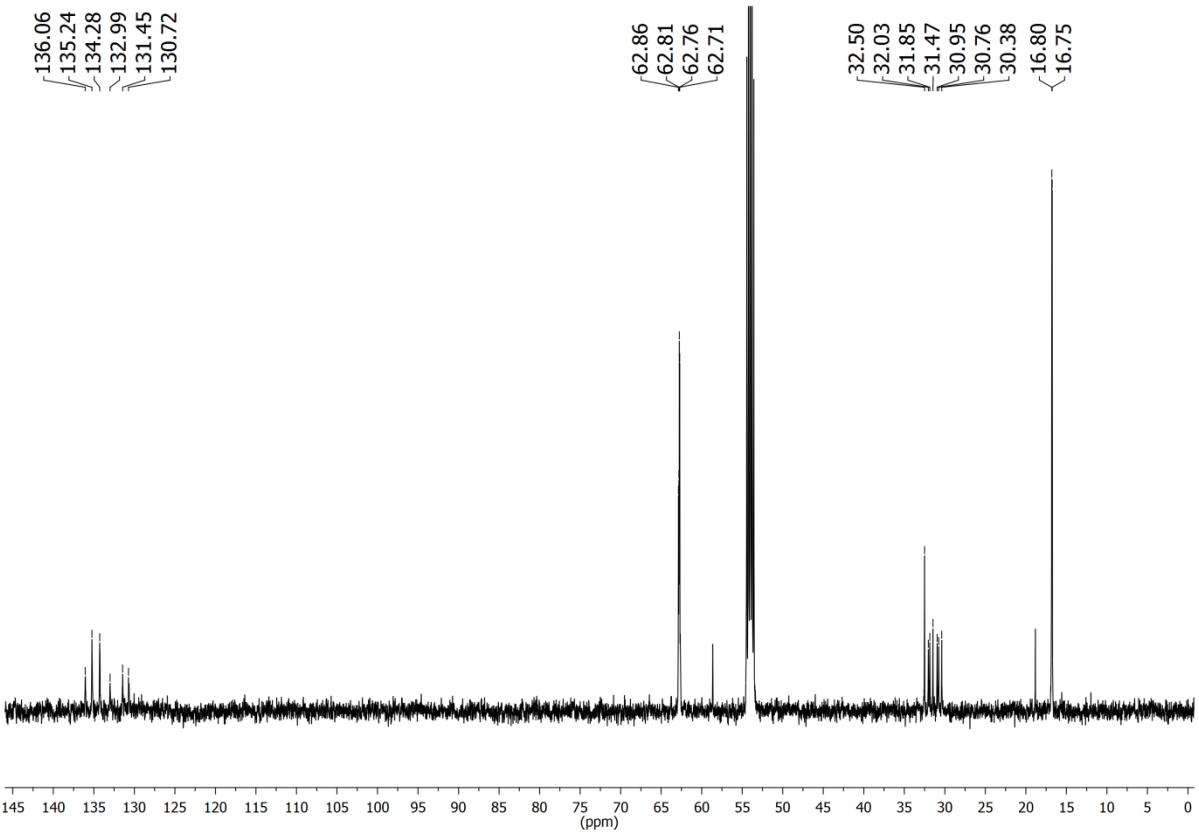

^{13}C-NMR (125 MHz, 300 K, CD_2Cl_2) of **6**

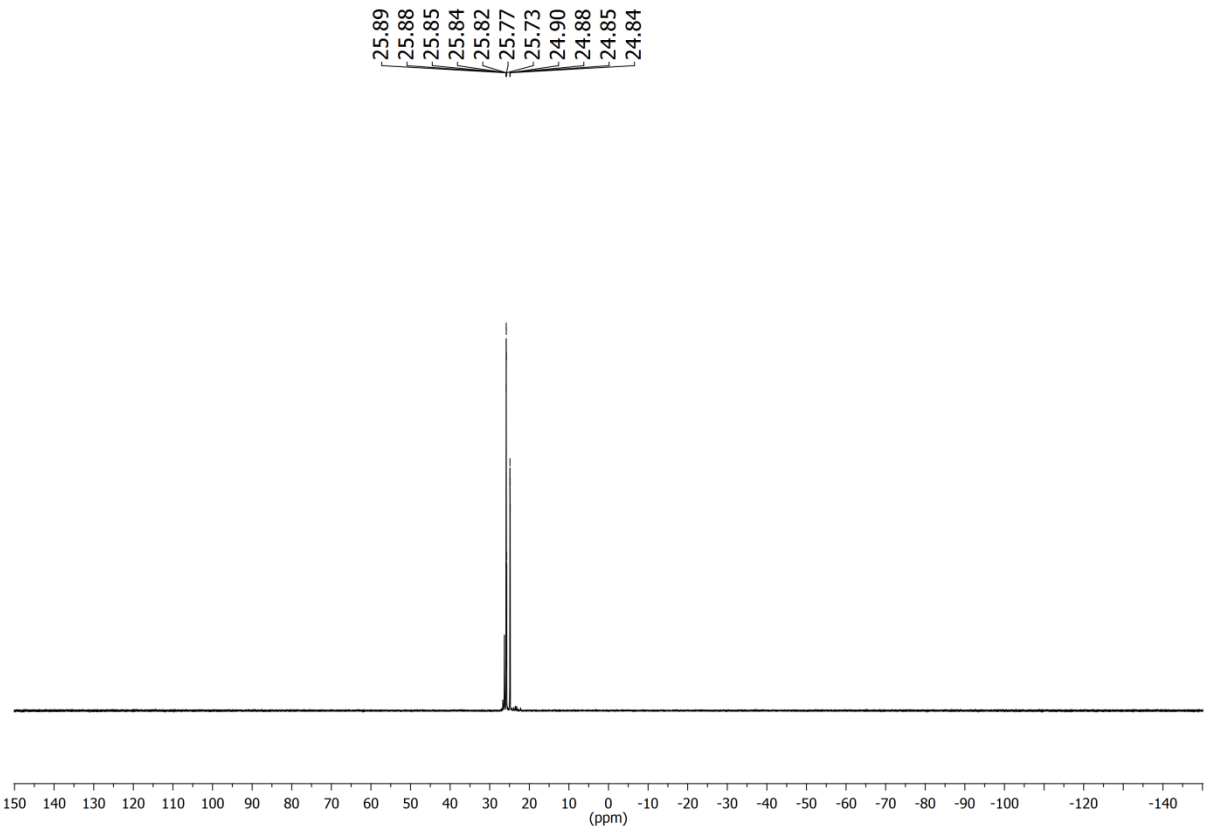

^{31}P-NMR (202 MHz, 300 K, CD_2Cl_2) of **6**

[5-(Phosphonomethyl)benzene-1,2,4-triyl]tris(methylsulfonic acid) (8)

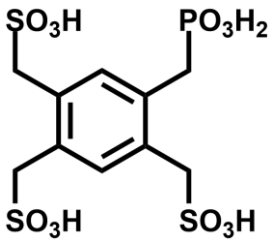

To a saturated aqueous solution of sodium sulfite (100 mL) was added water (25 mL) and [2,4,5-tris(bromomethyl)phenyl]methylphosphonic acid diethyl ester (**5**, 6.30 g, 12.43 mmol) dissolved in acetone (20 mL). The reaction mixture was stirred at 100 °C for 12 h. Acetone was removed in vacuo and conc. hydrochloric acid (100 mL) was added to the aqueous solution and the mixture was stirred at 120 °C for 2 d. The solvent was removed in vacuo and the residue was treated with dimethyl sulfoxide (200 mL) to dissolve the product. Undissolved sodium chloride was separated by filtration. The solution was poured into dichloromethane (2000 mL) and the precipitate was collected by filtration. To exchange the sodium ions, the residue was dissolved in water and rinsed over a column filled with ion-exchange resin (Dowex 50WX8 hydrogen form). The eluate was concentrated and dried for 24 h at 60 °C in a vacuum oven, to yield a colourless solid.

Yield: 3.59 g (7.91 mmol, 64 %)

M. p.: 250 °C (decomposition)

^{1}H-NMR (500 MHz, 300 K, DMSO-d6): δ = 8.80 (br. s, 5H, SO_3H, PO_3H_2), 7.09 (s, 1H, Ar-3-*H*), 7.08 (d, $^{4}J_{H\text{-}P}$ = 2.6 Hz, 1H, Ar-6-*H*), 4.09 (s, 2H, Ar-1-CH_2), 4.05 (s, 2H, Ar-2-CH_2), 4.00 (s, 2H, Ar-4-CH_2), 3.25 (d, $^{2}J_{H\text{-}P}$ = 21.0 Hz, 2H, Ar-5-CH_2) ppm.

^{13}C-NMR (125 MHz, 300 K, DMSO-d6): δ = 135.7 (d[d_P], $^{4}J_{C\text{-}P}$ = 2.0 Hz, Ar-3-*C*), 134.5 (d[d_P], $^{3}J_{C\text{-}P}$ = 4.9 Hz, Ar-6-*C*), 132.3 (s[d_P], $^{5}J_{C\text{-}P}$ = 3.1 Hz, Ar-2-*C*), 131.9 (s[d_P], $^{4}J_{C\text{-}P}$ = 3.8 Hz, Ar-1-*C*), 131.5 (s[d_P], $^{2}J_{C\text{-}P}$ = 9.0 Hz, Ar-5-*C*), 131.4 (s[d_P], $^{3}J_{C\text{-}P}$ = 5.7 Hz, Ar-4-*C*), 54.7 (t, Ar-4-*C*H_2), 54.6 (t, Ar-1-*C*H_2, Ar-2-*C*H_2), 32.3 (t[d_P], $^{1}J_{C\text{-}P}$ = 130.0 Hz, Ar-5-*C*H_2) ppm.

^{31}P-NMR (202 MHz, 300 K, DMSO-d6): 22.6 (s, 1P, *P*O_3H_2) ppm.

MS (ESI_{neg}): *m/z* = 453 $[M-H]^-$, 435 $[M-H_3O]^-$.

IR (ATR): $\tilde{\nu}$ = 2655, 2166 (br. O-H), 1655 (H_3O^+), 1508 (arom. C=C) cm^{-1}.

EA ($C_{10}H_{15}O_{12}PS_3$) (454.39): calcd. C 26.43 H 3.33 S 21.17;
($C_{10}H_{15}O_{12}PS_3 \cdot 4\ H_2O$) (526.45): calcd. C 22.81 H 4.40 S 18.27;
found C 22.61 H 4.55 S 18.40.

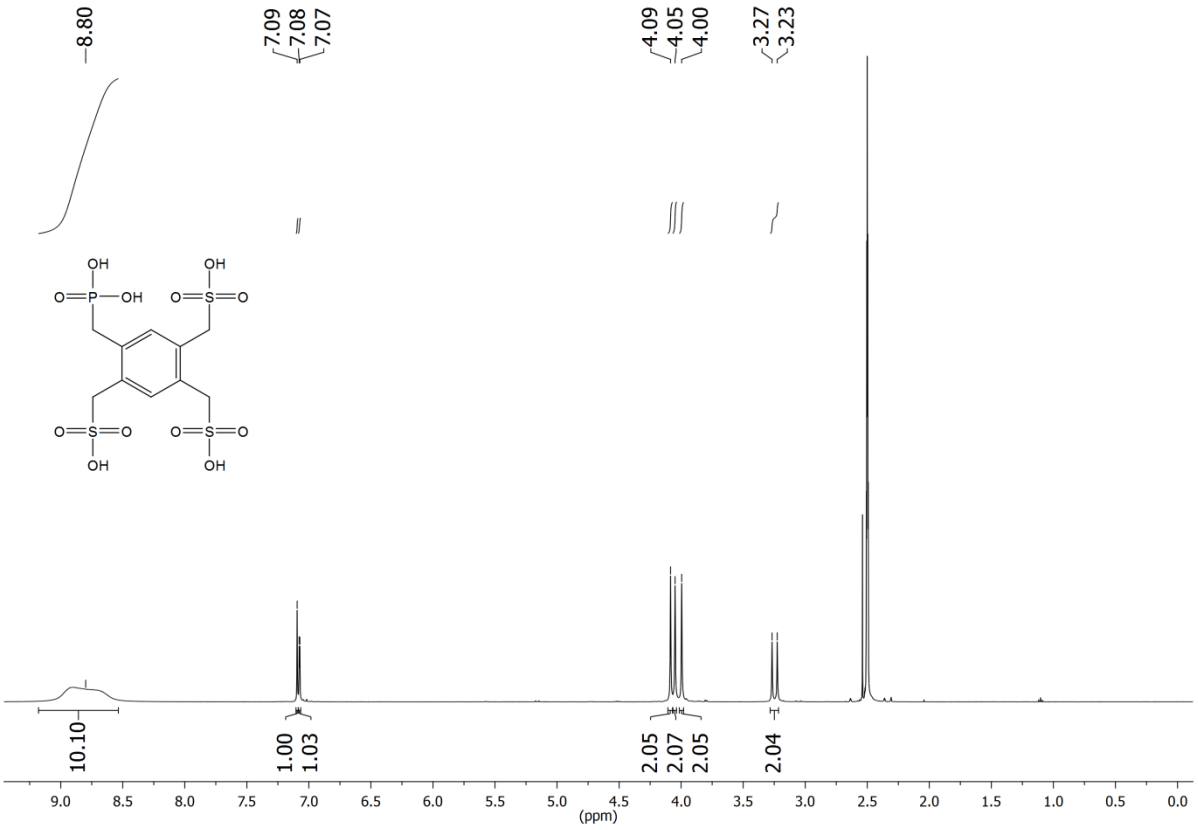

^{1}H-NMR (500 MHz, 300 K, DMSO-d6) of **8**

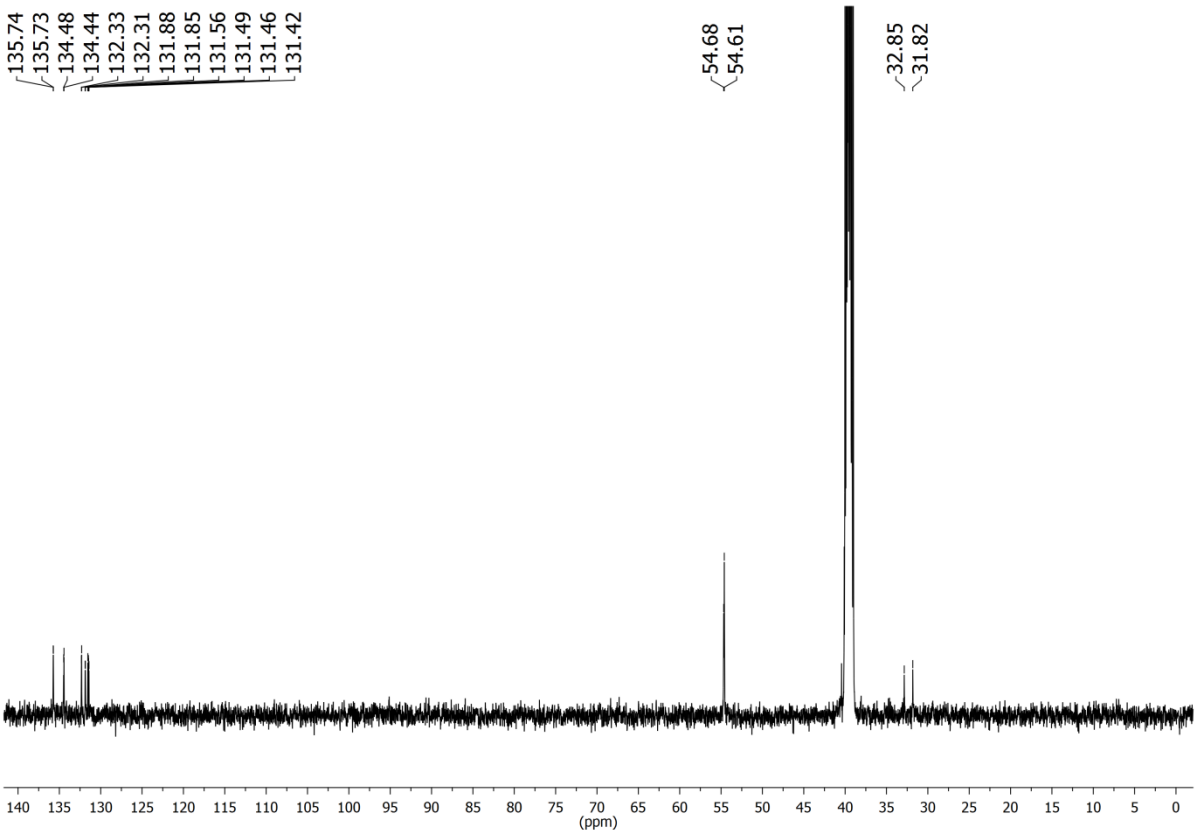

^{13}C-NMR (125 MHz, 300 K, DMSO-d6) of **8**

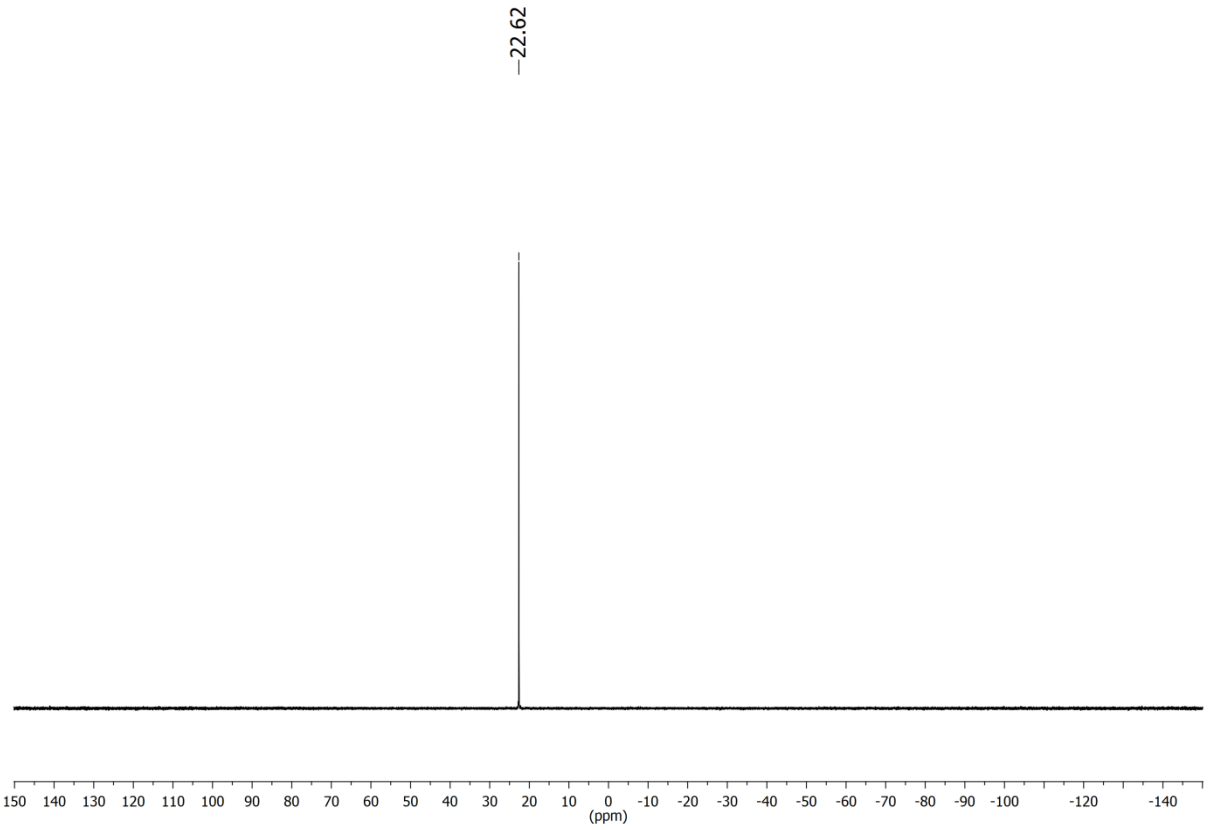

^{31}P-NMR (202 MHz, 300 K, DMSO-d6) of **8**

[2,5-Bis(phosphonomethyl)-benzene-1,4-diyl]bis(methylsulfonic acid) (9)

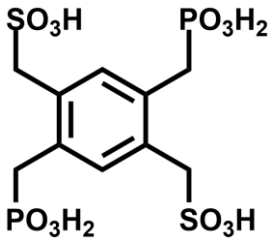

To a saturated aqueous solution of sodium sulfite (20 mL) was added water (5 mL) and [2,5-bis(bromomethyl)-benzene-1,4-diyl]bis(methylphosphonic acid diethyl ester) (**2**, 878 mg, 1.56 mmol) dissolved in acetone (15 mL). The reaction mixture was stirred at 100 °C for 12 h. Acetone was removed in vacuo and conc. hydrochloric acid (40 mL) was added to the aqueous solution and the mixture was stirred at 120 °C for 2 d. The solvent was removed in vacuo and the residue was treated with dimethyl sulfoxide (50 mL) to dissolve the product. Undissolved sodium chloride was separated by filtration. The solution was poured into dichloromethane (500 mL) and the precipitate was collected by filtration. To exchange the sodium ions, the residue was dissolved in water and rinsed over a column filled with ion-exchange resin (Dowex 50WX8 hydrogen form). The eluate was concentrated to give yellow oil which was dissolved in ethanol (3 mL). Acetonitrile (20 mL) was added and the solution

was kept at 5 °C for 2 h. The precipitate was filtered and dried for 24 h at 60 °C in a vacuum oven, to yield a colourless solid.

Yield: 532 mg (1.17 mmol, 75 %)

M. p.: 285 °C (decomposition)

^{1}H-NMR (500 MHz, 300 K, DMSO-d6): δ = 10.46 (br. s, 6H, SO_3H, PO_3H_2), 7.08 (s, 2H, Ar-3,6-*H*), 3.97 (s, 4H, Ar-1,4-CH_2), 3.21 (d, $^{2}J_{H\text{-}P}$ = 19.7 Hz, 4H, Ar-2,5-CH_2) ppm.

^{13}C-NMR (125 MHz, 300 K, DMSO-d6): δ = 134.6 (d[m_P], Ar-3,6-*C*), 131.6 (s[m_P], Ar-2,5-*C*), 131.1 (s[m_P], Ar-1,4-*C*), 54.7 (t, Ar-1,4-*C*H_2), 32.3 (t[d_P], $^{1}J_{C\text{-}P}$ = 130.6 Hz, Ar-2,5-*C*H_2) ppm.

^{31}P-NMR (202 MHz, 300 K, DMSO-d6): 22.0 (s, 2P, *P*O_3H_2) ppm.

MS (ESI_{neg}): *m/z* = 453 $[M-H]^-$, 435 $[M-H_3O]^-$.

IR (ATR): $\tilde{\nu}$ = 2753, 2249 (br. O-H), 1667 (H_3O^+), 1510 (arom. C=C) cm^{-1}.

EA ($C_{10}H_{16}O_{12}P_2S_2$) (454.30): calcd. C 26.44 H 3.55 S 14.12;
($C_{10}H_{16}O_{12}P_2S_2 \cdot 0.33\ C_2H_6O \cdot 0.33\ H_2O$) (475.66): calcd. C 26.93 H 3.96 S 13.48;
found C 27.29 H 4.03 S 13.34.

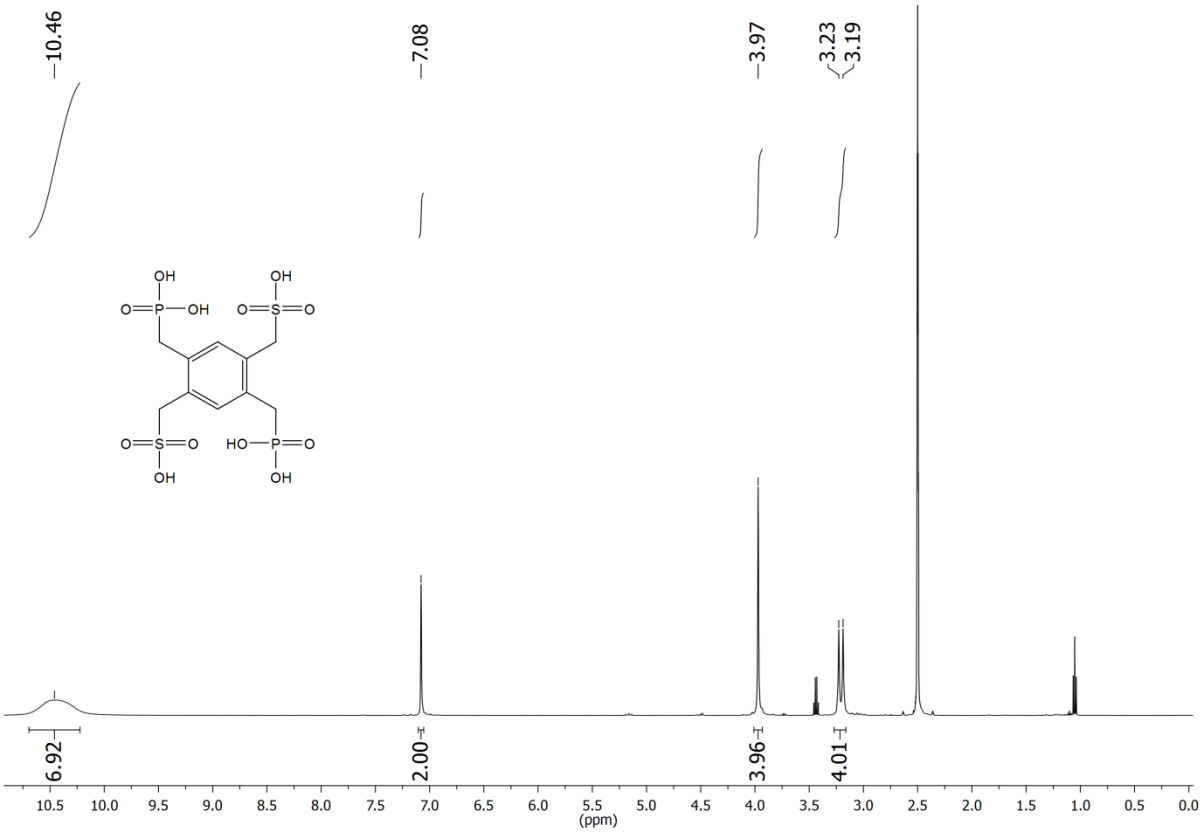

^{1}H-NMR (500 MHz, 300 K, DMSO-d6) of **9**

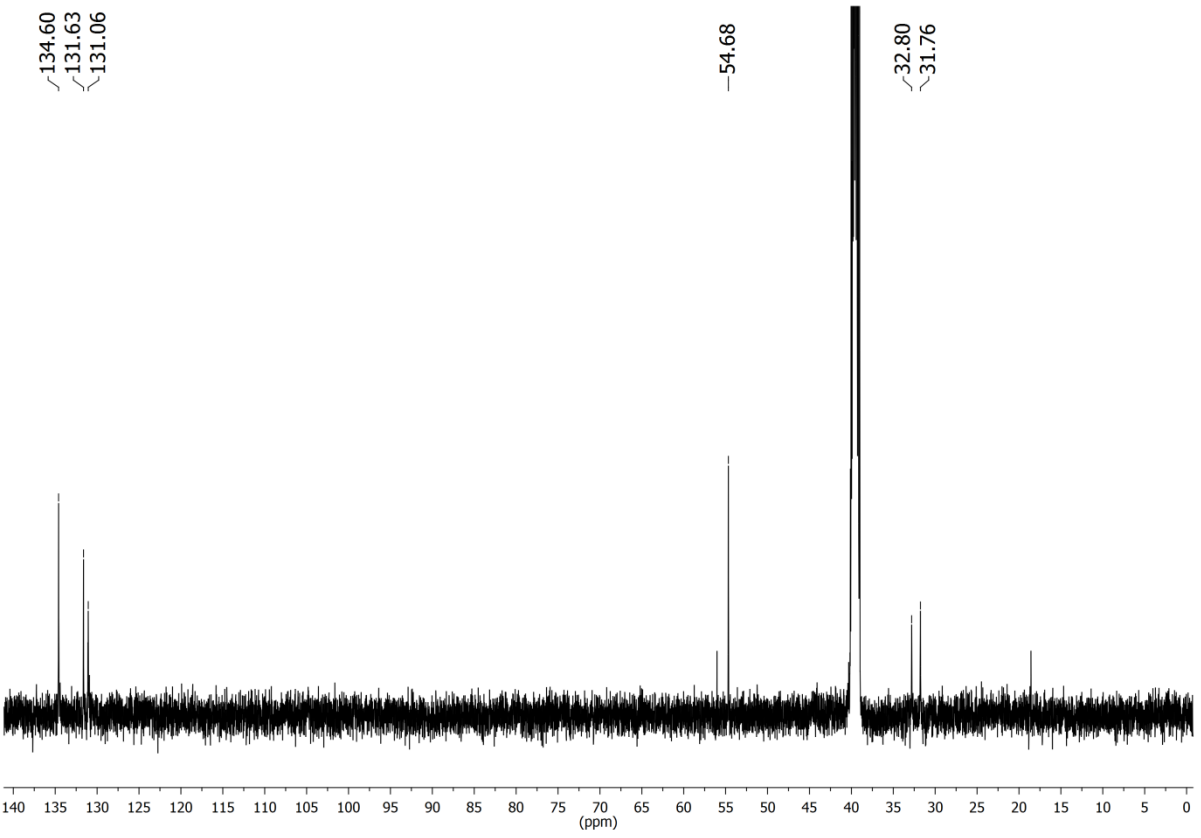

^{13}C-NMR (125 MHz, 300 K, DMSO-d6) of **9**

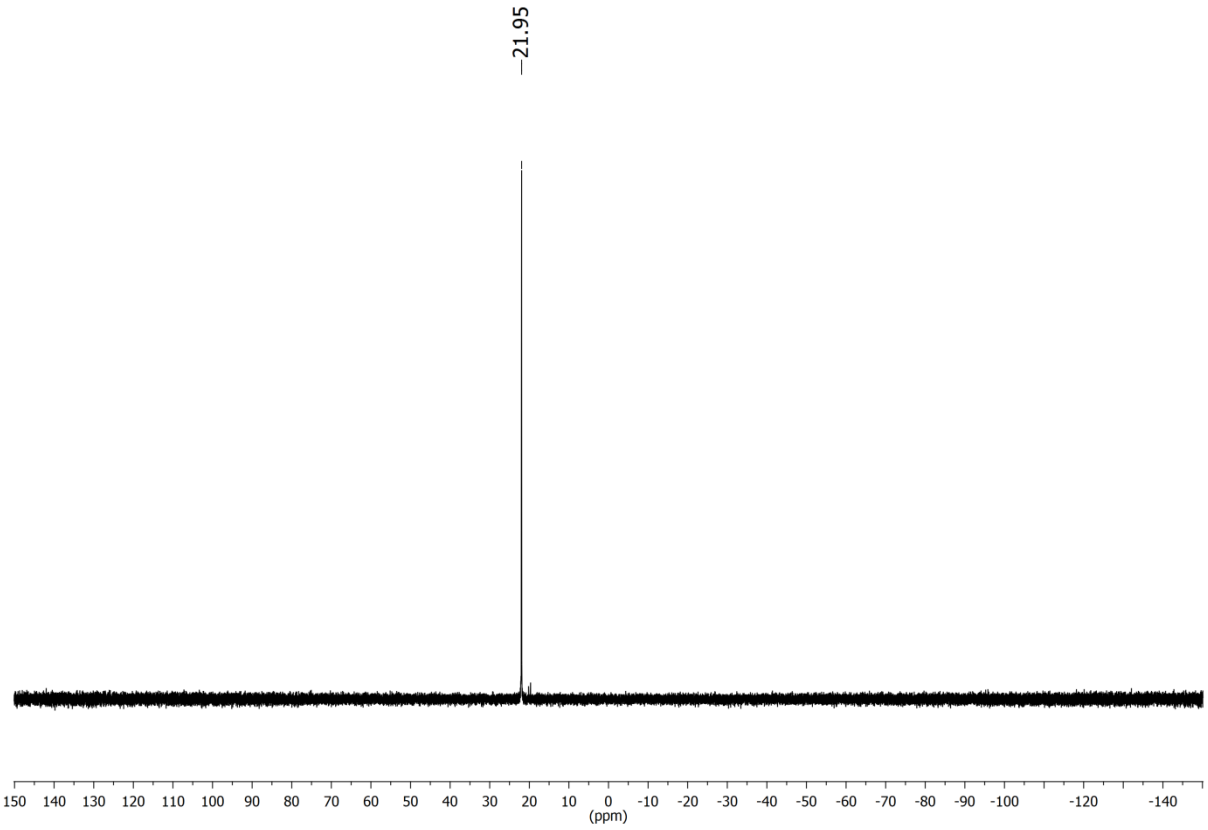

^{31}P-NMR (202 MHz, 300 K, DMSO-d6) of **9**

[4,5-Bis(phosphonomethyl)-benzene-1,2-diyl]bis(methylsulfonic acid) (10)

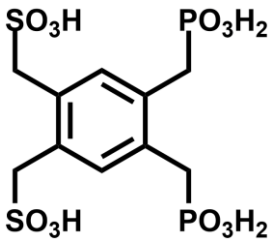

To a saturated aqueous solution of sodium sulfite (10 mL) was added water (2.5 mL) and [4,5-bis(bromomethyl)-benzene-1,2-diyl]bis(methylphosphonic acid diethyl ester) (**4**, 342 mg, 606 µmol) dissolved in acetone (10 mL). The reaction mixture was stirred at 100 °C for 12 h. Acetone was removed in vacuo and conc. hydrochloric acid (30 mL) was added to the aqueous solution and the mixture was stirred at 120 °C for 2 d. The solvent was removed in vacuo and the residue was treated with dimethyl sulfoxide (50 mL) to dissolve the product. Undissolved sodium chloride was separated by filtration. The solution was poured into dichloromethane (500 mL) and the precipitate was collected by filtration. To exchange the sodium ions, the residue was dissolved in water and rinsed over a column filled with ion-exchange resin (Dowex 50WX8 hydrogen form). The eluate was concentrated to give yellow oil, which was dissolved in ethanol (3 mL). Acetonitrile (20 mL) was added and the solution

was kept at 5 °C for 2 h. The precipitate was filtered and dried for 24 h at 60 °C in a vacuum oven, to yield a colourless solid.

Yield: 225 mg (495 µmol, 82 %)

M. p.: >300 °C

^{1}H-NMR (500 MHz, 300 K, DMSO-d6): δ = 9.95 (br. s, 6H, SO_3H, PO_3H_2), 7.07 (s, 2H, Ar-3,6-*H*), 4.03 (s, 4H, Ar-1,2-CH_2), 3.13 (d, $^{2}J_{H\text{-}P}$ = 20.3 Hz, 4H, Ar-4,5-CH_2) ppm.

^{13}C-NMR (125 MHz, 300 K, DMSO-d6): δ = 134.6 (d[m_P], Ar-3,6-*C*), 132.2 (s[m_P], Ar-1,2-*C*), 130.4 (s[m_P], Ar-4,5-*C*), 54.7 (t, Ar-1,2-*C*H_2), 32.3 (t[d_P], $^{1}J_{C\text{-}P}$ = 131.5 Hz, Ar-4,5-*C*H_2) ppm.

^{31}P-NMR (202 MHz, 300 K, DMSO-d6): 22.2 (s, 2P, *P*O_3H_2) ppm.

MS (ESI_{neg}): *m/z* = 453 $[M-H]^-$, 435 $[M-H_3O]^-$.

IR (ATR): $\tilde{\nu}$ = 2957 (br. O-H), 1657 (H_3O^+), 1513 (arom. C=C) cm^{-1}.

EA ($C_{10}H_{16}O_{12}P_2S_2$) (454.30): calcd. C 26.44 H 3.55 S 14.12;
($C_{10}H_{16}O_{12}P_2S_2 \cdot 0.2\ C_2H_6O \cdot 0.2\ H_2O$) (467.12): calcd. C 26.74 H 3.80 S 13.73;
found C 26.47 H 3.77 S 13.36.

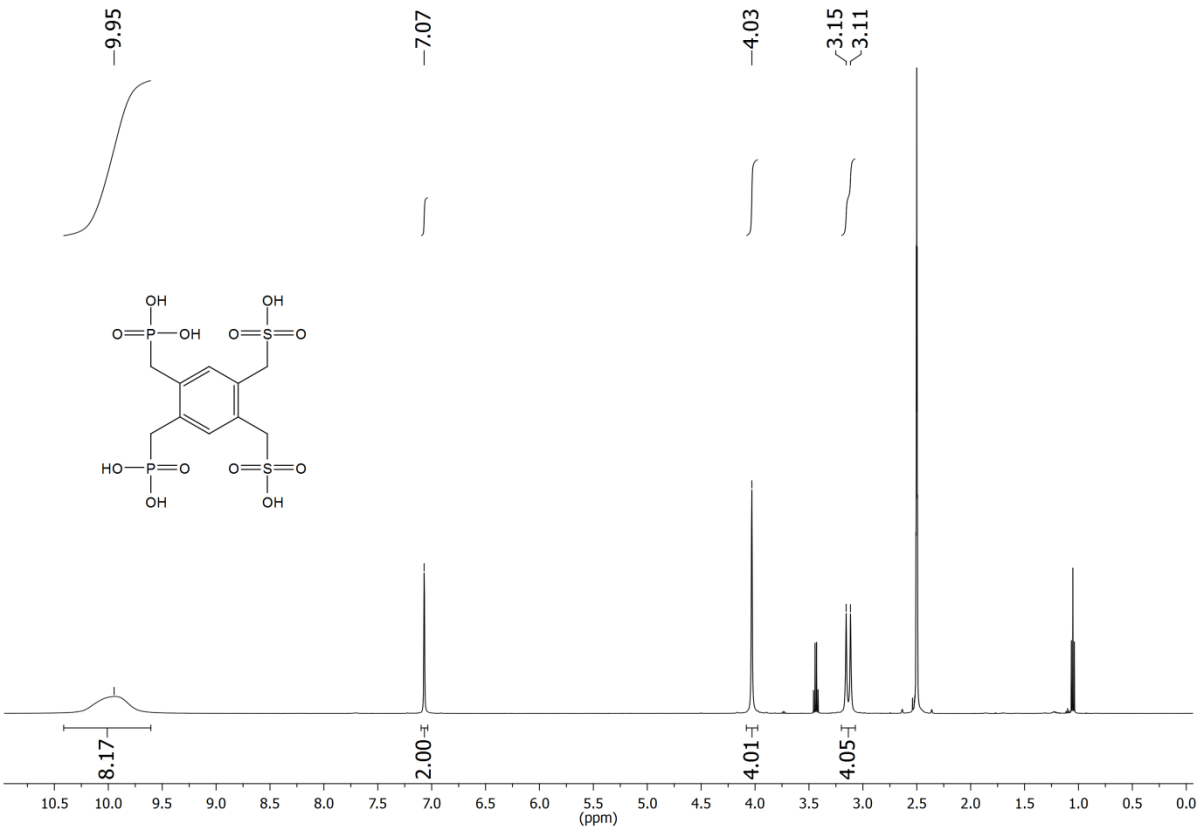

^{1}H-NMR (500 MHz, 300 K, DMSO-d6) of **10**

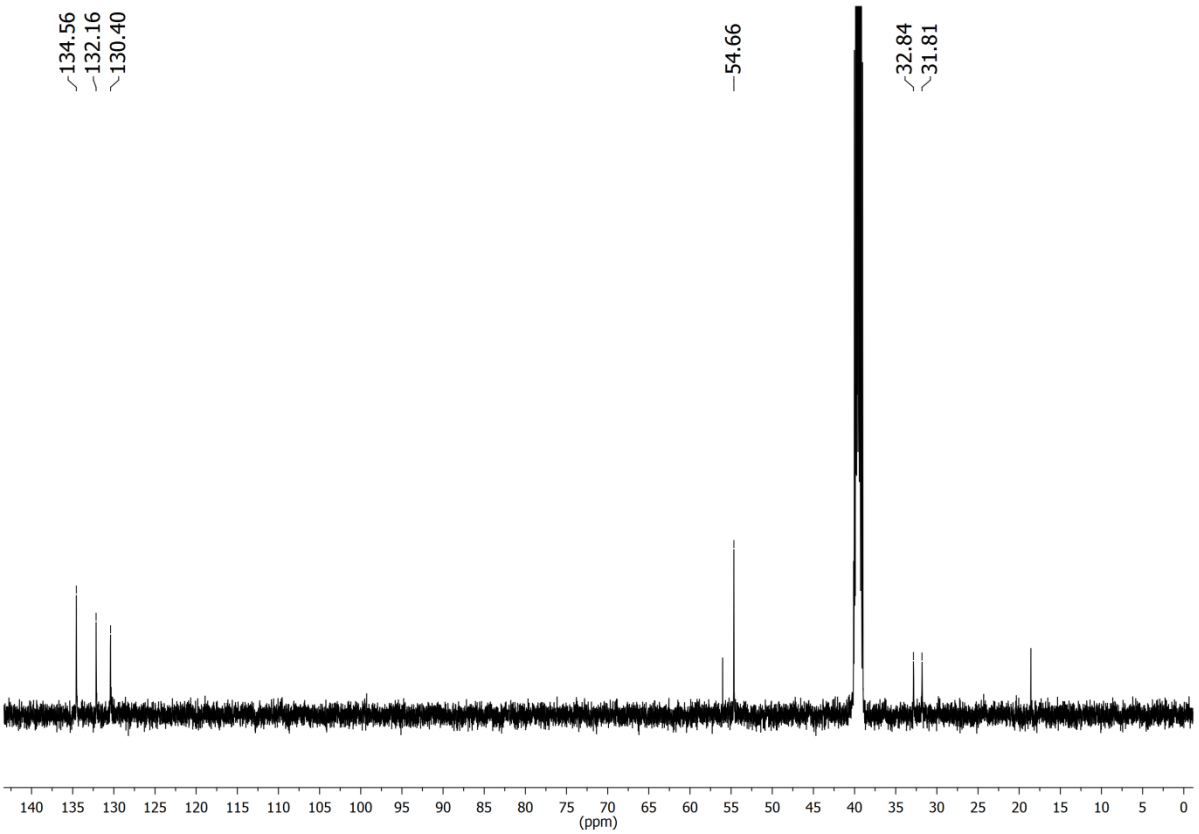

^{13}C-NMR (125 MHz, 300 K, DMSO-d6) of **10**

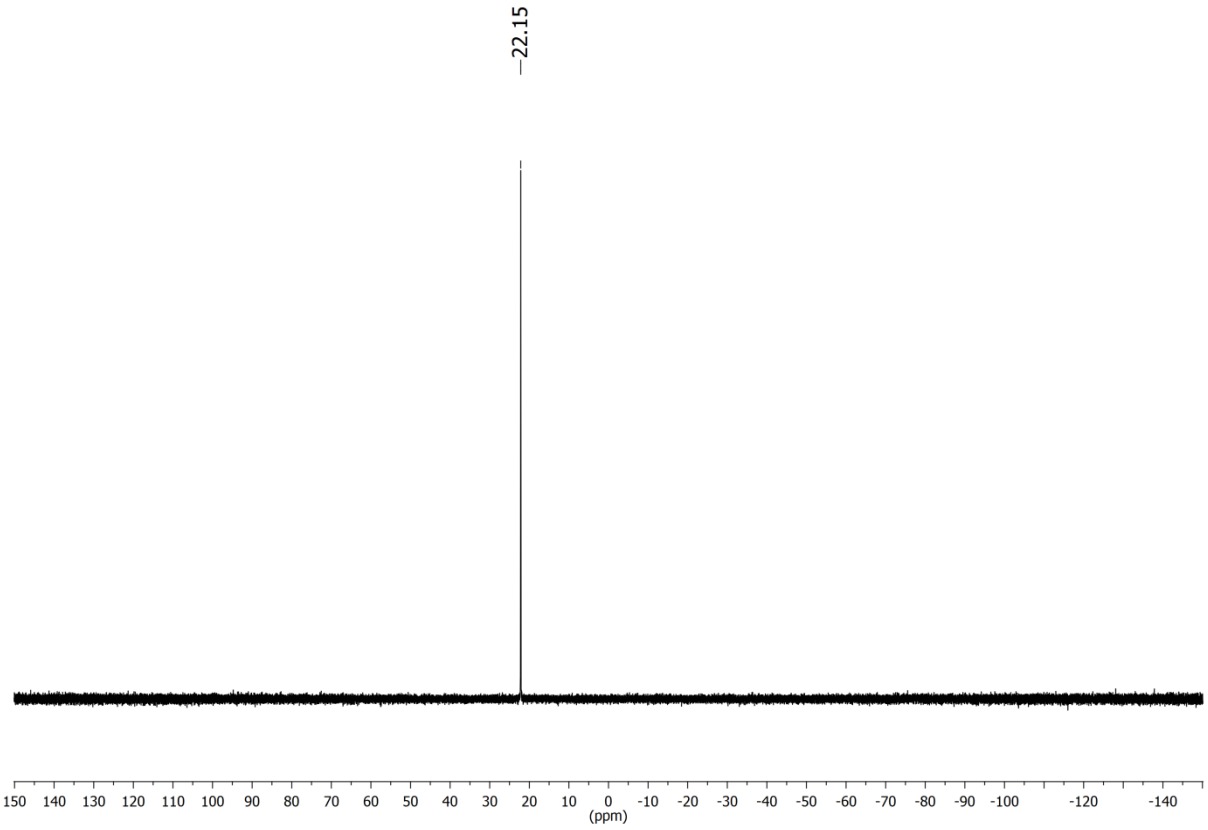

^{31}P-NMR (202 MHz, 300 K, DMSO-d6) of **10**

[2,4,5-Tris(phosphonomethyl)phenyl]methylsulfonic acid (11)

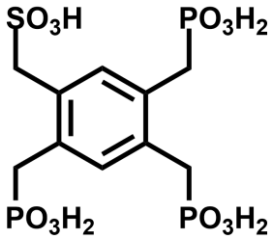

To a saturated aqueous solution of sodium sulfite (40 mL) was added water (10 mL) and [5-(bromomethyl)-benzene-1,2,4-triyl]tris(methylphosphonic acid diethyl ester) (**6**, 2.39 g, 3.85 mmol) dissolved in acetone (15 mL). The reaction mixture was stirred at 100 °C for 12 h. Acetone was removed in vacuo and conc. hydrochloric acid (40 mL) was added to the aqueous solution and the mixture was stirred at 120 °C for 2 d. The solvent was removed in vacuo and the residue was treated with dimethyl sulfoxide (100 mL) to dissolve the product. Undissolved sodium chloride was separated by filtration. The solution was poured into dichloromethane (1000 mL) and the precipitate was collected by filtration. To exchange the sodium ions, the residue was dissolved in water and rinsed over a column filled with ion-exchange resin (Dowex 50WX8 hydrogen form). The eluate was concentrated and dried for 24 h at 60 °C in a vacuum oven, to yield a colourless solid.

Yield: 1.52 g (3.35 mmol, 87 %)

M. p.: 246 °C

^{1}H-NMR (500 MHz, 300 K, DMSO-d6): δ = 8.08 (br. s, 7H, SO_3H, PO_3H_2), 7.09 (s, 1H, Ar-6-*H*), 7.06 (m_c, 1H, Ar-3-*H*), 3.90 (s, 2H, Ar-1-CH_2), 3.19 (d, $^{2}J_{H\text{-}P}$ = 20.3 Hz, 2H, Ar-2-CH_2), 3.11 (d, $^{2}J_{H\text{-}P}$ = 20.3 Hz, 4H, Ar-4,5-CH_2) ppm.

^{13}C-NMR (125 MHz, 300 K, DMSO-d6): δ = 134.8 (d[m_P], Ar-6-*C*), 133.4 (d[m_P], Ar-3-*C*), 131.6 (s[m_P], Ar-1-*C*), 131.3 (s[m_P], Ar-2-*C*), 130.6 (s[m_P], Ar-4-*C*), 129.9 (s[m_P], Ar-5-*C*), 54.7 (t, Ar-1-*C*H_2), 32.3 (t[d_P], $^{1}J_{C\text{-}P}$ = 129.8 Hz, Ar-2-*C*H_2), 32.2 (t[d_P], $^{1}J_{C\text{-}P}$ = 132.8 Hz, Ar-4,5-*C*H_2) ppm.

^{31}P-NMR (202 MHz, 300 K, DMSO-d6): 21.9 (m_c, 3P, *P*O_3H_2) ppm.

MS (ESI_{neg}): *m/z* = 453 [M -H]$^-$, 435 [M -H_3O]$^-$.

IR (ATR): $\tilde{\nu}$ = 2752, 2291 (br. O-H), 1505 (arom. C=C) cm^{-1}.

EA ($C_{10}H_{17}O_{12}P_3S$) (454.22): calcd. C 26.44 H 3.77 S 7.06;
found C 26.53 H 3.76 S 7.20.

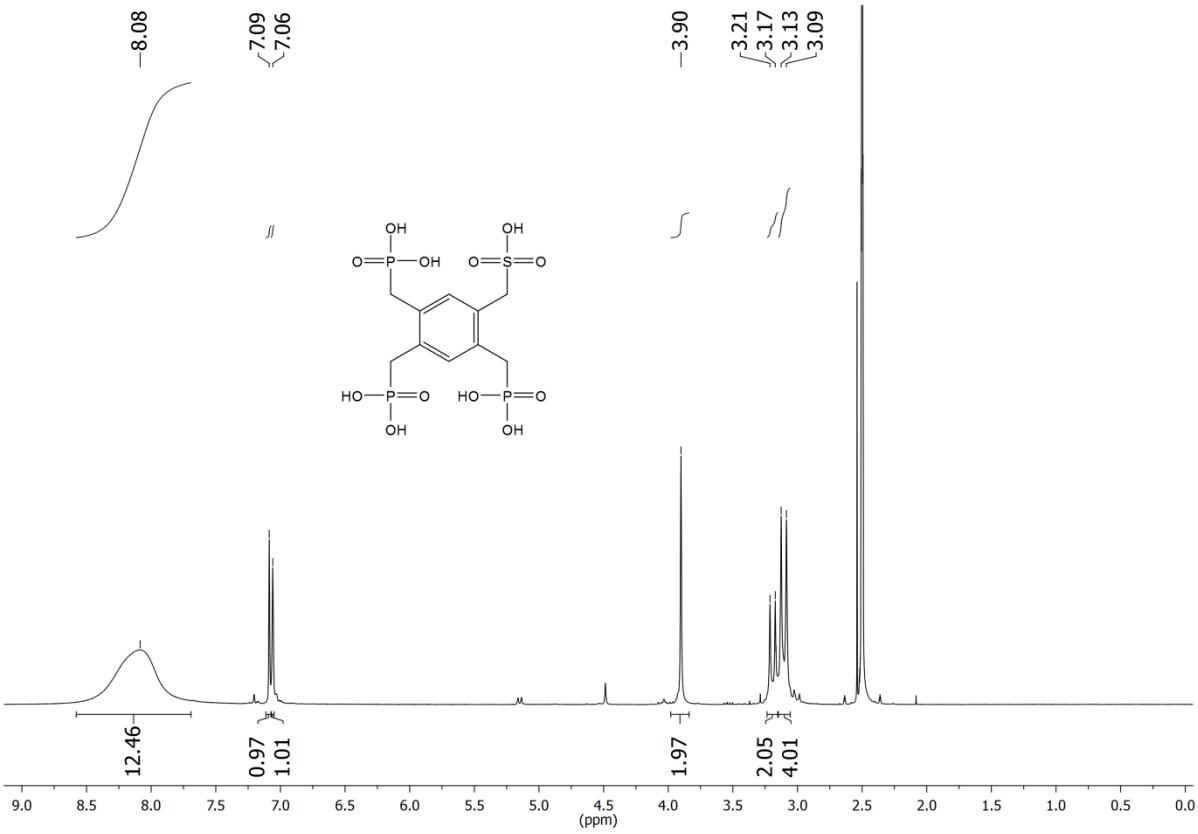

^{1}H-NMR (500 MHz, 300 K, DMSO-d6) of **11**

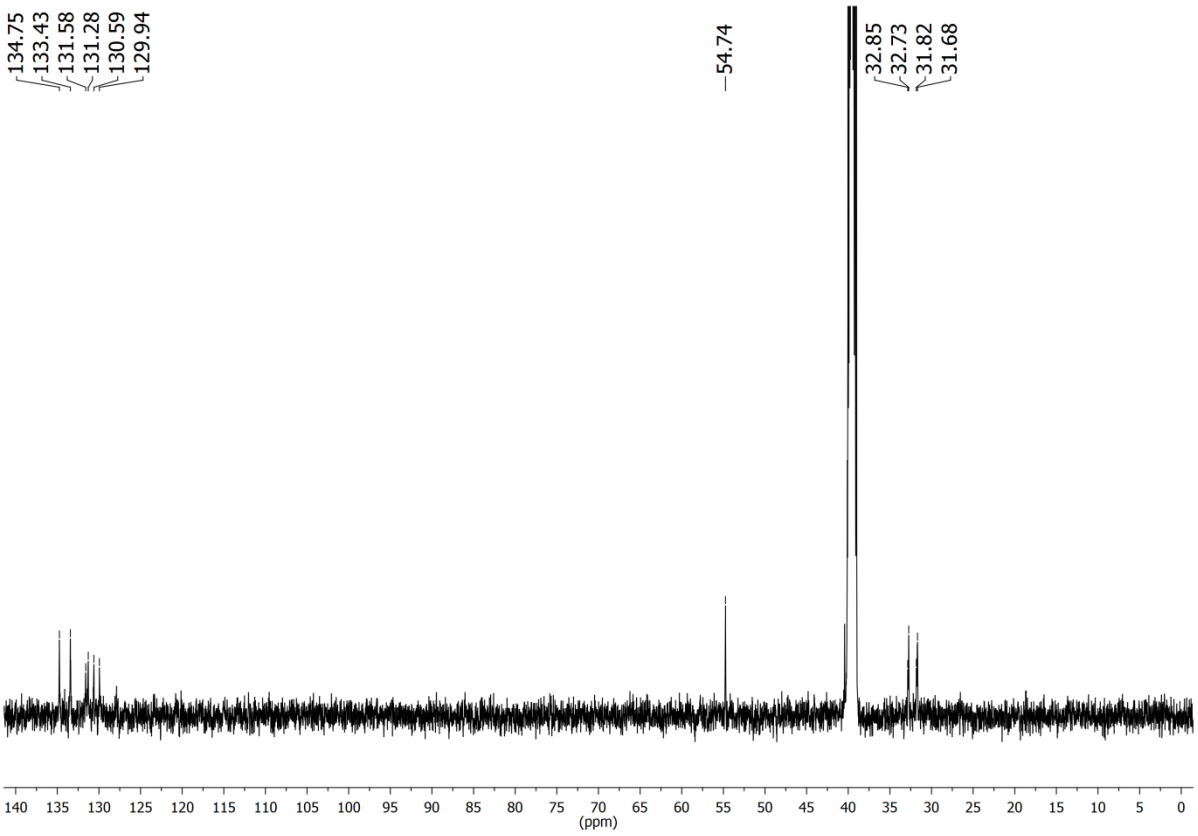

^{13}C-NMR (125 MHz, 300 K, DMSO-d6) of **11**

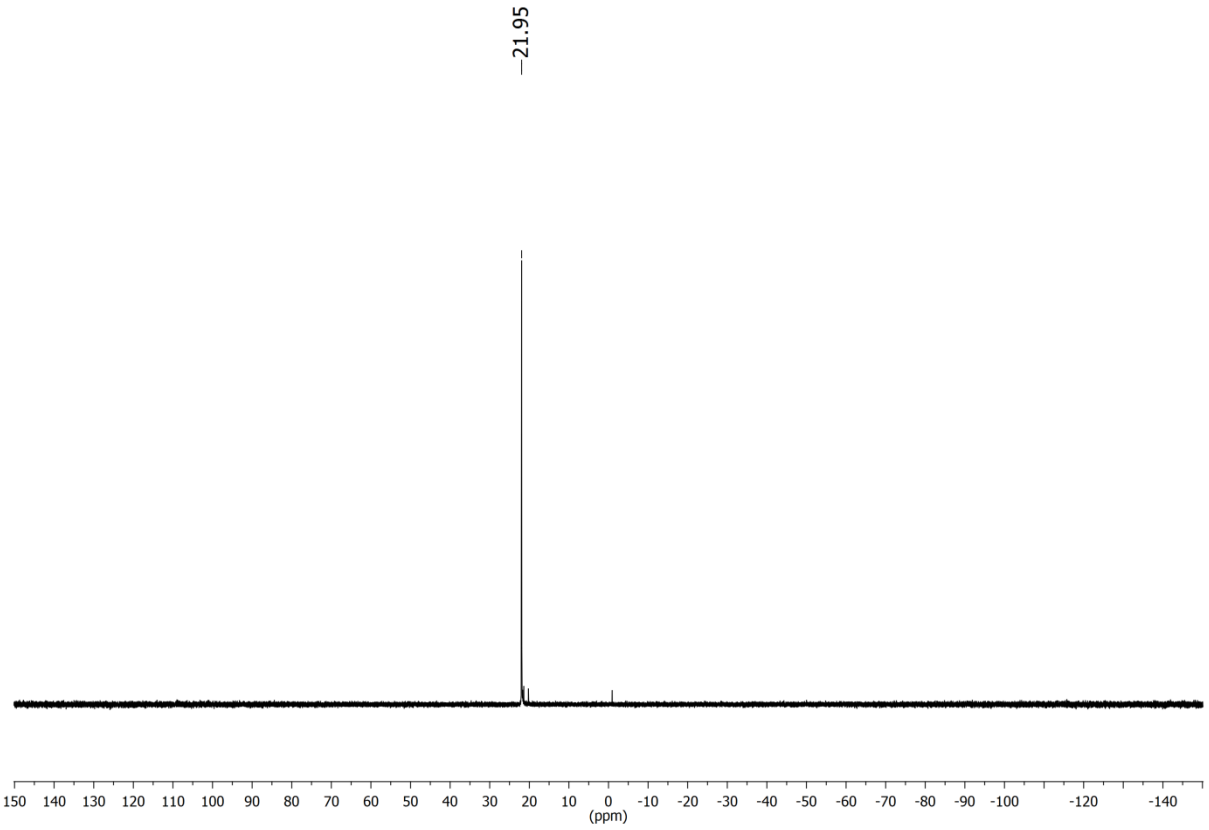

^{31}P-NMR (202 MHz, 300 K, DMSO-d6) of **11**

2,5-Dibromobenzenesulfonic acid (18)

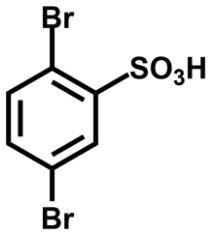

Fuming sulfuric acid (20 - 30 % SO_3) (10 mL) was added to 1,4-dibromobenzene (**17**, 5.0 g, 21.2 mmol) under nitrogen atmosphere. The suspension was stirred at 150 °C until it became a dark brown solution (ca. 2 h). The reaction mixture was poured carefully into ice-cold water (100 mL). After treating the mixture with saturated aqueous sodium hydrogen carbonate solution until pH = 7 was reached, the water was evaporated in vacuo and the residue was dried for 2 d at 60 °C in a vacuum oven. Methanol (1000 mL) was added to the dry solid and the suspension was heated to 60 °C. Undissolved sodium sulfate was separated by filtration and the solvent was evaporated in vacuo. The residue was mixed with 2 M aqueous sodium hydroxide (200 mL) and water (50 mL) to give a suspension, which was stirred at 50 °C for 1 h. After 15 h at room temp., the undissolved solid was filtered off to give the sodium salt as a colourless solid (2.60 g). Concentration of the mother liquor to 50 % of the volume led to precipitation. Filtration gave about 800 mg of additional product. To exchange the sodium ion, the combined residue was dissolved in water and rinsed over a column filled with ion-

exchange resin (Dowex 50WX8 hydrogen form). The eluate was concentrated and dried for 24 h at 60 °C in a vacuum oven, to yield a colourless solid.

Yield: 3.01 g (9.53 mmol, 45 %) (Lit.[2]: 86 % of the sodium salt)

M. p.: 138 °C

^{1}H-NMR (500 MHz, 300 K, DMSO-d6): δ = 8.00 (d, ^{4}J = 2.6 Hz, 1H, Ar-6-*H*), 7.53 (d, ^{3}J = 8.4 Hz, 1H, Ar-3-*H*), 7.42 (dd, ^{3}J = 8.4 Hz, ^{4}J = 2.6 Hz, 1H, Ar-4-*H*), 6.67 (br. s, 1H, SO_3H) ppm.

^{13}C-NMR (125 MHz, 300 K, DMSO-d6): δ = 148.8 (s, Ar-1-*C*), 135.9 (d, Ar-3-*C*), 132.8 (d, Ar-4-*C*), 131.4 (d, Ar-6-*C*), 119.8 (s, Ar-5-*C*), 118.7 (s, Ar-2-*C*) ppm.

MS (EI): *m/z* = 318, 316, 314 (52, 100, 50) $[M]^{+\cdot}$.

HRMS (EI): *m/z* = $C_6H_4{}^{79}Br_2O_3S$ calcd. 313.8248; found 313.8243 (Δ 1.5 ppm);
$C_6H_4{}^{79}Br^{81}BrO_3S$ calcd. 315.8227; found 315.8222 (Δ 1.7 ppm);
$C_6H_4{}^{81}Br_2O_3S$ calcd. 317.8207; found 317.8202 (Δ 1.6 ppm).

IR (ATR): $\tilde{\nu}$ = 3087 (aryl-H val.), 2900, 2169 (br., OH), 1673 (H_3O^+) cm^{-1}.

EA ($C_6H_4Br_2O_3S$) (315.97): calcd. C 22.81 H 1.28 S 10.15;
($C_6H_4Br_2O_3S \cdot 1\ H_2O$) (333.98): calcd. C 21.58 H 1.81 S 9.60;
found C 21.19 H 2.20 S 9.83.

^{1}H-NMR (500 MHz, 300 K, DMSO-d6) of **18**

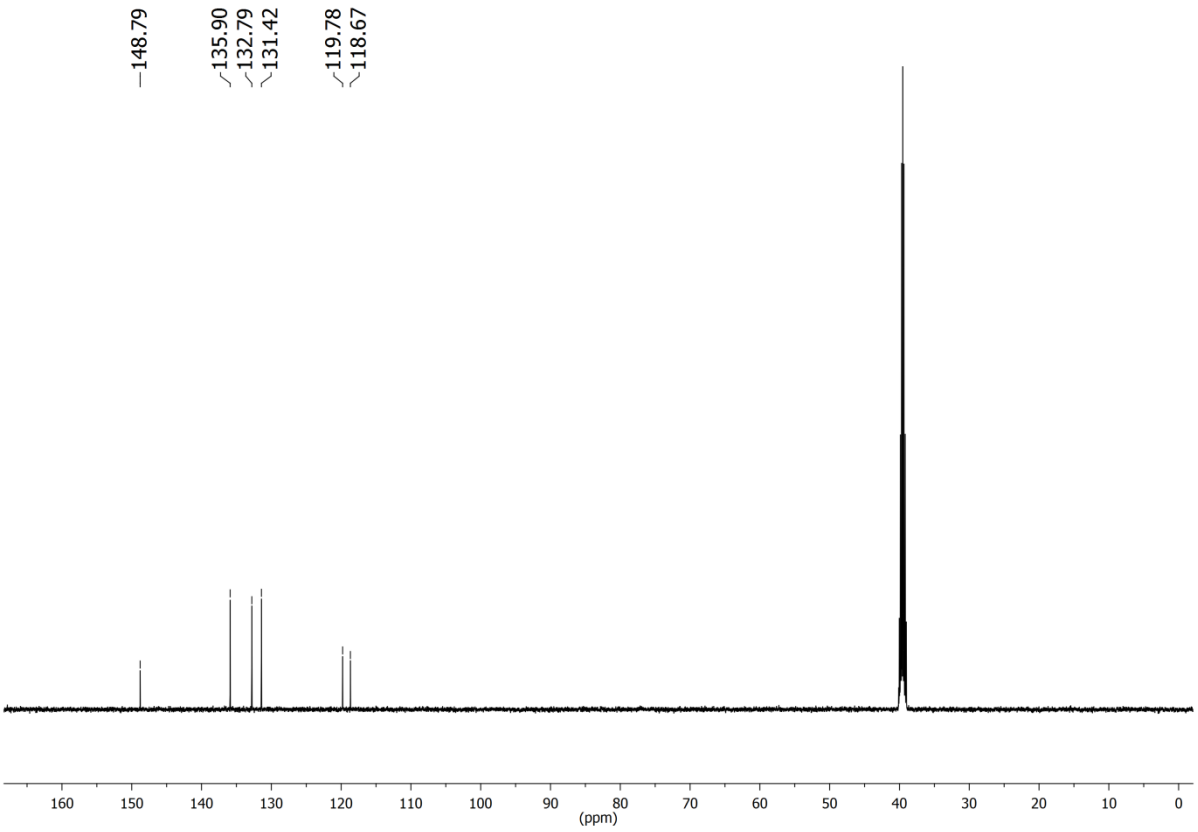

^{13}C-NMR (125 MHz, 300 K, DMSO-d6) of **18**

2,5-Diphosphonobenzenesulfonic acid (25)

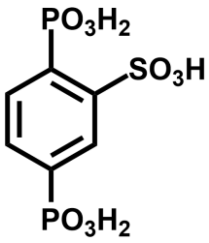

A solution of 2,5-dibromobenzenesulfonic acid (**18**, 1.93 g, 6.12 mmol) in water (50 mL) was treated with aqueous tetra-*n*-butylammonium hydroxide (40 % in water) until pH = 7 was reached. The solvent was removed in vacuo and the residue was dried in a vacuum oven at 60 °C for 12 h to obtain the respective tetra-*n*-butylammonium salt. Three microwave vials were charged each with salt (3 x 1.13 g, 3 x 2.03 mmol), palladium(II) chloride (3 x 36 mg, 3 x 203 µmol) and triethyl phosphite (3 x 4 mL, 3 x 16.7 mmol). The vials were irradiated in a microwave oven (max. 200 W, 220 °C) for 1 h. The combined dark brown solution was added to a mixture of ethyl acetate (100 mL) and water (100 mL) in a separatory funnel. The aqueous layer was washed with ethyl acetate (3 x 100 mL) and water was removed in vacuo. The residue was dissolved in a mixture of water (50 mL) and conc. hydrochloric acid (100 mL) and stirred for 12 h at 120 °C. After removing the solvent in vacuo, the residue was dissolved in acetone (50 mL) and mixed with four equivalents of sodium iodide (3.67 g, 24.5 mmol) dissolved in acetone (30 mL). The precipitate was collected by filtration and recrystallized from a mixture of ethanol and water. To exchange the sodium ions, the residue was dissolved in water and rinsed over a column filled with ion-exchange resin (Dowex 50WX8 hydrogen form). The eluate was concentrated and dried for 24 h at 60 °C in a vacuum oven, to yield a colourless solid.

Yield: 922 mg (2.90 mmol, 47 %)

M. p.: 172 °C

^{1}H-NMR (500 MHz, 300 K, DMSO-d6): δ = 8.26 (ddd, $J_{H\text{-}P}$ = 13.2 Hz, $J_{H\text{-}P}$ = 4.8 Hz, ^{4}J = 1.3 Hz, 1H, Ar-6-*H*), 8.04 (ddd, $J_{H\text{-}P}$ = 13.9 Hz, ^{3}J = 7.6 Hz, $J_{H\text{-}P}$ = 3.7 Hz, 1H, Ar-3-*H*), 7.79 (m_c, H, Ar-4-*H*), 6.79 (br. s, 5H, PO_3H_2, SO_3H) ppm.

^{13}C-NMR (125 MHz, 300 K, DMSO-d6): δ = 146.6 (s[$d_P d_P$], $J_{C\text{-}P}$ = 13.4 Hz, $J_{C\text{-}P}$ = 9.3 Hz, Ar-1-*C*), 137.0 (s[$d_P d_P$], $^{1}J_{C\text{-}P}$ = 137.0 Hz, $^{4}J_{C\text{-}P}$ = 2.6 Hz, Ar-5-*C*), 133.1 (d[$d_P d_P$], $J_{C\text{-}P}$ = 13.6 Hz, $J_{C\text{-}P}$ = 7.0 Hz, Ar-3-*C*), 132.5 (s[$d_P d_P$], $^{1}J_{C\text{-}P}$ = 164.3 Hz, $^{4}J_{C\text{-}P}$ = 2.9 Hz, Ar-2-*C*), 131.2 (d[$d_P d_P$],

$J_{C\text{-}P}$ = 12.3 Hz, $J_{C\text{-}P}$ = 9.5 Hz, Ar-4-*C*), 129.4 (d[$d_P d_P$], $^2J_{C\text{-}P}$ = 11.5 Hz, $^3J_{C\text{-}P}$ = 11.5 Hz, Ar-6-*C*) ppm.

^{31}P-NMR (202 MHz, 300 K, DMSO-d6): 10.5 (d, $^5J_{P\text{-}P}$ = 3.2 Hz, 1P, PO_3H_2), 9.3 (d, $^5J_{P\text{-}P}$ = ca. 3 Hz, 1P, PO_3H_2) ppm.

MS (ESI_{neg}): *m/z* = 953 $[3M - H]^-$, 635 $[2M - H]^-$, 317 $[M - H]^-$, 299 $[M - H_3O]^-$.

IR (ATR): $\tilde{\nu}$ = 2758, 2290 (br., OH), 1684 (H_3O^+) cm^{-1}.

EA ($C_6H_8O_9P_2S$) (318.13): calcd. C 22.65 H 2.53 S 10.08;
($C_6H_8O_9P_2S \cdot 2\ H_2O$) (354.17): calcd. C 20.35 H 3.42 S 9.05;
found C 20.53 H 3.21 S 9.26.

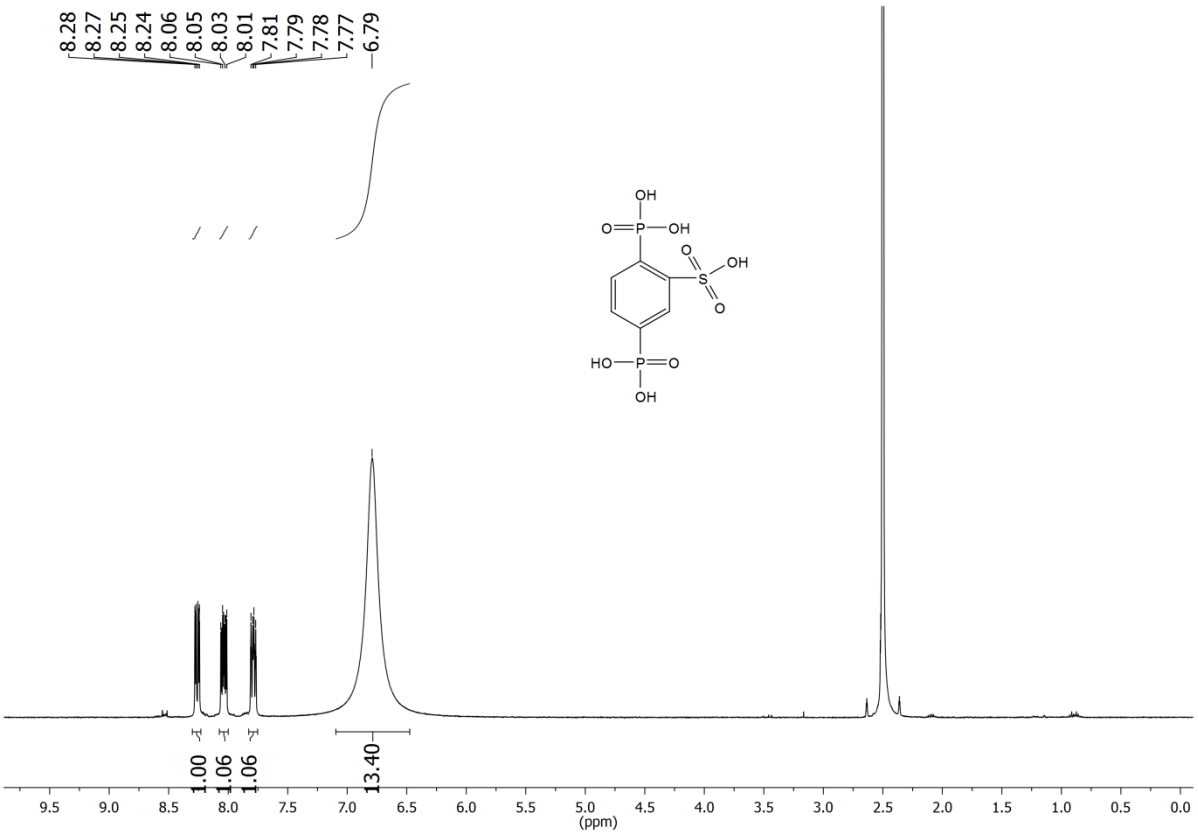

^{1}H-NMR (500 MHz, 300 K, DMSO-d6) of **25**

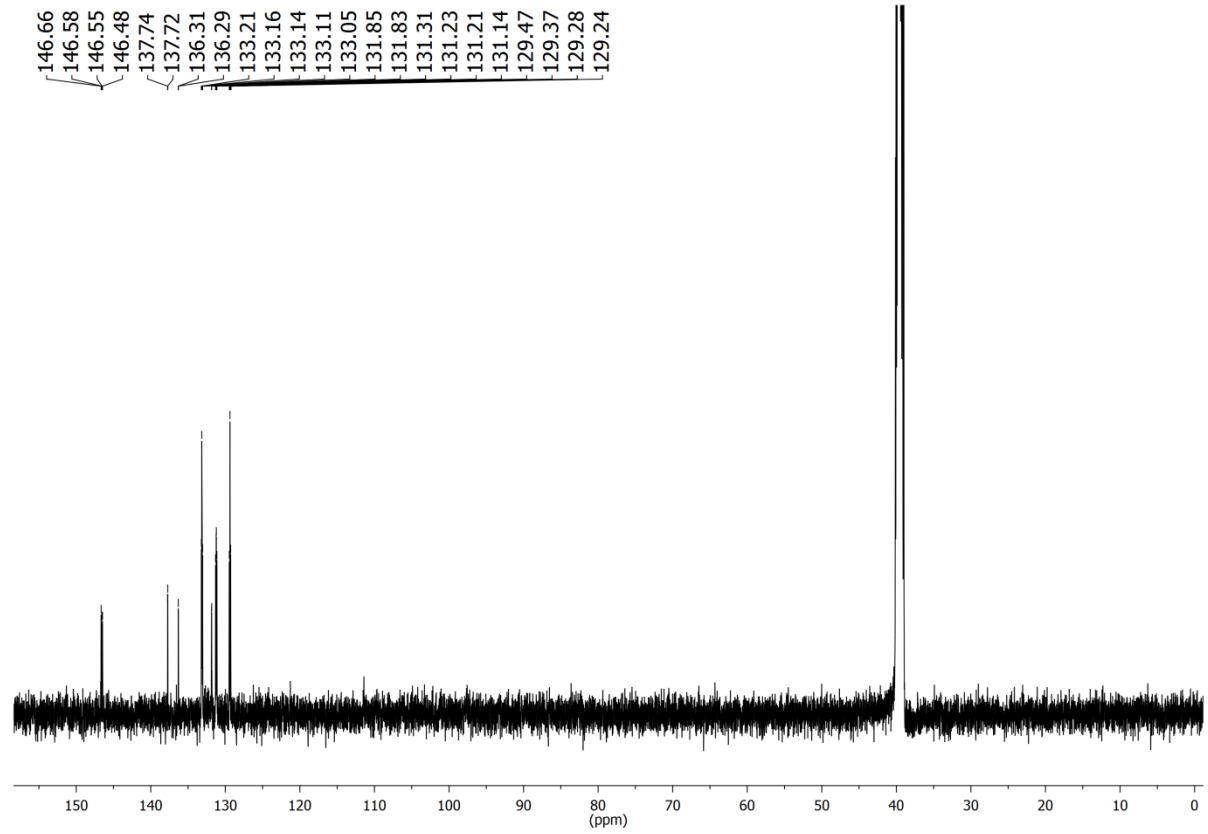

^{13}C-NMR (125 MHz, 300 K, DMSO-d6) of **25**

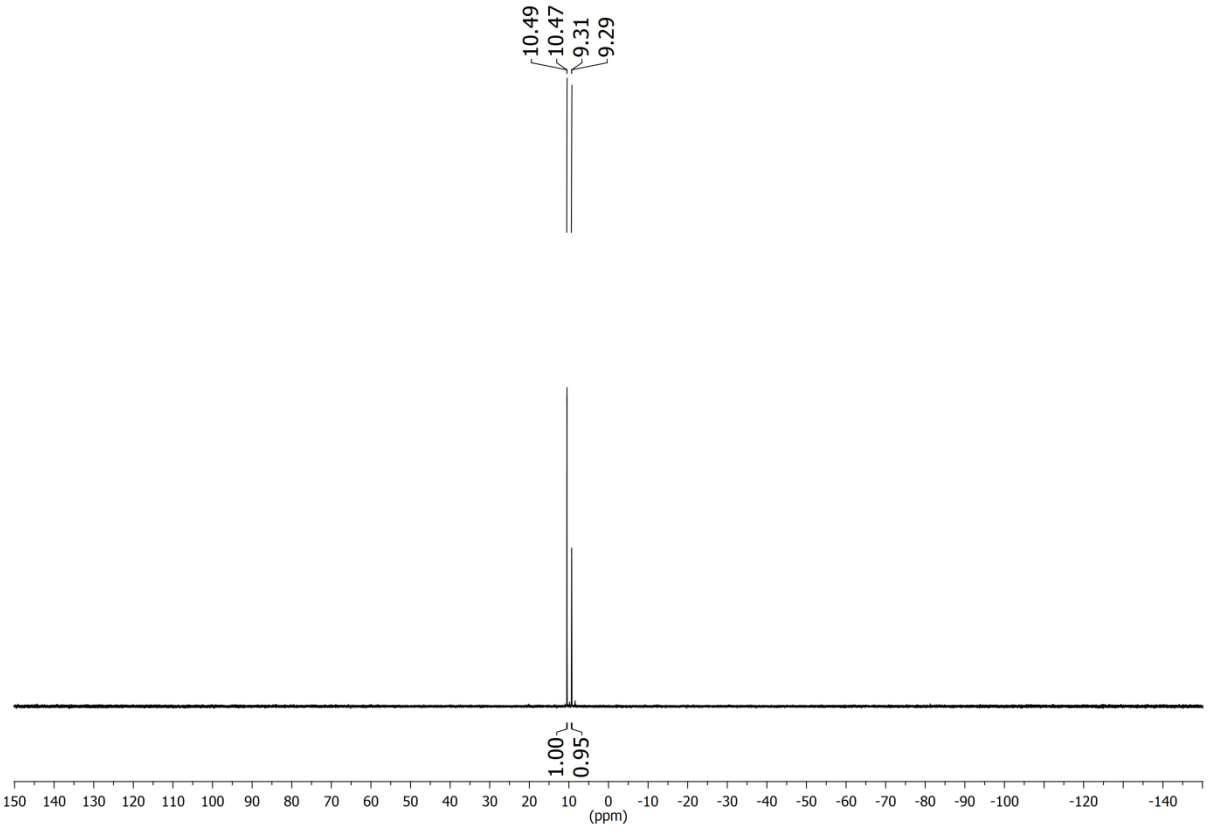

^{31}P-NMR (202 MHz, 300 K, DMSO-d6) of **25**

4,6-Dibromobenzene-1,3-disulfonic acid (22)

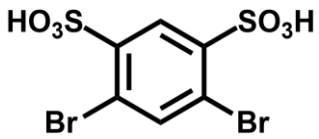

1,3-Dibromobenzene (**21**, 9.2 mL, 76.13 mmol) was added in portions to fuming sulfuric acid (65 % SO_3) (60 mL) and the reaction mixture was stirred for 5 h at 120 °C followed by 12 h at room temp. The mixture was poured carefully into ice-cold water (300 mL) and treated with sodium hydroxide until pH = 7 was reached. The water was removed in vacuo and the residue was dried for 2 d at 60 °C in a vacuum oven. Dimethyl sulfoxide (150 mL) was added to the dried solid and the suspension was stirred for 1 h at 60 °C. Undissolved sodium sulfate was removed by filtration and the filtrate was poured into dichloromethane (800 mL). Filtration of the precipitate and washing with dichloromethane (200 mL) gave a colourless solid. To exchange the sodium ions, the residue was dissolved in water and rinsed over a column filled with ion-exchange resin (Dowex 50WX8 hydrogen form). The eluate was concentrated and dried for 24 h at 60 °C in a vacuum oven, to yield a colourless solid.

Yield: 23.57 g (59.52 mmol, 78 %)

M. p.: 200 °C

^{1}H-NMR (500 MHz, 300 K, DMSO-d6): δ = 8.44 (s, 1H, Ar-2-*H*), 7.74 (s, 1H, Ar-5-*H*), 5.70 (br. s, 2H, SO_3*H*) ppm.

^{13}C-NMR (125 MHz, 300 K, DMSO-d6): δ = 145.4 (s, Ar-1,3-*C*), 137.6 (d, Ar-5-*C*), 129.4 (d, Ar-2-*C*), 119.9 (s, Ar-4,6-*C*) ppm.

MS (EI): *m/z* = 398, 396, 394 (56, 100, 49) $[M]^{+\cdot}$.

HRMS (EI): *m/z* = $C_6H_3{}^{79}Br_2O_6{}^{33}S^{34}S$ calcd. 395.7689; found 395.7686 (Δ 0.9 ppm).

IR (ATR): $\tilde{\nu}$ = 3101 (aryl-H val.), 2170 (br., OH), 1684 (H_3O^+), 1559, 1528 (arom. C=C) cm^{-1}.

EA ($C_6H_4Br_2O_6S_2$) (396.03): calcd. C 18.20 H 1.02 S 16.19;
($C_6H_4Br_2O_6S_2 \cdot 2\ H_2O$) (432.06): calcd. C 16.68 H 1.87 S 14.84;
found C 16.65 H 1.79 S 15.14.

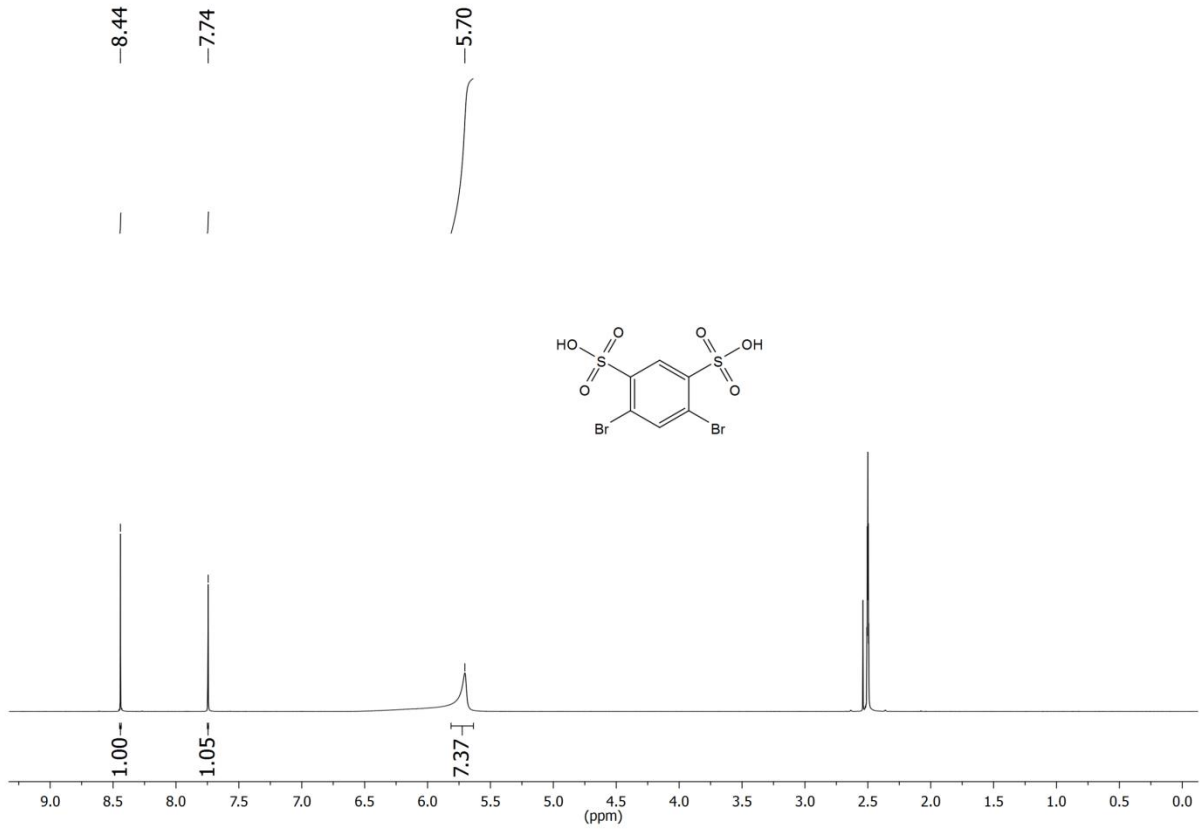

^{1}H-NMR (500 MHz, 300 K, DMSO-d6) of **22**

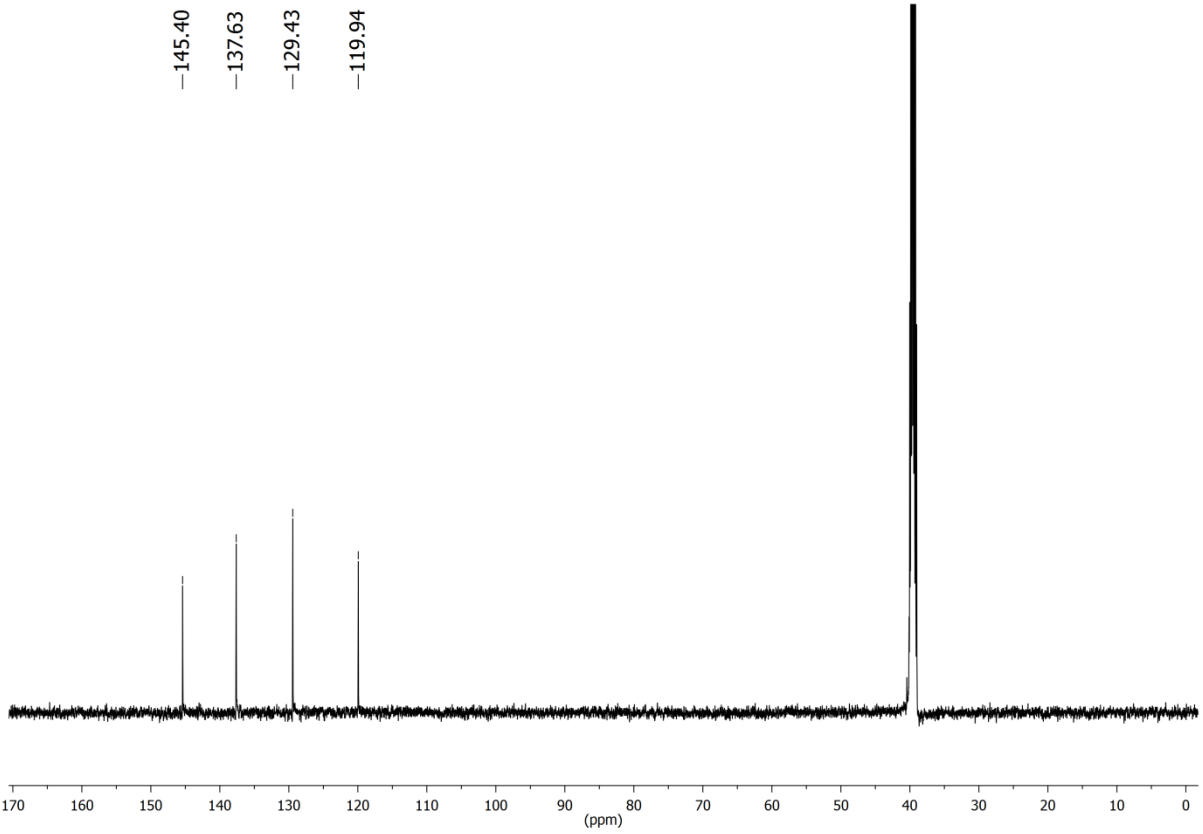

^{13}C-NMR (125 MHz, 300 K, DMSO-d6) of **22**

4,6-Diphosphonobenzene-1,3-disulfonic acid (27)

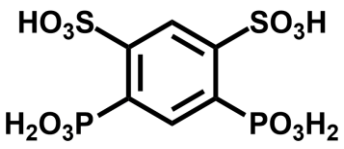

4,6-Dibromobenzene-1,3-disulfonic acid (**22**, 3.00 g, 7.57 mmol) dissolved in water (50 mL) was treated with aqueous tetra-*n*-butylammonium hydroxide (40 % in water) until pH = 7 was reached. The solvent was removed in vacuo and the residue was dried in a vacuum oven at 60 °C for 12 h to obtain the respective tetra-*n*-butylammonium salt. Four microwave vials were charged each with salt (4 x 1.66 g, 4 x 1.89 mmol), palladium(II) chloride (4 x 34 mg, 4 x 189 µmol) and triethyl phosphite (4 x 5 mL, 4 x 20.9 mmol). The vials were irradiated in a microwave oven (max. 200 W, 220 °C) for 60 min. The combined dark brown solution was added to a mixture of ethyl acetate (150 mL) and water (150 mL) in a separatory funnel. The aqueous layer was washed with ethyl acetate (3 x 150 mL) and water was removed in vacuo. The residue was dissolved in a mixture of water (100 mL) and conc. hydrochloric acid (200 mL) and stirred for 12 h at 120 °C. After removing the solvent in vacuo, the residue was dissolved in acetone (100 mL) and mixed with five equivalents of sodium iodide (5.67 g, 37.85 mmol) dissolved in acetone (50 mL). The precipitate was collected by filtration and recrystallized from a mixture of ethanol and water. To exchange the sodium ions, the residue was dissolved in water and rinsed over a column filled with ion-exchange resin (Dowex 50WX8 hydrogen form). The eluate was concentrated and dried for 24 h at 60 °C in a vacuum oven, to yield a colourless solid.

Yield: 987 mg (2.48 mmol, 33 %)

M. p.: >300 °C

^{1}H-NMR (500 MHz, 300 K, DMSO-d6): δ = 8.61 (t, $^{3}J_{H\text{-}P}$ = 13.9 Hz, 1H, Ar-5-*H*), 8.47 (t, $^{4}J_{H\text{-}P}$ = 4.6 Hz, 1H, Ar-2-*H*), 6.31 (br. s, 6H, PO_3H_2, SO_3H) ppm.

^{13}C-NMR (125 MHz, 300 K, DMSO-d6): δ = 149.0 (s[$d_P d_P$], $J_{C\text{-}P}$ = 9.9 Hz, $J_{C\text{-}P}$ = 3.5 Hz, Ar-1,3-*C*), 138.8 (d[t_P], $^{2}J_{C\text{-}P}$ = 8.9 Hz, Ar-5-*C*), 130.8 (s[$d_P d_P$], $^{1}J_{C\text{-}P}$ = 166.3 Hz, $^{3}J_{C\text{-}P}$ = 11.3 Hz, Ar-4,6-*C*), 126.8 (d[t_P], $^{3}J_{C\text{-}P}$ = 10.8 Hz, Ar-2-*C*) ppm.

^{31}P-NMR (202 MHz, 300 K, DMSO-d6): 8.6 (s, 2P, PO_3H_2) ppm.

MS (ESI_{neg}): *m/z* = 795 $[2M - H]^-$, 397 $[M - H]^-$, 379 $[M - H_3O]^-$.

IR (ATR): $\tilde{\nu}$ = 3127 (aryl-H val.), 2753, 2257, (br., OH), 1654 (H_3O^+) cm^{-1}.

EA ($C_6H_8O_{12}P_2S_2$) (398.20): calcd. C 18.10 H 2.03 S 16.11;
($C_6H_8O_{12}P_2S_2 \cdot 3\ H_2O$) (452.24): calcd. C 15.93 H 3.12 S 14.18;
found C 16.28 H 3.30 S 13.85.

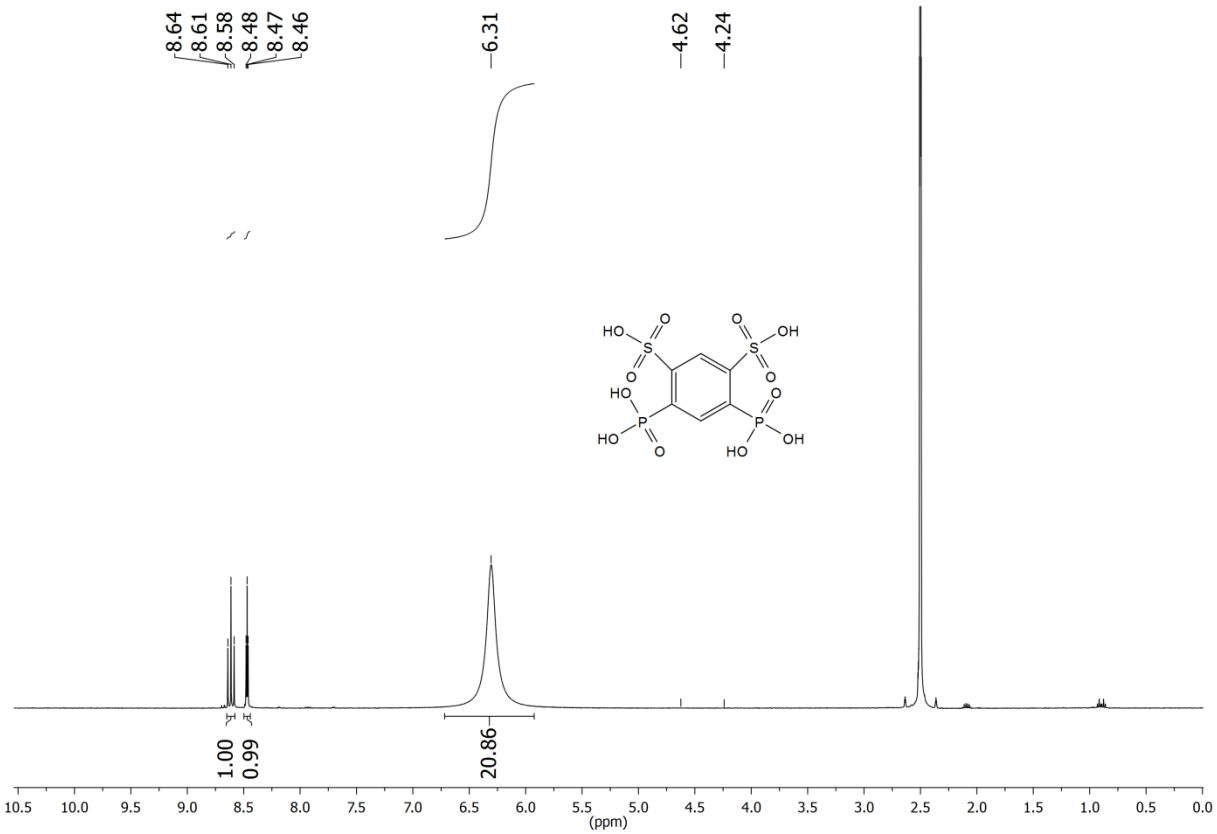

^{1}H-NMR (500 MHz, 300 K, DMSO-d6) of **27**

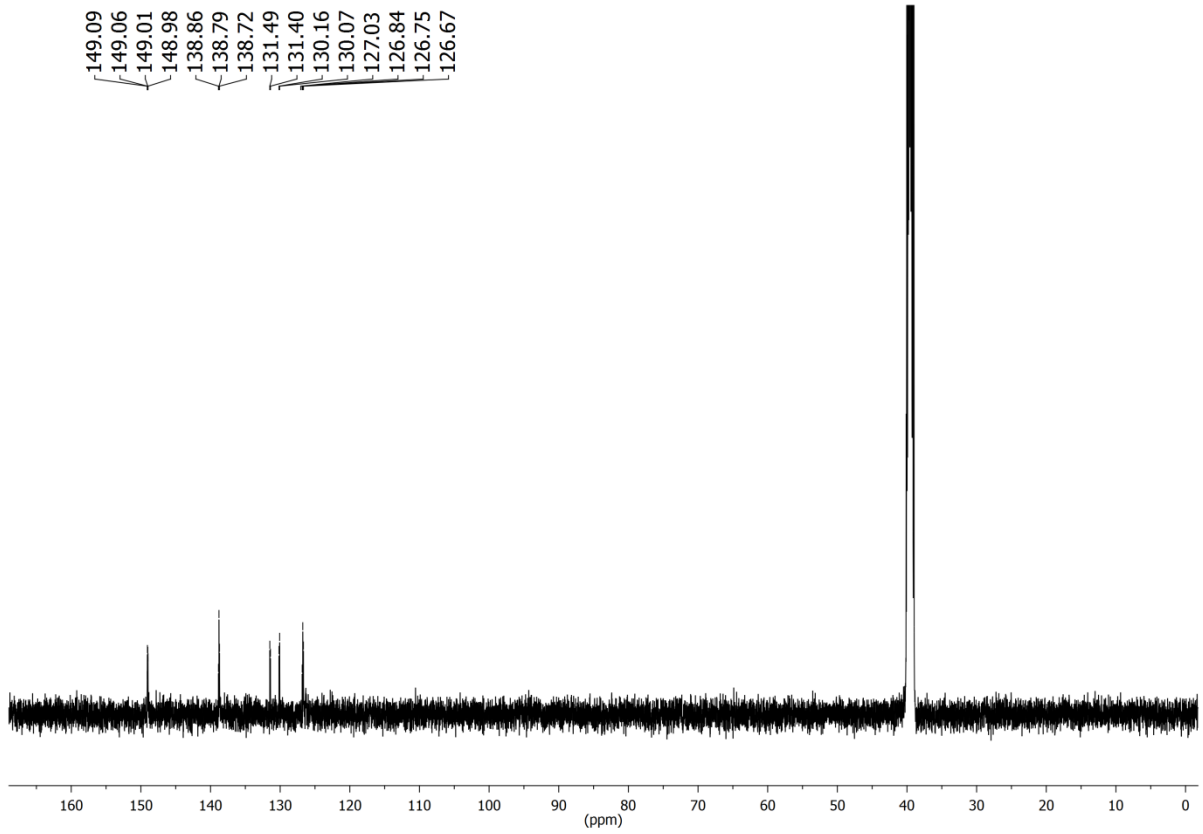

^{13}C-NMR (125 MHz, 300 K, DMSO-d6) of **27**

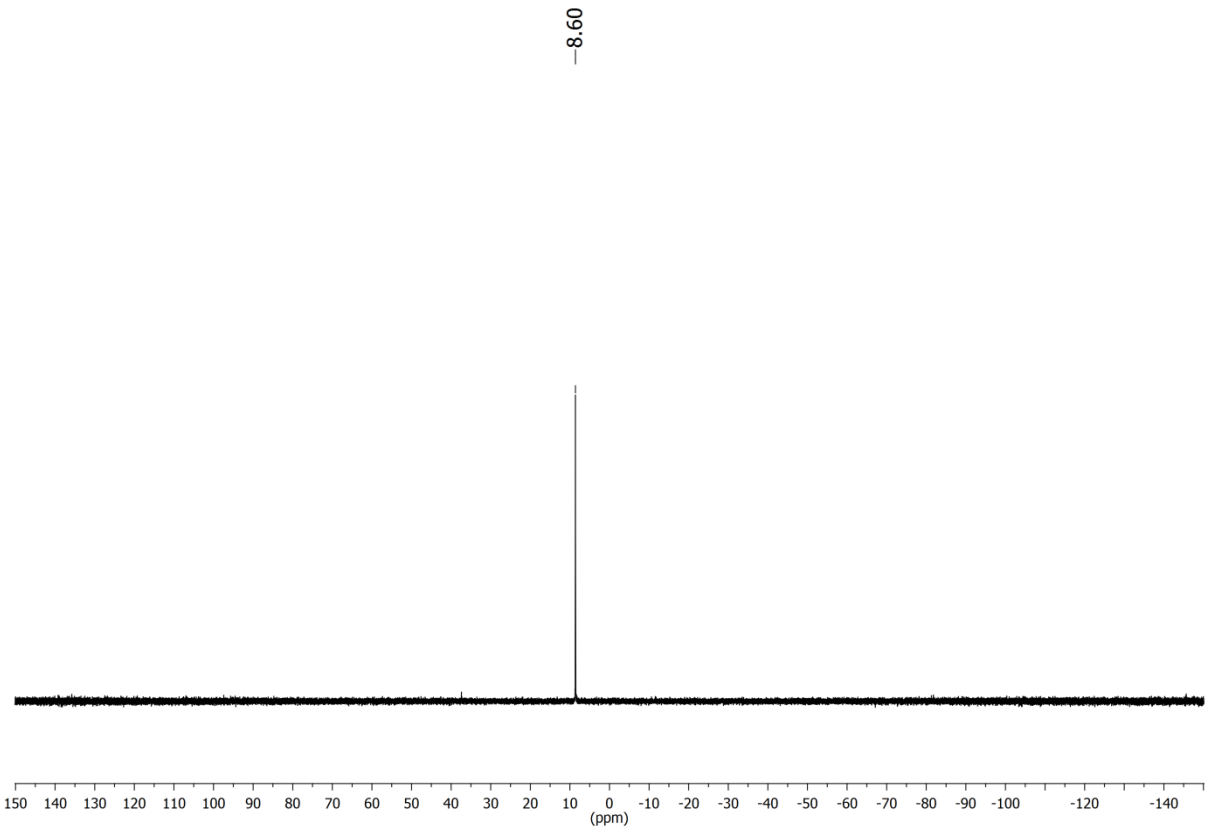

^{31}P-NMR (202 MHz, 300 K, DMSO-d6) of **27**

Procedure for the synthesis of disulfonic acids 19 and 20

A suspension of 1,4-dibromobenzene (**17**, 10.00 g, 42.39 mmol) and fuming sulfuric acid (20 - 30 % SO_3) (40 mL) was stirred for 24 h at 200 °C. The brown solution was poured into ice-cold water (300 mL) and treated with sodium carbonate until pH = 7 was reached. Water was removed in vacuo and the residue was dried for 2 d at 60 °C in a vacuum oven. *N*,*N*-Dimethylformamide (200 mL) was added to the dried solid and the suspension was stirred for 6 h at 60 °C. Undissolved sodium sulfate was removed by filtration and the DMF was evaporated in vacuo. The obtained solid was dried for 5 d at 60 °C in a vacuum oven. The residue, which is a mixture of 2,5-dibromobenzene-1,3-disulfonic acid disodium salt and 2,5-dibromobenzene-1,4-disulfonic acid disodium salt, was extracted with ethanol using Soxhlet extraction. Because the 2,5-dibromobenzene-1,4-disulfonic acid sodium salt is insoluble in ethanol, it stayed in the extraction thimble and was investigated by ^{1}H- and ^{13}C-NMR to determine the extraction time. When only pure 2,5-dibromobenzene-1,4-disulfonic acid sodium salt was left in the thimble, the extraction was stopped. The colourless solid in the thimble was dried for 1 d at 60 °C in a vacuum oven. Evaporation of ethanol in vacuo from the filtrate gave pure 2,5-dibromobenzene-1,3-disulfonic acid sodium salt. The residue was dried for 1 d at 60 °C in a vacuum oven to give a colourless solid. To exchange the sodium ions, the respective sodium salt was dissolved in water and rinsed over a column filled with ion-exchange resin (Dowex 50WX8 hydrogen form). The eluate was concentrated and dried for 24 h at 60 °C in a vacuum oven, to yield a colourless solid in both cases.

2,5-Dibromobenzene-1,3-disulfonic acid (19)

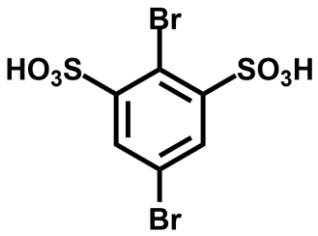

Yield: 10.64 g (26.9 mmol, 63 %)

M. p.: 220 °C

^{1}H-NMR (500 MHz, 300 K, DMSO-d6): δ = 8.02 (s, 2H, Ar-4,6-*H*), 5.29 (br. s, 2H, SO_3*H*) ppm.

^{13}C-NMR (125 MHz, 300 K, DMSO-d6): δ = 150.4 (s, Ar-1,3-*C*), 131.4 (d, Ar-4,6-*C*), 118.3 (s, Ar-5-*C*), 117.2 (s, Ar-2-*C*) ppm.

MS (EI): *m/z* = 398, 396, 394 (56, 100, 49) $[M]^{+\cdot}$, 316, 314, 312 (74, 94, 36) $[M - H_2O_3S]^{+\cdot}$, 235, 233 (79, 47) $[M - H_2O_3S - Br]^{+\cdot}$.

HRMS (EI): *m/z* = $C_6H_4{}^{79}Br_2O_6S_2$ calcd. 393.7816; found 393.7813 (Δ 0.8 ppm);
$C_6H_4{}^{79}Br^{81}BrO_6S_2$ calcd. 395.7796; found 395.7795 (Δ 0.2 ppm);
$C_6H_4{}^{81}Br_2O_6S_2$ calcd. 397.7775; found 317.7774 (Δ 0.3 ppm).

IR (ATR): $\tilde{\nu}$ = 2518, 2163 (br., OH), 1749, 1630 (H_3O^+), 1548 (arom. C=C) cm^{-1}.

EA ($C_6H_4Br_2O_6S_2$) (396.03): calcd. C 18.20 H 1.02 S 16.19;
($C_6H_4Br_2O_6S_2 \cdot 2\ H_2O$) (432.06): calcd. C 16.68 H 1.87 S 14.84;
found C 17.05 H 1.89 S 15.09.

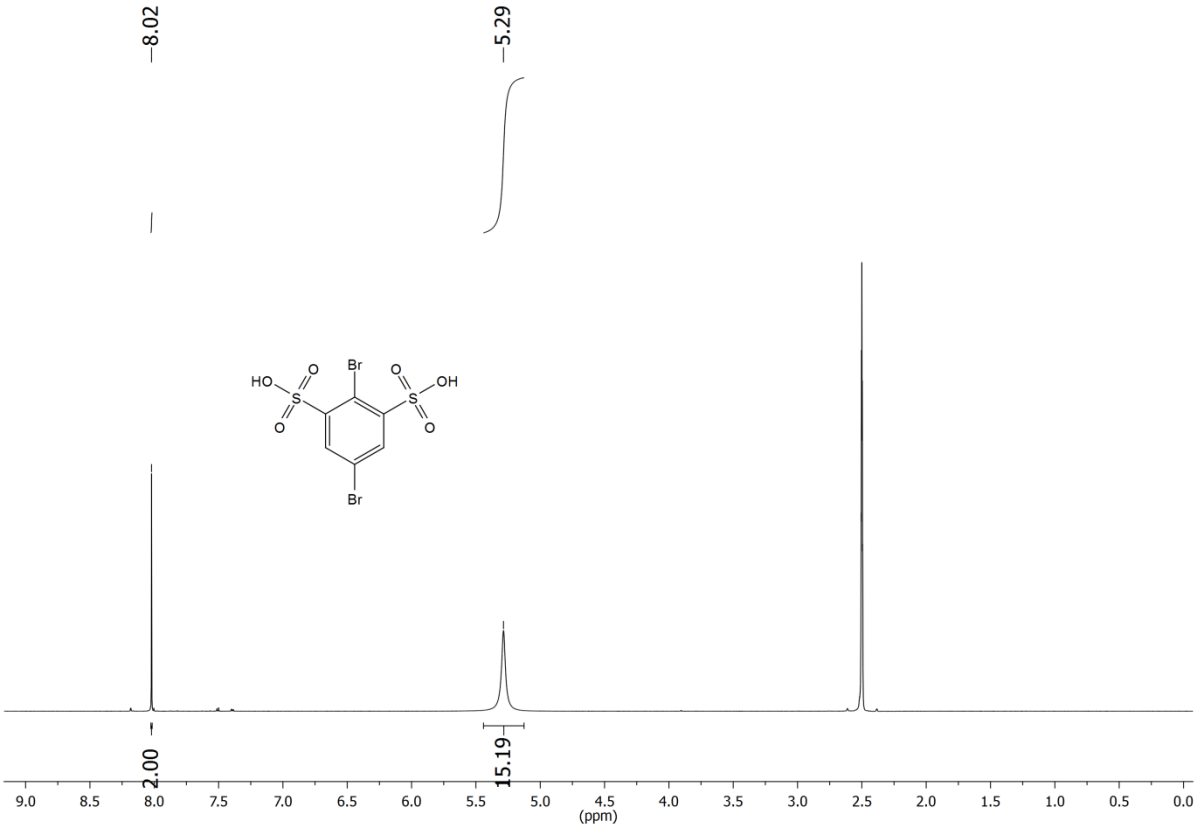

^{1}H-NMR (500 MHz, 300 K, DMSO-d6) of **19**

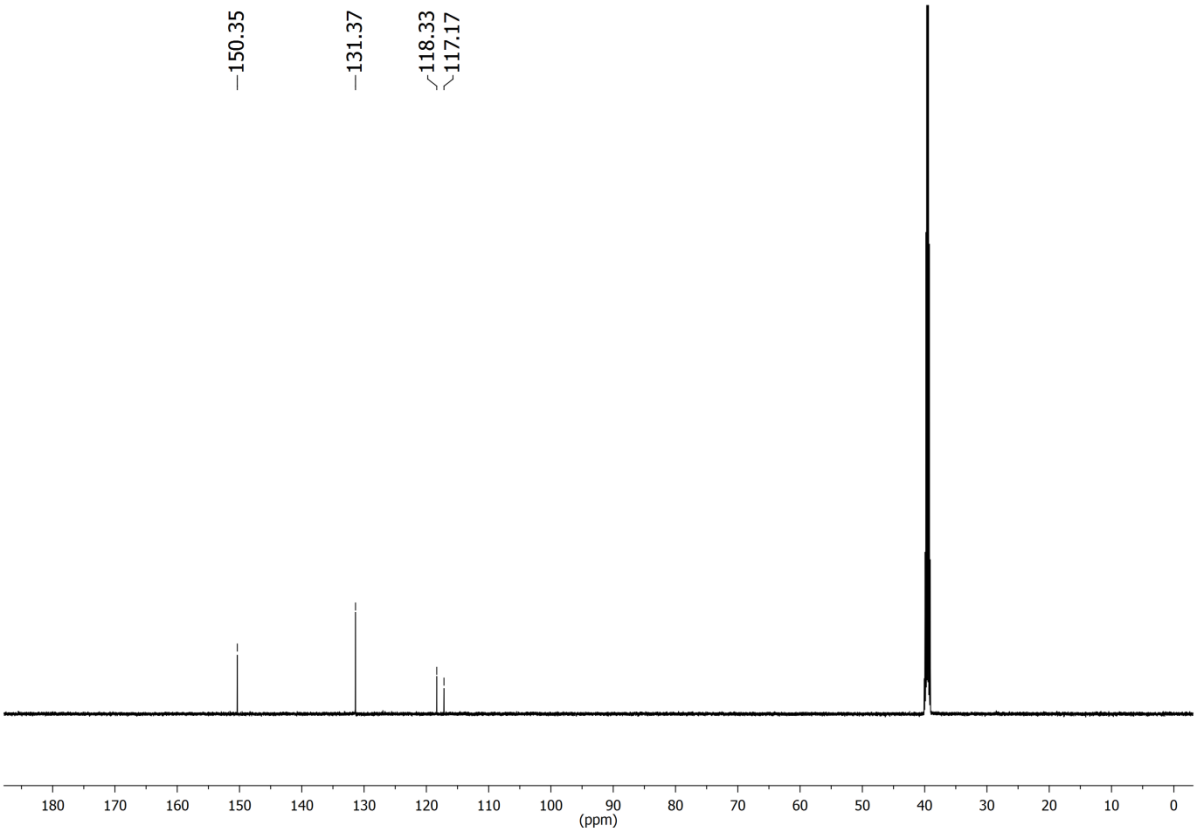

^{13}C-NMR (125 MHz, 300 K, DMSO-d6) of **19**

2,5-Dibromobenzene-1,4-disulfonic acid (20)

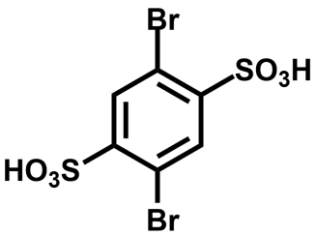

Yield: 4.56 g (11.5 mmol, 27 %) (Lit.[3]: 38 % of the sodium salt)

M. p.: >300 °C

^{1}H-NMR (500 MHz, 300 K, DMSO-d6): δ = 8.00 (s, 2H, Ar-3,6-*H*), 4.59 (br. s, 2H, SO_3*H*) ppm.

^{13}C-NMR (125 MHz, 300 K, DMSO-d6): δ = 148.0 (s, Ar-1,4-*C*), 134.0 (d, Ar-3,6-*C*), 117.5 (s, Ar-2,5-*C*) ppm.

MS (EI): *m/z* = 398, 396, 394 (40, 71, 35) $[M]^{+\cdot}$, 318, 316, 314 (18, 23, 12) $[M - O_3S]^{+\cdot}$, 157 (100) $[MH - O_3S - 2Br]^{+\cdot}$.

HRMS (EI): *m/z* = $C_6H_4{}^{79}Br_2O_6S_2$ calcd. 393.7816; found 393.7803 (Δ 3.3 ppm);
$C_6H_4{}^{79}Br^{81}BrO_6S_2$ calcd. 395.7796; found 395.7786 (Δ 2.5 ppm);
$C_6H_4{}^{81}Br_2O_6S_2$ calcd. 397.7775; found 317.7767 (Δ 2.0 ppm).

IR (ATR): $\tilde{\nu}$ = 3112 (aryl-H val.), 2480, 2082 (br., OH), 1697 (H_3O^+) cm^{-1}.

EA ($C_6H_4Br_2O_6S_2$) (396.03): calcd. C 18.20 H 1.02 S 16.19;
($C_6H_4Br_2O_6S_2 \cdot 2\ H_2O$) (432.06): calcd. C 16.68 H 1.87 S 14.84;
found C 16.99 H 1.90 S 14.92.

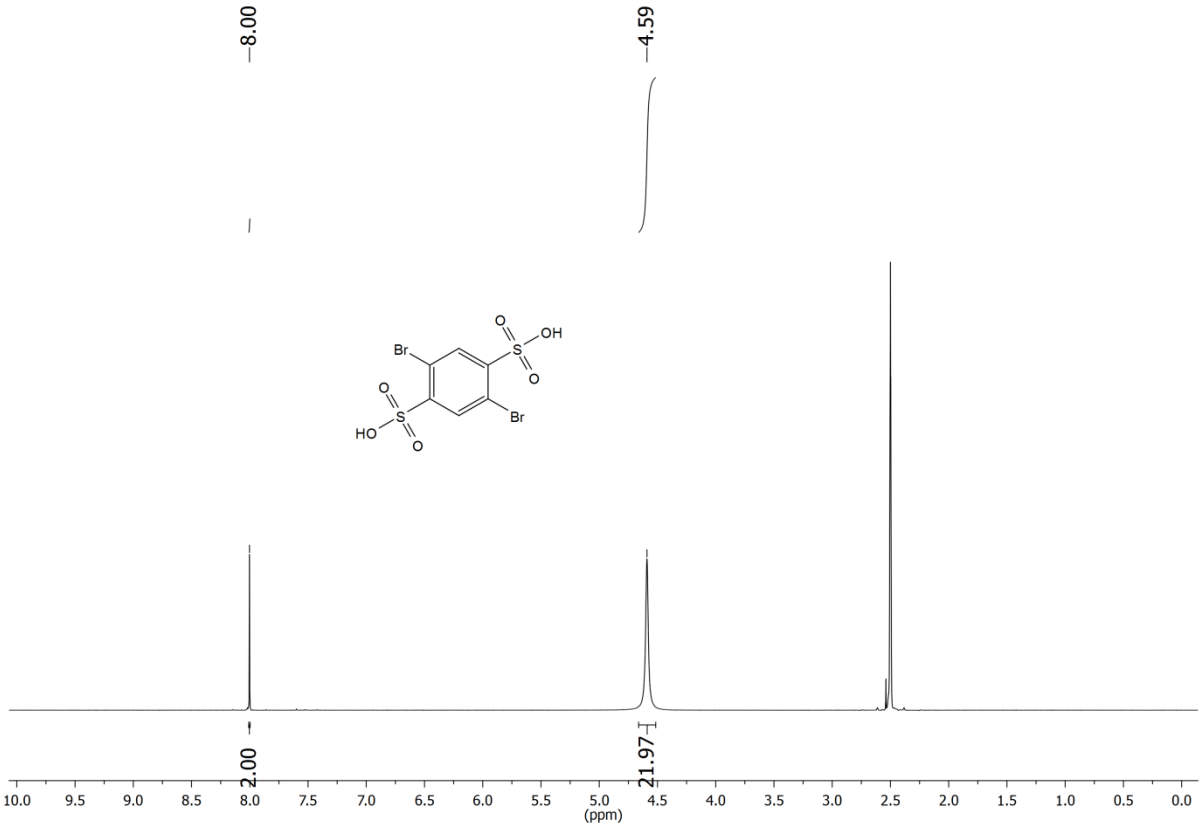

^{1}H-NMR (500 MHz, 300 K, DMSO-d6) of **20**

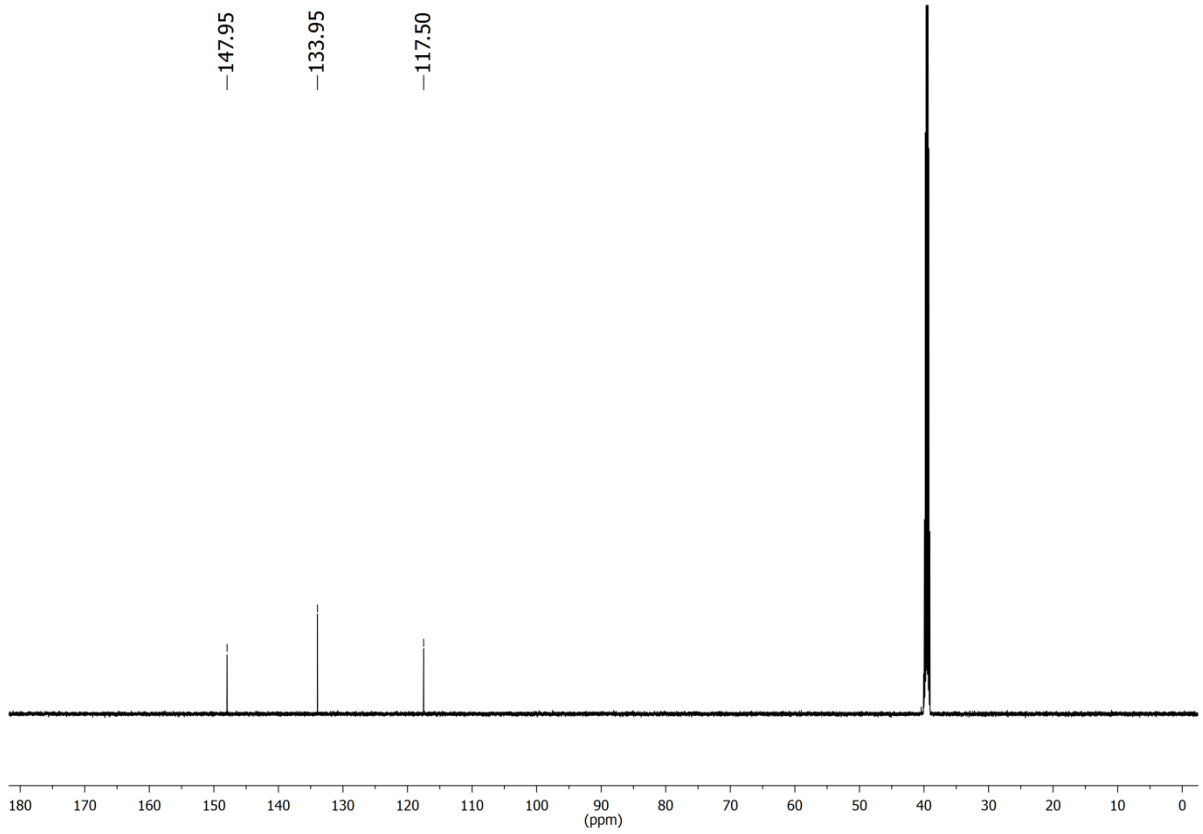

^{13}C-NMR (125 MHz, 300 K, DMSO-d6) of **20**

2,5-Diphosphonobenzene-1,3-disulfonic acid (28)

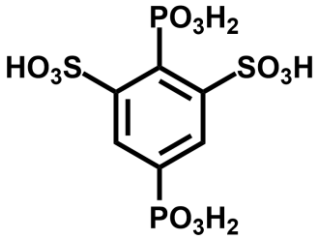

A solution of 2,5-dibromobenzene-1,3-disulfonic acid (**19**, 861 mg, 2.17 mmol) in water (20 mL) was treated with aqueous tetra-*n*-butylammonium hydroxide (40 % in water) until pH = 7 was reached. The solvent was removed in vacuo and the residue was dried in a vacuum oven at 60 °C for 12 h to obtain the respective tetra-*n*-butylammonium salt. Two microwave vials were charged each with salt (2 x 955 mg, 2 x 1.09 mmol), palladium(II) chloride (2 x 19 mg, 2 x 109 µmol) and triethyl phosphite (2 x 4 mL, 2 x 16.7 mmol). The vials were irradiated in a microwave oven (max. 200 W, 220 °C) for 60 min. The combined dark brown solution was added to a mixture of ethyl acetate (100 mL) and water (100 mL) in a separatory funnel. The aqueous layer was washed with ethyl acetate (3 x 100 mL) and water was removed in vacuo. The residue was dissolved in a mixture of water (50 mL) and conc. hydrochloric acid (100 mL) and stirred for 12 h at 120 °C. After removing the solvent in

vacuo, the residue was dissolved in acetone (50 mL) and mixed with five equivalents of sodium iodide (1.63 g, 10.9 mmol) dissolved in acetone (30 mL). The precipitate was collected by filtration and recrystallized two times from a mixture of ethanol and water. To exchange the sodium ions, the residue was dissolved in water and rinsed over a column filled with ion-exchange resin (Dowex 50WX8 hydrogen form). The eluate was concentrated and dried for 24 h at 60 °C in a vacuum oven, to yield a colourless solid.

Yield: 42 mg (105 µmol, 5 %)

M. p.: 158 °C

^{1}H-NMR (500 MHz, 300 K, DMSO-d6): δ = 8.48 (dd, $^{3}J_{H\text{-}P}$ = 13.1 Hz, $^{4}J_{H\text{-}P}$ = 3.6 Hz, 2H, Ar-4,6-*H*), 5.78 (br. s, 6H, PO_3H_2, SO_3H) ppm.

^{13}C-NMR (125 MHz, 300 K, DMSO-d6): δ = 148.6 (s[$d_P d_P$], $J_{C\text{-}P}$ = 12.8 Hz, $J_{C\text{-}P}$ = 8.3 Hz, Ar-1,3-*C*), 136.3 (s[$d_P d_P$], $^{1}J_{C\text{-}P}$ = 180.6 Hz, $^{4}J_{C\text{-}P}$ = 2.7 Hz, Ar-5-*C*), 131.9 (d[$d_P d_P$], $^{2}J_{C\text{-}P}$ = 11.1 Hz, $^{3}J_{C\text{-}P}$ = 11.1 Hz, Ar-4,6-*C*), 129.5 (s[$d_P d_P$], $^{1}J_{C\text{-}P}$ = 161.1 Hz, $^{4}J_{C\text{-}P}$ = 2.9 Hz, Ar-2-*C*) ppm.

^{31}P-NMR (202 MHz, 300 K, DMSO-d6): 9.2 (d, $^{5}J_{P\text{-}P}$ = 3.7 Hz, 1P, PO_3H_2), 7.2 (m_c, 1P, PO_3H_2) ppm.

MS (ESI_{neg}): *m/z* = 795 $[2M - H]^-$, 397 $[M - H]^-$, 379 $[M - H_3O]^-$.

IR (ATR): $\tilde{\nu}$ = 2785, 2219 (br., OH), 1694 (H_3O^+) cm^{-1}.

EA ($C_6H_8O_{12}P_2S_2$) (398.20): calcd. C 18.10 H 2.03 S 16.11;
($C_6H_8O_{12}P_2S_2 \cdot 1\ H_2O$) (416.21): calcd. C 17.31 H 2.42 S 15.41;
found C 17.66 H 2.45 S 15.11.

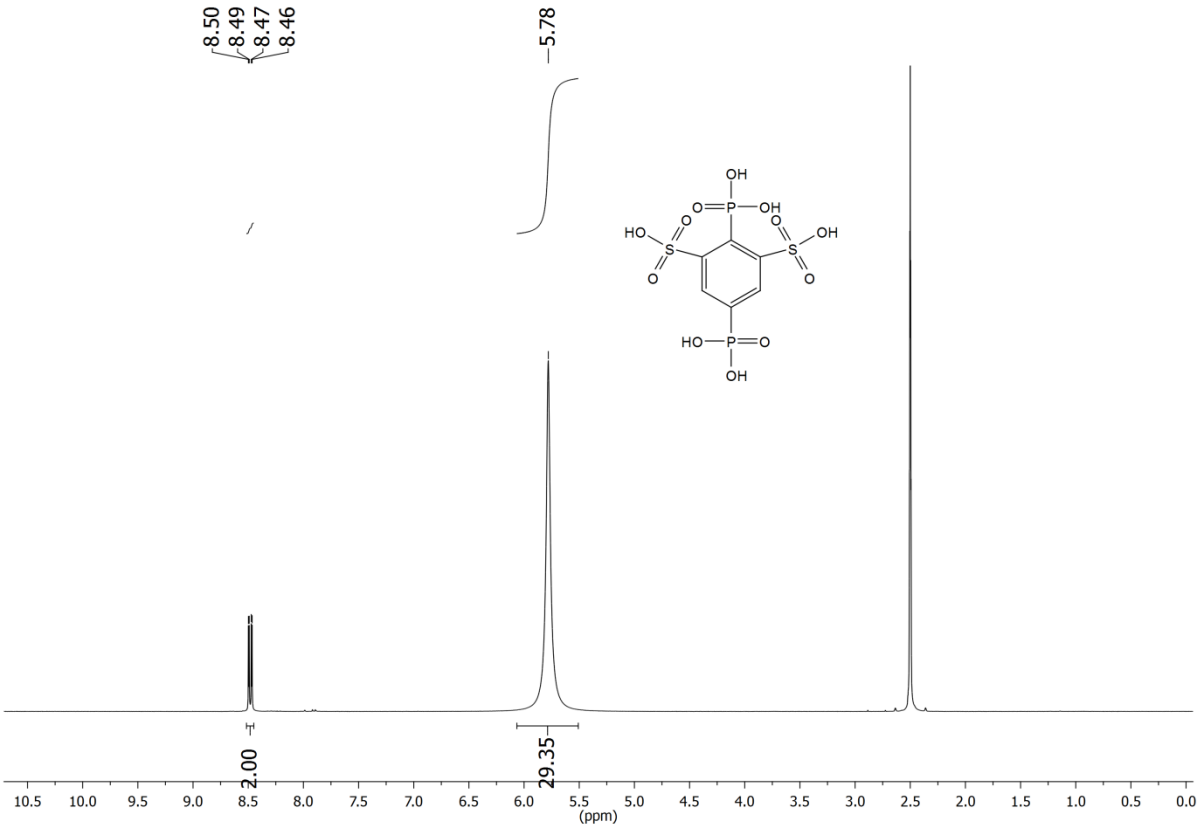

^{1}H-NMR (500 MHz, 300 K, DMSO-d6) of **28**

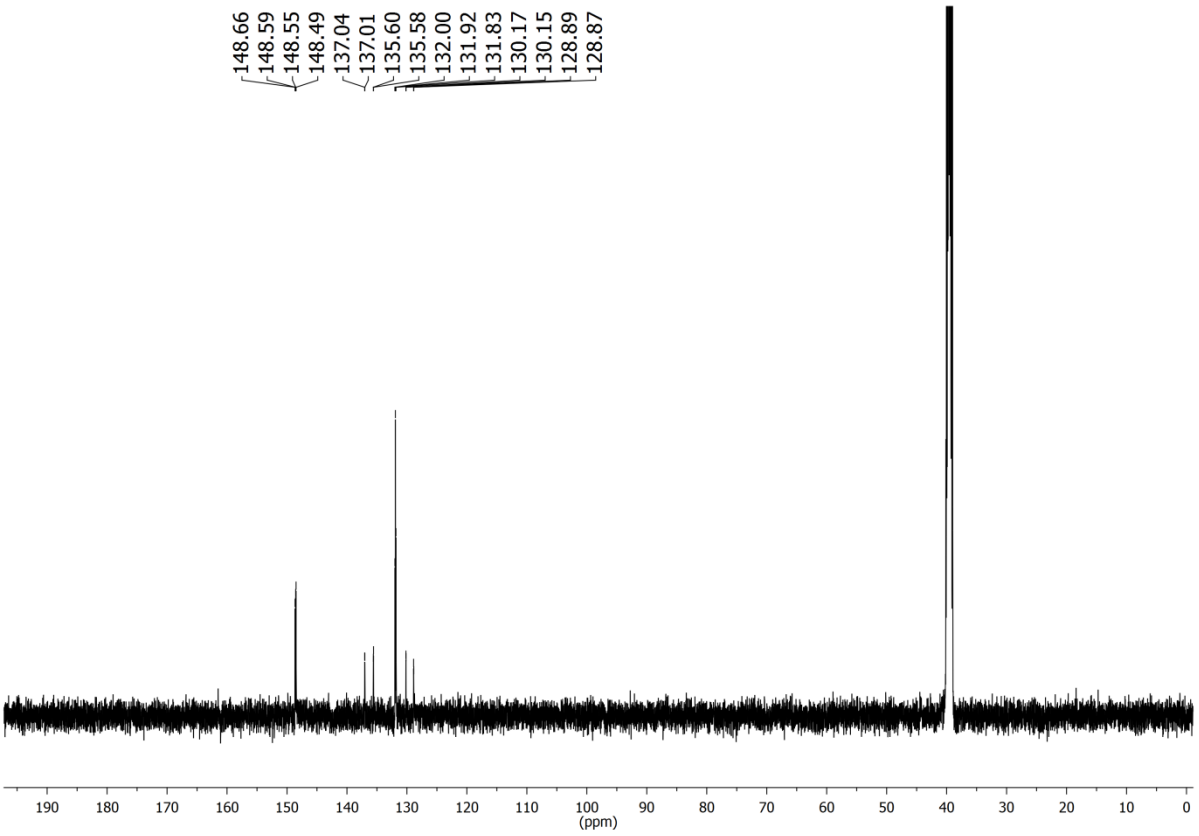

^{13}C-NMR (125 MHz, 300 K, DMSO-d6) of **28**

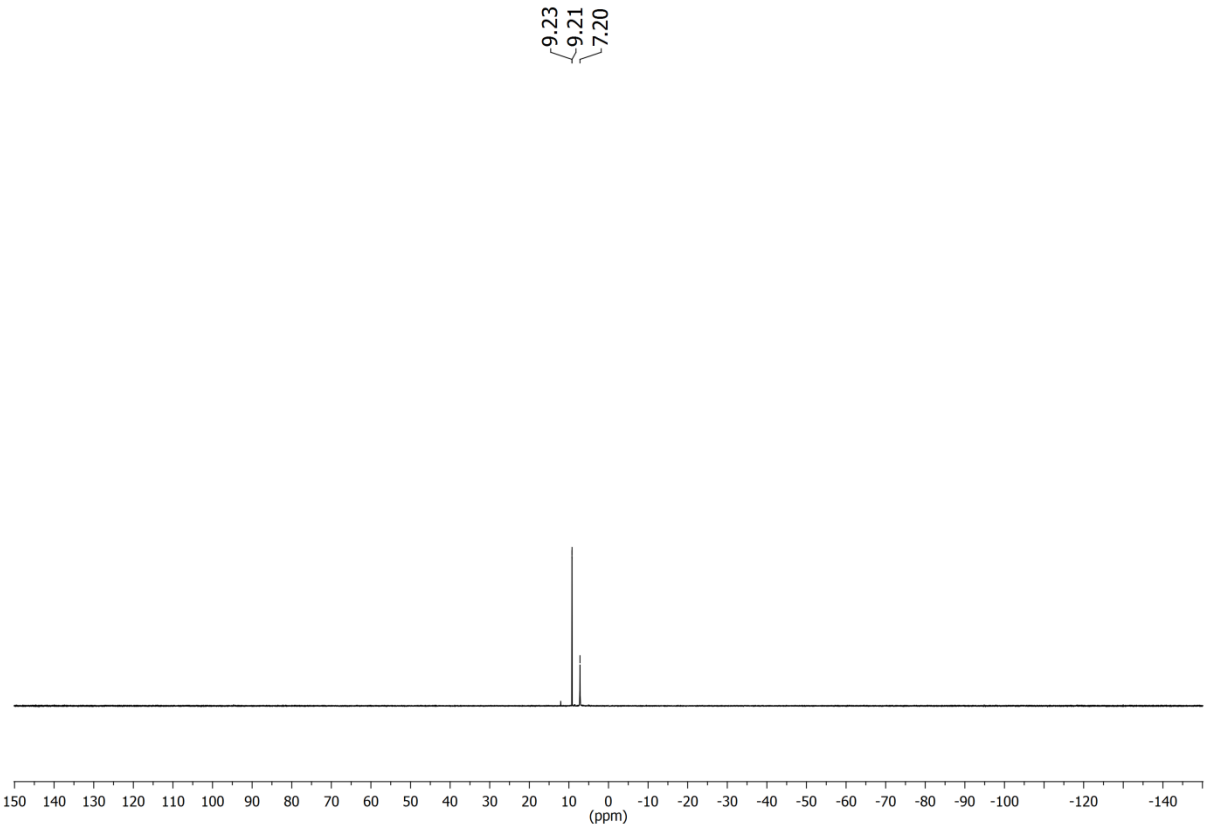

^{31}P-NMR (202 MHz, 300 K, DMSO-d6) of **28**

2,5-Diphosphonobenzene-1,4-disulfonic acid (26)

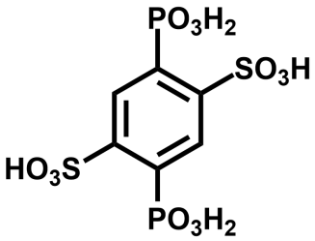

2,5-Dibromobenzene-1,4-disulfonic acid (**20**, 469 mg, 1.18 mmol) dissolved in water (20 mL) was treated with aqueous tetra-*n*-butylammonium hydroxide (40 % in water) until pH = 7 was reached. The solvent was removed in vacuo and the residue was dried in a vacuum oven at 60 °C for 12 h to obtain the respective tetra-*n*-butylammonium salt. A microwave vial was charged with salt (1.04 g, 1.18 mmol), palladium(II) chloride (21 mg, 118 µmol) and triethyl phosphite (4 mL, 16.7 mmol). The vial was irradiated in a microwave oven (max. 200 W, 220 °C) for 60 min. The dark brown solution was added to a mixture of ethyl acetate (100 mL) and water (100 mL) in a separatory funnel. The aqueous layer was washed with ethyl acetate (3 x 100 mL) and water was removed in vacuo. The residue was dissolved in a mixture of water (15 mL) and conc. hydrochloric acid (30 mL) and stirred for 12 h at 120 °C. After removing the solvent in vacuo, the residue was dissolved in acetone (15 mL) and mixed with

five equivalents of sodium iodide (884 mg, 5.90 mmol) dissolved in acetone (10 mL). The precipitate was collected by filtration and recrystallized from a mixture of ethanol and water. To exchange the sodium ions, the residue was dissolved in water and rinsed over a column filled with ion-exchange resin (Dowex 50WX8 hydrogen form). The eluate was concentrated and dried for 24 h at 60 °C in a vacuum oven, to yield a colourless solid.

Yield: 187 mg (470 µmol, 40 %)

M. p.: >300 °C

^{1}H-NMR (500 MHz, 300 K, DMSO-d6): δ = 9.35 (br. s, 6H, PO_3H_2, SO_3H), 8.53 (m_c, 2H, Ar-3,6-*H*) ppm.

^{13}C-NMR (125 MHz, 300 K, DMSO-d6): δ = 147.7 (s[m_P], Ar-1,4-*C*), 133.06 (s[d_Pd_P], $^{1}J_{C\text{-}P}$ = 165.4 Hz, $^{4}J_{C\text{-}P}$ = 2.8 Hz, Ar-2,5-*C*), 133.05 (d[t_P], $^{2}J_{C\text{-}P}$ = 9.8 Hz, Ar-3,6-*C*) ppm.

^{31}P-NMR (202 MHz, 300 K, DMSO-d6): 8.5 (s, 2P, PO_3H_2) ppm.

MS (ESI_{neg}): *m/z* = 795 $[2M - H]^-$, 397 $[M - H]^-$, 379 $[M - H_3O]^-$.

IR (ATR): $\tilde{\nu}$ = 2796, 2250, (br., OH), 1683 (H_3O^+) cm^{-1}.

EA ($C_6H_8O_{12}P_2S_2$) (398.20): calcd. C 18.10 H 2.03 S 16.11;
($C_6H_8O_{12}P_2S_2 \cdot 0.4H_2O \cdot 0.2C_2H_6O$) (414.62): calcd. C 18.54 H 2.43 S 15.47;
found C 18.67 H 2.30 S 15.58.

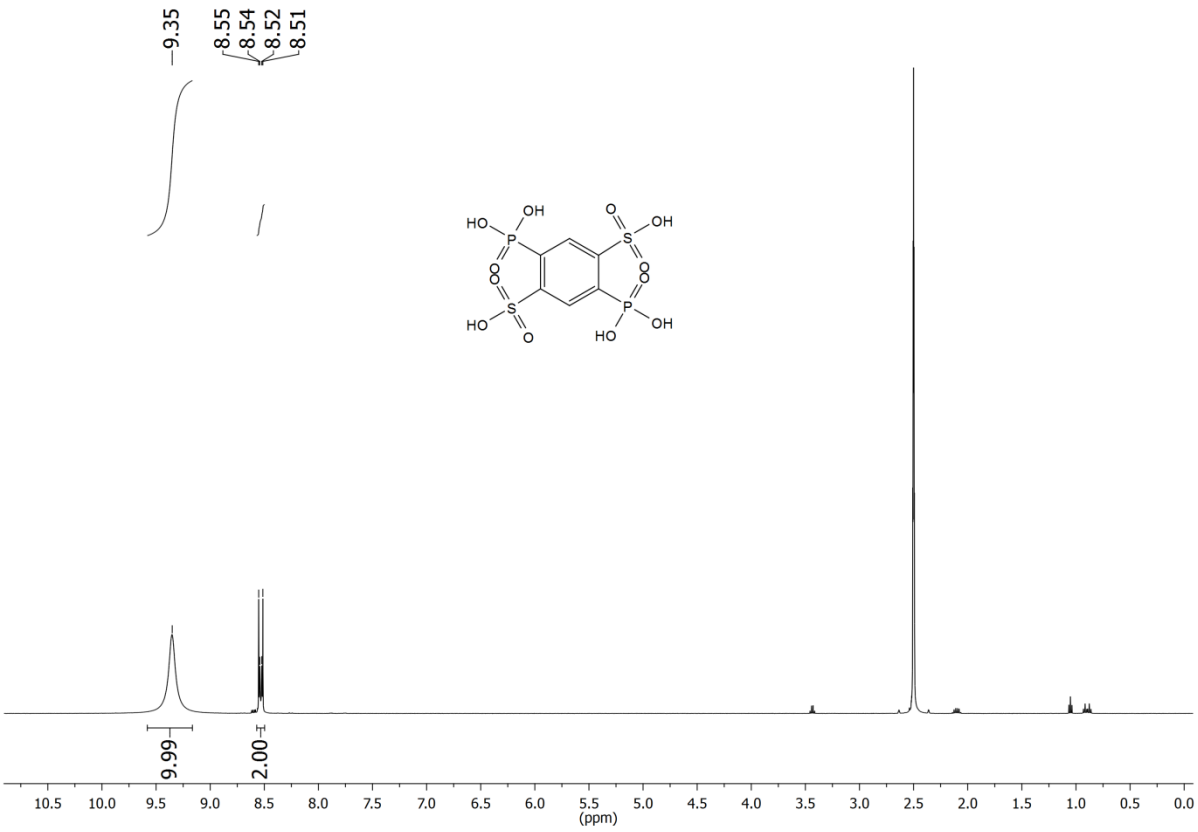

^{1}H-NMR (500 MHz, 300 K, DMSO-d6) of **26**

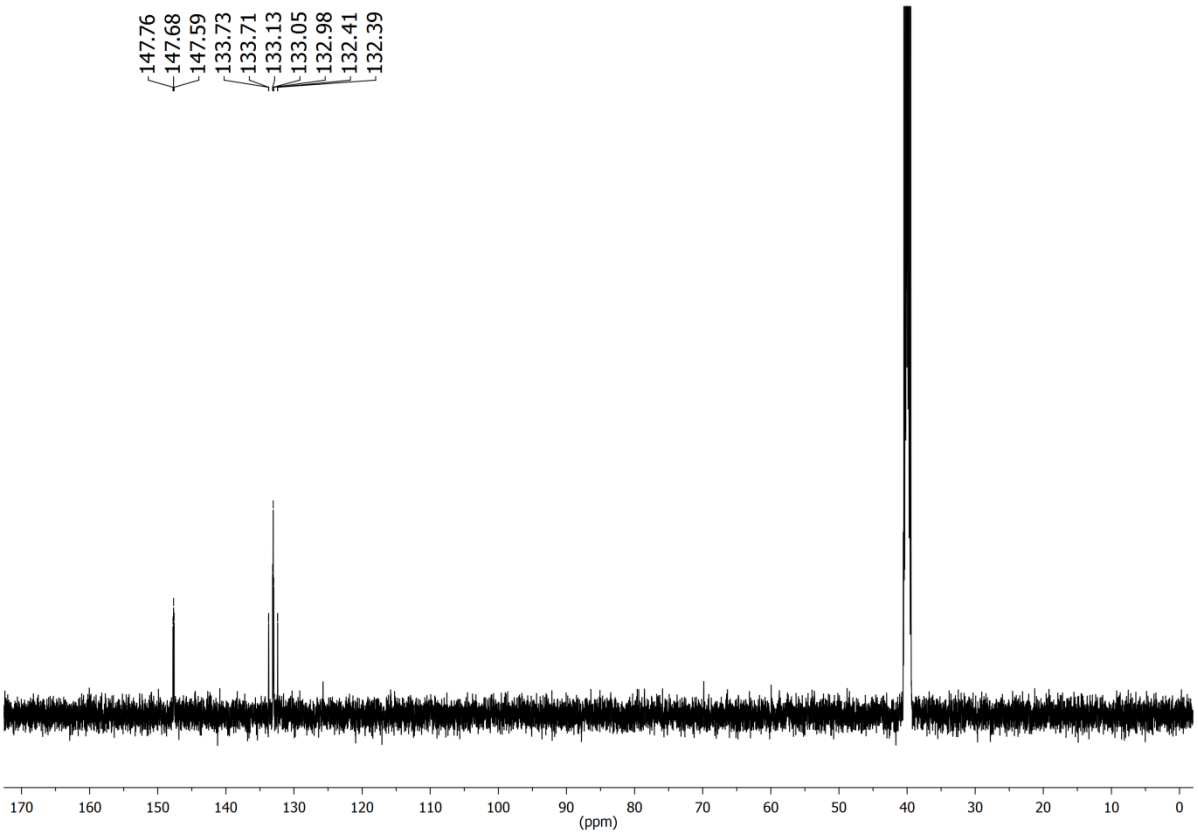

^{13}C-NMR (125 MHz, 300 K, DMSO-d6) of **26**

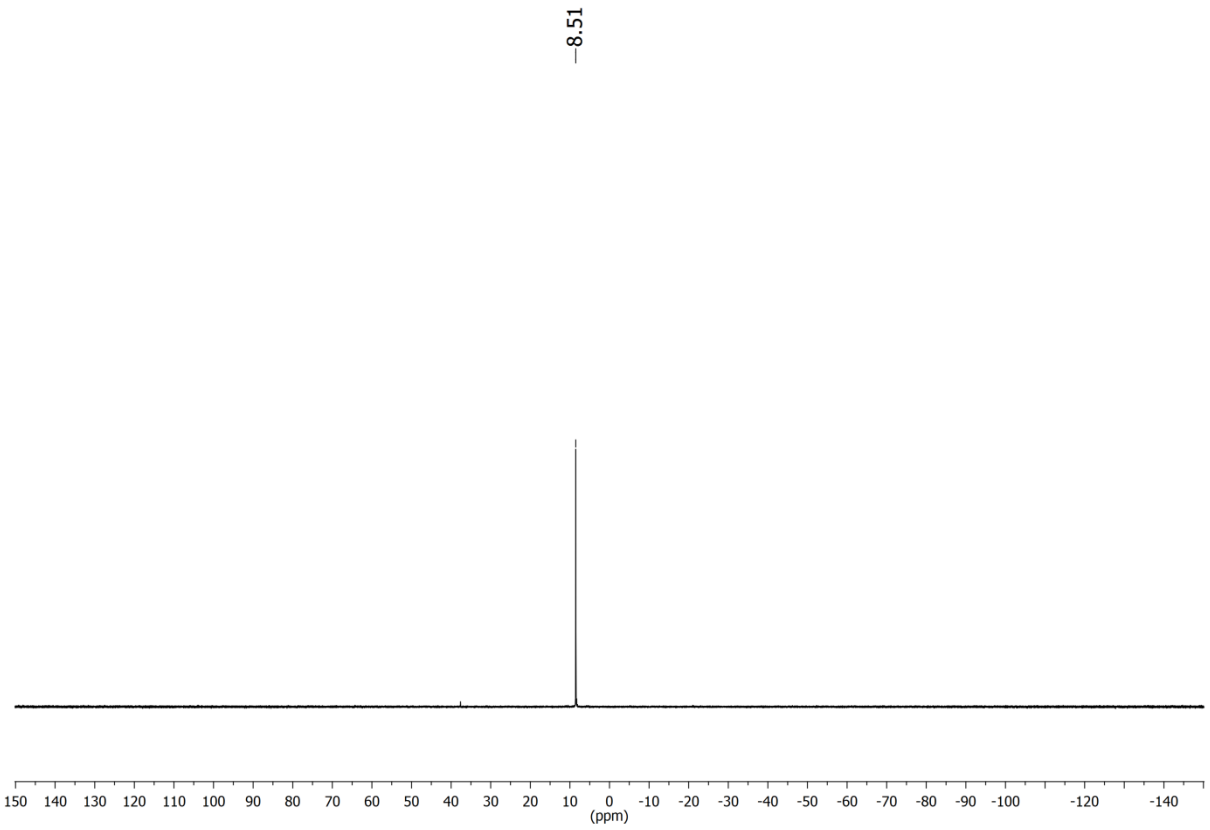

^{31}P-NMR (202 MHz, 300 K, DMSO-d6) of **26**

5-Bromobenzene-1,3-disulfonic acid (13)

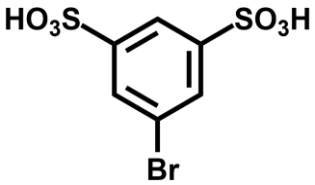

To conc. sulfuric acid (40 mL) was added benzene-1,3-disulfonic acid disodium salt (**12**, 10.0 g, 35.44 mmol) and the suspension was stirred until everything was dissolved. *N*-bromosuccinimide (6.94 g, 38.98 mmol) was added in portions and the reaction mixture was stirred for 12 h at room temp..The solution was poured into water (500 mL) and neutralized with calcium hydroxide. Undissolved calcium sulfate was removed by filtration. After removing the water in vacuo, the residue was dried in a vacuum oven at 60 °C for 12 h. To remove impurities of unreacted benzene-1,3-disulfonic acid disodium salt, the residue was dissolved in water (250 mL) and tetra-*n*-butylammonium bromide (25.1 g, 77.88 mmol) was added. The aqueous solution was extracted with dichloromethane (3 x 150 mL) and the organic layer was dried with magnesium sulfate. After removing the solvent in vacuo, the residue was dissolved in acetone (50 mL) and mixed with four equivalents of sodium iodide (21.22 g, 141.6 mmol) dissolved in acetone (100 mL). The precipitate was collected by

filtration and washed with acetone (250 mL). To exchange the sodium ions, the residue was dissolved in water and rinsed over a column filled with ion-exchange resin (Dowex 50WX8 hydrogen form). The eluate was concentrated and dried for 24 h at 60 °C in a vacuum oven, to yield a colourless solid.

Yield: 9.34 g (29.5 mmol, 83 %)

M. p.: 134 °C

^{1}H-NMR (500 MHz, 300 K, DMSO-d6): δ = 7.84 (t, ^{4}J = 1.4 Hz, 1H, Ar-2-*H*), 7.63 (d, ^{4}J = 1.4 Hz, 2H, Ar-4,6-*H*), 6.80 (br. s, 2H, SO_3H) ppm.

^{13}C-NMR (125 MHz, 300 K, DMSO-d6): δ = 150.0 (s, Ar-1,3-*C*), 128.1 (d, Ar-4,6-*C*), 122.0 (d, Ar-2-*C*), 120.1 (s, Ar-5-*C*) ppm.

MS (EI): *m/z* = 318, 316 (100, 94) $[M]^{+\cdot}$.

HRMS (EI): *m/z* = $C_6H_5{}^{79}BrO_6S_2$ calcd. 315.8711; found 315.8705 (Δ 1.8 ppm);
$C_6H_5{}^{81}BrO_6S_2$ calcd. 317.8690; found 317.8686 (Δ 1.5 ppm).

IR (ATR): $\tilde{\nu}$ = 3081 (aryl-H val.), 2634, 2187, (br., OH), 1685 (H_3O^+) 1568 (arom. C=C) cm^{-1}.

EA ($C_6H_5BrO_6S_2$) (317.13): calcd. C 22.72 H 1.59 S 20.22;
($C_6H_5BrO_6S_2 \cdot 2\ H_2O$) (353.16): calcd. C 20.41 H 2.57 S 18.16;
found C 20.58 H 2.49 S 17.98.

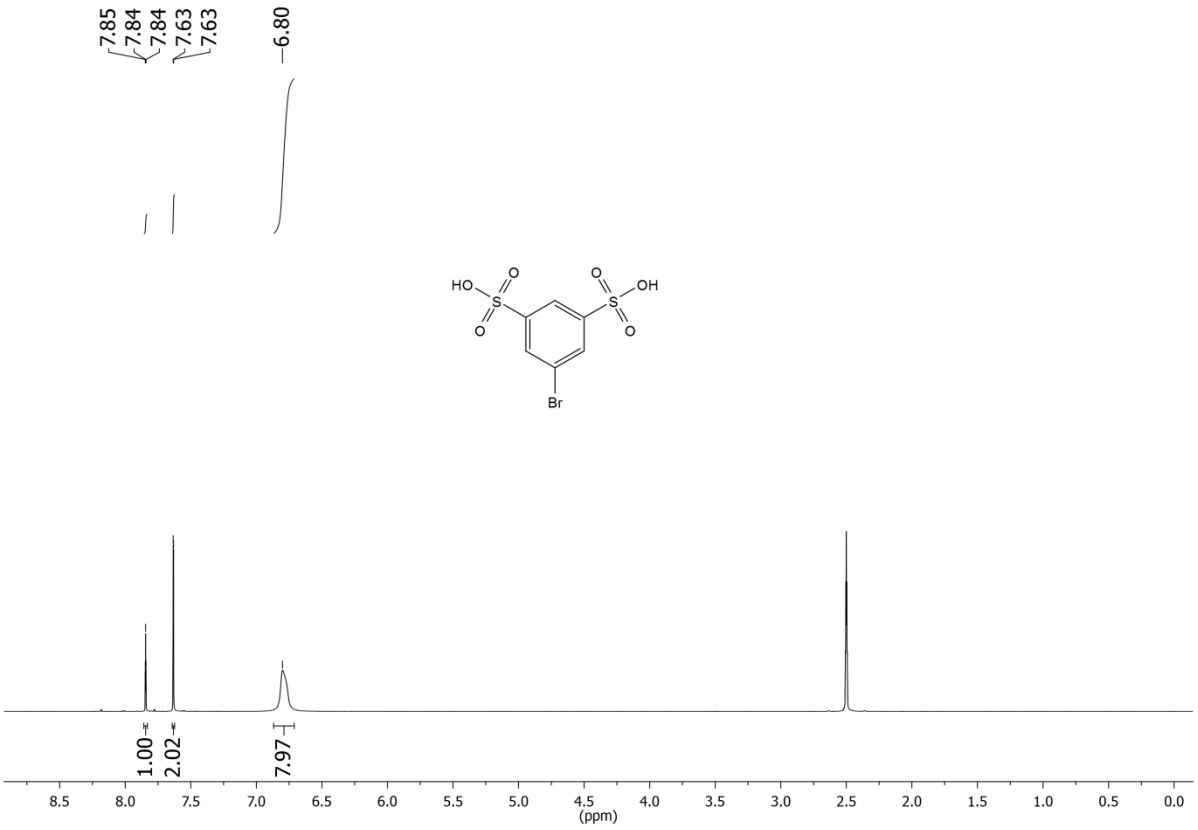

^{1}H-NMR (500 MHz, 300 K, DMSO-d6) of **13**

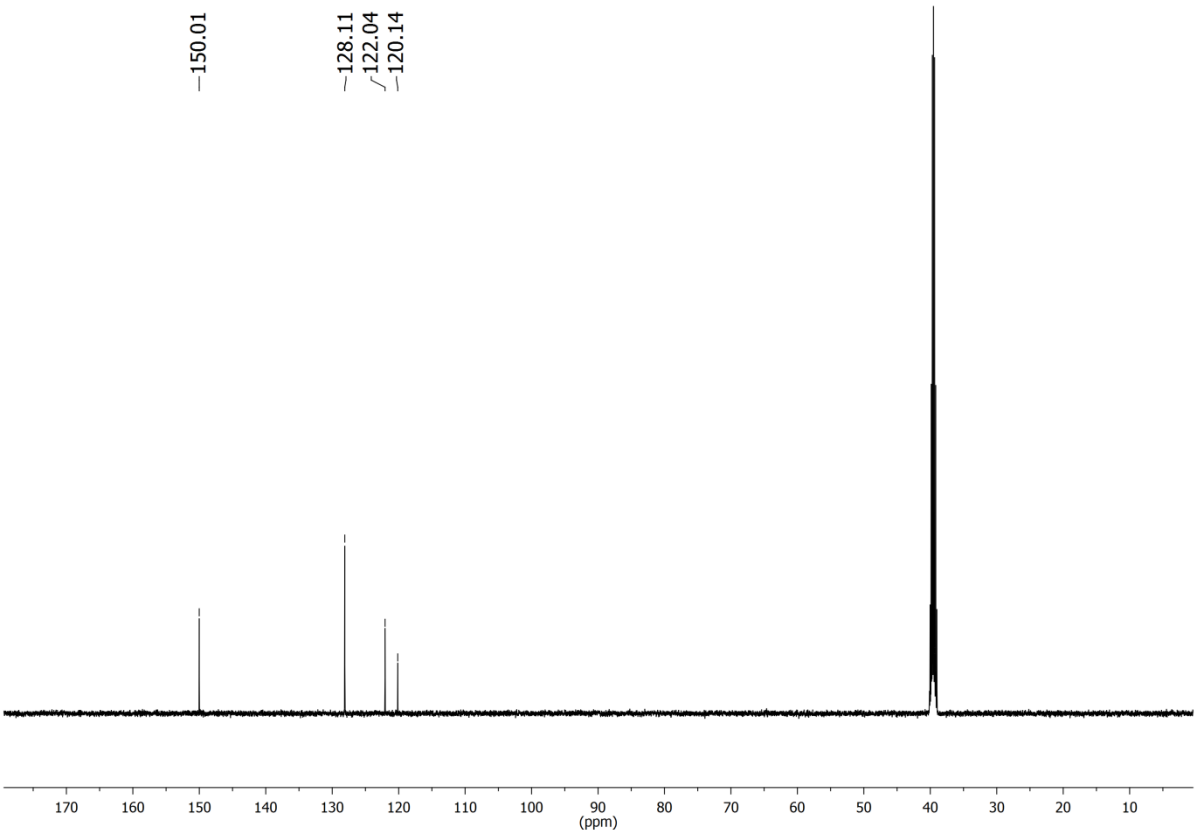

^{13}C-NMR (125 MHz, 300 K, DMSO-d6) of **13**

5-Phosphonobenzene-1,3-disulfonic acid (23)

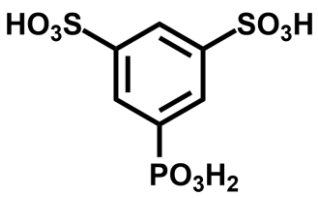

5-Bromobenzene-1,3-disulfonic acid (**13**, 992 mg, 2.75 mmol) dissolved in water (20 mL) was treated with aqueous tetra-*n*-butylammonium hydroxide (40 % in water) until pH = 7 was reached. The solvent was removed in vacuo and the residue was dried in a vacuum oven at 60 °C for 12 h to obtain the respective tetra-*n*-butylammonium salt. Two microwave vials were charged with salt (2 x 1.09 g, 2 x 1.37 mmol), palladium(II) chloride (2 x 24 mg, 2 x 137 µmol) and triethyl phosphite (2 x 4 mL, 2 x 16.7 mmol). The vials were irradiated in a microwave oven (max. 200 W, 220 °C) for 60 min. The combined solution was added to a mixture of ethyl acetate (100 mL) and water (100 mL) in a separatory funnel. The aqueous layer was washed with ethyl acetate (3 x 100 mL) and water was removed in vacuo. The residue was dissolved in a mixture of water (20 mL) and conc. hydrochloric acid (40 mL) and stirred for 12 h at 120 °C. After removing the solvent in vacuo, the residue was dissolved in acetone (25 mL) and mixed with five equivalents of sodium iodide (1.65 g, 10.99 mmol) dissolved in acetone (20 mL). The precipitate was collected by filtration and washed with ethanol (150 mL). To exchange the sodium ions, the residue was dissolved in water and rinsed over a column filled with ion-exchange resin (Dowex 50WX8 hydrogen form). The eluate was concentrated and dried for 24 h at 60 °C in a vacuum oven, to yield a colourless solid.

Yield: 684 mg (2.15 mmol, 78 %)

M. p.: 225 °C

^{1}H-NMR (500 MHz, 300 K, DMSO-d6): δ = 8.76 (br. s, 4H, PO_3H_2, SO_3H), 7.99 (dt, ^{4}J = 1.7 Hz, $^{5}J_{H\text{-}P}$ = 1.0 Hz, 1H, Ar-2-*H*), 7.91 (dd, $^{3}J_{H\text{-}P}$ = 13.0 Hz, ^{4}J = 1.7 Hz, 1H, Ar-4,6-*H*) ppm.

^{13}C-NMR (125 MHz, 300 K, DMSO-d6): δ = 147.5 (s[d_P], $^{3}J_{C\text{-}P}$ = 13.8 Hz, Ar-1,3-*C*), 133.06 (s[d_P], $^{1}J_{C\text{-}P}$ = 180.0 Hz, Ar-5-*C*), 127.9 (d[d_P], $^{2}J_{C\text{-}P}$ = 11.2 Hz, Ar-4,6-*C*), 125.4 (d[d_P], $^{4}J_{C\text{-}P}$ = 2.5 Hz, Ar-2-*C*) ppm.

^{31}P-NMR (202 MHz, 300 K, DMSO-d6): 12.2 (s, 1P, PO_3H_2) ppm.

MS (ESI_{neg}): *m/z* = 635 $[2M - H]^-$, 317 $[M - H]^-$, 299 $[M - H_3O]^-$.

IR (ATR): $\tilde{\nu}$ = 2743, 2198 (br., OH), 1684 (H_3O^+), 1588 (arom. C=C) cm^{-1}.

EA ($C_6H_7O_9PS_2$) (318.22): calcd. C 22.65 H 2.22 S 20.15;
($C_6H_7O_9PS_2 \cdot 1\ H_2O$) (336.23): calcd. C 21.43 H 2.70 S 19.07;
found C 21.25 H 2.63 S 18.94.

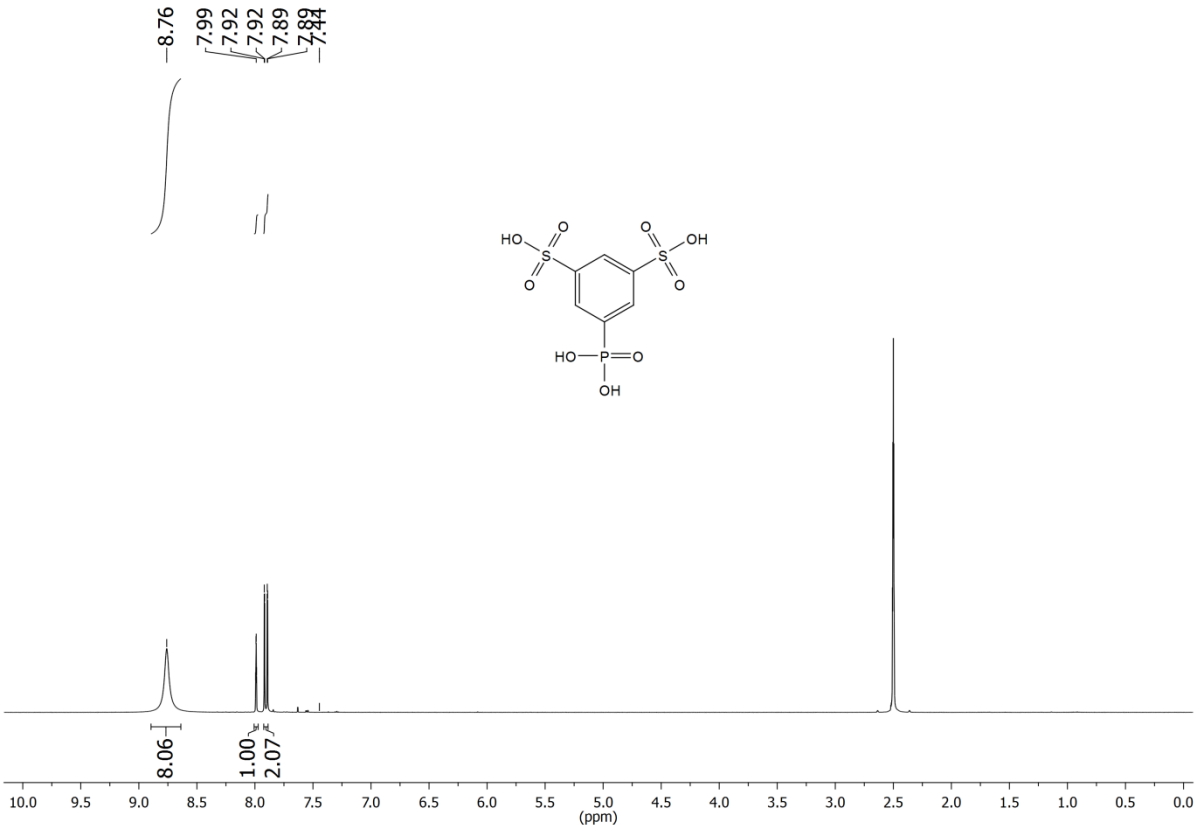

^{1}H-NMR (500 MHz, 300 K, DMSO-d6) of **23**

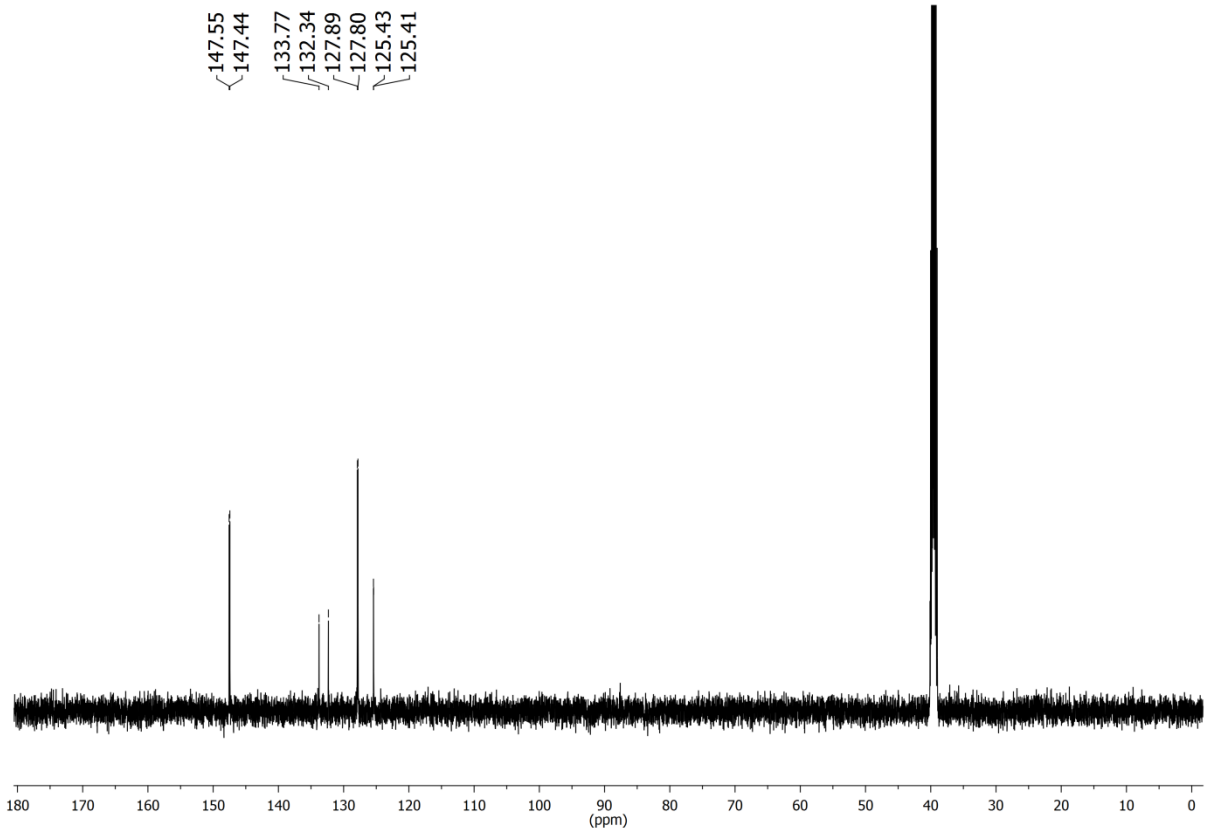

^{13}C-NMR (125 MHz, 300 K, DMSO-d6) of **23**

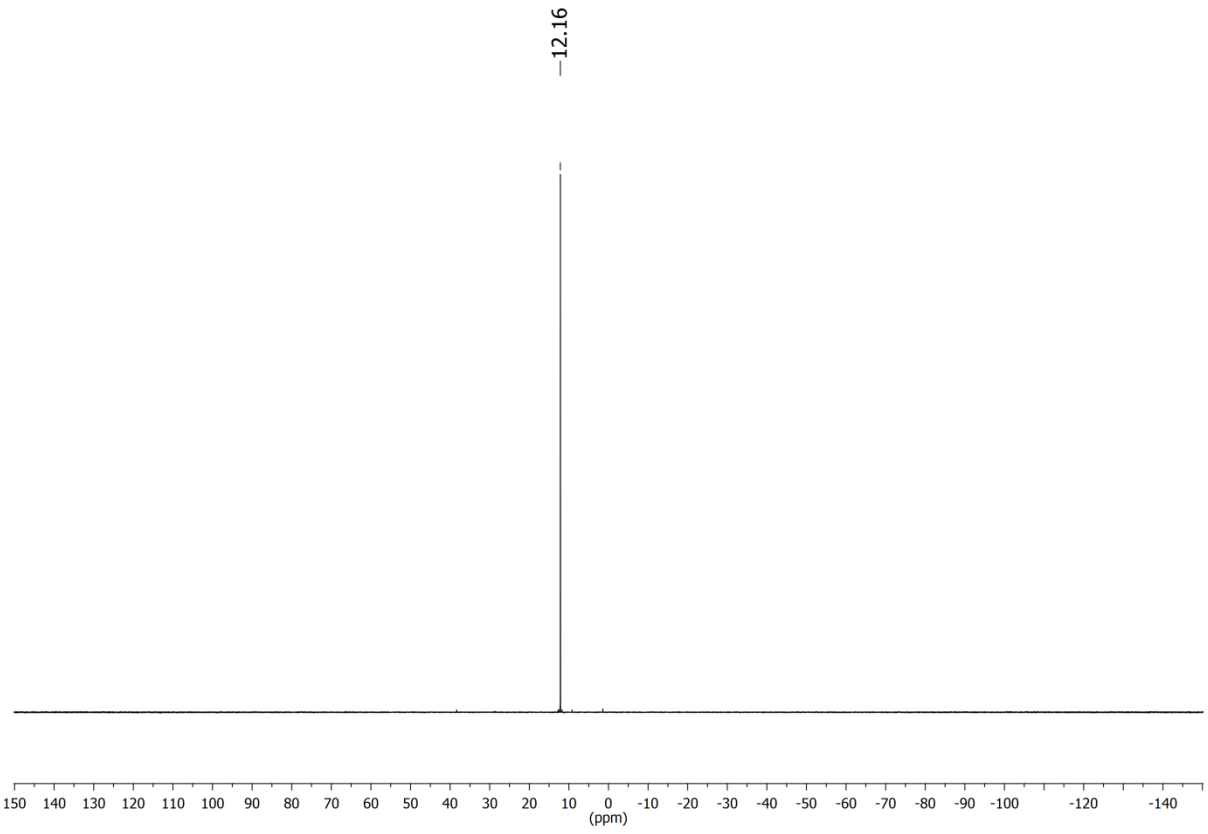

^{31}P-NMR (202 MHz, 300 K, DMSO-d6) of **23**

3,5-Dibromobenzenesulfonic acid (16)

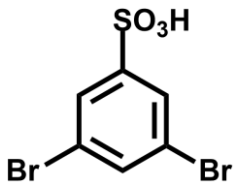

Under nitrogen, 3,5-dibromo-1-(trimethylsilyl)benzene (**14**, 2.86 g, 9.28 mmol) was dissolved in 1,2-dichloroethane (20 mL) and trimethylsilyl chlorosulfonate (1.86 mL, 12.08 mmol) was added. The reaction mixture was stirred for 2 d at 90 °C. After adding 2 M aqueous sodium hydroxide (15 mL), the mixture was stirred at room temp. for 1 h. Water (100 mL) and dichloromethane (100 mL) were added and the aqueous layer was washed with dichloromethane (3 x 100 mL). The aqueous layer was treated with conc. sulfuric acid until pH = 7 was reached. Tetra-*n*-butylammonium iodide (5.15 g, 13.9 mmol) was dissolved in the aqueous layer to transfer the product ions into the organic layer by extraction with dichloromethane (3 x 100 mL). After drying with magnesium sulfate, the solvent was removed in vacuo. The residue was dissolved in acetone (20 mL) and mixed with two equivalents of sodium iodide (2.78 g, 18.58 mmol) dissolved in acetone (30 mL). A precipitate formed within 12 h and was separated by filtration. To exchange the sodium ion, the residue was dissolved in water and rinsed over a column filled with ion-exchange resin (Dowex 50WX8 hydrogen form). The eluate was concentrated and dried for 24 h at 60 °C in a vacuum oven, to yield a colourless solid.

Yield: 2.49 g (7.88 mmol, 85 %)

M. p.: 133 °C

^{1}H-NMR (500 MHz, 300 K, DMSO-d6): δ = 7.80 (t, ^{4}J = 1.8 Hz, 1H, Ar-4-*H*), 7.68 (d, ^{4}J = 1.8 Hz, 2H, Ar-2,6-*H*), 7.66 (br. s, 1H, SO_3H) ppm.

^{13}C-NMR (125 MHz, 300 K, DMSO-d6): δ = 151.9 (s, Ar-1-*C*), 133.4 (d, Ar-4-*C*), 127.5 (d, Ar-2,6-*C*), 122.0 (s, Ar-3,5-*C*) ppm.

MS (EI): *m/z* = 318, 316, 314 (52, 100, 50) $[M]^{+\cdot}$, 237, 235, 233 (13, 31, 16) $[M - HO_3S]^{+\cdot}$.

HRMS (EI): *m/z* = $C_6H_4{}^{79}Br_2O_3{}^{34}S$ calcd. 315.8206; found 315.8212 (Δ 1.8 ppm);
$C_6H_4{}^{79}Br\,{}^{81}BrO_3S$ calcd. 315.8227; found 315.8212 (Δ 5.0 ppm).

IR (ATR): $\tilde{\nu}$ = 3065 (aryl-H val.), 2554, 2187 (br., OH), 1666 (H_3O^+), 1560 (arom. C=C) cm^{-1}.

EA ($C_6H_4Br_2O_3S$) (315.97): calcd. C 22.81 H 1.28 S 10.15;
($C_6H_4Br_2O_3S \cdot 1\ H_2O$) (333.98): calcd. C 21.58 H 1.81 S 9.60;
found C 21.82 H 1.69 S 9.77.

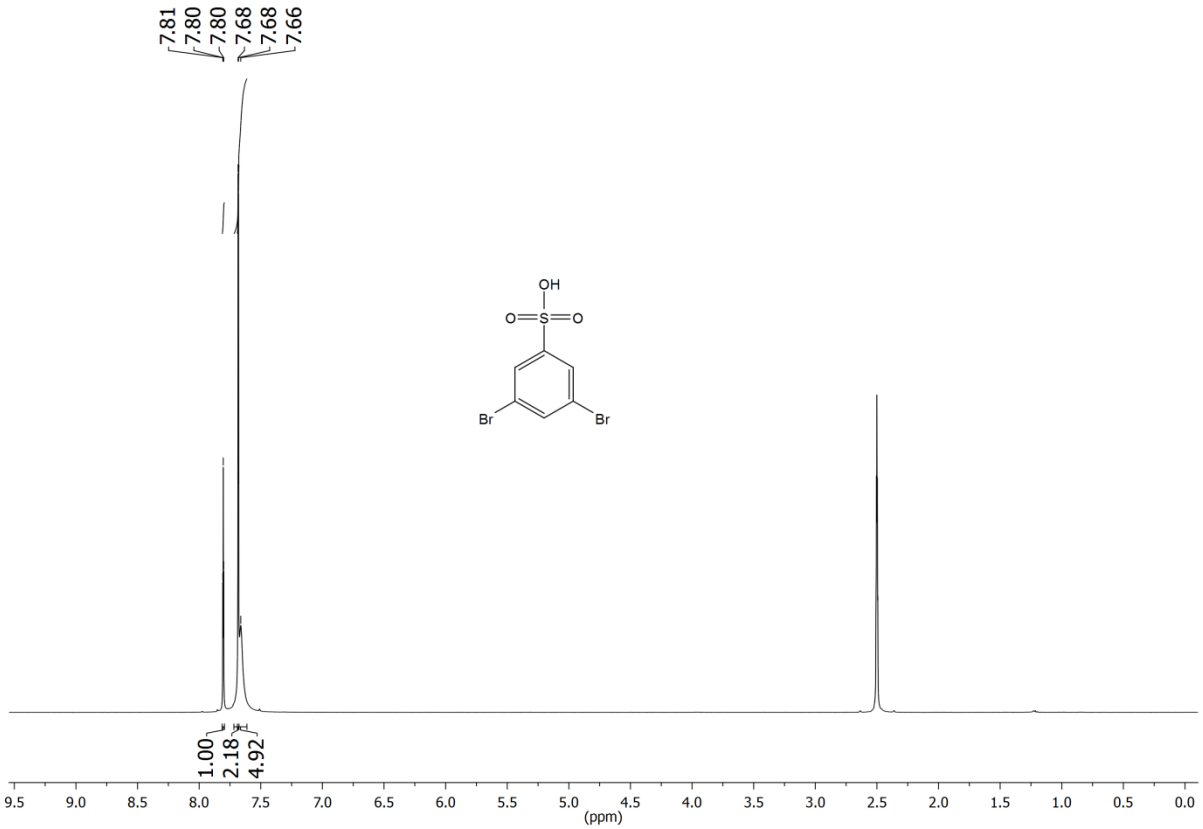

^{1}H-NMR (500 MHz, 300 K, DMSO-d6) of **16**

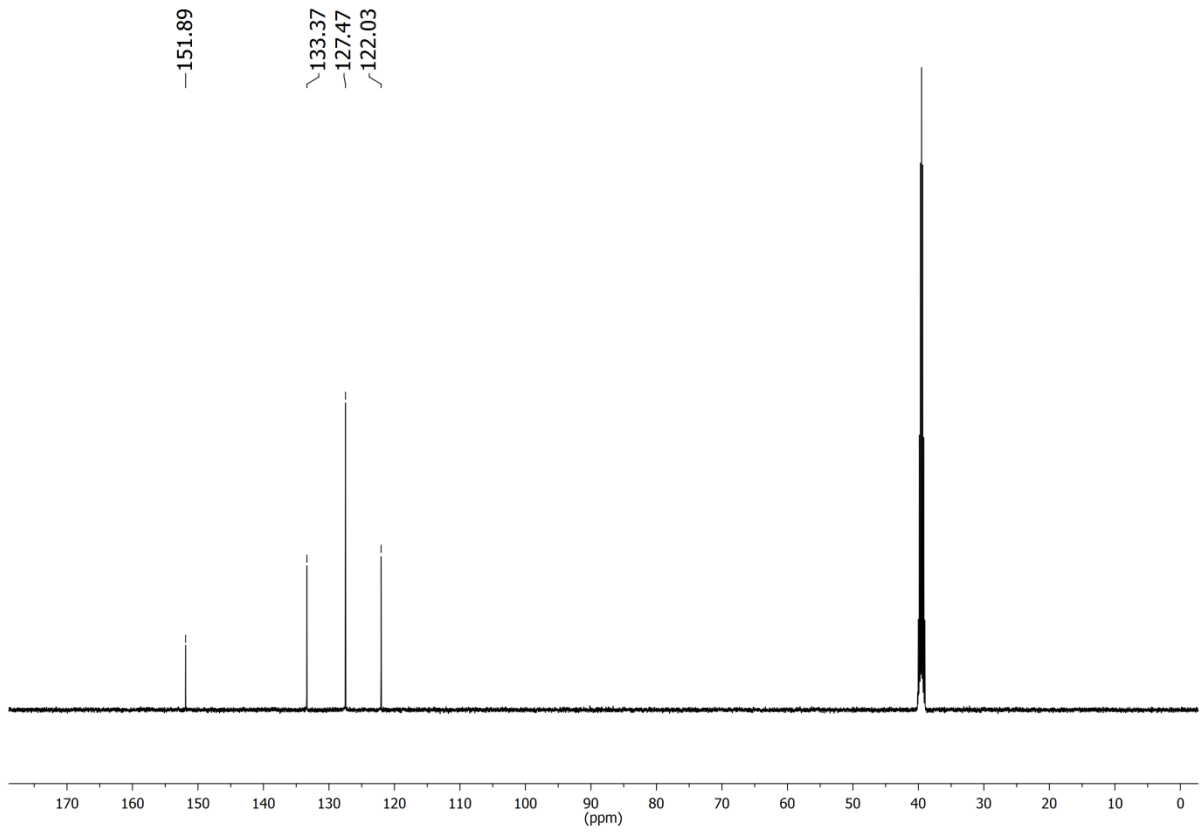

^{13}C-NMR (125 MHz, 300 K, DMSO-d6) of **16**

3,5-Diphosphonobenzenesulfonic acid (24)

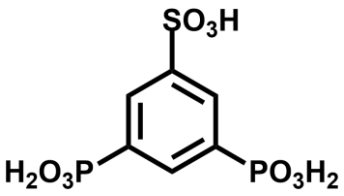

3,5-Dibromobenzenesulfonic acid (**16**, 1.76 g, 5.59 mmol) dissolved in water (40 mL) was treated with aqueous tetra-*n*-butylammonium hydroxide (40 % in water) until pH = 7 was reached. The solvent was removed in vacuo and the residue was dried in a vacuum oven at 60 °C for 12 h to obtain the respective tetra-*n*-butylammonium salt. Three microwave vials were charged with salt (3 x 1.03 g, 3 x 1.86 mmol), palladium(II) chloride (3 x 33 mg, 3 x 186 µmol) and triethyl phosphite (3 x 4 mL, 3 x 16.7 mmol). The vials were irradiated in a microwave oven (max. 200 W, 220 °C) for 60 min. The combined solution was added to a mixture of ethyl acetate (100 mL) and water (100 mL) in a separatory funnel. The aqueous layer was washed with ethyl acetate (3 x 100 mL) and water was removed in vacuo. The residue was dissolved in a mixture of water (40 mL) and conc. hydrochloric acid (80 mL) and stirred for 12 h at 120 °C. After removing the solvent in vacuo, the residue was dissolved in acetone (40 mL) and mixed with four equivalents of sodium iodide (3.35 g, 22.38 mmol)

dissolved in acetone (20 mL). The precipitate was collected by filtration and washed with ethanol (150 mL). To exchange the sodium ions, the residue was dissolved in water and rinsed over a column filled with ion-exchange resin (Dowex 50WX8 hydrogen form). The eluate was concentrated and dried for 24 h at 60 °C in a vacuum oven, to yield a colourless solid.

Yield: 1.11 g (3.49 mmol, 62 %)

M. p.: 292 °C

^{1}H-NMR (500 MHz, 300 K, DMSO-d6): δ = 9.91 (br. s, 5H, PO_3H_2, SO_3H), 8.06 (m_c, 2H, Ar-2,6-*H*), 7.96 (tt, $^{3}J_{H\text{-}P}$ = 12.6 Hz, ^{4}J = 1.4 Hz, 1H, Ar-4-*H*) ppm.

^{13}C-NMR (125 MHz, 300 K, DMSO-d6): δ = 147.8 (s[t_P], $^{3}J_{C\text{-}P}$ = 13.2 Hz, Ar-1-*C*), 133.7 (s[d_Pd_P], $^{1}J_{C\text{-}P}$ = 180.1 Hz, $^{3}J_{C\text{-}P}$ = 12.7 Hz, Ar-3,5-*C*), 132.6 (d[t_P], $^{2}J_{C\text{-}P}$ = 10.8 Hz, Ar-4-*C*), 130.0 (d[m_P], Ar-2,6-*C*) ppm.

^{31}P-NMR (202 MHz, 300 K, DMSO-d6): 11.6 (s, 2P, PO_3H_2) ppm.

MS (ESI_{neg}): *m/z* = 317 $[M-H]^-$.

IR (ATR): $\tilde{\nu}$ = 3074 (aryl-H val.), 2657, 2226 (br., OH), 1587 (arom. C=C) cm^{-1}.

EA ($C_6H_8O_9P_2S$) (318.13): calcd. C 22.65 H 2.53 S 10.08;
found C 22.70 H 2.54 S 10.03.

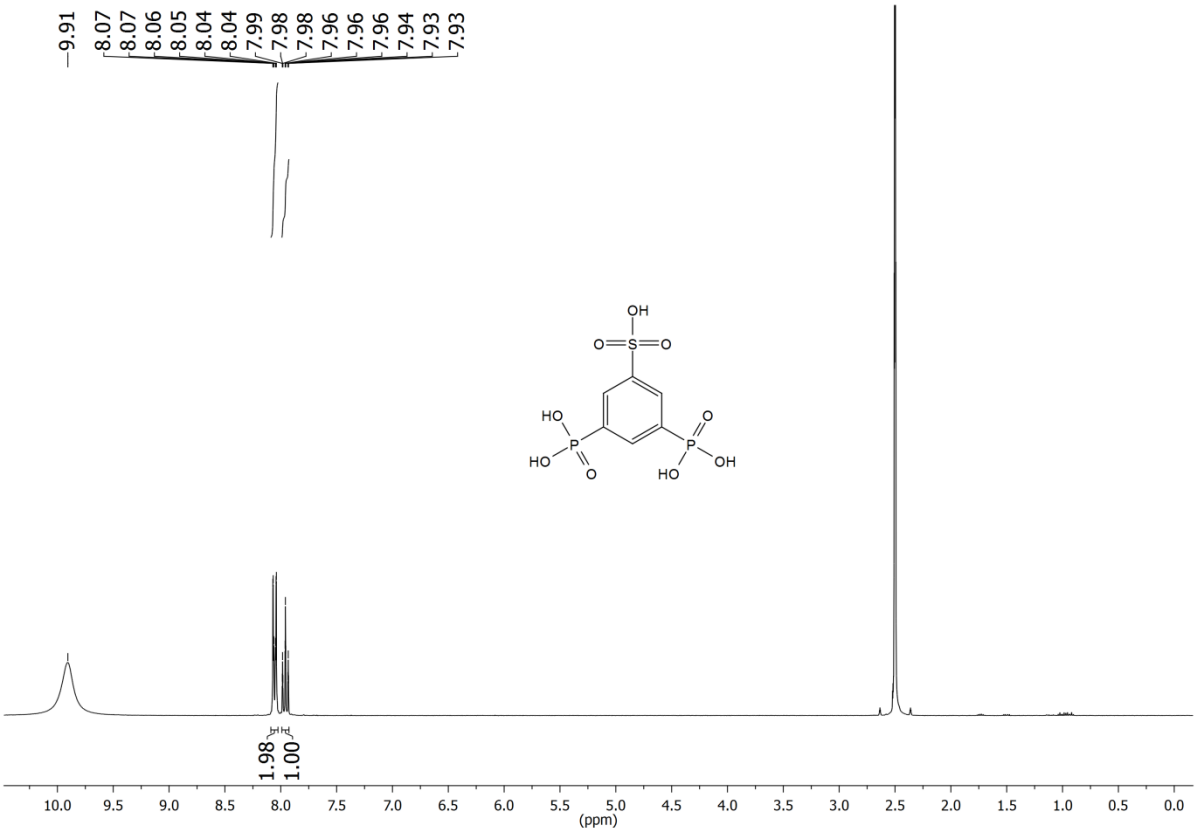

^{1}H-NMR (500 MHz, 300 K, DMSO-d6) of **24**

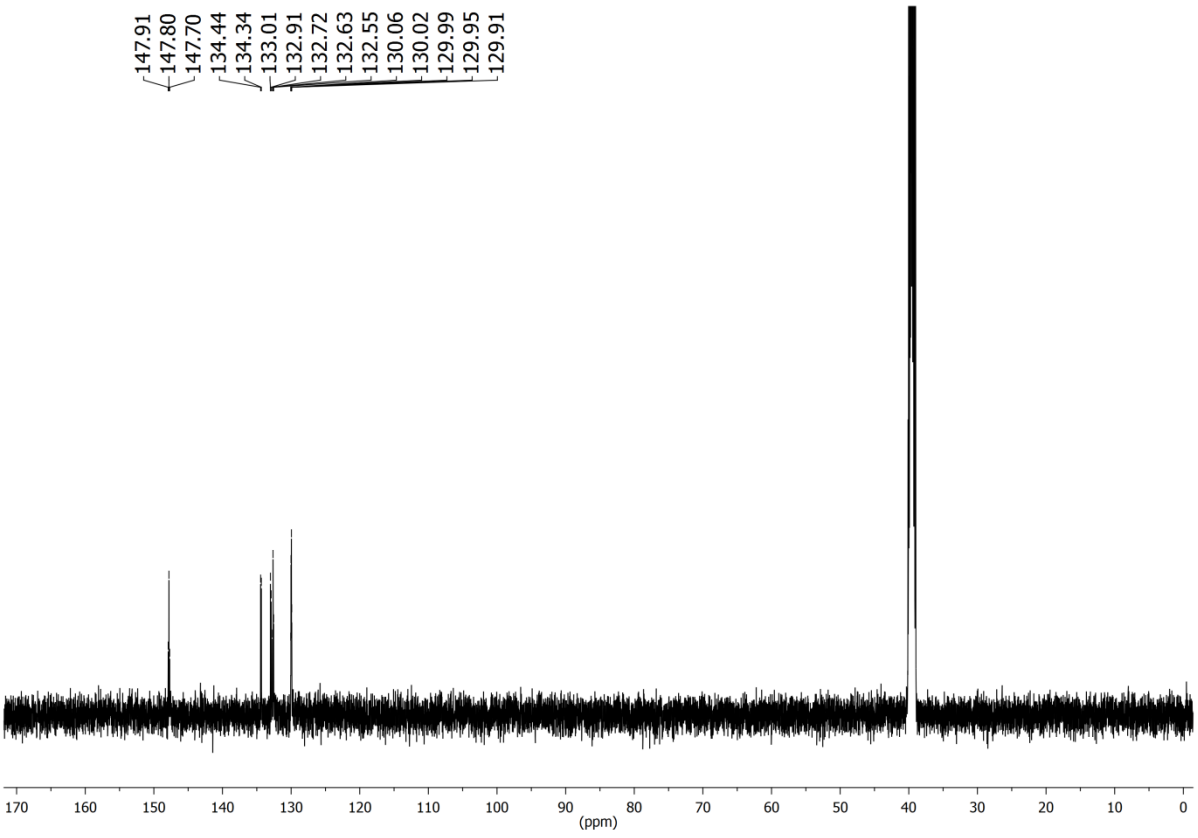

^{13}C-NMR (125 MHz, 300 K, DMSO-d6) of **24**

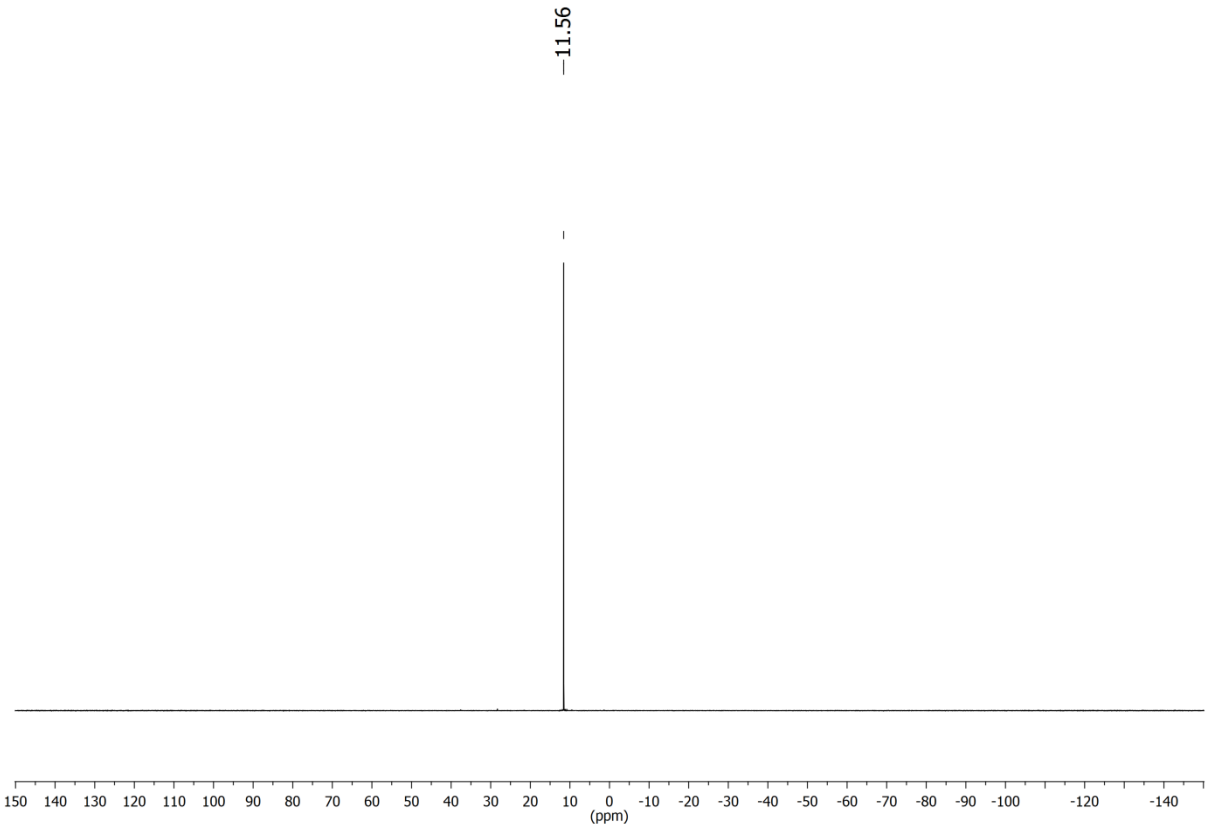

^{31}P-NMR (202 MHz, 300 K, DMSO-d6) of **24**

2. Synthesis and characterization of $[La_4(H_2L)_3(H_2O)_8]$

Synthesis procedure

Using high-throughput methods, the following optimized synthesis was established. A mixture of [2,5-bis(phosphonomethyl)-benzene-1,4-diyl]bis(methylsulfonic acid) (**9**, 15.4 mg, 340 µmol), $La(NO_3)_3 \cdot 6H_2O$ (14.7 mg, 340 µmol) and 1.5 mL H_2O was heated to 160 °C within 2 h. After 84 h at 160 °C, the sample was cooled to room temperature within 12 h and the resulting yellowish crystals were filtered off, washed with H_2O and dried in air.

Structure solution and refinement

The crystal structure of $[La_4(H_2L)_3(H_2O)_8]$ was determined from single-crystal X-ray diffraction data. X-ray diffraction measurements were performed on a Stoe IPDS diffractometer equipped with an image-plate detector using Mo-K_α radiation (λ=71.073 pm). The crystal structure was solved in the space group *C2/m* by direct methods with the program SHELXT-2014 and refined using the program SHELXL-2014[4]. The functional groups $–SO_3^-$ and $–PO_3H^-$ have very similar coordination properties and in addition, phosphorus and sulfur can

hardly be distinguished by X-ray diffraction due to the very similar scattering power. In our structure refinement, the linker molecules are located on special positions (Wyckoff letter 4i and 2a with site symmetry *m* and *2/m*, respectively) and thus the atomic positions of the P/S atoms were refined with an occupancy of 0.5 each, utilizing the EADP and EXYZ commands. Numerical absorption correction was carried out by using XShape and XRed[5]. The electron density inside the pores was removed via SQUEEZ by Platon[6].

Table S13 Results of the crystal structure determination of $[La_4(H_2L)_3(H_2O)_8]$.

Formula	$La_4S_6P_6C_{30}O_{44}H_{46}$
Crystal system	monoclinic
Space group	*C2/m*
a (Å)	20.047(4)
b (Å)	11.357(2)
c (Å)	18.677(4)
α (°)	90
β (°)	118.51(3)
γ (°)	90
V (Å³)	3736.3(16)
Z	6
Abs. coeff. (mm^{-1})	2.625
Crystal size (mm)	0.133 x 0.106 x 0.06
Reflections collected Symmetry independent	19490 / 4470
R_{int}	0.0691
No. of parameters	218
R1 [$I > 2\sigma(I)$], R1 (all data)	0.0696, 0.0762
wR2 [$I > 2\sigma(I)$], *wR2* (all data)	0.1919, 0.1954
Largest diff. peak (e $Å^{-1}$)	-1.38 / 1.83

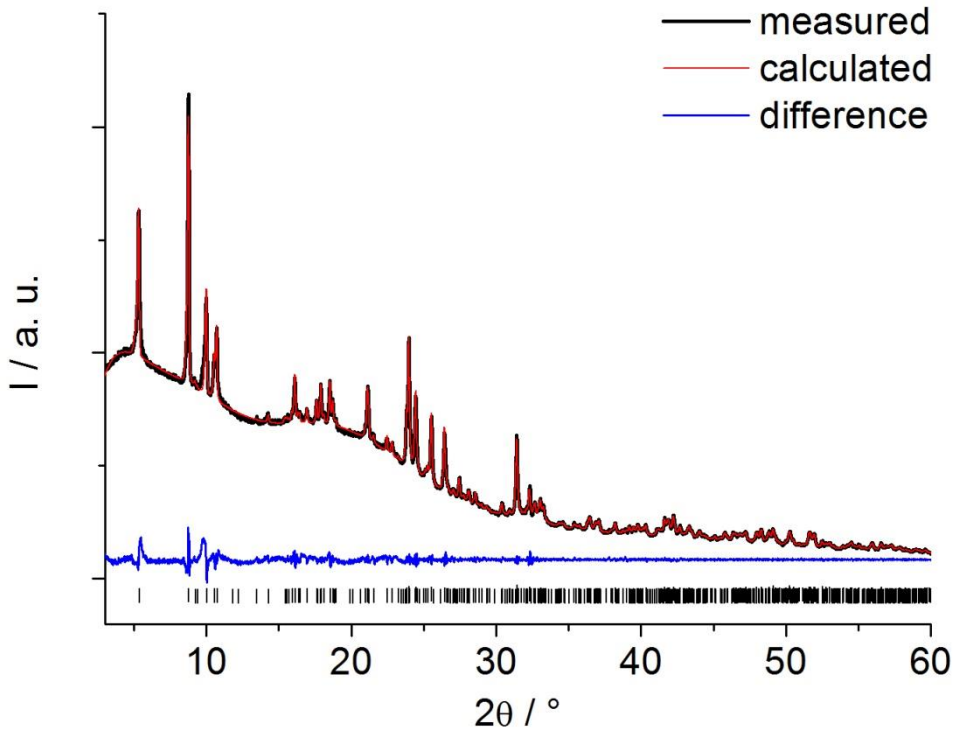

Figure S45: Pawley-Fit of $[La_4(H_2L)_3(H_2O)_8]$. Measured and calculated PXRD data, the difference of both and the allowed reflections are shown in black, red, blue and as black bars, respectively.

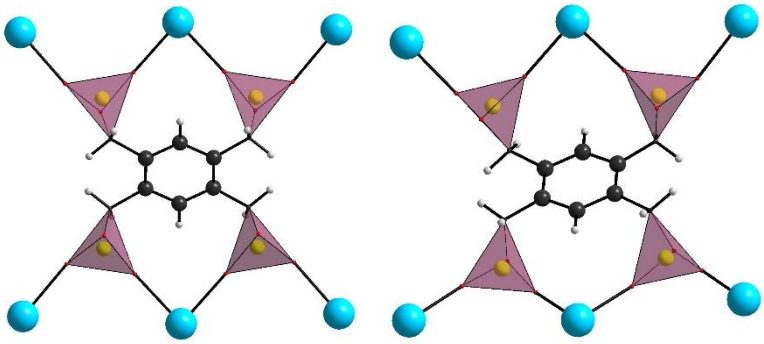

Figure S2: Representation of the two crystallographically independent linker molecules connecting six La^{3+} ions each via sulfonate/phosphonate groups. Lanthanum atoms are shown in teal, oxygen atoms in red, sulfur / phosphor in yellow, carbon atoms in black and hydrogen in white.

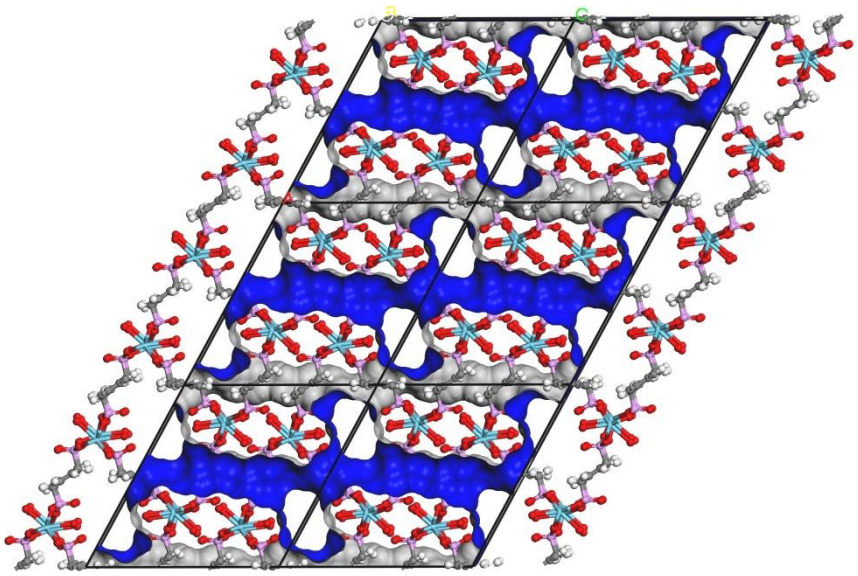

Figure S3: Representation of 1D channels in $[La_4(H_2L)_3(H_2O)_8]$ along the *b* axis. Lanthanum atoms are shown in teal, oxygen atoms in red, and carbon atoms in gray. The Connolly surface was calculated with a probe diameter of 2.6 Å (kinetic diameter of H_2O) using Materials Studio and is shown in blue/gray.[7]

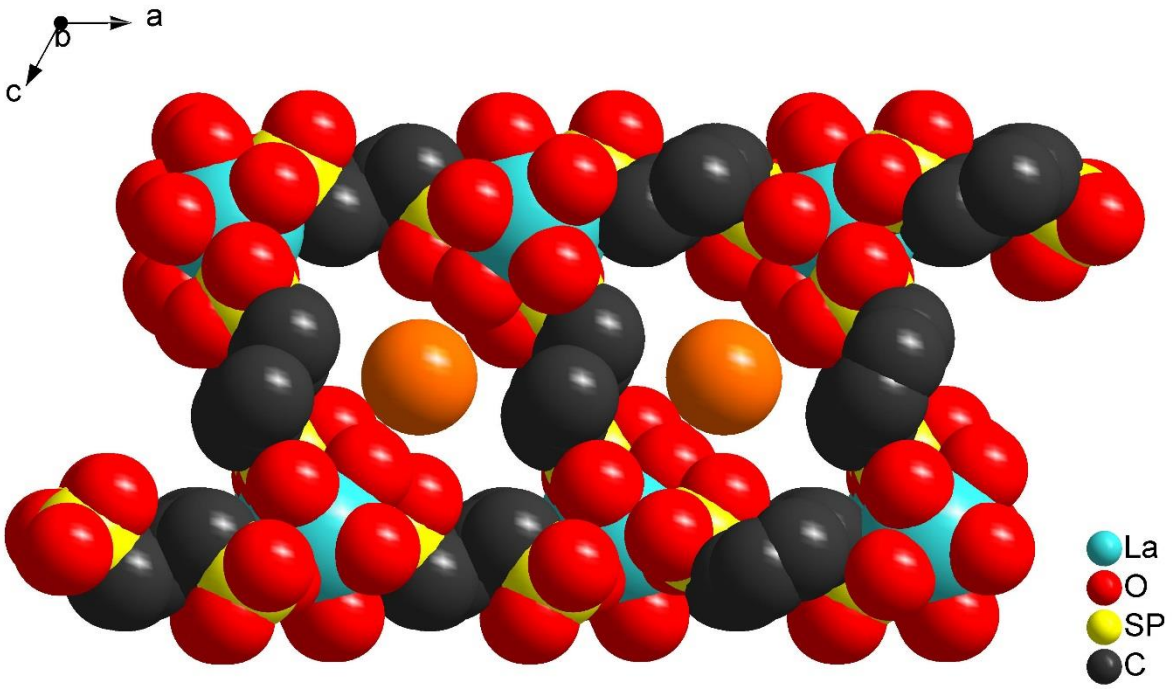

Figure S4: Space filling representation of 1D channels in $[La_4(H_2L)_3(H_2O)_8]$ along the *b* axis. The orange sphere with a diameter of 3.8 Å is used for easier visualisation. Lanthanum atoms are shown in teal, oxygen atoms in red, sulfur and phosphor in yellow and carbon atoms in black.

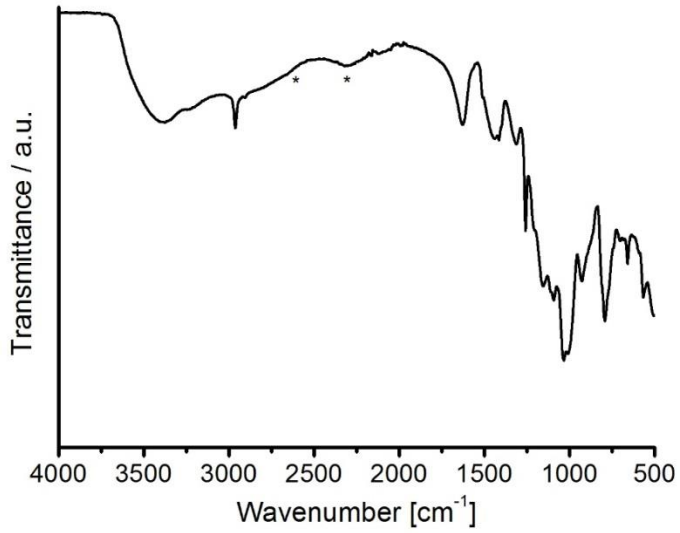

Figure S5: IR spectrum of $[La_4(H_2L)_3(H_2O)_8]$. A broad band between 4000 and ~2500 cm^{-1} is visible and most likely attributed to water molecules as suggested by single-crystal X-ray diffraction. In addition, C-H stretching vibrations of the CH_2 groups are around ~2970 and ~2910 cm^{-1} Within the region of 2650 and 2300 cm^{-1} pronounced signals for the presence of protonated phosphonate groups can be found (marked with a *), which supports the finding of the single-crystal X-ray diffraction data.[8] The sharp Signal at 1630 cm^{-1} is assigned to the deformation vibration of water.

Table S14: Possible hydrogen bonds (oxygen ⋯ oxygen distance) within the crystal structure of $[La_4(H_2L)_3(H_2O)_8]$.

Atoms	Atomic distance [Å]
La1-O1 ⋯ O10	3.082
La2-O2 ⋯ O10	2.976

3. References

1 H. Kawai, T. Umehara, K. Fujiwara, T. Tsuji and T. Suzuki, *Angew. Chem.*, 2006, **118**, 4387-4392; *Angew. Chem. Int. Ed.*, 2006, **45**, 4281–4286.

2 M. F. Teasley, US Pat., 20120004387A1, 2012.

3 M. H. Litt and J. Kang, US Pat., 20090259013A1, 2009.

4 G. M. Sheldrick, *Acta Crystallogr., Sect. C: Struct. Chem.*, 2015, **71**, 3-8.

5 Stoe & Cie, XShape and XRed., Darmstadt, Germany, 1998.

6 A. L. Spek, *Acta Crystallogr., Sect. D: Biol. Crystallogr.*, 2009, **65**, 148-155.

7 *Materials Studio v4.1*, Accelrys Software Inc.

8 a) H. Silvia Martínez-Tapia, A. Cabeza, S. Bruque, P. Pertierra, S. García-Granda and M. A. G. Aranda, *J. Solid State Chem.*, 2000, **151**, 122-129;
b) A. Cabeza, M. A. G. Aranda and S. Bruque, *J. Mat. Chem.,* 1999, **9**, 571-578.

9 P. Atorngitjawat, R. J. Klein and J. Runt, *Macromolecules*, 2006, **39**, 1815–1820.

4.2 PSM von Cr-MIL-101-Derivaten zur Implementierung von Phosphonsäure-Gruppen

Ein anderer Ansatz zur Darstellung protonenleitfähiger MOFs ist die postsynthetische Modifikation. Durch den postsynthetischen Einbau von organischen Säuregruppen könnte eine Koordination am Metall-Ion vermieden werden und die Protonenleitfähigkeit eines MOFs eventuell verbessert werden. Die postsynthetische Modifikation zur Darstellung von MOFs mit freien Carbon- und Sulfonsäure-Gruppen ist bereits mehrfach beschrieben (s. Kapitel 1.2). Vor allem MOFs mit Sulfonsäure-Gruppen zeigen großes Potential als protonenleitfähige Materialien.[149] Ein Beispiel ist der durch postsynthetische Modifikation erhaltene UiO-66(SO_3H)$_2$.[157] Die Protonenleitfähigkeit dieses MOFs gilt bis heute als eine der höchsten, die je für einen MOF gemessenen wurde.

Obwohl Phosphonsäure-Gruppen eine ähnlich hohe Acidität wie Sulfonsäure-Gruppen besitzen und der positive Einfluss von Phosphonsäure-Gruppen auf die Protonenleitfähigkeit schon in mehreren MOFs beobachtet wurde (s. Kapitel 1.3), ist bis heute nur eine PSM zum Einbau von Phosphonsäure-Gruppen in MOFs bekannt.[150] Hierbei ist zu erwähnen, dass die Phosphonsäure-Gruppen zwar postsynthetisch durch Hydrolyse der jeweiligen Ethylester erhalten wurden, aber die Phosphonsäurediethylester-Gruppen schon vor der MOF-Synthese am Linker vorlagen. Die einzige erfolgreiche PSM zur Implementierung von Phosphonsäurediethylester-Gruppen wurde 2016 von VAN DER VOORT beschrieben.[181] In diesem Fall wurden die Ester jedoch nicht hydrolysiert. In den folgenden Kapiteln sollen neue, postsynthetische Möglichkeiten zur Implementierung von Phosphonsäure-Gruppen aufgezeigt und diskutiert werden.

Um ein möglichst breites Spektrum an postsynthetischen Test-Reaktionen durchführen zu können, wurde ein MOF ausgewählt, der sich durch eine hohe thermische und chemische Stabilität auszeichnet und mit einer großen Variation an funktionellen Gruppen ausgestattet werden kann. Dafür empfahl sich das erstmals von FÉREY beschriebene poröse Cr-MIL-101[182], welches aus $Cr(NO_3)_3$ und Terephthalsäure (BDC) dargestellt wird. Cr-MIL-101 besitzt Poren mit einer Größe von 30 bis 34 Å, die wiederrum durch Porenfenster von 12 bis 16 Å erreicht werden können. Es besitzt eine thermische Stabilität bis zu 275 °C und konnte seine chemische Stabilität bereits unter sehr extremen postsynthetischen Modifikationen wie z.B. Sulfonierung[183–185] oder Nitrierung[109] unter Beweis stellen. Außerdem ist bis heute eine

Vielzahl an präsynthetisch funktionalisierten Cr-MIL-101-Derivaten bekannt.[186] Für die postsynthetische Modifikation zur Implementierung von Phosphonsäure-Gruppen wurden folgende drei Cr-MIL-101-Derivate ausgewählt: unfunktionalisierter Cr-MIL-101, Cr-MIL-101-Br und Cr-MIL-101-NH_2. Die Synthesen der MOFs wurden von THOMAS HOMBURG durchgeführt.

4.2.1 Generelle Methoden zur Darstellung von organischen Phosphonsäuren

Das folgende Kapitel soll einen Überblick über Synthesemethoden der organischen Chemie zur Darstellung von Phosphonsäuren geben. Dabei wird, aufgrund der zur Verfügung stehenden MOFs, hauptsächlich auf Methoden eingegangen, die Phosphonsäure-Gruppen durch Ausbildung von Kohlenstoff-Phosphor-Bindungen und Stickstoff-Phosphor-Bindung darstellen. Auch die Möglichkeit, Phosphonsäure-Gruppen mit Hilfe anderer funktioneller Gruppen einzuführen, wird besprochen. Da fast alle bekannten Synthesemethoden zur Darstellung von organischen Phosphonsäuren auf der Synthese der jeweiligen Phosphonsäurealkylester basieren, wird zunächst nur die Darstellung von Phosphonsäuredialkylestern beschrieben. Auf mögliche Methoden zur Hydrolyse der Ester wird erst im Anschluss eingegangen.

Zur Darstellung von Kohlenstoff-Phosphor-Bindungen ist eine Vielzahl an Methoden bekannt.[187] Je nach Hybridisierung des reaktiven Kohlenstoff-Atoms können unterschiedliche Methoden verwendet werden. Eine der bekanntesten Methoden zur Darstellung von Phosphonsäuredialkylestern an sp^3-hybridisierten Kohlenstoffatomen ist die Arbuzov-Reaktion.[188] Dabei wird ein Alkylhalogenid mit z. B. Triethylphosphit (oder anderen Trialkylphosphiten) umgesetzt und der jeweilige Alkylphosphonsäurediethylester erhalten. Eine andere Möglichkeit ist die Michaelis-Becker-Reaktion[189,190]. Auch in diesem Fall dienen Alkylhalogenide als Elektrophil und werden mit Dialkylphosphiten und einer Base zum jeweiligen Phosphonsäureester umgesetzt. Andere Beispiele sind die Palladium-katalysierte Kreuzkupplungsreaktion von Benzylhalogeniden mit Dialkylphosphiten[191,192] und die Umsetzung von Grignard- oder Organolithium-Verbindungen mit Chlorphosphorsäurediethylester[193–195].

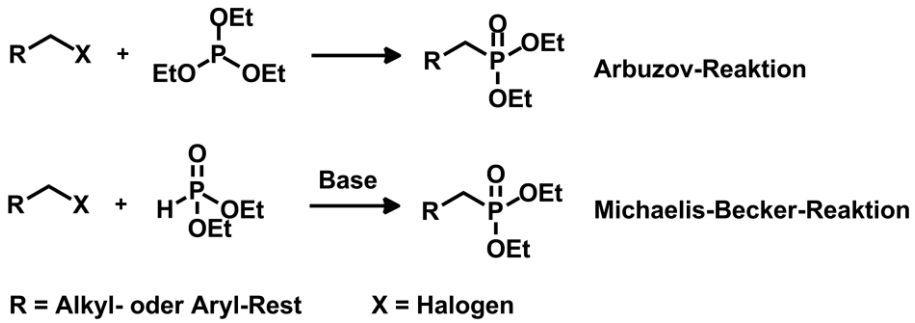

Abb. 27: Umsetzung von Alkylhalogeniden in einer Arbuzov-Reaktion bzw. einer Michaelis-Becker-Reaktion.

Für die R Ausbildung einer Kohlenstoff-Phosphor-Bindung an sp^2-hybridisierten Kohlenstoffatomen sind diverse Metall-katalysierte Kupplungsreaktionen bekannt. Dabei können Arylhalogenide mit Dialkylphosphiten oder Trialkylphosphiten unter Einfluss von Palladium-[196–199], Nickel-[200,201] oder Kupfer[202,203]-Katalysatoren zu den jeweiligen Arylphosphonsäuredialkylestern umgesetzt werden. Eine andere Möglichkeit zur Synthese von Arylphosphonsäureestern ist die oxidative Kupplung aromatischer Verbindungen mit Dialkylphosphiten. Als Katalysator kann Mangan(II)diacetat oder Mangan(III)triacetat verwendet werden.[204,205] Außerdem sind Darstellungen von Phosphonsäureestern ausgehend von Carbonylverbindungen [206,207] und α,β-ungesättigten Carbonylverbindungen[208,209] bekannt.

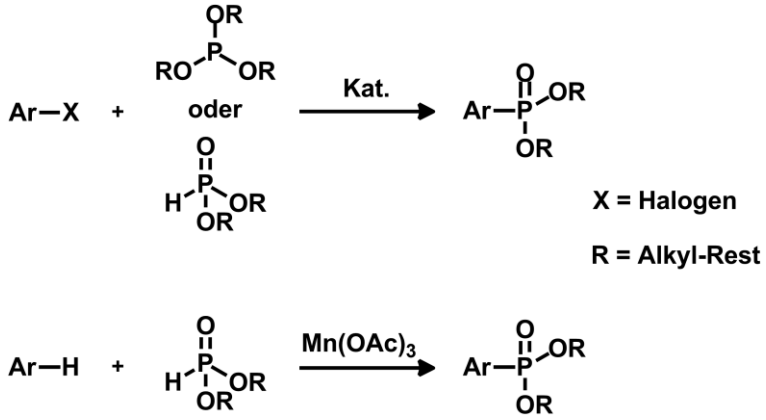

Abb. 28: Darstellung aromatischer Phosphonsäureester aus Arylhalogeniden mittels Metall-katalysierter Kreuzkupplungsreaktionen (oben) und durch oxidative Kupplung am Aromaten (unten).

Zuletzt sei noch auf die Darstellung von Phosphonsäureestern an sp-hybridisierten Kohlenstoffatomen eingegangen. Mittels Kupfer-katalysierter Kupplung können terminale Alkine mit Dialkylphosphiten zu den jeweiligen Alkinphosphonsäuredialkylestern umgesetzt werden.[210] Ausgehend von den gleichen Edukten können mit Palladium-[211,212], Nickel-[213]

und Molybdän-[214]Katalysatoren außerdem Phosphonsäureester an die Dreifachbindung addiert werden.

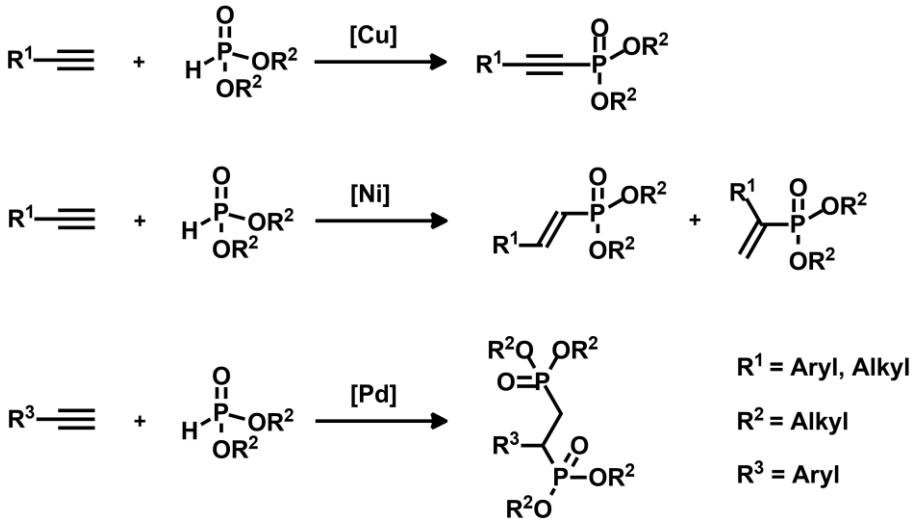

Abb. 29: Unterschiedliche Möglichkeiten der Umsetzung von Alkinen mit Dialkylphosphiten in Metall-katalysierten Kupplungsreaktionen.

Eine weitere Möglichkeit, Phosphonsäureester einzuführen, ist die Umsetzung von organischen Aminen zu Phosphorsäureamiden. Die Darstellung kann unter anderem durch nukleophile Substitution an einem Chlorphosphorsäuredialkylester erfolgen. Auch für die Umsetzung mit Dialkylphosphiten sind verschiedene Synthesebedingungen zur Darstellung von Phosphorsäureamiden bekannt. Bei der Atherton-Todd-Reaktion[215,216] wird aus dem Dialkylphosphit mit Hilfe einer Base und Tetrachlorkohlenstoff der, für die nukleophile Substitution benötigte, Chlorphosphorsäuredialkylester *in situ* erzeugt. Andere Beispiele sind oxidative Kupplungen mit Kupfer(I)salzen[217] oder elementarem Iod[218] als Katalysator.

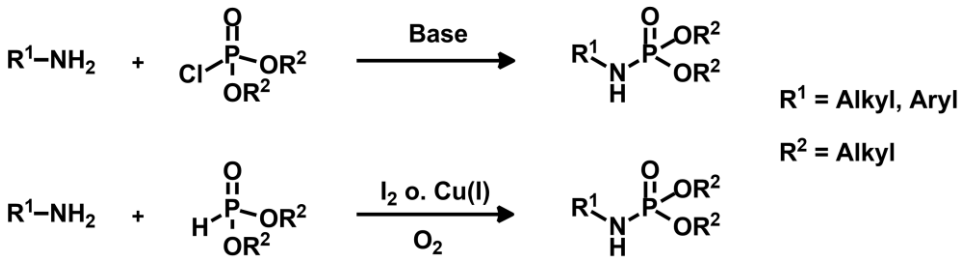

Abb. 30: Darstellung von Phosphorsäureamiden mittels nucleophiler Substitution (oben) oder oxidativer Kupplung (unten).

Ist die direkte Darstellung eines Phosphonsäureesters am gewünschten Molekül nicht möglich, könnten Precursor-Verbindungen verwendet werden. Als Precursor werden im Folgenden Moleküle bezeichnet, die neben einer Phosphonsäureester-Gruppe noch eine

weitere funktionelle Gruppe besitzen. Die zweite funktionelle Gruppe dient zur Verknüpfung des Precursors mit der gewünschten Verbindung. So könnte z. B. eine aminofunktionalisierte Verbindung mit einem Carbonsäurechlorid-Precusor zu einem Amid umgesetzt werden, welches eine Phosphonsäureester-Gruppe besitzt. Die Darstellung von Phosphonsäureestern ist bei dieser Methode lediglich durch die Reaktivität der Ausgangsverbindung und die Verfügbarkeit der Precusor limitiert. So wäre z. B. auch die Umsetzung von einem Amin mit cyclischen Phosphonsäureestern, analog der Umsetzung mit Sultonen (s. Kap. 1.2), denkbar. Allerdings ist die Synthese von cyclischen Phosphonsäureestern und deren Umsetzung mit Aminen bis heute kaum untersucht.[219]

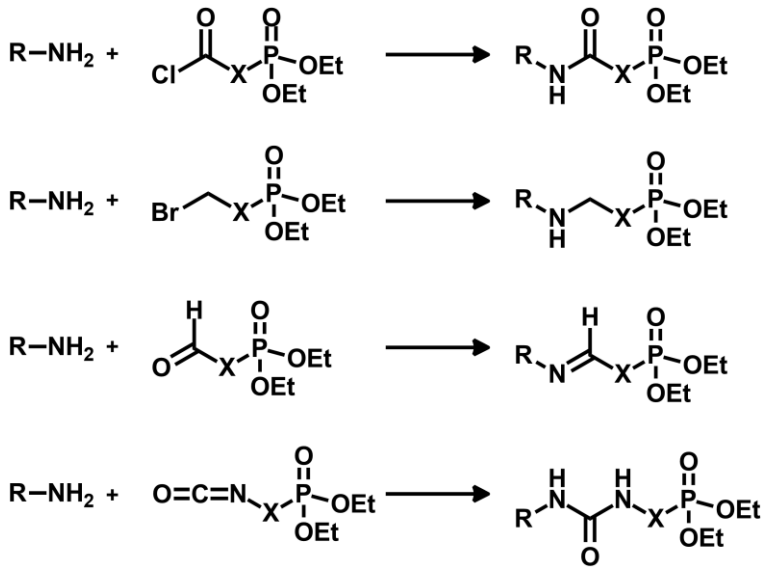

Abb. 31: Umsetzung eines Amins mit einer Precusor-Verbindung, um Phosphonsäureester-Gruppen einzuführen.

Für die Hydrolyse der Phosphonsäureester zu den jeweiligen Phosphonsäuren eignen sich zwei unterschiedliche Arten von Reagenzien. Entweder können wässrige Lösungen von starken anorganischen Säuren wie z. B. HCl oder HBr verwendet werden oder bestimmte Trimethylsilylhalogenide. Die Hydrolyse mit HCl oder HBr verläuft zwar in guten Ausbeuten, jedoch können die extremen Bedingungen zu unerwünschten Nebenreaktionen führen. Der Vorteil von Trimethylsilylhalogeniden ist, dass die Esterspaltung bei Raumtemperatur und in organischen Lösungsmitteln durchgeführt werden kann. Nachteile sind die etwas schlechteren Ausbeuten im Vergleich zu den anorganischen Säuren und ebenfalls eventuelle Nebenreaktionen.[187]

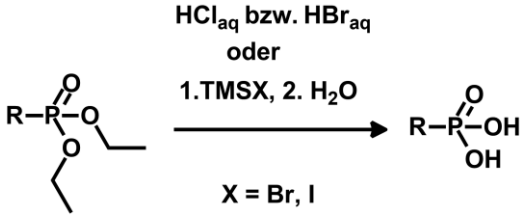

Abb. 32: Esterspaltung am Beispiel eines Phosphonsäurediethylesters.

4.2.2 Vorversuche mit den Methylestern der Linker

Viele der genannten Methoden können nicht direkt auf die postsynthetische Modifikation eines MOFs übertragen werden, da nicht bekannt ist, ob die jeweiligen Linker unter den angegebenen Synthesebedingungen umgesetzt werden können. Außerdem können nur Synthesebedingungen gewählt werden, bei denen das MOF stabil bleibt. Um die Reaktivität der Linker gegenüber den verschiedenen Methoden zu testen, wurden Vorversuche mit den Methylestern der jeweiligen Linker durchgeführt. Die Methylester wurden gewählt, da sie eine bessere Löslichkeit in organischen Lösungsmitteln im Vergleich zu den Carbonsäure-Derivaten besitzen und generell eine bessere Handhabbarkeit in Bezug auf Aufreinigungsmethoden wie z. B. Chromatographie besitzen. Ist die Modifikation mit einer Phosphonsäureester-Gruppe erfolgreich, kann die Verbindung außerdem als Referenz für auf gleichem Wege modifizierte MOFs dienen. In den folgenden Abschnitten werden sowohl erfolgreiche als auch fehlgeschlagene Umsetzungen von Terephthalsäuredimethylester (**1**), 2-Bromterephthalsäuredimethylester (**6**) und 2-Aminoterephthalsäuredimethylester (**8**) diskutiert.

Terephthalsäuredimethylester

Basierend auf der in Kapitel 4.2.1 beschriebenen oxidativen Kupplung mit $Mn(OAc)_3$ wurde versucht, eine Phosphonsäureester-Gruppe direkt am Aromaten einzuführen. Da in der Literatur[205] schon ähnliche Moleküle auf diese Weise erfolgreich umgesetzt wurden, wurden die Synthesebedingungen mit kleinen Variationen adaptiert. Terephthalsäuredimethylester (**1**), $Mn(OAc)_3 \cdot 2H_2O$ und Diethylphosphit (**2**) wurden in Essigsäure für 12 h bei 60 °C gerührt. Nach Aufarbeitung und säulenchromatographischer Reinigung konnte der gewünschte Phosphonsäurediethylester **3** mit einer Ausbeute von 20 % isoliert werden.

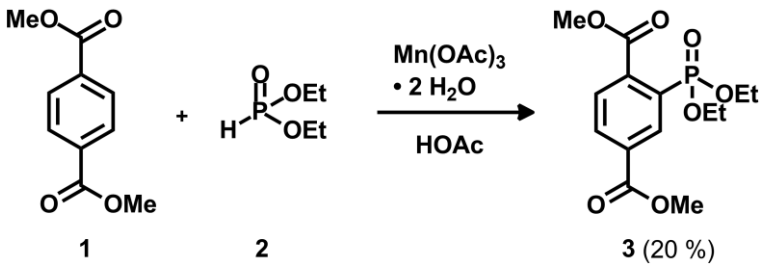

Abb. 33: Synthese des Phosphonsäurediethylesters **3** mittels oxidativer Kupplung.

Ein weiterer Ansatz basiert auf der von GOESTEN beschriebenen Chlormethylierung am Cr-MIL-101.[149] VAN DER VOORT nutzte und erweiterte diese PSM, um Phosphonsäureester-Gruppen in das Cr-MIL-101 einzuführen.[181] Diese vielversprechenden Ergebnisse sollten in Vorversuchen mit dem Terephthalsäuredimethylester (**1**) reproduziert werden und zusätzlich neue Methoden zur Implementierung von Phosphonsäureester-Gruppen an der Chlormethyl-Gruppe ausprobiert werden. Da für den Terephthalsäuredimethylester (**1**) keine Chlormethylierungen in der Literatur bekannt sind, wurden die gleichen Synthesebedingungen verwendet, die zur Modifizierung von Cr-MIL-101 beschrieben sind. Dafür wurde Terephthalsäuredimethylester (**1**) mit Methoxyacetylchlorid (**4**) und Aluminiumtrichlorid in Nitromethan bei 100 °C gerührt. Jedoch konnte, trotz Variation der Reaktionstemperatur und Reaktionsdauer, keine Umsetzung des Edukts **1** beobachtet werden. Weitere Versuche der Chlormethylierung wurden direkt am Cr-MIL-101 durchgeführt (s. Kap.4.2.3).

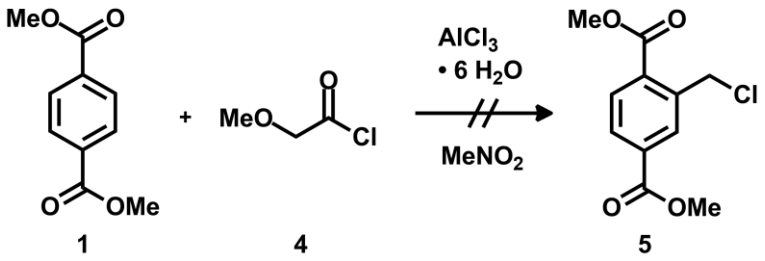

Abb. 34: Eine Chlormethylierung des Terephthalsäuredimethylesters (**1**) mit Methoxyacetylchlorid (**4**) war nicht erfolgreich.

2-Bromterephthalsäuredimethylester

Für die Umsetzung des 2-Bromterephthalsäuredimethylesters (**6**) wurden zwei unterschiedliche Palladium-katalysierte Kreuzkupplungsreaktionen ausprobiert. Zunächst soll auf die zuerst von HIRAO[197] beschriebene Kreuzkupplung von Arylhalogeniden mit Diethylphosphit (**2**) eingegangen werden. 2-Bromterephthalsäuredimethylester (**6**) wurde

analog einer literaturbekannten[220] Synthese (Literatur geht von 2-Iodterephthalsäuredimethylester aus) mit Diethylphosphit (**2**), Triethylamin als Base, $Pd(PPh_3)_4$ als Katalysator und Ethanol als Lösungsmittel umgesetzt. Eine Reaktionskontrolle per Dünnschichtchromatographie (DC) zeigte jedoch auch nach 24 h unter Rückfluss keine vollständige Umsetzung. Basierend auf den Ergebnissen von STAWINSKI[198] bezüglich Mikrowellen-assistierter Synthese konnte die Umsetzung und die Reaktionszeit optimiert werden. Mit Toluol als Lösungsmittel und $Pd(dppf)Cl_2$ als Katalysator wurde nach 15 min in der Mikrowelle (max. 200 W, 150 °C) eine vollständige Umsetzung beobachtet.

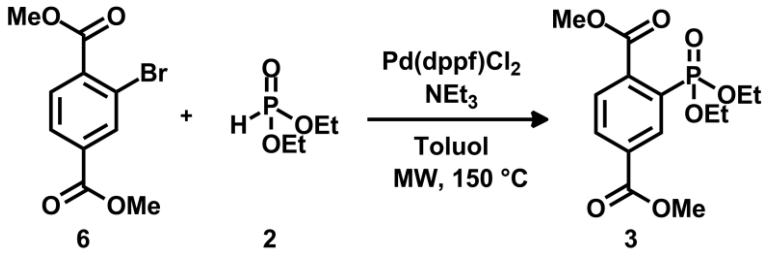

Abb. 35: Mikrowellen-assistierte Synthese des Phosphorsäurediethylesters **3** mit Diethylphosphit (**2**).

Eine andere Möglichkeit zur Darstellung von Arylphosphonsäureestern ist die von TAVS[200] beschriebene Reaktion von Arylhalogeniden mit Triethylphosphit (**7**) und Nickeldichlorid als Katalysator. Nachteile dieser Reaktion sind die extremen Reaktionsbedingungen (200 °C) und die hohe Empfindlichkeit von $NiCl_2$ gegenüber Luftfeuchtigkeit. Im Jahr 2003 berichtete VILLEMIN[199] von kürzeren Reaktionszeiten durch Mikrowellen-assistierte Synthese und von höheren Ausbeuten mit Palladiumdichlorid als Katalysator. Basierend auf diesen Ergebnissen wurde 2-Bromterephthalsäuredimethylester (**6**) mit Triethylphosphit (**7**) und $PdCl_2$ in einer Mikrowellen-gestützten Synthese umgesetzt. Triethylphosphit (**7**) dient hierbei gleichzeitig als Reaktionspartner und Lösungsmittel. Reaktionskontrolle nach 20 min mittels DC zeigte, dass die Umsetzung sowohl bei 150 °C als auch 170 °C nicht vollständig war. Ein weiterer Versuch bei 200 °C führte letztlich zu einer vollständigen Umsetzung.

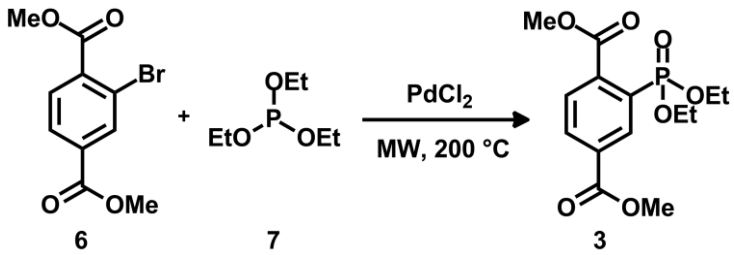

Abb. 36: Optimierte Synthesebedingungen zur Darstellung des Phosphorsäurediethylesters **3** mit Triethylphosphit (**7**) und $PdCl_2$.

2-Aminoterephthalsäuredimethylester

Angelehnt an eine Literaturvorschrift[218] zur Darstellung von aromatischen Phosphorsäureamiden wurde 2-Aminoterephthalsäuredimethylester (**8**) mit Diethylphosphit (**2**) und elementarem Iod als Katalysator umgesetzt. Dabei ist entscheidend, dass die Reaktion unter Anwesenheit von Sauerstoff bzw. Luftsauerstoff durchgeführt wird, da sonst keine Umsetzung stattfindet. Mit Dichlormethan als Lösungsmittel wurde das gewünschte Phosphorsäureamid **9** nach Aufarbeitung und säulenchromatographischer Reinigung in einer Ausbeute von 27 % erhalten.

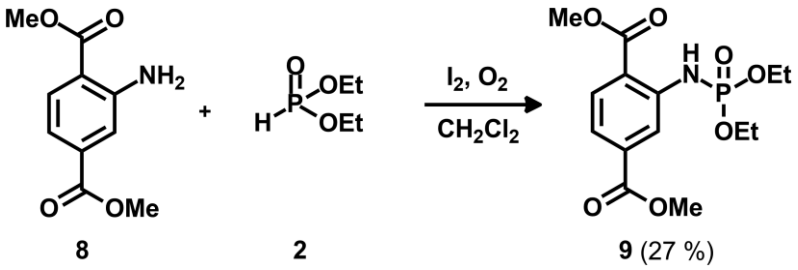

8 2 **9** (27 %)

Abb. 37: Oxidative Kupplung zur Darstellung des literaturunbekannten Phosphorsäureamids **9**.

Eine andere Möglichkeit das Phosphorsäureamid **9** zu synthetisieren, ist die Umsetzung von 2-Aminoterephthalsäuredimethylester (**8**) mit Chlorphosphorsäurediethylester (**10**). Mit Dichlormethan als Lösungsmittel und Triethylamin als Base konnte das Phosphorsäureamid **9** nach Aufarbeitung und säulenchromatographischer Aufreinigung in einer Ausbeute von 18 % erhalten werden.

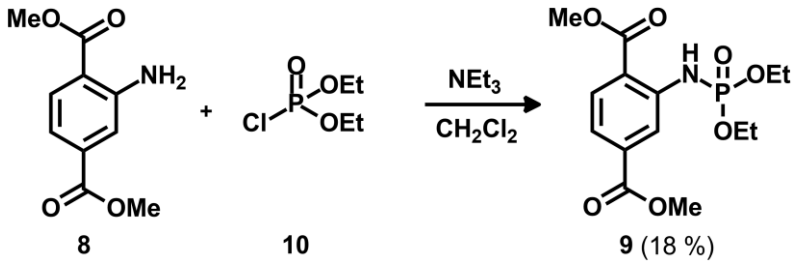

8 10 **9** (18 %)

Abb. 38: Nukleophile Substitution zur Darstellung des Phosphorsäureamids **9**.

Analog zur nukleophilen Substitution am Chlorphosphorsäurediethylester (**10**) wurde versucht, 2-Aminoterephthalsäuredimethylester (**8**) mit einer äquimolaren Menge Phosphoroxychlorid (**11**) umzusetzen. Durch eine anschließende Hydrolyse mit Wasser sollte die jeweilige Phosphorsäureamid-Gruppe erhalten werden. Ob das gewünschte Produkt **12** entstanden war, konnte aufgrund von diversen Nebenprodukten nicht eindeutig geklärt werden. Eine säulenchromatographische Trennung war nicht erfolgreich. Die große Anzahl an

Verunreinigungen lässt vermuten, dass eine Mischung aus einfach-, zweifach- und dreifach-substituierten Phosphoroxychloriden entstanden sein könnte.

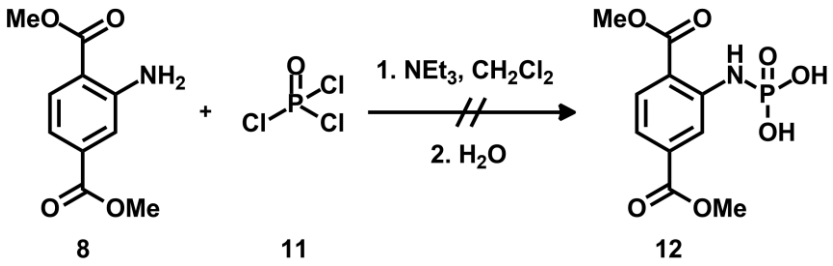

Abb. 39: Fehlgeschlagene Umsetzung mit Phosphoroxychlorid (**11**).

Auf Optimierungen der Reaktionsbedingungen wurde im Rahmen der Vorversuche größtenteils verzichtet. Die Vorversuche sollten zeigen, dass eine Umsetzung der Linker-Moleküle unter den gewählten Bedingungen möglich ist. Notwendige Reaktionsoptimierungen wurden erst während der postsynthetischen Modifizierung vorgenommen.

4.2.3 Postsynthetische Modifikation von Cr-MIL-101-Derivaten

Auf Basis der Vorversuche wurden postsynthetische Modifikationen am Cr-MIL-101, Cr-MIL-101-Br und Cr-MIL-101-NH_2 durchgeführt. Zum Nachweis der potentiellen Modifikationen am Linker wurde das MOF zunächst mit Natronlauge aufgelöst, die Cr^{3+}-Ionen abgetrennt und die Linker mittels NMR-Spektroskopie untersucht. Das Abtrennen der Cr^{3+}-Ionen ist entscheidend, da paramagnetische Metall-Ionen zu einer starken Linienverbreiterung im NMR-Spektrum führen. ^{31}P-NMR-Spektren wurden für alle Verbindungen aufgenommen (s. Kapitel 6.3), werden aber im folgenden Kapitel nicht näher diskutiert, da die Aussagekraft aufgrund von Verunreinigungen oft nur gering ist. Genaue Details zur Durchführung der jeweiligen Modifikationen sind in Kapitel 6.2.2 zu finden.

Cr-MIL-101

Eine Chlormethylierung von Cr-MIL-101 wurde schon mehrfach in der Literatur[149,181] beschrieben und deshalb trotz fehlgeschlagener Vorversuche ausprobiert. Jedoch konnte unter den angegebenen Reaktionsbedingungen keine Umsetzung beobachtet werden. Auch die Variation der Reaktionsbedingungen (höhere Reaktionstemperatur, längere Reaktionszeiten) führte nicht zum Erfolg.

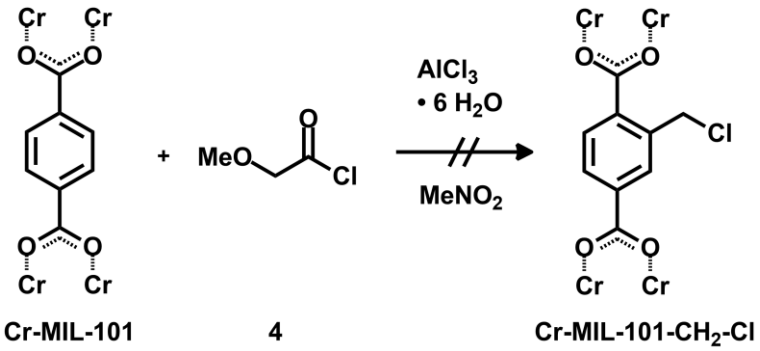

Abb. 40: Eine literaturbekannte[149] Chlormethylierung von Cr-MIL-101 war im Rahmen dieser Arbeit nicht erfolgreich.

Da die Umsetzung des Terephthalsäuredimethylesters (**1**) mit Diethylphosphit (**2**) und $Mn(OAc)_3$ erfolgreich war, wurde versucht, Cr-MIL-101 unter den gleichen Bedingungen umzusetzen. Jedoch konnte sowohl bei 60 °C als auch bei 100 °C nach 12 h Rühren keine Modifizierung beobachtet werden. Da zusätzlich die Abtrennung des schlecht löslichen $Mn(OAc)_3$ vom MOF schwierig war, wurden keine weiteren Versuche zur Optimierung unternommen.

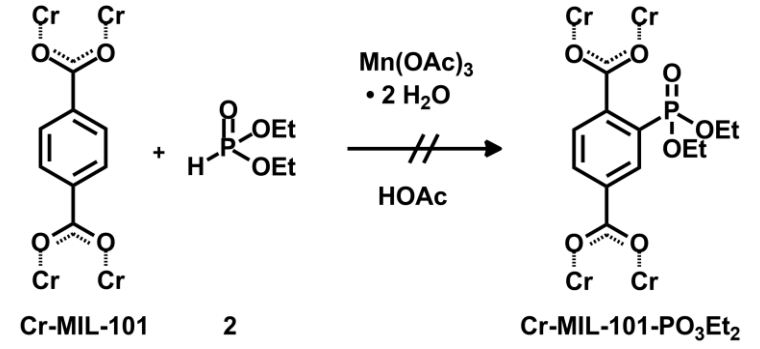

Abb. 41: Eine oxidative Kupplung am Cr-MIL-101 war nicht erfolgreich.

Cr-MIL-101-Br

Analog der Vorversuche wurde versucht, Cr-MIL-101-Br sowohl mit Diethylphosphit (**2**) als auch mit Triethylphosphit (**7**) zum Cr-MIL-101-PO_3Et_2 umzusetzen. Dafür wurde Cr-MIL-101-Br in einer Mikrowellen-gestützten Synthese mit Diethylphosphit (**2**), $Pd(dppf)Cl_2$, Triethylamin und Toluol für 15 min bei 150 °C gerührt.

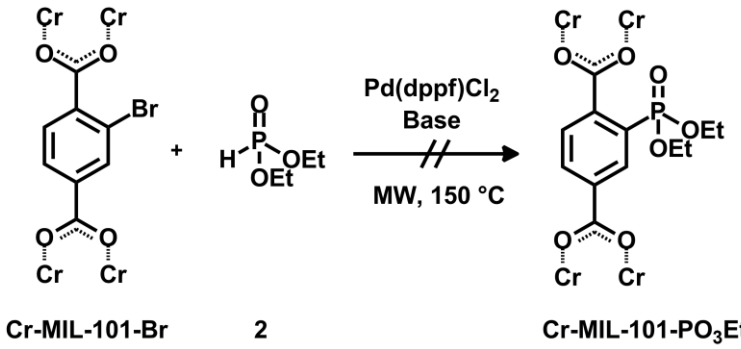

Abb. 42: Bei der Palladium-katalysierten Kreuzkupplung mit Diethylphosphit (**2**) konnte trotz Variation der Reaktionsbedingungen keine Umsetzung von Cr-MIL-101-Br beobachtet werden.

NMR-spektroskopische Untersuchungen des aufgelösten MOFs zeigten, dass nur unmodifizierter Cr-MIL-101-Br vorlag. Weitere Versuche wurden durchgeführt, in denen sowohl Reaktionszeit, -temperatur, Lösungsmittel, Base und Katalysator variiert wurden (s. Tab. 1). Unter keiner der Bedingungen konnte eine Umsetzung zum Cr-MIL-101-PO_3Et_2 beobachtet werden. In einigen Fällen konnte Terephthalsäure nach der Reaktion nachgewiesen werden. Dies lässt vermuten, dass der Palladiumkatalysator zwar in die Kohlenstoff-Brom-Bindung insertiert, aber nicht mit der jeweiligen Phosphor-Spezies weiterreagiert.

Tab. 1: Übersicht der Reaktionsbedingungen von Cr-MIL-101-Br mit Diethylphosphit (**2**).

Katalysator	Base	Lösungsmittel	Zeit (min)	Temperatur (°C)
$Pd(dppf)Cl_2$	NEt_3	Toluol	15	150
$Pd(dppf)Cl_2$	NEt_3	Toluol	60	200
$Pd(dppf)Cl_2$	NEt_3	DMF	60	200
$Pd(dppf)Cl_2$	KOAc	THF	60	200
$Pd(PPh_3)_4$	NEt_3	EtOH	60	200

Analog zum Vorversuch wurde Cr-MIL-101-Br mit Triethylphosphit (**7**) und $PdCl_2$ als Katalysator umgesetzt. Die Reaktionsmischung wurde für 60 min bei 200 °C in der Mikrowelle gerührt.

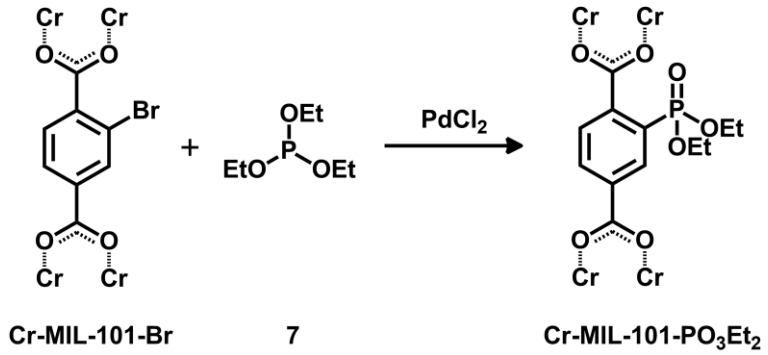

Abb. 43: Palladium-katalysierte Kreuzkupplung mit Triethylphosphit (**7**).

Nach geeigneter Aufarbeitung wurde das MOF im Basischen aufgelöst und mittels ^{1}H-NMR-Spektroskopie untersucht. Dabei wurden zusätzlich zu den Signalen der Bromterephthalsäure auch Signale für Terephthalsäure und eine weitere Spezies beobachtet. Um die unbekannte Spezies zu identifizieren, sollten die Carbonsäuremethylester-Gruppen von **3** hydrolysiert werden und das ^{1}H-NMR-Spektrum mit der unbekannten Spezies verglichen werden. Unter basischen Bedingungen wurde Phosphonsäuremonoethylester **13** und unter sauren Bedingungen Phosphonsäure **14** erhalten. In beiden Fällen werden die Carbonsäuremethylester zu Carbonsäuren hydrolysiert.

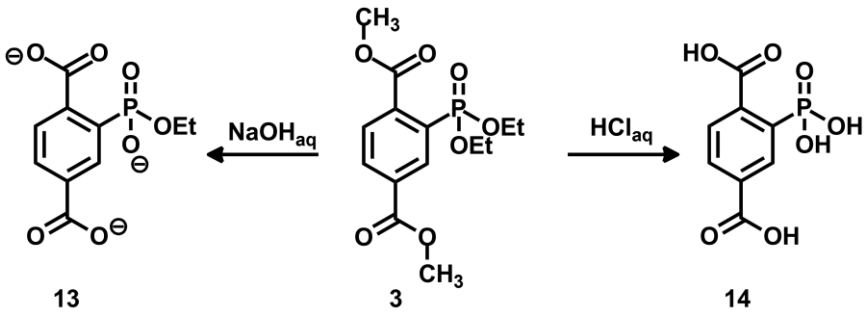

Abb. 44: Hydrolyse des Phosphonsäurediethylesters **3**.

Die ^{1}H-NMR-Spektren wurden trotzdem verglichen und zeigten, dass es sich im Fall der unbekannten Spezies um den Phosphonsäuremonoethylester **13** handelt. Es wird vermutet, dass der Monoethylester **13** erst beim Auflösen des MOFs im basischen Milieu entstanden ist und zuvor der jeweilige Diethylester vorlag.

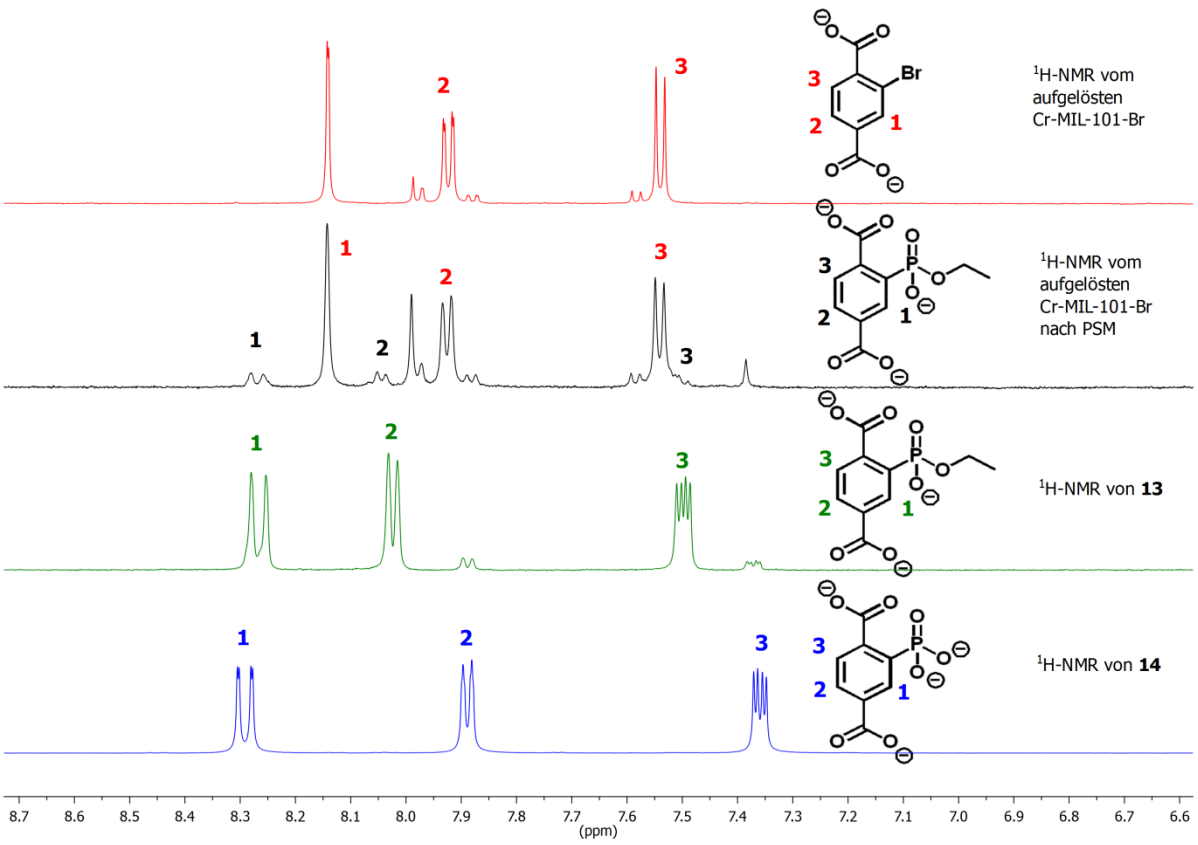

Abb. 45: Vergleich von ^{1}H-NMR-Spektren zur Identifizierung des Monoethylesters **13**.

Die Ergebnisse zeigen, dass die postsynthetische Modifikation zur Implementierung einer Phosphonsäurediethylester-Gruppe erfolgreich war. Durch die Messung eines Röntgendiffraktogramms konnte außerdem gezeigt werden, dass die Struktur nach der postsynthetischen Modifikation erhalten wurde (s. Kapitel 6.2.2). Der Umsatz lag jedoch lediglich bei 23 %. Davon konnten 15 % dem Phosphonsäurediethylester und 8 % der Terephthalsäure zugeordnet werden. Es wurde versucht, durch Variation der Reaktionsbedingungen einen höheren Umsatz zu erzielen. Neben der Reaktionszeit wurde die Menge des Triethylphosphits (**7**) und die Menge des Katalysators variiert. Es konnte jedoch kein Trend zu höheren Umsätzen ausgemacht werden. Die Optimierungsversuche zeigten vielmehr, dass sich der Umsatz, bei gleicher MOF-Charge und gleichen Reaktionsbedingungen, um bis zu 20 % unterscheiden kann. Auch das Verhältnis von Terephthalsäure zu Phosphonsäurediethylester war nicht beeinflussbar und bei jedem Ansatz unterschiedlich. Zusammenfassend kann man sagen, dass die postsynthetische Modifikation zwar erfolgreich, aber nicht reproduzierbar war. Dabei variierte der allgemeiner Umsatz zwischen 14 und 34 % und der Umsatz zum Phosphonsäurediethylester zwischen 7 und 25 %. Ein möglicher Grund für die große Variation ist, dass die Reaktion bevorzugt an der Oberfläche des MOFs abläuft. Da das MOF vor der Reaktion nicht gemörsert wurde, könnte

die unterschiedliche Größe der Kristalle einen Einfluss auf den Umsatz gehabt haben. Dies wurde im Rahmen dieser Arbeit jedoch nicht genauer untersucht.

Cr-MIL-101-NH_2

Zur Darstellung eines MOFs mit Phosphorsäureamid-Gruppen wurde von Cr-MIL-101-NH_2 ausgegangen. Dieser sollte zunächst analog der Vorversuche in einer oxidativen Kupplung mit Diethylphosphit (**2**) umgesetzt werden. Dafür wurde Cr-MIL-101-NH_2 in Dichlormethan vorgelegt und mit Diethylphosphit (**2**) und elementarem Iod für 12 h in Sauerstoff- bzw. Luftsauerstoff-Atmosphäre gerührt. Es konnte sowohl bei Raumtemperatur als auch unter Rückfluss keine Umsetzung beobachtet werden. Weitere Optimierungsversuche wurden nicht durchgeführt.

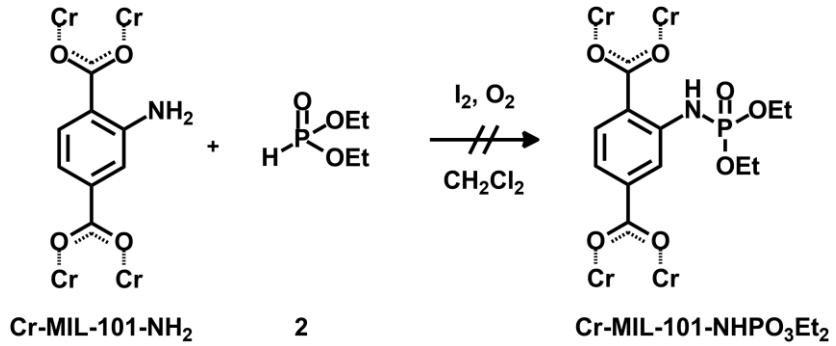

Abb. 46: Die Darstellung von Cr-MIL-101-$NHPO_3Et_2$ in einer oxidativen Kupplung war nicht erfolgreich.

Eine andere Möglichkeit zur Darstellung von Phosphorsäureamiden ist die nukleophile Substitution an Phosphorsäurechloriden. Analog zu den Vorversuchen kann Cr-MIL-101-NH_2 mit Chlorphosphorsäurediethylester (**10**) oder Phosphoroxychlorid (**11**) umgesetzt werden. Obwohl die Umsetzung mit Phosphoroxychlorid (**11**) in den Vorversuchen nicht erfolgreich war, wurde dieser Syntheseweg für Cr-MIL-101-NH_2 trotzdem ausprobiert. Dieser Weg hat den Vorteil, dass bei erfolgreicher Umsetzung eine Zwischenstufe erhalten wird, die durch Hydrolyse mit Wasser oder Hydroxid-Ionen ein Phosphorsäureamid mit freier Phosphonsäuregruppe ergibt. Mehrfachsubstitutionen am Phosphoroxychlorid (**11**) sollten nicht auftreten, da die Aminogruppen der Linker im MOF räumlich voneinander getrennt vorliegen.

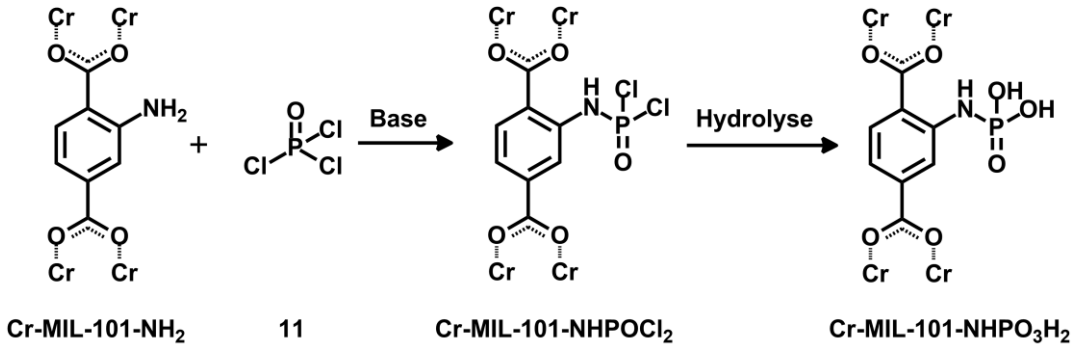

Abb. 47: Darstellung von Cr-MIL-101-$NHPO_3H_2$.

Für die Umsetzung von Cr-MIL-101-NH_2 mit Phosphoroxychlorid (**11**) wurden unterschiedliche Reaktionsbedingungen und der Einfluss einer Base untersucht.

Tab. 2: Postsynthetische Modifikation von Cr-MIL-101-NH_2 mit $POCl_3$ (**11**, min. 10 Äq.) unter Einfluss einer Base (min. 10 Äq.) mit Toluol als Lösungsmittel. (MW = Mikrowellensynthese)

Ansatz	Base	Verhältnis $POCl_3$: Base	Temperatur	Zeit	Umsatz
1	keine	-	Raumtemp.	24 h	0 %
2	NEt_3	1 : 1	Raumtemp.	24 h	0 %
3	keine	-	80 °C	24 h	0 %
4	NEt_3	1 : 1	80 °C	24 h	20 %
5	NEt_3	1 : 3	100 °C	48 h	20 %
6	Pyridin	4 : 1	120 °C	12 h	16 %
7	Pyridin	1 : 1	120 °C	12 h	18 %
8	NEt_3	1 : 1	105 °C (MW)	1 h	21 %
9	NEt_3	8 : 1	105 °C (MW)	1 h	23 %
10	Pyridin	8 : 1	105 °C (MW)	1 h	49 %

Die Untersuchungen zeigten, dass nach 24 h bei Raumtemperatur sowohl mit als auch ohne Base keine Umsetzung erfolgte (Ansatz 1 und 2). Erhöht man die Temperatur auf 80 °C, kann mit Triethylamin als Base ein Umsatz von 20 % mittels ^{1}H-NMR-Spektroskopie beobachtet werden (Ansatz 4). Ohne Base findet auch nach 24 h bei 80 °C keine Reaktion statt (Ansatz 3). In einem weiteren Ansatz wurde Reaktionszeit, -temperatur und die Menge an

Triethylamin erhöht, was jedoch nicht zu einer Erhöhung des Umsatzes führte (Ansatz 5). Mit Pyridin als Base konnte nach 12 h Rühren bei 120 °C ein vergleichbarer Umsatz beobachtet werden (Ansatz 6 und 7). Weitere Untersuchungen mit Mikrowellen-gestützter Synthese führten mit Triethylamin als Base nur zu einer geringfügigen Erhöhung des Umsatzes (Ansatz 8 und 9). Mit Pyridin als Base konnte der Umsatz bei gleichen Synthesebedingungen auf 49 % verbessert werden (Ansatz 10). Dabei wurde ein achtfacher Überschuss an Phosphoroxychlorid (**11**) gegenüber Pyridin verwendet. Zusammenfassend lässt sich sagen, dass das Verhältnis von Base zu Phosphoroxychlorid (**11**) keinen ersichtlichen Einfluss auf den Umsatz hat. Die Mikrowellen-gestützte Synthese mit Pyridin erwies sich als vielversprechender Ansatz zur Darstellung von Phosphorsäureamid-Gruppen.

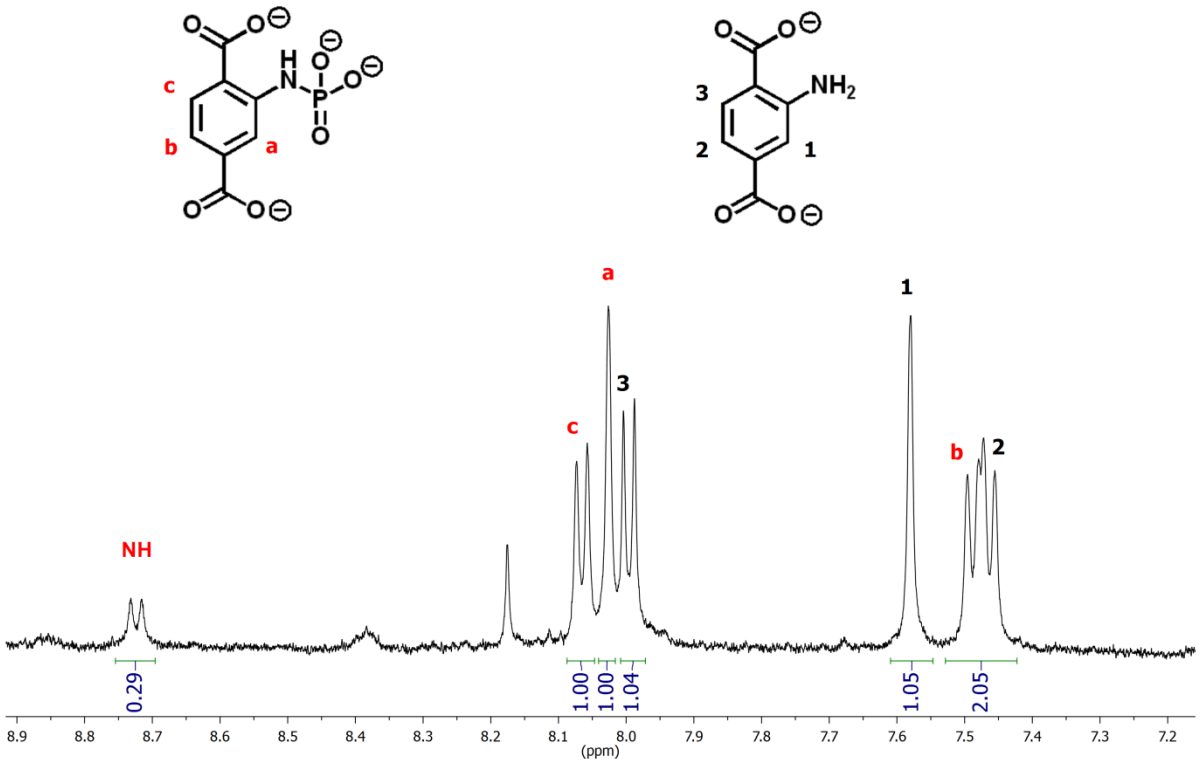

Abb. 48: ^{1}H-NMR-Spektrum des aufgelösten MOF nach der Synthese von Cr-MIL-101-NH_2 mit $POCl_3$ (**11**) zeigt einen Umsatz von 49 %.

Ein entscheidender Schritt bei der postsynthetischen Modifikation von Cr-MIL-101-NH_2 mit Phosphoroxychlorid (**11**) ist die Aufarbeitung. Dafür muss der modifizierte MOF zunächst gründlich mit wasserfreien organischen Lösungsmitteln gewaschen werden, um die Base und unreagiertes Phosphoroxychlorid (**11**) möglichst vollständig abzutrennen. Bei der anschließenden Hydrolyse mit Wasser wurde, vermutlich aufgrund der hohen

Reaktionswärme und den sehr aciden Bedingungen, häufig ein Auflösen des MOFs beobachtet. Im Rahmen dieser Arbeit wurden die modifizierten MOFs, nach dem Waschen mit organischen Lösungsmitteln, direkt mit Natronlauge behandelt. Dies sollte zum einen die entstandenen Phosphorsäurechloride hydrolysieren und zum anderen den MOF auflösen, um NMR-spektroskopische Untersuchungen durchführen zu können. Ob die Struktur des MOFs nach der postsynthetischen Modifikation noch intakt ist, wurde nicht untersucht. Dafür muss in weiteren Arbeiten zunächst eine Möglichkeit zur „milden" Hydrolyse gefunden werden.

Während die gerade erwähnten Versuche zur Implementierung von Phosphonsäure-Gruppen auf der postsynthetischen Darstellung von Phosphorsäureamiden beruhen, soll im folgendem eine andere Möglichkeit, basierend auf der in Kapitel 4.2.1 erwähnten Precusor-Methode, beschrieben werden. Analog einer literaturbekannten[221] Heck-Kupplung von Cr-MIL-101-NH_2 mit endständigen Alkenen sollten Phosphonsäurediethylester-Gruppen in den MOF implementiert werden. Dafür wurde Cr-MIL-101-NH_2 zunächst mit HBF_4 und $NaNO_2$ in das Diazonium-Salz Cr-MIL-101-$N_2^+BF_4^-$ überführt. Anschließend wurde der diazotierte MOF in einer Heck-Kupplung mit $Pd(OAc)_2$, $CaCO_3$ und Allylphosphonsäurediethylester (**15**) umgesetzt.

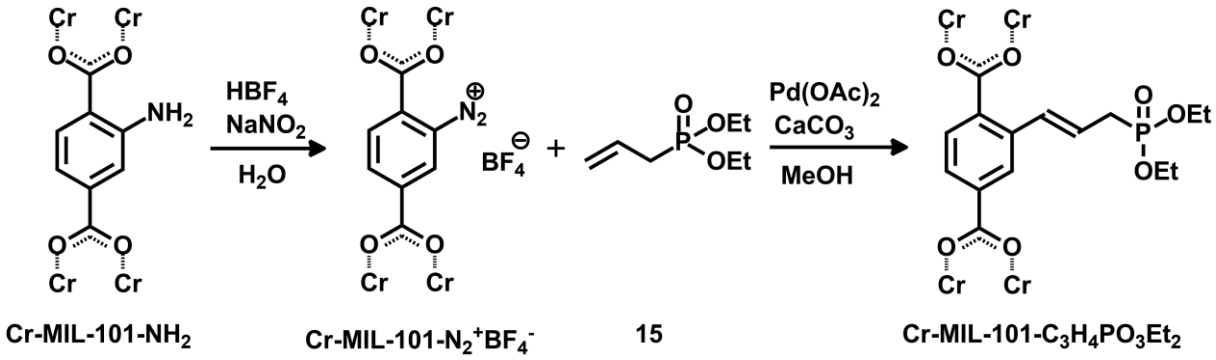

Abb. 49: Diazotierung von Cr-MIL-101-NH_2 und anschließende Heck-Kupplung.

Nach Auflösen des MOFs mit einer 2M-Natriumhydroxid-Lösung zeigte das ^{1}H-NMR-Spektrum eine Mischung aus dem gewünschten Produkt der Heck-Kupplung und Terephthalsäure. Die Abwesenheit von 2-Aminoterephthalsäure bedeutet, dass die Diazotierung quantitativ abgelaufen sein muss. Die oxidative Addition des Palladiumkatalysators muss ebenfalls quantitativ abgelaufen sein, da keine Nebenprodukte der Phenol-Verkochung nachgewiesen werden konnten. Einen Vergleich der Integrale im ^{1}H-NMR-Spektrum ergab ein Umsatz von 58 % für das Produkt der Heck-Kupplung. Durch die basischen Bedingungen beim Auflösen des MOFs wurde der Phosphonsäurediethylester zum jeweiligen Monoester hydrolysiert. Linkermoleküle, die nicht in einer Heck-Kupplung

umgesetzt wurden, konnten als Terephthalsäure identifiziert werden. Ein Vergleich der Röntgenpulverdiffraktogramme von Cr-MIL-101-NH_2 und Cr-MIL-101-$C_3H_4PO_3Et_2$ zeigte, dass die Struktur während der postsynthetischen Modifikation erhalten geblieben ist (s. Kapitel 6.2.2).

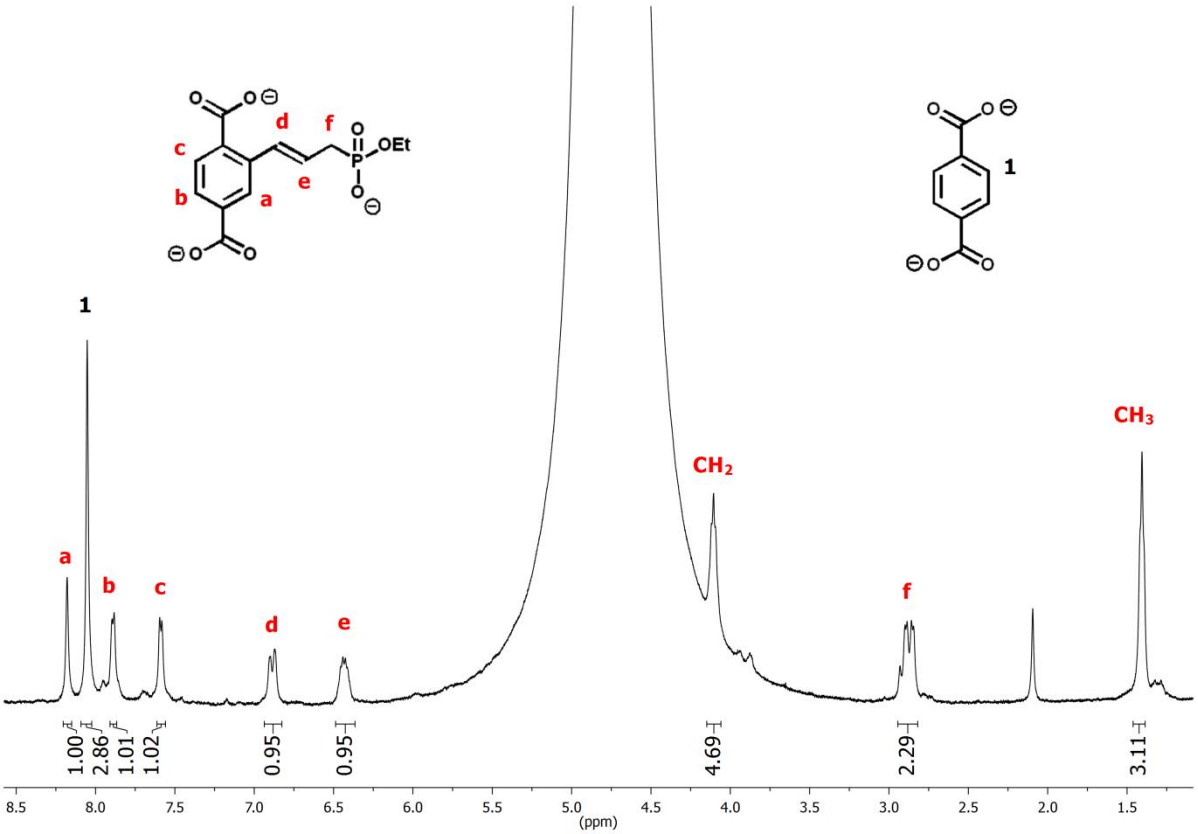

Abb. 50: ^{1}H-NMR-Spektrum nach dem Auflösen des Cr-MIL-101-$C_3H_4PO_3Et_2$ in $NaOH_{aq}$.

Im Rahmen dieser Arbeit sollten neue postsynthetische Methoden zur Implementierung von Phosphonsäure-Gruppen in einen MOF entwickelt werden. Bei zwei der gewählten Methoden konnte ein Umsatz zum jeweiligen Phosphonsäurediethylester nachgewiesen werden. Zur Darstellung von MOFs mit freien Phosphonsäure-Gruppen sind jedoch noch weitere Untersuchungen bezüglich der Hydrolyse von Phosphorsäurechloriden und der Hydrolyse von Phosphonsäurediethylestern notwendig. Zusätzlich wurde ein Überblick über Synthesemethoden zur Darstellung von Phosphonsäuredialkylestern bzw. Phosphonsäuren gegeben.

5 Zusammenfassung und Ausblick

Die Ergebnisse der prä- und postsynthetischen Modifikation zur Darstellung von funktionalisierten IRMOFs und protonenleitfähigen MOFs sind in den folgenden Kapiteln zusammengefasst. Ergebnisse bezüglich der Synthese von funktionalisierten Triazin-Linkern und der postsynthetischen Modifikation eines funktionalisierten IRMOFs werden in Kapitel 5.1 zusammengefasst. In Kapitel 5.2 werden die Ergebnisse bezüglich der Synthese neuer Phosphosulfonsäure-Linker und in Kapitel 5.3 die Ergebnisse zur Implementierung von Phosphonsäure-Gruppen in Cr-MIL-101-Derivate zusammengefasst.

5.1 Funktionalisierte Triazin-Linker: Synthese und PSM

Ein Ziel dieser Arbeit war die Synthese von erweiterten und funktionalisierten Triazin-Linkern. Diese sollten für die Darstellung von isoretikularen MOFs zur Verfügung gestellt werden. Dafür wurden sowohl literaturbekannte als auch literaturunbekannte Triazin-Linker synthetisiert.

Die Erweiterung der von KLINKEBIEL[172] beschriebenen TAPB-Linker erfolgte ausgehend von Tribromtriazin **V1-3a**, **V1-3b** oder **V1-3c** und Biphenylboronsäureester **V1-18**. Dafür wurde jedes der Tribromtriazine **V1-3a**, **V1-3b** oder **V1-3c** mit jeweils drei Äquivalenten des Biphenylboronsäureester **V1-18** in einer Suzuki-Kupplung umgesetzt. Die jeweiligen Trimethylester **V1-19a**, **V1-19b** und **V1-19c** konnten erfolgreich in Ausbeuten von 24 % [**V1-19a**], 16 % [**V1-19a**] und 81 % [**V1-19a**] erhalten werden. Sowohl der unfunktionalisierte Trimethylester **V1-19a** als auch der nitrofunktionalisierte Trimethylester **V1-19b** konnte in guten Ausbeuten zur entsprechenden Tricarbonsäure **V1-20a** (99 %) bzw. **V1-20b** (79 %) hydrolysiert werden. Der methoxyfunktionalisierte Trimethylester **V1-19c** wurde mit geschmolzenen Pyridinhydrochlorid umgesetzt. Auf diese Weise konnten gleichzeitig die Methylester-Gruppen und der Methylether gespalten werden. Der hydroxyfunktionalisierte Tricarbonsäure-Linker **V1-20c** konnte in einer Ausbeute von 62 % isoliert werden.

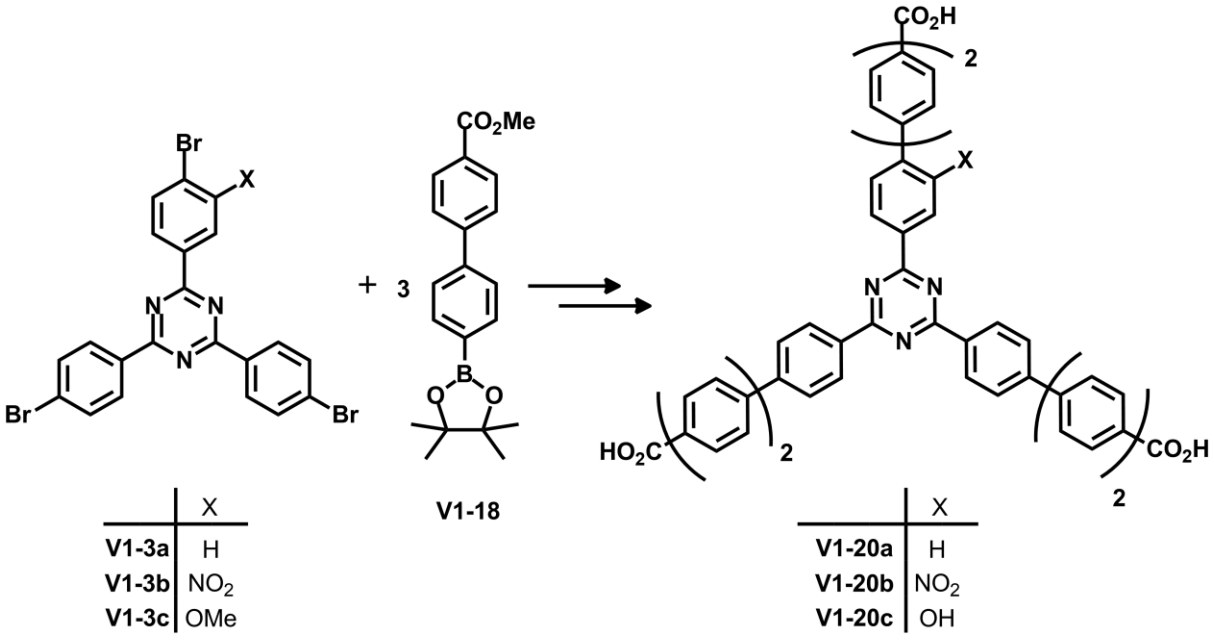

	X
V1-3a	H
V1-3b	NO_2
V1-3c	OMe

	X
V1-20a	H
V1-20b	NO_2
V1-20c	OH

Abb. 51: Synthese der erweiterten Triazin-Linker **V1-20a**, **V1-20b** und **V1-20c**.

Die Spaltung eines Methylethers mit Pyridinhydrochlorid konnte außerdem erfolgreich zur Darstellung des hydroxyfunktionalisierten H_3TAPB-Linker **V1-17e** genutzt werden. Dieser konnte ausgehend vom Trimethylester **V1-16c** in einer Ausbeute von 52 % erhalten werden.

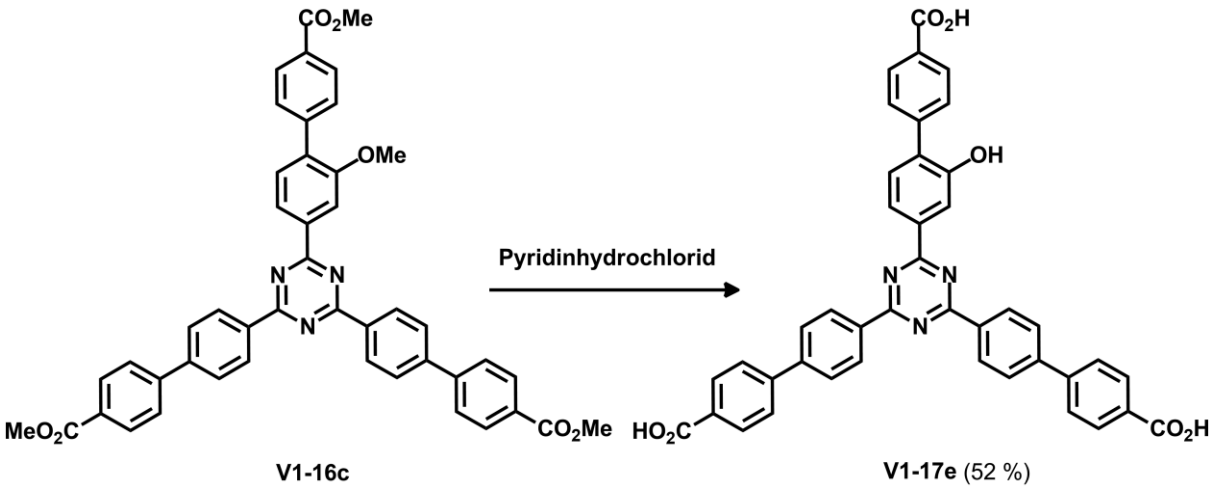

Abb. 52: Darstellung des hydroxyfunktionalisierten H_3TAPB-Linker **V1-17e**.

Die funktionalisierten H_3TATB-Linker **V2-5a**, **V2-5b**, **V2-5c** und **H_3TATB-NH_2(*ortho*)** und der **H_3TAPB-OMe**-Linker wurden erfolgreich im Multigrammmaßstab synthetisiert und für die Darstellung von MOFs zur Verfügung gestellt.

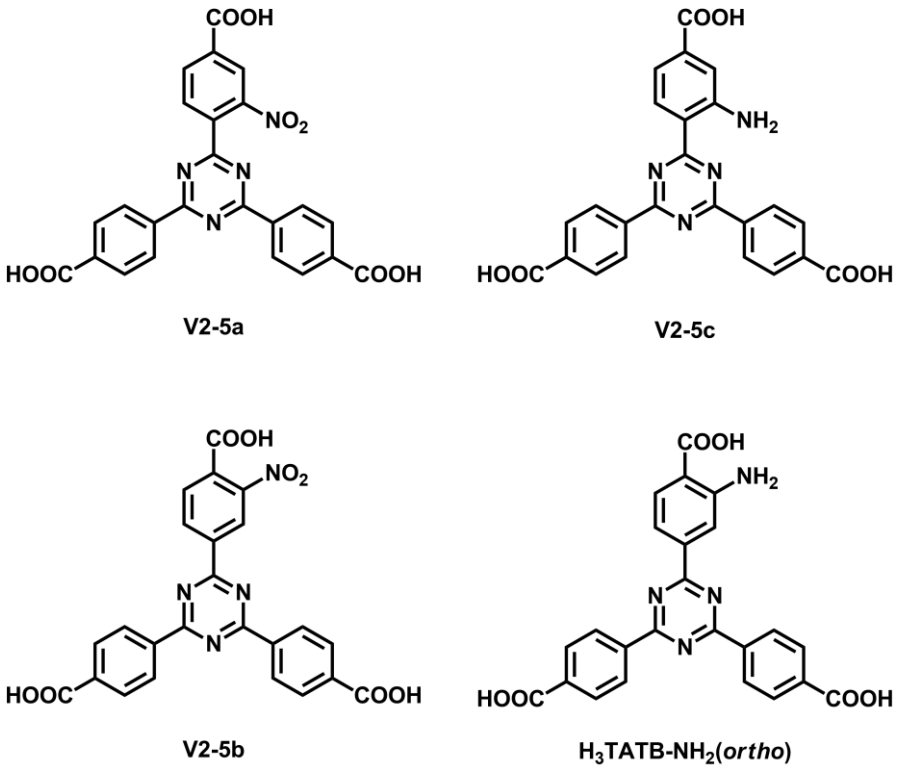

Abb. 53: Funktionalisierte H_3TATB-Linker **V2-5a**, **V2-5b**, **V2-5c** und **H_3TATB-NH_2(*ortho*)**.

Der *meta*-substituierte H_3TATB-NH_2(*m*)-Linker **V2-5c** wurde von ERIKA VIRMANI (geb. MÜHLBAUER) und STEFAN WUTTKE erfolgreich mit $Cu(NO_3)_2$•$3H_2O$ zu einem MOF mit PCN-6-Struktur umgesetzt. Die nitrofunktionalisierten Triazin-Linker **V2-5a** und **V2-5b** sowie der **H_3TAPB-OMe**-Linker wurden von ERIKA VIRMANI zur Darstellung neuer Eisen(III)-basierter Misch-Linker-MOFs mit MIL-143-Struktur verwendet. Mit Hilfe des aminofunktionalisierten **H_3TATB-NH_2(*ortho*)** wurde von MILAN KÖPPEN ein Bismut-MOF (CAU-7-TATB-NH_2) mit CAU-7-Struktur dargestellt.

Aufgrund der Verfügbarkeit von aminofunktionalisiertem CAU-7-TATB-NH_2 sollten außerdem Methoden zur postsynthetischen Modifikation entwickelt werden. Dafür wurden verschiedene, für Amino-MOFs etablierte, postsynthetische Modifikationen untersucht (s. Kapitel 1.2). CAU-7-TATB-NH_2 konnte erfolgreich mit Essigsäureanhydrid, Valeriansäureanhydrid, Bernsteinsäureanhydrid, Phthalsäureanhydrid und 1,3-Propansulton umgesetzt werden. Der Funktionalisierungsgrad variierte je nach Reaktionspartner zwischen 33 % und 79 %. Mit Hilfe von Röntgenpulverdiffraktogrammen konnte, für jeden der fünf modifizierten MOFs, ein Erhalt der Struktur bestätigt werden. Durch die Umsetzung mit Bernsteinsäureanhydrid, Phthalsäureanhydrid und 1,3-Propansulton konnten außerdem organische Säuregruppen in die Struktur implementiert werden. Dies sind die ersten beschriebenen Beispiele für eine postsynthetische Modifikation an einem Bismut-MOF.

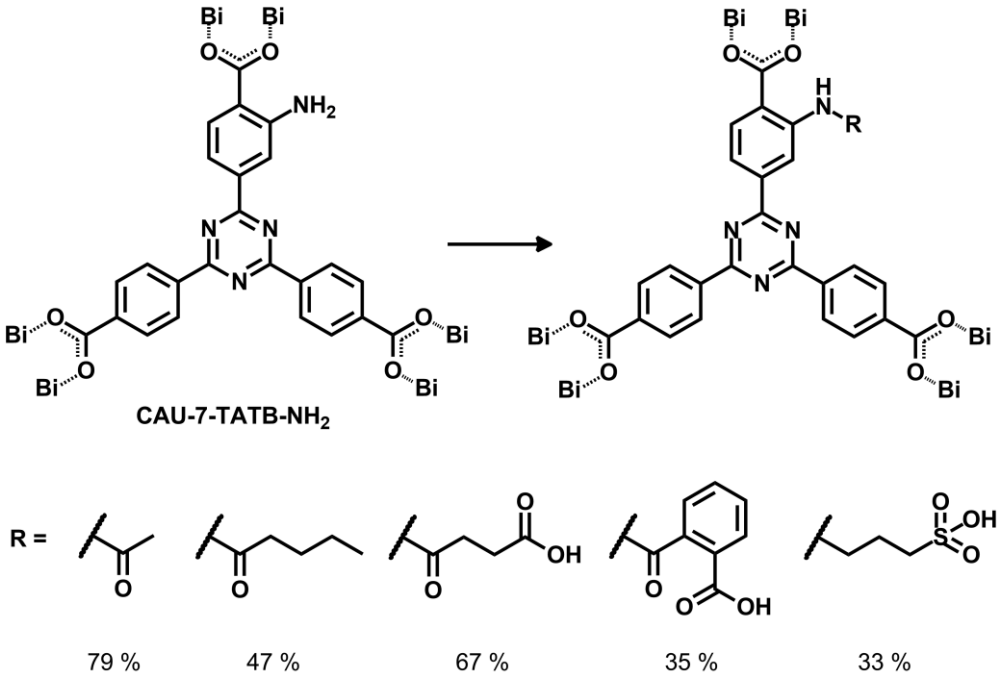

Abb. 54: PSM am CAU-7-TATB-NH_2 mit unterschiedlichen Anhydriden und 1,3-Propansulton.

Zusätzlich wurden postsynthetische Modifikationen mit Methansulfonsäurechlorid, Acetylchlorid und Ethylisocyanat ausprobiert. Dabei wurde entweder ein Auflösen oder eine Zersetzung der Struktur beobachtet.

5.2 Synthese von Phosphosulfonsäure-Linkern

Ein weiteres Ziel dieser Arbeit war die Synthese von Phosphosulfonsäure-Linkern zur Darstellung von protonenleitfähigen MOFs. Für die Darstellung dieser Linker wurden zwei unterschiedliche Syntheserouten entwickelt.

Ausgehend von Tetrakis(brommethyl)benzol (**M3-1**) wurde im Rahmen dieser Arbeit eine Syntheseroute zur Darstellung von vier Phosphosulfonsäure-Linkern entwickelt. Dafür wurde Tetrakis(brommethyl)benzol (**M3-1**) in einer nukleophilen Substitution zunächst mit zwei Äquivalenten Triethylphosphit umgesetzt. Unter den gewählten Reaktionsbedingungen wurde ein Gemisch aus unsubstituierten sowie einfach-, zweifach-, dreifach- und vierfach-substituiertem Tetrakis(brommethyl)benzol erhalten.

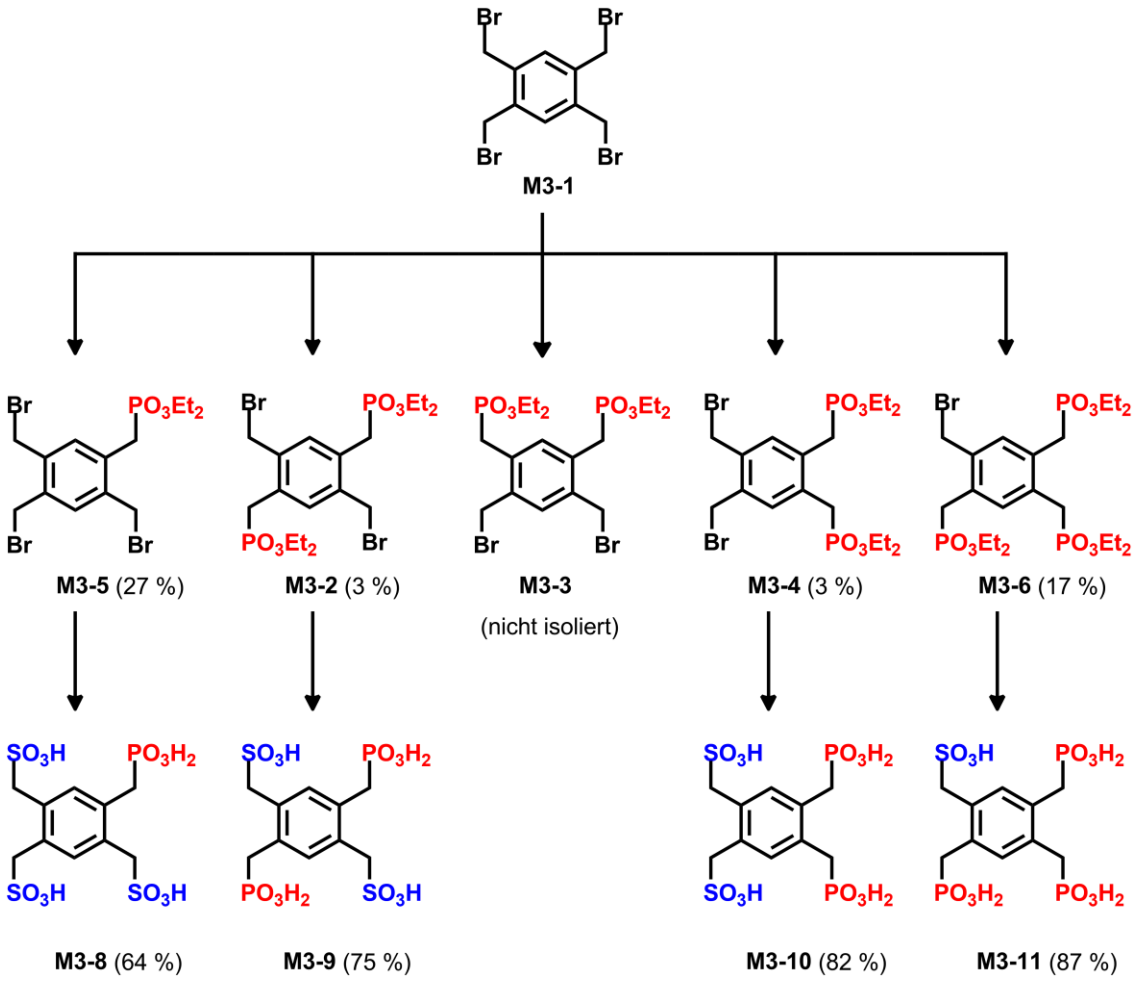

Abb. 55: Syntheseübersicht zur Darstellung der Phosphosulfonsäure-Linker **M3-8**, **M3-9**, **M3-10** und **M3-11**.

Mit Hilfe einer säulenchromatographischen Reinigung konnten der Monophosphonsäure-diethylester **M3-5** und der Triphosphonsäurediethylester **M3-6** vom Reaktionsgemisch abgetrennt und in einer Ausbeute von 27 % bzw. 17 % isoliert werden. Zusätzlich wurde ein

Gemisch der schwierig zu trennenden Diphosphonsäurediethylester **M3-2**, **M3-3** und **M3-4** erhalten. Mittels Kristallisation und anschließender säulenchromatographischer Reinigung konnten die Diphosphonsäurediethylester **M3-2** und **M3-4** zwar vom Gemisch abgetrennt werden, aber nur in geringen Ausbeuten von jeweils 3 % isoliert werden. Der Diphosphonsäurediethylester **M3-3** konnte zwar NMR-spektroskopisch nachgewiesen werden, eine Isolierung war jedoch nicht erfolgreich. Durch Umsetzung mit Natriumsulfit und anschließender Hydrolyse der Phosphonsäurediethylester-Gruppen konnten die Phosphosulfonsäure-Linker **M3-8**, **M3-9**, **M3-10** und **M3-11** in guten Ausbeuten dargestellt werden.

Ein anderer Ansatz zur Darstellung von Phosphosulfonsäure-Linkern ist die direkte Verknüpfung von Phosphonsäure- und Sulfonsäure-Gruppen mit einem Benzol-Ring. Im Rahmen dieser Arbeit wurde eine Syntheseroute zur Darstellung von tri- und tetrasubstituierten Phosphosulfonsäure-Linkern entwickelt. In einem ersten Syntheseschritt wurden verschiedene Brom-substituierte Benzolsulfonsäuren synthetisiert, welche anschließend in einer Palladium-katalysierten Kreuzkupplung mit Triethylphosphit umgesetzt wurden. Die erhaltenen Phosphonsäurediethylester-Gruppen wurden durch Hydrolyse in die jeweiligen Phosphonsäure-Gruppen überführt.

Die trisubstituierten Brombenzolsulfonsäuren **M3-13**, **M3-16** und **M3-18** konnten durch Bromierung, *ipso*-Sulfonierung oder Sulfonierung in guten Ausbeuten dargestellt werden.

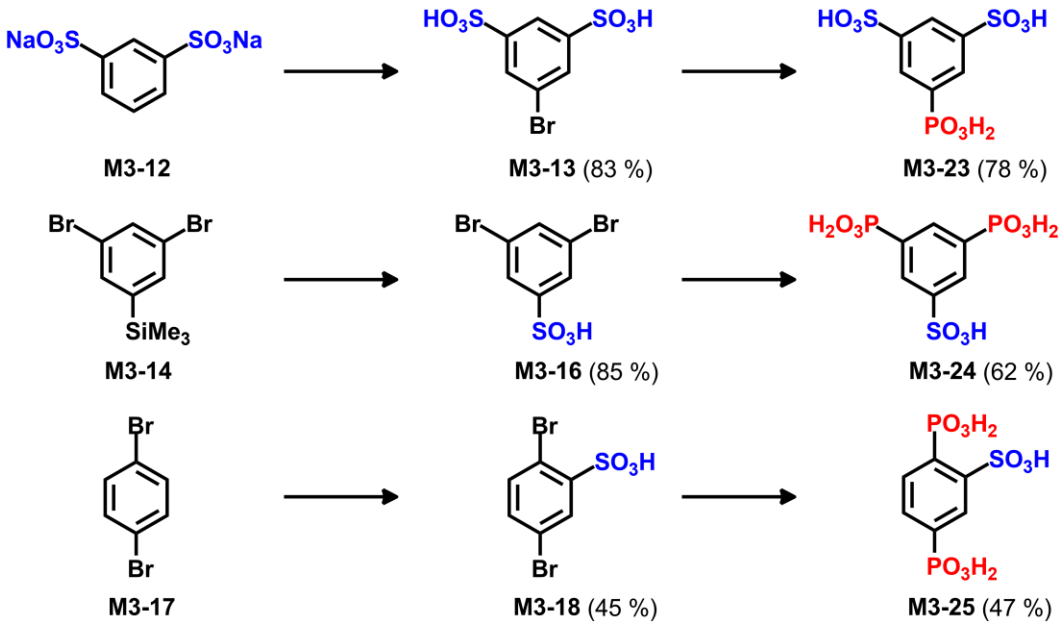

Abb. 56: Synthese der trisubstituierten Phosphosulfonsäure-Linker **M3-23**, **M3-24** und **M3-25**.

Phosphonsäure-Gruppen konnten erfolgreich durch Mikrowellen-gestützte Kreuzkupplung mit Triethylphosphit und anschließende Hydrolyse eingeführt werden. Die trisubstituierten Phosphosulfonsäure-Linker **M3-23**, **M3-24** und **M3-25** wurden in guten Ausbeuten isoliert. Durch Sulfonierung von 1,4-Dibrombenzol **M3-17** und 1,3-Dibrombenzol **M3-21** konnten die drei tetrasubstituierten Brombenzolsulfonsäuren **M3-19**, **M3-20** und **M3-22** dargestellt werden. Nach anschließender Kreuzkupplung und Hydrolyse wurden die tetrasubstituierten Phosphosulfonsäure-Linker **M3-23**, **M3-24** und **M3-25** isoliert.

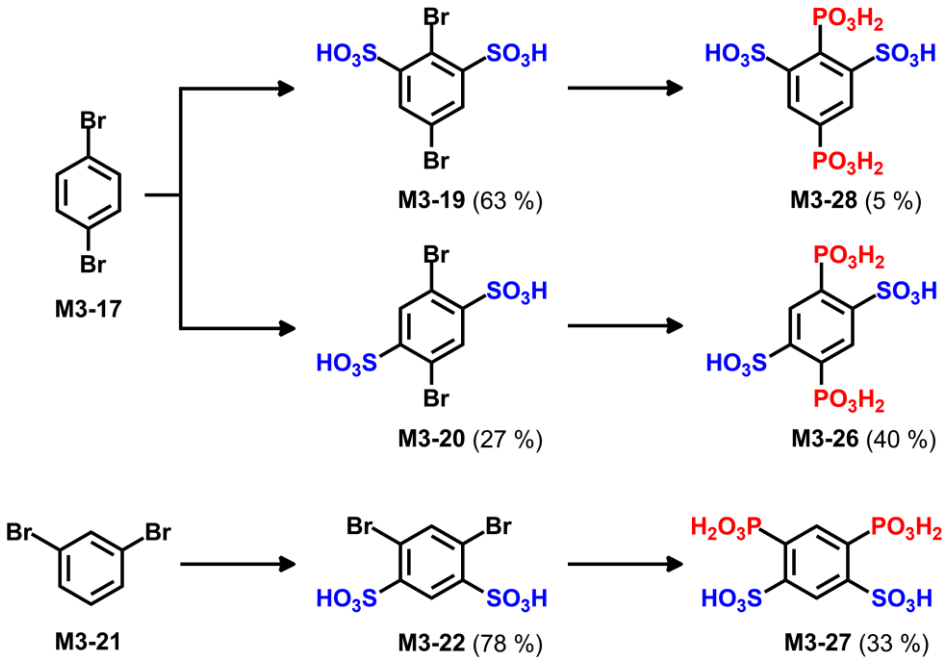

Abb. 57: Synthese der tetrasubstituierten Phosphosulfonsäure-Linker **M3-26**, **M3-27** und **M3-28**.

Die Phopshosulfonsäure-Linker **M3-9**, **M3-10, M3-11** und **M3-26** konnte bereits erfolgreich zur Darstellung verschiedener Lanthan-MOFs bzw. CPs verwendet werden.[222,223]

5.3 PSM von Cr-MIL-101-Derivaten

Ein weiteres Ziel dieser Arbeit war die Entwicklung von postsynthetischen Methoden zur Implementierung von Phosphonsäure-Gruppen in verschiedene Cr-MIL-101-Derivate (Cr-MIL-101, Cr-MIL-101-Br, Cr-MIL-101-NH_2). Dafür wurden zunächst Vorversuche zum Einführen von Phosphonsäurediethylester-Gruppen durchgeführt. Um die Reaktionskontrolle zu vereinfachen, wurde von den Dimethylestern der Linker-Moleküle Terephthalsäure (Cr-MIL-101), 2-Bromterephthalsäure (Cr-MIL-101-Br) und 2-Aminoterephthalsäure (Cr-MIL-101-NH_2) ausgegangen.

Terephthalsäuredimethylester (**1**) konnte erfolgreich, in einer oxidativen Kupplung mit Diethylphosphit (**2**), funktionalisiert werden. Der Phosphonsäurediethylester **3** konnte mit einer Ausbeute von 20 % isoliert werden.

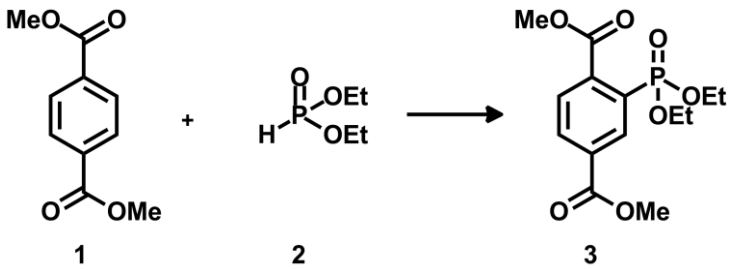

Abb. 58: Oxidative Kupplung zur Darstellung des Phosphonsäurediethylester **3**.

2-Bromterephthalsäuredimethylester (**6**) konnte in einer Palladium-katalysierten Kreuzkupplung mit Triethylphosphit (**7**) ebenfalls zum Phosphonsäurediethylester **3** umgesetzt werden.

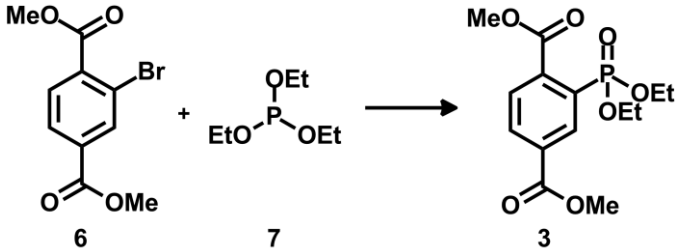

Abb. 59: Palladium-katalysierte Kreuzkupplung zur Darstellung des Phosphonsäurediethylester **3**.

Das Einführen von Phosphonsäurediethylester-Gruppen am 2-Aminoterephthalsäure-dimethylester (**8**) konnte erfolgreich durch nukleophile Substitution oder oxidative Kupplung erreicht werden. Die oxidative Kupplung erfolgte durch Umsetzung des 2-Aminoterephthalsäuredimethylesters (**8**) mit Diethylphosphit unter Einfluss von

elementarem Iod und Luftsauerstoff. Das Phosphorsäureamid **9** konnte nach säulenchromatographischer Reinigung mit einer Ausbeute von 27 % isoliert werden.

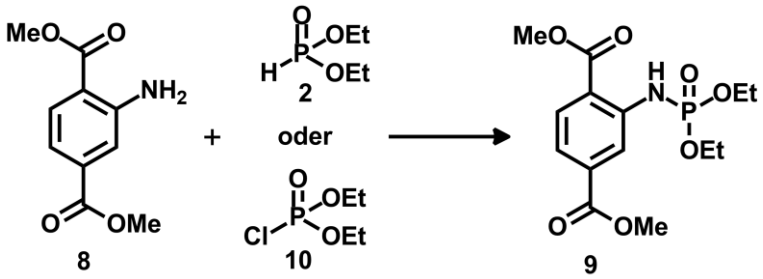

Abb. 60: Synthese des Phosphorsäureamids **9** mittels oxidativer Kupplung (27 %) oder nukleophiler Substitution (18 %).

Zusätzlich konnte das Phosphorsäureamid **9** durch nukleophile Substitution des Chlorphosphorsäurediethylester (**10**) mit 2-Aminoterephthalsäuredimethylester (**8**) dargestellt werden.

Auf Basis der erfolgreichen Vorversuche wurden postsynthetische Modifikationen an Cr-MIL-101-Derivaten durchgeführt. Die Implementierung von Phosphonsäurediethylester-Gruppen mittels oxidativer Kupplung war sowohl für den Cr-MIL-101 als auch für den Cr-MIL-101-NH_2 nicht erfolgreich.

Bei der postsynthetischen Modifikation des Cr-MIL-101-Br mit Triethylphosphit (**7**) konnte eine Umsetzung der 2-Bromterephthalsäure-Linker beobachtet werden. NMR-spektroskopische Untersuchungen nach Auflösen des MOFs zeigten, dass sich die 2-Bromterephthalsäure sowohl zum gewünschten Phosphonsäurediethylester als auch zur Terephthalsäure umgesetzt hatte.

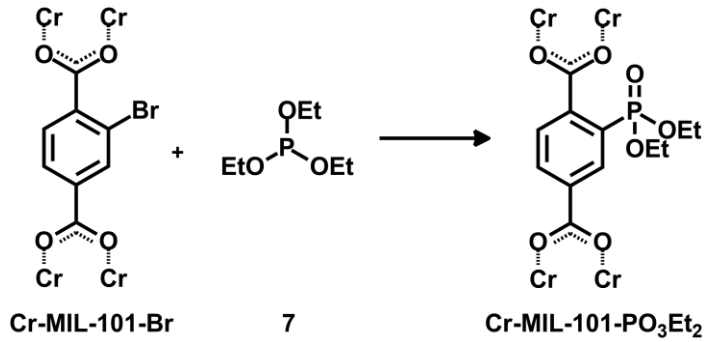

Abb. 61: Palladium-katalysierte Kreuzkupplung zur postsynthetischen Implementierung von Phosphonsäure-diethylester-Gruppen.

Die Umsetzung zum Phosphonsäurediethylester variierte je nach Ansatz zwischen 7 % und 25 %. Röntgenpulverdiffraktogramme vom modifizierten MOF bestätigen, dass die Struktur nach der posytsynthetischen Modifikation intakt geblieben ist.

Basierend auf den Vorversuchen zur nukleophilen Substitution konnte Cr-MIL-101-NH_2 erfolgreich mit Phosphoroxychlorid (**11**) modifiziert werden. Durch Optimierung der Reaktionsbedingungen konnte eine Umsetzung von bis zu 49 % erreicht werden.

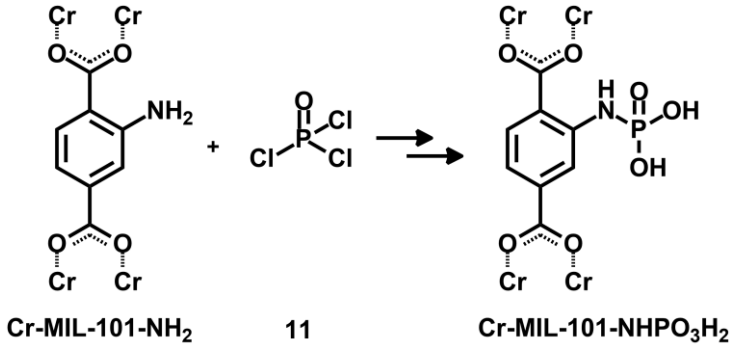

Abb. 62: Nukleophile Substitution mit Phosphoroxychlorid (**11**) und anschließende Hydrolyse.

Ausgehend von Cr-MIL-101-NH_2 konnte außerdem eine Heck-Kupplung zur Implementierung von Phosphonsäurediethylester-Gruppen etabliert werden. Dafür wurde die Aminogruppe von Cr-MIL-101-NH_2 zunächst in ein Diazionium-Salz überführt und dieses anschließend in einer Heck-Kupplung mit Allylphosphonsäurediethylester (**15**) umgesetzt. NMR-spektroskopische Untersuchungen zeigten eine Umsetzung von 58 % für das Produkt der Heck-Kupplung.

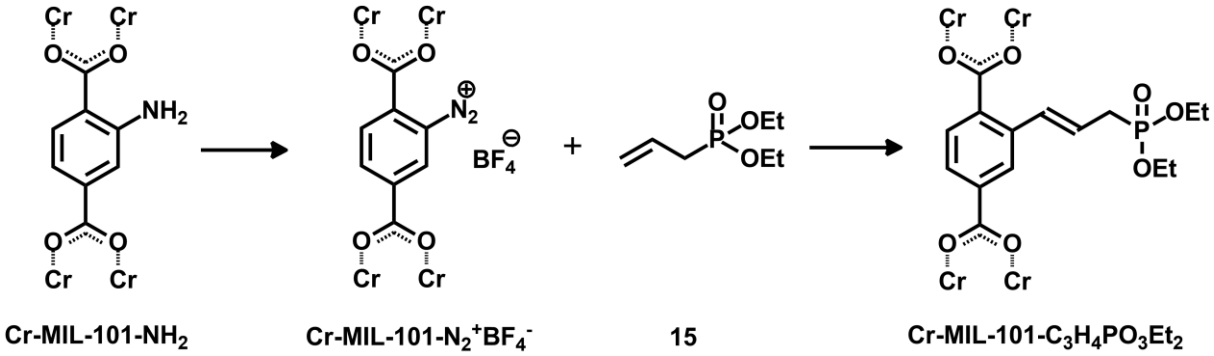

Abb. 63: Heck-Kupplung zur Implementierung von Phosphonsäurediethylester-Gruppen.

5.4 Ausblick

Im Rahmen dieser Arbeit wurden Methoden zur prä- und postsynthetischen Darstellung von funktionalisierten IRMOFs und protonenleitfähigen MOFs entwickelt. Für die präsynthetische Darstellung wurden funktionalisierte Triazin-Linker bzw. Phosphosulfonsäure-Linker synthetisiert. Die postsynthetischen Reatkionen erfolgten an präsynthetisch funktionalisierten MOFs.

Um den Pool an funktionalisierten Triazin-Linkern noch zu erweitern, könnte die in dieser Arbeit etablierte Methode zur Darstellung von hydroxyfunktionalisierten Triazin-Linkern genutzt werden, um hydroxyfunktionalisierte H_3TATB-Linker zu synthetisieren. Zusätzlich könnte versucht werden, den nitrosubstituierten Linker **V1-20b** durch Reduktion in den entsprechenden aminosubstituierten Linker zu überführen.

Weitere Arbeiten sollten sich zunächst mit der Darstellung von MOFs basierend auf den in dieser Arbeit beschriebenen Triazin- und Phosphosulfonsäure-Linkern beschäftigen. Dabei sollten vor allem die physikalischen und chemischen Eigenschaften dieser MOFs in Hinblick auf potentielle Anwendungen untersucht werden. MOFs, basierend auf den beschriebenen Phosphosulfonsäure-Linkern, könnten als protonenleitfähige Materialien oder heterogene Brønsted-acide Katalysatoren eingesetzt werden. Die funktionalisierten Triazin-Linker sollten zur Darstellung weiterer isoretikularer MOFs verwendet werden. Durch Variation der Linkergröße, der funktionellen Gruppen oder durch postsynthetische Modifikation könnten auf diesem Weg MOFs mit definierten Poreneigenschaften (Acidität, Porengröße, Polarität, katalytische Aktivität) dargestellt werden.

Die in dieser Arbeit gezeigten Ansätze zur postsynthetischen Implementierung von Phosphonsäure-Gruppen sollten in folgenden Arbeiten weiter untersucht und optimiert werden. Dabei muss vor allem eine Methode zur Hydrolyse der Phosphonsäurediethylester-Gruppen entwickelt werden. Für die vielversprechende Umsetzung des Cr-MIL-101-NH_2 mit Phosphoroxychlorid (**11**) muss ebenfalls eine Methode zur Hydrolyse der entstandenen Phosphonsäurechlorid-Gruppen gefunden werden, bei der sich das MOF nicht auflöst. In weiteren Arbeiten könnten außerdem andere Methoden zur Implementierung von Phosphonsäure-Gruppen bzw. Phosphonsäurediethylester-Gruppen ausprobiert werden. Ein Überblick über mögliche Methoden ist in Kapitel 4.2.1 gegeben.

6 Experimenteller Teil

6.1 Allgemeine Hinweise

6.1.1 Verwendete Geräte

Schmelzpunktbestimmung

Schmelzpunktbestimmungsgerät der Fa. Gallenkamp.

NMR-Spektroskopie

FT-NMR-Spektrometer DRX 500, (^{1}H: 500 MHz, ^{13}C: 125 MHz, ^{31}P: 202 MHz), Fa. Bruker.

Alle Spektren wurden, wenn möglich, mit Hilfe des nicht vollständig deuterierten Lösungsmittels referenziert. Die chemischen Verschiebungen δ sind in ppm und die Kopplungskonstanten J in Hertz (Hz) angegeben. Kopplungen mit Phosphor-Atomen werden im ^{1}H-NMR mit $J_{H\text{-}P}$ und im ^{13}C-NMR mit $J_{C\text{-}P}$ gekennzeichnet. Alle Spektren wurden bei 300 K gemessen. Bei literaturunbekannten Substanzen wurden einige Signale mit Hilfe zweidimensionaler Messmethoden (COSY, HSQC, HMBC) zugeordnet. Die Spinmultiplizitäten im ^{1}H-NMR (Singulett, Dublett, Triplett, Quartett, Multiplett und zentriertes Multiplett) wurden mit s, d, t, q, m und m_c abgekürzt. Im ^{13}C-NMR geben die Abkürzungen den Strukturtyp des Kohlenstoffatoms an (s: quartär, d: tertiär, t: sekundär, q: primär). Für Kopplungen mit Phosphor-Atomen wird im ^{13}C-NMR die jeweilige Multiplizität in eckigen Klammern und mit einem „P“ im Index angegeben. Zur Charakterisierung von literaturbekannten Strukturen wurden lediglich ^{1}H-NMR-Spektren und für phosphorhaltige Strukturen zusätzlich ein ^{31}P-NMR angefertigt. Bei der Auswertung der NMR-Spektren wurden „Ar“ als Abkürzung für Aryl verwendet.

Massenspektrometrie

Applied Biosystems Mariner 5280 (ESI).

JEOL AccuTOF GCV 4G (HRMS, Elektronenstoß-Ionisation erfolgte bei 70 eV).

IR-Spektroskopie

Perkin Elmer Spectrum 100 mit Golden Gate Diamond ATR Einheit A531-G.

Röntgenbeugung

STOE-Stadi-P Combi Diffraktometer.

Synthese-Mikrowelle

Discover SP Mikrowellen-System mit Explorer 12 Hybrid-Autosampler.

6.1.2 Verwendete Chemikalien

Die folgenden Chemikalien wurden käuflich erworben oder dem Laborbestand entnommen und ohne weitere Reinigung eingesetzt.

Chemikalie	Hersteller	Reinheit
Allylphosphonsäurediethylester	Sigma Aldrich	98 %
Aluminiumchlorid-Hexahydrat	Merck	97 %
2-Aminoterephthalsäuredimethylester	Alfa Aesar	97 %
1,1-Bis(diphenylphosphin)ferrocen-palladiumdichlorid	ABCR	99.9 %
2-Bromterephthalsäuredimethylester	TCI	98 %
Calciumcarbonat	Merck	99 %
Chlorphosphorsäurediethylester	Fluka	97 %
Diethylphosphit	ABCR	94 %
Essigsäure	Merck	99.8 %
Iod	Laborbestand	reinst
Magnesiumsulfat	Grüssing	reinst
Mangan(III)acetat-Dihydrat	Sigma Aldrich	97 %
Methoxyacetylchlorid	Sigma Aldrich	97 %

Natriumhydrogencarbonat	Grüssing	99 %
Natriumhydroxid	Merck	99.9 %
Natriumnitrit	Laborbestand	reinst
Palladium(II)acetat	TCI	98%
Palladium(II)chlorid	Alfa Aesar	99%
Phosphoroxychlorid	Sigma Aldrich	99 %
Pyridin	Acros	98 %
Salpetersäure	Acros	65 %
Salzsäure	Merck	37 %
Terephthalsäuredimethylester	Sigma Aldrich	99 %
Tetrafluorborsäure	Alfa Aesar	48 %
Triethylamin	Fisher Scientific	99.5 %
Triethylphosphit	Alfa Aesar	98 %

6.1.3 Verwendete Lösungsmittel

Die folgenden Lösungsmittel wurden vor der Verwendung durch Destillation gereinigt und gegebenenfalls unter Verwendung des angegebenen Trockenmittels getrocknet. Wasserfreies Dichlormethan wurde unter Stickstoffatmosphäre aus einer Trocknungsanlage bezogen (PureSolv MD3 Solvent Purification System, Fa. Inert).

Lösungsmittel	**Trockenmittel/Indikator**	**Hersteller**
Aceton	Molekularsieb, 3 Å	BCD.
Cyclohexan		BCD
Dichlormethan		BCD
Dichlormethan, HPLC grade	PureSolv MD3	Prolabo
Essigsäureethylester		BCD
Ethanol		Walther CMP

Methanol		BCD
Toluol	Molekularsieb, 4 Å	BCD

6.1.4 Adsorbentien für Chromatographie

Für säulenchromatographische Reinigungen wurde Kieselgel der Fa. Macherey-Nagel mit einer Korngröße von 0.04-0.063 mm verwendet.

Dünnschichtchromatographie wurde mit DC-Aluminiumfolien (Kieselgel 60 F_{254}) der Fa. Merck durchgeführt.

Die angegebenen R_f-Werte beziehen sich auf das Ergebnis aus der Dünnschichtchromatographie.

6.2 Synthesen

6.2.1 Vorversuche

6.2.1.1 2-(Diethoxyphosphonyl)terephthalsäuredimethylester (3)

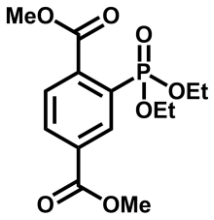

Vorschrift A:

Terephthalsäuredimethylester (**1**, 500 mg, 2,575 mmol) und Mangan(III)triacetat-Dihydrat (2.07 g, 7.73 mmol) wurden in Eisessig (10 mL) vorgelegt und mit Diethylphosphit (**2**, 663 µL, 5.15 mmol) versetzt. Die Reaktionsmischung wurde für 12 h bei 60 °C gerührt. Anschließend wurde Wasser (50 mL) zugegeben und mit Ethylacetat (3 x 50 mL) extrahiert. Die vereinigten org. Extrakte wurden mit ges. Natriumchlorid-Lösung (50 mL) gewaschen, über Magnesiumsulfat getrocknet und das Lösungsmittel i. Vak. entfernt. Der Rückstand wurde mittels Säulenchromatographie (Kieselgel, Cyclohexan/Ethylacetat = 1:1, R_f = 0.12) gereinigt. Ein farbloser Feststoff wurde erhalten.

Ausbeute: 170 mg (515 µmol, 20 %).

Vorschrift B:

2-Bromterephthalsäuredimethylester (**6**, 50.0 mg, 183 µmol), Diethylphosphit (**2**, 94 µL, 732 µmol) und Triethylamin (100 µL, 732 µmol) wurden in einem Mikrowellen-Vial vorgelegt und mit Toluol (2 mL) versetzt. Anschließend wurde Pd(dppf)Cl_2 (1.4 mg, 1.8 µmol) zugegeben und das Vial in einer Synthese-Mikrowelle für 15 min bei 150 °C (max. 200 W) bestrahlt. Die Reaktionsmischung wurde mittels Dünnschichtchromatographie (DC) untersucht.

Ausbeute: Die Ausbeute wurde nicht bestimmt. Mittels DC-Untersuchung konnte das gewünschte Produkt **3** nachgewiesen werden. Die Abwesenheit von Edukt **6** deutet auf eine vollständige Umsetzung hin.

Vorschrift C:

2-Bromterephthalsäuredimethylester (**6**, 50.0 mg, 183 µmol) und Triethylphosphit (**7**, 200 µL, 1.17 mmol) wurden in einem Mikrowellen-Vial vorgelegt und mit $PdCl_2$ (3.2 mg, 18 µmol) versetzt. Das Vial wurde in einer Synthese-Mikrowelle für 20 min bei 200 °C (max. 200 W) bestrahlt. Die Reaktionsmischung wurde mittels Dünnschichtchromatographie (DC) untersucht.

Ausbeute: Die Ausbeute wurde nicht bestimmt. Mittels DC-Untersuchung konnte das gewünschte Produkt **3** nachgewiesen werden. Die Abwesenheit von Edukt **6** deutet auf eine vollständige Umsetzung hin.

^{1}H-NMR (500 MHz, $CDCl_3$): 8.59 (ddd, $^3J_{H\text{-}P}$ = 14.3 Hz, ^4J = 1.7 Hz, ^5J = 0.4 Hz, 1H, Ar-3-*H*), 8.23 (m_c, 1H, Ar-5-*H*), 7.75 (ddd, ^3J = 8.0 Hz, $^4J_{H\text{-}P}$ = 4.8 Hz, ^5J = 0.4 Hz, 1H, Ar-6-*H*), 4.27 - 4.09 (m, 4H, C*H*$_2$), 3.95 (s, 6H, CO_2CH_3), 1.35 (td, ^3J = 7.1 Hz, $^4J_{H\text{-}P}$ = 0.5 Hz, 6H, C*H*$_3$) ppm.

^{31}P-NMR (202 MHz, $CDCl_3$): 14.6 (s, 1P, Ar-*P*) ppm.

6.2.1.2 2-Phosphoterephthalsäure (14)

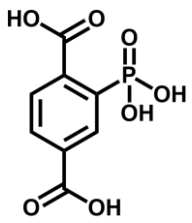

2-(Diethoxyphosphonyl)terephthalsäuredimethylester (**3**, 100 mg, 303 µmol) wurde mit Wasser (4.5 mL) und konz. Salzsäure (1.5 mL) versetzt und für 72 h bei 80 °C gerührt. Beim Abkühlen der Reaktionslösung auf Raumtemp. fiel ein farbloser Feststoff aus. Dieser wurde abfiltriert und i. Vak. getrocknet.

Ausbeute: 72 mg (293 µmol, 97 %).

Schmp.: 298 °C (Lit.[224]: 296 - 298 °C)

^{1}H-NMR (500 MHz, D_2O/NaOD): 7.98 (dd, $^3J_{H\text{-}P}$ = 12.2 Hz, ^4J = 1.5 Hz, 1H, Ar-3-*H*), 7.58 (br. d, ^3J = 7.9 Hz, 1H, Ar-5-*H*), 7.05 (dd, ^3J = 7.9 Hz, $^4J_{H\text{-}P}$ = 3.5 Hz, 1H, Ar-6-*H*) ppm.

^{31}P-NMR (202 MHz, D_2O/NaOD): 9.24 (s, 1P, Ar-*P*) ppm.

MS (ESI_{pos}): *m/z* = 247 $[M + H]^+$, 229 $[M - OH]^+$.

6.2.1.3 2-(Diethoxyphosphonylamino)terephthalsäuredimethylester (9)

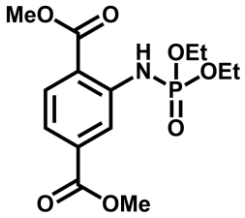

Vorschrift A:

2-Aminoterephthalsäuredimethylester (**8**, 100 mg, 478 µmol), Diethylphosphit (**2**, 123 µL, 955 µmol) und Iod (4.0 mg, 15.7 µmol) wurden vorgelegt und mit Dichlormethan (5 mL) versetzt. Die Reaktionsmischung wurde unter Luftsauerstoff für 12 h bei Raumtemp. gerührt. Anschließend wurde Ethylacetat (10 mL) und Wasser (10 mL) zugegeben. Die wässr. Phase wurde mit Ethylacetat (3 x 10 mL) extrahiert. Die vereinigten org. Extrakte wurden mit ges. Natriumchlorid-Lösung (40 mL) gewaschen und über Magnesiumsulfat getrocknet. Das Lösungsmittel wurde i. Vak. entfernt und der Rückstand mittels Säulenchromatographie (Kieselgel, Cyclohexan/Ethylacetat = 1:1, R_f = 0.17) gereinigt. Ein farbloser Feststoff wurde erhalten.

Ausbeute: 44 mg (127 µmol, 27 %).

Vorschrift B:

Unter Stickstoffatmosphäre wurden 2-Aminoterephthalsäuredimethylester (**8**, 100 mg, 478 µmol) und Triethylamin (70 µL, 505 µmol) in wasserfr. Dichlormethan (2 mL) vorgelegt und die Reaktionsmischung auf 0 °C abgekühlt. In einem Tropftrichter wurde wasserfr. Dichlormethan (2 mL) vorgelegt und Chlorphosphorsäurediethylester (**10**, 80 µL, 574 µmol) zugegeben. Diese Lösung wurde innerhalb von 15 min zugetropft und die Reaktionsmischung für 12 h bei Raumtemp. gerührt. Anschließend wurde Wasser (20 mL) zugegeben und weitere 5 h bei Raumtemp. gerührt. Die wässr. Phase wurde mit Dichlormethan (3 x 10 mL) extrahiert Die vereinigten org. Extrakte wurden mit ges. Natriumhydrogencarbonat-Lösung (40 mL) gewaschen, über Magnesiumsulfat getrocknet und das Lösungsmittel wurde i. Vak. entfernt. Der Rückstand wurde mittels Säulenchromatographie (Kieselgel, Cyclohexan/Ethylacetat = 1:1, R_f = 0.17) gereinigt. Ein farbloser Feststoff wurde erhalten.

Ausbeute: 30 mg (87 µmol, 18 %).

Schmp.: 64 °C.

^{1}H-NMR (500 MHz, $CDCl_3$): 9.17 (d, $^{2}J_{H\text{-}P}$ = 10.0 Hz, 1H, N*H*), 8.10 (d, ^{4}J = 1.5 Hz, 1H, Ar-3-*H*), 8.04 (dd, ^{3}J = 8.3 Hz, $^{5}J_{H\text{-}P}$ = 1.5 Hz, 1H, Ar-6-*H*), 7.57 (dd, ^{3}J = 8.3 Hz, ^{4}J = 1.5 Hz, 1H, Ar-5-*H*), 4.30 - 4.10 (m, 4H, CH_2), 3.93 (2s, 6H, CO_2CH_3), 1.35 (t, ^{3}J = 7.0 Hz, 6H, CH_3) ppm.

^{13}C-NMR (125 MHz, $CDCl_3$): 168.2 (s, 1-Ar-*C*O_2Me), 166.2 (s, 4-Ar-*C*O_2Me), 144.1 (s[d_P], $^{2}J_{C\text{-}P}$ = 1.8 Hz, Ar-2-*C*), 135.4 (s, Ar-4-*C*), 131.4 (d, Ar-6-*C*), 120.9 (d, Ar-5-*C*), 119.1 (d[d_P], $^{3}J_{C\text{-}P}$ = 2.2 Hz, Ar-3-*C*), 117.5 (s[d_P], $^{3}J_{C\text{-}P}$ = 9.4 Hz, Ar-1-*C*), 63.5 (t[d_P], $^{2}J_{C\text{-}P}$ = 5.4 Hz, P-O-*C*H_2), 52.67, 52.63 (2q, 1,4-Ar-CO_2*C*H_3), 16.3 (q[d_P], $^{3}J_{C\text{-}P}$ = 6.7 Hz, P-O-CH_2*C*H_3) ppm.

^{31}P-NMR (202 MHz, $CDCl_3$): 0.33 (s, 1P, NH-*P*) ppm.

HRMS (EI): *m/z* = $C_{14}H_{20}NO_7P$ ber. 345.0977; gef. 345.0977 (Δ <0.2 ppm).

IR (ATR): $\tilde{\nu}$ = 3245 (N-H Valenzschw.), 2956 (aliph. C-H-Valenzschw.), 1720, 1689 (C=O-Valenzschw.), 1576, 1507 (arom. C=C-Valenzschw.), 1297 (P=O), 1259, 1234 (C-O-Valenzschw.) cm^{-1}.

6.2.2 Postsynthetische Modifikationen

6.2.2.1 Probenvorbereitung für NMR-spektroskopische Untersuchungen

Die Untersuchung der postsynthetisch modifizierten Cr-MIL-101-Derivate erfolgte mit Hilfe der NMR-Spektroskopie. Dafür wurde der jeweilige MOF mit einer 2M-Natriumhydroxid-Lösung versetzt. Die Suspension wurde geschüttelt, bis eine klare grüne Lösung entstand. Anschließend wurde die Lösung mit 6M Salzsäure versetzt, bis ein pH-Wert zwischen 8 und 10 erreicht wurde. Unter diesen Bedingungen fielen die Cr^{3+}-Ionen als Chrom(III)hydroxid aus, welches durch Zentrifugieren und Abdekantieren abgetrennt werden konnte. Die abdekantierte Lösung wurde i. Vak. eingeengt. Der Rückstand wurde mit D_2O oder einer 4%-igen Lösung von NaOD in D_2O gelöst und NMR-spektroskopisch untersucht. Der Umsatz einer postsynthetischen Modifikation wurde durch Vergleich der Integrale von unmodifizierten und modifizierten Linkern bestimmt.

6.2.2.2 PSM von Cr-MIL-101-Br mit Triethylphosphit (7)

Cr-MIL-101-Br (20 mg) wurde in einem Mikrowellen-Vial vorgelegt und mit Triethylphosphit (**7**, 0.2 mL) und $PdCl_2$ (5.0 mg) versetzt. Die Suspension wurde in einer Synthese-Mikrowelle für 60 min bei 200 °C (max. 200 W) gerührt. Nach dem Abkühlen wurde die Reaktionsmischung zentrifugiert und die überstehende Lösung abgetrennt. Der grüne Feststoff wurde nacheinander mit Dichlormethan (3 x 10 mL), Ethanol (3 x 10 mL) und Wasser (3 x 10 mL) gewaschen. Dafür wurde der Feststoff mit dem jeweiligen Lösungsmittel versetzt und 10 min mit einem Vortex-Schüttler geschüttelt. Anschließend wurde das Lösungsmittel durch Zentrifugieren abgetrennt. Dieser Vorgang wurde mit jedem Lösungsmittel dreimal durchgeführt. Zuletzt wurde das MOF für 24 h bei 60 °C im Vakuumofen getrocknet und nach dem Auflösen mit 2M-Natriumhydroxid-Lösung NMR-spektroskopisch untersucht.

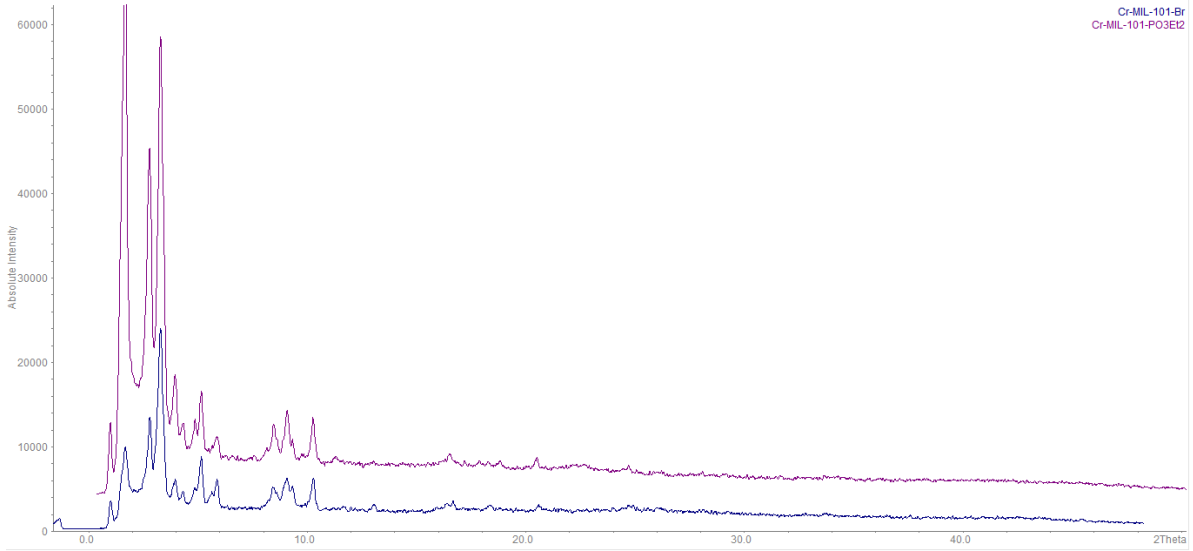

Abb. 64: Vergleich der Röntgenpulverdiffraktogramme von Cr-MIL-101-Br (unten) und Cr-MIL-101-PO_3Et_2 (oben).

6.2.2.3 PSM von Cr-MIL-101-NH_2 mit Phosphoroxychlorid (11)

Cr-MIL-101-NH_2 (10 mg), Pyridin (60 µL) und wasserfr. Toluol (2 mL) wurden in einem Mikrowellen-Vial vorgelegt und mit Phosphoroxychlorid (**11**, 500 µL) versetzt. Das Vial wurde in einer Synthese-Mikrowelle für 60 min auf 105 °C (max. 200 W) erhitzt. Nach dem Abkühlen wurde die Suspension zentrifugiert und die überstehende Lösung abgetrennt. Der Rückstand wurde nacheinander mit wasserfr. Toluol (3 x 10 mL), wasserfr. Dichlormethan (3 x 10 mL) und wasserfr. Aceton (3 x 10 mL) gewaschen. Dafür wurde der Feststoff mit dem jeweiligen Lösungsmittel versetzt und 10 min mit einem Vortex-Schüttler geschüttelt.

Anschließend wurde das Lösungsmittel durch Zentrifugieren abgetrennt. Dieser Vorgang wurde mit jedem Lösungsmittel dreimal durchgeführt. Nach dem letzten Waschvorgang wurde der Rückstand mit 2M-Natriumhydroxid-Lösung versetzt und NMR-spektroskopisch untersucht.

6.2.2.4 PSM von Cr-MIL-101-NH_2 mit Allylphosphonsäurediethylester (15)

Cr-MIL-101-NH_2 (70 mg) wurde mit einer 20%-igen, wässr. HBF_4-Lösung (1.4 mL) und einer wässr. Natriumnitrit-Lösung (32 mg in 1 mL Wasser) versetzt und für 3 h bei Raumtemp. gerührt. Die Suspension wurde zentrifugiert und die überstehende Lösung abgetrennt. Der Rückstand wurde mit Methanol (2 x 10 mL) gewaschen. Dafür wurde der Feststoff mit Methanol versetzt und 10 min mit einem Vortex-Schüttler geschüttelt. Anschließend wurde das Lösungsmittel durch Zentrifugieren abgetrennt und der Vorgang wiederholt. Der gewaschene Feststoff wurde in Methanol (1.6 mL) vorgelegt und mit Allylphosphonsäurediethylester (**15**, 280 µL, 1.60 mmol), $CaCO_3$ (8 mg, 80 µmol) und $Pd(OAc)_2$ (1.8 mg, 8.0 µmol) versetzt. Die Reaktionsmischung wurde für 48 h bei Raumtemp. gerührt. Anschließend wurde die Suspension zentrifugiert und die überstehende Lösung abgetrennt. Der Rückstand wurde nacheinander mit 5%-iger Salpetersäure (3 x 10 mL), Methanol (3 x 10 mL) und Dichlormethan (3 x 10 mL) gewaschen. Zuletzt wurde das MOF für 24 h bei 60 °C im Vakuumofen getrocknet und nach dem Auflösen mit 2M-Natriumhydroxid-Lösung NMR-spektroskopisch untersucht.

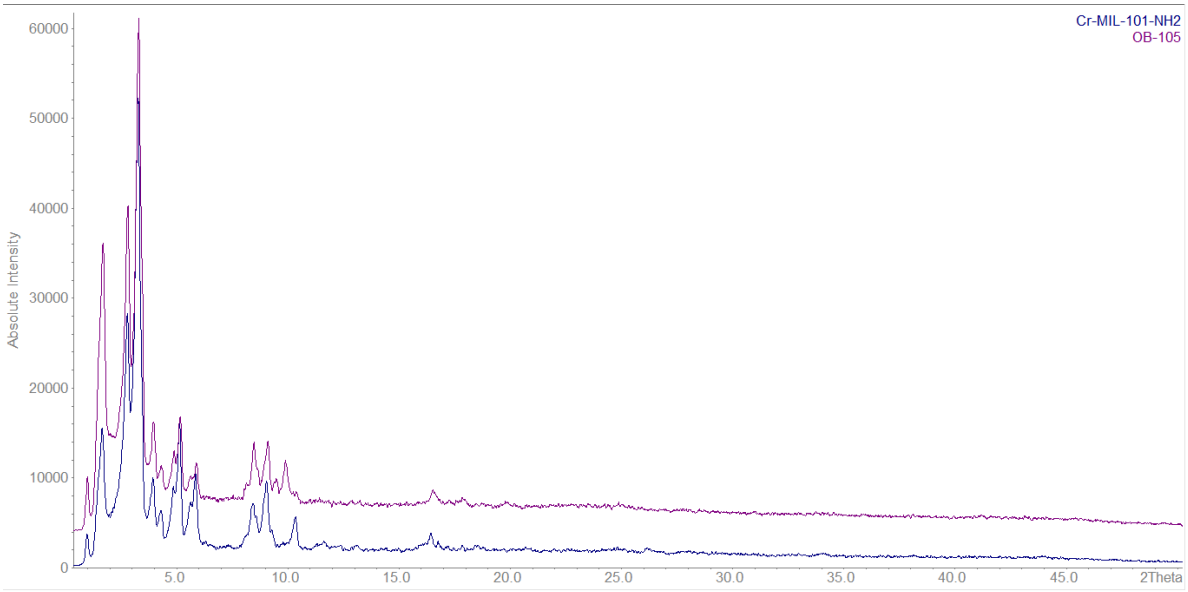

Abb. 65: Vergleich der Röntgenpulverdiffraktogramme von Cr-MIL-101-NH_2 (unten) und Cr-MIL-101-$C_3H_4PO_3Et_2$ (oben).

6.3 NMR-Spektren

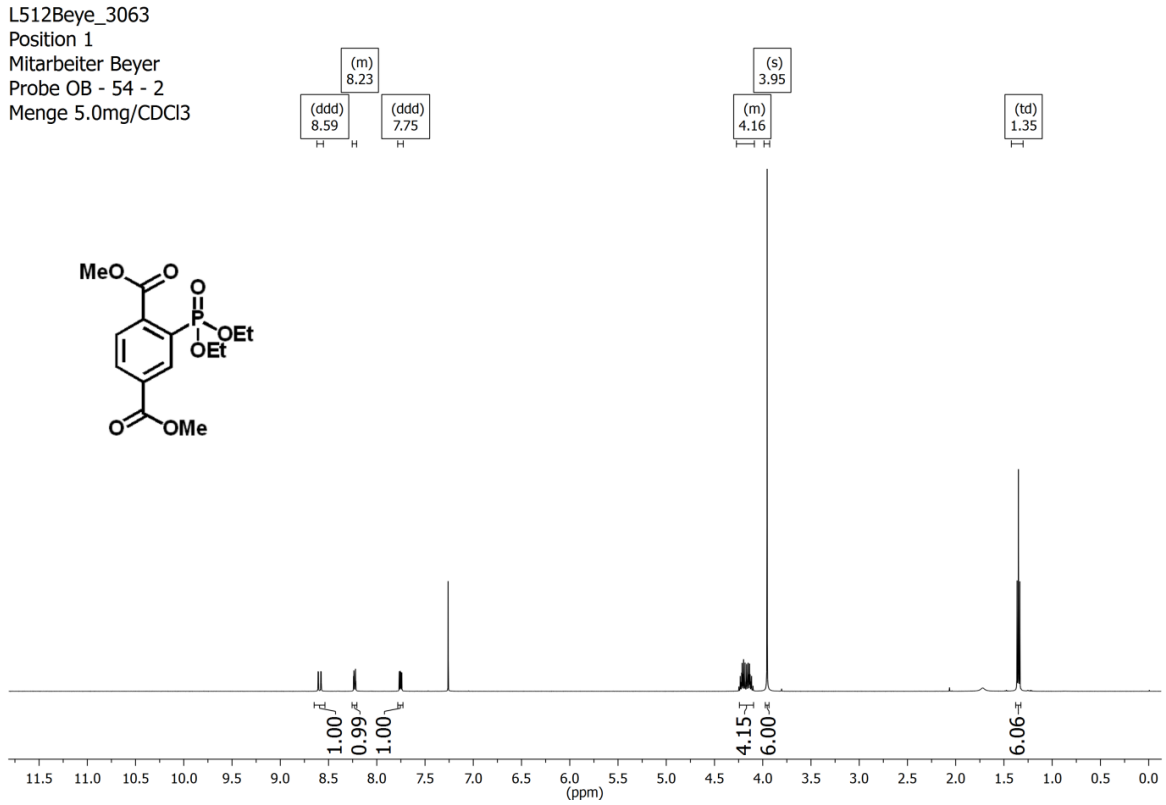

Abb. 66: ^{1}H-NMR-Spektrum von 2-(Diethoxyphosphonyl)terephthalsäuredimethylester (**3**).

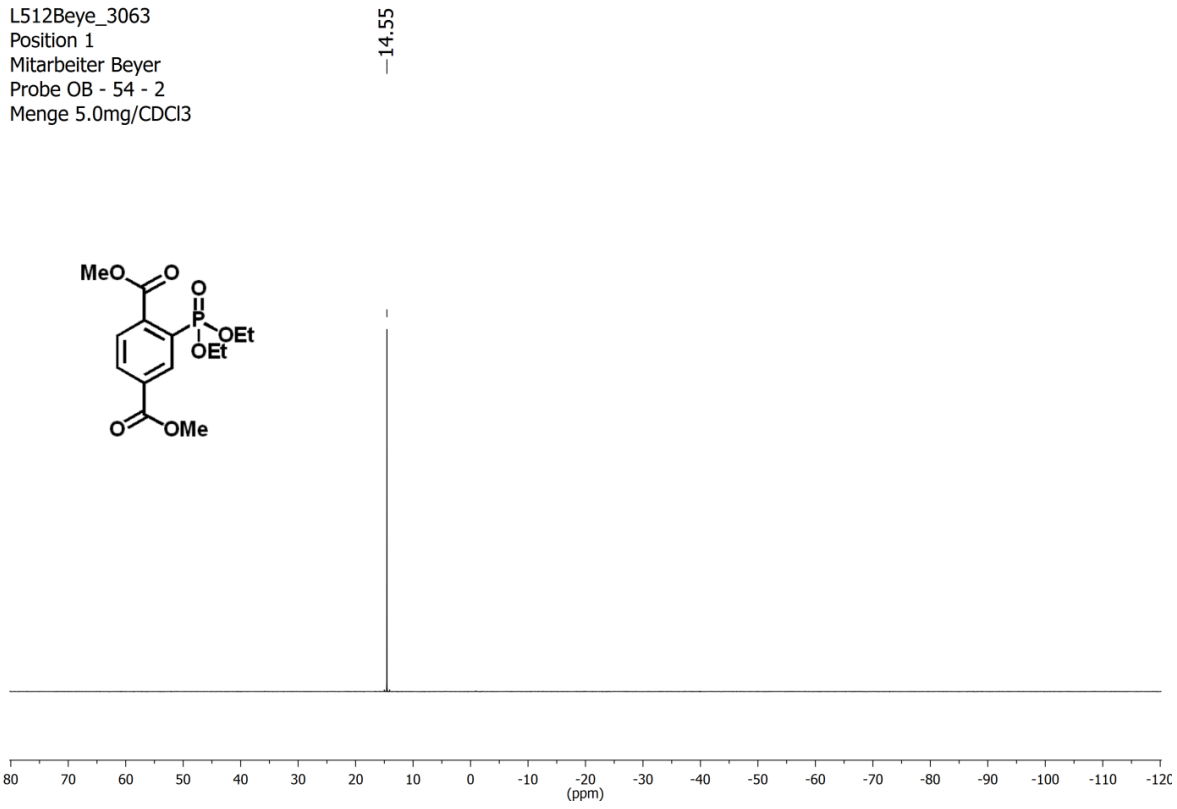

Abb. 67: ^{31}P-NMR-Spektrum von 2-(Diethoxyphosphonyl)terephthalsäuredimethylester (**3**).

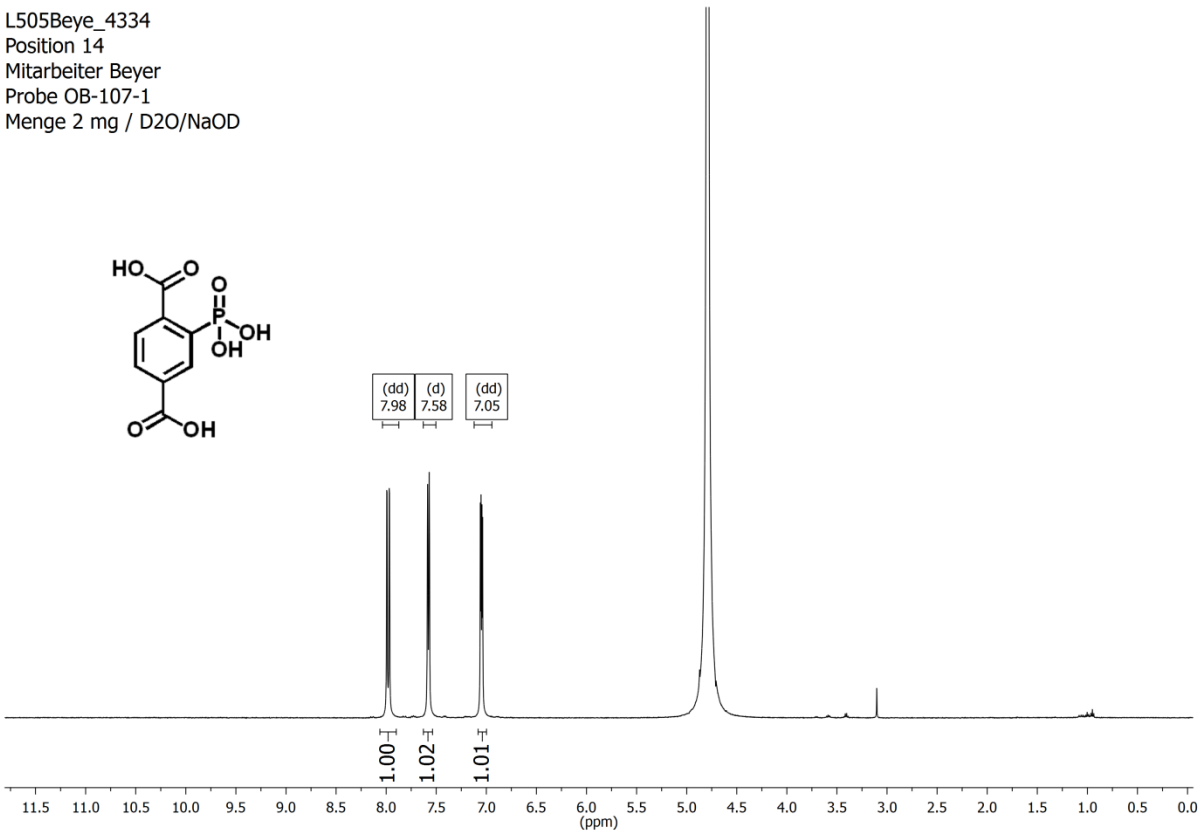

Abb. 68: ^{1}H-NMR-Spektrum von 2-Phosphoterephthalsäure (**14**).

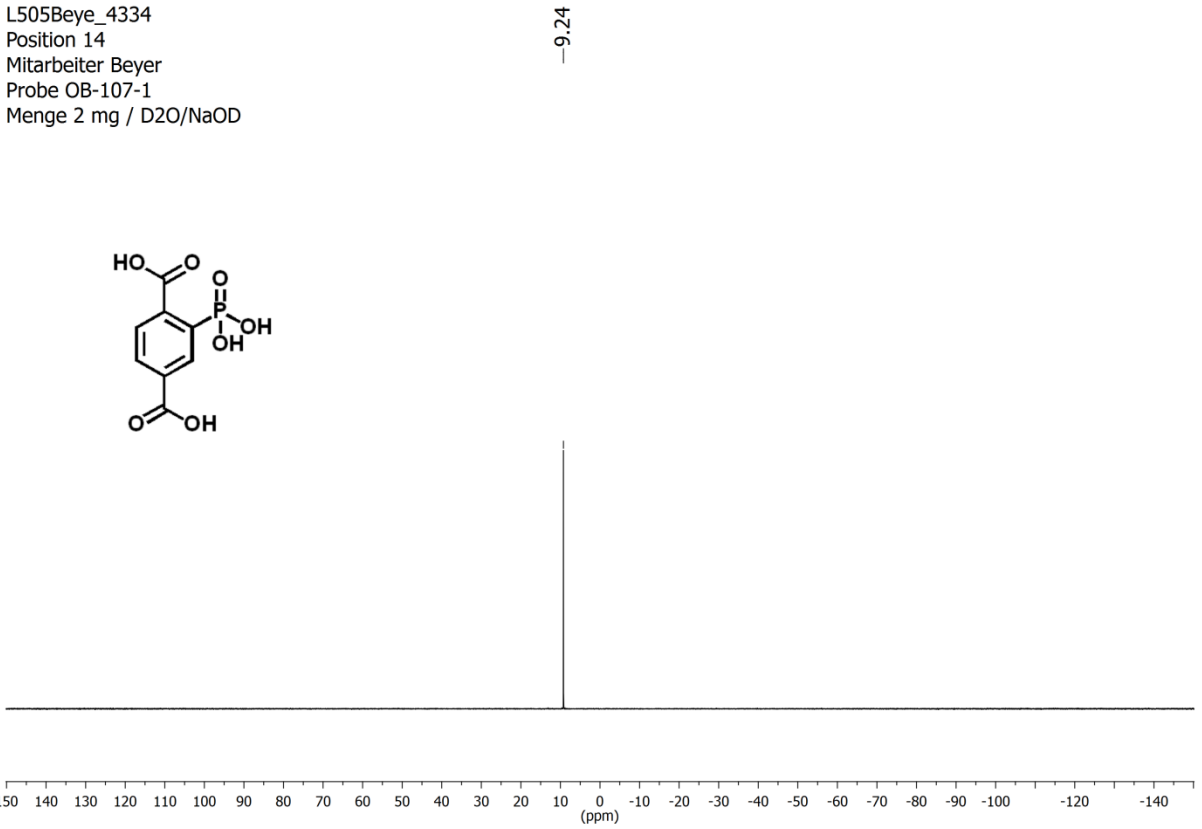

Abb. 69: ^{31}P-NMR-Spektrum von 2-Phosphoterephthalsäure (**14**).

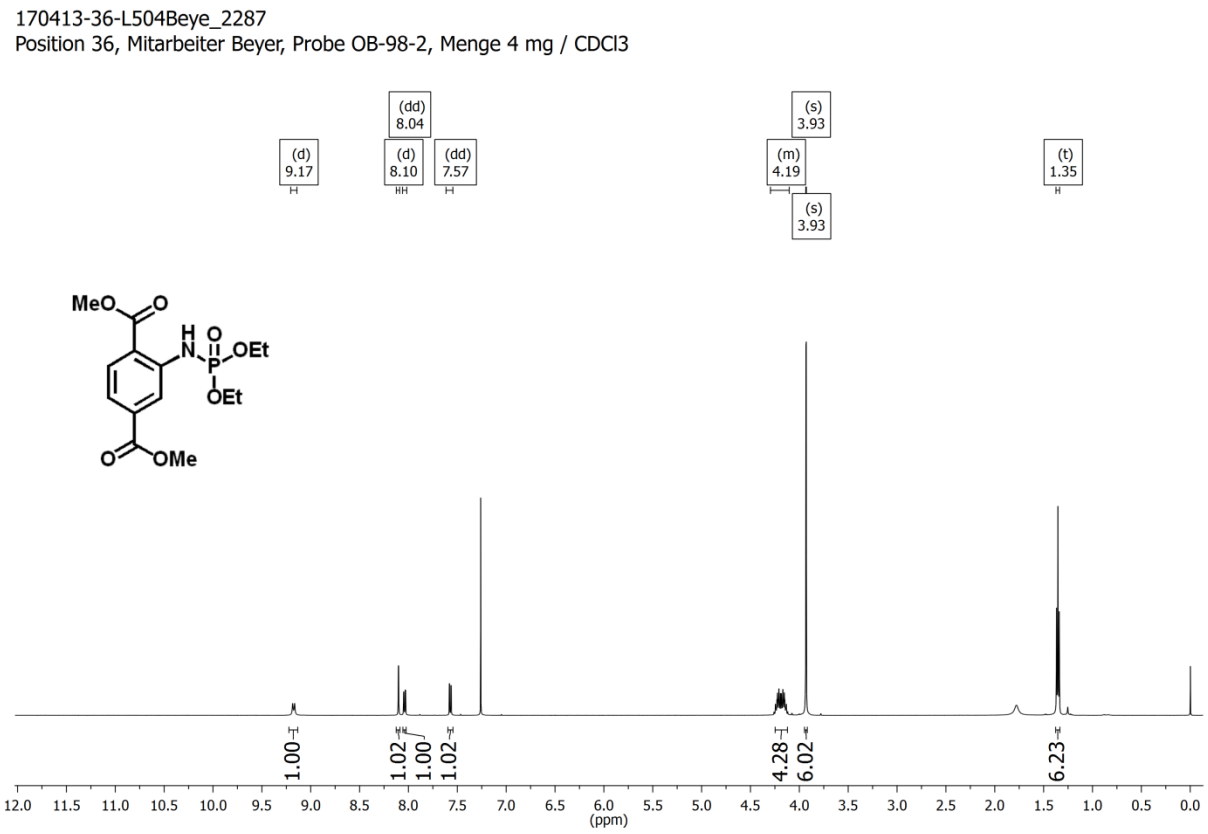

Abb. 70: ^{1}H-NMR-Spektrum von 2-(Diethoxyphosphonylamino)terephthalsäuredimethylester (**9**).

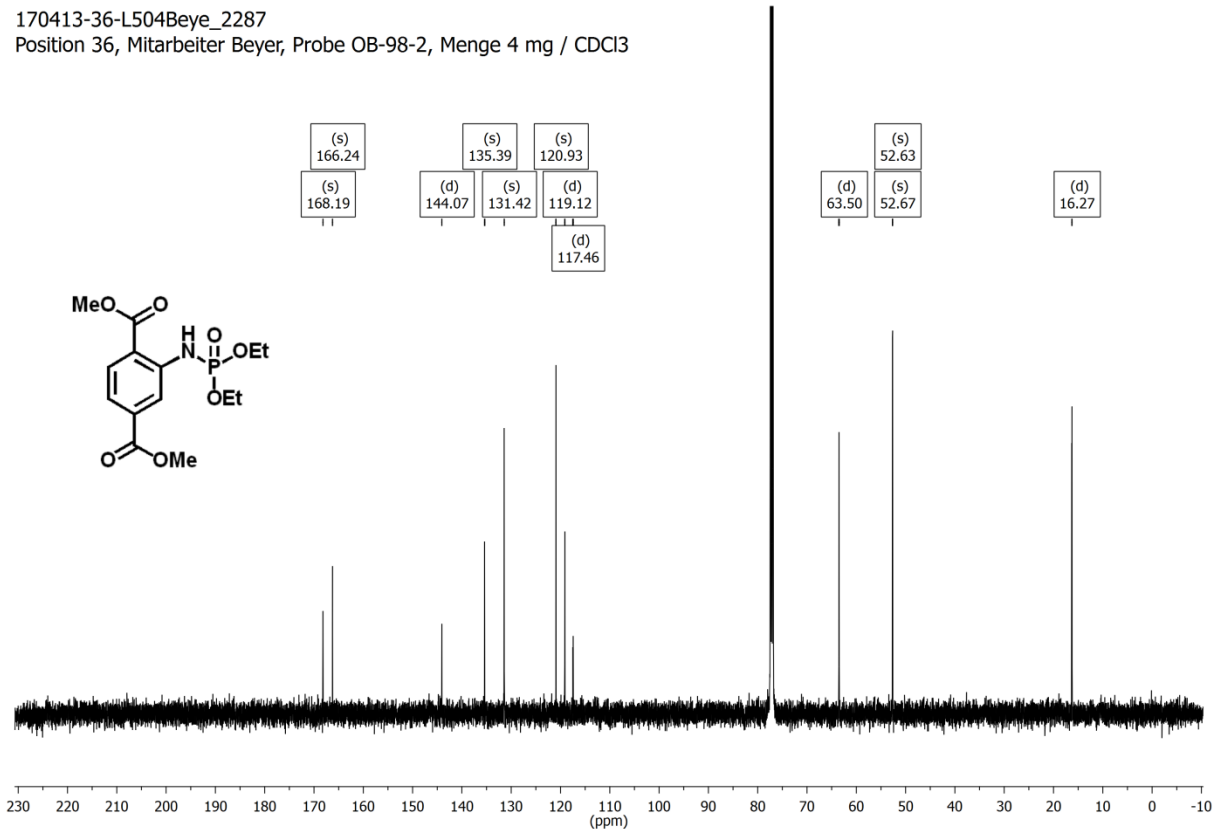

Abb. 71: ^{13}C-NMR-Spektrum von 2-(Diethoxyphosphonylamino)terephthalsäuredimethylester (**9**).

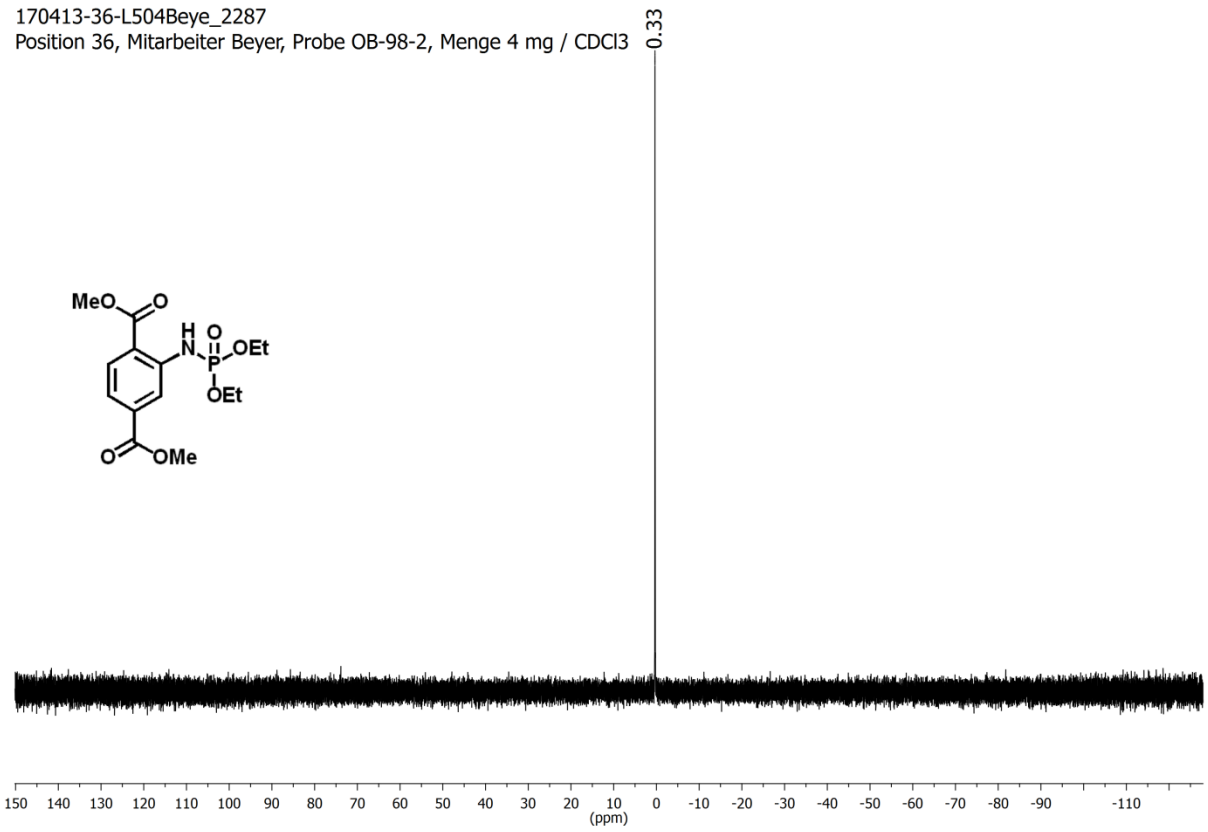

Abb. 72: ^{31}P-NMR-Spektrum von 2-(Diethoxyphosphonylamino)terephthalsäuredimethylester (**9**).

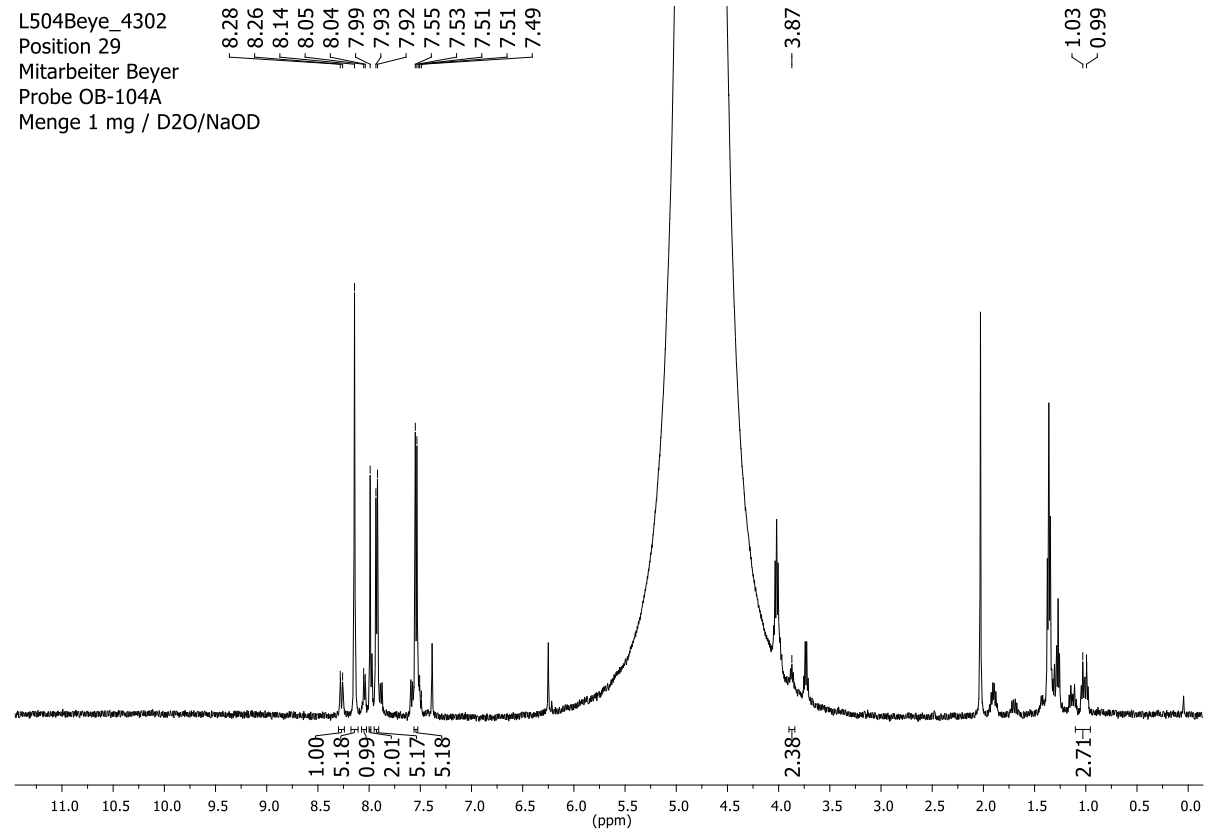

Abb. 73: ^{1}H-NMR-Spektrum nach dem Auflösen von Cr-MIL-101-PO_3Et_2.

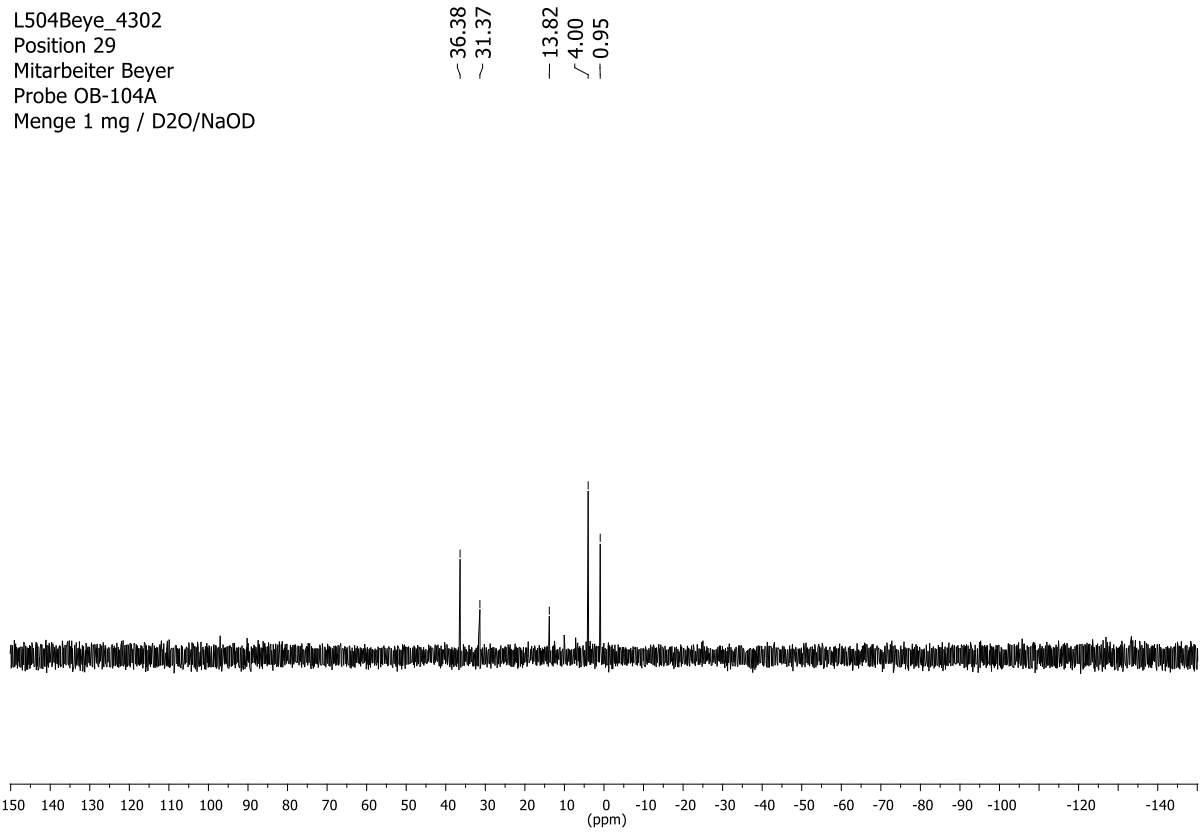

Abb. 74: ^{31}P-NMR-Spektrum nach dem Auflösen von Cr-MIL-101-PO_3Et_2.

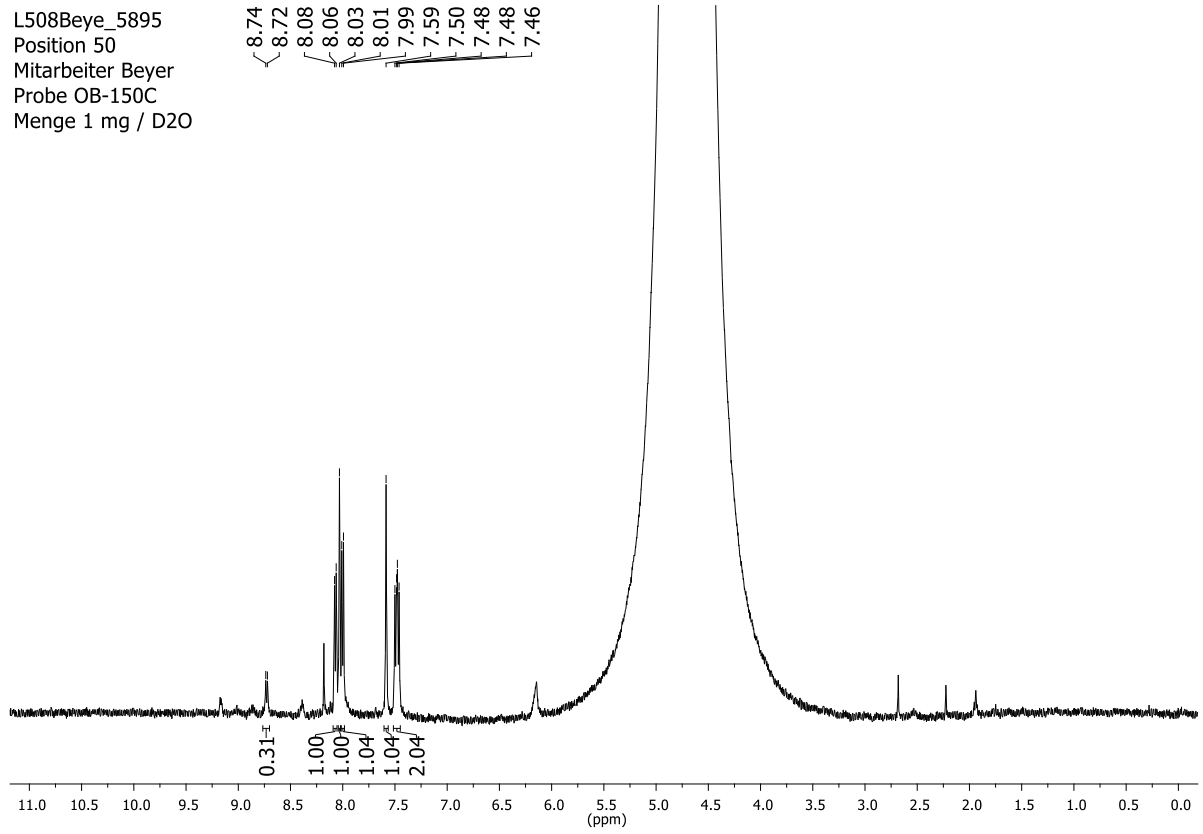

Abb. 75: ^{1}H-NMR-Spektrum nach dem Auflösen von Cr-MIL-101-$NHPO_3H_2$.

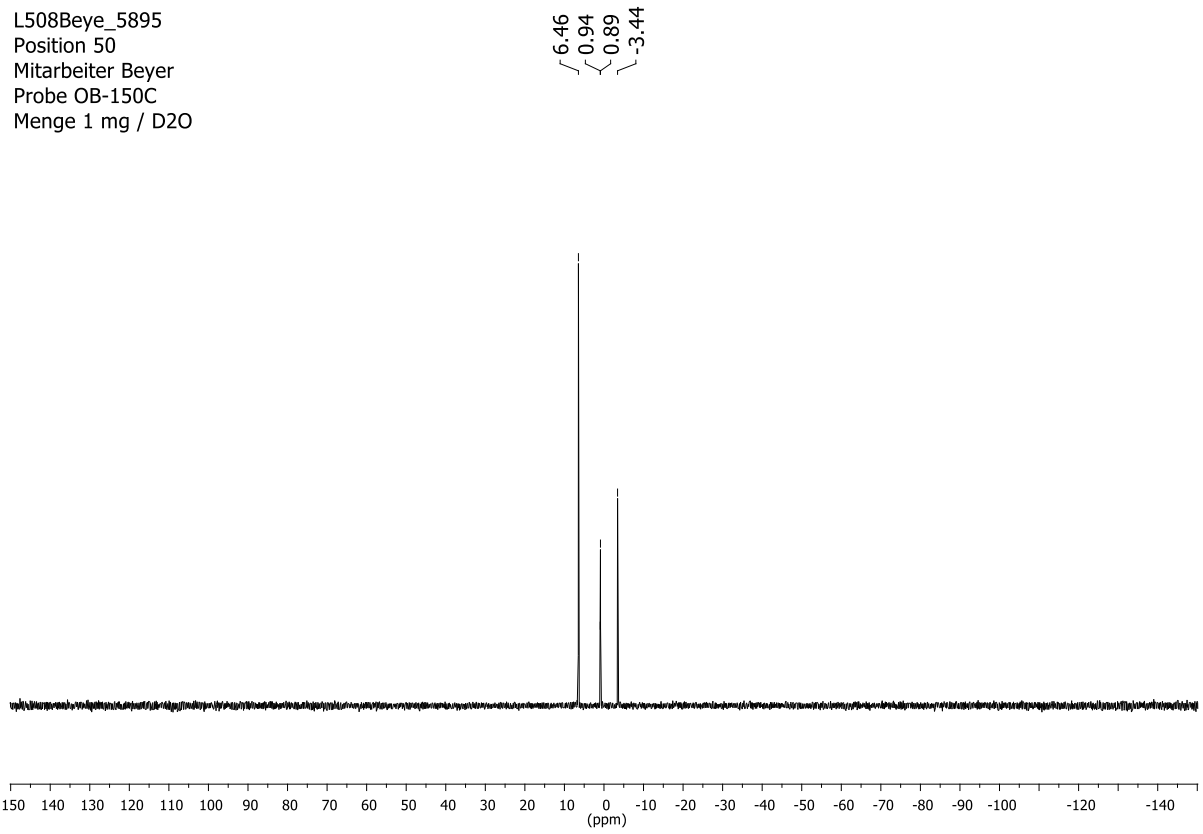

Abb. 76: ^{31}P-NMR-Spektrum nach dem Auflösen von Cr-MIL-101-$NHPO_3H_2$.

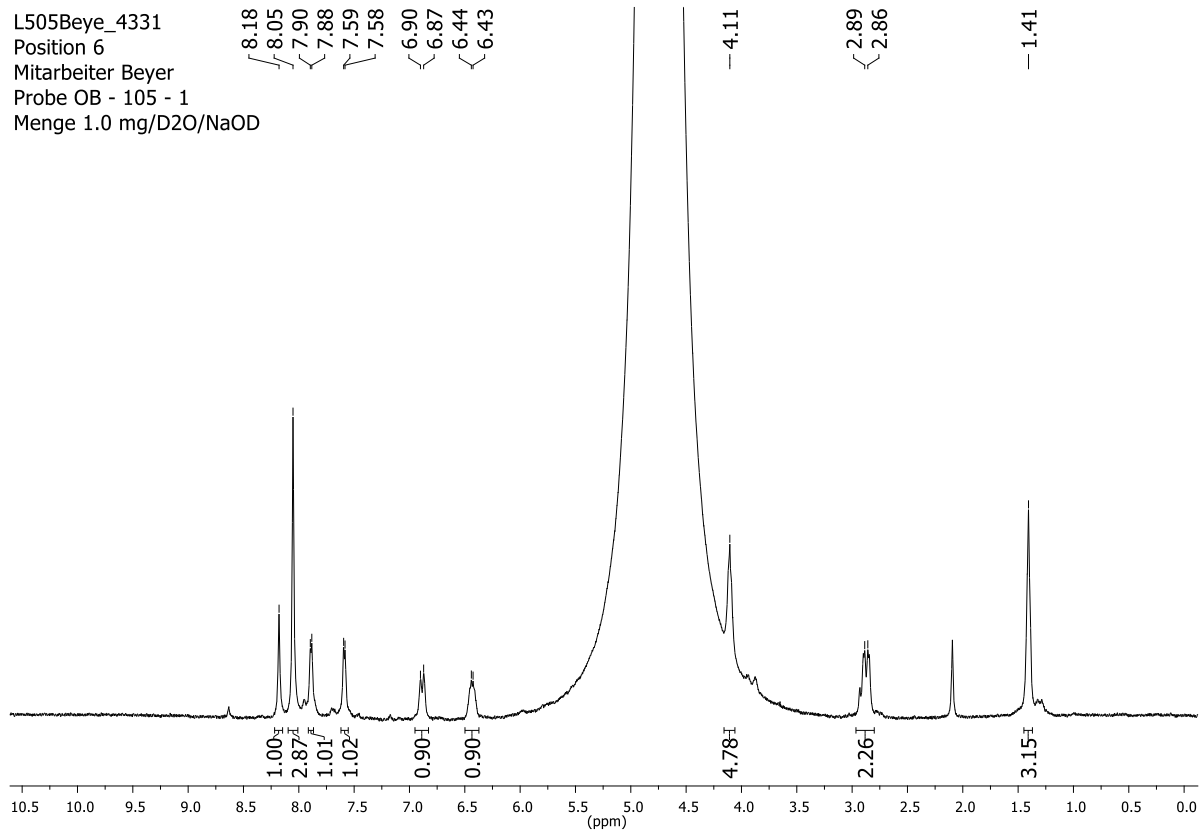

Abb. 77: ^{1}H-NMR-Spektrum nach dem Auflösen von Cr-MIL-101-$C_3H_4PO_3Et_2$.

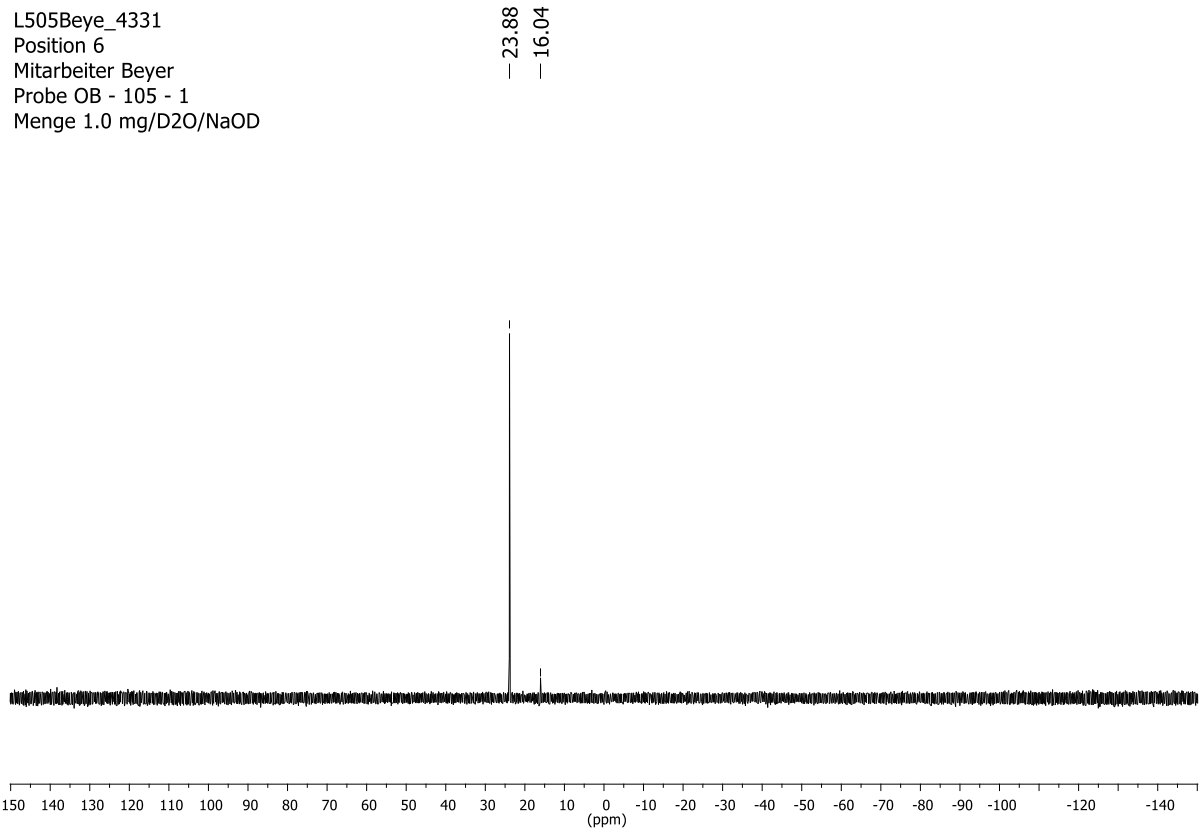

Abb. 78: ^{31}P-NMR-Spektrum nach dem Auflösen von Cr-MIL-101-$C_3H_4PO_3Et_2$.

7 Literaturverzeichnis

[1] D. Farrusseng, *Metal-Organic Frameworks*, John Wiley & Sons, Hoboken, **2011**.

[2] S. Kaskel, *The chemistry of metal-organic frameworks. Synthesis, characterization, and applications*, Wiley - VCH Verlag GmbH & Co. KGaA, Weinheim, **2016**.

[3] H.-C. J. Zhou, S. Kitagawa, *Chem. Soc. Rev.* **2014**, *43*, 5415–5418.

[4] H. Furukawa, K. E. Cordova, M. O'Keeffe, O. M. Yaghi, *Science* **2013**, *341*, 1230444.

[5] H.-C. Zhou, J. R. Long, O. M. Yaghi, *Chem. Rev.* **2012**, *112*, 673–674.

[6] A. Y. Robin, K. M. Fromm, *Coord. Chem. Rev.* **2006**, *250*, 2127–2157.

[7] S. Kitagawa, R. Kitaura, S. Noro, *Angew. Chem.* **2004**, *116*, 2388–2430, *Angew. Chem. Int. Ed.* **2004**, *43*, 2334–2375.

[8] S. R. Batten, N. R. Champness, X.-M. Chen, J. Garcia-Martinez, S. Kitagawa, L. Öhrström, M. O'Keeffe, M. P. Suh, J. Reedijk, *CrystEngComm* **2012**, *14*, 3001–3004.

[9] S. R. Batten, N. R. Champness, X.-M. Chen, J. Garcia-Martinez, S. Kitagawa, L. Öhrström, M. O'Keeffe, M. Paik Suh, J. Reedijk, *Pure Appl. Chem.* **2013**, *85*, 1715–1724.

[10] M. P. Suh, H. J. Park, T. K. Prasad, D.-W. Lim, *Chem. Rev.* **2012**, *112*, 782–835.

[11] K. Sumida, D. L. Rogow, J. A. Mason, T. M. McDonald, E. D. Bloch, Z. R. Herm, T.-H. Bae, J. R. Long, *Chem. Rev.* **2012**, *112*, 724–781.

[12] R. B. Getman, Y.-S. Bae, C. E. Wilmer, R. Q. Snurr, *Chem. Rev.* **2012**, *112*, 703–723.

[13] J.-R. Li, J. Sculley, H.-C. Zhou, *Chem. Rev.* **2012**, *112*, 869–932.

[14] J.-R. Li, R. J. Kuppler, H.-C. Zhou, *Chem. Soc. Rev.* **2009**, *38*, 1477–1504.

[15] Y.-B. Huang, J. Liang, X.-S. Wang, R. Cao, *Chem. Soc. Rev.* **2017**, *46*, 126–157.

[16] A. H. Chughtai, N. Ahmad, H. A. Younus, A. Laypkov, F. Verpoort, *Chem. Soc. Rev.* **2015**, *44*, 6804–6849.

[17] M. Yoon, R. Srirambalaji, K. Kim, *Chem. Rev.* **2012**, *112*, 1196–1231.

[18] J. Lee, O. K. Farha, J. Roberts, K. A. Scheidt, S. T. Nguyen, J. T. Hupp, *Chem. Soc. Rev.* **2009**, *38*, 1450–1459.

[19] P. Horcajada, R. Gref, T. Baati, P. K. Allan, G. Maurin, P. Couvreur, G. Ferey, R. E. Morris, C. Serre, *Chem. Rev.* **2012**, *112*, 1232–1268.

[20] R. C. Huxford, J. Della Rocca, W. Lin, *Curr. Opin. Chem. Biol.* **2010**, *14*, 262–268.

[21] E. Coronado, G. Minguez Espallargas, *Chem. Soc. Rev.* **2013**, *42*, 1525–1539.

[22] L. E. Kreno, K. Leong, O. K. Farha, M. Allendorf, R. P. van Duyne, J. T. Hupp, *Chem. Rev.* **2012**, *112*, 1105–1125.

[23] B. F. Hoskins, R. Robson, *J. Am. Chem. Soc.* **1989**, *111*, 5962–5964.

[24] B. F. Hoskins, R. Robson, *J. Am. Chem. Soc.* **1990**, *112*, 1546–1554.

[25] O. M. Yaghi, G. Li, H. Li, *Nature* **1995**, *378*, 703–706.

[26] O. M. Yaghi, H. Li, M. Eddaoudi, M. O'Keeffe, *Nature* **1999**, *402*, 276–279.

[27] S. S. Chui, *Science* **1999**, *283*, 1148–1150.

[28] K. S. Walton, R. Q. Snurr, *J. Am. Chem. Soc.* **2007**, *129*, 8552–8556.

[29] S. Brunauer, P. H. Emmett, E. Teller, *J. Am. Chem. Soc.* **1938**, *60*, 309–319.

[30] S. S. Kaye, A. Dailly, O. M. Yaghi, J. R. Long, *J. Am. Chem. Soc.* **2007**, *129*, 14176–14177.

[31] S. Xiang, W. Zhou, J. M. Gallegos, Y. Liu, B. Chen, *J. Am. Chem. Soc.* **2009**, *131*, 12415–12419.

[32] Bildnachweis: T. Boehle (lizensiert nach CCSA-3.0).

[33] N. Stock, S. Biswas, *Chem. Rev.* **2012**, *112*, 933–969.

[34] J. Cravillon, S. Münzer, S.-J. Lohmeier, A. Feldhoff, K. Huber, M. Wiebcke, *Chem. Mater.* **2009**, *21*, 1410–1412.

[35] L. Huang, *Microporous Mesoporous Mater.* **2003**, *58*, 105–114.

[36] D. J. Tranchemontagne, J. R. Hunt, O. M. Yaghi, *Tetrahedron* **2008**, *64*, 8553–8557.

[37] Y. Zhao, K. Li, J. Li, *Z. Naturforsch.* **2010**, 976–998.

[38] N. A. Khan, S. H. Jhung, *Coord. Chem. Rev.* **2015**, *285*, 11–23.

[39] J. Klinowski, F. A. A. Paz, P. Silva, J. Rocha, *Dalton Trans.* **2011**, *40*, 321–330.

[40] Z. Ni, R. I. Masel, *J. Am. Chem. Soc.* **2006**, *128*, 12394–12395.

[41] J. H. Bang, K. S. Suslick, *Adv. Mater.* **2010**, *22*, 1039–1059.

[42] T. Friščić, *J. Mater. Chem.* **2010**, *20*, 7599–7605.

[43] U. Mueller, H. Puetter, M. Hesse, M. Schubert, H. Wessel, J. Huff, M. Guzmann, (BASF Aktiengesellschaft), Method for electrochemical production of a crystalline porous metal organic skeleton material, 2. June 2005, *patent application*, WO2005/049892.

[44] P. M. Forster, N. Stock, A. K. Cheetham, *Angew. Chem.* **2005**, *117*, 7780–7784, *Angew. Chem. Int. Ed.* **2005**, *44*, 7608–7611.

[45] R. Banerjee, A. Phan, B. Wang, C. Knobler, H. Furukawa, M. O'Keeffe, O. M. Yaghi, *Science* **2008**, *319*, 939–943.

[46] N. Stock, *Microporous Mesoporous Mater.* **2010**, *129*, 287–295.

[47] T. Ahnfeldt, J. Moellmer, V. Guillerm, R. Staudt, C. Serre, N. Stock, *Chem. Eur. J.* **2011**, *17*, 6462–6468.

[48] O. M. Yaghi, M. O'Keeffe, M. Kanatzidis, *J. Solid State Chem.* **2000**, *152*, 1–321.

[49] O. M. Yaghi, H. Li, C. Davis, D. Richardson, T. L. Groy, *Acc. Chem. Res.* **1998**, *31*, 474–484.

[50] S. Kitagawa, M. Kondo, *Bull. Chem. Soc. Jpn.* **1998**, *71*, 1739–1753.

[51] S. R. Batten, R. Robson, *Angew. Chem.* **1998**, *110*, 1558–1595, *Angew. Chem. Int. Ed.* **1998**, *37*, 1460–1494.

[52] O. M. Yaghi, M. O'Keeffe, N. W. Ockwig, H. K. Chae, M. Eddaoudi, J. Kim, *Nature* **2003**, *423*, 705–714.

[53] N. W. Ockwig, O. Delgado-Friedrichs, M. O'Keeffe, O. M. Yaghi, *Acc. Chem. Res.* **2005**, *38*, 176–182.

[54] M. Eddaoudi, D. B. Moler, H. Li, B. Chen, T. M. Reineke, M. O'Keeffe, O. M. Yaghi, *Acc. Chem. Res.* **2001**, *34*, 319–330.

[55] D. J. Tranchemontagne, J. L. Mendoza-Cortes, M. O'Keeffe, O. M. Yaghi, *Chem. Soc. Rev.* **2009**, *38*, 1257–1283.

[56] Reprinted with permission from *Acc. Chem. Res.* **2011**, *44*, 123–133. Copyright 2010 American Chemical Society.

[57] H. Li, M. Eddaoudi, T. L. Groy, O. M. Yaghi, *J. Am. Chem. Soc.* **1998**, *120*, 8571–8572.

[58] P. D. C. Dietzel, R. Blom, H. Fjellvåg, *Eur. J. Inorg. Chem.* **2008**, 3624–3632.

[59] S. R. Caskey, A. G. Wong-Foy, A. J. Matzger, *J. Am. Chem. Soc.* **2008**, *130*, 10870–10871.

[60] N. L. Rosi, J. Kim, M. Eddaoudi, B. Chen, M. O'Keeffe, O. M. Yaghi, *J. Am. Chem. Soc.* **2005**, *127*, 1504–1518.

[61] Reprinted from *Chem. Eng. Sci.* **2011**, *66*, 163–170, Copyright 2010, with permission from Elsevier.

[62] H. Deng, S. Grunder, K. E. Cordova, C. Valente, H. Furukawa, M. Hmadeh, F. Gandara, A. C. Whalley, Z. Liu, S. Asahina, H. Kazumori, M. O'Keeffe, O. Terasaki, J. F. Stoddart, O. M. Yaghi, *Science* **2012**, *336*, 1018–1023.

[63] M. Eddaoudi, J. Kim, N. Rosi, D. Vodak, J. Wachter, M. O'Keeffe, O. M. Yaghi, *Science* **2002**, *295*, 469–472.

[64] Reproduced from *Chem. Soc. Rev.* **2014**, *43*, 5561–5593 with permission of The Royal Society of Chemistry.

[65] H. K. Chae, D. Y. Siberio-Perez, J. Kim, Y. Go, M. Eddaoudi, A. J. Matzger, M. O'Keeffe, O. M. Yaghi, *Nature* **2004**, *427*, 523–527.

[66] H. Furukawa, N. Ko, Y. B. Go, N. Aratani, S. B. Choi, E. Choi, A. O. Yazaydin, R. Q. Snurr, M. O'Keeffe, J. Kim, O. M. Yaghi, *Science* **2010**, *329*, 424–428.

[67] H. Furukawa, Y. B. Go, N. Ko, Y. K. Park, F. J. Uribe-Romo, J. Kim, M. O'Keeffe, O. M. Yaghi, *Inorg. Chem.* **2011**, *50*, 9147–9152.

[68] From *Science* **2010**, *329*, 424–428. Reprinted with permission from AAAS.

[69] Z. Miao, Y. Luan, C. Qi, D. Ramella, *Dalton Trans.* **2016**, *45*, 13917–13924.

[70] R. Kuang, L. Zheng, E. Cottrill, N. Pan, Y. Chi, J. Shi, C. Zhang, X. Chen, *RSC Adv.* **2016**, *6*, 97399–97403.

[71] C.-Y. Sun, X.-L. Wang, C. Qin, J.-L. Jin, Z.-M. Su, P. Huang, K.-Z. Shao, *Chem. Eur. J.* **2013**, *19*, 3639–3645.

[72] X.-S. Wang, J. Liang, L. Li, Z.-J. Lin, P. P. Bag, S.-Y. Gao, Y.-B. Huang, R. Cao, *Inorg. Chem.* **2016**, *55*, 2641–2649.

[73] Q. Gao, X.-L. Zhao, Z. Chang, J. Xu, X.-H. Bu, *Dalton Trans.* **2016**, *45*, 6830–6833.

[74] L. Zhang, J. Qian, W. Yang, X. Kuang, J. Zhang, Y. Cui, W. Wu, X.-Y. Wu, C.-Z. Lu, W.-Z. Chen, *J. Mater. Chem. A* **2015**, *3*, 15399–15402.

[75] D. Tian, X.-L. Zhou, Y.-H. Zhang, Z. Zhou, X.-H. Bu, *Inorg. Chem.* **2015**, *54*, 8159–8161.

[76] G. Brunet, D. A. Safin, I. Korobkov, A. Cognigni, M. Murugesu, *Cryst. Growth Des.* **2016**, *16*, 4043–4050.

[77] Y.-H. Han, Z.-Y. Zhou, C.-B. Tian, S.-W. Du, *Green Chem.* **2016**, *18*, 4086–4091.

[78] S. Pal, A. Bhunia, P. P. Jana, S. Dey, J. Mollmer, C. Janiak, H. P. Nayek, *Chem. Eur. J.* **2015**, *21*, 2789–2792.

[79] A. Abbasi, T. Moradpour, K. van Hecke, *Inorg. Chim. Acta* **2015**, *430*, 261–267.

[80] H. Zhang, D. Chen, H. Ma, P. Cheng, *Chem. Eur. J.* **2015**, *21*, 15854–15859.

[81] J. Wang, W. Sun, S. Chang, H. Liu, G. Zhang, Y. Wang, Z. Liu, *RSC Adv.* **2015**, *5*, 48574–48579.

[82] X. Zhang, Y.-Z. Zhang, D.-S. Zhang, B. Zhu, J.-R. Li, *Dalton Trans.* **2015**, *44*, 15697–15702.

[83] X. Zhang, Y. Zhang, H. Hu, Z. Chen, Z. Yuan, *Inorg. Chem. Commun.* **2015**, *55*, 65–68.

[84] D. Feng, T.-F. Liu, J. Su, M. Bosch, Z. Wei, W. Wan, D. Yuan, Y.-P. Chen, X. Wang, K. Wang, X. Lian, Z.-Y. Gu, J. Park, X. Zou, H.-C. Zhou, *Nat. Commun.* **2015**, *6*, 1–8.

[85] W. Gao, F. Xing, D. Zhou, M. Shao, S. Zhu, *Inorg. Chem. Commun.* **2011**, *14*, 601–605.

[86] D. Sun, S. Ma, Y. Ke, T. M. Petersen, H.-C. Zhou, *Chem. Commun.* **2005**, 2663–2665.

[87] S. Ma, H.-C. Zhou, *J. Am. Chem. Soc.* **2006**, *128*, 11734–11735.

[88] X.-B. Liu, Z.-Y. Xiao, A. Huang, W. Wang, L.-L. Zhang, R.-M. Wang, D.-F. Sun, *Z. Anorg. Allg. Chem.* **2016**, *642*, 31–35.

[89] J. Li, H.-R. Fu, J. Zhang, L.-S. Zheng, J. Tao, *Inorg. Chem.* **2015**, *54*, 3093–3095.

[90] D. Sun, S. Ma, Y. Ke, D. J. Collins, H.-C. Zhou, *J. Am. Chem. Soc.* **2006**, *128*, 3896–3897.

[91] S. Ma, D. Sun, M. Ambrogio, J. A. Fillinger, S. Parkin, H.-C. Zhou, *J. Am. Chem. Soc.* **2007**, *129*, 1858–1859.

[92] L. Han, L. Qin, L.-P. Xu, W.-N. Zhao, *Inorg. Chem.* **2013**, *52*, 1667–1669.

[93] D. Sun, Y. Ke, D. J. Collins, G. A. Lorigan, H.-C. Zhou, *Inorg. Chem.* **2007**, *46*, 2725–2734.

[94] X.-B. Liu, Z.-Y. Xiao, M.-H. Zhang, L.-L. Zhang, R.-M. Wang, D.-F. Sun, *Z. Anorg. Allg. Chem.* **2015**, *641*, 1781–1785.

[95] X. Wang, M. Chen, M. Du, *Inorg. Chem.* **2016**, *55*, 6352–6354.

[96] X. Zhang, L. Fan, Z. Sun, W. Zhang, W. Fan, L. Sun, X. Zhao, *CrystEngComm* **2013**, *15*, 4910–4916.

[97] J. Rong, W. Zhang, J. Bai, *CrystEngComm* **2016**, *18*, 7728–7736.

[98] S. Ma, D. Yuan, X.-S. Wang, H.-C. Zhou, *Inorg. Chem.* **2009**, *48*, 2072–2077.

[99] S. Ma, X.-S. Wang, D. Yuan, H.-C. Zhou, *Angew. Chem.* **2008**, *120*, 4198–4201, *Angew. Chem. Int. Ed.* **2008**, *47*, 4130–4133.

[100] Y. K. Park, S. B. Choi, H. Kim, K. Kim, B.-H. Won, K. Choi, J.-S. Choi, W.-S. Ahn, N. Won, S. Kim, D. H. Jung, S.-H. Choi, G.-H. Kim, S.-S. Cha, Y. H. Jhon, J. K. Yang, J. Kim, *Angew. Chem.* **2007**, *119*, 8378–8381, *Angew. Chem. Int. Ed.* **2007**, *46*, 8230–8233.

[101] A. Klinkebiel, O. Beyer, B. Malawko, U. Lüning, *Beilstein J. Org. Chem.* **2016**, *12*, 2267–2273.

[102] B. Chen, M. Eddaoudi, S. T. Hyde, M. O'Keeffe, O. M. Yaghi, *Science* **2001**, *291*, 1021–1023.

[103] http://rcsr.anu.edu.au/.

[104] Adapted with permission from *Inorg. Chem.* **2011**, *50*, 9147–9152. Copyright 2011 American Chemical Society.

[105] S. M. Cohen, *J. Am. Chem. Soc.* **2017**, *139*, 2855–2863.

[106] S. M. Cohen, *Chem. Rev.* **2012**, *112*, 970–1000.

[107] K. K. Tanabe, S. M. Cohen, *Chem. Soc. Rev.* **2011**, *40*, 498–519.

[108] Z. Wang, S. M. Cohen, *Chem. Soc. Rev.* **2009**, *38*, 1315–1329.

[109] S. Bernt, V. Guillerm, C. Serre, N. Stock, *Chem. Commun.* **2011**, *47*, 2838–2840.

[110] Z. Wang, S. M. Cohen, *J. Am. Chem. Soc.* **2007**, *129*, 12368–12369.

[111] K. K. Tanabe, Z. Wang, S. M. Cohen, *J. Am. Chem. Soc.* **2008**, *130*, 8508–8517.

[112] M. Savonnet, D. Bazer-Bachi, N. Bats, J. Perez-Pellitero, E. Jeanneau, V. Lecocq, C. Pinel, D. Farrusseng, *J. Am. Chem. Soc.* **2010**, *132*, 4518–4519.

[113] M. Savonnet, E. Kockrick, A. Camarata, D. Bazer-Bachi, N. Bats, V. Lecocq, C. Pinel, D. Farrusseng, *New J. Chem.* **2011**, *35*, 1892–1897.

[114] G. Tuci, A. Rossin, X. Xu, M. Ranocchiari, J. A. van Bokhoven, L. Luconi, I. Manet, M. Melucci, G. Giambastiani, *Chem. Mater.* **2013**, *25*, 2297–2308.

[115] Y. Goto, H. Sato, S. Shinkai, K. Sada, *J. Am. Chem. Soc.* **2008**, *130*, 14354–14355.

[116] A. D. Burrows, C. G. Frost, M. F. Mahon, C. Richardson, *Angew. Chem.* **2008**, *120*, 8610–8614, *Angew. Chem. Int. Ed.* **2008**, *47*, 8482–8486.

[117] W. Morris, C. J. Doonan, H. Furukawa, R. Banerjee, O. M. Yaghi, *J. Am. Chem. Soc.* **2008**, *130*, 12626–12627.

[118] K. Hindelang, A. Kronast, S. I. Vagin, B. Rieger, *Chem. Eur. J.* **2013**, *19*, 8244–8252.

[119] K. Hindelang, S. I. Vagin, C. Anger, B. Rieger, *Chem. Commun.* **2012**, *48*, 2888–2890.

[120] M. Kandiah, S. Usseglio, S. Svelle, U. Olsbye, K. P. Lillerud, M. Tilset, *J. Mater. Chem.* **2010**, *20*, 9848–9851.

[121] Z. Wang, K. K. Tanabe, S. M. Cohen, *Inorg. Chem.* **2009**, *48*, 296–306.

[122] Z. Wang, S. M. Cohen, *J. Am. Chem. Soc.* **2009**, *131*, 16675–16677.

[123] J. G. Nguyen, S. M. Cohen, *J. Am. Chem. Soc.* **2010**, *132*, 4560–4561.

[124] S. J. Garibay, S. M. Cohen, *Chem. Commun.* **2010**, *46*, 7700–7702.

[125] S. J. Garibay, Z. Wang, K. K. Tanabe, S. M. Cohen, *Inorg. Chem.* **2009**, *48*, 7341–7349.

[126] S. J. Garibay, Z. Wang, S. M. Cohen, *Inorg. Chem.* **2010**, *49*, 8086–8091.

[127] T. Gadzikwa, O. K. Farha, K. L. Mulfort, J. T. Hupp, S. T. Nguyen, *Chem. Commun.* **2009**, 3720–3722.

[128] K. K. Tanabe, S. M. Cohen, *Angew. Chem.* **2009**, *121*, 7560–7563, *Angew. Chem. Int. Ed.* **2009**, *48*, 7424–7427.

[129] M. Savonnet, S. Aguado, U. Ravon, D. Bazer-Bachi, V. Lecocq, N. Bats, C. Pinel, D. Farrusseng, *Green Chem.* **2009**, *11*, 1729–1732.

[130] Q. Yan, Y. Lin, P. Wu, L. Zhao, L. Cao, L. Peng, C. Kong, L. Chen, *ChemPlusChem* **2013**, *78*, 86–91.

[131] A. Modrow, D. Zargarani, R. Herges, N. Stock, *Dalton Trans.* **2012**, *41*, 8690–8696.

[132] J. S. Costa, P. Gamez, C. A. Black, O. Roubeau, S. J. Teat, J. Reedijk, *Eur. J. Inorg. Chem.* **2008**, 1551–1554.

[133] E. Dugan, Z. Wang, M. Okamura, A. Medina, S. M. Cohen, *Chem. Commun.* **2008**, 3366–3368.

[134] C. Volkringer, S. M. Cohen, *Angew. Chem.* **2010**, *122*, 4748–4752, *Angew. Chem. Int. Ed.* **2010**, 49, 4644–4648.

[135] C. J. Doonan, W. Morris, H. Furukawa, O. M. Yaghi, *J. Am. Chem. Soc.* **2009**, *131*, 9492–9493.

[136] M. J. Ingleson, J. P. Barrio, J.-B. Guilbaud, Y. Z. Khimyak, M. J. Rosseinsky, *Chem. Commun.* **2008**, 2680–2682.

[137] A. D. Burrows, L. L. Keenan, *CrystEngComm* **2012**, *14*, 4112–4114.

[138] K. M. L. Taylor-Pashow, J. Della Rocca, Z. Xie, S. Tran, W. Lin, *J. Am. Chem. Soc.* **2009**, *131*, 14261–14263.

[139] J. Jiang, O. M. Yaghi, *Chem. Rev.* **2015**, *115*, 6966–6997.

[140] S. Biswas, J. Zhang, Z. Li, Y.-Y. Liu, M. Grzywa, L. Sun, D. Volkmer, P. van der Voort, *Dalton Trans.* **2013**, *42*, 4730–4737.

[141] L. Wang, M. Yang, Z. Shi, Y. Chen, S. Feng, *J. Solid State Chem.* **2005**, *178*, 3359–3365.

[142] M. Lin Foo, S. Horike, T. Fukushima, Y. Hijikata, Y. Kubota, M. Takata, S. Kitagawa, *Dalton Trans.* **2012**, *41*, 13791–13794.

[143] G. Akiyama, R. Matsuda, H. Sato, M. Takata, S. Kitagawa, *Adv. Mater.* **2011**, *23*, 3294–3297.

[144] L.-J. Zhou, W.-H. Deng, Y.-L. Wang, G. Xu, S.-G. Yin, Q.-Y. Liu, *Inorg. Chem.* **2016**, *55*, 6271–6277.

[145] H. Liu, F.-G. Xi, W. Sun, N.-N. Yang, E.-Q. Gao, *Inorg. Chem.* **2016**, *55*, 5753–5755.

[146] R. S. Andriamitantsoa, J. Wang, W. Dong, H. Gao, G. Wang, *RSC Adv.* **2016**, *6*, 35135–35143.

[147] D. Britt, C. Lee, F. J. Uribe-Romo, H. Furukawa, O. M. Yaghi, *Inorg. Chem.* **2010**, *49*, 6387–6389.

[148] Z. Miao, C. Qi, A. M. Wensley, Y. Luan, *RSC Adv.* **2016**, *6*, 67226–67231.

[149] M. G. Goesten, J. Juan-Alcañiz, E. V. Ramos-Fernandez, K. B. Sai Sankar Gupta, E. Stavitski, H. van Bekkum, J. Gascon, F. Kapteijn, *J. Catal.* **2011**, *281*, 177–187.

[150] M. Carboni, C. W. Abney, S. Liu, W. Lin, *Chem. Sci.* **2013**, *4*, 2396–2402.

[151] X. Meng, H.-N. Wang, S.-Y. Song, H.-J. Zhang, *Chem. Soc. Rev.* **2017**, *46*, 464–480.

[152] P. Ramaswamy, N. E. Wong, G. K. H. Shimizu, *Chem. Soc. Rev.* **2014**, *43*, 5913–5932.

[153] K.-D. Kreuer, *Chem. Mater.* **2014**, *26*, 361–380.

[154] J. M. Taylor, K. W. Dawson, G. K. H. Shimizu, *J. Am. Chem. Soc.* **2013**, *135*, 1193–1196.

[155] S. Kim, K. W. Dawson, B. S. Gelfand, J. M. Taylor, G. K. H. Shimizu, *J. Am. Chem. Soc.* **2013**, *135*, 963–966.

[156] X.-Y. Dong, R. Wang, J.-B. Li, S.-Q. Zang, H.-W. Hou, T. C. W. Mak, *Chem. Commun.* **2013**, *49*, 10590–10592.

[157] W. J. Phang, H. Jo, W. R. Lee, J. H. Song, K. Yoo, B. Kim, C. S. Hong, *Angew. Chem.* **2015**, *127*, 5231–5235, *Angew. Chem. Int. Ed.* **2015**, *54*, 5142–5146.

[158] M. Feyand, C. F. Seidler, C. Deiter, A. Rothkirch, A. Lieb, M. Wark, N. Stock, *Dalton Trans.* **2013**, *42*, 8761–8770.

[159] S. Pili, S. P. Argent, C. G. Morris, P. Rought, V. Garcia-Sakai, I. P. Silverwood, T. L. Easun, M. Li, M. R. Warren, C. A. Murray, C. C. Tang, S. Yang, M. Schroder, *J. Am. Chem. Soc.* **2016**, *138*, 6352–6355.

[160] J. M. Taylor, R. K. Mah, I. L. Moudrakovski, C. I. Ratcliffe, R. Vaidhyanathan, G. K. H. Shimizu, *J. Am. Chem. Soc.* **2010**, *132*, 14055–14057.

[161] P. Ramaswamy, N. E. Wong, B. S. Gelfand, G. K. H. Shimizu, *J. Am. Chem. Soc.* **2015**, *137*, 7640–7643.

[162] M. Bazaga-Garcia, R. M. P. Colodrero, M. Papadaki, P. Garczarek, J. Zon, P. Olivera-Pastor, E. R. Losilla, L. Leon-Reina, M. A. G. Aranda, D. Choquesillo-Lazarte, K. D. Demadis, A. Cabeza, *J. Am. Chem. Soc.* **2014**, *136*, 5731–5739.

[163] T. Kundu, S. C. Sahoo, R. Banerjee, *Chem. Commun.* **2012**, *48*, 4998–5000.

[164] P. Maniam, C. Näther, N. Stock, *Eur. J. Inorg. Chem.* **2010**, 3866–3874.

[165] A. Sonnauer, M. Feyand, N. Stock, *Cryst. Growth Des.* **2009**, *9*, 586–592.

[166] A. Sonnauer, C. Nather, H. A. Hoppe, J. Senker, N. Stock, *Inorg. Chem.* **2007**, *46*, 9968–9974.

[167] Z.-Y. Du, A. V. Prosvirin, J.-G. Mao, *Inorg. Chem.* **2007**, *46*, 9884–9894.

[168] F. Adani, M. Casciola, D. J. Jones, L. Massinelli, E. Montoneri, J. Rozière, R. Vivani, *J. Mater. Chem.* **1998**, *8*, 961–964.

[169] A. F. Benedetto, P. J. Squattrito, F. Adani, E. Montoneri, *Inorg. Chim. Acta* **1997**, *260*, 207–216.

[170] V. Zima, J. Svoboda, K. Melánová, L. Beneš, M. Casciola, M. Sganappa, J. Brus, M. Trchová, *Solid State Ionics* **2010**, *181*, 705–713.

[171] J. Pan, S. Wang, M. Xiao, M. Hickner, Y. Meng, *J. Membr. Sci.* **2013**, *443*, 19–27.

[172] A. Klinkebiel, *Dissertation* **2015**, Christian-Albrechts-Universität zu Kiel.

[173] D. J. Hoffart, S. A. Dalrymple, G. K. H. Shimizu, *Inorg. Chem.* **2005**, *44*, 8868–8875.

[174] M. Krüger, H. Reinsch, A. K. Inge, N. Stock, *Microporous Mesoporous Mater.* **2017**, *249*, 128-136.

[175] E. Mühlbauer, A. Klinkebiel, O. Beyer, F. Auras, S. Wuttke, U. Lüning, T. Bein, *Microporous Mesoporous Mater.* **2015**, *216*, 51–55.

[176] A. Coelho, *TOPAS Academic 4.1*, Coelho Software, **2007**.

[177] M. Feyand, E. Mugnaioli, F. Vermoortele, B. Bueken, J. M. Dieterich, T. Reimer, U. Kolb, D. de Vos, N. Stock, *Angew. Chem.* **2012**, *124*, 10519–10522, Angew. Chem. Int. Ed., 2012, 51, 10373–10376.

[178] T. Düren, F. Millange, G. Férey, K. S. Walton, R. Q. Snurr, *J. Phys. Chem. C* **2007**, *111*, 15350–15356.

[179] *Materials Studio 5.5.3*, Accelrys Software Inc., **2010**.

[180] V. Favre-Nicolin, R. Černý, *J. Appl. Crystallogr.* **2002**, *35*, 734–743.

[181] J. de Decker, J. de Clercq, P. Vermeir, P. van der Voort, *J. Mater. Sci.* **2016**, *51*, 5019–5026.

[182] G. Ferey, C. Mellot-Draznieks, C. Serre, F. Millange, J. Dutour, S. Surble, I. Margiolaki, *Science* **2005**, *309*, 2040–2042.

[183] J. Chen, K. Li, L. Chen, R. Liu, X. Huang, D. Ye, *Green Chem.* **2014**, *16*, 2490–2499.

[184] Z. Li, G. He, Y. Zhao, Y. Cao, H. Wu, Y. Li, Z. Jiang, *J. Power Sources* **2014**, *262*, 372–379.

[185] M. Saikia, L. Saikia, *RSC Adv.* **2016**, *6*, 15846–15853.

[186] M. Lammert, S. Bernt, F. Vermoortele, D. E. de Vos, N. Stock, *Inorg. Chem.* **2013**, *52*, 8521–8528.

[187] C. S. Demmer, N. Krogsgaard-Larsen, L. Bunch, *Chem. Rev.* **2011**, *111*, 7981–8006.

[188] A. K. Bhattacharya, G. Thyagarajan, *Chem. Rev.* **1981**, *81*, 415–430.

[189] V. André, H. Lahrache, S. Robin, G. Rousseau, *Tetrahedron* **2007**, *63*, 10059–10066.

[190] R. J. Cohen, D. L. Fox, J. F. Eubank, R. N. Salvatore, *Tetrahedron Lett.* **2003**, *44*, 8617–8621.

[191] G. Lavén, J. Stawinski, *Synlett* **2009**, 225–228.

[192] G. Lavén, M. Kalek, M. Jezowska, J. Stawinski, *New J. Chem.* **2010**, *34*, 967–975.

[193] C. W. Barfoot, J. E. Harvey, M. N. Kenworthy, J. P. Kilburn, M. Ahmed, R. J. Taylor, *Tetrahedron* **2005**, *61*, 3403–3417.

[194] P. Sampson, G. B. Hammond, D. F. Wiemer, *J. Org. Chem.* **1986**, *51*, 4342–4347.

[195] H. Zhang, R. Tsukuhara, G. Tigyi, G. D. Prestwich, *J. Org. Chem.* **2006**, *71*, 6061–6066.

[196] T. Hirao, T. Masunaga, Y. Ohshiro, T. Agawa, *Tetrahedron Lett.* **1980**, *21*, 3595–3598.

[197] T. Hirao, T. Masunaga, N. Yamada, Y. Ohshiro, T. Agawa, *Bull. Chem. Soc. Jpn.* **1982**, *55*, 909–913.

[198] M. Kalek, A. Ziadi, J. Stawinski, *Org. Lett.* **2008**, *10*, 4637–4640.

[199] D. Villemin, A. Elbilali, F. SimÉon, P.-A. Jaffrès, G. Maheut, M. Mosaddak, A. Hakiki, *J. Chem. Res. (S)* **2003**, 436–437.

[200] P. Tavs, *Chem. Ber.* **1970**, *103*, 2428–2436.

[201] T. M. Balthazor, R. C. Grabiak, *J. Org. Chem.* **1980**, *45*, 5425–5426.

[202] D. Gelman, L. Jiang, S. L. Buchwald, *Org. Lett.* **2003**, *5*, 2315–2318.

[203] S. Thielges, P. Bisseret, J. Eustache, *Org. Lett.* **2005**, *7*, 681–684.

[204] O. Tayama, A. Nakano, T. Iwahama, S. Sakaguchi, Y. Ishii, *J. Org. Chem.* **2004**, *69*, 5494–5496.

[205] W. Xu, J.-P. Zou, W. Zhang, *Tetrahedron Lett.* **2010**, *51*, 2639–2643.

[206] M. Hatano, S. Suzuki, E. Takagi, K. Ishihara, *Tetrahedron Lett.* **2009**, *50*, 3171–3174.

[207] R. G. de Noronha, P. J. Costa, C. C. Romão, M. J. Calhorda, A. C. Fernandes, *Organometallics* **2009**, *28*, 6206–6212.

[208] E. Maerten, S. Cabrera, A. Kjaersgaard, K. A. Jorgensen, *J. Org. Chem.* **2007**, *72*, 8893–8903.

[209] D. Zhao, Y. Yuan, A. S. C. Chan, R. Wang, *Chem. Eur. J.* **2009**, *15*, 2738–2741.

[210] Y. Gao, G. Wang, L. Chen, P. Xu, Y. Zhao, Y. Zhou, L.-B. Han, *J. Am. Chem. Soc.* **2009**, *131*, 7956–7957.

[211] A. Allen, D. R. Manke, W. Lin, *Tetrahedron Lett.* **2000**, *41*, 151–154.

[212] L.-B. Han, M. Tanaka, *J. Am. Chem. Soc.* **1996**, *118*, 1571–1572.

[213] L.-B. Han, C. Zhang, H. Yazawa, S. Shimada, *J. Am. Chem. Soc.* **2004**, *126*, 5080–5081.

[214] A. I. Kuramshin, A. A. Nikolaev, R. A. Cherkasov, *Mendeleev Commun.* **2005**, *15*, 155–156.

[215] F. R. Atherton, H. T. Openshaw, A. R. Todd, *J. Chem. Soc.* **1945**, 660–663.

[216] S. S. Le Corre, M. Berchel, H. Couthon-Gourves, J.-P. Haelters, P.-A. Jaffres, *Beilstein J. Org. Chem.* **2014**, *10*, 1166–1196.

[217] Y. Zhou, J. Yang, T. Chen, S.-F. Yin, D. Han, L.-B. Han, *Bull. Chem. Soc. Jpn.* **2014**, *87*, 400–402.

[218] B. A. Dar, N. A. Dangroo, A. Gupta, A. Wali, M. A. Khuroo, R. A. Vishwakarma, B. Singh, *Tetrahedron Lett.* **2014**, *55*, 1544–1548.

[219] H. Stutz, H.-G. Henning, *Z. Chem.* **1975**, *15*, 52–54.

[220] V. Benin, S. Durganala, A. B. Morgan, *J. Mater. Chem.* **2012**, *22*, 1180–1190.

[221] T. Liu, J.-X. Che, Y.-Z. Hu, X.-W. Dong, X.-Y. Liu, C.-M. Che, *Chem. Eur. J.* **2014**, *20*, 14090–14095.

[222] T. Homburg, *Aktuelle Arbeiten*, Christian-Albrechts-Universität zu Kiel.

[223] S. Wöhlbrandt, *Aktuelle Arbeiten*, Christian-Albrechts-Universität zu Kiel.

[224] N. Ivan, V. Benin, A. B. Morgan, *Synth. Commun.* **2013**, *43*, 1831–1836.